

Regd. No. C-1139

# INDIAN JOURNAL OF PHYSICS

**VOL. 38**

AND

**PROCEEDINGS**

OF THE

Indian Association for the Cultivation of Science, Vol. 47

*(Edited in Collaboration with the Indian Physical Society)*

( With Twelve Plates )

Published by the Registrar, Indian Association for the Cultivation of Science,  
Jadavpur, Calcutta 32 and printed by Kalipada Mukherjee, Eka  
Press, 204/1, B. T. Road, Calcutta

**1964**

## BOARD OF EDITORS

K. BANERJEE	S. R. KHASTGIR
G. N. BHATTACHARYA	D. S. KOTHARI
D. M. BOSE	B. D. NAG CHOUDHURI
S. N. BOSE	K. R. RAO
S. D. CHATTERJEE	D. B. SINHA
P. S. GILL	S. C. SIRKAR
B. N. SRIVASTAVA	A. BOSE ( <i>Secretary</i> )

## EDITORIAL COLLABORATORS

PROF. R. K. ASUNDI, PH.D., F.N.I.  
PROF. D. BASU, PH.D.  
PROF. J. N. BHAR, D.Sc., M.I.E.R.E., F.N.I.  
PROF. V. G. BHIDE, PH.D.(Nag.), PH.D.(Lond)  
PROF. H. N. BOSE  
PROF. S. K. CHAKRABORTY, D.Sc., F.N.I.  
DR. J. S. CHATTERJEE,  
DR. K. DAS GUPTA, PH.D.,  
PROF. N. N. DAS GUPTA, PH.D., F.N.I.  
DR. J. DHAR, D.Phil. (Sc)  
PROF. A. K. DUTTA, D.Sc., F.N.I.,  
DR. S. DUTTA MAZUMDAR, D.Sc.,  
PROF. C. S. GHOSH, M.Sc., S.M., F.N.I. M.I.E.E.,  
PROF. S. GHOSH, D.Sc., F.N.I.  
PROF. S. N. GHOSH, D.Sc.,  
PROF. S. GUPTA, M.Sc., F.N.I.  
PROF. D. N. KUNDU, PH.D., F.N.I.  
PROF. R. C. MAZUMDAR, PH.D., F.N.I.  
PROF. A. MOOKHERJEE, D.Sc.,  
PRINCIPAL Y. G. NAIK, PH.D.,  
PROF. S. R. PALIT, D.Sc., F.R.I.C., F.N.I.  
PROF. H. RAKSHIT, S.Sc., F.N.P., F.I.T.E. F.N.I.  
PROF. A. SAHA, D.Sc., F.N.I.  
PROF. VIKRAM A. SARABHAI, M.A., PH.D., F.N.I.  
PROF. A. K. SENGUPTA, D.Sc.  
PROF. NAND LAL SINH, D.Sc.,  
PROF. M. S. SINHA, D.Sc., F.N.I.  
DR. N. R. TAWDE, PH.D., F. INST. P. M.I. NUC. E.F.A.Sc. F.N.I.  
DR. P. VENKATESWARLU.



## CONTENTS

### No. 1 January

	PAGE
1. Thermal Conductivity of the Slowly Reacting System $2\text{HI} \rightleftharpoons \text{H}_2 + \text{I}_2$ —B. N. Srivastava and P. K. Chakraborti .. .. .	1
2. "Double Emission of Heavy Fragments ( $Z \geq 3$ ) in the Disintegration of Emulsion Nuclei"—G. C. Deka and K. M. Pathak .. .. .	7
3. Electrical Conductivity of Single Crystals of Ilmenite—A. -K. Mukerjee .. .. .	10
4. A Convenient and Direct Method of Finding the Principal Ionic Susceptibilities of Triclinic Crystals—U. S. Ghosh and S. Mitra .. .. .	19
5. X-Ray Method of Determining the Amplitude Factors of Organic Liquids—T. Ratho, S. Torasia and J. C. Mohanty .. .. .	28
6. A new Approach to the Solution of Switching Functions having Cyclic Prime Implicant Tables—A. K. Choudhury, Sunil Ranjan Das and M. S. Basu .. .. .	31

### LETTERS TO THE EDITOR—

1. Molecular Orbital Theory of Trigonalally Distorted $[\text{Co}, 6\text{H}_2\text{O}^{2+}]$ Complex—L. C. Jackson and R. Rai .. .. .	49
2. A short note on a Transition in Chromium Potassium Sulphate Alum—S. Mitra and S. K. Dutta Roy .. .. .	51
3. Validity of the Phase Shift Calculation of Electron Scattering by Brysk Method—D. M. Bhattacharya and N. C. Sil .. .. .	53
4. A note on the Transformation of Manganite—D. R. Dasgupta .. .. .	55
5. On Nuclear Binding Energies—A. K. Dutta, B. Pal, P. Ganguly and D. Banerjee .. .. .	

### No. 2. February

7. An Analysis of the J-Phenomenon in X-Rays. Part I—Hirendra Kumar Pal .. .. .	61
8. Effect of Complex Formation on the Intensities of Raman Lines—N. Rajeswara Rao and K. V. Ramanaiah .. .. .	79
9. A 19 cm Debye-Scherrer Camera for Working between $400^\circ\text{K}$ and $106^\circ\text{K}$ —Siddhartha Roy .. .. .	82
10. On Heat Transfer in Nucleate Boiling (I)—S. P. Basu .. .. .	87
11. Excess Thermodynamic Functions of Binary Mixture: Systems Fluorobenzene+Toluene—S. N. Bhattacharyya and Asok Kumar Mukherjee .. .. .	93

	Page
12. Experimental Study of Duration of Contact of a Transversely Impinging Load on Cantilever—B. B. Banerjee .. .. .	99
13. Distribution of Positive Ions in the F-Region—S. N. Ghosh, K. D. Sharma and A. Sharma .. .. .	106

## LETTERS TO THE EDITOR—

6. Analysis of Gamma-Ray Spectrum of Radioactive Fallout over Calcutta—Sushil Kr. Das, Prabir K. Sandell, R. C. Sastri and S. D. Chatterjee .. .. .	118
7. Molecular Orbital Theory of the Ligand Field in Tetrahedrally Coordinated $Ni^{2+}$ Complexes—R. Rai and S. Mitra .. .. .	121

**No. 3. March**

14. On a Method of Simplification of Switching Functions for Synthesis of three Level Circuits—A. K. Choudhury and S. R. Das .. .. .	125
15. Change in the Shape of a Molecule During the Formation of Hydrogen Bond—N. Rajeswara Rao and K. V. Ramanaiah .. .. .	144
16. Locking Phenomena in Phase Locked Oscillators—N. B. Chakrabarti and B. N. Biswas .. .. .	148

## LETTERS TO THE EDITOR—

8. Ultraviolet Absorption of Carbonate and Bicarbonate Ions—A. Mookherji and S. P. Tandon .. .. .	174
9. Preliminary Observations on a Reversible Structural Change in Cobalt Fluosilicate Hexahydrate—Siddhartha Ray .. .. .	176
10. A Short Note on Ligand Field Theory of the Magnetic Anisotropy and Susceptibility of $Fe^{2+}$ Tutton Salts—B. Bhattacharyya .. .. .	178

**No. 4. April**

17. Raman Spectra of Benzene and Carbon-Disulphide at $-209^{\circ}C$ —S. C. Sirakar, D. K. Mukherjee and P. K. Bishui .. .. .	181
18. On Rumer's Invariant Theory of Gravitational Waves—K. D. Krori .. .. .	190
19. Dielectric Absorption at 3 cm. in some Higher Alkyl Phenols—G. C. Hiramath and K. Suryanarayana Rao .. .. .	194
20. Application of Electrostatic Model of Hydrogen Bond to Hydrogen Bonding in some Aliphatic Alcohols and Phenol Compounds in Solutions of Polar Solvents—G. S. Kastha and K. C. Medhi .. .. .	205
21. The Emission Band Spectrum of $AsO$ —M. Venkataramanaiah and S. V. J. Lakshman .. .. .	209
22. The Refractive Index and the Absorption Index for the Propagation of Radio Wave in the Ionosphere in some Special Cases—T. S. N. Murty and S. R. Khastgir .. .. .	214

**LETTERS TO THE EDITOR—**

- |  |     |
|--|-----|
| 11. Estimation of the Crystalline Electric Field and Evaluation of $g$ -Factors in $\text{CuSO}_4 \cdot 5\text{H}_2\text{O}$ —A. Narasimhamurthy and D. Premaswarup .. | 225 |
| 12. Ionospheric Disturbances Accompanying Non-Crochet and Crochet Associated Flares—S. D. Deshpande .. .. .  | 229 |

**No. 5. May**

- |   |     |
|---|-----|
| 23. Cohesive Energies and other Properties of Ionic Crystals I. Alkali Halides—M. N. Sharma and M. P. Madan .. .. . | 231 |
| 24. A new Multiplier using Dead-Band Type Nonlinearity—A. K. Nath, N. G. Nath and A. K. Choudhury .. .. .           | 241 |
| 25. A Transistor Sawtooth Generator—R. R. Dutta Gupta ..  | 250 |
| 26. A Simple Computer for Fourier Analysis and Synthesis—J. Das and P. Dasgupta .. .. .                             | 265 |

**LETTERS TO THE EDITOR—**

- |   |     |
|---|-----|
| 13. Ultraviolet Absorption of Chlorate Bromate and Iodate Ions—A. Mookherji and S. P. Tandon .. .. .  | 278 |
| 14. Molecular Orbital Theory of the Magnetic Properties of the Tetrahedral Copper Complex, $\text{Cs}_2\text{CuCl}_4$ —R. Chatterjee, S. Lahiry, U. S. Ghosh and S. Mitra .. .. . | 280 |

**No. 6 June**

- |  |     |
|--|-----|
| 27. On the Angle of Inclination of the Equivalent Lightning Channel—H. Bhattacharya and Manoranjan Rao .. .. .                                       | 283 |
| 28. Mean Amplitudes of Vibration of some Trigonal Bipyramidal Pentachlorides—G. Nagarajan .. .. .  | 289 |
| 29. Cohesive Energies and other Properties of Ionic Crystals—2. Halides of Copper, Silver, Thallium and Ammonia—M. N. Sharma and M. P. Madan .. .. . | 305 |
| 30. Some Approximations of Signals and Informations—J. Das ..  | 311 |
| 31. On the Determination of Distortion in Nuclear Emulsions—Prem K. Aditya .. .. .   | 326 |

**No. 7. July**

- |  |     |
|--|-----|
| 32. Ligand Field Theory of Magnetic Anisotropy and Susceptibility of $\text{Fe}^{2+}$ Tutton Salts—B. D. Bhattacharyya .. .. . | 331 |
| 33. On the Thermal Expansion in $\text{Cu}_3\text{Au}$ Alloy—B. N. Dey and S. P. Sen Gupta .. .. .                             | 341 |
| 34. Coupled Wave Equations in Magneto-Ionic Theory—S. K. Banerjee and S. R. Khastgir .. .. .                                   | 347 |

	PAGE
35. Orientations of the Orthorhombic $g$ -Tensors and their Magnitudes in $\text{Cu}(\text{KSO}_4)_2 \cdot 6\text{H}_2\text{O}$ Crystals—A. Bose; U. S. Ghosh, R. N. Bagehi and A. K. Pal .. .. .	361

LETTERS TO THE EDITOR—

15. X-Ray Analysis of Radio Active Fall-out over Calcutta—Prabir Kumar Sandell, J. Mukherjee and Sushil K. Das .. .. .	376
16. The Crystal Structure of Pyrocatechol—S. K. Talapatra .. .. .	379

**No. 8. August**

36. Electron Mobility in a Magnetic Field—S. N. Sen and R. N. Gupta .. .. .	383
37. Cohesive Energy, Compressibility and Thermal Expansion of Diatomic Crystals—C. M. Kachhava and S. C. Saxena .. .. .	388
38. On the $\beta \rightarrow \beta'$ Transformation in CuSn Alloy—B. N. Dey and M. A. Quader .. .. .	398
39. Dynamic Elastic Modulus and Damping Coefficient of some Indian Timbers—W. J. John and M. M. Lal .. .. .	401
40. An Antiproton Event—G. C. Deka and T. D. Goswami .. .. .	409
41. On the Dependence of the time of Relaxation of Nitrobenzene in Solutions in non polar Solvents on the Viscosity of the Solutions—J. Bhattacharyya, (Miss) B. Sinha, S. B. Roy and G. S. Kastha .. .. .	413

LETTERS TO THE EDITOR—

17. A Note on the Franck-Condon Factors of $\text{Vo} (\text{A}^2\Delta\text{-X}^2\Delta)$ Band System—N. Sreedhara Murthy, T. K. Sreerango Setty and Miss K. V. Sumathi .. .. .	428
18. Exchange Narrowing of DPPH Line Shape in ESR—B. N. Mishra .. .. .	430
19. Cobalt X-Ray Absorption Spectrum in Pink and Blue Solutions of Cobalt (II) Chloride—Chintamani Mande and A. R. Chetal .. .. .	433

**No. 9. September**

42. Reflection and Transmission Properties of a Stratified Plasma—J. Basu .. .. .	435
43. X-Ray Diffraction Study of Cellulose Degradation—W. J. John, B. C. Biswas and S. S. Krishnan .. .. .	453
44. Correlation of Dissociation Energy and Molecular Constants of Diatomic Molecules—S. P. Tandon and Kamala Tandon .. .. .	460
45. Low Angle X-Ray Measurements on Densely Packed Colloidal Systems—Wool—T. Ratho .. .. .	475

LETTERS TO THE EDITOR—

20. A Preliminary Note on Magnetic Susceptibility and Anisotropy in Tetrahedrally Coordinated $\text{Co}^{++}$ Ion—S. Kumar, S. Mitra and R. Rai .. .. .	481
--	-----

**No. 10 October**

46.	A Note on the Hydrogen Bonding in Isomeric Aminopyridines in Relation to their Basicities—K. C. Medhi and G. S. Kastha ..	483
47.	Stability of a Gravitating Fluid Layer of Uniform Thickness in the Presence of Coriolis Force and a Magnetic Field—B. B. Chakrabarty ..	490
48.	Low Energy, Nuclear Bursts of Cosmic Rays at Sea Level—S. R. Ganguly and S. D. Chatterjee .. .. .	499
49.	Effect of Electrolytic Currents on a Current Carrying Conductor—M. S. Gaur, G. P. Bhatnagar and V. S. Dubey .. ..	509

LETTERS TO THE EDITOR—

21.	On Nuclear Excitation and Formation Energies, (IV)—A. K. Dutta, B. Pal, P. Ganguly and D. Banerjee .. .. .	518
22.	Nuclear Energy and Nuclear Characteristics (V)—A. K. Dutta ..	522
23.	On Nuclear Structure and Nuclear Moments (VI)—A. K. Dutta ..	527
24.	Quasi-Crystalline Structure and Interrelation between Nuclear Moments (VII)—A. K. Dutta .. .. .	531

**No. 11 November**

50.	A Miniature Joule-Thomson Cascade Liquefier Cryostat for Helium—B. N. Srivastava, J. K. N. Sharma, S. Chatterjee and S. K. Sen ..	535
51.	Dielectric Absorption of 7.7 mm Microwaves in some Polar Liquids (Part I—Alkyl Benzenes)—J. Bhattacharyya, S. B. Roy and G. S. Kastha .. .. .	545
52.	Study of Properties of Flexible Artificial Dielectric—S. S. Gupta and M. N. Sharma .. .. .	555
53.	Simultaneous Oscillations at three Frequencies in a Regenerative Circuit with a Limiter type Non-Linear Element—B. N. Biswas ..	561

LETTERS TO THE EDITOR—

25.	Velocity of Ultrasonic waves in Solutions of Electrolytes—a Comment—M. Suryanarayana .. .. .	583
26.	Preparation and Crystallographic Studies of Strontium Plutonate—D. M. Chakraborty and N. C. Jayadevan .. ..	585
27.	Phase Transformation in Erbium Ethyl Sulphate Single Crystal with Lowering of Temperature—T. Mookherji .. ..	587

**No. 12 December**

54.	The Effects of Gaussian Noise on the Frequency Response Characteristics of a Nonlinear Feedback Control System—Asim K. Sen ..	589
55.	Determination of the Dielectric Constant of a Tubular Material at 3KMc/s—S. K. Sen, J. Basu and A. K. Ghoshal .. ..	601

	<b>PAGE</b>
56. On the Infrared Spectra of Fluoro-, Chloro-, Bromo-, and Iodobenzene in the Vapour State—S. C. Sirkar, D. K. Mukherjee and P. K. Bishui .. .. .	610
57. Oriented Transformation of Magnesite—D. R. Dasgupta ..	623
58. A Study of the Angle of Spread of the Downcoming Radio-Waves—N. N. Sen .. .. .	627
59. Influence of Inelastic Cross Section on Multiple Coulomb Scattering—Prem K. Aditya .. .. .	630
 LETTERS TO THE EDITOR—	
28. Identification of Alpha-Emitters in Radioactive Fallout—S. D. Chatterjee, S. K. Mondal, S. K. Das and N. C. Ghosh .. ..	635

# AUTHOR INDEX

AUTHOR	SUBJECT	PAGE
Aditya, P. K.	On the determination of distortion in nuclear emulsions	326
	Influence of inelastic cross section on multiple Coulomb scattering	630
Bagchi, R. N.	see Bose, A.	
Banerjee, B. B.	Experimental study of duration of contact of a transversely impring- ing load on cantilever	99
Banerjee, D.	see Dutta, A. K.	
Banerjee, S. K. and Khastgir, S. R.	Coupled wave equations in magneto- ionic theory	347
Basu, J.	Reflection and transmission proper- ties of a stratified plasma	435
” ”	see Sen, S. K.	
Basu, M. S.	see Choudhury, A. K.	
Basu, S. P.	On heat transfer in nucleate boiling (I)	87
Bhatnagar, G. P.	see Gaur, M. S.	
Bhattacharya, B.	A short note on ligand field theory of the magnetic anisotropy and susceptibility of $\text{Fe}^{2+}$ Tutton salts (L)	178
Bhattacharya, B. D.	Ligand field theory of magnetic ani- sotropy and susceptibility of $\text{Fe}^{2+}$ Tutton salts	331
Bhattacharya, D. M. and Sil, N. C.	Validity of the phase shift calculation of electron scattering by Brysk method (L)	53
Bhattacharya, H. and Rao, M.	On the angle of inclination of the equivalent lighting channel	283
Bhattacharya, J., Sinha, B., Roy, S. B. and Kastha, G. S.	On the dependence of the time of relaxation of nitrobenzene in solu- tions in non polar solvents on the viscosity of the solutions	413
Bhattacharya, J., Roy, S. B. and Kastha, G. S.	Dielectric absorption of 7.7 mm microwaves in some polar liquids (Part I-Alkyl Benzenes)	545
Bhattacharya, S. N. and Mukherjee, A. K.	Excess thermodynamic functions of binary mixture : systems fluoro- benzene + toluene	93

AUTHOR	SUBJECT	PAGE
Biswas, B. C.	see John, W. J.	
Biswas, B. N.	Simultaneous oscillations at three frequencies in a regenerative circuit with a limiter type non-linear element.	561
	see Chakrabarti, N. B.	
Bishui, P. K.	see Sirkar, S. C.	
Bose, A., Ghosh, U. S., Bagchi, R. N. and Pal, A. K.	Orientations of the orthorhombic $g$ -tensors and their magnitudes in $\text{Cu}(\text{KSO}_4)_2 \cdot 6\text{H}_2\text{O}$ crystals	361
Chakrabarty, B. B.	Stability of gravitating fluid layer of uniform thickness in the presence of coriolis force and a magnetic field	490
Chakraborty, D. M. and Jayadevan, N. C.	Preparation and crystallographic studies of strontium plutonate(L)	585
Chakravarti, N. B. and Biswas, B. N.	Locking phenomena in phase locked oscillators	148
Chakravorty, P. K.	see Srivastava, B. N.	
Choudhury, A. K., Das, S. R. and Basu, M. S.	A new approach to the solution of switching function having cyclic prime implicant tables	31
Choudhury, A. K. and Das, S. R.	On a method of simplification of switching functions for synthesis of three level circuits	125
Choudhury, A. K.	see Nath, A. K.	
Chatterjee, R., Lahiry, S., Ghosh, U. S. and Mitra, S	Molecular orbital theory of the magnetic properties of the tetrahedral copper complex, $\text{Cs}_2\text{CuCl}_4$ (L)	280
Chatterjee, S.	See Srivastava, B. N.	
Chatterjee, S. D., Mondal, S. K., Das, S. K. and Ghosh, N. C.	Identification of alpha emitters in Radioactive fallout (L)	635
Chatterjee, S, D,	see Das, S. K.	
” ”	see Ganguly, S. R.	
Chetal, A. R.	see Mande, C.	
Das, J.	Some approximations of signals and informations	311
Das, S. K., Sandell, P. K., Sastri, R. C. and Chatterjee, S. D.	Analysis of gamma-ray spectrum of radioactive fallout over Calcutta (L)	118
Das, S. K.	see Chatterjee, S. D.	
	see Sandell, P. K.	



AUTHOR	SUBJECT	PAGE
Das, S. R.	see Choudhury, A. K.	
Das, J. and Dasgupta, P.	A simple computer for Fourier analysis and synthesis	265
Dasgupta, D. R.	A note on the transformation of Manganite (L)	55
Dasgupta, D. R.	Oriented transformation of magnesite	623
Dasgupta, P.	see Das, J.	
Deka, G. C. and Pathack, K.M.	Double emission of heavy fragments ( $Z \geq 3$ ) in the disintegration of emulsion nuclei	7
Deka, G. C. and Goswami, T. D.	An antiproton event	409
Dey, B. N. and Sengupta, S. P.	On the thermal expansion of $\text{Cu}_3\text{Au}$ alloy	341
Dey, B. N. and Quader, M. A.	On the $\beta \rightarrow \beta'$ transformation in $\text{CuSn}$ alloy	398
Despande, S. D.	Ionospheric disturbances accompanying non-crochet and crochet associated flares (L)	229
Dubey, V. S.	see Gaur, M. S.	
Dutta, A. K., Pal, B., Ganguly, P and Banerjee, D.	On nuclear binding energies (L)	57
Dutta, A. K., Pal, B., Ganguly, P and Banerjee, D.	On nuclear excitation and formation energies (IV) (L)	518
Dutta, A. K.	Nuclear energy and nuclear characteristic (V) (L)	522
	On nuclear structure and nuclear moments (VI) (L)	527
	Quasi-crystalline structure and interrelation between nuclear moments (VII) (L)	531
Dutta Gupta, R. R.	A transistor sawtooth generator	250
Dutta Roy, S. K.	see Mitra, S.	
Ganguly, P	see Dutta, A. K.	
Ganguly, S. R. and Chatterjee, S. D.	Low energy nuclear bursts of cosmic rays at sea level	499
Gaur, M. S., Bhatnagar, G. P. and Dubey, V. S.	Effect of Electrolytic currents on a current carrying conductor	509
Ghosh, S. N., Sharma, K. D. and Sharma, A.	Distribution of positive ions in the F-region	106
Ghosh, U. S. and Mitra, S.	A convenient and direct method of finding the principal ionic susceptibilities of triclinic crystals	19

AUTHOR	SUBJECT	PAGE
Ghosh, U. S.	see Bose, A.	
" "	see Chatterjee, R.	
Goswami, T. D.	see Deka, G. C.	
Gupta, S. S. and Sharma, M. N.	Study of properties of flexible artificial dielectric	555
Gupta, R. N.	see Sen, S. N.	
Ghosal, A. K.	see Sen, S. K.	
Ghosh, N. C.	see Chatterjee, S. D.	
Hiremath, G. C. and Suryanarayana Rao, K.	Dielectric absorption at 3 cm in some higher alkyl phenols	194
Jackson, L. C. and Rai, R.	Molecular orbital theory of trigonally distorted $[\text{Co. } 6\text{H}_2\text{O}^{2+}]$ complex (L) see Chakraborty, D. M.	49
Jayadevan, N. C.	X-Ray diffraction study of Cellulose degradation	453
John, W. J., Biswas, B. C., Krishnan, S. S.	Dyanamic elastic modulus and damping coefficient of some Indian timbers	401
John, W. J. and Lal, M. M.	Cohesive energy, compressibility and thermal expansion of diatomic crystal	388
Kachhava, C. M. and Saxena, S. C.	Application of electrostatic model of hydrogen bond to Hydrogen bonding in some aliphatic alcohols and phenol compounds in solutions of polar solvents	205
Krori, K. D.	On Rumer's invariant theory of gravitational waves	190
Kastha, G. S.	see Bhattachar, J.	
" "	see Medhi, K. C.	
Khastgir, S. R.	see Murty, Y. S. N.	
" "	see Banerjee, S. K.	
Krishnan, S. S.	see John, W. J.	
Kumar, S., Mitra, S. and Rai, R.	A preliminary note on magnetic susceptibility and anisotropy in tetrahedrally coordination $\text{Co}^{++}$ ion (L)	481
Lahiry, S.	see Chatterjee, R.	
Lakshman, S. V. J.	see Venkataramanaiah, M.	
Lal, M. M.	see John, W. J.	
Madon, M. P.	see Sharma, M. N.	
Mando, C. and Chetal, A. R.	Cobalt X-ray absorption spectrum in pink and blue solutions of cobalt (II) chloride (L)	433

AUTHOR	SUBJECT	PAGE
Medhi, K. C. and Kastha, G. S.	A note on the Hydrogen bonding in isomeric aminopyridines in relation to their basicities	483
Medhi, K. C.	see Kastha, G. S.	
Misra, B. N.	Exchange narrowing of DPPH line shape in ESR (L)	430
Mitra, S. and Dutta Roy, S. K.	A short note on a transition in chromium potassium sulphate alum (L)	51
Mitra, S.	see Ghosh, U. S.	
" "	see Rai, R.	
	see Chatterjee, R.	
	see Kumar, S.	
	see Ratho, T.	
Mohanty, J. C.		
Mookherji, A and Tandon, S. P.	Ultraviolet absorption of carbonate and bicarbonate ions (L)	174
Mookherji, A and Tandon, S. P.	Ultraviolet absorption of chlorate bromate and iodate ions (L)	278
Mookherji, T.	Phase transformation in erbium ethyl sulphate single crystal with lowering of temperature (L)	587
Mondal, S. K.	see Chatterjee, S. D.	
Mukherjee, A. K.	Electrical conductivity of single crystal of ilmenite	10
Mukherjee, A. K.	see Bhattacharya, S. N.	
Mukherjee, D. K.	see Sirkar, S. C.	
Mukherjee, J.	see Sandol, P.	
Murthy, Y. S. N. and Khastgir, S. R.	The refractive index and the absorption index for the propagation of radio wave in the ionosphere in some special cases	214
Nagarajan, G.	Mean amplitudes of vibration of some trigonal bipyramidal pentachlorides	289
Narasimhamurty, A. and Premaswarup, D.	Estimation of the crystalline electric field and Evaluation of <i>g</i> -factors in $\text{CuSO}_4 \cdot 5\text{H}_2\text{O}$ (L)	225
Nath, A. K., Nath, N. G. and Chaudhury, A. K.	A few multiplier using dead band type nonlinearity	241
Nath, N. G.	see Nath, A. K.	
Pal, A. K.	see Bose, A.	
Pal, B.	see Dutta, A. K.	

AUTHOR	SUBJECT	PAGE
Pal, H. K.	An analysis of the J-phenomenon in X-rays Part I	61
Pathak, K. M.	see Deka, G. C.	
Premaswarup, D.	see Narasimhamurty, A.	
Quader, M. A.	see Dey, B. N.	
Rai, R.	see Jackson, L. C.	
Rai, R.	see Kumar, S.	
Rai, R. and Mitra, S.	Molecular orbital theory of the ligand field in tetrahedrally co-ordinated Ni <sup>2+</sup> complexes (L)	121
Rajeswara Rao, N. and Ramanaiah, K. V.	Effect of complex formation on the intensities of Raman lines	79
Rajeswara Rao, N. and Rmanaiah, K. V.	Change in the shape of a molecule during the formation of hydro- gen bond	144
Ramanaiah, K. V.	see Rajeswara Rao, N.	
Rao, M.	see Bhattacharya, H.	
Ratho, T. Torasia, S. and Mohanty, J. C.	X-ray method of determining the amplitude factors of organic liquids	28
Ratho, T.	Two angle X-ray measurements on density packed colloidal systems- wool	475
Ray, S.	Preliminary observations on a re- versible structural change in cobalt fluosilicate hexahydrate (L)	176
Roy, S.	A 19 cm Debye-Scherrer camera for working between 400°K and 106°K	82
Roy, S. B.	see Bhattacharya, J.	
Sandel, P. K. Mukherjee, J. and Das, S. K.	X-ray analysis of radio active fall- out over Calcutta (L)	376
Sandel, P. K.	see Das, S. K.	
Sastri, R. C.	see Das S. K.	
Saxena, S. C.	see Kachhava, C. M.	
Sen, A. K.	The effects of Gaussian noise on the frequency response characteristics of a nonlinear Feedback control system	598
Sen, N. N.	A study of the angle of spread of the down coming radio-waves	627

AUTHOR	SUBJECT	PAGE
Sen, S. K., Basu, J. and Ghosal, A. K.	Determination of the dielectric constant of a tabular material at 3KMc/s	601
Sen, S. K.	see Srivastava, B. N.	
Sen, S. N. and Gupta, R. N.	Electron mobility in a magnetic field	383
Sengupta, S. P.	see Dey, B. N.	
Sharma, A.	see Ghosh, S. N.	
Sharma, J. K. N.	see Srivastava, B. N.	
Sharma, K. D.	see Ghosh, S. N.	
Sharma, M. N. and Madan, M. P.	Cohesive energies and other properties of ionic crystal- I. Alkali halides	231
	Cohesive energies and other properties of ionic crystals- 2. Halides of copper, silver, thallium and ammonia	305
Sharma, M. N.	see Gupta, S. S.	
Sil, N. C.	see Bhattacharya, D. M.	
Sinha, B.	see Bhattacharya, J.	
Sirkar, S. C., Mukherjee, D. K. and Bishui, P. K.	Raman spectra of benzene and carbon-disulphide at 209°C	181
Sirkar, S. C., Mukherjee, D. K. and Bishui, P. K.	On the infrared spectra of fluoro-, chloro-, bromo-, and iodobenzene in the vapour state	610
Sreedhara Murthy, N., Sreeranga Setty, T. K. and Sumathi, K. V.	A note on the Frank-Condon factors of $V_0(A^2\Delta-X^2\Delta)$ band system (L)	428
Sreeranga Setty, T. K.	see Sreedhara Murthy, N.	
Srivastava, B. N. and Chakraborti, P. K.	Thermal conductivity of the slowly reacting system $2HI \rightleftharpoons H_2 + I_2$	1
Srivastava, B. N., Sharma, J. K. N., Chatterjee, S. and Sen, S. K.	A miniature Joule-Thomson cascade liquefier cryostat for helium	535
Sumathi, K. V.	see Sreedhara Murthy, N.	
Suryanarayana, M.	Velocity of ultrasonic waves in solutions of electrolytes- a comment (L)	583

AUTHOR	SUBJECT	PAGE
Suryanarayana Rao, K.	see Hiremath, G. C.	
Talapatra, S. K.	The crystal structure of pyrocatechol (L)	379
Tandon, K.	see Tandon, S. P.	
Tandon, S. P. and Tandon, K.	Correlation of dissociation energy and molecular constants of diatomic molecules	460
Tandon, S. P.	see Mookherji, A.	
Torasia, S.	see Ratho, T.	
Venkataramanaiah, M. and Lakshman, S. V, J.	The emission band spectrum of AsO	209

# SUBJECT INDEX

SUBJECT	AUTHOR	PAGE
Alpha-emitters in radioactive fallout-- Identification of (L)	S. D. Chatterjee, S. K. Mondal, S. K. Das and N. C. Ghosh	635
Amplitude Factors of Organic Liquids- X-ray method of determining	T. Ratho, S. Torasia and J. C. Mohanty	28
Angle of inclination of the equivalent lightning channel—On the	H. Bhattacharya and Monoranjan Rao	283
Angle of spread of the downcoming Radio-waves,—A study of	N. N. Sen	627
Antiproton event—An	G. C. Deka and T. D. Goswami	409
Approximations of signals and infor- mations—Some	J. Das	311
$\beta$ — $\beta'$ Transformation in CuSn alloy- —on the	B. N. Dey and M. A. Quader	398
Cellulose degradation—X-ray diffrac- study of	W. J. John, B. C. Biswas and S. S. Krishnan	453
Cobalt X-ray absorption spectrum in pink and blue solutions of cobalt (II) chloride (L)	Chintamani mande and A. R. Chetal	433
Cohesive energies and other Properties of ionic crystals 1. Alkali halides	M. N. Sharma and M. P. Madan	231
Cohesive energies and other properties of ionic crystals 2. Halides of copper silver, thallium and Ammonia	M. N. Sharma and M. P. Madan	305
Cohesive energy, compressibility and thermal expansion of diatomic crystals	C. M. Kachhava and S. C. Saxena	388
Coupled wave equations in Magneto- ionic theory	S. K. Banerjee and S. R. Khastgir	347
Crystal structure of pyrocatechol—The (L)	S. K. Talapatra	379
Crystalline electric field and evaluation g-factors in $\text{CuSO}_4 \cdot 5\text{H}_2\text{O}$ (L)	A. Narasimhamurthy and D. Premaswarup	225

SUBJECT	AUTHOR	PAGE
Debye-Scherrer Camera for working between 400°K and 106°K—A 19 cm	Siddhartha Roy	82
Dependence of the time of relaxation of nitrobenzene in solutions in non-polar solvents on the viscosity of the solutions	J. Bhattacharyya, (Miss) B. Sinha, S. B. Roy and G. S. Kastha	413
Dielectric absorption at 3 cm. in some higher Alkyl phenols	G. C. Hiremath and K. Suryanarayana Rao	194
Dielectric absorption of 7.7 mm micro-waves in some polar liquids (Part I—Alkyl benzenes)	J. Bhattacharyya, S. B. Roy and G. S. Kastha	545
Dielectric constant of a Tabular material at 3KMc/s—Determination of the	S. K. Sen, J. Basu and A. K. Ghosal	601
Dissociation energy and molecular constants of diatomic molecules—Correlation of	S. P. Tandon and Kamala Tandon	460
Distortion in nuclear emulsions—On the determination of	Prem K. Aditya	326
Double emission of heavy fragments ( $Z \geq 3$ ) in the disintegration of emulsion nuclei	G. C. Deka and K. M. Pathak	7
Duration of contact of a transversely impinging load on cantilever—Experimental study of	B. B. Banerjee	99
Dynamic elastic modulus and damping coefficient of some Indian timbers	W. J. John and M. M. Lal	401
Electrical conductivity of single crystals of ilmenite	A. K. Mukherjee	10
Electrolytic currents on a current conductor—Effect of	M. S. Gaur, G. P. Bhatnagar and V. S. Dubey	509
Electron mobility in a magnetic field	S. N. Sen and R. N. Gupta	383
Electrostatic model of hydrogen bond to hydrogen bonding in some aliphatic		



SUBJECT	AUTHOR	PAGE
alcohols and phenol compounds in solutions of polar solvents—Application of	G. S. Kastha and K. C. Medhi	205
Emission band spectrum of AsO—The	M. Venkataramanaiah and S. V. J. Lakshman	209
Excess thermodynamic functions of binary mixture : Systems fluorobenzene +toluene	S. N. Bhattacharyya and Asok Kumar Mukherjee	93
Exchange narrowing of DPPH line shape in ESR (L)	B. N. Misra	430
Flexible Artificial Dielectric—Study of properties of.	S. S. Gupta and M. N. Sharma	555
Frankoo-Condon factors of $V_0(A^2 \nabla > X^2 \nabla)$ band system—A note on the (L)	N. Sreedhara Murthy, T. K. Sreeranga Setty and Miss K. V. Sunathi	428
Gamma-ray spectrum of radioactive fall-out over Calcutta—Analysis of (L)	Sushil Kr. Das, Prabir K. Sandell, R. C. Sastri and S. D. Chatterjee.	
Gaussian noise on the frequency response characteristics of a nonlinear feedback control system—The effects of	Asim K. Sen	589
Gravitating fluid layer of uniform thickness in the presence of coriolis force and a magnetic field—Stability of a	B. B. Chakrabarty	490
Heat transfer in nucleate boiling (1)—On	S. P. Basu	87
Hydrogen bonding in isomeric aminopyridines in relation to their basicities—A note on the	K. C. Medhi and G. S. Kastha	483
Inelastic cross section on multiple coulomb scattering—Influence of	P. K. Aditya	630
Infrared spectra of fluoro, chloro-bromo-, and iodobenzene in the vapour state—On the	S. C. Sirkar, D. K. Mukherjee and P. K. Bishui	610

SUBJECT	AUTHOR	PAGE
Debye-Scherrer Camera for working between 400°K and 106°K—A 19 cm	Siddhartha Roy	82
Dependence of the time of relaxation of nitrobenzene in solutions in non-polar solvents on the viscosity of the solutions	J. Bhattacharyya, (Miss) B. Sinha, S. B. Roy and G. S. Kastha	413
Dielectric absorption at 3 cm. in some higher Alkyl phenols	G. C. Hiremath and K. Suryanarayana Rao	194
Dielectric absorption of 7.7 mm micro-waves in some polar liquids (Part I—Alkyl benzenes)	J. Bhattacharyya, S. B. Roy and G. S. Kastha	545
Dielectric constant of a Tabular material at 3KMc/s—Determination of the	S. K. Sen, J. Basu and A. K. Ghosal	601
Dissociation energy and molecular constants of diatomic molecules—Correlation of	S. P. Tandon and Kamala Tandon	460
Distortion in nuclear emulsions—On the determination of	Prem K. Aditya	326
Double emission of heavy fragments ( $Z \geq 3$ ) in the disintegration of emulsion nuclei	G. C. Deka and K. M. Pathak	7
Duration of contact of a transversely impinging load on cantilever—Experimental study of	B. B. Banerjee	99
Dynamic elastic modulus and damping coefficient of some Indian timbers	W. J. John and M. M. Lal	401
Electrical conductivity of single crystals of ilmenite	A. K. Mukherjee	10
Electrolytic currents on a current carry-conductor—Effect of	M. S. Gaur, G. P. Bhatnagar and V. S. Dubey	509
Electron mobility in a magnetic field	S. N. Sen and R. N. Gupta	383
Electrostatic model of hydrogen bond to hydrogen bonding in some aliphatic		

SUBJECT	AUTHOR	PAGE
alcohols and phenol compounds in solutions of polar solvents—Application of	G. S. Kastha and K. C. Medhi	205
Emission band spectrum of AsO—The	M. Venkataramanaiah and S. V. J. Lakshman	209
Excess thermodynamic functions of binary mixture : Systems fluorobenzene +toluene	S. N. Bhattacharyya and Asok Kumar Mukhorjee	93
Exchange narrowing of DPPH line shape in ESR (L)	B. N. Misra	430
Flexible Artificial Dielectric—Study of properties of.	S. S. Gupta and M. N. Sharma	555
Frankoo-Condon factors of $V_0(A^2 \nabla > X^2 \nabla)$ band system —A note on the (L)	N. Sreedhara Murthy, T. K. Sreeranga Setty and Miss K. V. Sumathi	428
Gamma-ray spectrum of radioactive fall-out over Calcutta—Analysis of (L)	Sushil Kr. Das, Prabir K. Sandell, R. C. Sastri and S. D. Chatterjee.	
Gaussian noise on the frequency response characteristics of a nonlinear feedback control system—The effects of	Asim K. Sen	589
Gravitating fluid layer of uniform thickness in the presence of coriolis force and a magnetic field—Stability of a	B. B. Chakrabarty	490
Heat transfer in nucleate boiling (I)—On	S. P. Basu	87
Hydrogen bonding in isomeric aminopyridines in relation to their basicities—A note on the	K. C. Medhi and G. S. Kastha	483
Inelastic cross section on multiple coulomb scattering—Influence of	P. K. Aditya	630
Infrared spectra of fluoro,chloro-bromo-, and iodobenzene in the vapour state —On the	S. C. Sirkar D. K. Mukherjee and P. K. Bishui	610

SUBJECT	AUTHOR	PAGE
Intensities of Raman lines --Effect of complex formation on the	N. Rajeswara Rao and K. V. Ramanaiah	79
Ionospheric disturbances accompanying non-crochet and crochet associated flares (L)	S. D. Despande	229
J.—phenomenon in X-rays. Part I—An analysis of	Hirendra Kumar Pal†	61
Joule-Thomson cascade liquefier cryostat for helium—A miniature	B. N. Srivastava, J. K. N. Sharma, S. Chatterjee and S. K. Sen	535
Ligand field theory of the magnetic anisotropy and susceptibility of $\text{Fe}^{2+}$ tutton salts—A short note on (L)	B. Bhattacharyya	178
Ligand field theory of magnetic anisotropy and susceptibility of $\text{Fe}^{+2}$ tutton salts	B. D. Bhattacharyya	331
Locking Phenomena in Phase locked oscillators	N. B. Chakrabarti and B. N. Biswas	148
Magnetic susceptibility and anisotropy in tetrahedrally co-ordinated $\text{Co}^{++}$ ion (L)	S. Kumar, S. Mitra and R. Rai	481
Mean amplitudes of vibration of some trigonal bipyramidal pentachlorides	G. Nagarajan	289
Molecular orbital theory of the ligand field in tetrahedrally co-ordinated $\text{Ni}^{2+}$ complexes (L)	R. Rai and S. Mitra	121
Molecular orbital theory of the magnetic properties of the tetrahedral copper complex. $\text{Cs}_2\text{CuCl}_4$ (L)	R. Chatterjee, S. Lahiry U. S. Ghosh and S. Mitra	280
Molecular orbital Theory of Trigonally distorted ( $\text{Co}, 6\text{H}_2\text{O}^{2+}$ ) complex (L)	L. C. Jackson and R. Rai	49
Multiplier using dead-band type nonlinearity—A new	A. N. Nath, N. G. Nath and A. K. Choudhury	241
Nuclear binding energies—On (L)	A. K. Dutta, B. Pal, P. Ganguly and D. Banerjee	57

# *Subject Index*

*xix*

SUBJECT	AUTHOR	PAGE
Nuclear bursts of cosmic rays at Sea level.—Low energy	S. R. Ganguly and S. D. Chatterjee	499
Nuclear energy and nuclear characteristics (V) (L)	A. K. Dutta,	522
Nuclear excitation and formation energies, (IV) (L)	A. K. Dutta, B. Pal, P. Ganguly and D. Banerjee	518
Nuclear moments (VII)—Quasi-crystalline structure and interrelation between (L)	A. K. Dutta	531
Nuclear structure and nuclear moments (V)—On (L)	A. K. Dutta	522
Oriented transformation of magnesite	D. R. Dasgupta	623
Orientations of the orthorhombic <i>g</i> -tensors and their magnitudes in $\text{Cu}(\text{KSO}_4)_2 \cdot 6\text{H}_2\text{O}$ crystals	A. Bose, U. S. Ghosh, R. N. Bagchi and A. K. Pal	361
Phase Transformation in erbium ethyl sulphate single crystal with lowering of temperature (L)	T. Mookherji	587
Positive ions in the F-region—Distribution of	S. N. Ghosh, K. D. Sharma and A. Sharma	106
Principal ionic susceptibilities of triclinic crystals—A convenient and direct method of finding	U. S. Ghosh and S. Mitra	19
Radio Active Fall-out over Calcutta—X-ray analysis of (L)	Prabir Kumar Sandell, J. Mukherjee and Sushil K. Das	376
Raman spectra of benzene and carbon—Disulphide at $-209^\circ\text{C}$	S. C. Sirkar, D. K. Mukherjee and P. K. Bishui	181
Reflection and transmission properties of a stratified plasma	J. Basu	435

SUBJECT	AUTHOR	PAGE
Refractive index and the absorption index for the propagation of radio wave in the ionosphere in some special cases	Y. S. Murty and S. R. Khastgir	214
Reversible Structural change in cobalt fluosilicate hexahydrate—Preliminary observations on (L)	Siddhartha Ray	176
Rumer's invariant theory of gravitational waves—On	K. D. Krori	190
Shape of molecule during the formation of hydrogen bond —Change in the	N. Rajeswara Rao and K. V. Ramanaiah	144
Simple computer for Fourier analysis and synthesis	J. Das and P. Dasgupta	265
Simultaneous oscillations at three frequencies in a regenerative circuit with a limiter type non-linear element	B. N. Biswas	561
Strontium plutonate —Preparation and crystallographic studies of (L)	D. M. Chakraborty and N. C. Jayadevan	585
Switching functions for synthesis of three level circuits—On a method of simplification of	A. K. Chaudhury and S. R. Dass	125
Switching functions having cyclic prime implicant tables—A new approach to the solution of	A. K. Choudhury, Sunil Rajan Das and M. S. Basu	31
Thermal conductivity of the slowly reacting system $2\text{HI} \rightleftharpoons \text{H}_2 + \text{I}_2$	B. N. Srivastava and P. K. Chakraborti	1
Thermal expansion in $\text{Cu}_3\text{Au}$ alloy—On the	B. N. Dey and S. P. Sen Gupta	341
Transformation of manganite—A note on the (L)	D. R. Dasgupta	55
Transistor sawtooth generator—A	R. R. Dutta Gupta	250
Transition in Chromium potassium sulphate alum—A short note on a (L)	S. Mitra and S. K. Dutta Roy	51
Ultrasonic waves in solutions of electrolytes—a comment—Velocity of (L)	M. Suryanarayana	583

# *Subject Index*

*xxi*

SUBJECT	AUTHOR	PAGE
Ultraviolet absorption of carbonate and bicarbonate ions (L)	A. Mookherji and S. P. Tandon	174
Ultraviolet absorption of Chlorate bromate and iodate ions (L)	A. Mookherji and S. P. Tandon	278
Validity of the phase shift calculation of electron scattering by Brysk method (L)	D. M. Bhattacharya and N. C. Sil	53
X-ray measurements on densely packed colloidal systems—wool—Low angle	T. Ratho	475





# THERMAL CONDUCTIVITY OF THE SLOWLY REACTING SYSTEM $2\text{HI} \rightleftharpoons \text{H}_2 + \text{I}_2$

B. N. SRIVASTAVA AND P. K. CHAKRABORTI

INDIAN ASSOCIATION FOR THE CULTIVATION OF SCIENCE, CALCUTTA-32

(Received, January 24, 1964)

**ABSTRACT.** The thermal conductivity of the dissociating system  $2\text{HI} \rightleftharpoons \text{H}_2 + \text{I}_2$  has been measured between 175°C and 205°C at a pressure below 1 atm. The absolute hot-wire method and an all-glass apparatus with a glass diaphragm manometer has been employed. The experimental conductivity values have been compared with the values calculated from the theoretical expression developed by Srivastava *et al.* for a slowly reacting system. Fair agreement has been obtained between the experimental and the calculated values.

## INTRODUCTION

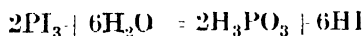
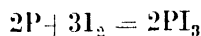
The study of the thermal conductivity of chemically reacting gaseous systems is of considerable interest both from the theoretical and the experimental point of view. Several workers (Hirschfelder, 1957*a*; Butler and Brokaw, 1957) have investigated this problem theoretically assuming the condition of local chemical equilibrium to hold. However, the experimental investigations with different reacting systems (Coffin, 1959; Srivastava and Barua, 1961; Barua and Chakraborti, 1962) have proved the inadequacy of the local equilibrium theory. This is due to the fact that the reaction rate for almost all chemical reactions are not fast enough to maintain the condition of local chemical equilibrium. The problem of non-equilibrium heat transfer in reacting gases has been considered theoretically by Franck and Spalthoff (1954); Seerest and Hirschfelder (1961) and Brokaw (1961).

Seerest and Hirschfelder (1961) have considered two types of chemical reactions, viz : (1) Moderately fast reactions and (2) slow reactions. Srivastava, Barua and Chakraborti (1963) have attempted to interpret the experimental heat conductivity data (Barua and Chakraborti, 1962) for the system  $2\text{NO}_2 \rightleftharpoons 2\text{NO} + \text{O}_2$  by extending the theory of Seerest and Hirschfelder (1961) for slowly reacting systems.

In the present paper we have reported the thermal conductivity of dissociating hydrogen iodide, the reaction rate for which is known to be slow (Sullivan, 1959). The experimental values have been compared with the values calculated on the basis of the expressions developed by Srivastava, Barua and Chakraborti (1963).

## PREPARATION OF HYDROGEN IODIDE

Pure HI was obtained by the action of water on a mixture of red phosphorus and re-sublimed iodine according to the reaction



By constructing a suitable glass apparatus, HI was first purified by passing it over moist red phosphorus and  $\text{P}_2\text{O}_5$  in succession. The purified HI was liquefied in the collecting tube by placing it in an alcohol-liquid oxygen bath. The liquid HI was then solidified by placing the collecting tube in another alcohol-liquid oxygen bath and the system was evacuated. The resulting pure HI was then distilled into ampoules which were sealed off. The ends of the ampoules were made so thin that they could be easily broken by mere tilting.

## APPARATUS AND THEORY

The method employed for the thermal conductivity measurements is the thick-wire-variant of the hot-wire method. An all-glass apparatus with a glass diaphragm manometer described earlier in detail has been used to avoid all complications due to spurious chemical reactions. The theory and procedure of the experiment have already been fully described elsewhere (Kannuliuk and Carman, 1952; Srivastava and Barua, 1960). The constants of the apparatus at different temperatures are given in Table I.

TABLE I

Constants of the conductivity cell at different temperatures

Constants	Temperature in °C			
	175	185	195	205
Resistance of the cell-wire $R_0$ in $\Omega$	2.6060	2.6583	2.7116	2.7640
Temperature coefficient of resistance " $\alpha$ " of the platinum wire in $^{\circ}\text{C}^{-1}$	0.00199	0.00198	0.00192	0.00190
Thermal conductivity " $\lambda$ " of the platinum wire in $\text{cal. cm}^{-1} \text{sec}^{-1} \text{.}^{\circ}\text{C}^{-1}$	0.1748	0.1749	0.1750	0.1752
Cell constant $(1-C)$	0.9788	0.9779	0.9778	0.9775
Length of the cell wire $(2l)$	11.014 cm.			
Radius of the cell wire $(r_1)$	0.005 cm.			
Internal diameter of the cell $(2r_2)$	0.3220 cm.			
External diameter of the cell $(2r_3)$	0.6021 cm.			

## EXPERIMENTAL RESULTS

A typical set of observations taken at  $175^{\circ}\text{C}$  is given in Table II. In the table  $K_u$  is the apparent thermal conductivity and  $K'_u$  is that obtained after

reduction to the bath temperature. The temperature coefficient of the thermal conductivity of the reacting system was obtained from the values of the thermal conductivity calculated on the basis of the slow reaction theory.  $K'$  is the value obtained after correcting for radiation loss, temperature jump and wall effects.  $K$  is the thermal conductivity obtained after correcting for the asymmetry in the cell construction by the relation  $K = K'(1-C)$ . The factor  $(1-C)$  was obtained from the measurements of the thermal conductivity of neon by taking the data of Kannuluik and Carman (1952) as standard.

TABLE II  
Observations taken for the thermal conductivity  $K$  at 175°C  
in cal. cm<sup>-1</sup>, sec<sup>-1</sup>, °C<sup>-1</sup>

$P$ in cm. of Hg.	$I$ in mA	$(R - R_0)$ in $m\Omega$	$K_u \times 10^5$	$K'_u \times 10^5$	$K' \times 10^5$	$K \times 10^5$
19.18	105.64	58.00	2.91	2.90	2.89	2.83
25.68	106.55	58.91	2.92	2.91	2.90	2.84
61.46	105.65	57.91	2.82	2.81	2.80	2.74

TABLE III  
Experimental and calculated values\* of the thermal conductivity of the  
system  $2\text{HI} \rightleftharpoons \text{H}_2 + \text{I}_2$  expressed in cal. cm<sup>-1</sup>, sec<sup>-1</sup>, °C<sup>-1</sup>

$T$ in °C	$P$ in cm. of Hg.	$T_H$ in °C	$T_e$ in °C	$x_2$	$x_3$	$\frac{(1-x_1)}{2}$	$K_{expt}$ $\times 10^5$	$K_{cal}$ $\times 10^5$	$(K_{HI})_{cal}$ $\times 10^5$
	19.18	182.0	178.8		0.0156		2.83	2.57	.....
175.0	25.68	181.6	.....		.....		2.84	.....	2.20
	61.46	182.0	.....		.....		2.74	.....	.....
	19.42	194.5	.....		.....		2.92	.....	.....
185.0	26.46	194.4	189.0		0.0163		2.92	2.63	2.25
	62.60	195.2	.....		.....		2.96	.....	.....
	19.54	206.0	.....		.....		3.00	.....	.....
195.0	26.69	202.1	198.5		0.0167		3.01	2.73	2.30
	65.01	202.5	.....		.....		3.02	.....	.....
	19.81	216.4	210.5		0.0171		3.12	2.85	.....
205.0	27.09	216.1	.....		.....		3.11	.....	2.35
	67.45	216.6	.....		.....		3.12	.....	.....

\*columns 4, 5 and 7 were calculated for only one value of  $T'$  corresponding to a  $T_e$  value. The values are, therefore, indicated against the particular  $T_H$  value.

## COMPARISON WITH THEORY

Following the procedure of Srivastava *et. al.* (1963) we get for the slowly reacting system  $2\text{HI} \rightleftharpoons \text{H}_2 + \text{I}_2$

$$x_2 x_3 / x_1^2 = \int_{T_H}^{T_c} K_c \frac{k_r}{T^2} \exp[\beta(T_H - T)] dT \bigg/ \int_{T_H}^{T_c} \frac{k_r}{T^2} \exp[\beta(T_H - T)] dT \quad \dots (1)$$

where  $x_1$ ,  $x_2$  and  $x_3$  are the molefractions of HI,  $\text{H}_2$ , and  $\text{I}_2$  respectively,  $K_c$  is the equilibrium constant for the hydrogen iodide dissociation,  $k_r$  is the rate constant for the reverse reaction  $\text{H}_2 + \text{I}_2 \rightarrow 2\text{HI}$ ,  $T_H$  and  $T_c$  are the temperatures of the hot and the cold surfaces respectively and  $\beta$  is given by

$$\beta = [2 \ln(r_2/r_1)]/(T_H - T_c), \quad \dots (2)$$

where  $r_1$  and  $r_2$  are the radii of the cell-wire and the cell respectively.

Further we have the relations

$$x_1 + x_2 + x_3 = 1 \quad \dots (3)$$

$$x_2 = x_3 = (1 - x_1)/2 \quad \dots (4)$$

The experimental values of the equilibrium constant  $K_c$  at different temperatures are given by Stegmüller (1910). Sullivan (1959) has given the experimental  $k_r$  values at different temperatures. The temperature of the hot surface,  $T_H$  can be calculated from

$$R_H = R_c \{1 + \alpha(T_H - T_c)\}, \quad \dots (5)$$

where  $R_H$  and  $R_c$  are the values of the resistance of the hot wire at  $T_H$  and  $T_c$  respectively. The values of  $\alpha$  and some of the typical values of  $(R_H - R_c)$  are given in Table I and Table II respectively.

The thermal conductivity of a chemically reacting gas mixture assuming local chemical equilibrium can be represented as

$$K = K_f + K_R, \quad \dots (6)$$

where  $K_R$  is the contribution of the chemical reaction to the thermal conductivity. For a slowly reacting system  $K_R$  is negligible. However,  $K_f$  will depend upon the chemical reaction rate as the steady state composition of the gas mixture (given by Eq. (1)) in the cell is dependent on the reaction rate.  $K_f$  is given by

$$K_f = K_{\text{mix(mon)}} + K_{\text{mix(int)}} \quad \dots (7)$$

$K_{\text{mix(mon)}}$  is the thermal conductivity of the mixture when it is assumed to be composed of monatomic molecules only.  $K_{\text{mix(int)}}$  is the contribution of the internal degrees of freedom. The value of  $K_{\text{mix(mon)}}$  was calculated to the first

approximation from the expression given by Brokaw (1958) and  $K_{mix(int)}$  was calculated from the expression given by Hirschfelder (1957b).

In all our calculations we have used Lennard-Jones (12 : 6) potential model. The force constants for the different components were taken from Hirschfelder, Curtiss and Bird (1954). The steady state composition at any particular temperature is pressure independent and its value was obtained by calculating the integrals in Eq. (1) numerically by using Simpson's one-third rule. The experimental specific heat values were obtained from the standard tables.

The results thus obtained are shown in Table III. Column 5 in the table gives the composition as calculated from Eq. (1) with the help of Eqs. (3) and (4). In column 8 of this table the conductivity values for undissociated hydrogen iodide are given. Comparison of columns (6) and (8) shows that there has been appreciable dissociation. Column 4 represents the temperature to which the composition presented in column 5 would correspond if there were thermodynamical equilibrium. It is to be noted that this temperature is almost equal to the mean of  $T_c$  and  $T_H$ . To examine this point further, a hypothetical calculation was performed for  $T_c = 175^\circ\text{C}$  and  $T_H = 225^\circ\text{C}$ . These calculations also showed that the equilibrium temperature was somewhat less than the mean of  $T_c$  and  $T_H$ . The actual value of  $T_e$  was found to be  $195^\circ\text{C}$ . Thus the average composition corresponds to a point nearer the colder surface for this cylindrical geometry but for plane geometry Hirschfelder found it to be farther from the cold surface.

#### CONCLUSIONS

It may be seen from Table III that the experimental values of the thermal conductivity of the system are consistently higher than the calculated values. A part of this discrepancy may be attributed to the effect of the dissociation of molecular iodine. A rough estimate of this effect shows that the contribution due to this may amount to about 3% at the highest temperature.

It should also be mentioned that in the temperature range of our present measurements the dissociation of HI is quite small. Further experiments with this system over a larger range of temperature will be of much interest.

#### REFERENCES

- Barua, A. K. and Chakraborti, P. K., 1962, *J. Chem. Phys.*, **36**, 2817.  
Brokaw, R. S., 1958, *J. Chem. Phys.*, **29**, 391.  
Brokaw, R. S., 1961, *J. Chem. Phys.*, **35**, 1569.  
Butler, J. N. and Brokaw, R. S., 1957, *J. Chem. Phys.*, **26**, 1636.  
Coffin, K. P., 1959, *J. Chem. Phys.*, **31**, 1290.  
Franek, E. U. and Spalthoff, W., 1954, *Z. Elektrochem.*, **58**, 374.  
Hirschfelder, J. O., Curtiss, C. F. and Bird, R. B., 1954, *Theory of Gases and Liquids*, John Wiley & Sons, Inc., New York.  
Hirschfelder, J. O., 1957a, *J. Chem. Phys.*, **26**, 274, 282.

- Hirschfelder, J. O., 1957b, *Sixth International Symposium on Combustion* (Reinhold Publishing Corp., New York, 1957).
- Kanmuhik, W. G. and Cauman, E. H., 1952, *Proc. Phys. Soc.* (London), **B65**, 701.
- Scarborough, J. B., 1954, *Numerical Mathematical Analysis*, John Hopkins Press, Baltimore.
- Secrest, D. and Hirschfelder, J. O., 1961, *Phys. Fluids*, **4**, 61.
- Srivastava, B. N., and Barua, A. K., 1960, *J. Chem. Phys.*, **32**, 427.
- Srivastava, B. N. and Barua, A. K., 1961, *J. Chem. Phys.*, **35**, 329.
- Srivastava, B. N., Barua, A. K. and Chakraborti, P. K., 1963, *Trans. Faraday Soc.*, **59**, 2522.
- Stegmuller, 1910, *Z. Elektrochem.*, **16**, 85.
- Sullivan, J. H., 1959, *J. Chem. Phys.*, **30**, 1292.

# “DOUBLE EMISSION OF HEAVY FRAGMENTS ( $Z \geq 3$ ) IN THE DISINTEGRATION OF EMULSION NUCLEI”

G. C. DEKA, AND K. M. PATHAK,

DEPARTMENT OF PHYSICS, COTTON COLLEGE, GAUHATI, ASSAM

(Received August 13, 1963)

## Plate I

**ABSTRACT.** Among 405 ‘hammer’ tracks which are observed in the interactions of 4.6 GeV/C negative pions with heavy emulsion nuclei, 12 cases are found, each to be associated with either two ‘hammer’ tracks or one hammer and a heavy fragment ( $Z \geq 3$ ). Our analysis indicates independent production rather than associated production of such fragments.

## INTRODUCTION

For the last few years it has been a subject of interest for the workers to see the emission of two or more fragments in an energetic disintegration of heavy emulsion nuclei. For instance, Lovera (1949) and Perkins (1950) looked for the emission of double or triple fragments of  $Z \geq 3$  in interactions produced by Cosmic Rays using photographic plates; they observed a tendency of associated production of two fragments. Gorichev *et al.* (1961) have analysed the emission frequency of a fragments accompanied by one or more fragments and concluded that the fragments are emitted independently. Gajewski *et al.* (1962) have studied double emission of Li-<sup>8</sup>-fragments in the disintegrations produced by 9 GeV protons. They have observed the emission of 8 double ‘hammer’ tracks in 188 cases. They have, however, noticed the indication of independent emission of such fragments, the frequency of emission of which depends on the excitation energy of the disintegrating nucleus. While studying the various properties of ‘hammer’ tracks and hyperfragments we also looked for double emission of ‘hammer’ tracks and other heavy fragments ( $Z \geq 3$ ).

## EXPERIMENTAL PROCEDURE

Ilford G5 emulsions were exposed to a separated negative pion beam of energy 4.6 GeV/C at the Berkeley Bevatron. The emulsion stack was processed and developed at the Bristol Physics Laboratory. Plates were area scanned under low magnification to observe double stars, ‘hammer’ tracks and stars with one or more heavy fragments. Altogether 51,609 stars have been examined by following black prongs of all the stars up to their end or to the points where they leave the

pellicle. Ends of the tracks are closely examined under higher magnification for any secondary track. As soon as a 'hammer' track is seen, the other prongs of the stars are also examined carefully for their charge. A track produced by a particle of charge  $Z \geq 3$  can ordinarily be distinguished from the rest by studying  $\delta$ -rays and tapering length. The particles which leave the plate are not followed further. It is because the number of such heavy tracks is small, and they are generally too short to travel very far. No star with more than two heavy fragments is observed in our sample.

Number of stars examined.....	51,609
Number of 'hammer' tracks.....	405
No. of stars with double 'hammer'.....	8
No. of stars with a 'hammer' track and a heavy fragment .....	4

TABLE I  
Details of the events

No.	Parent star size	Range of the tracks in microns		Angles with the primary dir.		Angle between the two fragments
		Hammer	Hammer	1	2	
		1	2			
1	15 + 2 $\pi^-$	30.74	50.43	83.7°	64.2°	147.9°
2	15 + 0 $\pi^-$	72.57	313.70	83.0°	116.6°	199.6°
3	11 + 1 $\pi^-$	101.30	516.60	102.7°	74.8°	27.9°
4	12 + 3 $\pi^-$	2219.0	246.3	91.5°	77.5°	14.0°
5	20 + 5 $\pi^-$	112.8	19.2	38.1°	68.6°	30.5°
6	19 + 4 $\pi^-$	47.25	110.9	75.8°	19.4°	56.4°
7	17 + 4 $\pi^-$	35.96	103.57	104.7°	82.1°	186.8°
8	18 + 2 $\pi^-$	445.0	19.5	20.0°	54.0°	34.0°
		Hammer	Fragment			
9	15 + 3 $\pi^-$	162.4	33.5	36.2°	15°	51.2°
10	22 + 2 $\pi^-$	124.7	70.1	57.7°	130°	187.7°
11	15 + 3 $\pi^-$	38.7	45.0	128.0°	60°	68°
12	18 + 2 $\pi^-$	38.84	58.1	43°	70°	27°







*Average number of black prongs for different types of stars :-*

For, all stars.....	14
stars with one 'hammer'.....	13
star with two 'hammers' or one 'hammer' plus one fragment.....	15

Microphotographs of two stars having double hammer tracks are reproduced in Plate 1.

## DISCUSSION .

The number of events obtained so far by us is not sufficient for the investigation of emission frequency, angular distribution etc. of the fragments. As such it is not possible to give a clear cut picture as regards the manner in which the fragments are produced and emitted during such interactions. It is, however, noticed that in eleven out of twelve cases fragments are of unequal ranges. This is most probably due to the fact that the fragments are emitted at different instant during evaporation of the excited nucleus, the longer being emitted at the beginning and the shorter towards the end of the process. It is also seen from our experimental observations given in the above table that there exists no angular relation between the fragments. Hence it appears as if such heavy fragments are emitted independently during the evaporation process.

## ACKNOWLEDGMENT

The authors are grateful to Prof. C. F. Powell, F.R.S., University of Bristol, for his kindly lending them the emulsion stack. They are also indebted to the Department of Atomic Energy for the annual financial support for the research project.

## REFERENCES

- Gajewski, W., Pniewski, J., Pniewski, T., Sieminska, J., Soltan, M., Soltynski, K., Suchorzewska, J., Rep. No. 286/VI (1961), Warsaw.  
 Gorichev, P. A., Lozhkin, O. V., Perfilov, N. A., Yakovlev, Y. P., 1961. *ZETF*, **41**, 327.  
 Lovera, G., 1949, *Nuovo. Cim.*, **6**, 233.  
 Perkins, D. H., 1950, *Proc. Royal Soc.*, **203**, 399.

# ELECTRICAL CONDUCTIVITY OF SINGLE CRYSTALS OF ILMENITE

A. K. MUKERJEE

DEPARTMENT OF MAGNETISM, INDIAN ASSOCIATION FOR THE CULTIVATION OF SCIENCE,  
JADAVPUR, CALCUTTA-32

(Received October 14, 1963)

**ABSTRACT.** The electrical conductivities of the ferromagnetic single crystals of naturally occurring rhombohedral crystals of ilmenite were measured from room temperature upto 880°K for currents in the symmetry plane and in direction perpendicular to it. The study revealed that (i) the substance is a symmetric varistor with negative temperature coefficient of resistance, (ii) the non-ohmic nature of the current-voltage characteristics vanished at about 500°K; (iii) two breaks were observed in the  $\log \sigma - 1/T$  curve.

## INTRODUCTION

Ilmenite (mainly  $\text{FeTiO}_3$ ) is one of the chief iron and titanium bearing minerals usually found as rhombohedral crystals associated with hematite ( $\text{Fe}_2\text{O}_3$ ) and magnetite ( $\text{Fe}_3\text{O}_4$ ). These crystals which are very hard ( $H5\frac{1}{2} - 6$ ) have conchoidal fracture and cleavage along  $\{0001\}$  and  $\{0112\}$  (Dana 1894). These have almost iron black colour with metallic or submetallic lustre.

The magnetic properties of synthetically prepared powdered samples of ilmenite, which are only  $\text{FeTiO}_3$ , have been studied by some workers (Chevallier *et al.* 1953, 55; Kume 1955, Bozorth *et al.* 1957; Ishikawa and Akimoto 1958) and have been found to be antiferromagnetic but very few have (Chevallier *et al.* 1955, Bizette and Tsai 1956, Kume 1955) worked with natural crystals of ilmenite which is often known to be ferromagnetic possibly owing to the inclusion of some magnetite or a solid solution of some hematite.

The electrical conductivity, on the other hand, has been studied only by a single group of workers, namely Ishikawa and Sawada (1956) and that too with synthetic powdered samples. They worked within the temperature range of 90°K to 1073°K and observed that direct current resistivity decreased throughout this range and can according to them be represented above room temperature by the relation  $\rho = \rho_0 \exp (+E/2kT)$  where  $\rho$  is the resistivity at any temperature within the stated limit and  $\rho_0$  and  $E$  have different values within different temperature ranges of the above limit.

On an examination of their results it is found that  $E$ , the activation energy for a particular sample, has three different values while for others only two such values.

The values of  $E$  within approximately same temperature range of two powder samples do not agree. It would appear that the samples being semiconducting, surface effects between different grains of the sample will, as is well known, be appreciable. In addition to this the directional effect of electrical conductivity cannot be observed with powders. It has therefore been decided to study the electrical conductivities of naturally occurring single crystals of ilmenite as a part of our general programme of studying the different properties of Indian minerals.

The present communication gives a preliminary report of observations on the electrical conductivities of single crystals of natural ilmenite which we obtained from the collection in this laboratory of late Prof. K. S. Krishnan.

## EXPERIMENTAL

### (a) *Preparation of the samples*

Before the samples are actually prepared for electrical measurements, these were examined by X-rays in order to test the reported crystal structure and also to ascertain the percentage of the ingredients of the sample, which contained somewhat more than 80% of  $\text{FeTiO}_3$ . Then small blocks of the specimen were fractured out from a larger single crystal by gently striking and tapping. The cleavage occurred along the  $c$ -plane and these blocks were ground with fine emery powder to thin rectangular tablets having the flat faces parallel to the  $c$ -plane. During the time of grinding the thickness was continuously checked for uniformity by a micrometer gauge.

These blocks were then electroplated with copper from a specially prepared electroplating solution. For measurement of electrical conductivity along the  $c$ -plane, electroplating is done over appreciable areas at the two ends on all sides of the specimen and for measurements in a perpendicular direction over two flat faces only, by coating the unwanted portions with wax.

### (b) *Holders for measurement of Conductivities*

The holders for measurement of electrical conductivities along and perpendicular to the  $c$ -plane are in principle the same as those used by Dutta (1953) for the measurement of conductivities of graphite excepting that for  $c$ -plane measurements point contact was used instead of flat contact and for measurements in a perpendicular direction the glass insulating bush was replaced by syndanyo ones.

### (c) *Electrical measurements*

The electrical measurements were taken in the same manner as described by Dutta (1953) and can be classified as follows.

(i) Observation of the D.C. current-voltage characteristics along  $c$ -plane and in perpendicular direction at room and different high temperatures produced

in a cylindrical electric oven wound with nichrome wire, giving temperatures upto about 1000°C.

(ii) Measurement of the electrical conductivities along the above two directions at different high temperatures.

In addition to these, a test for detecting the presence of any rectification effect has to be made since from (i) above, the current-voltage relation has been found to be non-ohmic at room temperature. This was observed for current along both direction of the crystal. For *c*-plane a flat contact was placed at one end on the flat surface of the crystal which is electroplated and a copperplated tungsten whisker on the same surface at the other end. For perpendicular directions one flat surface was entirely electroplated and the whisker was placed on the other surface.

## RESULTS

The result of the X-ray examination of the samples revealed that the present mineral contains more than 80% of  $\text{FeTiO}_3$ , the rest being magnetite and hematite.

The results of various electrical measurements at room temperature as well as higher temperatures are shown in the following Table (I) and graphs. Here  $\sigma_{||}$  and

TABLE I  
Electrical conductivities at room temperature

Samples	Conductivity in $\Omega^{-1} \text{ cm}^{-1}$	
	$\sigma_{  }$	$\sigma_{\perp}$
C <sub>1</sub>	.38	.022
C <sub>2</sub>	.11	.016
C <sub>3</sub>	.20	.018

$\sigma_{\perp}$  represent the electrical conductivities along and perpendicular respectively to the *c*-plane.

## DISCUSSION

It is observed from the results of measurements (Fig. 1-4) that at room temperature for currents passing both along and perpendicular to the *c*-plane, the relationship between the current passing through the crystal and the corresponding voltage drop across the specimen is non-ohmic. In view of this finding the samples were naturally tested for the presence of any rectification effect in them and it was observed that for currents along both the directions (along the plane and perpendicular to it), the current—voltage characteristic though non-ohmic in nature is

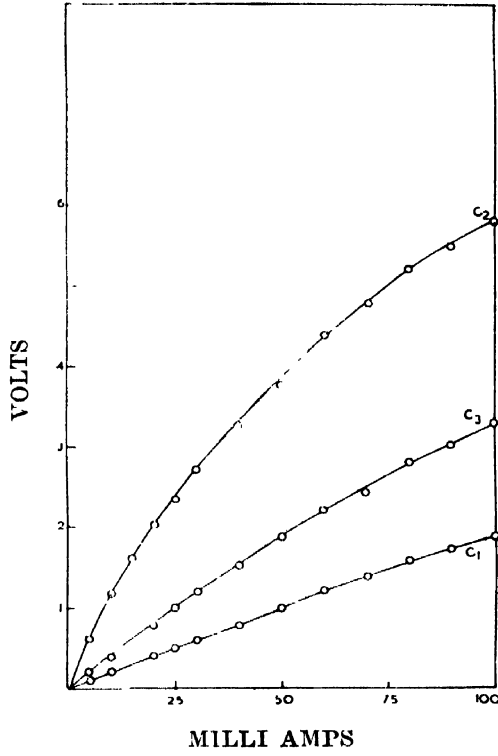


Fig. 1. Current-Voltage characteristics for three crystals in the c-plane with extended contacts at both ends.

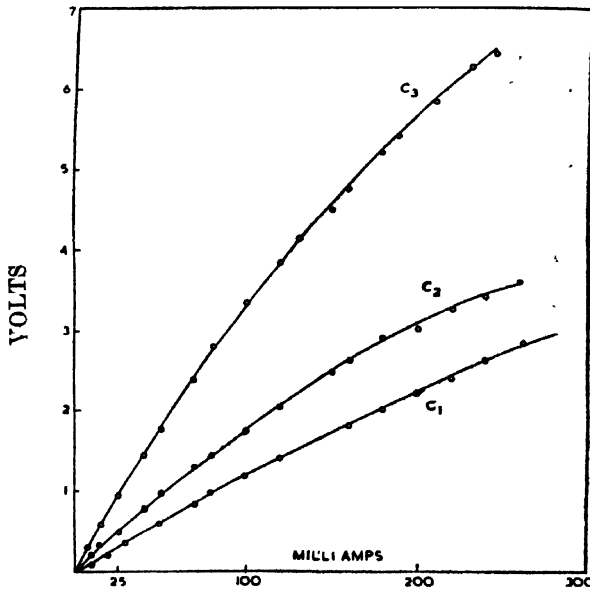


Fig. 2. Current-Voltage characteristics for three crystals perpendicular to the c-plane with extended contacts at both ends.

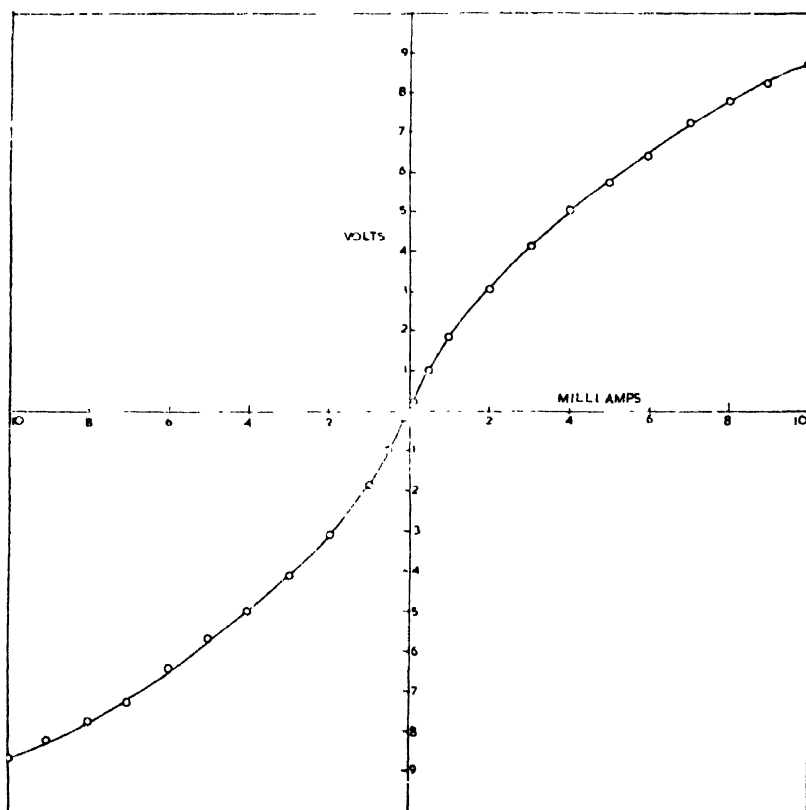


Fig. 3. Current-Voltage characteristic in the c-plane with extended contact at one end and a point contact at the other for direct and reverse currents

practically symmetrical for both forward and backward currents. Therefore the samples which will be shown subsequently to be semi-conductors are symmetrical varistors.

For finding the electrical conductivities at room temperature, the conductivities are calculated in the usual way from the linear portion of the current-voltage characteristics at very low voltage. Following this the values of  $\sigma_{||}$  and  $\sigma_{\perp}$  have been obtained for room temperature. It is observed that the electrical anisotropy i.e.  $\sigma_{||}/\sigma_{\perp}$  is sufficiently large i.e. about 15.

The current-voltage characteristics reported above have been studied at different high temperatures and it was observed that the non-ohmic nature gradually decreased as the temperature was raised and ultimately vanished about 500°K and thereafter the behaviour was perfectly ohmic (see Figs. 5, 6).

The conductivities at different temperatures were obtained so long the behaviours were non-ohmic in the manner already indicated. From a study of the temperature variation of the conductivities ( $\log_e \sigma$  versus  $100/T$ , see figs. 7, 8), it is observed that there are two distinct breaks in the curves at which both  $\sigma_{||}$  and  $\sigma_{\perp}$  undergo



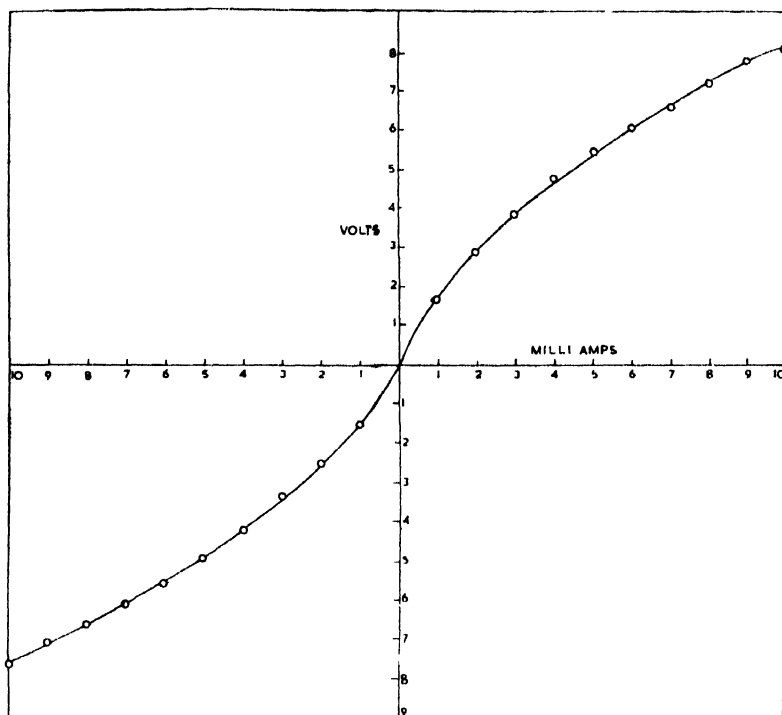


Fig. 4. Current-Voltage characteristics perpendicular to the *c*-plane with extended contact at one end and point contact at the other for direct and reverse currents.

very sharp changes. The temperatures are quite sharply marked and the conductivities perfectly reversible with temperature. It has been not yet possible to associate the breaks with any other physical properties. Moreover, it has been found

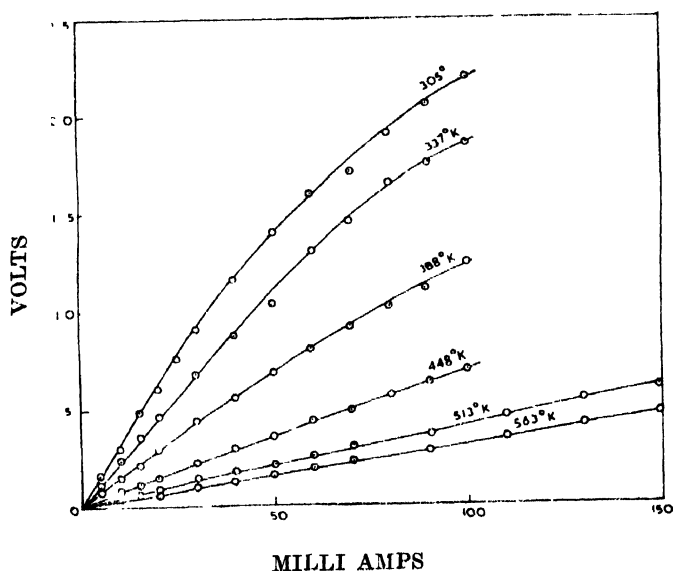


Fig. 5. Current-Voltage characteristics in *c*-plane at different temperatures above room temperature with extended contacts at both ends.

Roth, J. P., 1957, Proceedings of the International Symposium on the Theory of Switching, Part I, in the Annals of the Computation Laboratory of Harvard University, XXIX, 57.

Svoboda, A., 1957, *Ibid.*, 293.

Scheinman, A. H., 1962, *Bell System Technical Journal*, 41, 1337.

Urbano, R. H. and Mueller, R. K., 1956, *Trans. Inst. Radio Engrs.*, N. Y., EC-5, 126.

Veitch, E. W., 1952, *Proceedings of the Association for Computing Machinery*, Pittsburgh, 127.

# Letters to the Editor

The Board of Editors does not hold itself responsible for opinions expressed in the letters published in this section. The notes containing short reports of original investigations communicated to this section should not contain many figures and should not exceed 500 words in length. The contributions reaching the Secretary by the 15th of any month may be expected to appear in the issue for the next month. No proof will be sent to the author.

## 1

### MOLECULAR ORBITAL THEORY OF TRIGONALLY DISTORTED $[\text{Co}, 6\text{H}_2\text{O}^{2+}]$ COMPLEX

L. C. JACKSON\* AND R. RAI

DEPARTMENT OF MAGNETISM, INDIAN ASSOCIATION FOR THE CULTIVATION OF SCIENCE,  
CALCUTTA-32

(Received January 9, 1964)

Under an octahedral field of type  $O_h$ ,  $3d^7$   $^4F$  ground state of  $\text{Co}^{2+}$  ion splits up into two triplets  $^4T_{1g}$ ,  $^4T_{2g}$  and a singlet  $^4A_{2g}$  of successively increasing energies. There is another term  $^1P(^4T_{1g})$  arising from the same configuration  $3d^7$  of the free ion, which lies about  $20,000 \text{ cm}^{-1}$  above  $^4T_{1g}$  in crystals (Abragam *et al*, 1951). So that the lowest triplet state contains an admixture of  $^4P$  through the effective orbital Lande  $g$ -factors  $\alpha, \alpha'$  (Bose *et al*, 1961), which are appreciably different in crystals from the value  $3/2$  for the free ion  $F$ -state. For trigonal distortion of the octahedron, the appropriate Hamiltonian is given by

$$H = V_{\text{trig}} + \alpha u_{\xi} s_{\xi} + \alpha' (u_{\xi} s_{\xi} + u_{\eta} s_{\eta})$$

where the effect of Spin-orbit interaction takes the form  $\Sigma(us)_i$  (Bose *et al*, 1960). Operating above Hamiltonian over the appropriate trigonal orbital states for the

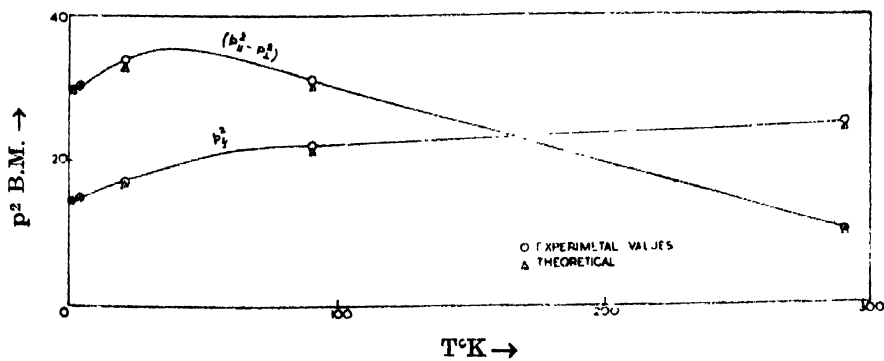


Fig. 1

\* Royal Military College, Canada, Kingston, Ontario, Canada.

lowest triplet (Bose *et al*, 1963) formed by mixing of the central *d*- and surrounding *p*-orbitals, we get the energies and wave-functions for lowest six Kramer's doublets, ready for magnetic perturbation.

Thus we have derived a very complicated expression for the principal ionic magnetic susceptibilities  $K_i$  ( $i = \parallel$  or  $\perp$ ) along and perpendicular to the trigonal axis of the  $\text{CoSiF}_6 \cdot 6\text{H}_2\text{O}$  single crystal, which is identical for the single trigonally distorted  $[\text{Co}^{2+} \cdot 6\text{H}_2\text{O}]$  complex in the unit cell sp.gr  $C'_{2v}$  (Pauling 1930) on the basis of molecular orbital theory of Stevens (1953), Bose *et al*, (1960) and compared our theoretical with the experimental results by one of us (L.C.J.).

We had to increase the trigonal field coefficient  $\Delta$  with temperature, from a value of  $830 \text{ cm}^{-1}$  at  $1.67^\circ\text{K}$  to  $952 \text{ cm}^{-1}$  at  $90^\circ\text{K}$  and then decrease it to  $560 \text{ cm}^{-1}$  at  $290.4^\circ\text{K}$ ; the values for the spin-orbit coupling coefficient we have to take  $\zeta_{\parallel} = -137 \text{ cm}^{-1}$  and  $\zeta_{\perp} = 130 \text{ cm}^{-1}$  instead of free ion value  $-180 \text{ cm}^{-1}$ ; the other parameters—the effective orbital Lande factors  $\alpha = 1.242$ ;  $\alpha' = 1.495$  and orbital reduction factors  $k_{\parallel} = .975$   $k_{\perp} = .93$ .

The anisotropic reduction in spin-orbit coupling coefficient is due to overlap of the  $\text{Co}^{2+}$  charge clouds with *s* and *p* ligand charge clouds. The increase in  $\Delta$  below  $90^\circ\text{K}$  is, as observed earlier, due to thermal expansion or relaxation effects but the decrease above  $90^\circ\text{K}$  appears to be due to some kind of phase transition reversible in character, evidence for which is available from some of our recent measurements between  $90^\circ\text{K}$  and  $300^\circ\text{K}$  (Mazumdar *et al*). Details of the theoretical developments and experimental results will be published elsewhere.

#### ACKNOWLEDGMENT

The junior author (R. R.) is indebted to Prof. A. Bose, D.Sc., F.N.I. for suggesting the problem and guidance in the work. Many valuable discussions and suggestions by Dr. R. Chatterjee are also gratefully acknowledged.

#### REFERENCES

- Abragam, A. and Pryce, M. H. L., 1951, *Proc. Roy. Soc. A.*, **206**, 173.
- Bose, A., Chakravarty, A. S. and Chatterjee R., 1961, *Proc. Roy. Soc., A*, **261**, 43.
- Bose, A., Chakravarty, A. S. and Chatterjee, R., 1960, *Proc. Roy. Soc.* **255**, 145.
- Bose, A., Chatterjee, R. and Rai, R., 1963, *Proc. phys. Soc.* (communicated),
- Mazumdar, M. and Dutta, S. K., *Jour. Chem. Phys.* (Communicated)
- Pauling, L. C., 1930, *Zeits. F. Kristallographie* **72A**, 482.
- Stevens, K. W. H., 1953, *Proc. Roy. Soc., A* **219**, 542.

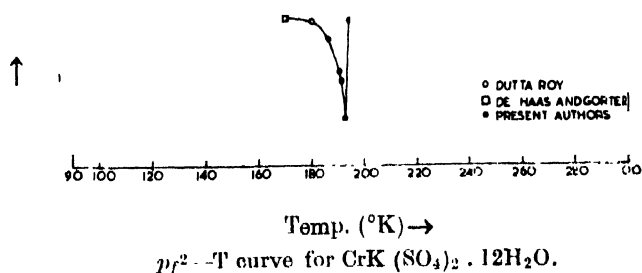
# A SHORT NOTE ON A TRANSITION IN CHROMIUM POTASSIUM SULPHATE ALUM

S. MITRA and S. K. DUTTA ROY\*

DEPARTMENT OF MAGNETISM, INDIAN ASSOCIATION FOR THE CULTIVATION OF SCIENCE,  
CALCUTTA-32

(Received December 13, 1964)

The single crystals of chrome alum  $\text{CrK}(\text{SO}_4)_2 \cdot 12\text{H}_2\text{O}$  being of the cubic class show no external magnetic anisotropy. The effective mean square moment ( $p_f^2$ ) when smoothly plotted against temperature is very nearly a straight line with a small slope to the temperature axis (See Fig. I, de Haas and Gorter, 1930; Serres, 1932) owing to the contribution from high frequency paramagnetism. However, a small curvature with a flat minimum is found in this curve near  $160^\circ\text{K}$  which is confirmed by Dutta Roy (1956) from his close and more accurate observation between  $200^\circ\text{K}$  and  $160^\circ\text{K}$  with measurement at  $20^\circ$  intervals. Some anomalies near  $200^\circ\text{K}$  in dielectric absorption (Griffiths and Powell, 1952) and paramagnetic resonance (Bleaney, 1951) and a multiplication of lines in absorption spectrum from  $290^\circ$  to  $77^\circ\text{K}$  (Spedding and Nutting 1934, Kraus and Nutting, 1941) have also been reported. We have, therefore, undertaken a detailed investigation of chrome alum with a new modified Curie balance and refined cryostatic system (Bose *et al.*, 1963) by means of which very accurate readings of susceptibility at intervals of a fraction of a degree can be taken. The  $p_f^2 - T$  curve is shown in Figure I.



The general nature of the curve is same as that of earlier workers. But a sharp discontinuity in the curve is clearly shown at  $192.5^\circ\text{K}$  which the earlier workers missed as they took readings at comparatively large intervals though departure from linearity in this region was apparent. The above transition

\* Formerly Pool Officer, Government of India; Present address : Department of Physics Indian Institute of Technology, Kharagpur.

is exactly reversible and reproducible with rising and falling temperatures. The deep violet colour of the crystal was observed to become light pink after the transition. The change in colour was also exactly reversible.

A detailed report of the work will be published very shortly elsewhere.

#### A C K N O W L E D G M E N T

Authors are grateful to Prof. A. Bose, D.Sc., F.N.I., for valuable discussions and guidance and one of us (S.M.) to the C.S.I.R. New Delhi, for the award of a Research Fellowship.

#### R E F E R E N C E S

- Bleaney, B., 1951, *Proc. Roy. Soc. A.*, **204**, 203.  
Bose, A., Dutta Roy, S. K., Ghosh, P. K. and Mitra, S., 1963, *Ind. Jour. Phys.* (in press).  
de Haas, W. J. and Gorter, G. J., 1929-30, *Com. Leiden*, no. 208C.  
Griffiths, J. H. E., and Powell, J. A., 1952, *Proc. Phy. Soc.*, **65**, 289.  
Krans, D. L. and Nutting, G. C., 1941, *J. Chem. Phys.*, **9**, 133.  
Sorres, A., 1932, *Ann. der. Phys.*, **17**, 1.  
Spedding, F. H. and Nutting, G. C., 1934, *J. Chem. Phys.*, **2**, 421.

# VALIDITY OF THE PHASE SHIFT CALCULATION OF ELECTRON SCATTERING BY BRYSK METHOD

D. M. BHATTACHARYA and N. C. SIL

DEPARTMENT OF THEORETICAL PHYSICS, INDIAN ASSOCIATION FOR THE CULTIVATION OF SCIENCE, JADAVPUR, CALCUTTA-32

(Received, October 21, 1963)

For a central potential  $V(r)$  the Born relation for the determination of phase shifts of elastic scattering is

$$\delta_l = -\frac{2km}{\hbar^2} \int_0^{\infty} r^2 j_l^2(kr) V(r) dr \quad \dots (1)$$

where  $k = \frac{(2mE)^{1/2}}{\hbar}$ ,  $E$  and  $m$  are the energy and the mass respectively of the incident particle.  $j_l(kr)$  and  $y_l(kr)$  are the spherical Bessel and Neumann functions respectively. Brysk (1962) has given an improved modification of equation (1) which is as follows

$$\tan \delta_l = \frac{-\frac{2km}{\hbar^2} \int_0^{\infty} r^2 j_l^2(kr) V(r) dr}{1 - \frac{2km}{\hbar^2} \int_0^{\infty} r^2 j_l(kr) y_l(kr) V(r) dr} \quad \dots (2)$$

Brysk after comparing the values of  $s$ -wave phase shift  $\delta_0$  obtained from the above relation and from exact calculation for the case of square well potential has found that equation (2) can be used to extend the calculation of  $s$ -wave phase shift to much lower energies where relation (1) fails totally and for higher energies relation (2) gives always better approximation than equation (1), at very high energies both the equations give the same exact result.

It may be worthwhile to investigate how the Brysk method fares for potentials other than the square well, for a screened coulomb potential as in the case of He atom, we have calculated  $\delta_0$  and  $\delta_1$  for incident energies at 5 e.v., 13.5 e.v. and 121.8 e.v. and have compared our theoretical values with those obtained by Born relation and the exact values obtained by Mc. Dougall (1932) by numerical method.

For He atom the field given by Hartree has been used. The integrals involved in the Brysk formula have been evaluated numerically and the results are tabulated as follows.

TABLE

Energy E in ev.	$\delta_0$			$\delta_1$		
	Present values	Born values	Exact values	Present values	Born values	Exact values
5 ev.	2.329	.380	1.659	.025	.013	.020
13.5 ev.	2.01	.57	1.40	.094	.04	.07
121.8 ev.	1.21	.75	.90	.44	.24	.27

A comparison of our calculated values with the values obtained by using Born relation and the exact values shows that both for  $\delta_0$  and  $\delta_1$  the Brysk method is somewhat superior to Born-approximation at 5 ev. and 13.ev.; but it fails to give a satisfactory result at 121.8 ev. where Born approximation gives values nearer to exact ones than does Brysk one.

Brysk has pointed out that it is not possible to assign a priori the limits of validity of the method and the probable error. He has, however, mentioned that his method should hold fairly good for a short range potential. In our case of the screened coulomb field, the Brysk phases exceed the values obtained exactly, whereas the Born relation gives results which are always less than the exact values.

Because of the rather slow decrease of the integral occurring in the denominator of equation (2) the values of the phases as given by the Brysk method is considerably higher than the exact values even at the moderately high energy of 121.8 ev. It may however be remarked that at very high energy where the value of the integral approaches zero, this approximation is expected to give result quite similar to that obtained by Born relation.

#### ACKNOWLEDGMENT

Authors are grateful to Prof. D. Basu for helpful discussions and valuable suggestions.

#### REFERENCES

- Brysk Henry, 1962, *Phys. Rev.*, **126**, 1589.  
 McDougall, J., 1932, *Proc. Roy. Soc.*, **A136**, 549.  
 Mott, N. F., and Massey, H. S. W., *The Theory of Atomic Collisions*, Second Edition, Chapter II.



## A NOTE ON THE TRANSFORMATION OF MANGANITE\*

D. R. DASGUPTA

GEOLOGICAL SURVEY OF INDIA, 29 CHOWRINGHEE, CALCUTTA-16

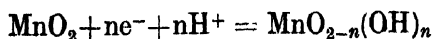
(Received, October 10, 1963)

Plate II, III and IV

The transformation of manganite during heat treatment has been studied by x-ray diffraction using single crystals. It is observed that a single crystal of manganite transformed into a single crystal of pyrolusite ( $\text{MnO}_2$ ) and then into a twinned crystal of  $\text{Mn}_2\text{O}_3$  at  $300^\circ\text{C}$  and  $500^\circ\text{C}$  respectively. The rotation photographs of a single crystal of manganite, before and after heating, are shown in Plates II-IV. All these photographs show that there are definite oriented relationships between the original and transformed phases. The relationship between manganite and pyrolusite has been found as follows :

[100]		[100]
Man		Pyro
[010]		[010]
Man		Pyro
[001]		[001]
Man		Pyro

Assuming the structure of manganite as that proposed by Buerger (1936), it can be seen that the transformation of manganite to pyrolusite (rutile like structure) took place by the removal of H from OH ions present in the manganite structure. This process would reduce the axial parameters in the  $a$  and  $c$  directions of manganite by one half together with a contraction along the  $b$  direction. The possibility of removal of H from OH ions has been proposed by Bernal (1960) in the case of manganese oxyhydroxides where hydrogen can enter or leave a system when there is a corresponding valency change of the positive ions. Recently, Feitknecht and his co-workers (1960) have shown that when  $\text{MnO}_2$  is reduced by  $\text{N}_2\text{H}_4$ , topochemical reactions take place by the migration of electrons and protons through the lattice without changing it much according to the following equation:



In that light the transformation of manganite to pyrolusite is just the reverse reaction.

\* Locality :—Ilfeld, Herz, Germany (Indian Museum, Reg. No. P. 57).

The next reaction, i.e. the transformation of pyrolusite to  $\text{Mn}_2\text{O}_3$ , also shows orientational relationship. A careful examination of Plate IV reveal that along the zero layer line sharp spots due to the reflections from 200, 400, 600, 620, 640 and 800 planes occur on the powder diffraction lines. The occurrence of these spots on the zero layer line indicates that the rotation axis is parallel to one of the crystallographic axes of the cubic crystal. There are also streaky spots along the zero layer line due to reflections from  $(hko)$  and  $(hhl)$  planes. This is due to the fact that the rotation axis is also parallel to one of the  $[110]$  axes of the cubic crystal. Periodicities, corresponding to  $[100]$  and  $[110]$  directions, are also observed in the same photograph. Thus, like cryptomelane to  $\text{Mn}_2\text{O}_3$  transformation (Fauling, Zwicker and Forgeng, 1960), the oriented relationship between pyrolusite and  $\text{Mn}_2\text{O}_3$  can be written as

$$\begin{array}{llll} [100] & || & [110] & \text{and} & [100] \\ \text{Pyro} & & & & \text{Mn}_2\text{O}_3 \\ [010] & || & [110] & \text{and} & [010] \\ \text{Pyro} & & & & \text{Mn}_2\text{O}_3 \\ [001] & || & [001] & & \\ \text{Pyro} & & \text{Mn}_2\text{O}_3 & & \end{array}$$

However, the complex nature of the  $\text{Mn}_2\text{O}_3$  structure, with different orientations of the  $\text{MnO}_6$  octahedra within it, stands in the way of understanding the mechanism of the transformation.

The work has been carried out in the Mineral Physics Section of the Central Petrological Laboratories of the Geological Survey of India. The author is very much grateful to Dr. M. V. N. Murty, Superintending Geologist, for his sincere encouragement during the progress of the work. His thanks are also due to all his colleagues for various helpful discussions.

#### REFERENCES

- Bernal, J. D. 1960, *Schw. Archiv.* 26 Jahr. Nr 2, 69.  
 Buerger, M. J. 1936, *Zeit. Krist.*, **95**, 163.  
 Faulring, W., Zwicker, W. K. and Forgeng, W. D., 1960, *Amer. Min.*, **45**, 943.  
 Feitknecht, W., Oswald, H. R. and Feitknecht-Steimann, U., 1960, *Helv. Chim. Acta.* **43**, 1947.

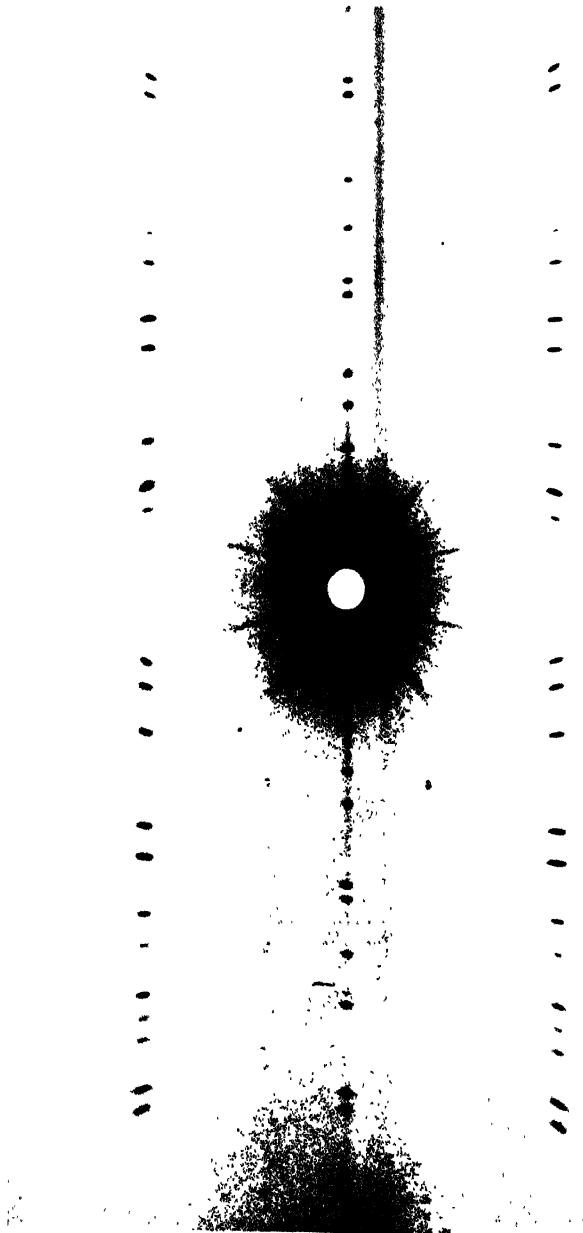


Fig. 1. X-ray rotation photograph of a single crystal of manganite taken along the 001 direction with Mn-filtered Fe-radiation. (Camera radius = 3 cms )



# ON NUCLEAR BINDING ENERGIES

A. K. DUTTA, B. PAL, P. GANGULY and D. BANERJEE

PALIT LABORATORY OF PHYSICS, CALCUTTA UNIVERSITY

92, ACHARYA PRAFULLA CHANDRA ROAD, CAL-9.

(Received January 10, 1964)

In a previous communication. (Dutta and others, 1963) the relationship for the binding energies of the most strongly bound nuclei of different mass numbers have been obtained in the form :

$$E = B(A) + F(Z) + F(I), \quad \dots (a)$$

a combination of base function and two periodic functions in nearly opposite phase.

It had been indicated that some modification would be necessary to make them correspond to the nuclei with optimum energy and optimum neutron number. Modifications have also been found necessary to satisfy the requirements of the weakly bound nuclei and excited nuclei, where one of these periodic functions,  $F(Z)$ , plays an important role. The modified equations, given later on, obtain the positions of the minima and the maxima as well as the associated amplitudes, slightly varying from the previously obtained values. The maxima, and minima positions in mass numbers of the periodic function  $F(Z)$  and the amplitude  $a_z$ , at the corresponding positions, are tabulated below :

	min	max	min	max	min	max	min	max	min	max
$A(F_z)$	16	27	40	61	90	117	140	177	208	237
$a_z$	16.7	10.9	10.9	10.9	16.7	10.9	12.5	10.9	16.7	10.9

The binding energies of the set of nuclei of a particular odd mass number as well as those for the even-even nuclei of an even mass number, are known to be determined by a relation of the approximate form :

$$E = E_0 + \beta(N - N_0)^2 \quad \dots (b)$$

where  $N_0$  is the optimum neutron number for the given mass number and  $\beta$  is the neutron proton exchange energy. It is also known that a simple quadratic relation of this type, with constant  $E_0$ ,  $\beta$  and  $N_0$  values, does not work satisfactorily for all the nuclei of a given mass number, when the isobaric nuclei are large in number. We have kept the quadratic form and have tried to obtain relations for the changes in  $\beta$  and  $N_0$  values with  $N$ .

In accordance with the quadratic form of relationship, the  $\beta$ -values for odd mass nuclei are determined by the mean deviation of the energies of the nearest isobaric neighbours on the two sides, from the energy of the most strongly bound one, obtainable from available tables (Konig *et al.* 1962). Thus, when  $x$ ,  $1-x$  and  $1-x$  are the fractional and nonintegral numbers to measure the changes in neutron numbers of the most strongly bound one and its neighbours from the optimum neutron number, the mean energy deviation from that for the most strongly bound nuclei would be given by

$$\frac{1}{2}\beta\{(1+x)^2 - x^2 + (1-x)^2 - x^2\} = \beta \quad (c)$$

The  $N_0$  values corresponding to it and named as  $N_0^*$  are determined from the relationship,

$$N_0^* = \frac{1}{2}(N_1 + N_2) - \frac{1}{2\beta}(E_2 - E_1) \quad (d)$$

which follows from the relationship,

$$E_2 - E_1 = \beta\{(N_2 - N_0)^2 - (N_0 - N_1)^2\}$$

a consequence of relation (b) with  $N_2 = N_1 + 1$ .

It has been obtained that the  $\beta$  values and the  $N_0^*$  values, calculated from the nearest neighbours of the odd-mass nuclei are composed of two parts : a function  $\beta(A)$  or  $N_0^*(A)$  dependent on mass numbers only, superposed by contributions of a periodic function,  $\beta(S)$  or  $N_0^*(S)$ .  $\beta(S)$  have been subdivided into three components  $\beta(S_1)$ ,  $\beta(S_2)$  and  $\beta(S_3)$ . The periodic function  $F(Z)$  with modulated amplitude gives the  $\beta(S_1)$  values. There is a strong enhancement of the  $\beta(S)$  values at the minima of the function  $F(Z)$  which is represented as  $\beta(S_2)$ . A combinational effect of the maxima of the  $F(Z)$  function and minima of the  $F(I)$  function, give further minor and irregular decrease in  $\beta$ -values near  $F(Z)$  maxima positions, represented by  $\beta(S_3)$ . The effect of  $F(I)$  minima may be better described by specifying the nuclei, that comes back to the periodic curve maxima.

The  $\beta$ -values calculated from next to nearest neighbour for odd masses, as also from the even-even isobaric nuclei, generally, agree. It also shows that  $\beta(S)$ -part of the  $\beta$ -values decrease with larger  $\Delta N = |N_0 - N|$  values. It is expressed by the factor  $\sigma(\Delta N)$ , in the following. It implies that the effect of the superposed periodic structure becomes weaker, as we go away from the optimum-neutron-number condition of the nuclei.

It has also been noted that  $N_0$  values change to larger magnitudes as we increase  $\Delta N$  values, implying a larger percentage of optimum neutron number, corresponding to weakly bound nuclei.

For the odd-odd nuclei, we can take the  $N_0^*$  value as the mean of the values of the previous and following odd-mass nuclei. It enables one to calculate  $\beta$  and  $E'_0$  values from the two equations obtained from relation (b). The  $\beta$  values,

so obtained, are in general agreement with the values expected from the previous and the following mass number's  $\beta$  values. These  $\beta$  and  $N_0^*$  values enable one to calculate the  $E_0$  value for the even-even nucleus. It gives us the correction  $C_{00} = E_0 - E'_0$ , for the odd-odd nuclei of any particular even-mass number.

It may be observed that the enhancement and decrease of  $\beta$  values at the minima and maxima of the  $F(Z)$  curve, is alike in nature to general excitation characteristics associated with potential energy levels and indicates the possibility of correlating nuclear excitation with the  $\beta$ -values. This has been taken up in the next communication.

The complete set of relations and the tabulated experimental and calculated values for all the isobars of some mass numbers are given below, as prototypes. Small adjustments of the relations are expected to give a closer agreement.

$$\begin{aligned} \text{Relations} \quad E &= E_0 + \beta(N - N_0)^2 \\ (0) \quad &\equiv B(A) + F_z + F_I + \beta(N - N_0)^2 \\ &= B(A) + a_z \cos \pi f(Z) - a_I \cos \pi \{f(Z) + \phi\} \\ &+ \{\beta(A) + \sigma(\Delta N) \cdot \Sigma \beta(S_i)\} \cdot \{N - N_0^* + \eta(\Delta N)\}^2 \end{aligned}$$

where,

$$\begin{aligned} (1) \quad B(A) &= -9.828.1 + 8.877 \times 10^{-3} A^2 + C_{ij} \text{ mev.} \\ C(ce) &= 32.2; C(e_o^e) = 33.0; C(oo) = 34 + 80A^{-1} \\ (2) \quad N_0^* &= .6302A - .01287A \cdot \exp(-7.95 \times 10^{-3} \cdot A) - .00155A \times \\ &\quad \cos \pi \{0.794 \sinh .0372(A - 104)\} \{1 - \tanh .6(A - 45)\} \\ &\quad \times \{1 - \tanh .6(A - 145)\} \\ \eta(\Delta N) &= 0.1 |N_0^* - N| - 0.1 \end{aligned}$$

It gives the increase in percentage of neutron number from about 50 at lower mass numbers to 63 for higher mass numbers with a superposed periodic variation in the range of mass numbers 40 to 150.

$$\begin{aligned} f(Z) &= -.051 + .0339A - 2 \exp -1.18 \times 10^{-3} \cdot A^2 + 0.3 \cdot \exp -3.43 \\ &\quad \times 10^{-3} \cdot (A - 140)^2. \end{aligned}$$

$$\begin{aligned} (3) \quad a_z &= 10.9 - 2.9 [\sin \pi 0.5f(Z) - \Sigma_i \exp -\alpha_i(A - A_i(F_z, \min))^2] \\ a_I &= 10 + 2.9 \sin \pi (.008A) + 2.3 \exp -2 \times 10^{-3} (A - 200)^2 \\ \phi &= -0.11 + .135 \cos \pi \{a_i \sinh b_i(A - A_{oi})\} \end{aligned}$$

$[\alpha_i = \frac{200}{T^2}; T = \text{period in mass number of } F_z, \text{ at the zone concerned. } a_i, b_i \text{ are associated constants with } A_{oi} \text{ for one period about } A_{oi} \text{ only. Associated constants } (A_{oi}; b_i; \alpha_i) \text{ are } (70; 3.42 \times 10^{-2}; 0.106); (186; 7.317 \times 10^{-2}; 0.226) \text{ and } (256; 8.625 \times 10^{-2}; 0.0636)]$

$$(4) \quad \beta(A) = 67.A^{-1} \exp b(A-52) \quad b = \begin{cases} -.01 & \text{for } A < 52 \\ +.0038 & \text{for } A > 52 \end{cases}$$

$$\sigma(\Delta N) = 0.6 + 0.6 \tanh(1.6 - 8\Delta N)$$

$$\beta(S_1) = \{0.95 - .6 \tanh .06(A-30) - .25 \tanh .12(A-145)\} \cos \pi f(Z)$$

$$\beta(S_2) = .08 a_z \exp -\gamma_i \{A - A_i(F_z \text{ min})\}^2$$

$$\beta(S_3) = -\{.45 - .15 \tanh(A-140)\} \exp -\gamma_i \{A' - A_i(F_z \text{ max})\}^2$$

$[\gamma_i = 80/T^2 A'$  refers to mass numbers 27, 31; 59; 113-115, which are affected by  $F_z$  max. Other nuclei in the regions obtain balanced effect due to  $F_z$  max and  $F_z$  min.]

TABLE I

Ele- ment	A	-E (exp) mev.	-E (Cal) mev.	Ele- ment	A	-E (exp) mev.	-E (Cal) mev.	Ele- ment	A	-E (exp) mev.	-E (Cal) mev.
C	15	106.5	108.3	Se	74	642.9	642.7	Er	170	1379.0	1379.8
N	15	115.5	116.7	Br	74	636.1	635.1	Tm	170	1377.8	1377.6
O	15	111.9	114.4	Kr	74	631.2	630.8	Yb	170	1378.0	1378.7
								Lu	170	1373.7	1373.6
C	16	110.8	112.5	Br	85	737.4	736.0				
N	16	118.0	118.3	Kr	85	739.5	738.6				
O	16	127.6	128.1	Rb	85	739.3	738.0	Tl	210	1640.9	1640.3
F	16	111.2	111.9	Sr	85	737.5	737.6	Pb	210	1645.6	1645.8
								Bi	210	1644.8	1644.5
S	35	298.8	297.6	Y	85	733.7	734.2	Po	210	1645.2	1644.0
Cl	35	298.2	297.3	Mo	99	852.0	854.1	At	210	1640.6	1639.6
Ar	35	291.4	292.4	Tc	99	852.6	854.4	Rn	210	1637.3	1637.1
Sc	50	432.3	431.8	Ru	99	852.1	853.5	Pa	235	1783.2	1784.2
Ti	50	437.8	437.8	Rh	99	849.2	850.3	U	235	1783.8	1784.2
V	50	434.8	434.6	Pd	99	844.6	845.3	Np	235	1782.9	1783.4
Cr	50	435.0	434.9	Te	130	1095.5	1096.3	Pu	235	1781.0	1780.8
Mn	50	426.9	425.3	I	130	1094.7	1094.8				
								Am	245	1841.4	1841.3
Ga	74	640.8	640.5	Xe	130	1096.9	1097.0	Cm	245	1841.5	1840.9
Ge	74	645.7	645.2	Cs	130	1093.1	1092.8	Bk	245	1839.9	1839.0
As	74	642.3	642.3	Ba	130	1092.8	1091.6	Cf	245	1837.6	1836.9

## REFERENCES

- Dutta, A. K., Pal, B., Gauguly, P., Banerjee, D, 1963. *Ind. J. Phys.* **37**, 543.  
 Konig, L. A., Mattauch, J. H., Wapstra, A. H., 1962, *Nuclear Physics*, **81**, 18.



## AN ANALYSIS OF THE J-PHENOMENON IN X-RAYS

## Part I.

HIRENDRA KUMAR PAL

DEPARTMENT OF PURE PHYSICS, CALCUTTA UNIVERSITY, CALCUTTA.

(Received January 8, 1963)

**ABSTRACT.** In this paper an attempt has been made to study some aspects of the *J*-phenomenon in X-rays from an analytical point of view. Some of the principal features of the phenomenon as well as the conditions governing the occurrence of the 'J-discontinuity' in two kinds of experiments have been discussed. It has been shown from theoretical considerations that the effect together with the associated features, is exactly what is expected under suitable circumstances. Barkla's concept of 'levels' of X-ray activity has not been considered in the present analysis.

## INTRODUCTION

It is well known that Barkla and his collaborators had observed under certain conditions discontinuities in X-ray absorption which at first were considered as an evidence of a *J*-series of characteristic X-radiation. It is also well known that later investigations led Barkla to discard this view but many incontrovertible facts were there which baffled explanation and Barkla classed them under the name, "*J*-phenomenon in X-rays".

The experimental results of Barkla *et al.* relate mainly to the absorption of heterogenous X-rays by matter. The two methods which were usually followed may be described as follows :

I. The mass-absorption coefficient of a heterogeneous beam of X-rays, from which the softer constituents had been eliminated by filtration, was determined as usual in two testing substances. The penetrating power of the incident beam was progressively increased and the mass-absorption coefficients in two substances were measured for each penetrating power. They were then plotted, one against the other in a graph.

II. A heterogeneous beam of X-rays was progressively hardened by passing it through an increasing thickness of a sheet of substance. The mass-absorption coefficient of the transmitted beam was then determined in either a similar substance or in a different substance and was plotted in a graph against the percentage of the incident radiation absorbed by the filter.

In the above two methods, the mass-absorption coefficient of the heterogeneous beam in any testing substance was measured in the usual way, i.e., by placing in its path, sheets of the testing substance and adjusting their thickness

till there was a 50% reduction in the intensity of the beam. If  $t$  represented the intercepting thickness, then the average mass-absorption coefficient would be given by  $\left(\frac{\mu}{\rho}\right) = \frac{1}{t} \log_e^2$ . The range of values for  $\left(\frac{\mu}{\rho}\right)_{AL}$  employed in the experiments under review was generally between 0.5 and 1.8 approximately, the corresponding wavelengths being nearly 0.29 Å and 0.48 Å respectively.

In both these methods, the graphs obtained can be classified as two distinct *alternative cases*, Cases *A* and *B*. In Case *B*, the graph was a continuous straight line and in Case *A* there were two and sometimes more, straight lines intervened by one or more discontinuity or discontinuities. The discontinuity or discontinuities observed in Case *A* constituted a notable feature of Barkla's *J*-phenomenon in X-rays.

The *J*-discontinuities had been observed times without number under various experimental conditions. It had been observed with an intense, narrow pencil of primary rays, or a weak, wide pencil of scattered rays; with heterogeneous radiations or approximately homogeneous radiations; with highly polarized or unpolarized radiations; with the same tube, but rays proceeding along different directions or with different tubes excited in similar or different ways. It had been observed by different investigators with different testing substances and by various testing methods. Again, under precisely the same conditions, it had not been observed by others and even by the same observers.

The principal features of the discontinuity-phenomenon may be outlined as follows :

(i) The discontinuity-phenomenon, when it occurred, occurred at a critical penetrating power of the radiation (as measured by the mass-absorption coefficient) which was characteristic of the testing substance and independent of the previous history of the radiation. The critical penetrating power changed slightly with the material of the testing element.

(ii) A number of discontinuities called  $J_1, J_2, J_3, \dots$  etc., each at its own critical frequency, was observed.

(iii) The discontinuity was very abrupt.

(iv) The discontinuity or discontinuities depended on some factors which could not be identified.

Amongst those who reported failures to reproduce the *J*-discontinuity were Dunbar (1925, 1928), Worsnop (1927), Alexander (1930), Backhurst (1932) and a few others. Their results represented only one of the two *alternative cases* (Case *B*) and could add nothing to our knowledge. Such a result was neither more nor less real and hence could not adequately prove or disprove the phenomenon itself.

In order to explain the phenomenon, Barkla had introduced a new concept of two (or more) discrete 'levels' of X-ray activity (absorption) and postulated sudden transformation, under proper circumstances, from one 'level' to another, depending upon the complex heterogeneous beam taken as a whole. This concept was not however acceptable. Barkla himself had admitted a number of times that much more experimental work would be necessary for any final explanation which would be convincing.

In the present investigations, an attempt has been made, on the basis of the heterogeneity of the X-ray beam, to give a consistent and comprehensive interpretation of all the experimental results which had been obtained by Barkla and his collaborators. It is significant that it has not been necessary to invoke Barkla's new concept in the interpretation given by the author. The present paper deals with the results of experimental investigations, embodied in the paper on "The J-phenomenon in X-rays—Part I" by Barkla (1925).

#### THEORETICAL CONSIDERATION

A mathematical treatment of the problems on heterogeneous X-rays, is extremely difficult in view of the fact that the beam concerned covers a wide range of wavelength lying between a known lower limit and an uncertain upper limit and also because the energy-distribution over this range is not known with any degree of precision. Besides, the distribution function itself may also vary from tube to tube, depending on many factors.

Truly speaking, there is no one wavelength for a heterogeneous beam. Yet for the sake of convenient reference, it is customary to assign to it, what is called an 'equivalent wavelength', based on its mass-absorption coefficient in some substance, as though the beam were monochromatic. This is not entirely satisfactory. As the absorption coefficient itself is determined somewhat arbitrarily (from a 50% reduction in the intensity) and as it varies with the nature of the testing element, the wavelength deduced from it should naturally be arbitrary to some extent and dependent on the testing material. However, the most important point for consideration is the fact that by this process of measurement, the very structure of the radiation is changed and the change is different with different testing materials. Thus the spectrum of the radiation emerging from the testing substance is different in minute details from that incident on it. As the emergent beam is richer in harder rays on account of the greater absorption of the softer constituents by the material of the tester, the average or the 'equivalent' wavelength on the emergent side is definitely shorter than on the incident side. Under the circumstances, the question naturally arises: To which portion of the beam, the incident or the emergent, should we ascribe the mass-absorption coefficient determined experimentally? Although the usual convention is to attribute it to the incident portion, the emergent one has an equal claim upon it. Such a

problem, of course, does not arise in the case of a perfectly homogeneous beam, where the emergent beam is identical with the incident beam, except that it is of less intensity. A little reflection will suggest that, for a heterogeneous beam, the mass-absorption coefficient should belong neither to the incident side, nor to the emergent. More appropriately it should correspond to an intermediate wavelength which the beam has somewhere inside the testing absorber.

*The Effective Wavelength of the heterogeneous radiation*

This intermediate wavelength, which we shall call 'effective' wavelength  $\lambda_{eff}$  can be interpolated from the following relation holding good between the mass-absorption coefficient and the wavelength of a monochromatic radiation, lying within the range of wavelengths with which we are concerned :

$$\frac{\mu}{\rho} = A + B\lambda^3 \quad \dots (1)$$

This is a linear relationship between  $\mu/\rho$  and  $\lambda^3$ , where  $A$  and  $B$  are constants depending on the nature of the testing material. The constant  $A$  may also depend upon the geometry of the measuring arrangement. The approximate values of  $A$  and  $B$ , computed for aluminium and copper from the standard data obtained with a narrow pencil of X-rays, may be written down as follows :

Aluminium	$A = 0.125$	$B = 14.1$
Copper	$A = 0$	$B = 153$

*The 'Discrepancy' between the Effective Wavelength and the Average Wavelength.*

We have now to probe into the relation corresponding to (1) between the measured  $(\mu/\rho)$  and the average wavelength  $\lambda'$  of the incident spectrum of a heterogeneous beam of X-rays. This 'average' wavelength is to be regarded as independent\* of the testing material. Obviously the 'effective' wavelength  $\lambda_{eff}$  falls short of the "average" wavelength  $\lambda'$  by a quantity 'e' so that

$$\lambda_{eff} = \lambda' - e \quad \dots (2)$$

Let  $e$  be called the 'discrepancy', which is necessarily a function of  $\lambda'$  and the nature of the absorbing material. For a monochromatic radiation,  $e$  is equal to zero, and for hard, filtered and heterogeneous radiations (such as were employed in the experiments under review) it is calculated to be small. Further, so long as the average wavelength of the latter remains unchanged, slight variations in their microscopic structure will be supposed to produce only a trivial change, if at all, in  $e$ —a change of second-order smallness which will be neglected.

\*Perhaps the 'average' wavelength  $\lambda'$  here may be best defined as follows :  $\lambda' = \frac{c}{\nu}$  where the average frequency  $\nu' = (\Sigma n.h.\nu)/(h.\Sigma n) = \text{Total energy}/(h \times \text{total number of photons})$ .

Now,  $\lambda_{eff}$  satisfies the equation :

$$\frac{\bar{\mu}}{\rho} = A + B\lambda_{eff}^3, \text{ which in view of (2)}$$

becomes :

$$\begin{aligned} \frac{\bar{\mu}}{\rho} &= A + B(\lambda' - e)^3 \\ &= A + B\lambda'^3(1 - 3e/\lambda'), \text{ since } e \ll \lambda' \end{aligned}$$

Deleting the dash upon  $\lambda$  for the sake of convenience, we shall henceforth write :

$$\frac{\bar{\mu}}{\rho} = A + B\lambda^3(1 - 3e/\lambda) \quad \dots (3)$$

where  $\lambda$  means now and hereafter the 'average' wavelength of the incident radiation. Putting  $\bar{\mu}/\rho = y$  and  $\lambda^3 = x$ , equation (3) takes the form

$$y = A + Bx - 3Bx^{2/3}e \quad \dots (3a)$$

Thus what was a straight line graph (*vide* equation 1) in the case of a monochromatic radiation becomes a curve\* in the case of a heterogeneous radiation, the equation to the curve being given by 3(a). Fig. 1 represents schematically the two graphs one above another.

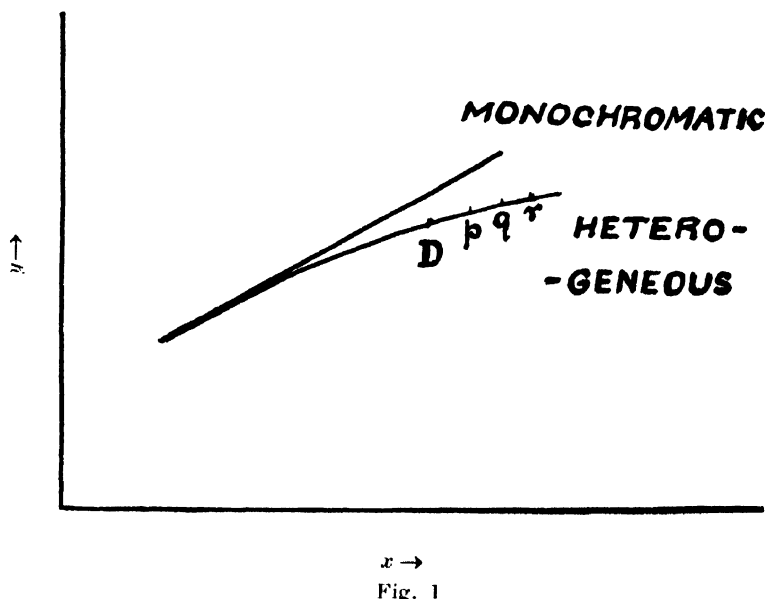


Fig. 1

Curvature of the graph for the heterogeneous beam

Differentiating equation (3a) successively with respect to  $x$ , we get :

$$y_1 = B(1 - 3x^{2/3}e_1 - 2x^{-1/3}e) \quad (4)$$

\*It should be stressed here, that the deviation of this curve from the linear course is nowhere great within the range of experimental wavelengths, as the term  $3e/\lambda$  in equation (3) is small compared to unity.

$$y_2 = -\frac{B}{3}(9x^{2/3}e_2 + 12x^{-1/3}e_1 - 2x^{-4/3}e) \quad \dots \quad (5)$$

and

$$y_3 = -Bx^{-7/3} \left( 3x^3e_3 + 6x^2e_2 - 2xe_1 + \frac{8}{9}e \right) \quad \dots \quad (6)$$

These differential coefficients cannot ordinarily be evaluated since  $e$ , as a function of  $x$ , is not known. In the present analysis, we shall suppose that for filtered, hard radiation,

$$e = ax + bx^2 + cx^3 \quad (\text{approx.}) \quad \dots \quad (7)$$

where  $a, b, c$  are positive constants, independent of  $x$  but dependent on the testing absorber.

Differentiating now equation (7), we have

$$\left. \begin{aligned} \frac{de}{dx} &= e_1 = a + 2bx + 3cx^2 \\ \frac{d^2e}{dx^2} &= e_2 = 2b + 6cx \\ \frac{d^3e}{dx^3} &= e_3 = 6c \end{aligned} \right\} \quad \dots \quad (8)$$

A justification for the function expressed by equation (7) arises from the fact that it satisfies the conditions that both  $e$  and  $de/dx$  should decrease with the decrease of  $\lambda$ , (i.e., with the decrease of  $x$ ) in conformity with the actual behaviour of the rays concerned.

Substituting in equation (5) the values of  $e$  and the differential coefficients from (7) and (8) respectively, we obtain after simplification,

$$y_2 = -\frac{2B}{3}(5ax^{-1/3} + 20bx^{2/3} + 44cx^{5/3}) \quad (9)$$

It is noted from this equation (9) that  $y_2$  is negative, so that the slope of the curve represented by (3a) decreases as  $x$  increases. Further, the rate of variation of the slope is comparatively great for small as well as for large values of  $x$  (i.e. of  $\lambda$ ). Hence this rate passes through a minimum at a certain medium wave length. If this minimum occurs within the experimental range of wave-length, a J-discontinuity will appear. The particular value of  $x$  at which such a minimum occurs can be calculated by putting  $y_3 = 0$  in equation (6), so that

$$0 = y_3 = -Bx^{-7/3} \left( 3x^3e_3 + 6x^2e_2 - 2xe_1 + \frac{8}{9}e \right)$$

or

$$3x^3e_3 + 6x^2e_2 - 2xe_1 + \frac{8}{9}e = 0 \quad \dots \quad (10)$$

The solution of the equation (10) gives the required value of  $x$ . The point on the curve corresponding to this minimum is denoted by  $D$ .

## DEDUCTIONS

### 1. *Monochromatic radiation.*

From equation (1) we have

$$\left(\frac{\mu}{\rho}\right)_X = A_X + B_X \lambda^3$$

and

$$\left(\frac{\mu}{\rho}\right)_Y = A_Y + B_Y \lambda^3,$$

where the subscripts  $X$  and  $Y$  refer to two different testing substances. Eliminating  $\lambda^3$  between these equations,

$$\left(\frac{\mu}{\rho}\right)_X = \left(A_Y - \frac{B_X}{B_Y} A_Y\right) + \frac{B_X}{B_Y} \left(\frac{\mu}{\rho}\right)_Y \quad (11)$$

This is a continuous linear relation between  $(\mu/\rho)_X$  and  $(\mu/\rho)_Y$ . If in a particular case,  $X$  represents aluminium and  $Y$  copper, then  $A_Y \approx 0$ ,

so that

$$\left(\frac{\mu}{\rho}\right)_{Al} = A_{Al} + \frac{B_{Al}}{B_{Cu}} \left(\frac{\mu}{\rho}\right)_{Cu}.$$

### 2. *Heterogeneous radiations*

#### CASE I.

*Relation between the mass-absorption coefficients in two absorbing substances when the incident beam is progressively hardened*

We have already seen that for a particular assumed functional relation between  $e$  and  $x$  in the case of a penetrating filtered radiation, there occurs a point  $D$  on the  $y-x$  curve at which the rate of decrease of the slope is minimum. If such is actually the case under the unknown and correct functional relation also, the rate of variation in the slope close to the point  $D$  and on either side of it, will also be near the minimum. A set of points  $p, q, r$  may, therefore, be taken on the curve close to and on one side of  $D$ , such that they may be regarded as practically lying on a straight line of short length. Similarly, we may take another set of points on the other side of  $D$  and they lie on another straight line of short length.

Now consider together the two curves  $(y_X - x)$  and  $(y_Y - x)$  for the two absorbers  $X$  and  $Y$  with their own  $D$ -points,  $D_X$  and  $D_Y$ . We shall suppose here that  $D_X$  and  $D_Y$  are sensibly one above the other. Taking the short straight lines passing through the points  $p, q, r$  lying on the same side (L.H.S., say) of

$D_X$  and  $D_Y$  in the two curves, it is shown below that, over a small range, the relation between  $y_X$  and  $y_Y$  is linear, when  $x$  is eliminated between them. It is evident from equation (3) that the assumption of a short length of the curve being practically straight means that  $e/\lambda$  is fairly constant with a mean value  $K$  over that length, so that on the L.H.S. of the  $D$ -points we have :

$$y_X = \left( \frac{\bar{\mu}}{\rho} \right)_X = A_X + B_X \lambda^3 \left( 1 - \frac{3e_X}{\lambda} \right) = A_X + B_X (1 - 3K_X)x \quad \dots (11a)$$

$$\text{and} \quad y_Y = \left( \frac{\bar{\mu}}{\rho} \right)_Y = 0 + B_Y \lambda^3 \left( 1 - \frac{3e_Y}{\lambda} \right) = B_Y (1 - 3K_Y)x$$

where  $X$  is taken to represent aluminium and  $Y$  copper.

Eliminating  $x$  between the above two equations, we have,

$$y_X = A_X + \frac{B_X}{B_Y} y_Y \{1 - 3(K_X - K_Y)\}$$

where  $K_X$  and  $K_Y$  are small compared to unity. Putting  $\alpha = (K_X - K_Y) = \text{const.}$ , we get

$$y_X = A_X + \frac{B_X}{B_Y} (1 - 3\alpha)y_Y \quad (12)$$

This equation represents a straight line graph for  $y_X$  plotted against  $y_Y$ . The slope of the straight line is given by  $\frac{B_X}{B_Y} (1 - 3\alpha)$  and the intercept on the  $y_X$ -axis by  $A_X$ .

Similarly, on the R. H. S. of the  $D$ -points on the two curves, we have another straight line represented by the equation

$$y_X = A_X + \frac{B_X}{B_Y} (1 - 3\beta)y_Y \quad (13)$$

where  $\beta = (K'_X - K'_Y) = \text{const.}$  The slope of this straight line is given by  $\frac{B_X}{B_Y} (1 - 3\beta)$ , and the intercept on the  $y$ -axis, again by  $A_X$ .

If  $\alpha$  and  $\beta$  are different, equations (12) and (13) represent two different straight lines with different slopes but equal intercepts.

It is not possible to say which of  $\alpha$  and  $\beta$  is greater. If however we assume  $\beta > \alpha$ , the two straight lines agree with Barkla's in their configurations : The former straight line is on the shorter wavelength side and the latter on the longer wavelength side of the  $D$ -points, there being a discontinuity in the region corresponding to these points. This is the well known ' $J$ -discontinuity' which is illustrated in Fig. 2. In case if one  $D$ -point  $D_X$  is within the experimental range of wavelengths and the other  $D_Y$  outside but not far away then also  $J$ -step may appear. Here  $\alpha = (K_X - K_Y)$  and  $\beta = (K'_X - K'_Y)$ .



A point in support of the theory advanced may be noted here. The experimental value of the intercept  $A_X$  for aluminium (obtained from Barkla's Figs. 1, 4 and 9 by extrapolation) agrees remarkably well with the theoretical, which is about 0.125. As for the other testing substances, such as paper or gold, reliable data for comparison are not available. Further, the smallness of  $\alpha$  and  $\beta$  can be verified if their values are estimated from the slopes of the two straight lines with the help of equations (12) and (13). For example, in the case of Al-Cu pair, in Barkla's Fig. 1, the values of  $\alpha$  and  $\beta$  are computed as -.033 and +.023 respectively.

### *Position of the J-discontinuity*

According to the present view, the position of the  $J$ -discontinuity in the graph (Fig. 2), is determined by the  $D$ -point. To get the  $x$ -coordinate of this point we have to solve equation (10), which is :

$$3x^3e_3 + 6x^2e_2 - 2xe_1 + \frac{8}{9}e = 0$$

Assuming the functional relation given in (7) and substituting in equation (10), the values of  $e$  and its differential coefficients from (7) and (8) respectively, we get, after simplification,

$$a + 8bx + 44cx^2 = 0 \quad \dots (14)$$

This leads to

$$x = (-2b \pm \sqrt{4b^2 + 11ac})/22c$$

Since the coefficients  $a, b, c$  are all positive, the negative sign before the radical is inadmissible, for that would make  $x$  negative, which is absurd. Hence

$$x_D = (-2b + \sqrt{4b^2 + 11ac})/22c \quad (15)$$

An approximate solution of equation (14) might at once be obtained, if we could neglect the term  $44cx^2$  which is likely to be small as compared to the other two terms. In that case

$$x_D \approx a/8b, \text{ for the absorber } X$$

and

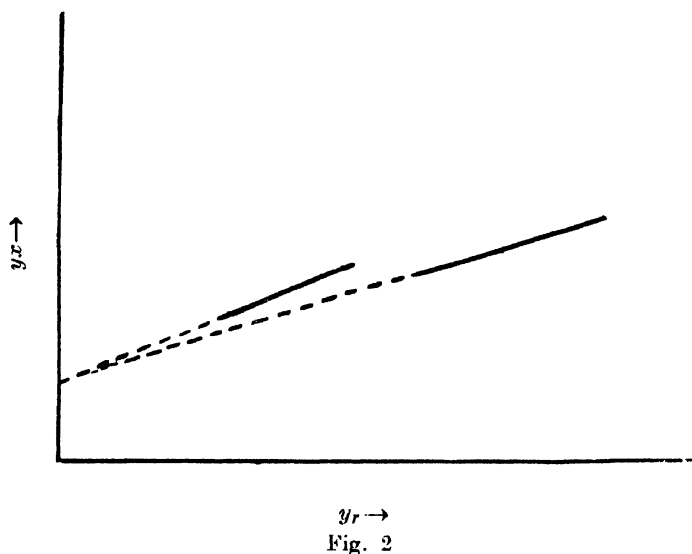
$$x_D' \approx a'/8b', \text{ for the absorber } Y \quad (16)$$

It is evident that  $D_X$  and  $D_Y$  will lie one above the other in Fig. 1, to the extent the values of  $a/b$  and  $a'/b'$  approach each other and the position of the  $J$ -discontinuity in Fig. 2, will be determined accordingly.

### *Critical Mass-absorption Coefficient for the J-discontinuity*

It is noted from equation (15) that the position of the  $D$ -point should be

characteristic of the absorbing material, since the constants  $a, b, c$  are characteristic of that material. This explains why the discontinuity in Fig. 2, should occur



at a critical value of  $(\mu/\rho)$  for the absorber concerned. The fact that the  $J$ -discontinuity appears at some critical value of  $(\bar{\mu}/\rho)$  of the absorber is a characteristic feature of the  $J$ -phenomenon. This critical value may be calculated with help of equation (3a), i.e.,

$$\left( \frac{\bar{\mu}}{\rho} \right)_j = y_j = A + Bx_j - 3Bx_j e_j \quad \dots (17)$$

where the subscript 'j' refers to the  $J$ -discontinuity and where

$$e_j = ax_j + bx_j^2 + cx_j^3$$

and

$$x_j = x_D = (-2b + \sqrt{4b^2 + 11ac})/22c$$

obtained from equations (7) and (15) respectively. Thus  $(\mu/\rho)_j$  turns out to be a function of  $a, b$ , and  $c$ , which again depend on the absorbing substance. As the nature of variation of  $a, b, c$  with the material of the substance is not known due to insufficiency of available data, it is not possible to find how  $\lambda_j$  should change with the testing material. But Barkla's experimental values,  $\lambda_{j_3} = 0.335 \text{ \AA}$  for aluminium and  $0.315 \text{ \AA}$  for copper, enable us to compute roughly, from equation (16), the ratio  $a/b$  for these elements. They are 0.3 for aluminium and 0.25 for copper. It may be mentioned here that on the basis of the function proposed in (7), the  $J$ -discontinuity, when it occurs, should appear at a *medium* wavelength. Actually in Barkla's experiments, the discontinuity was found to be within the experimental range,  $0.29 \text{ \AA} - 0.48 \text{ \AA}$ , and the value of the critical wavelength at which the discontinuity appeared varied from  $0.30 \text{ \AA}$  (gold) to  $0.39 \text{ \AA}$  (carbon).

*Constancy of the Critical Penetrating Power*

It is seen from equation (16) that the average wavelength at which the *J*-discontinuity occurs is given, to a rough approximation, by  $(a/8b)^{1/3}$  which is a constant for a given absorber. But this average wavelength is also a measure of the macroscopic complexion of the heterogeneous radiation. The occurrence of the *J*-discontinuity is thus conditional upon the availability and constancy of this complexion within the scope of the experiment and not upon the individual wavelengths constituting the incident beam. This is the reason why, with beams obtained in so many diverse ways, their critical penetrating power should turn out so constant, when measured with any substance.

*J-step*

Referring to our Fig. 2, if  $y'_Y$  be the abscissa of the discontinuity, then the corresponding ordinates belonging to the two straight lines represented by the equations (12) and (13) are given by

$$AX + \frac{B_X}{B_Y} (1-3\alpha)y'_Y$$

and

$$AX + \frac{B_X}{B_Y} (1-3\beta)y'_Y$$

respectively and their difference is

$$3 \frac{B_X}{B_Y} (\beta-\alpha)y'_Y$$

This is the *J*-step.

The percentage step-up compared to  $y'_Y$

$$= \left\{ 3 \frac{B_X}{B_Y} (\beta-\alpha)y'_Y \times 100 \right\} / y'_Y = 300 \frac{B_X}{B_Y} (\beta-\alpha).$$

*Multiple discontinuities*

The occurrence sometimes of more than one discontinuity in course of a single experiment, is in the light of the present analysis, suggestive of the existence of a corresponding number of *D*-points along the whole length of the curve ( $y-x$ ) represented by equation (3a) and brought under experimental observation. The  $a, b, c$ —values over different segments of the curve, are, in that case, different. We are, however, inclined to the view that the double discontinuities in Barkla's Fig. 3, p. 1041, is possibly due to  $D_X$  and  $D_Y$  being somewhat separated along  $x$ -direction.

## CASE II

*Relation between the mass-absorption coefficient and the fraction of the radiation absorbed, when the given incident beam is increasingly filtered*

Let  $Z$  denote the fraction of the radiation cut off by the filter and  $(\mu/\rho)_X$  the mass-absorption coefficient of the transmitted beam, as measured with the testing substance  $X$ . Then the average wavelength  $\lambda$  of the transmitted beam is a function of  $Z$ . We can therefore write :

$$x = \psi(Z) \text{ or } Z = f(x), \text{ say} \quad (18)$$

where  $x = \lambda^3$ , as before.

Since the wavelength emerging from the filter is the wavelength incident on the testing substance we also have from (11a) near the  $D$ -point :

$$y_X - (\mu/\rho)_X = A_X + B_X x (1 - 3K_X) \quad (19)$$

The required relation between  $(\mu/\rho)_X$  and  $Z$  will be obtained by eliminating  $x$  between equations (18) and (19). Although the exact form of the function  $f$  in (18) is not known, yet the conditions to be satisfied by it are quite definite and may be utilised in ascertaining the general run of the curve  $(Z-x)$  in (18). The conditions are :

- (i) As  $Z$  increases,  $x$  decreases.
- (ii) As  $Z$  increases,  $dx/dZ$  decreases and hence  $dZ/dx$  increases numerically.
- (iii) When  $Z = 0$ ,  $x = x_0$  (corresponding to the unfiltered radiation).
- (iv) When  $Z = 1$ ,  $x$  has a minimum value which is not zero.

These are illustrated in the above Fig. 3, where the curve  $O'PQ$  represents the equation  $Z = f(x)$ , and the curve  $RPS$  represents equation (3a). The  $Z$ -axis and  $y$ -axis are represented by the L.H.S. and R.H.S. vertical lines respectively. The points  $Q$  and  $P$ , on the curve  $O'PQ$  correspond to 100 per cent and 50 per cent reduction in intensity respectively. As the actual experiments under consideration (Barkla's Figs. 10 and 11) were performed with a radiation filtered till the intensity was cut off by 50%, i.e., till  $Z$  increased from zero to 0.5, they are necessarily confined to the region of the diagram (Fig. 3), lying on the R.H.S. of  $P$  only. The  $D$ -point described in Case I previously and assumed present, is also shown (encircled) on the curve  $RPS$  and lying somewhere between  $P$  and  $S$ . The abscissa  $x$  is drawn on a scale somewhat exaggerated.

It may be pointed out that so far as the  $J$ -discontinuity is concerned, an exact knowledge of the function  $f$  is not essential. In view of the smallness of the

part O'P( $\Delta\lambda = 0.1 \text{ \AA}$  approx), the function may be regarded as practically linear. We may assume that the curve O'PQ is concurrent with a small portion of a parabola with a large latus rectum.

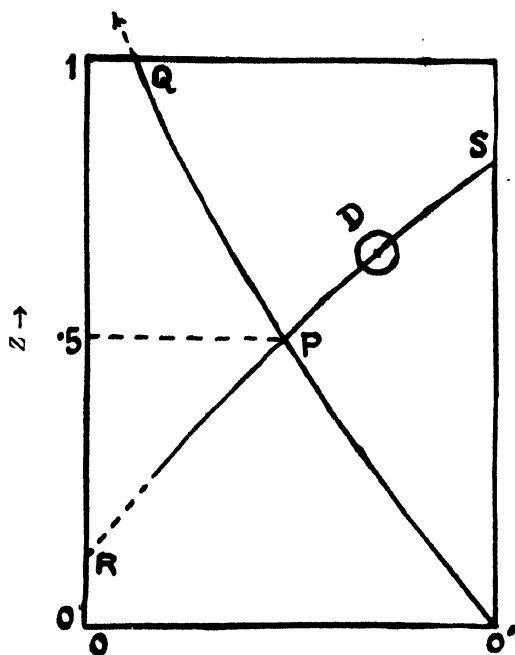


Fig. 3

Accordingly, for the curve O'PQ, we write

$$(a_1 - Z)^2 = b_1(x + \sigma) \quad (20)$$

where  $a_1$ ,  $b_1$  and  $\sigma$  are constants depending on the filtering material,  $b_1$  being the latus rectum. This equation will be found to satisfy all the conditions, enumerated above. Thus

when  $Z \rightarrow 1(\text{max})$ ,  $x$  is minimum in keeping with (iv), and assuming  $Z \ll a_1$ ,

$\frac{dZ}{dx}$  is negative in keeping with (i), since  $\frac{dZ}{dx} = -\frac{b_1}{2(a_1 - Z)}$ , also as  $Z$  increases,

$\frac{dZ}{dx}$  increases in magnitude, in keeping with (ii) and further, when  $Z = 0$ ,  $x = \text{max.}$

$= x_0$ , agreeing with (iii) so that from (20) we have,

$$a_1^2 = b_1(x_0 + \sigma) \quad \dots (21)$$

Therefore, from (20) and (21), the equation to the curve O'PQ satisfying all the required conditions (i), (ii), (iii) and (iv), may be written down also as :

$$\left( \frac{a_1 - Z}{a_1} \right)^2 = \frac{x + \sigma}{x_0 + \sigma}$$

$$\text{or} \quad \left(1 - \frac{Z}{a_1}\right)^2 = \frac{x + \sigma}{x_0 + \sigma}$$

$$\frac{2Z}{a_1} = \frac{x + \sigma}{x_0 + \sigma} \quad (\text{approximate})$$

$$\text{or} \quad Z = -\frac{a_1}{2} \cdot \frac{x - x_0}{x_0 + \sigma} = f(x) \quad \dots \quad (22)$$

The above is practically a linear relationship between  $Z$  and  $x$ . Hence the portion O'P of the curve is straight to the extent that the values of  $Z$  and  $a_1$  conform to the assumed condition.

Taking O'P to be approximately straight and considering the short segments of the curve PS on either sides of  $D$  (supposed present) close to it, as linear, we may now eliminate  $x$  between the equations (19) and (22) and obtain :

$$y_X = \{A_X + B_X x_0 (1 - 3K_X)\} - \left\{ \frac{2}{a_1} (x_0 + \sigma) B_X (1 - 3K_X) \right\} Z \quad \dots \quad (23)$$

The required relation between  $y_X$  and  $Z$  is thus linear. But as the values of the constant  $K_X$  are different for the two sides of 'D' (*vide* Case I), the straight line in (23) splits up into two different (non-collinear) straight lines represented by

$$(i) \quad y_X = \{A_X + B_X x_0 (1 - 3K'_X)\} - \left\{ \frac{2}{a_1} (x_0 + \sigma) B_X (1 - 3K'_X) \right\} Z$$

$$\text{and} \quad (ii) \quad y_X = \{A_X + B_X x_0 (1 - 3K''_X)\} - \left\{ \frac{2}{a_1} (x_0 + \sigma) B_X (1 - 3K''_X) \right\} Z \quad \dots \quad (24)$$

where  $K'_X$  belongs to the left hand side of 'D' and  $K''_X$  to the right hand side in Fig. 3, or in other words  $K'_X$  corresponds to the shorter wavelength side of 'D' (and hence to larger values of  $Z$ ) and  $K''_X$  to the longer wavelength side (and hence to smaller values of  $Z$ ).

Now,  $K_X (= e_X/\lambda)$  increases with  $\lambda$  for a filtered radiation, which is apparent from equation (7). Therefore,  $K''_X > K'_X$ . Hence the 'intercept' and the 'slope' of the straight line (i) are respectively greater than the corresponding quantities of the straight line (ii), the two straight lines being, of course, intervened by a discontinuity initiated by the  $D$ -point, exactly as in Case I. This is the  $J$ -discontinuity in Case II. The two straight lines agree in all essential features with those illustrated by Barkla in his Figs. 10 and 11, pp. 1047-1048.

It is evident that here also the  $J$ -discontinuity should be formed at the same critical penetrating power characteristic of the testing element, as in Case I and this corresponds to

$$x_j = \{-2b + \sqrt{4b^2 + 11ac}\}/22c$$

$$\approx \frac{a}{8b} \quad (\text{vide Eqns. 15 and 16})$$

This feature, viz. the constancy of the critical penetrating power had been verified in Barkla's experiments.

The above treatment is a general one, in as much as it does not take into consideration the actual material of the filter; i.e., whether the material of the filter is the same as or different from that of the testing substance for measuring the mass-absorption coefficient. Analysis reveals that if there is a *D*-point, there should appear a discontinuity. In Barkla's experiments, however, discontinuity occurred only when the materials of the filter and the testing substance were identical, i.e., when both were aluminium or both copper. But the discontinuity was missing when the filter was aluminium and the testing substance copper. This according to the present view, only means that the *D*-point was either absent in that case, or was situated close to P (or S) but outside the segment PS (Fig. 3). The linear relation between  $(\mu/\rho)_{Cu}$  and  $Z_{.47}$  (Fig. 10, Barkla), suggests that the latter alternative should hold.

#### VERIFICATIONS

The fact that the theory advanced here has yielded results in general accord with the experimental findings of Barkla, amply bears out the correctness of the various assumptions made previously in that connection. A further justification may be had from an actual examination of the experimental data furnished below.

With the help of Barkla's Fig. 10 (lower diagram) and Fig. 11, together with our equations (21 and 24), it is possible to make the following computations :

(a) For Aluminium-Aluminium pair,

$$K_1 - K'_X \approx 0.057, \quad b_1/a_1 \approx 32, \quad a_1 > 1.58, \quad b_1 = 50.5,$$

and since  $Z < 0.5, \quad Z^2/a_1^2 < 0.1.$

(b) For Copper-Copper pair,

$$K''_X - K'_X \approx 0.093, \quad b_1/a_1 \approx 17.7, \quad a_1 > 2.17, \quad b_1 > 38.5$$

and since  $Z < 0.5, \quad \frac{Z^2}{a_1^2} < 0.06$

#### *Absence of the J-discontinuity*

We shall now discuss the circumstances leading to the non-appearance or absence of the *J*-discontinuity. Evidently, where the 'discrepancy'  $e$  is either zero or very small, the *D*-point is absent or practically so. Hence a discontinuity is not to be expected there. This is so

- (i) with a beam of X-rays which is strictly monochromatic for which  $e = 0$ ,
- (ii) with a beam of heterogeneous X-rays which has been excessively filtered and consequently rendered more or less homogeneous, when  $e$  becomes insignificant and

- (iii) with a method of measurement where the absorption coefficient of the filtered heterogeneous beam is determined arbitrarily from insufficient absorption—say, 25% instead of 50% as usual—within the testing substance, thus making  $e$  too small.

Case (ii) here, was nicely illustrated by Dunbar's (1925) failures and (iii) by Barkla's Fig. 8 (lower diagram). In all these cases, the graph  $(y_X - y_Y)$  was found to be linear as expected from Equation (11).

There is a fourth case in which the discontinuity may not appear. If the  $D$ -points do not fall within the range of wavelengths studied, but are yet not far away, only one side of the  $D$ -points can be considered. In such a case we should expect a single continuous straight line for the  $(y_X - y_Y)$  graph, instead of two, intervened by the discontinuity. A fifth case for no discontinuity may arise if  $\alpha = \beta$  (*vide* equation 12 and 13) when the two straight lines should merge into one, even with the  $D$ -point present within the experimental range. (See Barkla's Fig. 4. for unfiltered radiation and the upper diagram of Fig. 10.).

Barkla and his collaborators had observed that the  $J$ -discontinuity sometimes occurred and sometimes did not occur under what appeared to be essentially identical conditions. This may be expected when the beam of X-rays concerned is in a state of unsteadiness. Irregular changes in the structure of the radiation may, at times, render the plotted points misleading and unreliable with a consequent obliteration of the  $J$ -step. (See Barkla's Fig. 2, p. 1040). Further it can be suggested that the 'discrepancy'-coefficients,  $a, b, c$  (in Equation 7) of an absorbing material may sometimes be affected by variations in some special factor or factors which have not been identified and controlled. The  $D$ -points may be sensitive to such variations, even when all other conditions are steady, appearing sometimes at the right places and sometimes moving beyond them. These considerations may explain, to some extent, the elusive nature of the  $J$ -discontinuity.

#### SUMMARY AND CONCLUSIONS

In the foregoing analysis of the  $J$ -phenomenon, we have accepted the hypothesis put forward by Barkla that a heterogeneous beam of X-rays behaves like an 'atmosphere' of radiation considered as an integrated whole for which its mass-absorption coefficient appears to be more fundamental than its individual wavelengths. It has been supposed that the mass-absorption coefficient of a heterogeneous beam of X-rays in an absorbing substance corresponds to some intermediate wavelength which the beam has somewhere inside the absorber. Since the softer constituents of the heterogeneous beam are increasingly filtered off as the beam passes through the absorber, this intermediate or the effective wavelength must needs be slightly less than the average wavelength. Expressing this 'discrepancy' between the effective wavelength and the average wavelength



as a suitable function of the latter, represented by (7), the *J*-discontinuity has been shown to be associated with the so-called *D*-point on the  $(\bar{\mu}/\rho - \lambda^3)$ -curve, where the rate of the variation of the slope is minimum (or zero as at a point of inflexion), the small segments of the curve lying on both sides of '*D*' and close to it, being regarded as straight lines. The position of the *J*-discontinuity, the critical mass-absorption coefficient for the discontinuity, the constancy of this critical value for a particular absorbing substance and its dependence on the material of the absorber and the magnitude of the *J*-step have been fully discussed in terms of the 'discrepancy' coefficients. Quantitative agreement has been shown in some cases between the results of the analysis and the experimental results of Barkla and his collaborators.

The absence of the *J*-discontinuity and the circumstances leading to it have been discussed in some details. Suggestions have also been made to explain the elusive nature of the *J*-discontinuity.

In conclusion, it is to be noted that Barkla's interpretation of the experimental results on the *J*-phenomenon in X-rays in terms of 'levels' of X-ray activity has not been considered in the present investigation. Barkla's fruitful idea that in the phenomena concerning a heterogeneous beam of X-rays, it is the average constitution of the beam that counts above every thing, is however recognised in the analysis detailed in this paper.

#### ACKNOWLEDGMENT

The author is indebted to late Prof. C. G. Barkla, F.R.S., N.L., for affording him all facilities for experimental researches in his laboratory at Edinburgh, U. K. and giving him helpful guidance during the period 1935-37. His best thanks are also due to Prof. S. R. Khastgir, Khaira Professor of Physics, University of Calcutta, for valuable discussions.

#### REFERENCES

- Alexander, 1930, *Proc. Phys. Soc.* **13**, 82.
- Backhurst, I., 1932, *Phil. Mag.* **13**, 28.
- Barkla, C. G., 1916, *Bakerian lecture*—*Phil. Trans.* 1917.
- „ 1923, *Nature*, **112**, Nov. 17, 723.
- „ 1924, *Nature* **22**.
- „ 1925, *Phil. Mag.* **49**, 1033.
- „ and White, 1917, *Phil. Mag.* **34**, 270.
- „ and Sale, 1923, *Phil. Mag.* **45**, 748.
- „ and Mackenzie, 1925, *Nature*, **115**, 942.
- „ and Khastgir, 1925, *Phil. Mag.* **49**, 251.
- „ and Khastgir, 1925, *Phil. Mag.* **50**, 1115.
- Compton, A. H., 1924, *Nature*, **113**, 160.
- Crowther, 1921, *Phil. Mag.* **42**, 719.
- Dauvillier, 1920, *Ann. d. Phys.* **13**, 49.

- (iii) with a method of measurement where the absorption coefficient of the filtered heterogeneous beam is determined arbitrarily from insufficient absorption—say, 25% instead of 50% as usual—within the testing substance, thus making  $e$  too small.

Case (ii) here, was nicely illustrated by Dunbar's (1925) failures and (iii) by Barkla's Fig. 8 (lower diagram). In all these cases, the graph  $(y_X - y_Y)$  was found to be linear as expected from Equation (11).

There is a fourth case in which the discontinuity may not appear. If the  $D$ -points do not fall within the range of wavelenths studied, but are yet not far away, only one side of the  $D$ -points can be considered. In such a case we should expect a single continuous straight line for the  $(y_X - y_Y)$  graph, instead of two, intervened by the discontinuity. A fifth case for no discontinuity may arise if  $\alpha = \beta$  (*vide* equation 12 and 13) when the two straight lines should merge into one, even with the  $D$ -point present within the experimental range. (See Barkla's Fig. 4. for unfiltered radiation and the upper diagram of Fig. 10.).

Barkla and his collaborators had observed that the  $J$ -discontinuity sometimes occurred and sometimes did not occur under what appeared to be essentially identical conditions. This may be expected when the beam of X-rays concerned is in a state of unsteadiness. Irregular changes in the structure of the radiation may, at times, render the plotted points misleading and unreliable with a consequent obliteration of the  $J$ -step. (See Barkla's Fig. 2, p. 1040). Further it can be suggested that the 'discrepancy'-coefficients,  $a, b, c$  (in Equation 7) of an absorbing material may sometimes be affected by variations in some special factor or factors which have not been identified and controlled. The  $D$ -points may be sensitive to such variations, even when all other conditions are steady, appearing sometimes at the right places and sometimes moving beyond them. These considerations may explain, to some extent, the elusive nature of the  $J$ -discontinuity.

#### SUMMARY AND CONCLUSIONS

In the foregoing analysis of the  $J$ -phenomenon, we have accepted the hypothesis put forward by Barkla that a heterogeneous beam of X-rays behaves like an 'atmosphere' of radiation considered as an integrated whole for which its mass-absorption coefficient appears to be more fundamental than its individual wavelengths. It has been supposed that the mass-absorption coefficient of a heterogeneous beam of X-rays in an absorbing substance corresponds to some intermediate wavelength which the beam has somewhere inside the absorber. Since the softer constituents of the heterogeneous beam are increasingly filtered off as the beam passes through the absorber, this intermediate or the effective wavelength must needs be slightly less than the average wavelength. Expressing this 'discrepancy' between the effective wavelength and the average wavelength

as a suitable function of the latter, represented by (7), the  $J$ -discontinuity has been shown to be associated with the so-called  $D$ -point on the  $(\bar{\mu}/\rho - \lambda^3)$ -curve, where the rate of the variation of the slope is minimum (or zero as at a point of inflexion), the small segments of the curve lying on both sides of ' $D$ ' and close to it, being regarded as straight lines. The position of the  $J$ -discontinuity, the critical mass-absorption coefficient for the discontinuity, the constancy of this critical value for a particular absorbing substance and its dependence on the material of the absorber and the magnitude of the  $J$ -step have been fully discussed in terms of the 'discrepancy' coefficients. Quantitative agreement has been shown in some cases between the results of the analysis and the experimental results of Barkla and his collaborators.

The absence of the  $J$ -discontinuity and the circumstances leading to it have been discussed in some details. Suggestions have also been made to explain the elusive nature of the  $J$ -discontinuity.

In conclusion, it is to be noted that Barkla's interpretation of the experimental results on the  $J$ -phenomenon in X-rays in terms of 'levels' of X-ray activity has not been considered in the present investigation. Barkla's fruitful idea that in the phenomena concerning a heterogeneous beam of X-rays, it is the average constitution of the beam that counts above every thing, is however recognised in the analysis detailed in this paper.

#### ACKNOWLEDGMENT

The author is indebted to late Prof. C. G. Barkla, F.R.S., N.L., for affording him all facilities for experimental researches in his laboratory at Edinburgh, U. K. and giving him helpful guidance during the period 1935-37. His best thanks are also due to Prof. S. R. Khastgir, Khaira Professor of Physics, University of Calcutta, for valuable discussions.

#### REFERENCES

- Alexander, 1930, *Proc. Phys. Soc.* **13**, 82.
- Backhurst, L., 1932, *Phil. Mag.* **13**, 28.
- Barkla, C. G., 1916, *Bakerian lecture—Phil. Trans.* 1917.
- „ 1923, *Nature*, **112**, Nov. 17, 723.
- „ 1924, *Nature* **22**.
- „ 1925, *Phil. Mag.* **49**, 1033.
- „ and White, 1917, *Phil. Mag.* **34**, 270.
- „ and Sale, 1923, *Phil. Mag.* **45**, 748.
- „ and Mackenzie, 1925, *Nature*, **115**, 942.
- „ and Khastgir, 1925, *Phil. Mag.* **49**, 251.
- „ and Khastgir, 1925, *Phil. Mag.* **50**, 1115.
- Compton, A. H., 1924, *Nature*, **113**, 160.
- Crowther, 1921, *Phil. Mag.* **42**, 719.
- Dauvillier, 1920, *Ann. d. Phys.* **13**, 49.

- Duane and Shimizu, 1919, *Phys. Rev.* **14**, 389.  
Dunbar, 1925, *Phil. Mag.* **49**, 210.  
„ 1928, *Phil. Mag.* V. 962.  
Gaertner, 1927, *Phys. Zeits.* **28**, 493.  
Khastgir and Watson, 1925, *Nature* **115**, 604.  
„ 1925, *Nature* **116**, 47.  
Nipper, 1925, *Nature*, **116**, 12.  
Owen, 1918, *Proc. Roy. Soc. A.* **94**, 339.  
Richtmyer, 1921, *Phys. Rev.* **17**, 434.  
„ 1921, *Phys. Rev.* **18**, 13.  
„ 1922, *Phys. Rev.* **19**, 418.  
„ and Grant 1920, *Phys. Rev.* **15**, 447.  
Siogbahn. 1925, *Nature*, **111**, 11.  
„ and Wmgardt, 1920, *Phys. Zeits.* **21**, 83.  
Watson. 1924-25, *Proc. Roy. Soc. of Edinburgh.* **45**, 48.  
Williams, 1918, *Proc. Roy. Soc.* **94**, 567.  
Worsnop, 1927, *Proc. Roy. Soc.* **39**, 305.

# EFFECT OF COMPLEX FORMATION ON THE INTENSITIES OF RAMAN LINES

N. RAJESWARA RAO AND K. V. RAMANAIAH

DEPARTMENT OF PHYSICS, OSMANIA UNIVERSITY, HYDERABAD

(Received, November 29, 1963)

**ABSTRACT.** On adding 5N ammonium nitrate to 13N nitric acid,  $\nu = 1300$  of nitric acid is found to decrease instead of increasing in intensity contrary to what is required by the law of mass action. To understand this, it is postulated that a complex like  $\text{HNO}_3\text{NO}_3$  is formed and it is surmised that when a complex is formed the bond stretching oscillation of a Raman line is decreased while it is known that the corresponding infra-red line decreases in intensity, during the formation of a complex.  $\nu = 1680$  of acetic acid also is found to behave in a similar way.

## INTRODUCTION

In recent years (Coggeshall, 1950 and Venkataramaiah and Puranik, 1962) it has been observed that the intensity of the line corresponding to any bond which is attached to another molecule due to hydrogen bond formation is increased. In fact, quantitative estimates of the intensities as related to the shift in the frequency of the bond due to hydrogen bond formation have been made. Now we report a few cases to say that the corresponding Raman line decreases in intensity.

*Nitric acid:* One of us (1943) reported many years back that when to a solution of bisulphate a sulphate is added,  $\nu = 1040 \text{ cm}^{-1}$  corresponding to the  $\text{HSO}_4$  ion decreases in intensity, contrary to the law of mass action, while addition of an acid brightens it as expected. Similar observation is made in a solution of nitric acid using  $\text{NH}_4\text{NO}_3$  and  $\text{HClO}_4$  as sources of  $\text{NO}_3$  and  $\text{H}$  ions.

TABLE I

	I(1050)	I(1300)
$\text{NH}_4\text{NO}_3$ (5N)	7.0	—
$\text{HNO}_3$ (13N)	3.6	6.2
$\text{HNO}_3$ (13N) + $\text{NH}_4\text{NO}_3$ (5N) }	5.8	5.2
$\text{HNO}_3$ (13N) + $\text{HClO}_4$ (5N) }	1.5	7.2

Table I shows that  $I(1300)$ , belonging to  $\text{HNO}_3$  molecules decreases in intensity from pure acid to nitrate mixture but brightens up in  $\text{HClO}_4$  mixture, similar to what is observed in the case of bisulphates. The microphotometric records demonstrate the effect clearly. (Fig. 1).

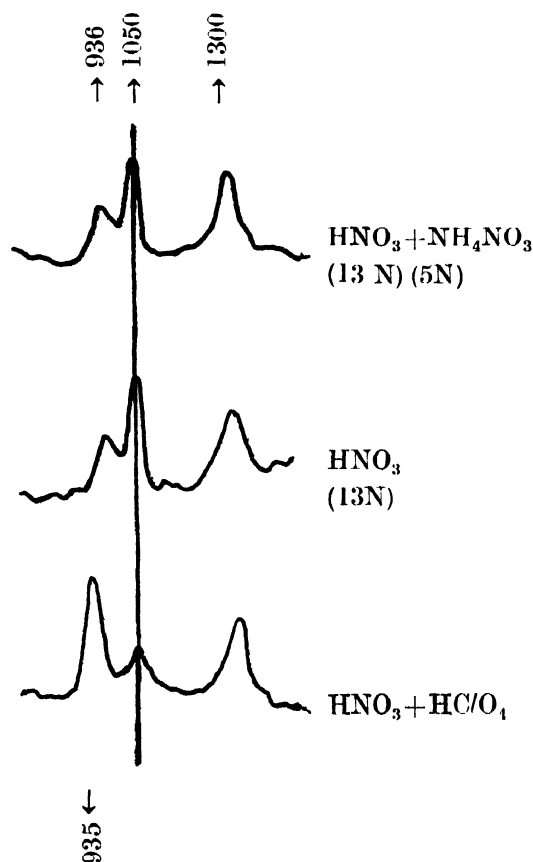


Fig. 1

In order to see whether the same result is reflected by the conductivity data, electrical conductivity of these mixtures is measured and the data given in

TABLE II

1	2	3	4	5	6	7	8	9	10
Temp °C	$\text{HNO}_3$	$\text{NH}_4\text{NO}_3$	Mixture	2+3 -4	5/2+3	$\text{HClO}_4$	Mixture	2/7-3	9/2+7
2	531.0	102.5	390.9	242.6	38.3%	355.6	377.8	508.8	57.4%
25	759.3	161.7	584.1	334.9	36.4%	515.2	554.5	720.0	56.5%
50	946.1	224.0	814.3	355.8	30.4%	642.1	692.9	895.3	56.4%

Conductivity in millimhos of nitric acid and its mixtures with ammonium nitrate and perchloric acid. Columns 6 and 10 show percentage decrease of conductivity in the mixtures.

Table II. Though, at these concentrations it is not possible to relate conductivity to the number of ions, qualitatively, it can be seen that nitrate ion also suppresses conductivity like the hydrogen ions, contrary to Raman effect data.

We are tempted to suggest formation of complex like  $\text{NO}_3\text{HNO}_3$  with a hydrogen bond between  $\text{NO}_3$  and  $\text{HNO}_3$ . This explains why  $\text{NO}_3$  helps suppression of conductivity to a large extent. The microphotometric records show that there is a line at  $d\nu = 936$  belonging to  $\text{HNO}_3$  molecules stronger in the nitrate mixture than in pure acid. This probably means that the decrease in the intensity of  $d\nu = 1300$  is not due to reduced number of  $\text{HNO}_3$  molecules but to the specific intensity (intensity per molecule) of the line decreasing due to hydrogen bond formation.

TABLE III

Solution	$d\nu = 446$	610	872	893	1270	1368	1680
Acetic acid pure	10	32	100	29	13	13	19
(2N) acid	15	32	100		15	20	52
Sodium acetate (2N)	13	17		100	37	70	0
acid and salt mixture 2N each	26	37	100	95	37	60	40

*Acetic acid* : A similar experiment is performed in mixtures of acetic acid and sodium acetate and the results given in Table III. The intensities are reduced to  $d\nu = 872$  taken as 100. It shifts to 893 in the spectra of salts. In the mixture, we see the two lines well separated. We want to point out to the large reduction in the intensity of  $d\nu = 1780$  attributed to  $C' = 0$  (Koteswaram, 1940) from 2N solution to pure acetic acid where dimers are known to form. Its reduction in the mixture is probably due to a complex like  $\text{H}_3\text{CCOOH} - \text{OCCC-CH}_3$  with hydrogen bond formation.

*Sulphuric acid* : 100% sulphuric acid contains about 18 moles per litre while water contains 54 moles. Yet, Raman spectrum of sulphuric acid does not show any OH band of detectable intensity, though water with 1/3 of the time given for the acid shows the band very well. It should be mentioned in this connection, however, that C. S. Venkateswaran (1938) reported a faint band at  $d\nu = 2794$  to 3172 for sulphuric acid. We are tempted to suggest that molecules in pure sulphuric acid are so intimately connected by hydrogen bonds that OH bond is very much reduced in intensity.

#### REFERENCES

- Coggeshall, N. D. 1950, *Jour. Chem. Phys.* **18**, 978.  
 Koteswaram, P. 1940, *Ind. Jour. Phys.* **14**, 353.  
 Rao, N. R. 1943, *Ind. Jour. Phys.* **17**, 5.  
 Venkataramaiah K. and Puranik, P. G. 1962, *Proc. Ind. Acad. Sci.*, **56**, 96.  
 Venkateswaran, C. S. 1938, *Proc. Ind. Acad. Sci.*, **7**, 13.

# A 19 CM DEBYE-SCHERRER CAMERA FOR WORKING BETWEEN 400°K AND 106°K

SIDDHARTHA RAY

DEPARTMENT OF MAGNETISM,  
INDIAN ASSOCIATION FOR THE CULTIVATION OF SCIENCE,  
CALCUTTA-32.

(Received February 1, 1964)

**ABSTRACT.** An adjustable temperature 19 cm Debye-Scherrer camera has been described, in which the specimen can be kept at any steady temperature from 106°K to 400°K, using liquid oxygen as refrigerant and with the help of a small heating element to counter-balance the cooling. Details of construction and performance have been described. The camera is designed for the main purpose of studying thermal expansion coefficients and phase transitions of various substances.

## INTRODUCTION

A scheme to investigate the thermal expansion of certain inorganic substances necessitated the construction of an X-ray camera, in which the powdered specimen may be kept at any steady temperature from about 90°K to about 400°K, for several hours at a stretch. Such a camera, using conduction cooling (and heating), has been designed and constructed in the workshop of this Association.

In the adjustable temperature X-ray cameras designed for work in low temperature regions, cooling of the specimen is achieved usually either by the flow of a cooled gas around the specimen, or by conduction. The latter method has been chosen for the present design, because of its easier and better adjustability, and possibility of attaining lower temperature, as well as due to the fact that in the present case of a camera using only powdered specimen, no great constructional complication arises. Also, it will be seen that the same accessories are used for attaining the moderately high range of temperatures necessary for the investigations envisaged.

## DESCRIPTION AND OPERATION OF THE CAMERA

The camera may be conveniently described under the two following heads : (1) the film-cylinder and collimator, and (2) the specimen-cooling system, and may be clearly understood with reference to fig. 1.

(1) The film-cylinder (A) is of a strictly uniform outside diameter of 19 cm., with cylindrical slots running almost all round the middle except two diametrically opposite parts, where the collimator (B) and the exit port (C) for the



direct X-ray beam are situated. Two strips of film are wrapped outside the cylinder over the slot, as is usual in standard cameras of similar diameter. The slots, along which the films are to be exposed, end in sharp edges, so that the

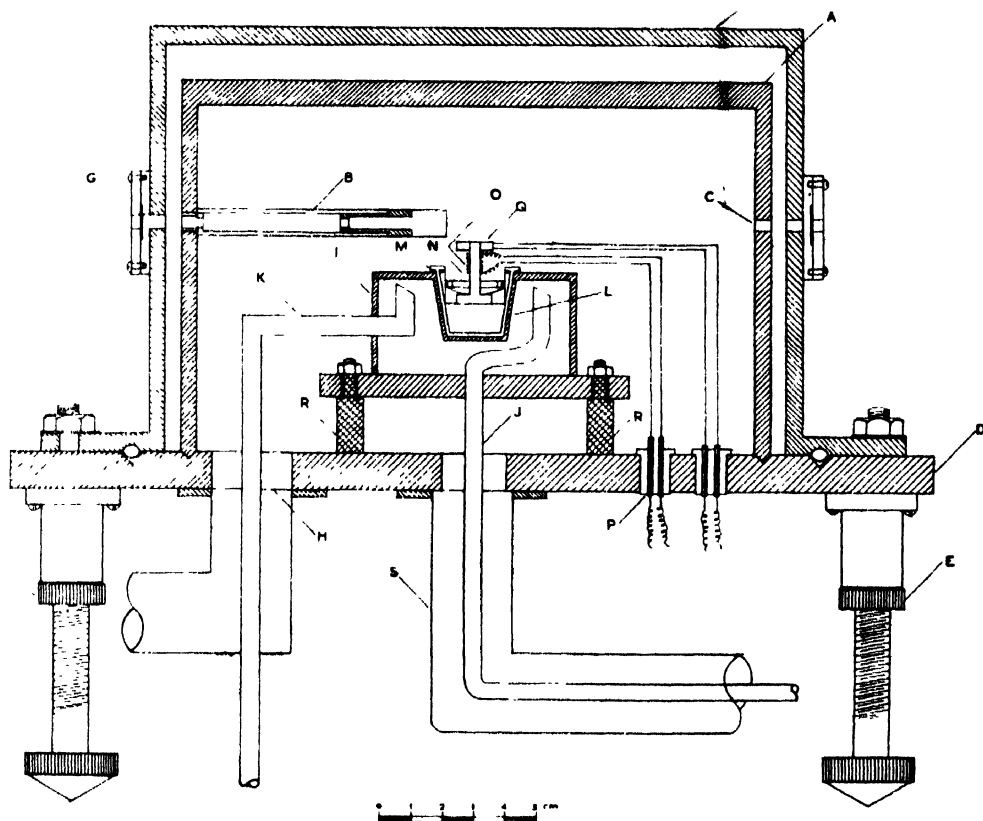


Fig. 1. The 19 cm adjustable temperature Debye-Scherrer camera.

- |                               |                                   |
|-------------------------------|-----------------------------------|
| A —film-cylinder              | K —liquid oxygen outlet tube      |
| B —collimator                 | L —copper cup                     |
| C —exit port for direct beam. | M —copper cone                    |
| D —base-plate                 | N —specimen-holder                |
| E —levelling screws           | O —heater                         |
| F —air-tight cover            | P —sealed exit for leads          |
| G —aluminium foil window      | Q —thermocouple                   |
| H —aperture for evacuation    | R —ebonite pillars                |
| I —liquid oxygen receptacle   | S —stainless-steel vacuum jacket. |
| J —liquid oxygen inlet tube   |                                   |

exposed parts on the films end in sharp lines, necessary for avoiding film-shrinkage error. Black paper pasted inside the cylinder along the slots and removable phosphor-bronze cover strips with black felt edges outside the cylinder make it a light-tight film carrier. The lower rim of the film-cylinder is chamferred to fit snugly into a circular V-groove on the Duralmin base-plate (D), so that it can be replaced in an identical position on the base plate, every time it is lifted and

removed to a darkroom for loading or developing the film. The base-plate is supported on three levelling screws (E).

The collimator (B) is attached to the film-cylinder. It projects wholly inside the cylinder, its axis coinciding with the diameter of the latter, and ends in a taper, so as not to obstruct diffracted rays from reaching the part of the film extending over the entire slotted region. The construction of the collimator is more or less the same as that described by Bradley, Lipson and Petch (1941), the two rectangular slits in this case being  $1/16''$  and  $1/32''$  in width.

An air-tight cylindrical brass cover (F), with a flange at the lower rim sealed with an O-ring in a groove on the base-plate, encloses the whole arrangement. The cover is furnished with aluminium foil windows (G) for entrance and exit of X-rays (a lead shutter is provided outside the exit window). The enclosure can be evacuated by a vacuum pump connected to an aperture (H) in the base-plate.

(2) The specimen-cooling arrangement consists of a cylindrical copper receptacle (I) for liquid oxygen. Two tubes (J, K) pass into the receptacle, sealed through the base-plate and running through a high vacuum line for sucking liquid oxygen in and the vapour out respectively. The upper cover of the receptacle has a conical cup (L) of copper attached to it in such a way that the cup projects wholly inside the receptacle. A solid copper cone (M) fits rather closely in the cup, and can be rotated smoothly. The specimen-holder (N) is a copper button fitted into a groove in the cone, with a spring and nut arrangement so that small displacements in all horizontal directions can be given to it. The pressure of the spring holds the button in the displaced position, the lower surface of the same being all the time pressed against the upper surface of the cone. This arrangement permits centering of the specimen mounted at the top of the specimen-holder, as well as ensures thermal conduction between the specimen and the liquid oxygen inside the receptacle.

On the stem of the copper button are wound a few turns of thin Nichrome wire, insulated by thin sheet of mica and Araldite. This serves as a heater element (O), and while the liquid oxygen in the receptacle tends to lower the temperature of the specimen, depending upon the rate of suction of the liquid and the small heat leakage from outside, different steady intermediate temperatures can be obtained by adjusting the current through this heater element. The hollow space inside the receptacle is filled with wire gauze for proper evaporation of oxygen and distribution of cold.

With no liquid oxygen in the receptacle, the heater is capable of maintaining different steady high temperatures of the specimen up to about  $400^{\circ}\text{K}$ . The connecting leads from the heater are kept free during centering of the specimen, so that the rotation of the cone is not obstructed, and are afterwards connected to the terminals provided at the camera base (P), and passing through polystyrene plugs sealed leak-tight to the base with Araldite. For measurement of tempera-

ture, a ring-shaped junction of a calibrated copper-constantan thermocouple (Q) is slipped on the stem of the specimen holder, just below the specimen, after centering has been secured. The e.m.f. of the couple is read off on a calibrated 6" dial millivoltmeter, each small division of which corresponds to about 2°K in the medium and high temperature ranges.

The liquid oxygen receptacle is mounted on three ebonite pillars (R) on the base-plate with suitable nuts and bolts. During this mounting, the rotation axis of the copper cone was made to coincide with the axis of the film-cylinder. This was checked optically, and once this arrangement was reliably ensured, centering of specimens reduced to the easy task of making them coincide with the axis of rotation of the copper cone.

The liquid oxygen inlet tube (J) is connected to the bottom centre of the receptacle. Inside the chamber, it reaches almost up to the upper cover. The exit tube (K) is attached to the side of the receptacle, and also reaches the same height inside. A stainless-steel jacket (S), in which vacuum is maintained along with that in the camera enclosure during operation, surrounds the whole length of the inlet tube from the camera-base to the liquid oxygen reservoir.

The liquid oxygen reservoir (not shown in the diagram) consists of a cylindrical container of German silver, placed in a 4-pint thermoflask with cotton linings. The container has four openings at the top. Through one of these, the vacuum-jacketted inlet tube enters the reservoir. The jacket fits closely at the entrance, and the inner tube reaches nearly the bottom of the container. A second opening is sealed with a graduated glass tube, closed at the top. The long, thin stem of a hollow glass float projects inside this tube, its position indicating the level of liquid oxygen in the reservoir. The third opening is used for pouring liquid oxygen in the container and is kept closed with a tight fitting cork during operation. The fourth opening connects the upper space over liquid oxygen level of the container to the atmosphere through a series of calcium chloride towers, so that when liquid oxygen is sucked out, only dry air can enter the reservoir.

A suction pump is connected to the free end of the exit tube outside the camera. With the specimen centered, the thermocouple ring placed in position, the connections to the heater secured, and the loaded film-cylinder replaced, the camera chamber is evacuated, and the suction pump started. The rate of suction is controlled by adjusting an air-leak in the pumping system. Liquid oxygen from the reservoir travels through the vacuum-jacketted tube towards the receptacle, and after the initial cooling off, tends to maintain a steady temperature which depends on the rate of heat leakage by radiation, and is finally balanced nicely by adjusting the heater current from a large 6 volt accumulator. Increasing the rate of flow of liquid oxygen and diminishing the heater current, successively lower temperatures are attained. For reaching the lowest tempera-

ture the heater is altogether cut out and oxygen allowed to accumulate in the receptacle. Owing to rather large radiation leakage and temperature gradient from the receptacle to the specimen, the lowest temperature reached was about 106°K.

During the many trial operations it has been found that the different temperatures of the specimen can be maintained satisfactorily steady for several hours over which an X-ray exposure is given, the maximum fluctuation never exceeding, and generally being less than .5°K. Five litres of liquid oxygen are found to be sufficient for 7 hours exposure of a specimen maintained at 106°K (not taking account of the period necessary to bring down the temperature of the specimen initially).

#### A C K N O W L E D G M E N T

The author expresses his deep sense of gratitude towards Prof. A. Bose, D.Sc., F.N.I., for his kind interest and encouraging guidance throughout the course of the work. His sincerest thanks are also due to Mr. A. K. Sarkar, Superintendent of the Association's Workshop, who with his team of excellent mechanics, carried out the actual constructions with all possible care.

#### R E F E R E N C E

Bradley, A. J., Lipson, H., and Petch, N. J., 1941, *J. Sci. Instrum.*, **18**, 216.

## ON HEAT TRANSFER IN NUCLEATE BOILING (I)

S. P. BASU

DEPARTMENT OF APPLIED PHYSICS, CALCUTTA UNIVERSITY,  
CALCUTTA*(Received February 25, 1964)*

**ABSTRACT.** Representative data of heat transfer coefficient for di-ethyl ether (B.P. 34.5°C) boiling on submerged horizontal tubes of copper, nickel and an alloy of Cu, Ni and Zinc, 3/16" in external diameter heated by enclosed electrical heaters have been obtained for a flux range upto 55000 Btu/hr. sq.ft. Data were obtained both for the commercial variety and purified liquid. The purity of the liquid is specified by data taken on electrical conductivity. To reduce the hysteresis effect, the liquid was stirred by a magnetic stirrer. The rotor speed was maintained at 650 r.p.m. and was determined by a stroboscope. After continued boiling the boiling curves showed to be almost straight lines for the heat flux range from 10,000 to 55,000 Btu/hr. sq.ft. The coefficient was found to be greater for the impure liquid than for the purified liquid at each heat flux.

## INTRODUCTION

Heat transfer between a submerged solid surface and a liquid boiling on it has been the subject of study of many investigators during recent years. A stimulating account of the art of boiling and the advancement towards the understanding of the boiling phenomena has been given by Drew and Mueller (1937), and J. W. Westwater (1956). Most of the boiling curves published show some hysteresis effect in the steady nucleate region and a very pronounced hysteresis effect at the threshold of nucleate boiling (Sinha, 1955). Regarding the effect of agitation on nucleate boiling Austin (1902) showed that stirring produced some increase in the heat transfer coefficient at moderate heat flux. Drew and Mueller (1937) confirmed Austin. Feeble agitation, on the other hand, has the advantage of decreasing the hysteresis effect without affecting the heat transfer coefficient at higher heat flux when the agitation produced by the columns of rising vapour bubbles is quite high. While reporting on heat transfer coefficient very little has been said by any worker about the purity of the liquid samples tried, though much has been said about the conditions of the heater surfaces. A point of interest in the problem should be to investigate how the purity condition of the liquid behaves in heat transfer and this is reported in the present work.

## EXPERIMENTAL APPARATUS

(1) *Construction of the heater*

Very thin walled (.004"), 3/16" diameter metal tubes were taken. Approximate lengths of the tubes were 7 cms. Glass insulated nicrome wires of gauge

No. 30 (dia. 0.026 cm) were placed within the tubes and were electrically heated. The technique employed for sealing the ends of the heater tube is shown in the schematic diagram shown in Fig. (1).

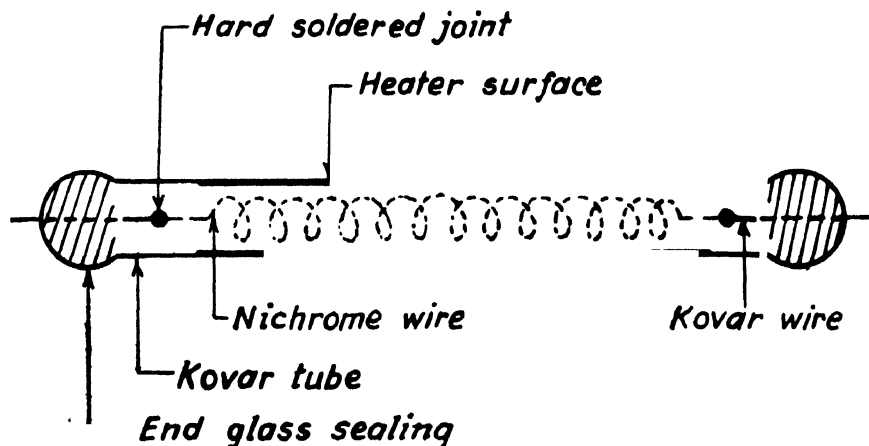


Fig. 1. Constructional details of the heaters.

The nichrome wire is hard soldered to a 'Kovar' wire. The 'Kovar' wire passes through a 'Kovar' tube of slightly smaller diameter than that of the heater tube. The 'Kovar' tube is soft soldered to the heater tube. Finally, the end is sealed with glass. The 'Kovar' wires serve as lead-in wires.

## (2) *Purification of the liquid :*

The chief impurities in commercial ether (Sp. gr. 0.72) are water, ethyl alcohol, traces of aldehyde, and in samples which have been exposed to the air and light for sometime or has been stored for a long time, ethyl peroxide. The ether was taken in a big separating funnel and was shaken vigorously with a saturated solution of ferrous sulphate. The ether was drained off and sufficient quantity of anhydrous calcium chloride was added to it. The mixture was allowed to stand for 24 hours with occasional shaking. Both the water and alcohol present were thus largely absorbed. The sample was then distilled doubly over phosphorus pentoxide. Sodium wires were inserted in the distilled ether to remove the last traces of moisture. Before use this ether was filtered. The purity of the sample was tested by experimentally studying its electrical conductivity.

## (3) *Stirring :*

The liquid was taken in a dewar and was stirred with the help of a magnetic stirrer. The method of magnetic stirring was adopted because it offered least contamination and also offered no path for heat leakage. For convenience of steady operation the conventional permanent magnet type of stirrer was modified to an electromagnet type of stirrer. The stirring element was a glass bead, cylindrical in shape, of length 2.8 cm and diameter 0.8 cm., in which was

embedded a magnetic core. The r.p.m. of the stirrer could be regulated by the simultaneous control of the speed and strength of the magnetic field. The r.p.m. was measured by a stroboscope (ORION-EMG, Type 2371/B)

#### (4) *Measurements*

Wedge shaped contact electrodes made of the same metals as those of the heater tubes placed at a fixed distance apart on an ebonite former were used to measure the p.d. between the contact points for a constant current sent through the tube material supplied from a battery which was continuously kept at constant e.m.f. by a battery charger. The resistance of the tube material was obtained by comparison with a standard low resistance. The temperature of the tube surface at each heat flux was evaluated from the resistance so determined (Sinha, 1955). The liquid temperature (bulk) was measured by 3 welded type single junction thermo-couples (copper-constantan). The p.d.'s were measured by a standardised Diesselhorst thermoelectric free potentiometer capable of reading upto 0.1  $\mu$ v. The actual measurements were taken down to 1 $\mu$ v.

#### *Experimental procedure*

The tube surfaces were very thoroughly cleansed by successive washing with acetone, benzene, carbon tetrachloride and finally with ether. Care was taken to avoid any contamination from grease. The liquid was charged into the dewar. The measuring current was then set in and the whole assembly was allowed to stand for sometime before the heating current was switched on. The heating current was increased in steps of 0.2 amp. and the corresponding p.d. between the electrodes were noted. After reaching a suitable maximum value the heating current was decreased in steps of 0.2 amp to test for hysteresis effect. The bulk liquid temperature was also measured in each step by means of three thermocouples inserted into the liquid at different depths. Between successive runs, the whole system was allowed to stand idle for about one hour. Several such runs were taken for each tube to test for reproducibility of results. Before performing a run the standardisation of the potentiometer was checked up each time.

### R E S U L T S

Experiments were performed with three copper tubes, two tubes of an alloy of Cu-nickel Zinc (5.88% Cu, 16.48% Ni and 77.50% Zinc) and one tube of Nickel supplied by Messrs. Johnson Matthey and Co. Ltd., London. Commercial ether (labelled, solvent) and the same after purification were used. Five runs were performed for each heater-liquid combination.

The values of  $\Delta t$  (temp. difference between the heater surface and bulk liquid) and  $h$  (heat transfer coefficient) as obtained in the present work for the different heaters, at a fixed heat flux viz. 45,000 Btu/hr.sq.ft. is shown in the

table below. The Graphs in Fig. Nos. 2, 3, 4 show the variation of heat flux with  $\Delta t$  and  $h$  vs  $\Delta t$  in the range of heat flux from 10,000 to 55,000 Btu/hr. sq.ft.

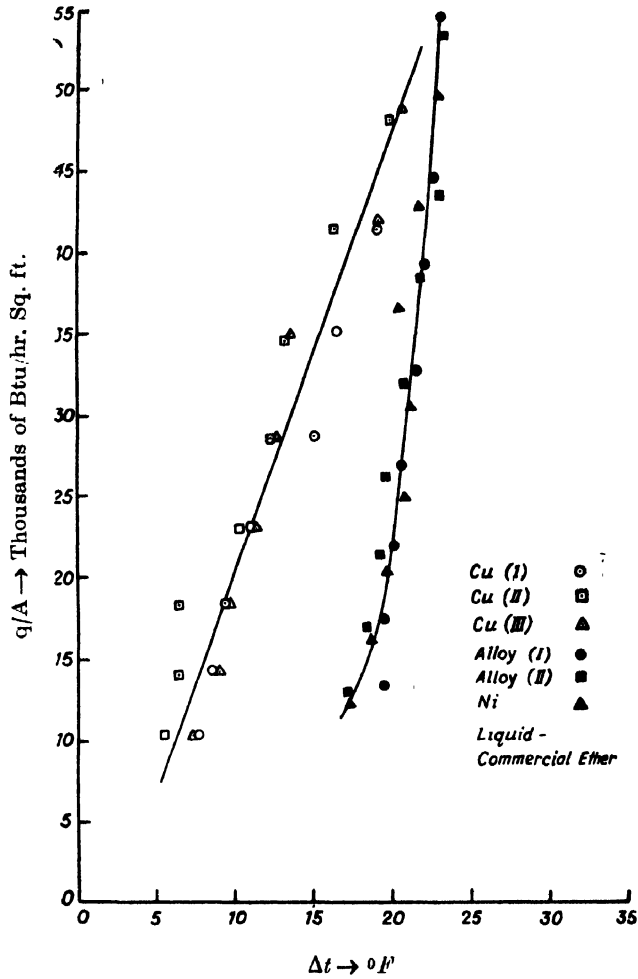


Fig. 2.  $q/A$  vs.  $\Delta t$  curves for commercial ether

TABLE I

Liquid :	Heater material	Heat flux Btu/hr. sq.ft.	$\Delta t$ °F	$h$ . Btu/hr. sq.ft.
Ether (Ordinary)	(i) Cu.	45,000	19	2365
	(ii) Cu-Ni-Zn. alloy and Nickel	„	22	2045
Ether (Purified)	(i) Cu.	„	21.25	2120
	(ii) Cu-Ni-Zn. alloy and Nickel	„	24.75	1820



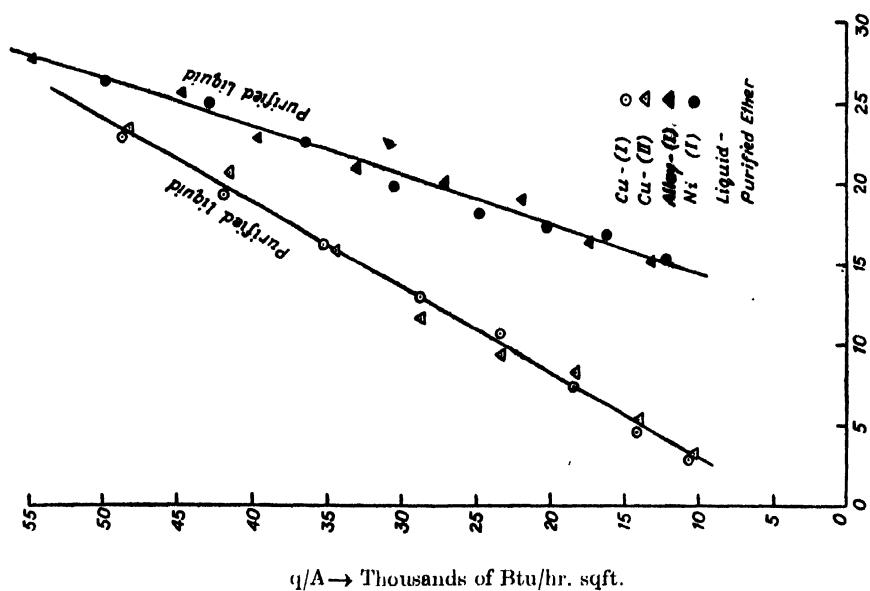


Fig. 3.  $q/A$  vs.  $\Delta t$  curves for pure ether.

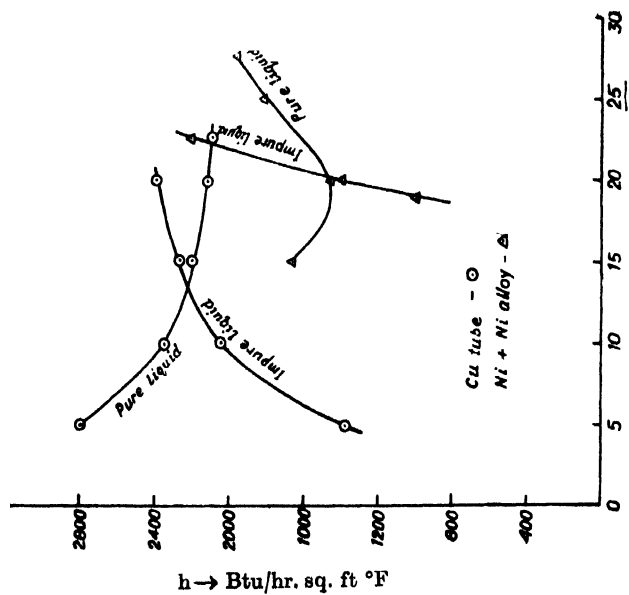


Fig. 4.  $h$  vs  $\Delta t$  curves.

## CONCLUSION

- (1) The variation of slopes in  $q/A$  vs  $\Delta t$  curves between the ordinary liquid and the liquid, when purified, is not much significant.
- (2) For the same tube and the same heat flux, the heat transfer coefficient decreased from impure to pure liquid.
- (3) The  $h \sim \Delta t$  curves did not follow similar patterns.

## ACKNOWLEDGMENT

The author is indebted to Dr. S. K. Sen of the Institute of Radio-Physics and Electronics for help in connection with the scaling of tubes. The work was carried out under the supervision of Dr. D. B. Sinha of the Department of Applied Physics, Calcutta University.

## REFERENCES

- Austin L., 1903, *Mitt. Forsch.* **7**, 75.
- Drew, T. B., and Mueller, A. C., 1937, *Trans. Am. Inst. Chem. Engrs.* **33**, 449.
- Westwater, J. W., Boiling of liquids, *Advances in Chemical Engineering*, 1956, Vol. 1, Academic Press, N. Y.
- Sinha, D. B., Ph. D. Thesis 1955, Department of Chemical Engineering, Imperial College of Science and Technology, London S.W.-7.

# EXCESS THERMODYNAMIC FUNCTIONS OF BINARY MIXTURE: SYSTEMS FLUOROBENZINE+TOLUENE

S. N. BHATTACHARYYA AND ASOK K. MUKHERJEE

INDIAN ASSOCIATION FOR THE CULTIVATION OF SCIENCE, JADAVPUR,  
CALCUTTA-32, INDIA

(Received February 10, 1964)

**ABSTRACT.** The excess enthalpy and the excess volume of mixing for the binary system Toluene+Fluorobenzene at 25°C. have been experimentally determined with the microcalorimeter and the pycnometer respectively. The results have been examined in the light of Bulescu's method and our modified approach reported earlier (Anantaraman *et. al.* 1961, 1962, 1963). An interesting feature of the present system is that the values of  $h^E$  and  $v^E$  are of opposite sign.

## INTRODUCTION

In continuation of our study on the accurate measurements of the thermodynamic excess functions of binary liquid mixtures, one component of which is slightly dipolar, and their interpretations in the light of the recent theories on the weak dipolar orientation, (Anantaraman, *et. al.* 1961, 1962, 1963) we report here the results of the study on the fluorobenzene-toluene system. Values of the excess enthalpy and the excess volume of mixing at 25°C are given and the results are analysed by our modified theoretical approach.

## EXPERIMENTAL

Experimental procedures adopted for the measurement of the excess enthalpy and the excess volume change were almost the same as described earlier except that the heating unit in the thermostat of the excess enthalpy measuring gadget was replaced by a freon gas operated cooling unit.

### *Purification of the Sample*

Fluorobenzene was prepared in this laboratory from the decomposition of stable salt benzene diazonium fluoborate by the method of Balz and Schiemann (1943). The distillate was separated from any phenol that had settled out. It was washed with 10% sodium hydroxide solution until the washings were almost colourless and then once with water. It was dried by shaking with crushed calcium chloride and then distilled in an all glass assembly. The middle fraction collected was further dried and distilled over a 40 plate fractionating column.

The purification of toluene was done in the same way as stated earlier (Anantaraman, *et. al.* 1963). Comparison of the densities of toluene and fluoro-

benzene measured in our laboratory with those from other standard works has been made in Table I.

TABLE I  
Densities of Pure Substances

Substance	Density, g/cm <sup>3</sup> (This work at 25°C)	Density, g/cm <sup>3</sup> (other determinations)	Ref.
Toluene	0.86271	0.86250	J. Timmermans, Physico-Chemical Constants of Pure Organic Compounds (Elsevier Publishing Co., 1950)
Fluorobenzene	1.0191	1.01919	

### RESULTS AND DISCUSSION

The excess heat and volume change of mixing were determined at 25°C to enable us to compare the experimental results directly with the theoretical predictions without taking recourse to any interpretations. In the present work certain drawbacks of earlier works in this respect have been avoided. The excess heat against the mole fraction shows a minimum of 55.0 J/mole occurring near  $x_A$  (mole-fraction of toluene) = 0.5

On the other hand, similar plot for excess volume shows a maximum of 0.035 C.C. near  $x_A = 0.35$ .

The excess heat can be best represented by the equation

$$\frac{h^E}{x_A x_B} = -220.4 - 7.75(x_A - x_B) + 28.5(x_A - x_B)^2 \text{ J/mole} \quad (I)$$

Although the plot of excess volume shows a pronounced asymmetric behaviour where the maximum has been shifted far towards the polar end of the scale, too much importance should not be given to the exact shape of this curve. This is due to the fact that excess volume is itself very small and consequently the error

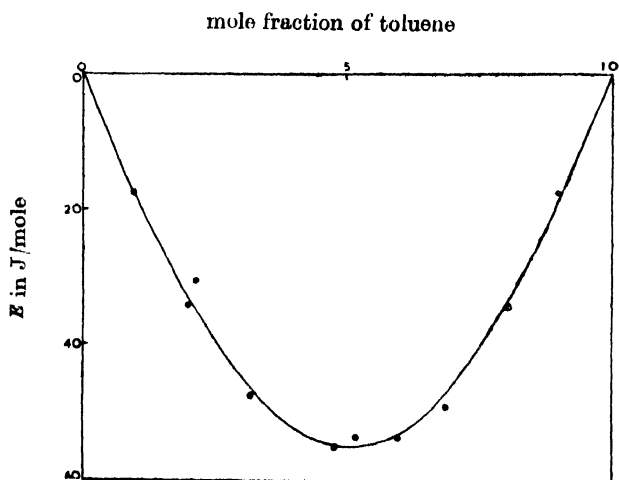


Fig. 1. Heats of mixing system : Toluene : Fluorobenzene—Temp. 25°C.

may be very large, particularly, at the both ends of the mole fraction scale. Due to this reason no empirical equation has been given for  $v^E$ . We satisfy ourselves with the value of  $v^E$  at  $x_A = 0.5$ . Table II and Table III give respectively the values of  $h^E$  and  $v^E$  measured at 25°C while figure 1 graphically represents the  $h^E$  data.

TABLE II

Heat of mixing

System : Toluene + Fluorobenzene

Temp.  $X_A$  = molefraction of toluene in the mixture, in J/mole

25°C

$X_A$	.0944	.1994	.2142	.3175	.4801	.5163	.5997	.6877
$h^E$	-17.6	-34.2	-30.0	-47.7	-55.1	-53.5	-53.5	-49.0
$X_A$					0.8038	0.9031		
$h^E$					-34.5	-17.6		

TABLE III

Volume change of mixing

System : Toluene + Fluorobenzene

Temp.

25°C

$x_A$  = mole fraction of toluene in the mixture ; in gm/mole.

$x_A$	0.0365	0.118	0.2748	0.3902	0.4887	0.6496	0.8619
$v^E$	+0.012	+0.011	+0.024	+0.027	+0.028	+0.020	+0.012
$x_A$	0.1819	0.3519	0.4696	0.5211			
$v^E$	+0.023	+0.031	+0.027	+0.030			

For a theoretical analysis we follow Anantaraman, Bhattacharyya and Palit, (1961) and treat the system as a mixture of polarizable dipolar and polarizable nonpolar molecules where each excess function consists of three terms such as

$$h^E = h_o^E + h_p^E(\text{pure dipolar}) + h_p^E(\text{polarizability}) \quad \dots (2)$$

The first term of the R. H. S. of (2) is the contribution of central forces and the remaining two terms are due to orientational forces of dipolar origin. The contribution due to polarizability can be neglected and we are left with the first two terms only. If one assumes, for unlike molecules, the combination of "Lorentz —Berthelot" type, one gets the Balescu's (1955) expressions for the excess functions of pure dipolar origin. The corresponding expressions for the central forces should then be taken from equation (10.7.5) of Prigogine (1957). On the other hand, if there is a deviation from the above mentioned combination rule we shall use Anantaraman, Bhattacharyya and Palit's equations (24 and 25) for pure dipolar contributions and use corresponding expressions from central forces from Prigogine taking account of this deviation. Table IV gives the critical constants of pure substance.

TABLE IV  
Critical constants of pure substance

Substance	$t_c$ °C	pc atmos.	$v_c$ cm <sup>3</sup> /mole
Toluene	320.6 <sup>9</sup>	41.6 <sup>9</sup>	304.9
Fluoro benzene	286.5 <sup>1</sup>	44.62 <sup>1</sup>	268.9

We have preferred to calculate  $\delta$  and  $\rho$  from critical constants of the pure components assuming that they obey the theorem of corresponding states. Only reliable value of  $t_c$  and  $p_c$  can be obtained for fluorobenzene and  $v_c$  of this component has been calculated from the empirical equation.

$$p_c = \frac{20.8T_c}{(V_c - 8)} \quad \dots (3)$$

where  $p_c$  is in atmosphere,  $T_c$  is absolute temperature and  $V_c$  indicates the critical molar volume. To maintain the uniformity and to reduce the errors same procedure has been adopted to obtain  $V_c$  of toluene. Table V illustrates the close agreement of  $\delta$  and  $\rho$  calculated from critical constants by two different methods, i. e.

$$1 + \delta = T_c^B / T_c^A \quad \dots (4)$$

$$= p_c^B V_c^B / p_c^A v_c^A \quad \dots (5)$$

and  $(1 + \rho)^3 = v_c^B / v_c^A \quad \dots (6)$

$$= p_c^A \cdot T_c^B / p_c^B T_c^A \quad \dots (7)$$

where  $A$  is the reference component in terms of which  $\rho$  and  $\delta$  have been expressed.

TABLE V  
Values of  $\delta$  and  $\rho$  calculated from two different equations

Reference Substance	1 + $\delta$			1 + $\rho$		
	from (4)	from (5)	mean	from (6)	from (7)	mean
Toluene	0.9426	0.9459	0.9443	0.9603	0.9596	0.9600
Fluorobenzene	1.0608	1.0572	1.0590	1.0413	1.0421	1.0417

The value of the dipolar perturbation  $\Gamma$  and all the configurational properties of the pure components at 25°C are taken from Anantaraman *et al.* (1963).

We first calculate the excess functions assuming that the "Lorentz-Brthelot" combination rule (i.e.  $\theta = \delta^2/8$ ) is obeyed. For an equimolecular mixture with  $\delta = 0.0577$  and  $\rho = -0.040$ , one obtains at 25°C.

$$h^E_o \text{ (Toluene as reference)} = 49.4 \text{ cal mole}^{-1},$$

$$\bar{h}^E_o \text{ (Fluorobenzene as reference)} = 50.2 \text{ cal mole}^{-1}$$

$$\bar{h}^E_o \text{ (average)} = 49.8 \text{ cal mole}^{-1}; h^E_p = 68.8 \text{ cal mole}^{-1}$$

$$h^E = +118 \text{ cal mole}^{-1}$$

$$v_0^E \text{ (Toluene as reference)} = 0.253 \text{ cm}^3 \text{ mole}^{-1}$$

$$v_0^E \text{ (fluorobenzene as reference)} = 0.251 \text{ cm}^3 \text{ mole}^{-1}$$

$$\bar{v}_0^E \text{ (average)} = 0.252 \text{ cm}^3 \text{ mole}^{-1}$$

$$v_p^E = 0.187 \text{ cm}^3 \text{ mole}^{-1}; \quad v^E = 0.439 \text{ cm}^3 \text{ mole}^{-1}$$

While the experimental values for an equimolar mixture at 25°C are :

$$h^E = -13.1 \text{ cal mole}^{-1}; \quad v^E = 0.03 \text{ cm}^3 \text{ mole}^{-1}.$$

The calculated results are thus not in agreement with experimental data ; even the sign of  $h^E$  has not been correctly predicted.

Next we assume deviation from "Lorentz-Berthelot" approximation and proceed with the Anantaraman *et al*'s treatment. We adjust  $\theta$  to fit  $h^E$  the excess function believed to be most accurately obtained experimentally. The excess volume  $v^E$  is then predicted using the value of  $\theta$  obtained in this way. One could, in principle, retain both  $\epsilon_{AB}$ , (i.e  $\theta$ ) for  $r_{AB}^0$  in the expressions of excess functions and then adjust them to obtain the best possible fit. But such a procedure would hardly be worth while here as the data available for this system would not be sufficient to compare these parameters for consistency.

Proceeding as mentioned we obtained  $\theta = +0.0207$  when toluene is taken as the reference substance, the value of  $\delta$  and  $\rho$  remaining unchanged as before. For an equimolar mixture at 25°C the calculated excess functions are :

$$h_0^E \text{ (toluene as reference)} = -85.8 \text{ cal mole}^{-1}$$

$$h_0^E \text{ (fluorobenzene as reference)} = -84.0 \text{ cal mole}^{-1}$$

$$\bar{h}_0^E \text{ (average)} = -84.9 \text{ cal mole}^{-1}$$

$$h_p^E = 71.8 \text{ cal mole}^{-1}$$

$$h^E = -13.1 \text{ cal mole}^{-1}$$

and  $v_0^E \text{ (toluene as reference)} = -0.107 \text{ cm}^3 \text{ mole}^{-1}$

$$v_0^E \text{ (fluorobenzene as reference)} = -0.104 \text{ cm}^3 \text{ mole}^{-1}$$

$$\bar{v}_0^E \text{ (average)} = 0.106 \text{ cm}^3 \text{ mole}^{-1}$$

$$v_p^E = 0.198 \text{ cm}^3 \text{ mole}^{-1}$$

$$v^E = 0.094 \text{ cm}^3 \text{ mole}^{-1}$$

We find that the predicted  $v^E$  is very close to the experimental result and the agreement is more or less satisfactory. As the absolute value of  $v^E$  is itself very small and as the theoretical value of  $v^E$  is obtained from the difference of two large quantities, a small error in any of the parameters used for theoretical calculation will cause here a large discrepancy between the experimental and the predicted result. The main source of error lies, of course, in the estimation of  $\rho$  and  $\delta$ , which may contain an uncertainty from 5 to 10%. Beside this, we have neglected the contribution from another important source, viz., the contributions of globular origin. The latter effect has been supposed to be appreciable for many similar systems\*. It is possible, in principle, to estimate this effect from the simul-

\*S. N. Bhattacharyya (unpublished results to be communicated shortly).

taneous measurement of all three major excess functions i.e.,  $g^E$ ,  $h^E$  and  $v^E$ . Work is in progress in this laboratory to obtain  $g^E$  of this system and to ascertain from it such effects. It might be mentioned in this connection that the excess functions of this system are very peculiar and interesting in the sense that they have opposite signs i.e.,  $h^E < 0$  and  $v^E > 0$ . Two other systems studied by Anantaraman *et al* (1961, 1963) might be recalled here for comparison. One is the "carbontetrachloride+chlorobenzene" system where  $h^E > 0$  and  $v^E < 0$  whereas in another, "chlorobenzene+toluene" both  $h^E$  and  $v^E$  have negative values. Most of the other system of this types have  $h^E > 0$  and  $v^E > 0$ . The fair success of the present approach to such an unusual set of excess functions again shows its validity and demonstrates clearly the complex nature of their origin.

#### ACKNOWLEDGMENT

The authors are grateful to Prof. S. R. Palit for his constant encouragement and many helpful suggestions during the course of the work. This work has been done under a C.S.I.R. scheme.

#### REFERENCES

- Anantaraman, A. V. Bhattacharyya S. N. and Palit, S. R. 1961, *Trans. Faraday Soc.*, **57**, 40.
- Anantaraman, A. V. Bhattacharyya S. N. and Palit, S. R. 1963, *Trans. Faraday Soc.*, **59**, 1101.
- Anantaraman, A. V. Bhattacharyya S. N. and Palit, S. R. 1963, *Ind. Jour. Chem.*, **1**, 459.
- Balescu R., 1955, *Acad. Roy. Belg., Cl. Sc.*, **41**, 1242.
- Bhattacharyya, S. N. Anantaraman A. V. and Palit, S. R. 1962, *Physica*, **28**, 633.
- Flood D. T. in "Organic Syntheses" Blat-(A. H. Editor), 1943, Collective Vol. 2, (John Wiley & Sons Inc., New York), pp. 295.
- Prigogine, I. 1957, "Molecular theory of Solutions" (North-Holland Publishing Company, Amsterdam,) Chapter XIV.
- Prigogine, I. *ibid*, pp. 215.
- Prigogine, I. *ibid*, pp. 196.
- Timmermans, J. 1950, "Physico-chemical constants of pure organic compounds" (Elsevier Publishing Co.) p. 152, 281.



# EXPERIMENTAL STUDY OF DURATION OF CONTACT OF A TRANSVERSELY IMPINGING LOAD ON CANTILEVER

B. B. BANERJEE

PHYSICS LABORATORY, UNIVERSITY COLLEGE OF ENGINEERING, BURLA (ORISSA).

(Received 11 July, 1963)

**ABSTRACT.** In this paper the variation of duration of contact for two metal hammers striking transversely a mild steel rod, fixed at one end from respective particular distances, has been photographically studied. The time is recorded by the shadow-graph of a light pointer attached to an electrically maintained tuning fork of frequency 100. The duration of impact has been found to vary discontinuously with striking distances measured from fixed end of the cantilever. The phenomenon of multiple or double contacts within the period of impact has been observed in almost all cases. This seems to be due to fluctuating pressures caused by reflected transverse waves from both ends producing reactions on the hammer. In every photograph the vibration curve of a section of the rod is fluctuating over the general sine curve. This shows that vibrations have set in the rod during impact itself. These observations will help settle many outstanding problems in the vibration of cantilevers and lead to a correct theoretical understanding of the problem.

## INTRODUCTION

Rayleigh and St.Venant by the help of the normal function tried to give theoretical explanation of the free vibration of a bar including a fixed-free bar permanently loaded at the free end. Morse has considered the case when the vibration is set up by initial velocity. Timoshenko has considered the Hertzian impact between the bar and transversely impinging load. M. Ghose and K. D. Roy tried to study the dynamics of the vibration of a bar excited by transverse impact of a load and obtained the expression for duration of impact. Their analysis is not however complete to explain the experimental facts which are observed and recorded in this paper. No detailed experimental observation has been on record so far. The results of the observations made in this paper may lead to correct theoretical approach to this problem.

## EXPERIMENTAL

In this paper we record some of our experimental observations of systematic study of the problem. The experimental study of the duration of impact for different mass of the hammer striking transversely at different points of a cantilever has been made by photographic method. The experimental arrangement for recording the duration of impact is similar to that adopted by M. Ghose

in the study of struck string. Elegance of this method over other methods is that the photograph obtained by a moving camera clearly records the complete behaviour of the cantilever at successive stages during impact.

A mild steel rod of length 90 cms. and diameter 1.27 cms. is fixed rigidly at one end in a heavy iron pillar, whose base being embedded in concrete in order to ensure that there is no yielding at the fixed end. The rod is found to remain horizontal. This has been thoroughly tested by the help of a spirit level. A pendulum with bifilar suspension is used for the impinging load. The shadows of the rod, the pointer of an electrically maintained tuning fork of frequency 100 for time base and the impinging load are simultaneously photographed on the moving photographic paper on trolley inside the camera box. The system is illuminated by an arc lamp from the top.

Ample precautions are taken during experiment such that the load strikes the rod perpendicularly and that there is no overlapping of the shadows of the load and the rod just before and after contact otherwise this would introduce serious error in the measurements. In order to obtain the simultaneous photograph of the impinging load and the rod, sufficient care has been taken in releasing the photo carrier with its trolley and the impinging load in time from their respective mechanical catches.

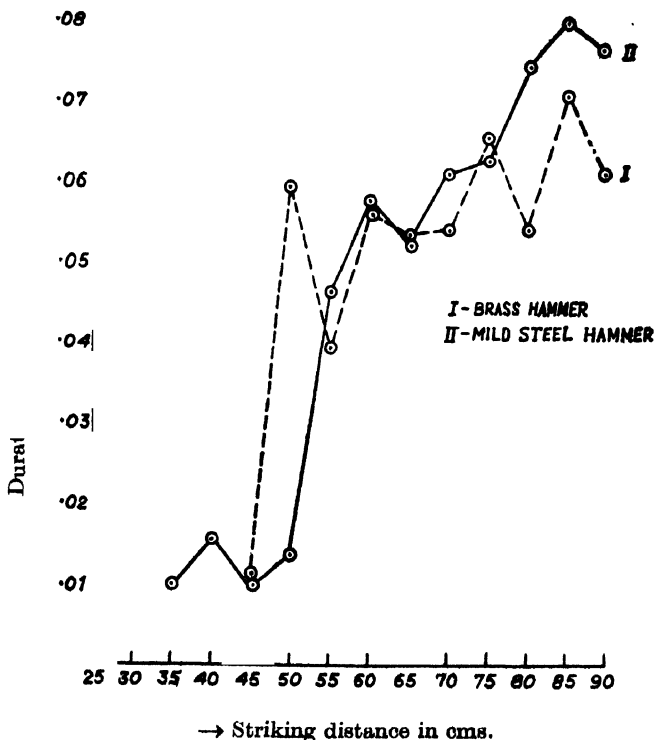


Fig. 1.

TABLE I

Brass hammer—Spherical.

Weight of hammer—240 gms.

Radius of curvature of surface of contact 1.905 cms.

Velocity before impact : 88.5 cms./sec.

Striking distance in cms.	Duration of successive contacts in secs.	Duration of separation in secs.	Duration of impact in secs.	Striking distance in cms.	Duration of successive contacts in secs.	Duration of separation in secs.	Duration of impact in secs.
45	.00304				.00199		
	.00442	.00361	.01107	70	.00263	.02493	.05421
					.00495	.01971	
	.00531			75	.00516		
50		.00374				.01683	
	.00621		.05960		.00865		.06659
		.03730				.00373	
	.00704				.03222		
55	.00599			80	.00319		
		.00221				.01263	
	.00345		.03965		.01236		.05385
		.02161				.00546	
	.00639				.02021		
60	.00513			85	.01208		
		.03243				.01220	
	.00370		.05558		.01997		.07097
		.01086				.00455	
	.00346				.02217		
65	.00527				.00597		
		.02195				.01089	
	.00740		.05351	89	.01168		
		.01542				.02266	.06165
	.00347				.00324		
						.00131	
					.00590		

The hammer is released mechanically from a fixed distance to keep the velocity of impact constant. It strikes the rod at a point the distance of which is measured from the fixed end of the rod. The observations are made at points 5 cms. apart, the last one being at 89 cms.

The measurements of duration of contact and duration of separation have been made by a comparator reading upto .0001 cm. The number of waves traced just overhead by the fork of frequency 100, within the same length of the hammer's shadow in contact with that of the rod, helps to measure the duration of impact or separation during impact.

## DISCUSSION AND RESULTS

The durations of impact for different struck points and for different hammers are given in tables I and II. It is found that in almost all cases there are double or multiple contacts before the hammers finally leave the rod. It is obvious that these phenomena are due to the influence of the reflected waves

from the ends that overtake the hammer. The duration of impact is a root of the pressure equation  $P = f(t) = 0$ , of the load. This equation may have multiple roots of which more than one may be real and positive. In that case it is more logical to define the real duration of impact as the greatest real positive root of the equation  $f(t) = 0$ . After this maximum value of the root, the pressure becomes negative, and the load leaves the rod completely.

TABLE II

Weight of hammer—mild steel—233 gms.

Radius of curvature of the surface of contact—2.432 cms.

Velocity before impact : 99 cms/sec.

Striking distance from fixed end in cms	Duration of successive contacts in secs.	Duration of separation in secs.	Total duration of Impact in secs.	Striking distance in cms.	Duration of successive contacts in secs.	Duration of separation in secs.	Total duration of Impact in secs.
35	.00386			65	.00819		
		.00297	.00994			.03531	.05217
	.00311				.00867		
40	.01044			70	.00443		
		.00253	.01588			.02242	
	.00291				.00850		.06160
					.01569	.01056	
45	.00283			75	.01108		
		.00297	.01054			.00738	.06246
	.00474				.04400		
50	.01371	×	.01371	80	.00268		
					.00441	.00306	
						.00980	.07409
					.05414		
55	.00482			85	.01091		
		.00344				.01743	
	.00555		.04619		.01865		.07980
		.02047				.01046	
	.01191				.02235		
60	.00667			89	.01124		
		.03117	.05766			.02029	
	.01982				.01570		
						.00953	.07680
					.00715		
						.00570	
					.00719		

Column (1) shows the position of contact on the rod measured from the fixed end. Column (2) shows the duration in seconds of respective contacts. Column (3) shows the duration of separation in seconds which is the time between two successive contacts. Column (4) shows the duration of impact, measured from the instant the hammer makes first contact with the rod to the time when it completely leaves it. It is same as the sum of the time of all the contacts and the time during which the load does not remain in contact with the rod as depicted by black patches within the shadow graph (Fig. 2).

Graphical representation (Fig. I) of variation of duration of impact with striking distance shows that duration of impact changes discontinuously with the striking distance and tends to minimum as the fixed end is approached. The two striking loads of different materials depict slightly different character in

Brass Hammer

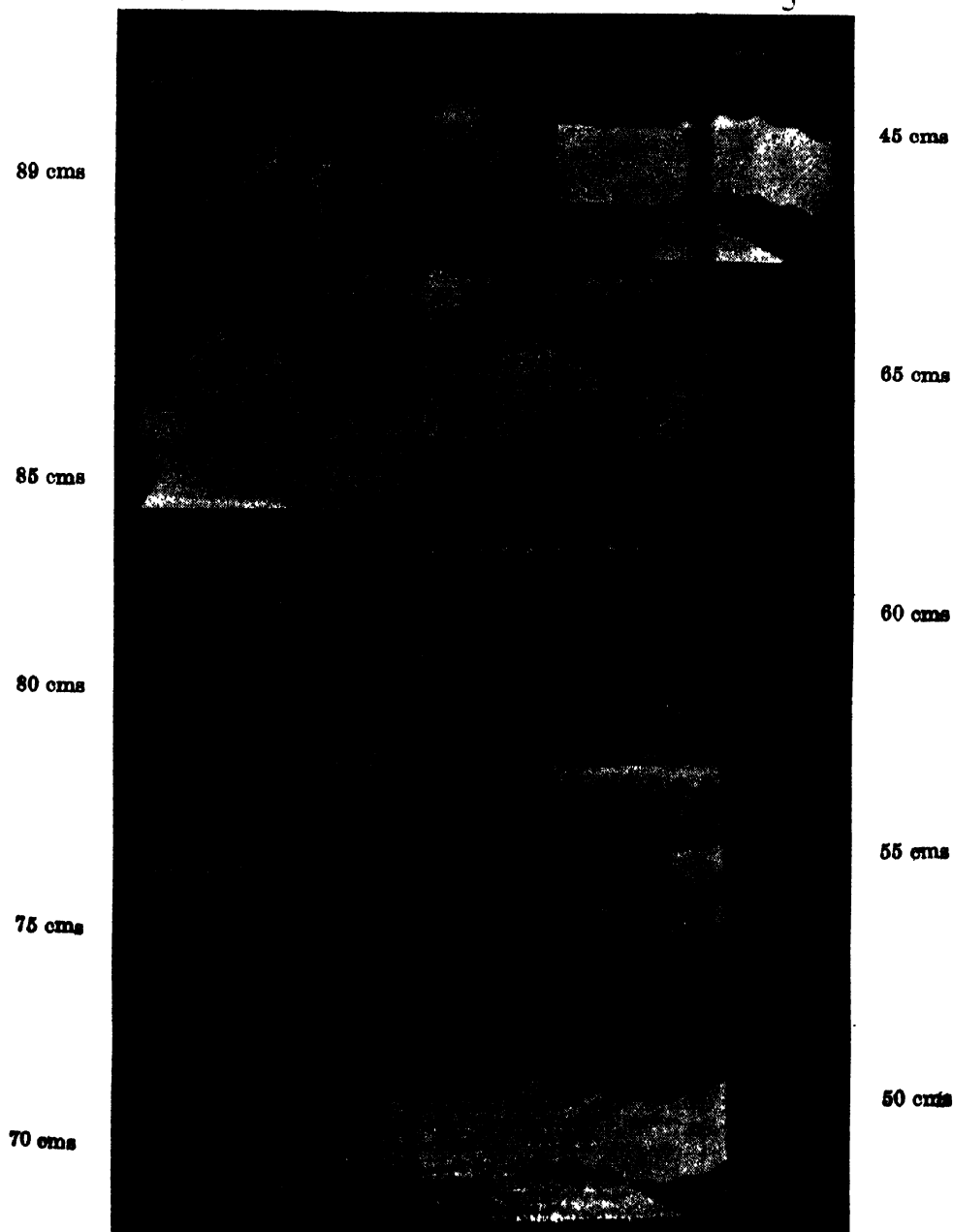


Fig. 2.

the behaviour of duration of impact though their general behaviours are similar. This difference may be due to the fact that they are different in weight and material and were impinged with different velocities.

It is evident from the observations of multiple contacts within the period of impact that pressure of impact fluctuates. This can not be explained by analyses given by Rayleigh, M. Ghose and K. D. Roy or Timoshenko. It suggests that transverse waves are generated in the rod which on travelling along the rod are

Mild Steel Hammer

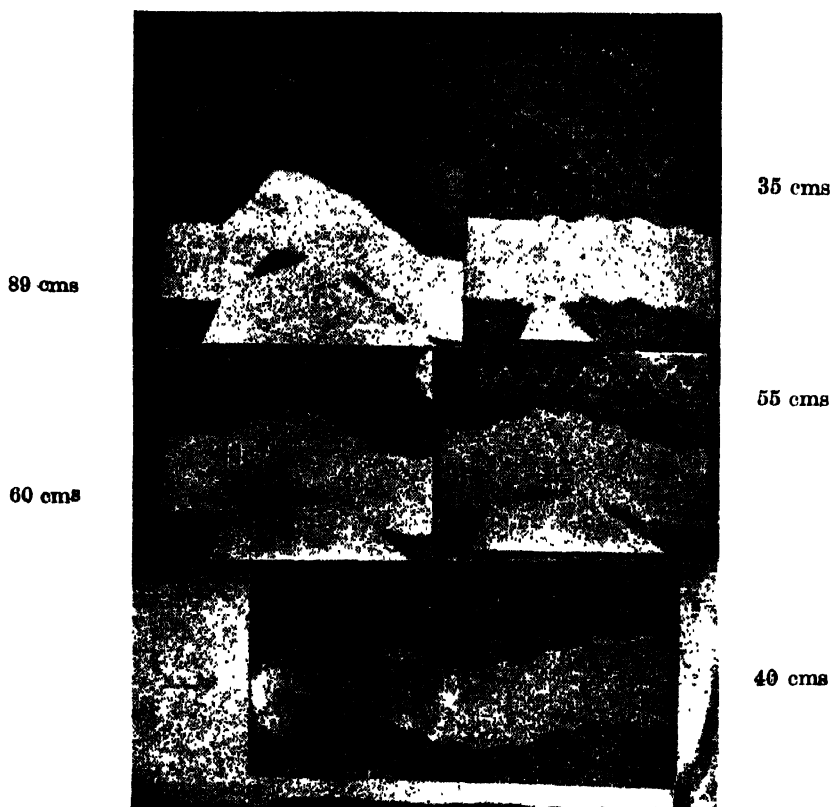


Fig. 3.

reflected from the ends and produce reaction on the load. In this way there may be successive reflections before the load completely leaves the rod; hence there are multiple contacts. None of the existing theories is able to explain the above fluctuations of pressure during impact as observed photographically.

The photographs show that the rod begins to vibrate as soon as impact begins. The vibration curves after impact show that some overtones are present along with the fundamental which is evident from fluctuating nature of vibrations over the general sine curve. The theoretical explanation of the same is in progress and

will be published in due course. Experimental study of the different aspects of the problem is also in progress and will be reported in short time.

#### ACKNOWLEDGMENT

My best thanks are due to Dr. M. Ghose, D.Sc., Vice-Principal and Head of Physics Department, City College, Calcutta, for his suggestion of the problem and continuous guidance during the course of this work. I extend my thanks to Sri B. Mohapatra, Principal, Utkal University College of Engineering, Burla. (Orissa) for his extending all facilities to me in preparing this paper.

#### REFERENCE

- Ghose, M. 1932, *Indian Journal of Physics*—Vol. 7, 5.  
Ghose M. and Roy K. D. 1952, *Indian Journal of Theoretical Physics*—Vol. XXVI, 9,  
Morse—Vibration and sound, Ch. IV.  
Rayleigh—Theory of Sound Vol. I, 168 and 182.  
St. Venant, 1883, *Théorie de l'élasticité des corps solides*, Paris, 298.  
Timoshenko—Vibration problems in Engineering, 411.

# DISTRIBUTION OF POSITIVE IONS IN THE F-REGION

S. N. GHOSH, K. D. SHARMA\* AND A. SHARMA

J. K. INSTITUTE OF APPLIED PHYSICS, UNIVERSITY OF  
ALLAHABAD, ALLAHABAD, INDIA.

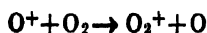
(Received January 1, 1964)

**ABSTRACT.** The distribution of positive ions in the F-region of the ionosphere is controlled mainly by the following processes:

- (a) photo-ionization of atmospheric constituents,
- (b) ion-atom interchange,
- (c) dissociative recombination of molecular ions with electrons and
- (d) diffusion and drift of ionization.

Of these processes, the rate of production of ions from photoionization can be calculated with a fair degree of accuracy from rocket data (Hinteregger, 1961) of the solar spectrum in the ultraviolet and x-ray regions. The rate coefficients of dissociative recombination process are known but the rate coefficients of ion-atom interchange reactions, which are responsible for reshuffling the ions, are not available. From the rocket-borne experimental determination of percentage of ion compositions (Johnson, 1961), the rate coefficients of these reactions are obtained.

In order to reproduce the known ion composition, the rate coefficients of ion-atom interchange reactions should vary with altitude. Assuming that the temperature dependence of the above process is analogous to that of a two-body chemical reaction, their altitude variation and activation energies are obtained. The rate coefficient of the reaction,



at 300°K is found to be  $3.07 \times 10^{-11}$  cm<sup>3</sup>/sec which agrees with the experimental value of  $2.5 \pm 0.4 \times 10^{-11}$  cm<sup>3</sup>/sec obtained by Dickinson and Sayers (1960) at the same temperature.

## INTRODUCTION

To understand many upper atmospheric phenomena, e.g., night airglow, aurora, twilight airglow etc., the processes controlling the distribution of ions and electrons in the upper atmosphere should be clearly understood. It has been realised by many workers (Martyn, 1959, Yonezawa and Takahashi, 1960, Bates and Nicolet, 1960, Hertzberg, 1961) that the following processes together with the diffusion of ions and electrons are mainly controlling the distribution of ions in the ionosphere.

- (1) photo-ionization of the atmospheric constituents,
- (2) ion-atom interchange, and
- (3) dissociative recombination of molecular ions with electrons.

---

\* Now at the Department of Physics, Jodhpur University, Jodhpur, India.



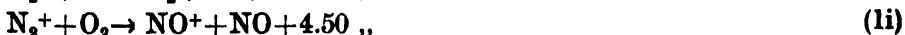
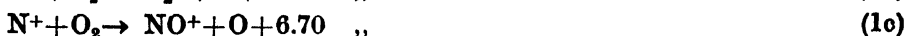
However, the relative contributions of these processes in controlling the distribution of ions in the ionosphere is not yet definitely known.

With the exception of the ion-atom interchange reactions, the rate coefficients of the above processes are known. In this paper from the rocket-borne experimental determination (Johnson, 1961) of the percentage of ion composition upto 220 km, the rate coefficients of these reactions are obtained. Using these rate coefficients, the ion distribution in the F-region is calculated upto 400 km. It is found that above 180 km, diffusion and ion drift must be taken into account to obtain the correct ion distribution with height.

#### DAYTIME IONOSPHERIC PROCESSES

The ionization of the upper atmospheric particles, which consists mainly of  $O_2$ ,  $N_2$ ,  $O$ ,  $N$  and  $NO$ , is caused by solar radiations in the X-ray and ultraviolet regions. Rates of production of ions by X-ray have been calculated by Ghosh and Sharma (1961). In addition to ionization by X-rays, Ghosh and Shardanand (1960, 1961) considered ionization by ultraviolet radiations and that produced by Auger electrons and photoelectrons.

Bates (1955) showed that primary photo-ions are reshuffled by the ion-atom interchange process. To obtain daytime ion distribution in the F-region, consider the possible ion-atom interchange reactions as given by Hertzberg (1961), namely,



The reaction  $O_2^+ + N \rightarrow NO + O^+$  which has been considered by Hertzberg has been neglected in our analysis as the reaction is endothermic (Bates and Nicolet, 1961).

The following recombination reactions are considered :



where (') signifies the excited species.

(Due to the high rate of photo-dissociation of negative ions, its presence has been neglected while considering the daytime equilibrium of positive ions).

The equations governing the daytime distribution of positive ions in the F-region are given by :

$$\begin{aligned}\dot{N} &= J_1a + J_2b + J_3c + J_4d + J_5e - N(\beta_1x_1 + \beta_2x_2 + \beta_3x_5) \\ &= q - N(\beta_1x_1 + \beta_2x_2 + \beta_3x_5)\end{aligned}\quad (3a)$$

where  $n(O_2)$ ,  $n(N_2)$ ,  $n(O)$ ,  $n(N)$  and  $n(NO)$  are denoted by  $a$ ,  $b$ ,  $c$ ,  $d$  and  $e$  respectively.  $n(O_2^+)$ ,  $n(N_2^+)$ ,  $n(O^+)$ ,  $n(N^+)$ ,  $n(NO^+)$  and  $n(e)$  are represented by  $x_1$ ,  $x_2$ ,  $x_3$ ,  $x_4$ ,  $x_5$  and  $N$  respectively.  $J_1$ ,  $J_2$ ,  $J_3$ ,  $J_4$  and  $J_5$  are the probabilities of photo-ionization of  $O_2$ ,  $N_2$ ,  $O$ ,  $N$  and  $NO$ .  $\beta_1$ ,  $\beta_2$  and  $\beta_3$  are the rate coefficients of dissociative recombination reactions (2a), (2b) and (2c) respectively.

If  $\alpha_r$  ( $r = 1, 2, 3, \dots, 9$ ) denotes the rate coefficients of ion-atom interchange reactions (1), we have

$$\dot{x}_1 = J_1a + \alpha_2ax_3 - x_1(\alpha_5d + \alpha_6b + \beta_1N) \quad \dots (3b)$$

$$\dot{x}_2 = J_2b - x_2(\alpha_7c + \alpha_8d + \alpha_9a + \beta_2N) \quad \dots (3c)$$

$$\dot{x}_3 = J_3c + \alpha_4ax_4 - x_3(\alpha_1b + \alpha_2a) \quad \dots (3d)$$

$$\dot{x}_4 = J_4d + \alpha_8dx_2 - x_4(\alpha_3a + \alpha_4a) \quad \dots (3e)$$

$$\dot{x}_5 = J_5e + \alpha_1bx_3 + \alpha_3ax_4 + x_1(\alpha_5d + \alpha_6b) + x_2(\alpha_7c + \alpha_9a) - \beta_3Nx_5 \quad \dots (3f)$$

Equations (3b) to (3f) can be written as,

$$\dot{x}_1 = -m_{11}x_1 + m_{13}x_3 + l_1 \quad \dots (4a)$$

$$\dot{x}_2 = -m_{22}x_2 + l_2 \quad \dots (4b)$$

$$\dot{x}_3 = -m_{33}x_3 + m_{34}x_4 + l_3 \quad \dots (4c)$$

$$\dot{x}_4 = -m_{44}x_4 + m_{42}x_2 + l_4 \quad \dots (4d)$$

$$\dot{x}_5 = -m_{55}x_5 + m_{51}x_1 + m_{52}x_2 + m_{53}x_3 + m_{54}x_4 + l_5 \quad \dots (4e)$$

where,

$$m_{11} = \alpha_5d + \alpha_6b + \beta_1N$$

$$m_{22} = \alpha_7c + \alpha_8d + \alpha_9a + \beta_2N$$

$$m_{33} = \alpha_1b + \alpha_2a$$

$$m_{44} = \alpha_3a + \alpha_4a$$

$$m_{55} = \beta_3N$$

$$m_{13} = \alpha_2a$$

$$m_{34} = \alpha_4a$$

$$m_{42} = \alpha_8d$$

$$m_{51} = \alpha_5d + \alpha_6b$$

$$m_{53} = \alpha_7c + \alpha_9a$$

$$m_{53} = \alpha_1b$$

$$m_{54} = \alpha_3a$$

$$l_1 = J_1a$$

$$l_2 = J_2b$$

$$l_3 = J_3c$$

$$l_4 = J_4d$$

$$l_5 = J_5e.$$

Denoting the initial concentrations of positive ions  $x_i^0$  ( $i = 1, 2, 3, 4, 5$ ), the solutions of equation (4) are obtained. For example, the solution of equation (4b) is given by

$$x_2 = \frac{l_2}{m_{22}} - \left( \frac{l_2}{m_{22}} - x_2^0 \right) e^{-m_{22} t} \quad \dots (5)$$

In a similar manner the other solutions can be obtained.

Substituting the numerical values of various quantities in equation (5), daytime distribution of ions at different altitudes can be calculated.

#### CALCULATION OF ION DISTRIBUTION FOR THE F-REGION

Using equation (5), the ion distribution in the F-region is calculated after determining the rates of production of ions and constants ( $m^s$ ) at different altitudes.

##### (a) Rates of production of ions

To determine the rates of production of ions, the following procedure is adopted :

The number of photons,  $n(h\nu)_z$ , incident per sq. cm per second corresponding to frequency  $\nu$  at an altitude  $z$  is given by,

$$n(h\nu)_z = n(h\nu)_\infty \exp \left( -\sum_i n(i)_z H_{iz} \sigma_{vi} \right) \quad \dots (6)$$

where,

$n(h\nu)_\infty$ —number of photons of frequency  $\nu$  at the top of the atmosphere,

$n(i)_z$ —particle concentration of  $i$ -th constituent at the altitude  $z$ ,

$H_{iz}$ —scale height of the  $i$ -th constituent at the altitude  $z$ ,

and  $\sigma_{vi}$ —absorption cross-section corresponding to frequency  $\nu$  for the  $i$ -th constituent.

The wavelength region 1000–100 Å, which is mainly responsible for the photo-ionization of F-region, is divided into intervals such that within each interval the absorption coefficient is practically constant. For oxygen and nitrogen atoms, the photo-ionization cross-sections given by Dalgarno and Parkinson (1960) were utilized. The absorption cross-section of  $O_2$  upto 500Å as given by Watanabe (1958) and below it those obtained by Weissler *et al* (1955), are taken. For  $N_2$  upto 303Å absorption cross-section given by Watanabe (1958) and below it those obtained by Weissler *et al* (1952) are assumed. Miller's (1957) model of atmospheric composition and scale heights as given in ARDC model atmosphere 1959 are used. Thorough mixing is assumed upto 150 km for  $O_2$  and upto 180 km for  $N_2$ , N and O. Above these heights diffusive equilibrium is considered. Values of  $n(h\nu)$  have been taken from the results of rocket-borne experiments extrapolated by Hinteregger (1961).

The rates of production of photo-ions produced due to ionization of the  $i$ -th constituent is calculated from the expression,

$$\sum_{\nu} n(h\nu)_z \cdot n(i)_z \cdot \sigma_{\nu i} = n(i)_z \sum_{\nu} n(h\nu)_z \cdot \sigma_{\nu i} = n(i)_z \cdot J_{iz}$$

where,  $J_{iz}$  is the probability of ionization of the  $i$ -th constituent at the altitude  $z$ .

The absorption coefficients and atmospheric composition as mentioned above have been used. The calculated rates of production of ions are given in Table I. The production of  $\text{NO}^+$  ions due to photo-ionization above 120 km has been neglected owing to the small density of NO molecules. The ionization due to solar X-rays is significant only below 160 km and is shown in Table I.

(b) *Determination of constants  $m^s$*

The constants  $m^s$  are controlled by rate coefficients of ion-atom interchange ( $\alpha^s$ ) and dissociative recombination ( $\beta^s$ ) processes. The electron density used in the calculations has been taken from rocket-borne experimental data obtained by Nisbet (1960). It is assumed that the rate coefficients of ion-atom interchange and dissociative recombination processes are constant. Taking known values of  $\beta^s$ ,  $\alpha^s$  are fixed at 150 km so as to give the observed percentage distribution of ions (Johnson, 1961). Using above values of  $\alpha^s$  and  $\beta^s$ , equilibrium time (Table II) is calculated for each ion and it is found that except for  $\text{O}^+$  and  $\text{NO}^+$  above 320 km, equilibrium is established within a short time. Taking above values of  $\alpha^s$  and  $\beta^s$ , the ion distributions are calculated up to 300 km. These distributions are compared with those obtained from Johnson's data (Fig. 1). It is found that,

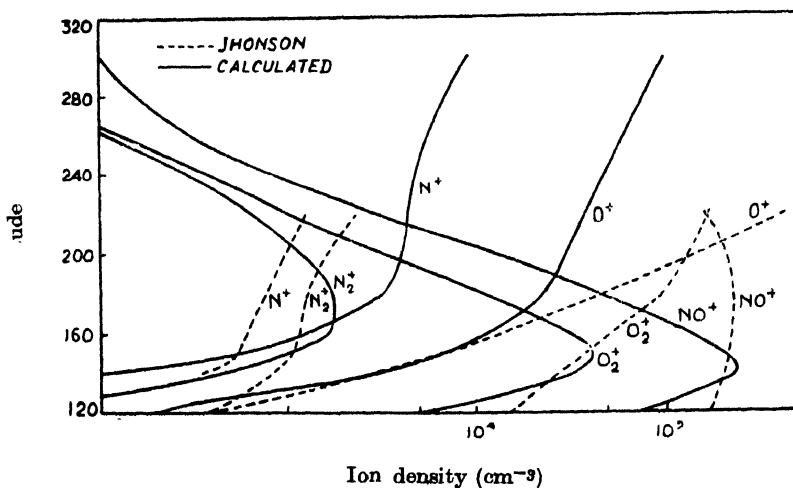


Fig. 1. The altitude variation of positive ions concentration in the F-region assuming the same rate coefficients for every altitude as that fixed for 150 km.

- (i) the calculated distributions do not agree with the observed distributions below and above 150 km and that the discrepancy between two distributions is greater above 180 km, and

TABLE I

Altitude (km)	$O_2^+$	Solar ultraviolet radiations		Rate of production of ions ( $\text{cm}^3 \text{ sec}^{-1}$ ) by Solar X-rays			
		$N_2^+$	$O^+$	$N^+$	$O_2^+$	$N_2^+$	$O^+$
1200	$1.28 \times 10^2$	$1.06 \times 10^2$	$1.66 \times 10^1$	$1.95 \times 10^{-1}$	$1.62 \times 10^2$	$5.53 \times 10^2$	$8.45 \times 10^2$
140	$1.78 \times 10^2$	$5.60 \times 10^3$	$1.05 \times 10^3$	$6.02 \times 10^1$	$4.12 \times 10^1$	$1.68 \times 10^2$	$2.45 \times 10^2$
150	$1.40 \times 10^2$	$5.94 \times 10^3$	$1.06 \times 10^3$	$9.15 \times 10^1$	$1.49 \times 10^1$	$7.70 \times 10^1$	$1.12 \times 10^2$
160	$6.34 \times 10^1$	$4.21 \times 10^3$	$6.44 \times 10^2$	$8.73 \times 10^1$	6.09	$3.77 \times 10^1$	$5.53 \times 10^1$
180	$2.86 \times 10^1$	$2.09 \times 10^3$	$2.52 \times 10^2$	$5.94 \times 10^1$			
200	$1.08 \times 10^1$	$8.99 \times 10^2$	$2.16 \times 10^2$	$3.88 \times 10^1$			
220	4.20	$3.95 \times 10^2$	$1.32 \times 10^2$	$2.48 \times 10^1$			
240	1.77	$1.83 \times 10^2$	$8.21 \times 10^1$	$1.62 \times 10^1$			
260	$8.01 \times 10^{-1}$	$9.09 \times 10^1$	$5.27 \times 10^1$	$1.09 \times 10^1$			
280	$3.87 \times 10^{-1}$	$4.74 \times 10^1$	$3.52 \times 10^1$	7.54			
300	$1.98 \times 10^{-1}$	$2.61 \times 10^1$	$2.43 \times 10^1$	5.36			
320	$1.06 \times 10^{-1}$	$1.51 \times 10^1$	$1.72 \times 10^1$	3.94			
340	$5.95 \times 10^{-2}$	9.00	$1.24 \times 10^1$	2.94			
360	$3.46 \times 10^{-2}$	5.54	9.13	2.24			
380	$2.07 \times 10^{-2}$	3.51	6.86	1.72			
400	$1.29 \times 10^{-2}$	2.30	5.26	1.35			

TABLE II

Equilibrium time (the time required to attain 1/e-th of the equilibrium concentration) for various ions

Altitude (km)	O <sub>2</sub> <sup>+</sup>	N <sub>2</sub> <sup>+</sup>	Time of equilibrium for		
			O <sup>+</sup>	N <sup>+</sup>	NO <sup>+</sup>
120	22.4 sec	0.22 sec	0.65 sec	11.96 sec	0.65 sec
160	1.03 mts	0.56 sec	28.8 sec	1.55 sec	28.8 sec
200	2.81 „	1.02 „	5.4 mts	9.35 „	5.4 mts
240	1.99 „	1.61 „	35.0 „	1.03 mts	25.0 „
280	1.15 „	1.43 „	2.65 hrs	4.80 „	2.65 „
320	1.16 „	1.57 „	9.53 „	17.67 „	9.53 „
360	1.61 „	2.25 „	28.61 „	54.33 „	28.61 „
400	2.21 „	3.12 „	75.56 „	2.44 hrs	75.56 „

TABLE III

Altitude Variation of the Effective Recombination Coefficient  $\alpha_{eff}$   
(assuming  $\beta_1^* = 1 \times 10^{-8} \text{ cm}^3/\text{sec}$ ,  $\beta_2^* = 4 \times 10^{-7} \text{ cm}^3/\text{sec}$  and  $\beta_3^*$  as follows)

Altitude (km)	$\beta_3(\text{cm}^3 \text{ sec}^{-1})$	$\alpha_{eff}(\text{cm}^3 \text{ sec}^{-1})$	
		Calculated	Havens <i>et al</i> (1954)
120	$5.5 \times 10^{-8}$	$5.0 \times 10^{-8}$	$1.6 \times 10^{-8}$
140	$1.5 \times 10^{-7}$	$1.4 \times 10^{-7}$	—
150	$1.3 \times 10^{-7}$	$1.1 \times 10^{-7}$	$1.6 \times 10^{-8}$
200	$7.5 \times 10^{-9}$	$4.4 \times 10^{-9}$	$2.0 \times 10^{-9}$
250	$3.0 \times 10^{-9}$	$1.1 \times 10^{-10}$	$1.3 \times 10^{-10}$
300	—	$1.1 \times 10^{-11}$	$1.6 \times 10^{-11}$
340	—	$7.2 \times 10^{-12}$	$5.0 \times 10^{-12}$
360	—	$7.5 \times 10^{-12}$	$3.0 \times 10^{-12}$
400	—	$7.4 \times 10^{-12}$	$1.8 \times 10^{-12}$

\*Bortner and Baulknight (1961) have recently reported that  $\beta_1$  and  $\beta_2$  are temperature dependent whereas  $\beta_3$  is independent of temperature. Their values are  $\beta_1 = 9.1 \times 10^{-5} \text{ T}^{-1}$ ,  $\beta_2 = 1.1 \times 10^{-5} \text{ T}^{-1/2}$  and  $\beta_3 = 1 \times 10^{-8}$ .

- (ii) total number of positive ions is not equal to electron density.

From above, it is clear that  $m^s$  should vary with altitude. It is generally agreed that dissociative recombination coefficients are constant (their dependance on temperature is not known, Bates and Nicolet, 1960). Therefore, keeping  $\beta^s$  constant,  $\alpha^s$  are fixed at each altitude to reproduce the observed ion distribution. It is found that  $\alpha^s$  increase upto 180 km and then decrease.  $\beta^s$  can be kept constant only upto 180 km and above it they have to be decreased together with  $\alpha^s$ . It should, however, be noted that effective recombination coefficient  $\alpha_{eff}$  calculated from the expression,

$$\alpha_{eff} = \frac{\beta_1 n(O_2^+) + \beta_2 n(N_2^+) + \beta_3 n(NO^+)}{N}$$

agrees with those obtained by Havens *et al* (1954) except for the  $F_1$ -layer (Table III)

The rate coefficient for dissociative recombination of  $NO^+$ ,  $\beta_3$ , could not be kept constant for all altitudes as assumed earlier. From Eqn. (3), it is seen that  $\beta_3$  appears in the last equation and is therefore solved at the end. If a fixed value of  $\beta_3$  (say  $1 \times 10^{-8}$  cm<sup>3</sup>/sec) is taken, the density of  $NO^+$  ions at lower altitudes exceeds the electron density which is not tenable.  $\beta_3$  has to be taken as high as  $1.5 \times 10^{-7}$  cm<sup>3</sup>/sec at 140 km which is decreased to  $2.3 \times 10^{-8}$  cm<sup>3</sup>/sec at 180 km in order to reproduce the observed distribution of  $NO^+$ .  $\beta_3$  as low as  $3.0 \times 10^{-9}$  cm<sup>3</sup>/sec, as suggested by Bates and Nicolet (1960), reproduces the observed distribution of  $NO^+$  above 180 km and is kept constant for higher altitudes.

Burkard (1962) has suggested that  $\beta_3$  should vary approximately linearly with temperature. In our analysis, we obtained that  $\beta_3$  increases approximately linearly with temperature (upto about 140 km) and that for higher temperatures it decreases exponentially with temperature. This variation in  $\beta_3$  may be due to the fact that we have assumed  $\beta_1$  and  $\beta_2$  independent of temperature whereas Bortner and Baulknight (1961) have shown that  $\beta_1 = 9.1 \times 10^{-5} T^{-1}$ ,  $\beta_2 = 1.1 \times 10^{-5} T^{-1/2}$  and  $\beta_3 = 1.0 \times 10^{-8}$  cm<sup>3</sup>/sec. The values of  $\beta_1$  and  $\beta_2$  used by us are, of course, of the same magnitude (in the F-region) as those reported by Bortner and Baulknight. However, further investigations are needed to verify these results.

From above, it seems that the situation above 180 km is not so simple as assumed above. It has been shown by many workers that above 180 km, diffusion and ion drift play an important role in the distribution of ions and electrons.

# RATE COEFFICIENTS OF ION-ATOM INTERCHANGE REACTIONS

The rate coefficients of ion-atom interchange reactions except for  $\alpha_2$  are not determined experimentally.  $\alpha_2$  has been measured by Dickinson and Sayers (1960) to be  $2.5 \pm 0.4 \times 10^{-11} \text{ cm}^3/\text{sec}$  at 300°K. Since the ion atom interchange is a two-body process, its coefficient is likely to increase with temperature analogous to the rate coefficient of two-body chemical process. Bates and Nicolet (1960) pointed out that the rate coefficients of these reactions should be an increasing function of temperature and that these might possess some activation energy or steric hinderance. We have, therefore, assumed that the rate coefficients vary as,

$$\alpha_r = C_r \exp (-E_r/RT)$$

where,  $r = 1, 2, 3, \dots 9$ ,  $R$  is the gas constant and  $E_r$  represents the activation energy. Graphs between  $\log_e \alpha_r$  and  $1/T$  (the values of  $\alpha_s$  are already fixed between 120–180 km) are found to be straight lines (Fig. 2). They are then extrapolated to obtain  $\alpha^s$  at higher altitudes (Table IV). From Fig. 2, it is seen that the magni-

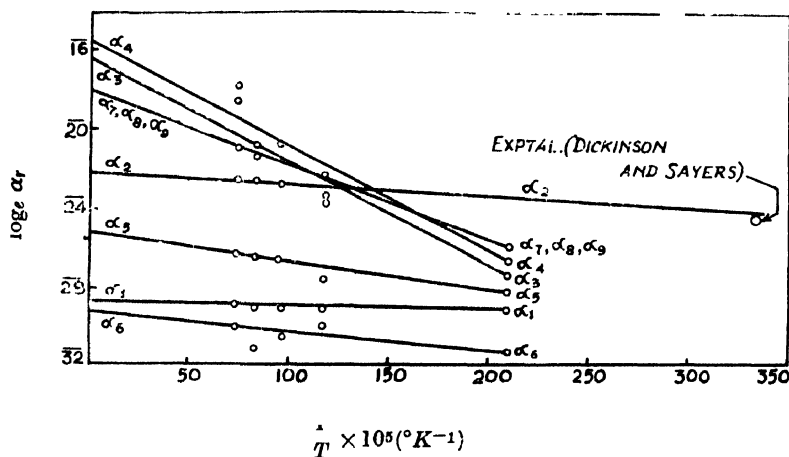


Fig. 2. The variation of rate coefficients of ion-atom interchange reactions with temperature.

tudes of  $\alpha^s$  do not differ appreciably above 200 km as  $1/T$  remains approximately constant (ARDC Model Atmosphere, 1959). The values of  $\alpha^s$  at 200 km have been used for higher altitudes.

From Table IV, it is seen that the rate coefficients  $\alpha_3$  and  $\alpha_4$  of ion-atom interchange reaction involving  $N^+$  ion and  $O_2$  vary between  $10^{-12}$  and  $10^{-9} \text{ cm}^3/\text{sec}$  and that their activation energies are very high i.e. 7.74 Kcal. Since the density of  $N^+$  ions is very small, the effect of these rate coefficients on the distribution of ions is small. The values of  $\alpha_3$  and  $\alpha_4$  above 180 km agree with the theoretically calculated order of  $10^{-9} \text{ cm}^3/\text{sec}$  for such a reaction (Bates and Nicolet, 1960). However, such a high value of rate coefficients has not been obtained for other



TABLE IV  
Temperature variation of rate coefficients of ion-atom interchange reactions. Quantities in  
parenthesis represent activation energies of reactions in Kcal

Altitude (km)	Temperature (°K)	$\alpha_1^*$ (0.47)	$\alpha_2^*$ (0.95)	$\alpha_3$ (7.74)	$\alpha_4$ (7.73)	$\alpha_5$ (1.59)	$\alpha_6^*$ (1.61)	$\alpha_7^*, \alpha_8, \alpha_9^*$ (3.56)
1200	477.0	$2.0 \times 10^{-13}$	$7.0 \times 10^{-11}$	$1.26 \times 10^{-12}$	$2.80 \times 10^{12}$	$1.0 \times 10^{13}$	$9.0 \times 10^{-14}$	$1.5 \times 10^{-11}$
140	849.9	$2.3 \times 10^{-13}$	$1.2 \times 10^{-10}$	$1.61 \times 10^{-10}$	$3.31 \times 10^{10}$	$5.0 \times 10^{12}$	$7.0 \times 10^{-13}$	$2.0 \times 10^{-10}$
150	1031.0	$2.4 \times 10^{-10}$	$1.3 \times 10^{-10}$	$5.07 \times 10^{-10}$	$1.02 \times 10^{-9}$	$6.0 \times 10^{-12}$	$9.0 \times 10^{-13}$	$4.0 \times 10^{-10}$
160	1207.0	$2.5 \times 10^{-13}$	$1.5 \times 10^{-10}$	$1.0 \times 10^{-9}$	$2.00 \times 10^{-9}$	$6.5 \times 10^{-12}$	$9.5 \times 10^{-13}$	$5.5 \times 10^{-10}$
180	1371.0	$3.0 \times 10^{-13}$	$1.6 \times 10^{-10}$	$1.77 \times 10^{-9}$	$3.76 \times 10^{-9}$	$7.0 \times 10^{-12}$	$1.0 \times 10^{-12}$	$7.5 \times 10^{-10}$
200	1404.0	$3.0 \times 10^{-13}$	$1.6 \times 10^{-10}$	$1.77 \times 10^{-9}$	$3.76 \times 10^{-9}$	$7.0 \times 10^{-12}$	$1.0 \times 10^{-12}$	$7.5 \times 10^{-10}$

\*M. H. Bortner and C. W. Baulknight (1961) in the Scientific Report No. 1 'Deionization kinetics', Contract No. AF19(604)—8820, AF Cambridge Research Center, Bedford, Mass., U.S.A. have reported that  $\alpha_1 = 5.0 \times 10^{-13}$ ,  $\alpha_2 = 2.5 \times 10^{-11}$ ,  $\alpha_3 = 0$ ,  $\alpha_7 = 1.0 \times 10^{-11}$  and  $\alpha_9 = 0$  cm<sup>3</sup>/sec.

reactions which usually vary between  $10^{-13}$  to  $10^{-10}$  cm<sup>3</sup>/sec. Table IV further shows that reactions involving the same ion have nearly equal activation energies.

The value of  $\alpha_2$  is found to be  $3.07 \times 10^{-11}$  cm<sup>3</sup>/sec at 300°K which agrees with the experimentally determined value ( $2.5 \pm 0.4 \times 10^{-11}$  cm<sup>3</sup>/sec) of Dickinson and Sayers (1960) at the same temperature. We obtained the values of  $\alpha_1$  and  $\alpha_2$  for 1415°K to be  $3.0 \times 10^{-13}$  cm<sup>3</sup>/sec and  $1.6 \times 10^{-10}$  cm<sup>3</sup>/sec respectively. Bates and Nicolet (1960) also found that  $\alpha_1$  and  $\alpha_2$  differ by two orders at 250 km which, according to ARDC model atmosphere, 1959, has a temperature of 1415°K. It should, however, be noted that the reactions (1a) and (1b) possess very small activation energies, and therefore, they seem to be important reactions in the ionosphere. Reaction (1a) is probably very important in the F<sub>2</sub> region where O<sup>+</sup> ions and N<sub>2</sub> molecules are in abundance. Through this reaction, O<sup>+</sup> ions are converted into NO<sup>+</sup> ions which readily dissociates ( $\beta_3 \sim 1.0 \times 10^{-8}$  cm<sup>3</sup>/sec) into nitrogen and oxygen atoms. The intensity variation of  $\lambda$  6300 with altitude in twilight and day airglow may be able to show the importance of the two controlling processes (1a) and (1b) in the higher region of the F-layer.

#### EFFECT OF DIFFUSION ON ION DISTRIBUTIONS\*

Using the above values of  $\alpha^s$  and  $\beta^s$  ion densities are calculated, which are found to be lower than the observed values above 180 km. The discrepancy can be accounted for, if diffusion and vertical drift are taken into consideration.

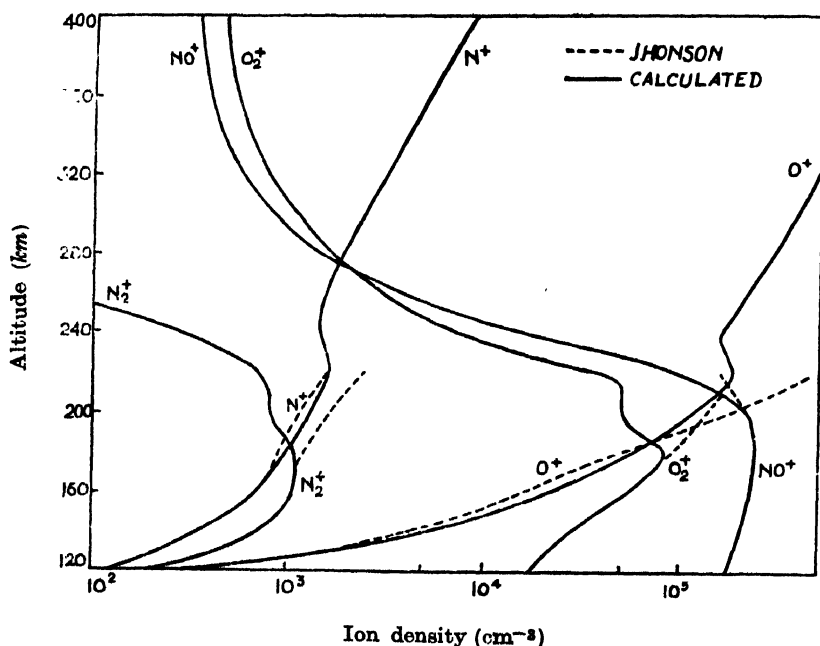


Fig. 3. The distribution of positive ions in the F-region of the ionosphere.

\*The diffusion of ions and electrons has been considered qualitatively by K. D. Sharma (D. Phil. thesis, University of Allahabad, 1962).

It is found that for altitudes between 200 and 220 km (above which the observed percentage ion distribution is not available), the discrepancy can be partially explained if the contribution due to diffusion is taken in the same proportion as the percentage of ions (Johnson, 1961) Fig. 3. To obtain more accurate agreement the vertical drift should also be considered.

#### EFFECT OF THE VERTICAL DRIFT

From the expression for the vertical drift, (Ferraro, 1961), we have

$$W = \frac{\delta}{\delta z} (Nw).$$

If it is assumed that the drift velocity,  $\omega$ , is constant at every altitude, we then have,

$$W = \frac{\delta N}{\delta z}$$

By assuming that the difference in the total number of positive ions and the electron density at 200 km is caused by the vertical drift,  $\omega$  is found to be about 16 metres/sec. This is of the same order as obtained by Ferraro (1961) in the F-region (10 metres/sec).

#### REFERENCES

- Aboud, A. A., Curtis, J. P., Mercure, R., and Rouse, W. A. 1955, *J. Opt. Soc. Am.*, **45**, 767.
- ARDC Model Atmosphere, 1959, Geophysical Research Directorate A. F., Cambridge Research Centre, Bedford, Mass., U.S.A.
- Bates, D. R. 1955, *Proc. Phys. Soc., London*, **A68**, 344.
- Bates, D. R., and Nicolet, M., 1960, *J. Atmos. Terr. Phys.*, **18**, 65.  
 „ 1961, *J. Atmos. Terr. Phys.* **21**, 286.
- Burkard, O. 1962, *J. Atmos. Terr. Phys.* **24**, 145.
- Bortner, M. H. and Baulknight C. W., 1961, Deionization Kinetics, Scientific Report No. 1, Contract No. AF19(604)-8820 AF Cambridge Research Centre.
- Dalgarno, A., 1958, *J. Atmos. Terr. Phys.*, **12**, 219.
- Dalgarno, A. and Parkinson, D., 1960, *J. Atmos. Terr. Phys.*, **18**, 335.
- Dickinson, P. H. G. and Sayers, J., 1960, *Proc. Phys. Soc.*, **76**, 137.
- Ghosh, S. N. and Sharma, K. D., 1961, *Planet. Space Sci.*, **8**, 9.
- Ghosh, S. N. and Shardanand, 1960, *Indian J. Phys.*, **34**, 516.  
 „ 1962, Progress Report 1960-61 JPK. Institute of Applied Physics, University of Allahabad, Allahabad, India.
- Havens, R. J., Friedman, H. and Hulbert, E. O., 1954, The Physics of the Ionosphere Conference, Cambridge, p. 237.
- Hertzberg, M., 1961, *J. Atmos. Terr. Phys.*, **20**, 177.
- Hinteregger, H. E., 1961, *J. Geophys. Res.* **66**, 2367.
- Johnson, C. Y., 1961, *Ann. Geophys.*, **17**, 100.
- Martyn, D. F., 1959, *Proc. Inst. Radio Engrs. NY.*, **47**, 147.
- Miller, J. E., 1957, *J. Geophys. Res.*, **62**, 351.
- Nisbet, J. S., 1960, *J. Geophys. Res.*, **65**, 2597.
- Watanabe, K., 1958, *Advances in Geophysics* Vol. 5, Academic Press, New York, p.153
- Weissler, G. L., Lees, P. and Mohr, E. I., 1952, *J. Opt. Soc. Am.*, **42**, 84.
- Yonezawa, T. and Takahashi, 1960, *J. Radio Res. Lab. (Japan)*, **7**, 335.

# *Letters to the Editor*

*The Board of Editors does not hold itself responsible for opinions expressed in the letters published in this section. The notes containing short reports of original investigations communicated to this section should not contain many figures and should not exceed 500 words in length. The contributions reaching the Secretary by the 15th of any month may be expected to appear in the issue for the next month. No proof will be sent to the author.*

## ANALYSIS OF GAMMA-RAY SPECTRUM OF RADIOACTIVE FALLOUT OVER CALCUTTA

SUSHIL KR. DAS, PRABIR K. SANDELL, R. C. SASTRI and  
S. D. CHATTERJEE

DEPARTMENT OF PHYSICS, JADAVPUR UNIVERSITY, CALCUTTA-32.

(Received February 25, 1964)

Systematic record of the intensity of  $\beta$  and  $\gamma$  rays emitted by precipitated samples of radioactive fallout has been maintained in our laboratory for over a couple of years. However, with the advent of the current monsoon season in May 1963, it was soon evident that the specific intensity of the rainborne radionuclides had increased considerably above the average value. Since the estimation of spectra necessitated somewhat more intense sources, the collected samples were grouped into fortnightly batches and assayed by direct measurement using a sodium iodide gamma scintillation spectrometer with a single-channel pulse height analyser (Type Philips P. W. 4082). The system was carefully calibrated with standard sources in a form simulating the samples to be assayed. Final measurements were, however, made with a NaI (3"  $\times$  3" bore hole) detector in conjunction with a Victoreen 800 channel Pulse-height analyser at the "Institut für Radiochemie en der Technischen Hochschule, München."

Fig. 1 shows the corrected  $\gamma$ -ray energy spectrum (range 0-2 Mev.), of a batch collected over a period of increased activity from June 1st to June 15, 1963, which was obtained after subtracting the background spectrum from the experimental curve. The radio-isotopes identified from the spectrum have been classified in Table A, in the order of increasing  $\gamma$ -energy.

Most of the radionuclides shown in Table A, have also been detected elsewhere by other groups of workers. For example, the Royal Cancer Hospital group

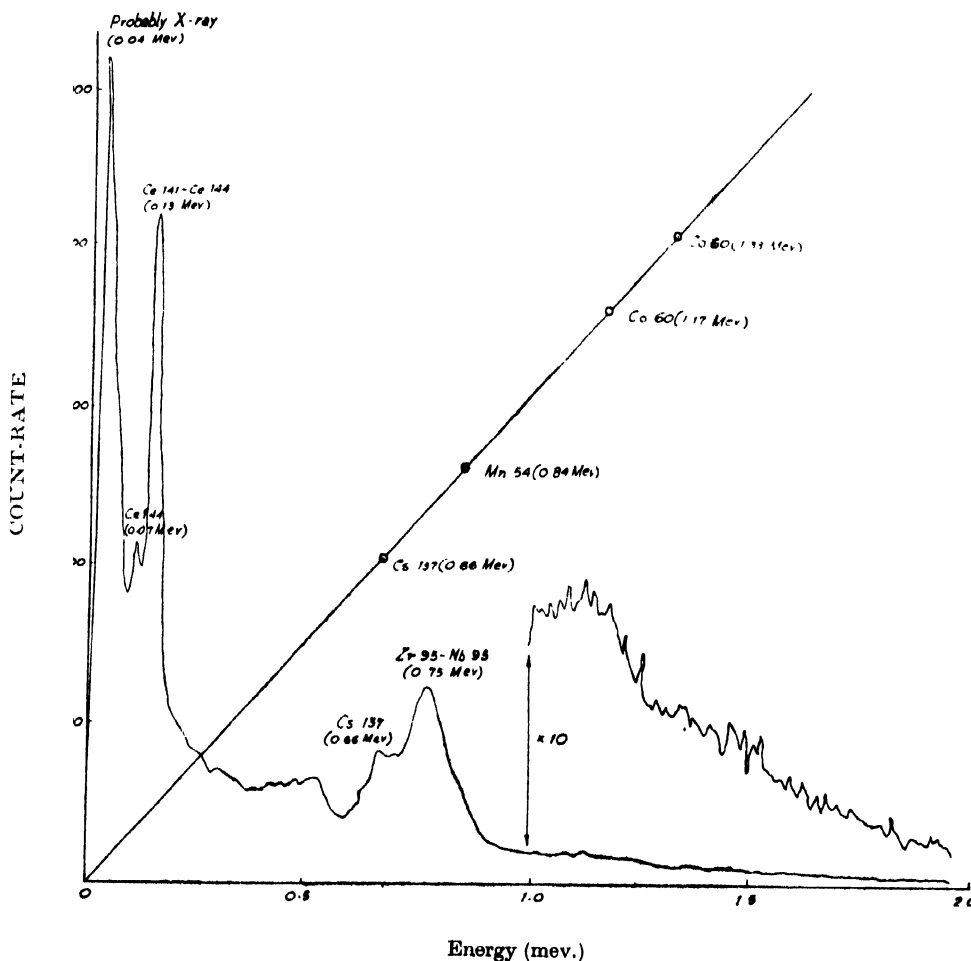


Fig. 1.

(Mayneord *et al.*, 1958, Anderson *et al.*, 1959, Anderson *et al.*, 1960) measuring radioactive fallout in London for a number of years, detected Cs-137, Ce-144, Zr-95, Nb-95, along with I-131, Ba-137m, Rh-106, Ru-103, Ba-140, La-140, and Pr-143. Working in Sweden, Aler *et al.*, (1956) detected the presence of Ce-141, Ce-144, Zr-95, Nb-95, Cs-137, and Ru-103. Vohra *et al.*, (1961) had also analysed the spectra of radioactive fallout at Bombay in 1960 after the French atomic test in Sahara and detected Ba-140, La-140, Zr-95, Nb95, Tc-99m, Ce-141, and Te-132.

TABLE A

Isotope	Energy (Mev)	Half-life
Ce-144	0.07	284d
Ce-141	0.13	30d
Ce-144	0.13	284d
Cs-137	0.66	30y
Zr-95	0.75	65d
Nb-95	0.75	35d

A fuller account of these measurements would be published elsewhere.

## REFERENCES

- Anderson, W., Bentley, R. E., Burton, L. K., Greutorex, C. A., 1960, *Nature*, **186**, 223.  
 Anderson, W., Bentley, R. E., Burton, L. K., Crookall, J. O., Greutorex, C. A., 1960, *Nature*, **186**, 925.  
 Mayneord, W. V., Anderson, W., Bentley, R. E., Burton, L. K., Crookall, J. O., Trott, N. G., 1958, *Nature*, **182**, 1473.  
 Aler, B., Bjornerstedt, R., Edvarson, K., Low, K., 1956, Forsvarets Forskningsanstalt., Avdelning 2, Dir., 2582-2092, Den 17/7.  
 Vohra, K. G., Bhatnagar, V. S., Rangarajan, C., 1961, *Ind. Jour. of Meteorology and Geophysics*, **12**, 250.

# MOLECULAR ORBITAL THEORY OF THE LIGAND FIELD IN TETRAHEDRALLY CO-ORDINATED $\text{Ni}^{2+}$ COMPLEXES

R. RAI AND S. MITRA

MAGNETISM DEPARTMENT,  
INDIAN ASSOCIATION FOR THE CULTIVATION OF SCIENCE  
JADAVPUR, CALCUTTA-32.

(Received, January 25, 1964)

A strong cubic ligand field splits the  $3d^8 {}^3F$  ground state of  $\text{Ni}^{2+}$  into three levels  ${}^3T_1$ ,  ${}^3T_2$  and  ${}^3A_2$  with separations of the order of  $10^4 \text{ cm}^{-1}$ . In tetrahedrally co-ordinated  $\text{Ni}^{2+}$  complexes, the cubic field coefficient is  $-4.9$  that of the octahedrally co-ordinated ones, so that (1) in the former the orbital triplets  ${}^3T_1$  lies lowest while in the latter it is the orbital singlet  ${}^3A_2$ ; also (2) the corresponding cubic separations in the former are less than half of those of the latter (Van Vleck, 1932; Gorter, 1932, Bleaney and Stevens, 1953).

A  $\text{Ni}^{2+}$  ion can be treated as a system consisting of two  $d$ -holes in which the three lowest states  ${}^3T_1(F)$ ,  ${}^3T_2(F)$  and  ${}^3A_2(F)$  arise out of  $(t_{2g})^2$ ,  $(t_{2g})^1(e_g)^1$  and  $(e_g)^2$  configurations respectively, so that the determinantal wavefunctions of the lowest triplet  ${}^3T_1(F)$  is

$$\begin{aligned}\psi_1 &= | t_o t_a | \\ \psi_2 &= | t_a t_b | \\ \psi_3 &= | t_b t_o | \end{aligned} \quad \dots \quad (1)$$

where  $t_a$ ,  $t_b$ ,  $t_o$  etc are single  $d$ -electron or hole orbitals in  $t_{2g}$  configuration, inclusive of the admixtures of excited  $3d^7 4p$  configuration orbitals (coming due to the absence of centre of inversion in the tetrahedral complexes) and of ligand  $s$ - and  $p$ -orbitals. Thus following Bates and others (Bates, 1962, Bates *et al*, 1962) and Wholfsberg and Helmutz (1952)

$$\begin{aligned}t_a = |xy> &= N \frac{1}{(1+\gamma^2)^{\frac{1}{2}}} \{dxy + \gamma |z>\} + \frac{\lambda}{2\sqrt{2}} \left\{ (\sigma_1 + \sigma_4 - \sigma_3) \right. \\ &\quad \left. + \frac{1}{2} (\pi_{x_3} + \pi_{x_2} - \pi_{x_1} - \pi_{x_4}) + \frac{\sqrt{3}}{4} (\pi_{y_4} + \pi_{y_1} - \pi_{y_2} - \pi_{y_3}) \right\} \end{aligned}$$

$$= |yz> = N \left[ \frac{1}{(1+\gamma^2)^{\frac{1}{2}}} \{dyz + \gamma |x>\} + \frac{\lambda}{2\sqrt{2}} \left\{ (\sigma_1 + \sigma_3 - \sigma_2 - \sigma_4) \right. \right.$$

$$\begin{aligned}
& + \frac{1}{2} (\pi x_4 + \pi x_2 - \pi x_1 - \pi x_3) + \frac{\sqrt{3}}{2} (\pi x_4 + \pi y_2 - \pi x_1 - \pi y_3) \Big\} \Big] \\
t_c = |xz\rangle = & N \left[ \frac{1}{(1+\gamma^2)^{\frac{1}{2}}} \{dxz + \gamma|y\rangle\} + \frac{\lambda}{2\sqrt{2}} (\sigma_1 + \sigma_2 - \sigma_3 - \sigma_4) \right. \\
& \left. + (\pi x_1 + \pi x_2 - \pi x_3 - \pi x_4) \Big\} \right]
\end{aligned}$$

where  $N$  is the normalizing factor;  $\lambda$  is a measure of amount of admixture of the ligand  $s$ - and  $p$ -orbitals with the central  $3d^8$  orbitals;  $dxz$  etc represent the large  $3d$  contributions and  $\gamma|z\rangle$  etc. the  $3d^8$   $4p$  contributions. Now if we choose trigonal axis as the axis of quantization, the appropriate orbital states for the lowest triplet is

$$\begin{aligned}
|+\rangle &= -\frac{1}{\sqrt{3}} [\omega|\psi_1\rangle + \omega^2|\psi_2\rangle + |\psi_3\rangle] \\
|0\rangle &= -\frac{1}{\sqrt{3}} [|\psi_1\rangle + |\psi_2\rangle + |\psi_3\rangle] \\
|-\rangle &= \frac{1}{\sqrt{3}} [\omega^2|\psi_1\rangle + \omega|\psi_2\rangle + |\psi_3\rangle]
\end{aligned}
\tag{3}$$

where

$$\omega = \exp \left( \frac{2\pi i}{3} \right)$$

and the appropriate Hamiltonian is

$$H = V_{trig} + \alpha u_{\xi} s_{\xi} + \alpha' (u_{\xi} s_{\xi} + u_{\eta} s_{\eta}) \tag{4}$$

where  $\alpha$  and  $\alpha'$  are the effective orbital Lande  $g$ -factors (Abragam *et al*, 1951) parallel and perpendicular to the trigonal axis and takes into account the effect of upper  ${}^3T_1(P)$ ,  ${}^3T_2(F)$  and  ${}^3A_2(F)$  with the lowest triplet  ${}^3T_1(F)$ . Operating upon wavefunctions (3) by above Hamiltonian and solving the secular determinant we get the resulting energies and wavefunctions, over which the magnetic perturbation  $H_1 = \beta H(L+2s)$  can be applied. Thus solving in detail the first order and second order magnetic perturbations as usual we have deduced an expression for the mean susceptibility for trigonally distorted  $Ni^{2+}$  tetrahedral complexes and have compared with experimental measurements on  $[Et_4N]_2[NiBr_4]$ . It may be mentioned here that  $[Et_4N]_2[NiBr_4]$  is a cubic crystal (space group  $P_{21}$ , with four ions in the unit cell,  $a = 15^\circ.5\text{\AA}$ ) and has a trigonal distortion of the



halogen tetrahedron round the  $\text{Ni}^{2+}$  ion, the trigonal axis passing through one halogen at the vertex of the tetrahedron and the  $\text{Ni}^{2+}$  ion and normal to the base formed by the other three equivalent halogens. (X-ray studies of Peter Pauling-reference by Gill *et al*, 1959)

TABLE.

Temp °K	$A_2$ $\text{cm}^{-1}$	$A_4$ $\text{cm}^{-1}$	$\Delta$ $\text{cm}^{-1}$			$k \times 10^6$ (Theo)	$k \times 10^6$ (Exp.)
300	291	80	- 780	0.94	1.67	5995	5986
260	282	88	- 900	0.90	1.69	6828	6840
180	265	95	-1020	0.876	1.71	9520	9536
140	254	102	-1096	0.84	1.73	11900	11909
100	245	110	-1110	0.761	1.76	15980	16000

From the above table we see that the agreement between the theoretical and experimental results is good, provided the second and fourth order trigonal field parameters  $A_2$  and  $A_4$  be allowed to change from  $291 \text{ cm}^{-1}$  and  $80 \text{ cm}^{-1}$  at room temperature to  $245 \text{ cm}^{-1}$  and  $110 \text{ cm}^{-1}$  at  $100^\circ\text{K}$ . These in turn change the trigonal separation  $\Delta$  from  $-780 \text{ cm}^{-1}$  to  $-1110 \text{ cm}^{-1}$ ,  $\alpha$  from .94 to .761 and  $\alpha'$  from 1.67 to 1.76. The values of the other parameters used are

$$Dq = 380 \text{ cm}^{-1}, \quad \zeta_{||} = -274 \text{ cm}^{-1} \quad \zeta_{\perp} = -217 \text{ cm}^{-1}$$

$$k_{||} = .95 \quad k_{\perp} = .80$$

where  $\zeta_{||}$  and  $\zeta_{\perp}$  are the effective spin-orbit coupling coefficients inclusive of the effects of  $3d^8$  and  $3d^74p$  configurational interaction and convalency overlap between the central orbitals of  $\text{Ni}^{2+}$  ion and  $s$  and  $p$  orbitals of the ligand atoms.  $k_{||}$  and  $k_{\perp}$  are the effective orbital reduction factors inclusive of the same interactions as above.

Details of the theoretical and experimental results will be published shortly elsewhere.

## ACKNOWLEDGMENT

The authors express their deep sense of gratitude to Prof. A. Bose, D.Sc., F.N.I. for his guidance and valuable suggestions.

## REFERENCES

- Abraham, A. and Pryce M. H. L. 1951, *Proc. Roy. Soc. A* **206**, 173.  
Bleaney, B. and Stevens K. W. H. 1953, *Reports on Prog. Phys.* **16**, 108.  
Bates, C. A. 1962, *Proc. Phys. Soc.* **78**, 69.  
Bates, C. A. Moore, W. S. Standley, K. J. and Stevens, K. W. H. 1962, *Proc. Phys. Soc.* **69**, 73.  
Gill M. S. and Nyholm R. S, 1959, *Jr. Chem. Soc.* 3997.  
Gorter, C. J. 1932, *Phys. Rev.* **42**, 427.  
Van Vleck J. H. 1932, *Phys. Rev.* **41**, 208.  
Wolfsberg, M. and Helm hol , L., 1952, *J. Chem. Phys.*, **20**, 837.

# ON A METHOD OF SIMPLIFICATION OF SWITCHING FUNCTIONS FOR SYNTHESIS OF THREE LEVEL CIRCUITS

A. K. CHOUDHURY AND S. R. DAS

INSTITUTE OF RADIO PHYSICS AND ELECTRONICS,  
UNIVERSITY OF CALCUTTA

(Received November 11, 1963)

**ABSTRACT.** A method of simplification of switching functions for synthesis of three-level circuits is presented. The method is an extension of the technique for simplification of switching functions for realising two-level circuits. The simplified expressions for synthesis of three-level circuits are obtained from the irredundant two-level covers of the functions by properly grouping the basic cells in the irredundant covers.

## INTRODUCTION

A switching function  $f(x_{n-1}, x_{n-2}, \dots, x_0)$  of  $n$  binary variables  $x_{n-1}, x_{n-2}, \dots, x_0$  can be written either as a sum of product terms or as a product of sum terms of the variables, the former being called the disjunctive normal form and the latter the conjunctive normal form of switching functions. Thus, when written as a sum of products, the switching function is expressed as

$$f(x_{n-1}, x_{n-2}, \dots, x_0) = \Sigma g_i \quad (1)$$

where  $g_i$ 's are each a product term of  $n$  or fewer number of variables. In this form, the switching function can be mechanised by a set of AND circuits feeding into an OR circuit. Alternatively, when the switching function is expressed as the product of the sum terms, the function is written as

$$f(x_{n-1}, x_{n-2}, \dots, x_0) = \Pi q_i \quad (2)$$

where  $q_i$ 's are the sum terms. This functional form is mechanised by a set of OR circuits feeding into an AND circuit. In the limiting case when the function can be expressed by a single product or sum term, a single AND or OR circuit is required for the mechanisation of the function. For certain functions, a two-level AND-OR realisation might give more economy than its OR-AND realisation in respect of the number of logical circuit elements (diodes or relay contacts). For others the reverse may be true. Methods have been suggested by several authors for obtaining the minimal two-level switching circuit in either of the two forms described above (Quine, 1952; 1955; Veitch, 1952; Karnaugh, 1953; Mc-

Cluskey, 1956; Urbano and Mueller, 1956; Roth, 1957; Svoboda, 1957; Mukhopadhyay, 1961; Choudhury and Basu, 1962).

It is well-known that many switching functions when mechanised by three-level OR-AND-OR or AND-OR-AND circuits require lesser number of logical circuit elements. For three-level circuit realisation a switching function is written as

$$f(x_{n-1}, x_{n-2}, \dots, x_0) = q_1 q_2 \dots + q_{1a} q_{2a} \dots + \dots \quad \dots \quad (3)$$

or as 
$$f(x_{n-1}, x_{n-2}, \dots, x_0) = (g_1 + g_2 + \dots)(g_{1a} + g_{2a} + \dots) \dots \quad (4)$$

where each of the terms of the form  $q_1 q_2 \dots$  or  $(g_1 + g_2 + \dots)$  is the product of the sum terms or the sum of the product terms respectively and can be realised by two-level circuits, the overall function being mechanised by three-level circuits. In the form of representation given in expression (3), the function is realised by an OR-AND-OR circuit whereas the form given in expression (4) can be mechanised by an AND-OR-AND circuit. The simplified three-level OR-AND-OR form of a switching function can be arrived at by splitting the function into a number of component functions and realising each of the component functions in OR-AND configuration. The simplified AND-OR-AND circuit realisation of the switching function can be obtained by first finding out the OR-AND-OR expression of the complementary function and then complementing the complementary function.

The available methods (Abhyankar, 1958; Veitch, 1959; Hurley, 1961) of realising OR-AND-OR or AND-OR-AND circuits of a switching function can be classified as

- (i) inhibiting method (Hurley, 1961),
- or (ii) pattern recognition in Veitch-Karnaugh maps (Veitch, 1959).

These methods though simple and straightforward suffer from the disadvantage that for their application one should be thoroughly acquainted with the functional patterns on the Veitch-Karnaugh map. Further, the difficulty of the pattern recognition in Veitch-Karnaugh map increases with the increase in the number of variables. In the present paper we shall suggest a method of obtaining simplified three-level expression of a switching function as a direct extension of the two-level minimisation process. The method mainly consists in finding the sets of basic  $k$ -cells of the function that are incident in  $(k+1)$ -cells. Only the basic cells in the irredundant covers of the function have to be searched for such incidence. A number of theorems has been proved in this connection, by the application of which three-level forms of a switching function are readily found out.

#### *n-Dimensional Cube as a Model of Switching Functions :*

With  $n$  binary variables,  $2^n$  different terms can be obtained where each term is a product of all the variables, either primed or unprimed. The terms can also

be represented as vertices of an  $n$ -cube. Such an  $n$ -cube is made up of cells of different dimensions (Urbano and Mueller, 1956; Svoboda, 1957), e.g.,

0-cell or vertex	a point	$k = 0$
1-cell	a line	$k = 1$
2-cell	a quadrilateral	$k = 2$
3-cell	a cube	$k = 3$
$k$ -cell		$k = k$

where  $k$  denotes the dimension of the cells. Total number of  $k$ -cells present in an  $n$ -cube is  ${}^nC_k \cdot 2^{n-k}$  where  $k$  may have any value from 0 to  $n$ . A switching function can be thought to be a collection of a set of vertices taken out of the  $2^n$  vertices of the  $n$ -cube. The cell complex and the basic cells of a given switching function will obviously depend on the vertices of the  $n$ -cube chosen for the representation of the function. If the form representing a switching function be an irredundant cover then the cell complex of the function consists of basic cells only. A minimal cover which consists of basic cells only is also an irredundant cover.

If any two vertices in the  $n$ -cube differ in  $k$  variables in their algebraic representations, then evidently they agree in  $(n-k)$  variables so that  $(n-k)$  variables are common in the algebraic representations of these two vertices. Since a  $k$ -cell requires  $(n-k)$  variables in its representation, there can be one and only one  $k$ -cell in the  $n$ -cube which can include those two vertices jointly. In such situations we will say that the vertices are incident in that particular  $k$ -cell. If in a function there are two basic  $k$ -cells, such that there are  $n-(k+1)$  variables common in their algebraic representation, there can be one and only one  $(k+1)$ -cell in the  $n$ -cube which includes these two  $k$ -cells jointly. These two  $k$ -cells are then similarly said to be incident in that particular  $(k+1)$ -cell.

Likewise if  $b$  basic  $k$ -cells of the  $n$ -cube are incident in a common  $(k+1)$ -cell, then in the disjunctive normal form of the function there will be disjunction of  $b$  terms where each term is the conjunction of  $(n-k)$  variables and these terms will have  $n-(k+1)$  variables common between them. The equivalent conjunctive normal form covering these basic  $k$ -cells will be the conjunction of two terms, one of which is the disjunction of  $b$  variables and the other conjunction of  $n-(k+1)$  variables.

#### *Basic Concepts and Theorems in Connection with Three-Level Simplification :*

Let us consider a cover of a switching function of  $n$  variables consisting only of  $b$  basic  $k$ -cells and let these basic  $k$ -cells be incident in a common  $(k+1)$ -cell. Then all these basic  $k$ -cells will be essential cells because if any of these basic  $k$ -cells is removed, then some of the vertices of the function will remain uncovered. The disjunction of these  $b$  terms representing  $b$ ,  $k$ -cells is the minimal form of the function. If we complement the function, multiply out the terms and drop all

the subsuming terms we will get the basic cells of the complementary function. In this complementary function also, all the basic cells will be essential cells since if any of these basic cells of the complementary function is dropped then the disjunction of the remaining basic cells will not be a cover of the complementary function.

Hence if  $b$  basic  $k$ -cells representing a switching function are incident in a common  $(k+1)$ -cell, then the minimal [AND-OR and OR-AND] expressions of the function can be written either as

$$f(x_{n-1}, x_{n-2}, \dots, x_0) = g_1 + g_2 + \dots + g_b = \text{Disjunction of } b \text{ terms where each term is the conjunction of } (n-k) \text{ variables... (5)}$$

$$\text{or as } f(x_{n-1}, x_{n-2}, \dots, x_0) = g_k \cdot q_l = [\text{Conjunction of } n-(k+1) \text{ variables}] \cdot [\text{Disjunction of } b \text{ variables}] \dots (6)$$

where the variables of  $g_k$  and  $q_l$  are all mutually exclusive.

Therefore if any switching function consists of  $b$  basic  $k$ -cells and if these  $k$ -cells are incident in a common  $(k+1)$ -cell, then the function may be mechanised by two different forms of two-level circuits. In one of the forms, we realise each of the  $b$   $k$ -cells separately so that the overall function can be mechanised by  $b$  AND circuits each with  $(n-k)$  inputs feeding into an OR circuit with  $b$  inputs. Alternatively, the function can be mechanised by an OR circuit with  $b$  inputs feeding into an AND circuit with  $(n-k)$  inputs. This second form of representation is evident from expression (6).

Total number of diodes required for the mechanisation of the function given in expression (5) i.e., as sum of  $b$   $k$ -cells is  $C_1 = [b(n-k) + b]$  whereas that required for the mechanisation of the function from expression (6) i.e., by an OR-AND circuit is  $C_2 = (n-k+b)$ . Table I gives the relative values of  $C_1$  and  $C_2$  for different values of  $n$ ,  $k$  and  $b$ .

TABLE I

$n$	$k$	$b$	$C_1$	$C_2$
4	1	2	8	5
5	1	2	10	6
6	1	2	12	7
7	1	2	14	8
8	1	2	16	9
4	2	2	6	4
5	2	2	8	5
6	2	2	10	6
7	2	2	12	7
8	2	2	14	8
4	2	3	9	5
5	2	3	12	6
6	2	3	15	7
7	2	3	18	8
8	2	3	21	9

A formal inspection of this table shows that economy can always be effected if a function be mechanised by an OR-AND circuit when the cell complex of the function is such that there are  $b$  basic  $k$ -cells incident in a  $(k+1)$ -cell.

If in an irredundant two-level cover of a switching function there are a number of different basic cells of which  $b$  basic  $k$ -cells are incident in a  $(k+1)$ -cell so that these  $k$ -cells can be realised in the OR-AND form, then the overall functional representation becomes a third-order expression and the function can be mechanised by a three-level OR-AND-OR circuit. To facilitate three-level realisations of switching function starting from its two-level irredundant covers, we shall discuss certain properties of the associated basic cells in the irredundant covers.

**Theorem 1 :** *The maximum number of basic  $k$ -cells that can be incident in a  $(k+1)$ -cell without covering all the vertices of the  $(k+1)$ -cell is  $(k+1)$ .*

*Proof :* When a number of basic  $k$ -cells are incident in a common  $(k+1)$ -cell, they can be represented as the product of two terms  $g_k q_l$  as shown in expression (6), where the variables of the terms are mutually exclusive. Of these two terms,  $g_k$  is a conjunction of  $n - (k+1)$  variables. So the disjunction terms  $q_l$  can consist of a maximum of  $(k+1)$  variables. Therefore the maximum number of basic  $k$ -cells that can be incident in a common  $(k+1)$ -cell without covering the  $(k+1)$ -cell is  $(k+1)$ .

**Theorem 2 :** *If  $b$  basic  $k$ -cells of a given function are incident in a common  $(k+1)$ -cell, the total number of different vertices covered by  $b$  basic  $k$ -cells is*

$$v_b = 2^k + 2^{k-1} + \dots + 2^{k-b+1} \quad \dots \quad (7)$$

*Proof :* If  $b$  basic  $k$ -cells are incident in a common  $(k+1)$ -cell they can be represented by the product of two terms  $g_k q_l$  as shown in expression (6) where  $g_k$  is the  $n - (k+1)$  variable term and  $q_l$  is the disjunction term  $(x_1 + x_2 + \dots + x_b)$  where the variables may be primed or unprimed. In this  $g_k x_1$  will cover  $2^k$  terms of the canonical form of the given function, corresponding to the vertices covered by the  $k$ -cell  $g_k x_1$ . Each such term covered by the  $k$ -cell  $g_k x_1$  is represented by the conjunction of  $n$  variables, either primed or unprimed. Of these  $n$  variables,  $(n-k)$  variables that are used for the representation of the  $k$ -cell  $g_k x_1$  are common for all the terms covered by the cell. Rest of the variables (i.e.,  $k$  variables) not included in the representation of the  $k$ -cell are present in their all possible combinations. Such is the case for the  $k$ -cell  $g_k x_2$ . Therefore of all the terms covered by the two  $k$ -cells, terms involving the variables  $g_k, x_1$  and  $x_2$  are common between the two  $k$ -cells. The number of such common terms is obviously

$$\frac{2^k}{2} \text{ or } 2^{k-1}$$

Therefore the total number of different terms or vertices covered by the two  $k$ -cells incident in a common  $(k+1)$ -cell but not covering a  $(k+1)$ -cell is

$$v_2 = 2^k + 2^{k-1}$$

If there are  $b$  basic  $k$ -cells incident in a  $(k+1)$ -cell, by similar argument it can be shown that the total number of different vertices covered by those  $b$  basic  $k$ -cells is

$$v_b = 2^k + 2^{k-1} + \dots + 2^{k-b+1}$$

The above result gives us a very easy procedure of testing whether a certain number of basic  $k$ -cells of a given switching function are incident in a common  $(k+1)$ -cell or not.

*Example :* Show whether the following two-cells are incident in a three-cell :

*Case (i).* Basic 2-cells of the function are :

$$(1) \quad (0, 1, 2, 3) = A$$

$$(2) \quad (0, 1, 4, 5) = B$$

$$(3) \quad (0, 1, 8, 9) = C$$

The total number of different terms covered by the three two-cells  $A$ ,  $B$ ,  $C$  is  $v_b = 8$ ; but for three two-cells to form part of a three-cell the total number of different terms to be covered should be  $v_b = 7$ . Therefore the three two-cells cannot be incident in a three-cell. But 2-cells  $(A, B)$  or  $(B, C)$  or  $(A, C)$  are incident in different 3-cells.

*Case (ii).* Basic two-cells of the function are :

$$(1) \quad (0, 1, 2, 3) = D$$

$$(2) \quad (0, 1, 4, 5) = E$$

$$(3) \quad (0, 2, 4, 6) = F$$

The total number of different terms covered by the three two-cells  $(D, E, F)$  is  $v_b = 7$ . Therefore these three two-cells are incident in a three cell.

We have already mentioned that if in an irredundant cover of a switching function, certain number of basic  $k$ -cells be incident in a common  $(k+1)$ -cell then those  $k$ -cells can be realised by OR-AND configuration with the net result that the overall function can be realised in three-level form and by such realisation economy may be achieved as compared to the two-level minimal form. The justification of starting from basic cells present in the irredundant covers as embracing a group of terms for three-level realisation lies in the fact that the total number of logical circuit elements (i.e., diodes) required to realise a basic  $(k+1)$ -cell as the sum of two or more  $k$ -cells is always greater than that required to realise the same as a  $(k+1)$ -cell, that is, as the conjunction of  $n-(k+1)$  variables.

We shall next show that by introducing redundant basic cells in the irredundant covers of switching functions, the resulting three-level realisations that we may obtain, will give under no circumstances economy as compared to the two-level realisations.



**Theorem 3 :** *If in an irredundant cover of a switching function consisting of a number of basic  $k$ -cells not incident in a  $(k+1)$ -cell, a  $k$ -cell is introduced from the subset of basic cells not included in the irredundant cover of the function, then by such incorporation of a redundant  $k$ -cell in the irredundant cover for three-level realisation, no economy is achieved.*

*Proof :* Since the  $k$ -cells present in the irredundant cover do not form part of a  $(k+1)$ -cell, therefore the number of common variables in the terms representing the  $k$ -cells should be less than  $(n-k-1)$ . If we now introduce a  $k$ -cell which can form part of a  $(k+1)$ -cell together with a  $k$ -cell already present in the irredundant cover, then  $(n-k-1)$  variables must be common between the two. And these  $(n-k-1)$  variables cannot be in common with any other  $k$ -cell. That is, by introducing one  $k$ -cell in the irredundant cover from the subsets of basic cells not included in the irredundant cover, we realise only one  $k$ -cell of the irredundant cover as being incident in a  $(k+1)$ -cell. Further, the total number of diodes required for realisation of a  $k$ -cell is equal to  $(n-k)$ . The total number of diodes required to realise two  $k$ -cells which are incident in a  $(k+1)$ -cell [as given in expression (6)], is  $(n+2-k)$  and is always greater than  $(n-k)$ . Therefore it follows that no economy can be effected in three-level realisation by incorporating a redundant  $k$ -cell in the irredundant cover.

If in an irredundant cover of a switching function, two or more of the basic  $k$ -cells are not incident in a  $(k+1)$ -cell, then ordinarily, under the conditions we are considering, we do not get any three-level cover. But certain operations and manipulation with the basic cells of this irredundant cover might lead to 3-level circuits with better economy over the irredundant two-level cover. The following theorem gives conditions under which such economic realisation might be possible.

**Theorem 4 :** *If in an irredundant cover of a switching function, the points that are uncovered due to the removal of a basic  $(k+1)$ -cell are covered by a  $k$ -cell belonging to the body of that basic  $(k+1)$ -cell and if this  $k$ -cell along with another basic  $k$ -cell in the irredundant cover be incident in a  $(k+1)$ -cell, then replacement of the basic  $(k+1)$ -cell by the  $k$ -cell which forms its part will lead to greater economy if the function is realised by a three-level circuit.*

*Proof :* Total number of diodes required for the realisation of the basic  $(k+1)$ -cell and the  $k$ -cell is

$$[n-(k+1)] + (n-k) + 2 = n-k+1 + n-k = 2(n-k) + 1$$

Total number of diodes required for the realisation of the two  $k$ -cells incident in a  $(k+1)$ -cell to replace these basic  $(k+1)$ -cell and  $k$ -cell is  $(n-k+2)$ . Since in the case that we are considering  $(n-k)$  will always be greater than one, the sum  $(n-k+2)$  will be always less than  $2(n-k)+1$ . It follows that under these conditions a three-level form will be more economical than the two-level irredundant form. If the irredundant cover under consideration happens to be a minimal

cover, then obviously the three-level circuit will require lesser number of circuit elements than the two-level circuit.

**Theorem 5 :** *In an irredundant cover, if a  $k$ -cell which is not included in a given  $(k+1)$ -cell can, along with  $k$ -cells of that  $(k+1)$ -cell be incident in different  $(k+1)$ -cells, then there can be only two different  $k$ -cells in the given  $(k+1)$ -cell with which it can so combine for incidence in two different  $(k+1)$ -cells.*

**Proof :** Total number of variables required to represent a  $(k+1)$ -cell is  $n-(k+1)$  whereas that required to represent a  $k$ -cell is  $(n-k)$ . If this  $k$ -cell along with a  $k$ -cell belonging to the body of the  $(k+1)$ -cell can be incident in a different  $(k+1)$ -cell, then these two  $k$ -cells can be represented as

$$g_k(x_i + x_j)$$

where the term  $g_k$  is the conjunction of  $n-(k+1)$  variables and  $x_i$  and  $x_j$  are single variable terms, all the variables being mutually exclusive. If such a representation is possible then it is evident that  $(n-k-2)$  variables must be common in the expression representing the  $(k+1)$ -cell and  $k$ -cell. Therefore it follows that in the body of the  $(k+1)$ -cell, there can be only two  $k$ -cells which can be incident in two different  $(k+1)$ -cells being combined with the existing  $k$ -cell.

As a consequence of theorems 4 and 5 it follows that if a  $k$ -cell belonging to the body of a basic  $(k+1)$ -cell be incident in a different  $(k+1)$ -cell being combined with the  $k$ -cells present in the irredundant cover, the total number of individual points or terms remaining uncovered by the withdrawal of the basic  $(k+1)$ -cell should not be greater than  $2^k/2$  i.e.,  $2^{k-1}$ . This evidently gives us a very easy method of recognising whether we can eliminate a  $(k+1)$ -cell and a  $k$ -cell and replace them by two  $k$ -cells which can be incident in a  $(k+1)$ -cell for economic three-level realisation. If the points remaining uncovered be greater than  $2^{k-1}$  then under no circumstances we can replace a basic  $(k+1)$ -cell in the irredundant cover by  $k$ -cells so as to be incident in different  $(k+1)$ -cells being combined with the existing basic  $k$ -cells. But if the points remaining uncovered due to such removal be less than  $2^{k-1}$ , then we may try to select  $k$ -cells from the body of that basic  $(k+1)$ -cell, such that these  $k$ -cells cover points remaining uncovered due to removal of the  $(k+1)$ -cell, and combine with the  $k$ -cells already present in the irredundant covers so as to be incident in different  $(k+1)$ -cells.

#### PROCEDURE FOR OBTAINING THREE-LEVEL COVERS

It is evident from the theorems proved earlier, that three-level realisations of switching functions can be obtained from its two-level irredundant covers. Detailed procedure for three-level simplification is given below :

(1) The prime implicants i.e., basic cells and the irredundant covers of the given switching function are first found out by any standard method (Quine, 1952; 1955; Veitch, 1952; Karnaugh, 1953; McCluskey, 1956; Urbano and

Mueller, 1956; Petrick, 1956; 1959; Roth, 1957; Svoboda, 1957; Ghazala, 1957; Mott, 1960; Mukhopadhyay, 1961; 1962; Choudhury and Basu, 1962; Mukherjee and Sarkar, 1963).

(2) Irredundant cover of the function is taken one at a time and then searched for whether different  $k$ -cells of the cover are incident in different  $(k+1)$ -cells. This can be done either comparing the algebraic expressions of the cells or by counting the total number of terms jointly covered by the cells. Depending on the nature of the function following different cases may arise in general.

*Case (i).*

All the  $k$ -cells that are present in the irredundant cover are such that each  $k$ -cell can combine with one or a group of  $k$ -cells to be incident in a distinct  $(k+1)$ -cell i.e., a  $k$ -cell does not share the parts of more than one  $(k+1)$ -cell. Method of finding three-level covers of such functions is illustrated by the following example.

*Example :*

Find the three-level cover of the five-variable switching function given by

$$f(x_4, x_3, x_2, x_1, x_0) = T = \Sigma (13, 14, 15, 16, 17, 18)$$

The basic cells of this function are

$$(1) \quad (16, 17)$$

$$(2) \quad (16, 18)$$

$$(3) \quad (13, 15)$$

$$\text{and} \quad (4) \quad (14, 15)$$

All the basic cells being essential basic cells, the only two-level irredundant cover (or the minimal cover) of this function is

$$C = (16, 17) + (16, 18) + (13, 15) + (14, 15)$$

The cost of realisation of this two-level minimal cover is 20 diodes.

To find the three-level cover from the irredundant cover  $C$ , we note that the one-cells (16, 17) and (16, 18) are incident in a two-cell and one-cells (13, 15) and (14, 15) are incident in another two-cell. Neither of these one-cells (16, 17), (16, 18), (13, 15), (14, 15) is incident in any other two-cell. The three-level cover is given by

$$C_m = (16, 17, 18) + (13, 14, 15)$$

which requires 14 diodes for its mechanisation. This gives a saving of 6 diodes over the two-level minimal form.

In some cases we will find that the basic  $k$ -cells of the function may be incident in different  $(k+1)$ -cells but the irredundant covers of the function are

such that in the covers each  $k$ -cell along with one or a group of  $k$ -cells is incident only in a distinct  $(k+1)$ -cell. Method of finding three-level covers of such functions is illustrated by the following example.

*Example :*

Find the three-level realisation of the following four variable switching function given by

$$f(x_3, x_2, x_1, x_0) = T = \Sigma(0, 1, 2, 5, 6, 7)$$

The basic cells of this function are:

(1)	(0, 1)
(2)	(0, 2)
(3)	(1, 5)
(4)	(2, 6)
(5)	(5, 7)
(6)	(6, 7)

The irredundant covers of the function are :

$$C_1 = (0, 1) + (0, 2) + (5, 7) + (6, 7)$$

$$C_2 = (0, 1) + (1, 5) + (2, 6) + (6, 7)$$

$$C_3 = (0, 2) + (1, 5) + (6, 7)$$

$$C_4 = (0, 1) + (2, 6) + (5, 7)$$

Of these irredundant covers,  $C_3$  and  $C_4$  represent the two-level minimal covers, cost of realisation of each of which is 12 diodes. Further, under the conditions we are considering (i.e., some of the  $k$ -cells of the cover being incident in  $(k+1)$ -cells, we do not get any three-level cover from these two minimal covers. But the irredundant covers  $C_1$  and  $C_2$  can be utilised to get three-level covers. In cover  $C_1$ , one-cells (0, 1) and (0, 2) are incident in a two-cell and one-cells (5, 7) and (6, 7) are incident in another two-cell, and these one-cells (0, 1), (0, 2), (5, 7) and (6, 7) are not incident in any other two-cells. The same is the case for cover  $C_2$ , where one-cells (0, 1) and (1, 5) are incident in a two-cell and one-cells (2, 6) and (6, 7) are incident in another two-cell. These three-level covers are

$$C_{1m} = (0, 1, 2) + (5, 6, 7)$$

$$C_{2m} = (0, 1, 5) + (2, 6, 7).$$

Cost of realisation of either of these three-level covers is 12 diodes which is the same as that required for the two-level minimal cover.

*Case (ii).*

In other cases, a  $k$ -cell may be incident in different  $(k+1)$ -cells along with different  $k$ -cells of the cover, that is, a  $k$ -cell will share parts of different

$(k+1)$ -cells along with different  $k$ -cells. The method of finding three-level covers for such functions is illustrated by the following example.

*Example :*

Find the economical three-level realisations of the following six-variable switching function:

$$f(x_5, x_4, x_3, x_2, x_1, x_0) = T = \Sigma(0, 1, 2, 3, 4, 5, 6, 7, 8, 9, 10, 11, 12, \\ 13, 14, 15, 16, 17, 18, 20, 21, 22, 24, \\ 25, 26, 28, 30, 32, 33, 34, 36, 37, 38, \\ 40, 41, 42, 44, 45, 48, 49, 50, 52, 53, \\ 54, 56, 57, 58, 60)$$

The basic cells of this function along with their algebraic representations are

- |     |   |             |
|-----|---|-------------|
| (1) | (0, 1, 2, 3, 4, 5, 6, 7, 8, 9, 10, 11, 12, 13, 14, 15)        | $-x_5'x_4'$ |
| (2) | (0, 1, 4, 5, 8, 9, 12, 13, 32, 33, 36, 37, 40, 41, 44, 45)    | $-x_4'x_1'$ |
| (3) | (0, 1, 4, 5, 16, 17, 20, 21, 32, 33, 36, 37, 48, 49, 52, 53)  | $-x_3'x_1'$ |
| (4) | (0, 1, 8, 9, 16, 17, 24, 25, 32, 33, 40, 41, 48, 49, 56, 57)  | $-x_2'x_1'$ |
| (5) | (0, 2, 4, 6, 8, 10, 12, 14, 16, 18, 20, 22, 24, 26, 28, 30)   | $-x_5'x_0'$ |
| (6) | (0, 2, 4, 6, 16, 18, 20, 22, 32, 34, 36, 38, 48, 50, 52, 54)  | $-x_3'x_0'$ |
| (7) | (0, 2, 8, 10, 16, 18, 24, 26, 32, 34, 40, 42, 48, 50, 56, 58) | $-x_2'x_0'$ |
| (8) | (0, 4, 8, 12, 16, 20, 24, 28, 32, 36, 40, 44, 48, 52, 56, 60) | $-x_1'x_0'$ |

All these basic cells being essential basic cells, only irredundant cover of the function is the disjunction of these essential basic cells.

To find the three-level covers from this two-level irredundant cover we shall search for  $k$ -cells of this cover incident in different  $(k+1)$ -cells. Here all the basic cells are four-cells and each of them is incident in different five-cells along with two or more of the remaining basic cells. If we designate the algebraic or numeric representation of the  $k$ -cells realised as being incident in  $(k+1)$ -cells by the term "three-level implicants", then the different three-level implicants that can be formed from the two-level basic cells of the irredundant cover of the given function will be

- (i)  $I = x_5'x_0' + x_5'x_4' = x_5'(x_0' + x_4')$
- (ii)  $J = x_5'x_4' + x_4'x_1' = x_4'(x_5' + x_1')$
- (iii)  $K = x_3'x_1' + x_3'x_0' = x_3'(x_1' + x_0')$
- (iv)  $L = x_2'x_1' + x_2'x_0' = x_2'(x_1' + x_0')$
- (v)  $M = x_4'x_1' + x_3'x_1' + x_2'x_1' + x_1'x_0' = x_1'(x_4' + x_3' + x_2' + x_0')$
- (vi)  $N = x_5'x_0' + x_3'x_0' + x_2'x_0' + x_1'x_0' = x_0'(x_5' + x_3' + x_2' + x_1')$

such that in the covers each  $k$ -cell along with one or a group of  $k$ -cells is incident only in a distinct  $(k+1)$ -cell. Method of finding three-level covers of such functions is illustrated by the following example.

*Example :*

Find the three-level realisation of the following four variable switching function given by

$$f(x_3, x_2, x_1, x_0) = T = \Sigma(0, 1, 2, 5, 6, 7)$$

The basic cells of this function are:

(1)	(0, 1)
(2)	(0, 2)
(3)	(1, 5)
(4)	(2, 6)
(5)	(5, 7)
(6)	(6, 7)

The irredundant covers of the function are :

$$C_1 = (0, 1) + (0, 2) + (5, 7) + (6, 7)$$

$$C_2 = (0, 1) + (1, 5) + (2, 6) + (6, 7)$$

$$C_3 = (0, 2) + (1, 5) + (6, 7)$$

$$C_4 = (0, 1) + (2, 6) + (5, 7)$$

Of these irredundant covers,  $C_3$  and  $C_4$  represent the two-level minimal covers, cost of realisation of each of which is 12 diodes. Further, under the conditions we are considering (i.e., some of the  $k$ -cells of the cover being incident in  $(k+1)$ -cells, we do not get any three-level cover from these two minimal covers. But the irredundant covers  $C_1$  and  $C_2$  can be utilised to get three-level covers. In cover  $C_1$ , one-cells (0, 1) and (0, 2) are incident in a two-cell and one-cells (5, 7) and (6, 7) are incident in another two-cell, and these one-cells (0, 1), (0, 2), (5, 7) and (6, 7) are not incident in any other two-cells. The same is the case for cover  $C_2$ , where one-cells (0, 1) and (1, 5) are incident in a two-cell and one-cells (2, 6) and (6, 7) are incident in another two-cell. These three-level covers are

$$C_{1m} = (0, 1, 2) + (5, 6, 7)$$

$$C_{2m} = (0, 1, 5) + (2, 6, 7).$$

Cost of realisation of either of these three-level covers is 12 diodes which is the same as that required for the two-level minimal cover.

*Case (ii).*

In other cases, a  $k$ -cell may be incident in different  $(k+1)$ -cells along with different  $k$ -cells of the cover, that is, a  $k$ -cell will share parts of different

$(k+1)$ -cells along with different  $k$ -cells. The method of finding three-level covers for such functions is illustrated by the following example.

*Example :*

Find the economical three-level realisations of the following six-variable switching function:

$$f(x_5, x_4, x_3, x_2, x_1, x_0) = T = \Sigma(0, 1, 2, 3, 4, 5, 6, 7, 8, 9, 10, 11, 12, \\ 13, 14, 15, 16, 17, 18, 20, 21, 22, 24, \\ 25, 26, 28, 30, 32, 33, 34, 36, 37, 38, \\ 40, 41, 42, 44, 45, 48, 49, 50, 52, 53, \\ 54, 56, 57, 58, 60)$$

The basic cells of this function along with their algebraic representations are

- |     |   |             |
|-----|---|-------------|
| (1) | (0, 1, 2, 3, 4, 5, 6, 7, 8, 9, 10, 11, 12, 13, 14, 15)        | $-x_5'x_4'$ |
| (2) | (0, 1, 4, 5, 8, 9, 12, 13, 32, 33, 36, 37, 40, 41, 44, 45)    | $-x_4'x_1'$ |
| (3) | (0, 1, 4, 5, 16, 17, 20, 21, 32, 33, 36, 37, 48, 49, 52, 53)  | $-x_3'x_1'$ |
| (4) | (0, 1, 8, 9, 16, 17, 24, 25, 32, 33, 40, 41, 48, 49, 56, 57)  | $-x_2'x_1'$ |
| (5) | (0, 2, 4, 6, 8, 10, 12, 14, 16, 18, 20, 22, 24, 26, 28, 30)   | $-x_5'x_0'$ |
| (6) | (0, 2, 4, 6, 16, 18, 20, 22, 32, 34, 36, 38, 48, 50, 52, 54)  | $-x_3'x_0'$ |
| (7) | (0, 2, 8, 10, 16, 18, 24, 26, 32, 34, 40, 42, 48, 50, 56, 58) | $-x_2'x_0'$ |
| (8) | (0, 4, 8, 12, 16, 20, 24, 28, 32, 36, 40, 44, 48, 52, 56, 60) | $-x_1'x_0'$ |

All these basic cells being essential basic cells, only irredundant cover of the function is the disjunction of these essential basic cells.

To find the three-level covers from this two-level irredundant cover we shall search for  $k$ -cells of this cover incident in different  $(k+1)$ -cells. Here all the basic cells are four-cells and each of them is incident in different five-cells along with two or more of the remaining basic cells. If we designate the algebraic or numeric representation of the  $k$ -cells realised as being incident in  $(k+1)$ -cells by the term "three-level implicants", then the different three-level implicants that can be formed from the two-level basic cells of the irredundant cover of the given function will be

- (i)  $I = x_5'x_0' + x_5'x_4' = x_5'(x_0' + x_4')$
- (ii)  $J = x_5'x_4' + x_4'x_1' = x_4'(x_5' + x_1')$
- (iii)  $K = x_3'x_1' + x_3'x_0' = x_3'(x_1' + x_0')$
- (iv)  $L = x_2'x_1' + x_2'x_0' = x_2'(x_1' + x_0')$
- (v)  $M = x_4'x_1' + x_3'x_1' + x_2'x_1' + x_1'x_0' = x_1'(x_4' + x_3' + x_2' + x_0')$
- (vi)  $N = x_5'x_0' + x_3'x_0' + x_2'x_0' + x_1'x_0' = x_0'(x_5' + x_3' + x_2' + x_1')$

Next we shall find the irredundant three-level covers of the two-level basic cells by utilising a table (Table II).

TABLE II

	I	J	K	L	M	N
$x'_5x'_0$	1					1
$x'_5x'_4$	1	1				
$x'_4x'_1$		1			1	
$x'_3x'_1$			1		1	
$x'_3x'_0$			1			1
$x'_2x'_1$				1	1	
$x'_2x'_0$				1		1
$x'_1x'_0$					1	1

In this table, the column headings indicate three-level implicants whereas the row headings indicate two-level basic cells, 1's in the subcharts denoting which particular group of two-level basic cells form three-level implicants. From this table, the three-level irredundant covers (Mukherjee and Sarkar, 1963) are found to be :

- (i) *IMKL*
- (ii) *IMN*
- (iii) *JNM*
- (iv) *JNKL*

From each of these three-level irredundant covers different three-level covers are found by eliminating those cells which occur more than once, thus introducing redundancy. Let us first take up the three-level irredundant cover *IMKL*. In this three-level irredundant cover, two-level basic cell  $x'_1x'_3$  occurs in both of the three-level implicants *M* and *K*. Similarly, two-level basic cell  $x'_1x'_2$  occurs in both of *M* and *L*. Since in the minimal three-level cover the same two-level basic cell cannot occur more than once, so to avoid redundancy, the three-level irredundant cover *IMKL* is expanded in the form of a table (Table III) as shown below. Here  $x'_1x'_3$  can occur either in *M* or *K* and with each occurrence of  $(x'_1x'_3)$  there are two possible choices of  $(x'_1x'_2)$  in either *M* or *L*. Hence altogether we get four possible configurations, giving four possible three-level covers.

TABLE III

I			M				K			L		
$x'_5(x'_0+x'_4)$			$x'_1(x'_4+x'_3+x'_2+x'_0)$				$x'_3(x'_1+x'_0)$			$x'_2(x'_1+x'_0)$		
1	1	1	1	1	0	0	1	1	1	1	1	1
1	1	1	1	1	0	1	1	1	1	1	0	1
1	1	1	1	1	1	0	1	1	0	1	1	1
1	1	1	1	1	1	1	1	1	0	1	1	0



From this, the three-level covers are :

$$\begin{aligned} C_{im_1} &= x'_5(x'_0+x'_4)+x'_1(x'_4+x'_0)+x'_3(x'_4+x'_0)+x'_2(x'_1+x'_0) \\ C_{im_2} &= x'_5(x'_0+x'_4)+x'_1(x'_4+x'_2+x'_0)+x'_3(x'_1+x'_0)+x'_2x'_0 \\ C_{im_3} &= x'_5(x'_0+x'_4)+x'_1(x'_4+x'_3+x'_0)+x'_3x'_0+x'_2(x'_1+x'_0) \\ C_{im_4} &= x'_5(x'_0+x'_4)+x'_1(x'_4+x'_3+x'_2+x'_0)+x'_3x'_0+x'_2x'_0 \end{aligned}$$

Similarly, expanding the cover  $IMN$ , we get

TABLE IV

I			M					N				
$x'_5(x'_0+x'_4)$			$x'_1(x'_4+x'_3+x'_2+x'_0)$					$x'_0(x'_5+x'_3+x'_2+x'_1)$				
1	1	1	1	1	1	1	1	1	0	1	1	0
1	1	1	1	1	1	1	0	1	0	1	1	1
1	0	1	1	1	1	1	1	1	1	1	1	0
1	0	1	1	1	1	1	0	1	1	1	1	1

From this, the simplest three-level covers are

$$\begin{aligned} C'_{jm_1} &= x'_5(x'_0+x'_4)+x'_1(x'_4+x'_3+x'_2+x'_0)+x'_0(x'_3+x'_2) \\ C'_{jm_2} &= x'_5(x'_0+x'_4)+x'_1(x'_4+x'_3+x'_2)+x'_0(x'_3+x'_2+x'_1) \\ C'_{jm_3} &= x'_5x'_4+x'_1(x'_4+x'_3+x'_2+x'_0)+x'_0(x'_5+x'_3+x'_2) \\ C'_{jm_4} &= x'_5x'_4+x'_1(x'_4+x'_3+x'_2)+x'_0(x'_5+x'_3+x'_2+x'_1) \end{aligned}$$

Likewise, the three-level covers from the irredundant covers  $JNM$  and  $JNKL$  are, respectively :

$$\begin{aligned} C'_{km_1} &= x'_4(x'_5+x'_1)+x'_0(x'_5+x'_3+x'_2+x'_1)+x'_1(x'_3+x'_2) \\ C'_{km_2} &= x'_4(x'_5+x'_1)+x'_0(x'_5+x'_3+x'_2)+x'_1(x'_3+x'_2+x'_0) \\ C'_{km_3} &= x'_4x'_5+x'_0(x'_5+x'_3+x'_2+x'_1)+x'_1(x'_4+x'_3+x'_2) \\ C'_{km_4} &= x'_4x'_5+x'_0(x'_5+x'_3+x'_2)+x'_1(x'_4+x'_3+x'_2+x'_0) \end{aligned}$$

and

$$\begin{aligned} C'_{lm_1} &= x'_4(x'_5+x'_1)+x'_0(x'_5+x'_1)+x'_3(x'_1+x'_0)+x'_2(x'_1+x'_0) \\ C'_{lm_2} &= x'_4(x'_5+x'_1)+x'_0(x'_5+x'_2+x'_1)+x'_3(x'_1+x'_0)+x'_2x'_1 \\ C'_{lm_3} &= x'_4(x'_5+x'_1)+x'_0(x'_5+x'_3+x'_1)+x'_3x'_1+x'_2(x'_1+x'_0) \\ C'_{lm_4} &= x'_4(x'_5+x'_1)+x'_0(x'_5+x'_3+x'_2+x'_1)+x'_3x'_1+x'_2x'_1 \end{aligned}$$

From an inspection of all these three-level covers, we see that the most economical three-level cover is

$$\begin{aligned} C_{min} &= x'_5(x'_0+x'_4)+x'_1(x'_4+x'_0)+x'_3(x'_1+x'_0)+x'_2(x'_1+x'_0) \\ &= (x'_4+x'_0)(x'_5+x'_1)+(x'_1+x'_0)(x'_3+x'_2) \end{aligned}$$

The three-level circuits of the switching functions, whose irredundant covers can be written in a compact form by following a procedure recently suggested by Mukherjee and Sarkar (1963), can be found readily even when the total number of such covers are very large.

These compact forms of representation aid in obtaining the three-level expressions of switching function without trying all the irredundant covers one at a time, which involves large amount of labour when the total number of such covers is very large. The following example will suggest the method of obtaining three-level expressions of switching function starting from its compact forms of irredundant expressions.

*Example :*

Find the economical three-level realisation of the seven-variable switching function given by

$$f(x_6, x_5, x_4, x_3, x_2, x_1, x_0) = T = \Sigma(0, 2, 5, 8, 10, 12, 13, 16, 18, 21, 24, 26, \\ 28, 29, 30, 32, 34, 37, 39, 40, 42, 45, 46, \\ 48, 50, 53, 55, 56, 58, 61, 64, 65, 67, 72, \\ 73, 77, 78, 79, 80, 81, 83, 88, 89, 91, 95, \\ 100, 102, 106, 107, 111, 114, 116, 120, \\ 122, 126, 127)$$

The basic cells of this function, along with their algebraic representations, are :

- |   |                            |       |
|---|----------------------------|-------|
| (1) (0, 2, 8, 10, 16, 18, 24, 26, 32, 34, 40, 42, 48, 50, 56 58)* | $= x'_6 x'_2 x'_0$         | $A^*$ |
| (2) (5, 13, 21, 29, 37, 45, 53, 61)*                              | $= x'_6 x_2 x'_1 x_0$      | $B^*$ |
| (3) (64, 65, 72, 73, 80, 81, 88, 89)                              | $= x'_6 x'_5 x'_2 x'_1$    | $C'$  |
| (4) (0, 8, 16, 24, 64, 72, 80, 88)                                | $= x_5 x'_2 x'_1 x'_0$     | $D$   |
| (5) (79, 95, 111, 127)  | $= x_6 x_3 x_2 x_1 x_0$    | $E$   |
| (6) (81, 83, 89, 91)  | $= x_6 x'_5 x_4 x'_2 x_0$  | $F$   |
| (7) (56, 58, 120, 122)  | $= x_5 x_4 x_3 x'_2 x'_0$  | $G$   |
| (8) (50, 58, 114, 122)*   | $= x_5 x_4 x'_2 x_1 x'_0$  | $H^*$ |
| (9) (42, 58, 106, 122)  | $= x_5 x_3 x'_2 x_1 x'_0$  | $I$   |
| (10) (37, 39, 53, 55)*  | $= x'_6 x_6 x'_3 x_2 x_0$  | $J^*$ |
| (11) (65, 67, 81, 83)*  | $= x_6 x'_5 x'_3 x'_2 x_0$ | $K^*$ |
| (12) (24, 56, 88, 120)  | $= x_4 x_3 x'_2 x'_1 x'_0$ | $L$   |
| (13) (24, 26, 28, 30)*  | $= x'_6 x'_5 x_4 x_3 x'_0$ | $M^*$ |
| (14) (12, 13, 28, 29)   | $= x'_6 x'_5 x_3 x_2 x'_1$ | $N$   |

(15)	$(8, 12, 24, 28) = x'_6 x'_5 x_3 x'_1 x'_0$	<i>O</i>
(16)	$(126, 127) = x_6 x_5 x_4 x_3 x_2 x_1$	<i>P</i>
(17)	$(122, 126) = x_6 x_5 x_4 x_3 x_1 x'_0$	<i>Q</i>
(18)	$(107, 111) = x_6 x_5 x'_4 x_3 x_1 x_0$	<i>R</i>
(19)	$(91, 95) = x_6 x'_5 x_4 x_3 x_1 x_0$	<i>S</i>
(20)	$(106, 107) = x_6 x_5 x'_4 x_3 x'_2 x_1$	<i>T</i>
(21)	$(78, 79)^* = x_6 x'_5 x'_4 x_3 x_2 x_1$	<i>U*</i>
(22)	$(77, 79) = x_6 x'_5 x'_4 x_3 x_2 x_0$	<i>V</i>
(23)	$(100, 116)^* = x_6 x_5 x'_3 x_2 x'_1 x'_0$	<i>W*</i>
(24)	$(100, 102)^* = x_6 x_5 x'_4 x'_3 x_2 x'_0$	<i>X*</i>
(25)	$(73, 77) = x_6 x'_5 x'_4 x_3 x'_1 x_0$	<i>Y</i>
(26)	$(42, 46)^* = x'_6 x_5 x'_4 x_3 x_1 x'_0$	<i>Z*</i>
(27)	$(13, 77) = x'_5 x'_4 x_3 x_2 x'_1 x_0$	

In the above, basic cells marked by asterisk are essential basic cells. Therefore these basic cells will occur in all the irredundant covers of the function.

The compact expressions for the irredundant forms of this function are given below.

$$(ABHJKMUWXZ) \begin{bmatrix} O \\ N \end{bmatrix} C \begin{bmatrix} V \\ Y \\ a \end{bmatrix} \begin{bmatrix} G \\ L \end{bmatrix} FEIR \begin{bmatrix} P \\ Q \end{bmatrix} \quad \dots \quad (i)$$

$$(ABHJKMUWXZ) \begin{bmatrix} O \\ N \end{bmatrix} C' \begin{bmatrix} V \\ Y \\ a \end{bmatrix} \begin{bmatrix} G \\ L \end{bmatrix} FET \begin{bmatrix} P \\ Q \end{bmatrix} \quad \dots \quad (ii)$$

$$(ABHJKMUWXZ) \begin{bmatrix} O \\ N \end{bmatrix} C \begin{bmatrix} V \\ Y \\ a \end{bmatrix} \begin{bmatrix} G \\ L \end{bmatrix} SIR \begin{bmatrix} P \\ QE \end{bmatrix} \quad \dots \quad (iii)$$

$$(ABHJKMUWXZ) \begin{bmatrix} O \\ N \end{bmatrix} C \begin{bmatrix} V \\ Y \\ a \end{bmatrix} \begin{bmatrix} G \\ L \end{bmatrix} STE \begin{bmatrix} P \\ Q \end{bmatrix} \quad \dots \quad (iv)$$

$$(ABHJKMUWXZ) \begin{bmatrix} O \\ N \end{bmatrix} C \begin{bmatrix} V \\ Y \\ a \end{bmatrix} \begin{bmatrix} G \\ L \end{bmatrix} STRP \quad \dots \quad (v)$$

$$(ABHJKMUWXZ) \begin{bmatrix} O \\ N \end{bmatrix} DYF \begin{bmatrix} G \\ L \end{bmatrix} IRE \begin{bmatrix} P \\ Q \end{bmatrix} \quad \dots \quad (vi)$$

$$(ABHJKMUWXZ) \begin{bmatrix} O \\ N \end{bmatrix} D Y F \begin{bmatrix} G \\ L \end{bmatrix} I R S P \quad \dots \quad \text{(vii)}$$

$$(ABHJKMUWXZ) \begin{bmatrix} O \\ N \end{bmatrix} D Y F \begin{bmatrix} G \\ L \end{bmatrix} T E \quad \dots \quad \text{(viii)}$$

$$(ABHJKMUWXZ) \begin{bmatrix} O \\ N \end{bmatrix} D Y F \quad T S R P \quad \text{(ix)}$$

In the expressions for the irredundant forms of the function it will be found that certain prime implicants are written in a column matrix. In order to obtain all the irredundant covers, each of these expressions has to be expanded. Of the prime implicants written in any column matrix, only one of the prime implicants taken at a time can be associated with other prime implicants of the expression. In the expression (i), the prime implicants  $A, B, H, J, K, M, U, W, X, Z, C, F, E, I, R$ , have to be associated with either  $O$  or  $N$  (but not with  $ON$  jointly). With these two different choices must be associated three different choices of

the prime implicants from the column matrix  $\begin{bmatrix} V \\ Y \\ a \end{bmatrix}$ , two different choices from the column matrix  $\begin{bmatrix} G \\ L \end{bmatrix}$  and two different choices from the column

matrix  $\begin{bmatrix} P \\ Q \end{bmatrix}$ . Thus a total of  $2 \times 3 \times 2 \times 2 = 24$  different irredundant covers of the function will be obtained from the expression (i).

To find three-level covers from these compact forms of irredundant covers, we shall first form the "three-level implicants" from the sets of prime implicants. These three-level implicants are :

- (1)  $CD = x'_5 x'_2 x'_1 (x_6 + x'_0)$
- (2)  $GH = x_5 x_4 x'_2 x'_0 (x_3 + x_1)$
- (3)  $GI = x_5 x_3 x'_2 x'_0 (x_4 + x_1)$
- (4)  $GL = x_4 x_3 x'_2 x'_0 (x_6 + x'_1)$
- (5)  $FK = x_6 x'_5 x'_2 x'_0 (x_4 + x'_3)$
- (6)  $MO = x'_6 x'_5 x_3 x'_0 (x_4 + x'_1)$
- (7)  $HI = x_5 x'_2 x_1 x'_0 (x_4 + x_3)$
- (8)  $NO = x'_6 x'_5 x_3 x'_1 (x_2 + x'_0)$
- (9)  $PQ = x_6 x_5 x_4 x_3 x_1 (x_2 + x'_0)$
- (10)  $RT = x_6 x_5 x'_4 x_3 x_1 (x'_2 + x_0)$
- (11)  $UV = x_6 x'_5 x'_4 x_3 x_2 (x_1 + x_0)$

$$(12) \quad VY = x_6x'_6x'_4x_3x_0(x_4+x'_1)$$

$$(13) \quad WX = x_6x_5x_3x'_2x'_0(x'_4+x'_1)$$

$$(14) \quad Ya = x'_5x'_4x_3x'_1x_0(x_5+x_2)$$

The simplified three-level forms are found out from the compact two-level irredundant forms in the following way. We have already observed that the irredundant cover

$$ABHJKMUWXZ \begin{bmatrix} O \\ N \end{bmatrix} C \begin{bmatrix} V \\ Y \\ a \end{bmatrix} \begin{bmatrix} G \\ L \end{bmatrix} FEIR \begin{bmatrix} P \\ Q \end{bmatrix} \quad \dots \quad (i)$$

when expanded will yield 24 different irredundant covers of the given function. Some prime implicants will be common in all the covers and the different covers are obtained from the combination of the prime implicants in the column matrix. Therefore for obtaining economic three-level circuits from the above expression (i), the expression is simplified by retaining only those prime implicants in the column matrix which can combine with others to form three-level implicants.

Following this procedure, the column matrix  $\begin{bmatrix} O \\ N \end{bmatrix}$  is simplified by retaining only the prime implicant  $O$ . Because from the list of the three-level implicants we find that the prime implicant  $N$  can combine with  $O$  only and in any irredundant cover  $O$  and  $N$  cannot occur jointly. Similarly, column matrix  $\begin{bmatrix} V \\ Y \\ a \end{bmatrix}$  is simplified by retaining only  $V$ .

Hence the expression (i) can be written as,

$$ABHJKMUWXZOCV \begin{bmatrix} G \\ L \end{bmatrix} FEIR \begin{bmatrix} P \\ Q \end{bmatrix} \quad \dots \quad (x)$$

Thus without checking all the 24 covers, by simple inspection, we have found out that out of the 24 irredundant covers only four need be tried for economic three-level circuit synthesis.

Now noting that  $W$  combines with  $X$ ,  $M$  with  $O$ ,  $F$  with  $K$ ,  $V$  with  $U$ ,  $G$  with either of  $H$  or  $I$ , each to give three-level implicants, the simplified three-level expression that can be written from the compact two-level irredundant cover (i) is

$$ABJZCER(WX)(MO)(FK)(VU) \begin{bmatrix} P \\ Q \end{bmatrix} \begin{bmatrix} (GH) & I \\ (GI) & H \\ (HI) & [G] \\ & [L] \end{bmatrix} \quad \dots \quad (xi)$$

where the expressions within the first brackets are three-level implicants. Similar three-level expressions can be obtained from other compact two-level irredundant covers. Total number of three-level covers that can be obtained by expanding the expression (xi) is  $2 \times 4 = 8$ .

All the three-level covers that can be obtained from the irredundant forms (i-ix) are given below, along with their cost numbers.

Three-level covers		Cost number	
(i)	$ABJZCER(WX)(MO)(FK)(VU)$	$\begin{bmatrix} P \\ Q \end{bmatrix} \begin{bmatrix} (GH) & I \\ (GI) & H \\ (HI) & \begin{bmatrix} G \\ L \end{bmatrix} \end{bmatrix}$	... 95
(ii)	$ABJZCET(WX)(MO)(FK)(VU)$	$\begin{bmatrix} P \\ Q \end{bmatrix} (GH)$	... 89
(iii)	$ABJKZCSR(WX)(MO)(VU)P$	$\begin{bmatrix} (GH) & I \\ (GI) & H \\ (HI) & \begin{bmatrix} G \\ L \end{bmatrix} \end{bmatrix}$	... 94
(iv)	$ABJKZCSTE$	$\begin{bmatrix} P \\ Q \end{bmatrix} (WX)(MO)(VU)(GH)$	... 94
(v)	$ABJKZCSP(WX)(MO)(VU)(GH)(RT)$		... 90
(vi)	$ABJUZYRE$	$\begin{bmatrix} P \\ Q \end{bmatrix} (WX)(MO)(FK) \begin{bmatrix} (GH) & I \\ (GI) & H \\ (HI) & \begin{bmatrix} G \\ L \end{bmatrix} \end{bmatrix}$	... 100
(vii)	$ABJUZYRSP(WX)(MO)(FK)$	$\begin{bmatrix} (GH) & I \\ (GI) & H \\ (HI) & \begin{bmatrix} G \\ L \end{bmatrix} \end{bmatrix}$	... 101
(viii)	$ABJUZYTE$	$\begin{bmatrix} P \\ Q \end{bmatrix} (WX)(MO)(FK)(GH)$	... 94
(ix)	$ABJUZYSP(WX)(MO)(FK)(GH)(RT)$		... 97

From the above three-level covers, we see that the most economical three-level cover is

$$\begin{aligned}
 C_m &= ABJEZCTP(WX)(MO)(VU)(GH)(FK) \\
 &= x'_6 x'_2 x'_0 + x'_6 x'_2 x'_1 x_0 + x_6 x'_5 x'_2 x'_1 + x'_6 x_5 x'_3 x_2 x_0 + x_6 x_3 x_2 x_1 x_0 \\
 &\quad + x_6 x_5 x_4 x_3 x_2 x_1 + x_6 x_5 x'_4 x_3 x'_2 x_1 + x'_6 x_5 x'_4 x_3 x_1 x'_0 + x'_6 x'_5 x_3 x'_0 (x_4 + x'_1) \\
 &\quad + x_6 x'_5 x'_4 x_3 x_2 (x_1 + x_0) + x_6 x'_5 x'_2 x_0 (x_4 + x'_3) + x_6 x_5 x'_3 x_2 x'_0 (x'_4 + x'_1) \\
 &\quad + x_6 x_4 x'_2 x'_0 (x_3 + x_1)
 \end{aligned}$$

## CONCLUSION

A simple and straightforward method is suggested for obtaining economic three-level circuit realisations of switching functions starting from the two-level irredundant covers. When the  $k$ -cells of the functions share the parts of different  $(K+1)$ -cells, it is possible to find the best three-level cover of the function by finding the three-level irredundant covers of the prime implicants which can form different three-level implicants. In cases where the function has a large number of two-level irredundant covers, if these covers can be written in compact forms, then the three-level covers of the function can be found very easily from the two-level irredundant covers without trying all of them at a time.

## ACKNOWLEDGMENT

The authors wish to express their indebtedness to Prof. J. N. Bhar, D.Sc., F.N.I., for guidance and keen interest in the work. One of the authors, Shri Das also thankfully acknowledges the award of a Research Fellowship by the U.G.C., Government of India, while doing the work (May–August 1962).

## REFERENCES

- Abhyankar, S., 1958, *Trans. Inst. Radio Engrs.*, N. Y., **EC-7**, 268.  
 Choudhury, A. K. and Basu, M. S., 1962, *Indian Journal of Physics*, **36**, 1; 1962, *Trans. Inst. Radio Engrs.*, N. Y., **EC-11**, 713.  
 Ghazala, M. J., 1957, *I.B.M. Journal of Research and Development*, **1**, 171.  
 Karnaugh, M., 1953, *Trans. A.I.E.E.*, Part I, **72**, 593.  
 Mott, T. H. (Jr.), 1961, *Trans. Inst. Radio Engrs.*, N. Y., **EC-9**, 245.  
 McCluskey, E. J. (Jr.), 1956, *Bell System Technical Journal*, **35**, 1417.  
 Mukhopadhyay, A., 1961, I.E.E. Monograph No. 487E; 1962, Doctoral Thesis to the University of Calcutta.  
 Mukherjee, T. and Sarkar, P., 1963, *Electronics and Control*, **14**, 563.  
 Petrick, S. R., 1956, Air Force Cambridge Research Center, Report No. AFCRC-TR-56-110; 1959, Proceedings of the International Conference on Information Processing, March (UNESCO Publication).  
 Quine, W. V., 1952, *American Mathematical Monthly*, **59**, 521; 1955, *American Mathematical Monthly*, **62**, 627.  
 Roth, J. P., 1957, Proceedings of the International Symposium on the Theory of Switching, Part I, in the Annals of the Computation Laboratory of Harvard University, **XXIX**, 57.  
 Svoboda, A., 1957, *Ibid.*, 293.  
 Urbano, R. H. and Mueller, R. K., 1956, *Trans. Inst. Radio Engrs.*, N. Y., **EC-5**, 126.  
 Veitch, E. W., 1952, *Proceedings of the Association for Computing Machinery*, Pittsburgh 127.

# CHANGE IN THE SHAPE OF A MOLECULE DURING THE FORMATION OF HYDROGEN BOND

N. RAJESWARA RAO AND K. V. RAMANAIAH

PHYSICS DEPARTMENT, OSMANIA UNIVERSITY, HYDERABAD

(Received November, 19, 1963)

## Plate V

**ABSTRACT.** Evidence is found to show that  $C=O$  bond frequency  $\nu=1710$  of monochloroacetic acid, the total symmetric line  $\nu=910$  of sulphuric acid and the total symmetric line 1050 of the nitrate ion in solution are found to decrease on depolymerisation due to heating, contrary to expectation. This goes against the assumptions usually made that the bond in question is unaffected by the presence of the other atoms in the molecules and the other molecules in the liquid. It is surmised that the molecules change their shape during the formation of a complex. The structure of the nitrate ion is pyramidal in solution at low temperature and it becomes plane on heating. This is taken to be a direct evidence for crystalline nature of hydration of ion in solution postulated by Lengyel.

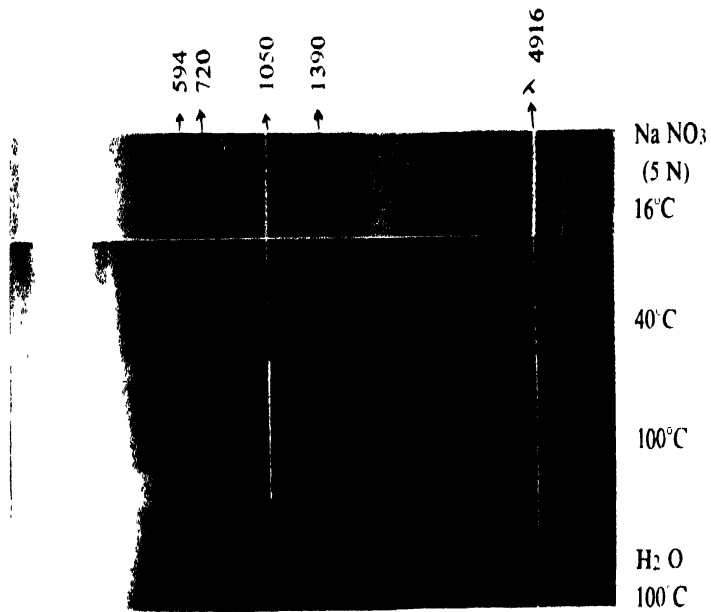
## INTRODUCTION

It is well known\* that during the formation of a complex by hydrogen bond, the stretching frequency of the bond, to which the proton from the neighbouring molecule is attached, is decreased. This change in the frequency is calculated in a number of cases, on the assumptions that (1) the bond in question is not affected by the other atoms in the molecules and (2) the molecules that are joining to form the complex are not influenced by the others in the liquid. We have, now gathered evidence to show that these assumptions are not quite justified.

1. Monochloroacetic acid: One of us (1944) reported on the changes in the  $C=O$  stretching frequency of this acid at various concentrations and temperatures. At  $10.5N$ , it shows a sharp maximum at  $\nu=1710$ . With dilution, a component appears at  $\nu=1617$  which increases in intensity while the peak at  $\nu=1710$  decreases. On heating the solution from  $30^{\circ}C$  to  $80^{\circ}C$ , also, the component at 1617 brightens up. As usual,  $\nu=1710$  is attributed to a dimer and  $\nu=1617$  to an unattached molecule, the hydrogen bond formation increasing the frequency contrary to general expectation. Most of the studies on complex formation by the application of Raman Effect depend on the shift of this line to lower frequency as, for instance, in the case of acetic acid (Kotaswaram, 1944), and trichloroacetic acid (N. R. Rao, 1943). Obviously, the  $C=O$  bond should not be regarded as if it is isolated.

\* Coggshall, 1950, Venkataramainah & Puranik, 1962





Raman spectra of nitrates at various temperatures and of water at 100°C. The shift of  $\lambda = 1050$  with temperature and its highest intensity at 100°C are seen. In the spectrum of nitrate at 100°C the water band is more intense than even for pure water.



2. Sulphuric acid : Raman spectrum of 100% sulphuric acid consists of four groups of lines  $\nu = 380, 490, 910$  and  $1150$  and  $1365$  forming the fourth group comparing the spectrum with that of  $\text{CCl}_4$ . In addition, we have a line at  $980$  and a faint band at  $3000$  which corresponds to OH band.  $\nu = 980$  disappears on heating the acid to  $350^\circ\text{C}$  or on adding a small amount of water—it is absent in 98% acid. Lines  $380$  and  $490$  are highly depolarised and  $910$  is highly polarised similar to the  $\nu 459$  of  $\text{CCl}_4$ , suggesting that it is of  $A_1$  type and total symmetric. It is found to shift from  $910$  at  $30^\circ\text{C}$  to  $890$  at  $350^\circ\text{C}$ , as seen from the microphotometric records in Fig. I. As, normally, separation of molecules takes place at higher temperature, this reduction in frequency is quite unexpected.

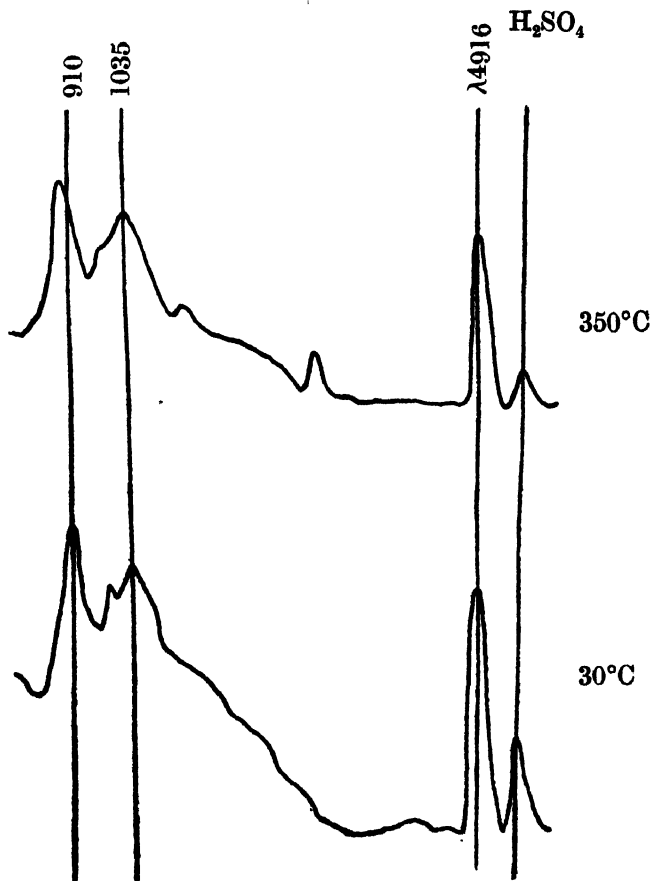


Fig. 1. Sulphuric acid at two temperatures. The shift of  $\nu = 910$  to lower frequency at higher temperature is seen.

3. Solution of Sodium nitrate : We wonder if we are dealing with molecules that are deformed during the formation of a complex. If this view is correct, we now cite a case where this is shown directly. Plate V shows Raman spectra of 5N sodium nitrate at  $16^\circ\text{C}$ ,  $40^\circ\text{C}$  and  $100^\circ\text{C}$  and pure water at  $100^\circ\text{C}$ . The first spectrum is taken separately and others with a Hartman diaphragm.

$\text{NO}_3$ , being of  $D_{3h}$  symmetry, is well known to show three Raman lines at  $\nu$  720, 1050, 1390. But, the spectrum at  $16^\circ\text{C}$  contains a faint line at 594 in addition, making one suspect whether the ion has become pyramidal on hydration. If so, using the formula, given by Herzberg,

$$\cos^2\beta = \frac{1}{\frac{4\nu_3^2 \nu_4^2}{\nu_1^2 \nu_2^2} + \frac{3m_y - m_x}{3m_y + m_x}}$$

where,  $\nu_1, \nu_2, \nu_3, \nu_4$  are respectively 1050, 594, 720, and 1390.  $m_y$  and  $m_x$  are masses of oxygen and nitrogen respectively,  $\beta = 72^\circ 12'$  for the angle between the axis of the pyramid and one of the NO bonds. This view is further supported by the fact that the total symmetric line 1050 shifts to lower frequency by  $10\text{ cm}^{-1}$  on increasing the temperature from  $16^\circ\text{C}$  to  $40^\circ\text{C}$  and by  $5\text{ cm}^{-1}$  for an increase from  $40^\circ\text{C}$  to  $100^\circ\text{C}$ .

A strong evidence for hydration is shown by the fact that this line increases both in intensity and width on heating. This is clearly demonstrated by the fact that  $\lambda 4916$  is of the same intensity at the two temperatures  $40^\circ\text{C}$  and  $100^\circ\text{C}$  while  $\nu = 1050$  is much brighter at  $100^\circ\text{C}$ . This is in accordance with the evidence shown earlier to the effect that the bond stretching line decreases in intensity on forming a complex.

Another point of interest is the large increase in the width of the line  $\nu = 1050$ . If the width of the line is due to inter-ionic Stark Effect, widening of the line at higher temperature may be due to (1) decrease in the dielectric constant at high temperature and (2) closer approach of the ions of opposite sign. According to the model of a solution proposed by S. Lengyel, ions in a solution are completely surrounded by molecules of water, the first shell by strong and regular hydrogen bonds and others by comparatively randomly oriented molecules of water, keeping the ions of opposite sign well separated. On increasing the temperature, however, the hydration shell breaks down, permitting the ions to come closer. This is, perhaps, the first direct spectroscopic evidence for the formation of crystalline hydrates of ions in solution.

Another consequence of hydration is its effect on the determination of the degree of dissociation of acids by applying Raman Effect first introduced by Rao (1930), and followed by a number of others. In this method, the intensity of the line  $\nu = 1050$  is measured in the spectra of nitric acid of various concentrations and assuming that it is proportional to the number of ions formed, the degree of dissociation is calculated. Now, if hydration is having some influence on the line, it introduces a large error in the determination of the degree of dissociation of the acid, especially at high concentrations as the amount of water available may not be sufficient to completely surround all the ions at all the concentrations.

Plate V shows another feature. Water band is stronger in the salt solution at  $100^\circ\text{C}$  than in the spectra on either side. It is well known that water band is

very wide and it is due to hydrogen bonded clusters. As the water is heated, the band becomes narrower due to the clusters breaking down. It is also known that on adding a salt or acid, again the band becomes narrow. Now, while the width of the band does not change from 40°C to 100°C of the salt solution, it is much stronger at 100°C, showing that while the structure breaks down completely even at 40°C in the salt solution the ions which are surrounded by water forming hydrogen bonds are not relieved from this bondage. The molecules in salt solution at 100°C are free compared to those in pure water at this temperature.

## REFERENCES

- Coggshall, N. D. 1950, *J. Chem. Phys.* **18**, 978.  
Cross, P. C., Burnham, J. and Leighton, P. A. 1938, *J. Am. Chem. Soc.* **59**, 1134-1147.  
Infrared and Raman Effect, By G. Herzberg, Page 162.  
Koteswaram, P. 1944, *Ind. J. Phys.* **14**, 353.  
Lengyel, S. 1963, *Acta Chemica, Tome* **337**, 87.  
Rao, N. R. 1944, *Ind. J. Phys.* **17**, 43.  
Rao, N. R., 1943, *Ind. Jour. Phys.* **17**, 332.  
Rao, I. R. 1930, *Proc. Roy. Soc.*, **33**, 632.  
Venkataramayya, K and Puranik, P. G. 1962, *Proc. Ind. Acad. Sci.* **56**, 96.

# LOCKING PHENOMENA IN PHASE LOCKED OSCILLATORS

N. B. CHAKRABARTI and B. N. BISWAS\*

INSTITUTE OF RADIO PHYSICS AND ELECTRONICS,  
UNIVERSITY OF CALCUTTA

(Received, August 29, 1963)

**ABSTRACT.** The operation of typical automatic phase control circuits has been studied with particular reference to locking range and time. The similarity of an injection synchronised oscillator with a slow acting amplitude stabilisation circuit to a standard APC system is pointed out. The pull-in phenomenon in APC circuits, with either sinusoidal or triangular comparators, incorporating low-pass filters in the feedback loop has been analysed. Expressions have been derived for the locking range and time of APC circuits using a sinewave comparator. Experimental results obtained for such circuits have been presented and are found to be in good agreement with the computed values.

## INTRODUCTION

A phase locked oscillator, as its name implies, is an oscillator the phase of which is locked to an input reference oscillation. It operates by detecting the phase difference between the two oscillations and controlling the frequency of the oscillator in correspondence to a measure of this phase difference after suitable filtering.

A phase locked oscillator is essentially a feedback device incorporating a narrow-band filter. Because of the narrow band feedback process it reduces internally generated noises and disturbances as well as disturbances appearing at the input. A phase-locked oscillator thus finds uses in noise- and jitter-free frequency synthesis and in frequency tracking. An *APC* circuit has a close similarity to injection synchronised oscillator where an oscillation of a desired frequency is injected into the oscillator. The amplitude and frequency of the injected voltage must be such as to quench the free oscillation, the quenching action being obtained through an instantaneous limiter type non-linearity which attenuates the weaker signal more than the stronger.

Because of the close similarity between the phase locked oscillator and the injection synchronised oscillator, this paper deals with some of the characteristics, such as the locking range and time, of both types of oscillator.

In section 2, a simple explanation of single frequency synchronisation phenomena is given and it is emphasised that it is imperative to use a limiter type charac-

---

\*Department of Physics, The University of Burdwan, Burdwan, West Bengal.

teristic. This is followed by a study in section 3 of the effect of low frequency time constant of the gain control arrangement of an injection synchronised oscillator. The similarity between this type of oscillator and a phase locked oscillator having a low pass filter in the loop has been pointed out.

The behaviour of a simple APC circuit with sinusoidal and linear phase comparators has been analysed in section 4. An explanation of pull-in effect is given in section 5 for APC loops with two different filters. From the accompanying analysis an approximate idea of the pulling range and time can be formed.

Expressions for locking time and range have been derived in section 6. Two types of filters have been considered in this connection—one with negligible high frequency gain and the other with finite high frequency gain. Simple but approximate relations for the locking range and time have been given. The practical results with regard to locking range in APC circuits with typical filter networks in the loop have been presented in section 7. These are in good agreement with the theoretical formulae.

#### SINGLE FREQUENCY DIRECT SYNCHRONISATION PHENOMENA

In this section, single frequency direct synchronisation in an oscillator of the type shown in Fig. 1 will be considered.

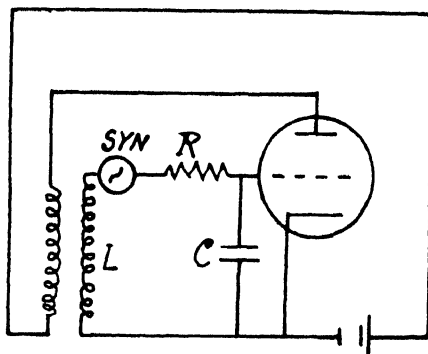


Fig. 1. Schematic diagram of a directly synchronised grid tuned oscillator.

The phenomenon of synchronisation in injection synchronised oscillators can be understood in the following way. Due to the mixing process provided by the inherent non-linearity between the grid voltage and the plate current in the tube circuit, the effective transconductance of the tube or the gain parameter has an in-phase as well as a quadrature component. The in-phase component modulates the amplitude of the free running oscillator and the quadrature component modulates the frequency of the oscillator. The magnitude of these quantities will depend on the relative amplitudes and the phase difference between the reference signal and the free running oscillator. If the frequency difference  $\Omega/2\pi$  between these signals is not large and the synchronising amplitude

is adequate, then it may be expected that the phase difference will attain a steady value  $\Phi_s$  and the phase of the free running oscillator will be locked in synchronism with that of the reference signal. The amplitude of the synchronising signal required for synchronising the free running oscillator depends not only on the difference of frequency between the free running oscillator and the reference signal but also on the amplitude of the free running oscillation.

Locking can also be considered as selection of the external signal and suppression of the internal. The suppression depends on the fact that when two non-coherent signals are applied to a limiter-type non-linear transference, the weaker signal is attenuated more than the stronger. One can understand the mechanism of weaker signal suppression by a reference to Fig. 2 which depicts relative transmission at two frequencies through a cubic type non-linearity,

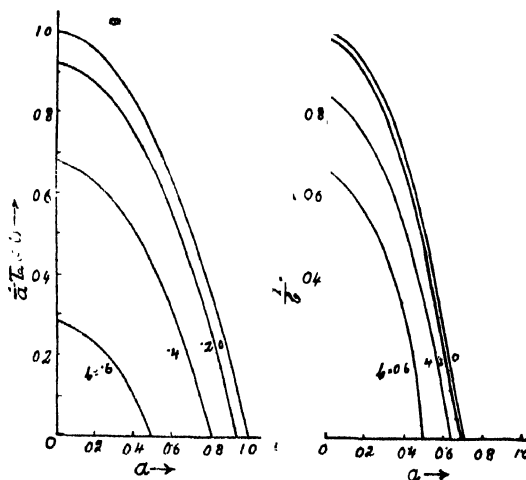


Fig. 2. Transmission characteristics of a limiter type non-linearity.

$$x_{out} = a_1 x_{in} - a_3 x_{in}^3. \quad \dots (2.1)$$

If we assume that  $x_{in}$  is of the form

$$x_{in} = a \cos \psi_1 + b \cos \psi_2, \quad \dots (2.2)$$

then the transmission of component at frequency  $\omega_1 = d\psi_1/dt$ , having the amplitude 'a' in presence of the another component at frequency  $\omega_2$  and of amplitude 'b' is

$$T_a(a, b) = [1 - 3/4(a^2 + 2b^2)]a. \quad \dots (2.3)$$

Similarly, for the component at frequency  $\omega_2$ ,

$$T_b(a, b) = b \left[ 1 - \frac{3}{4}(b^2 + 2a^2) \right]. \quad \dots (2.4)$$



On the other hand, if we assume an expansion-type characteristic such as given by

$$x_{out} = \exp(x_{in}) - \exp(-x_{in}), \quad \dots (2.5)$$

then the transmissions are given by

$$T_a(a, b) = 2I_1(a)I_0(b), \quad \dots (2.6)$$

and

$$T_b(a, b) = 2I_0(a)I_1(b). \quad \dots (2.7)$$

A plot of  $T_a(a, b)/a$  is shown in Fig. 3 from which one easily understands that this type of characteristic helps a weaker signal to build up.

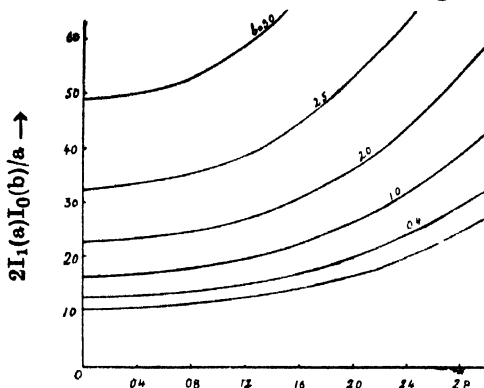


Fig. 3. Transmission characteristics of an expander type non-linearity.

It is evident, then, that a limiter type characteristic is preferable to an expander type characteristic so far as the interference reduction is concerned. In the case of limiter type characteristics, if we consider the same frequency synchronisation phenomena, it can be easily shown that the locking equation is given by,

$$\frac{d\Phi}{dt} = \Omega - K \sin \Phi, \quad (2.8)$$

where  $K$  is a constant which depends on 'a' and 'b' and  $\Omega$  is the initial frequency difference. It is to be noted that the process of synchronisation is due to instantaneous limiting and thus no filtering other than at r.f. is possible. In fact the value of  $K$  is given approximately by  $K = \frac{a}{b} \cdot \frac{\omega_0}{2Q}$  for single tuned circuit.

It is to be noted that if there are finite transmissions at other frequencies generated through the process of limiting then the statements made earlier in connection with interference reduction do not apply. If, for example, the component at frequency  $(2\omega_1 - \omega_2)$  has finite transmission then it can be shown that the amount of suppression obtainable is small. This is due to the fact that the input to the limiter in such a case shows too little amplitude modulation for limiting to be effective. In any event the oscillator should have a soft characteristic, that is, it should be a free oscillator even in the absence of any r.f. input excitation.

Thus oscillators working in any subharmonic mode should be free-running and not of the regenerative divider type.

### EFFECT OF LOW-FREQUENCY TIME CONSTANT OF THE GAIN CONTROL ARRANGEMENT ON THE PHASE EQUATION

In the previous case we have assumed instantaneous limiting due to which there was 'strong signal capture' and 'small signal rejection'. We shall now study the case when the limiting is not instantaneous. In most of the practical oscillator circuits the gain control arrangement is only partly instantaneous. For example, the R-C time constant in the self-bias circuit of an oscillator provides a slow-acting gain control circuit.

Let us suppose that the gain is controlled by the rectified envelope and the time constant of the circuit is  $T$  secs. Then the open loop equations can be written as (Fig. 4),

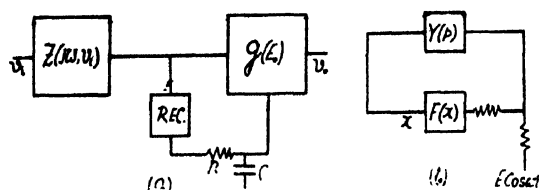


Fig. 4. Equivalent block diagram of a directly synchronised oscillator with a filter in the gain control circuit.

$$v_o = Z(j\omega, v_i) g(E_0) v_i \quad \dots (3.1)$$

and

$$T \frac{dE_0}{dt} = E_i - E_0 = \alpha v_i - E_0. \quad \dots (3.2)$$

where  $v_i$  and  $v_o$  are the input and output voltages respectively and  $E_i$  is the detected voltage and  $E_0$  is the control voltage.

Now let us suppose that  $v_i$  consists of two components one at an angular frequency  $\omega_1$  and the other at the angular frequency  $\omega_2$  of amplitudes 'a' and 'b' respectively. Then

$$v_i = a \cos \psi_1 + b \cos \psi_2. \quad \dots (3.3)$$

It can be shown that if the control characteristic is given by  $g(E_0) \approx (1 - \beta/E_0^2) g_0$ , the net transmissions at frequencies  $\omega_1$  and  $\omega_2$  are respectively

$$T_a(a, b) = a[1 - g_0(a^2 + b^2 + b^2 G_1 \cos \Phi_1)], \quad \dots (3.4)$$

$$\text{and} \quad T_b(a, b) = b[1 - g_0(a^2 + b^2 + a^2 G_1 \cos \Phi_1)], \quad \dots (3.5)$$

where  $G_1(\Delta\omega) \exp[j\Phi_1(\Delta\omega)]$  represents the filter transmission at the difference frequency  $\Delta\omega = \omega_1 \sim \omega_2$ . Hence from the above it is evident that if  $G_1 \cos \Phi_1 \neq 0$ , then there will be non-linear discrimination of one frequency against the another.

Similar conclusions apply for other types of gain control characteristics, like  $g(E_0) = g_0(1 - \beta |E_0|)$ .

Now for the loop shown in Fig. 4 the component 'a' at  $\omega_1$  should satisfy the following eq.

$$a \cos(\omega t + \Phi) \left[ F_a(a, b) + \frac{E}{a} \cos \Phi \right] + E \sin \Phi \sin(\omega_1 t + \Phi) = \frac{1}{y(p)} \cos(\omega_1 t + \Phi), \quad (3.6)$$

where

$$y(p) = \frac{\alpha p}{p^2 + \alpha p + \omega_0^2} \quad (3.7)$$

and  $E \cos(\omega_1 t + \Phi)$  is the external synchronising voltage. Now

$$\frac{1}{y(p)} = 1 + \frac{1}{\alpha} \left( p + \frac{\omega_0^2}{p} \right) \approx 1 + \frac{2}{\alpha} S + j \frac{\omega_1^2 - \omega_0^2}{2\omega_1}, \quad (3.8)$$

If we put  $p = j\omega_1 + S$

where  $S$  represents an operator in a slow time scale. The amplitude and phase equations are approximately given by

$$\frac{2}{a} \cdot \frac{da}{dt} = a \left[ F_a(a, b) - 1 \right] + E \cos \phi, \quad \dots \quad (3.9)$$

$$\frac{2}{\alpha} \cdot \frac{d\phi}{dt} = \frac{\omega_1^2 - \omega_0^2}{\alpha \omega_1} - \frac{E}{\omega_1} \sin \phi. \quad (3.10)$$

Hence from (3.2) and (3.10) we have,

$$\frac{2}{\alpha} \cdot \frac{d\phi}{dt} = - \frac{\omega_1^2 - \omega_0^2}{\alpha \omega_1} - \frac{\alpha_0}{E_0} \cdot \frac{E}{(1 + PT)} \sin \phi, \quad (3.11)$$

which can be rewritten in the form

$$\frac{d\phi}{dt} = \Omega - G(p) \frac{\omega_0}{2Q} \cdot \frac{E}{E_0} \sin \phi, \quad \dots \quad (3.12)$$

where  $G(p)$  represents the transfer function of a simple  $R-C$  lag filter. It is to be noted that Eq. (3.15) represents the APC equation with a simple  $R-C$  lag filter (see Sec. 5, 2). It is apparent that the maximum rate of the input frequency variation depends on the  $Q$  of the tuned circuit and the time constant of the gain control circuit. Experimental results for locking range for different values of

the  $RC$  product in the grid circuit of an oscillator are shown in Fig. 4(a). These confirm the theoretical findings.

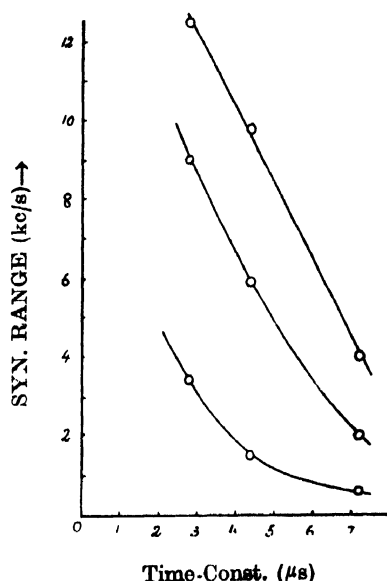


Fig. 4(a). Pull-in performance of the directly synchronised oscillator with a slow acting gain control arrangement. The variation of the locking range with the detector time constant is shown for three values of the synchronising voltage.

### THE SIMPLE APC CIRCUIT

In this section we shall consider the simple APC circuit shown in Fig. 5. It contains an oscillator whose output frequency is approximately equal to the desired

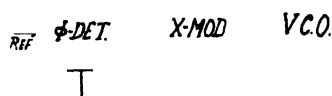


Fig. 5. Block diagram of a standard APC circuit.

frequency, a phase detector and a reactance modulator. The phase detector performs the function of an error detecting device in the sense that it detects the error between the instantaneous phases of the reference input and the oscillator.

APC loops can be classified into different categories depending on the nature of the signals and the type of comparator used. The signal may be continuous or interrupted. The comparator may be linear or sinusoidal. In the following analysis we will assume the signal to be continuous.

#### 4.1. APC Circuit with Sinusoidal Comparator :

We shall here analyse the behaviour of an APC circuit with a sinusoidal comparator. In this case the output of the phase detector  $\delta E$  is

$$\delta E = \mu \sin \phi, \quad (4.1)$$

where  $\phi$  is the instantaneous phase difference between the signals and  $\mu$  represents the gain of the phase detector in volts per radian. This output voltage tends to keep the output frequency of the oscillator constant through the reactance modulator, the sensitivity of which can be represented by

$$\beta = \delta\omega/\delta E. \quad (4.2)$$

Thus  $\beta$  represents the gain of the modulator in rad/sec per volt. Then the governing equation of the system is given by

$$\frac{d\phi}{dt} = \Omega - K \sin \phi, \quad \dots \quad (4.3)$$

where  $K = \mu\beta$ . If  $\Omega$ , the undisturbed beat angular frequency, is less than  $K$ , then there is a fixed value  $\phi = \phi_s$  for which  $d\phi/dt = 0$ , so that

$$\phi_s = \sin^{-1}(\Omega/K). \quad (4.4)$$

Thus if the initial detuning lies within the limiting synchronisation range ( $K$ ) then the phase of the output oscillation will be locked in phase in synchronism with the reference input. Solving Eq. (4.3), expressions for the instantaneous phase and frequency of the oscillator can be readily obtained.

If  $\Omega > K$  then the instantaneous phase and frequency are given by

$$\phi = 2 \tan^{-1} \left[ \frac{1}{\Omega/K} + \frac{\sqrt{(\Omega/K)^2 - 1}}{\Omega/K} \tan K \frac{\sqrt{(\Omega/K)^2 - 1}}{2} (t + t_0) \right] \dots \quad (4.5a)$$

$$\text{and} \quad \frac{d\phi}{dt} = K \left[ \left( \frac{\Omega}{K} \right)^2 - 1 \right] \frac{1}{(\Omega/K)^2 + \cos(2\psi - \beta_0)} \quad (4.5b)$$

$$\text{where} \quad \psi = K \frac{\sqrt{(\Omega/K)^2 - 1}}{2} (t + t_0)$$

$$\text{and} \quad \beta_0 = \tan^{-1} \sqrt{\left( \frac{\Omega}{K} \right)^2 - 1}.$$

Inside the pull-in range (i.e.  $\Omega < K$ ) the expression for the instantaneous phase is

$$\phi = 2 \tan^{-1} \left[ \frac{1}{\Omega/K} - \frac{\sqrt{1 - (\Omega/K)^2}}{\Omega/K} \tanh K \frac{\sqrt{1 - (\Omega/K)^2}}{2} (t + t_0) \right] \dots \quad (4.6)$$

A Fourier analysis of Eq. (4.5b) yields the values of the spectral components of the instantaneous frequency

$$\begin{aligned} \frac{d\phi}{dt} = K \sqrt{\left( \frac{\Omega}{K} \right)^2 - 1} [1 - 2r \cos(2\psi - \beta_0) + 2r^2 \cos 2(2\psi - \beta_0) - \\ \dots + (-1)^n 2r^n \cos n(2\psi - \beta_0)], \quad \dots \quad (4.7) \end{aligned}$$

where

$$r = \frac{\Omega}{K} - \sqrt{\left(\frac{\Omega}{K}\right)^2 - 1}.$$

It is clear from the study of Eq. (4.7) that the instantaneous frequency will show violent fluctuation as  $\Omega$  approaches  $K$  and the output will contain a large number of spectral components of significant amplitudes separated by the multiples of the beat frequency. The instantaneous phase for frequencies away from the cross-over (i.e.  $\Omega \gg K$ ) can be represented by the following approximate relation

$$\phi = \omega t + \alpha + m_1 \sin \omega t + m_2 \sin (2\omega t + \theta) \quad \dots (4.8)$$

The values of  $\omega$ ,  $\alpha$ ,  $m_1$ ,  $m_2$  and  $\theta$  can be determined by substituting the value of  $\phi$  given by Eq. 4.8 into Eq. 4.3 and equating components at different frequencies.

#### 4.2 Linear Phase Comparator :

We shall now consider the case where the instantaneous detected voltage is a symmetrical triangular function of the phase difference (Fig. 6). The loop equation now becomes

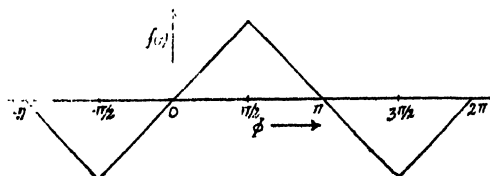


Fig. 6. Output of the linear phase comparator.

$$\frac{d\phi}{dt} = \Omega - K\phi, \quad -\pi/2 \leq \phi \leq +\pi/2 \quad \dots (4.9a)$$

and

$$\frac{d\phi}{dt} = \Omega - K(\pi - \phi), \quad +\pi/2 \leq \phi \leq 3\pi/2. \quad \dots (4.9b)$$

It may be mentioned that a symmetrical triangular comparator can be realised in practice by mixing two strongly limited r.f. voltages.

The period of the instantaneous beat frequency can be found by solving (4.9) and is given by

$$T = \frac{2}{K} \log_e \left( \frac{1+x}{1-x} \right), \quad \dots (4.10)$$

where

$$x = \frac{K\pi}{2\Omega}$$

If the comparator characteristic is triangular but asymmetric, i.e., the detected voltage is

$$V = K_1\phi, \quad -\phi_1 \leq \phi \leq \phi_1$$

and ...

$$V = K_2\phi, \quad (\pi - \phi_1) \leq \phi \leq (\phi_1 + \pi)$$

and the corresponding expression for a beat period is

$$T = \frac{1}{K_1} \log_e \frac{1 + \frac{K_1 \phi_1}{\Omega}}{1 - \frac{K_1 \phi_1}{\Omega}} + \frac{1}{K_2} \log_e \frac{1 + K_2 \frac{\pi + \phi_1}{\Omega}}{1 - K_2 \frac{\pi - \phi_1}{\Omega}} \quad (4.11)$$

The instantaneous beat frequency  $2\pi/T$  and also the discriminator output voltage for the case of a symmetrical triangular comparator have been plotted against  $\Omega T$  and compared with those of the case when the phase comparator is sinusoidal (Fig. 7). It will be observed that there is a close functional similarity between

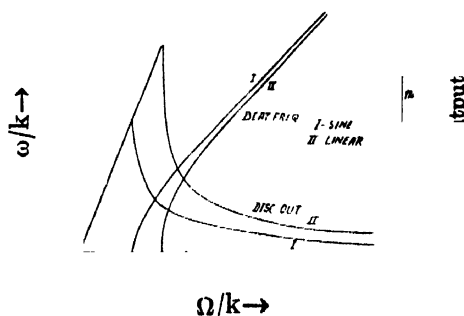


Fig. 7. Discriminator output and beat frequency vs. error characteristics.

an APC loop with a symmetrical triangular comparator and that with a sinusoidal comparator, although the range in the former is larger by a factor of  $\pi/2$ .

### APC LOOP WITH FILTER

It will be observed from the analysis in section 4 that for APC circuits without a filter incorporating either type of comparator the value of the locking ratio ( $\Omega/K$ ) determines completely their performance characteristics, viz., locking range, noise band-width and the nature of the response to transients of phase and frequency. Now it is considered desirable to be able to control these parameters independently of one another, in particular, to reduce the noise band-width. Incorporation of an appropriate low pass filter in the loop helps to achieve this. Inclusion of the filter network will, however, introduce the so-called pull-in phenomenon. The response to transients may no longer be deadbeat even if the difference frequency lies within the locking range and the instantaneous frequency may drift for a few beat cycles of continuously decreasing frequency till equilibrium is reached.

#### 5.1. Pull-in Effect in an APC Circuit with Filter and Symmetrical Triangular Comparator :

We shall now consider the pull-in phenomena in an APC circuit with symmetri-

cal triangular phase comparator and a low pass filter. Introduction of a filter in the feedback loop modifies Eq. (4.9) to the following equations :

$$\frac{d\phi}{dt} = \Omega - K \cdot G(p)\phi, \quad -\pi/2 \leq \phi \leq +\pi/2 \quad \dots (5.1)$$

$$\text{and} \quad \frac{d\phi}{dt} = \Omega - K \cdot G(p)(\pi - \phi), \quad +\pi/2 \leq \phi \leq 3\pi/2 \quad (5.2)$$

where  $G(p)$  stands for the filter-transfer function. For the filter network shown in Fig. 8(a) we have from equations (5.1) and (5.2)

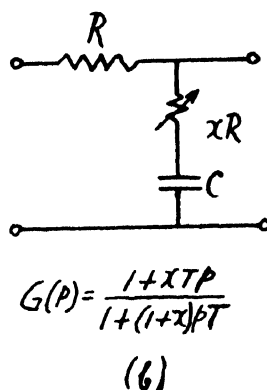
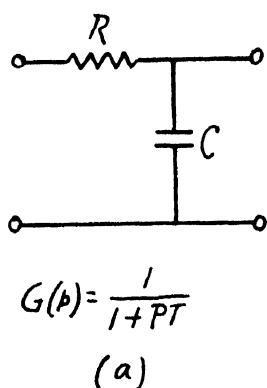


Fig. 8. Simple low pass filter :

(a) with negligible high frequency gain

(b) with finite high frequency gain.

$$\frac{d^2\phi_1}{dt^2} + \frac{1}{\alpha} \cdot \frac{d\phi_1}{dt} + \frac{K}{\alpha} \cdot \phi_1 = 0, \quad -\pi/2 \leq \phi \leq \pi/2 \quad \dots (5.3)$$

where

$$\phi_1 = \phi - \Omega/K$$

and

$$\frac{d^2\phi_2}{dt^2} + \frac{1}{\alpha} \cdot \frac{d\phi_2}{dt} - \frac{K}{\alpha} \phi_2 = 0, \quad +\pi/2 \leq \phi \leq 3\pi/2 \quad \dots (5.4)$$

where

$$\phi_2 = \phi - \Omega/K + \pi/2.$$

and

$$\alpha = R.C.$$

Combining (5.3) and (5.4) the phase equation of such a system can be written as

$$\frac{d^2\psi}{dt^2} + 2b \frac{d\psi}{dt} \pm C\psi = 0, \quad \dots (5.5)$$

Writing  $\omega = d\psi/dt$ , we have

$$\frac{d\omega}{d\psi} = 2b \mp C\psi/\omega. \quad \dots (5.6)$$



As an example, we shall consider the case when  $b = 0.5$  and  $C = 1$ . The 'phase-plane' plots for this case are shown in Fig. 9(a) and 9(b). Now when  $\phi$  lies between

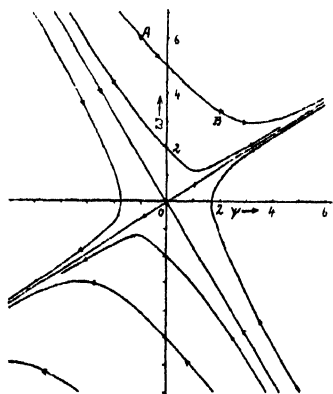


Fig. 9(a) Phase-plane trajectories.

$$\frac{d\omega}{d\psi} = -1 + \psi/\omega$$

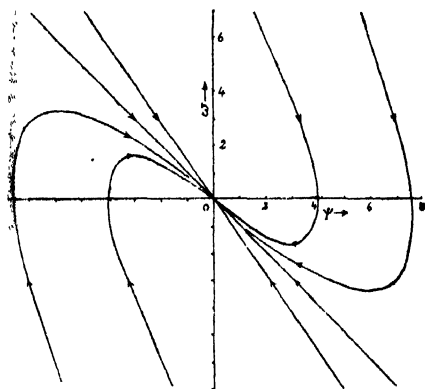


Fig. 9(b) Phase-plane trajectories

$$\frac{d\omega}{d\psi} = -2 - \psi/\omega$$

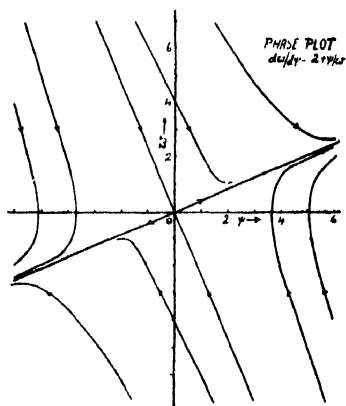


Fig. 9(c) Phase-plane trajectories.

$$\frac{d\omega}{d\psi} = -2 + \psi/\omega$$

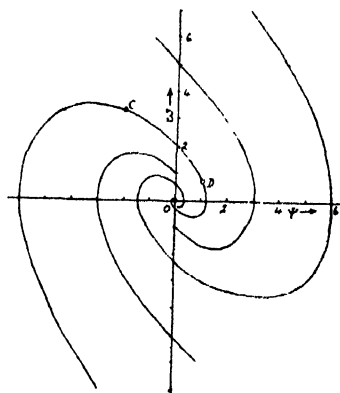


Fig. 9(d) Phase-plane trajectories.

$$\frac{d\omega}{d\psi} = -1 - \frac{\psi}{\omega}$$

$-\pi/2$  and  $+\pi/2$ ,  $\psi$  lies between  $-\pi/2 - \Omega/K$  and  $\pi/2 - \Omega/K$  and similarly when  $\phi$  lies between  $\pi/2$  and  $3\pi/2$ ,  $\psi$  lies between  $-\pi/2 + \Omega/K$  and  $\pi/2 + \Omega/K$ . On the assumption that  $\Omega/K = 0.5$ , Eq. (5.6) becomes

$$\frac{d\omega}{d\psi} = -1 - \psi/\omega, -2.07 \leq \psi \leq 1.07 \quad \dots (5.7)$$

and

$$\frac{d\omega}{d\psi} = -1 + \psi/\omega, -1.07 \leq \psi \leq 2.07 \quad \dots (5.8)$$

We may now consider a typical trajectory starting from  $\psi = -1.07$ ,  $\omega = 6$ . The trajectory will lie in the region defined by (5.8), till at the end of the interval  $AB$ ,  $\psi$  becomes 2.07 and the instantaneous beat frequency  $\omega$  becomes 3.3 (Fig. 9a). The next stretch of the trajectory starts from  $\psi = -2.07$ . Now at the end of this interval  $CD$  (Fig. 9b)  $\psi = 1.07$  and  $\omega$  is seen to be reduced to 0.8. During the next successive cycles the value of the terminal  $\omega$  continuously decreases (Figs. 9a and 9b) and ultimately the oscillator is pulled into synchronism. It thus requires a phase drift of about  $4\pi$  radians for the oscillator to synchronise. As the ratio  $\Omega/K$  is increased and is brought closer to unity, the oscillator takes more time to be synchronised. Now at the extreme case when  $\Omega/K = \pi/2$  it can be shown that the instantaneous beat frequency at first decreases but it does so upto a certain limit. To study the effect of different values of the  $RC$  product the trajectories for different values of ' $b$ ' will have to be drawn and the motion of  $(\omega, \psi)$  followed from the initial conditions through a required number of cycles till the equilibrium is attained.

Graphical construction, similar to those considered above, is possible for the filter network shown in Fig. 8(b). Here

$$G(p) = \frac{1 + \alpha p}{1 + \beta p}, \quad (5.9)$$

where

$$\alpha = xCR, \quad \beta = (1+x)CR.$$

Now taking, for example,  $K/\beta = 1$ , we have

$$\frac{d\omega}{d\psi} = -\frac{1 \pm \alpha K}{\beta} \mp \psi/\omega. \quad (5.10)$$

The pull-in mechanism here will be clear from a study of the appropriate plots (see Fig. 9) for different values of the time constants  $\alpha$  and  $\beta$ . The effect of different values of  $\alpha$  and  $\beta$  on the locking range and time will also be evident.

## 5.2. APC circuit with Filter and a Sinusoidal Comparator :

The governing equation of an APC circuit with a lowpass filter in the loop (Fig. 10) is given by the relation



Fig. 10. Block diagram of an APC system with filter.

$$\frac{d\phi}{dt} = \Omega - KG(p) \sin \phi, \quad \dots \quad (5.11)$$

where  $G(p)$  represents the gain function of the lowpass filter network normalised with respect to the maximum gain at zero frequency. As was pointed out in the discussion on the simple APC loop, the phase function contains not only the component at the fundamental beat frequency but also harmonic components. Now for a low pass filter it is logical to assume that the filter-transmission at the harmonic frequencies  $2\omega$ ,  $3\omega$  etc. is negligible. Then outside the pull-in range, the phase function (Cf. Eq. 4.7) takes the simple form

$$\phi = \omega t + \alpha + m \sin \omega t \quad \dots (5.12)$$

where  $\omega$  is the beat frequency.

The steady state loop equations then become

$$\omega = \Omega + J_1(m) - \frac{G_0 y}{\sqrt{\sin^2 \phi_1 + y^2 \cos^2 \phi_1}}, \quad \dots (5.13)$$

$$\text{and } \left[ \frac{m}{J_0(m) + J_2(m)} \right]^2 \left( \frac{\omega \cos \phi_1}{G_1} \right)^2 + \left[ \frac{m}{J_0(m) - J_2(m)} \right]^2 \left( \frac{\omega \sin \phi_1}{G_1} \right)^2 = K^2 \quad \dots (5.14)$$

where 
$$y = \frac{J_0(m) - J_2(m)}{J_0(m) + J_2(m)}$$

and  $J_n(m)$  is Bessel's Function of order 'n' and argument 'm', and  $\phi_1$  is the filter phase and  $G_0$  and  $G_1$  represent respectively d.c. and a.c. gains of the filter. These equations enable determination of  $\alpha$ ,  $\omega$  and  $m$  for a given  $\Omega$ . Now if the Eqs. (5.13) and (5.14) can be simultaneously satisfied for any value of the beat frequency  $\omega$  and a value of  $m$  less than unity, the system will not lock and will show stationary beats. On the other hand, 'instability', leading to synchronisation, will set in if the value of  $m$  demanded by the Eqs. (5.13) and (5.14) equals or exceeds unity.

The plots of the equations (5.13) and (5.14) for a simple  $R-C$  network are shown in Fig. 11. With the help of this figure one can find the variation of  $\omega$  and  $m$

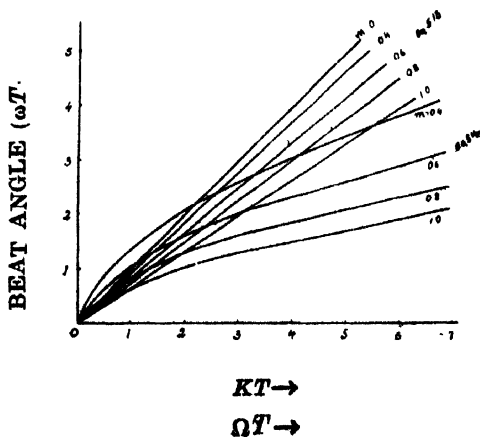


Fig. 11. Graph illustrating the evaluation of 'm' and 'ω' using Eqs. 5.13 and 5.14.

with time till the limiting value of the beat frequency corresponding to  $m = 1$  is reached, and also whether the system will synchronise or not.

#### LOCKING RANGE AND LOCKING TIME

An APC loop is characterised by the following parameters : (i) the locking range, (ii) the locking time and (iii) the noise bandwidth (see Appendix for an expression for the noise-bandwidth). The locking time can be thought of as composed of frequency pulling time and phase pulling time. Phase pulling time is the time taken by the loop to annul the discrepancy in phase between the input and the output, if the initial difference frequency is very small. Frequency pulling time, on the other hand, is the time required for equalisation of the frequency of the input and the output brought about by a gradual increase of the steady discriminator voltage. It should be remarked that the frequency pulling time is considerably larger than the phase pulling time. (The latter has been briefly analysed in the Appendix).

During the period of phase pulling, one may consider the APC loop as a semi-direct-current loop, while during the period of frequency pulling the loop is a combined A.C. and DC. one, and the A.C. gain characteristic assumes a significant role. Now there may arise two distinct cases—(a) one in which the limiting high frequency gain is zero and (b) the other in which it is finite. Whatever the case may be, in the long time process of frequency pulling there will be a steady drift of the difference frequency per beat cycle. The amount of this drift is determined by the initial difference frequency and the gain of the open loop at the beat frequency. The situation is best analysed by considering the phenomenon in a sequence of beat cycles. The phenomenon of frequency pulling in APC loops with two different types of filters mentioned above will be studied in some details in this section and expressions for locking range and time will then be derived.

##### 6.1. Filter with Finite A.C. Gain :

We shall assume that the gain function  $G(P)$  may be separated into two parts—high frequency gain  $G_H(P)$  and a low frequency portion  $G_L(p)$ , i.e.,

$$G(p) = G_H(p) + G_L(p). \quad \dots (6.1)$$

Further it will be assumed that the high frequency gain is considerably smaller than the low frequency gain. If the initial difference frequency  $\Omega$  is lower than  $KG_H$ , the phase will attain a steady value in a fairly short period. On the other hand, if  $\Omega > KG_H$  the system may still attain the equilibrium, but the time will be considerably longer. In the period of a beat cycle, the beat frequency may be considered to be constant. There will, however, be a steady drift of the value of this beat frequency over a number of such cycles. Now

$$\frac{d\phi}{dt} = (\Omega - KG_L \sin \phi) - KG_H \sin \phi. \quad \dots (6.2)$$

If the time constants involved in locking are long compared with a period of a beat cycle, we can write,

$$KG_H \sin \phi = -p\phi + \Omega - KG_L \sin \phi, \quad \dots (6.3)$$

Now putting  $\omega_1 = \Omega - KG_L \sin \phi,$

or,  $\bar{\omega}_1 = \Omega - KG_L \sin \phi. \quad \dots (6.4)$

We have from (6.3)

$$\omega_\beta = \sqrt{\bar{\omega}_1^2 - (KG_H)^2} + \bar{\omega}_1. \quad \dots (6.5)$$

So that  $KG_H \sin \phi = -\sqrt{\bar{\omega}_1^2 - (KG_H)^2} + \bar{\omega}_1. \quad \dots (6.6)$

This equation gives us the value of the effective difference frequency at a given time. Equations (6.4) and (6.6) yield

$$\bar{\omega}_1 = \Omega + \frac{G_L}{G_H} \left[ \sqrt{\bar{\omega}_1^2 - (KG_H)^2} - \bar{\omega}_1 \right]. \quad \dots (6.7)$$

Equation (6.7) can be written as a differential equation in  $\bar{\omega}_1$ , which can then be solved for evaluating frequency pulling time (Richman, 1954). For example, if

$$G(p) = m + \frac{1-m}{1+p \frac{y}{m} t_c},$$

where  $y = x T/t_c$ ,  $t_c = 1/\mu\beta = 1/K$  and  $m$  is ratio of a.c. gain to d.c. gain of the filter. Now replacing  $\sqrt{\bar{\omega}_1^2 - (mK)^2}$  by the approximate relation  $\frac{\bar{\omega}_1(\bar{\omega}_1 - mK)}{\bar{\omega}_1 - 0.84mK}$  and putting  $\bar{\omega}_1/mK = \rho$ ,  $\Omega/mK = \rho_0$  we have ultimately the following relations for the locking time and range :

$$\frac{mT}{yt_c} = \left[ -\frac{1}{2} \log_e (\rho^2 - 2b\rho + 0.84\rho_0) - \frac{2b-0.84}{2} \cdot \frac{1}{\sqrt{0.84\rho_0^2 - b^2}} \tan^{-1} \frac{\rho-b}{\sqrt{0.84\rho_0^2 - b^2}} \right] \rho_0 \quad \dots (6.8)$$

and  $\Omega/K \geq 0.16 + 0.84m, \quad \dots (6.9)$

where  $2b = \rho_0 + \frac{m-0.16}{m}$

### 6.2. Filter with Negligible High-Frequency Gain :

There may be systems in which there is no high frequency gain or the high frequency gain falls rapidly with frequency. An example is provided by a simple  $R-C$  filter (Rey, 1960). In this case, the loop equation reduces to

$$\frac{d\phi}{dt} = \Omega - \frac{K}{1+pT} \sin \phi, \quad \dots (6.10)$$

$$\text{or,} \quad T \frac{d^2\phi}{dt^2} + \frac{d\phi}{dt} + K \sin \phi = \Omega, \quad \dots (6.11)$$

Where  $T$  is the time constant. We may assume that

$$\dot{\phi} = \omega t + \alpha + m \sin(\omega t - \beta) \quad \dots (6.12)$$

Hence from these two equations we have

$$T \frac{d\omega}{dt} + \omega - K J_1(m) \sin \beta = \Omega, \quad \dots (6.13)$$

$$T \frac{d}{dt} (m\omega) + m \left( \omega - \frac{d\beta}{dt} \right) + K(J_0 + J_2) \sin \beta = 0, \quad \dots (6.14)$$

$$-T \left( \omega - \frac{d\beta}{dt} \right) \omega + \frac{dm}{dt} + K(J_0 - J_2) \cos \beta = 0. \quad \dots (6.15)$$

To a first order of approximation

$$K(J_0 + J_2) \sin \beta \simeq -m \left( \omega - \frac{d\beta}{dt} \right), \quad \dots (6.16)$$

$$\text{and} \quad K(J_0 - J_2) \cos \beta \simeq T \left( \omega - \frac{d\beta}{dt} \right). \quad \dots (6.17)$$

Therefore from the Eqs. (6.12), (6.16) and (6.17)

$$T \frac{d\omega}{dt} + \omega - K \frac{1}{2\sqrt{1+\omega^2 T^2}} = \Omega. \quad \dots (6.18)$$

from which locking range and time can be found out. Again from above, we have

$$m\omega = KG J_0(m). \quad \dots (6.19)$$

The locking range is given by

$$\Omega_{10} = KG \left( 1 + \frac{\cos \phi_F}{2G} \right), \quad \dots (6.20)$$

where  $\phi_F$  denotes the filter-phase angle.

The locking time can be found by evaluating

$$T_F = T \int_{\omega_{max}}^{KG} \frac{d\omega}{\Omega - F(\omega)} \quad (6.21)$$

where

$$\begin{aligned} F(\omega) &= \omega - \frac{K}{2} \frac{1}{\sqrt{1 + \omega^2 T^2}} \\ &= \omega - \frac{K}{2} |G(\omega)|. \end{aligned}$$

It should be mentioned that equations (6.19), (6.20) and (6.21) will apply for any APC loop with a filter having negligible asymptotic gain.

### 6.3. Derivation of Simple Expressions for Locking Range and Time :

Locking range and time can also be estimated from the following simple treatment. We shall here assume that the instantaneous phase contains : (i) a very slowly varying component  $\alpha$ , corresponding to a slow change of the average discriminator voltage, (ii) a component varying linearly with time at the rate of the beat angular frequency and (iii) a component periodic at the beat frequency. If we further assume that the significant component of the periodic part is the fundamental, the following equations are obtained to a first order of approximation:

$$\frac{d\alpha}{dt} = \Omega - \omega + KG_0 J_1(m) \sin \alpha, \quad (6.22)$$

$$\frac{dm}{dt} = -KG[(J_0 - J_2) \cos \alpha \cos \phi - (J_0 + J_2) \sin \alpha \sin \phi]; \quad (6.23)$$

$$\text{and} \quad m\omega = -KG[J_0 \sin(\alpha + \phi) + J_2 \sin(\alpha - \phi)]. \quad (6.24)$$

Using these equations (Eq. 6.22 to 6.24), one can derive an approximate equation for the average drift in frequency

$$\frac{d\alpha}{dt} : (\Omega - 0.8KG) - 0.2KG_0 \sin \alpha \quad (6.25)$$

where  $\bar{G}$  stands for the average value of the network gain over the range—d.c. to the initial difference frequency  $\Omega$ . The weighted averaging involved in this derivation has been done with due regard to the ranges over which the quantities vary. It is to be noted, for example, that the value of 'm' will be initially small, but after a while will approach unity.

Eq. (6.25) is identical in form with Eq. (4.3) and gives both the locking range and time. Thus assuming  $G_0 = 1$ , the initial difference frequency is given by

$$\Omega = K\bar{G} \quad \dots \quad (6.26)$$

The locking time can be found by evaluating

$$T_F = \int_{\alpha_i}^{\alpha_f} \frac{d\alpha}{\Omega_0 - K_0 \sin \alpha} \quad \dots (6.27)$$

$$\Omega_0 = \Omega - 0.8KG, \quad K_0 = .2KG_0$$

where  $\alpha_i$  and  $\alpha_f$  are the initial and final values of  $\alpha$ .

The initial value of  $\alpha$  can be found by putting  $dx/dt = 0$ ,  $dm/dt = 0$  in Eqs. (6.22) to (6.24). An working approximate value for  $\alpha_i$  is  $[\pi/2 - \phi(\Omega)]$ . The final value is obviously equal to  $\sin^{-1}(\Omega/K)$ . Using Eq. (6.27) it is now possible to find the locking time for a given difference frequency.

It will appear that the knowledge of the average gain  $G$  and the network phase  $\phi(\Omega)$  at  $\Omega$  is sufficient to obtain reasonably accurate estimates of the locking time and range (see Sec. 7). The value of  $G$  in Eqs. (6.26) and (6.25) can be found out either analytically or graphically. Analytical solutions are possible only in simple cases and one will have to take recourse to graphical techniques in cases when the network gain function contains a number of poles and zeros.

Graphical constructions for the filters (Figs. 8a and 8b) have been shown in Figs. 12 and 13 from which the evaluation of locking ratio ( $\Omega/K$ ) can be accomplished with the help of equation (6.26).

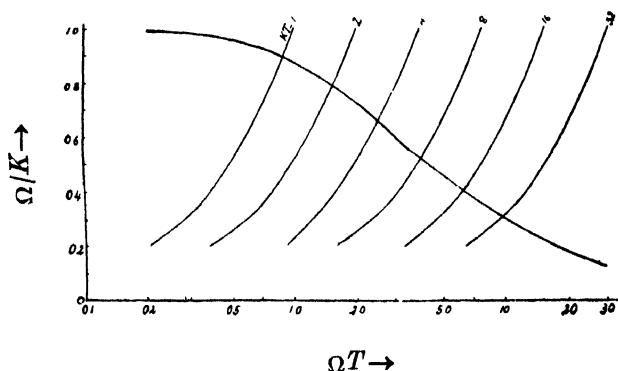


Fig. 12. Graphical determination of locking ratio for the simple R-C filter of Fig. 8(a)

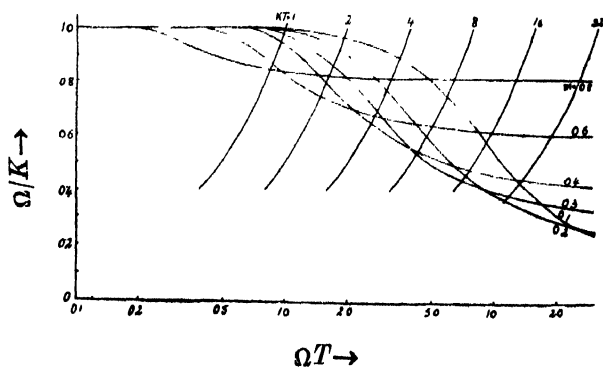


Fig. 13. Graphical determination of locking ratio for the filter of Fig. 8(b).



## EXPERIMENTAL SET-UP AND RESULTS

In this section we shall first describe the experimental set-up. This will be followed by a discussion of the results obtained and comparison of these with the results of the analysis presented in section 6.

Fig. 14 shows the experimental set-up for making measurements of the locking range ( $\Omega$ ) for two types of filters—one having negligible high frequency

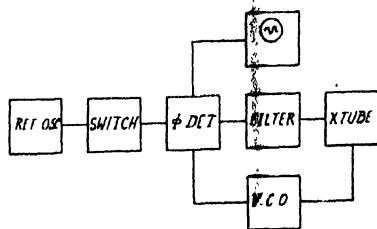


Fig. 14. Experimental set-up.

gain and the other having finite high frequency gain to check the theoretically derived results. The detailed circuit diagram is shown in Fig. 15. The phase shift of  $90^\circ$  required between the grid and the plate voltages in the reactance tube (4) has been achieved by means of a two stage R-C phase-shifter ( $R_{13}C_{13}R_{14}C_{14}$ )

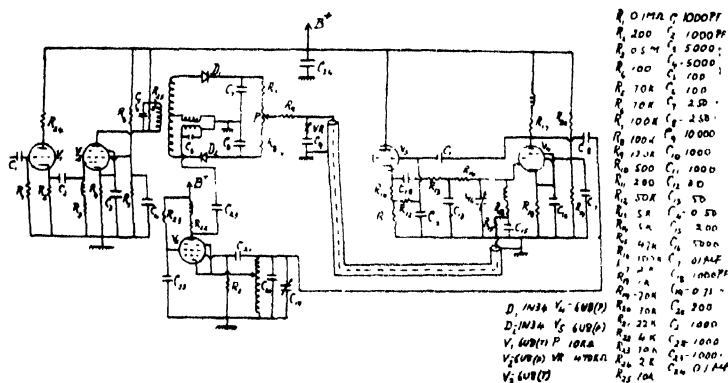


Fig. 15. Detailed circuit diagram of the system.

provided with a trimmer to effect accurate adjustments. This arrangement was adopted as it ensures negligible conductance loading of the reactance tube ( $V_4$ ). The oscillator to be synchronised is electron coupled tuned grid Hartely type ( $V_5$ ). The phase detector used is of the balanced demodulator type. Its output is the difference between the voltages  $|E_c + E_i|$  and  $|E_c - E_i|$  where  $E_c$  and  $E_i$  are proportional respectively to the oscillator and input synchronising voltages. For a successful operation of the circuit it is necessary to guarantee that the ratio of the magnitudes of the two voltages never approaches unity. The centre frequency of the oscillator and the input amplifier need be carefully adjusted to the same value. Further, the input amplifier for feeding the phase detector should have a flat top characteristics. Presence of a dip anywhere in its response characteris-

ties is likely to produce spurious effects and sometimes a type of oscillation. It is necessary to ensure that the time constant of the detector circuit be such that the  $r$ - $f$  filtering is adequate, yet is small enough as not to interact with the filter time constants. In fact the latter consideration sets the lowest limit to the minimum filter time constant usable. It has been found necessary to incorporate an  $r$ . $f$ . choke in the path from the detector-filter to the grid of the reactance tube to provide effective  $r$ . $f$ . decoupling. It should also be mentioned that large variations of resistance in the d.c. grid circuit should be avoided as it affects the sensitivity of the X-tube. The value of the limiting angular frequency of synchronisation ( $K$ ) obtaining in the circuit described is 10 kiloradian/sec.

In Fig. 16 the experimental values of the locking ratio ( $\Omega/K$ ) have been plotted against the product of the limit of synchronising frequency in radian per sec and the filter time constant of the network of Fig. 8a. The variation of time constant was here effected by changing the value of the capacitance  $C$ . It will be found that the experimental values are in close agreement with the corresponding values computed from Eq. (6.26) which are also shown in Fig. 16. The values of locking

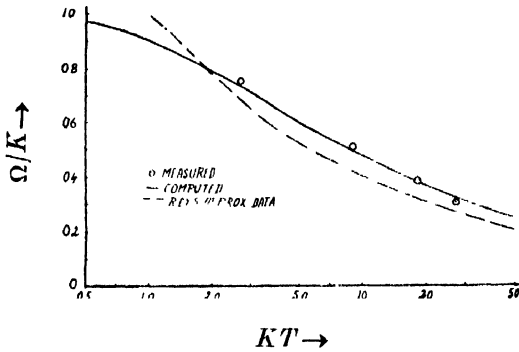


Fig. 16. Pull-in performance of the system with filter of Fig. 8(a).

ratio obtained by computations using Eq. (6.20) have been found to be close to but a little less than the experimental values.

In the APC circuit using the filter of Fig. 8b, the value of the ratio of the a.c./d.c. gain was varied by changing the value of  $XR$  and the time constant by

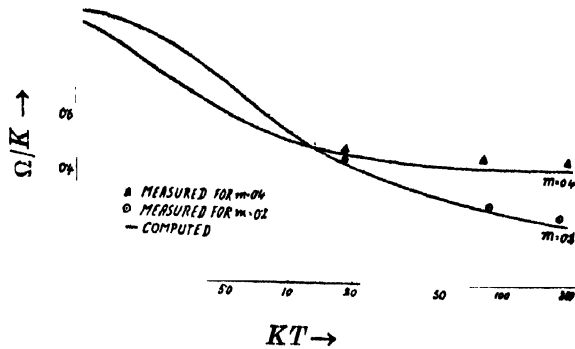


Fig. 17. Pull-in performance of the system with filter of Fig. 8(b).

changing the capacitance  $C$ . Fig. 17 shows the values of the locking ratio determined experimentally as well as those computed from Eq. (6.26) for this case. (Photographs showing transient pull-in for the filter of Fig. 8(b) are given in

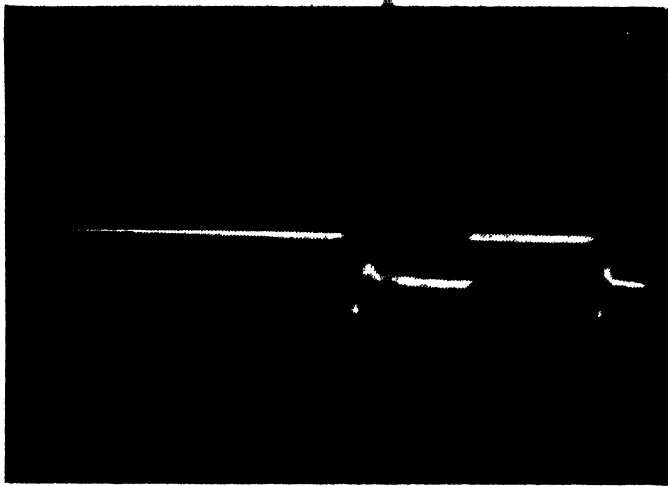


Fig. 18. (a) Photograph showing pull-in time for an APC circuit with the filter of Fig. 8(b) when the initial difference frequency is: 0.5 Kc/s below the centre frequency.

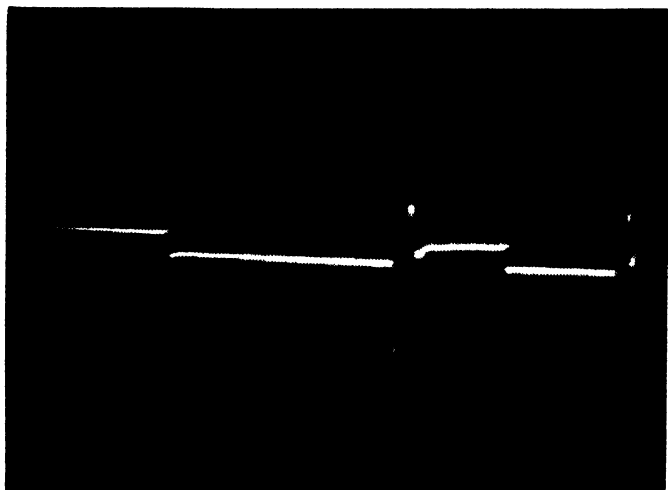


Fig. 18. (b) 0.5 Kc/s above the centre frequency.

Fig. 18). Here also the agreement is fairly close. If, however, Eq. (6.9) is used for computing the locking ratio, it will be found that the computed values agree with the experimental values for large values of  $T$  only. The discrepancy at low values of  $T$  arises from the fact that the difference between the high and the low frequency time constants is then small.

It can be concluded from the above results that Eq. (6.26) provides a simple

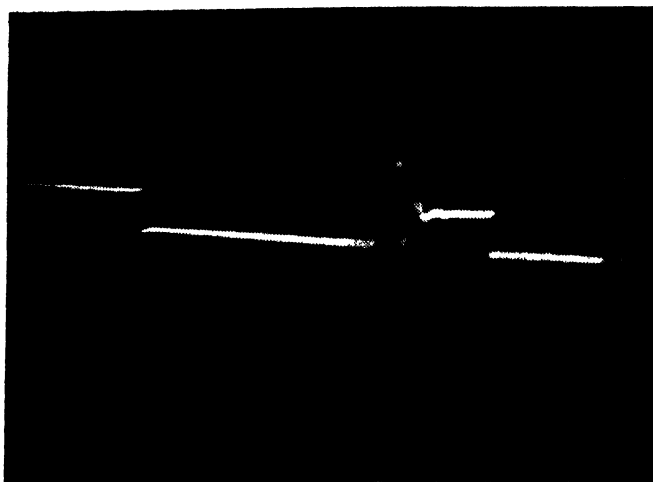


Fig. 18. (c) 1.0 Kc/s above the centre frequency.

yet fairly accurate relation for calculating the locking range and time of APC systems with filters of a wide class.

#### CONCLUDING REMARKS

The locking phenomenon in APC circuits with two different filter networks has been analysed for continuous synchronising signal at the input and their performance studied experimentally. The cases of interrupted wave synchronisation and the synchronisation with a signal having low S/N ratio will be considered in a future communication.

#### ACKNOWLEDGMENT

The authors wish to thank Prof. J. N. Bhar, D.Sc., F.N.I., for his kind interest and encouragement.

#### APPENDIX

##### A.1. *Response to a step-change in 'Ω' and phase Locking Range and Time*

We shall here consider the response of an APC circuit to a step change in the angular frequency 'Ω' applied to the input. If the instantaneous phase difference between the external input and the reference input is sufficiently small, then the governing equation of the loop is :

$$\frac{d\phi}{dt} \simeq \Omega - \frac{2}{\pi} \cdot KG(p) \cdot \phi. \quad (\text{A.1})$$

With this approximation one can readily find the minimum value of  $\phi$  so that the system never loses cycles by determining the condition that the resultant phase

on excitation by a step in frequency never exceeds  $\pm\pi/2$ . For the purpose one has only to find the amount of overshoot  $\gamma$  in the step response of

$$F(p) = - \frac{\Omega}{p[p + \frac{2}{\pi} K \cdot G(p)]} \quad \dots \quad (\text{A.2})$$

The value of the steady state phase  $\phi_s = \pi/2 \cdot \frac{\Omega}{K}$ . Hence the required condition is seen to be,

$$\frac{\pi}{2} \Omega (1+\gamma) < K\pi/2$$

i.e.,  $\Omega (1+\gamma) < K. \quad \dots \quad (\text{A.3})$

If this condition is satisfied one can find the phase locking time by calculating the time required for settling to a value within five per cent of the difference between the initial and final phases. Let us assume that a sudden step change in frequency is applied at  $t = 0$ , when the initial conditions are  $\phi = 0$ , and  $d\phi/dt = 0$ . Then Eq. (A.1) reduces to

$$[1 + (1+x)pT]p \cdot \phi(p) + \frac{2}{\pi} \cdot K \cdot (1+xpT)\phi(p) = \frac{\Omega}{p} [1 + (1+x)pT] \dots \quad (\text{A.4})$$

Substituting

$$T_1 = \frac{(1+x)T}{1 + \frac{2}{\pi} xKT}$$

and

$$K_1 = \frac{K}{1 + \frac{2}{\pi} xKT} \quad \dots \quad (\text{A.5})$$

and comparing (A. 4) with (A. 5) we have

$$\phi(p) = \frac{\Omega}{p} \cdot T_1 \left[ p + \frac{1}{(1+x)T} \right] \cdot \frac{1}{p^2 T_1 + p + 2/\pi K_1} \quad \dots \quad (\text{A.6})$$

or,

$$\phi(p) = \frac{\Omega T_1 \left[ p + \frac{1}{(1+x)T} \right]}{p[p + \alpha + j\beta][p + \alpha - j\beta]} \quad (\text{A.7})$$

where  $(\alpha \pm j\beta)$  are the roots of the polynomial  $p^2 T_1 + p + 2/\pi K_1 = 0$ . Hence the variation of phase function with time is given by

$$\phi(t) = \frac{\Omega T_1}{\alpha^2 + \beta^2} \left[ \frac{1}{(1+x)T} - \frac{e^{-\alpha t}}{\beta} \cdot A \sin(\beta t + \psi) \right], \quad (\text{A.8})$$

where,

$$A = \left[ \left\{ \frac{\alpha}{(1+x)T} - (\alpha^2 + \beta^2) \right\}^2 + \left( \frac{\beta}{(1+x)T} \right)^2 \right]^{\frac{1}{2}} \quad \dots \quad (\text{A.9})$$

and

$$\psi = \tan^{-1} \frac{\frac{\beta}{(1+x)T}}{\frac{\alpha}{(1+x)T} - (\alpha^2 + \beta^2)} \quad \dots \quad (\text{A.10})$$

From Eq. (A.8) the percentage overshoot will be found to be given by

$$\frac{\phi_m - \phi_s}{\phi_s} = \frac{A(1+x)T}{\beta} \cdot \sin \theta \cdot \exp [-(\pi + \theta - \psi) \cot \theta] \quad \dots \quad (\text{A.11})$$

where  $\phi_m$  and  $\phi_s$  are the maximum and steady state phase shifts respectively and

$$\theta = \tan^{-1}(\beta/\alpha) \quad \dots \quad (\text{A.12})$$

From Eqs. (A.3) and (A.11) the locking ratio is seen to be given by the approximate relation :

$$\frac{\Omega}{K} \simeq \frac{1}{1+q \cdot y} \quad \dots \quad (\text{A.13})$$

where

$$q = \frac{A}{\beta} \sin \theta \cdot \exp [-\pi + \theta - \psi] \cot \theta \quad \dots \quad (\text{A.14})$$

$$y = (1+x)T \quad \dots \quad (\text{A.15})$$

The instants when the phase equals  $\phi_s$  can be found from Eq. (A.8). Thus  $t_n = \frac{n\pi - \psi}{\beta}$ . An approximate value for the phase settling time can be written as

$$T_p \simeq \frac{1}{3\alpha} \cdot \log \left[ \frac{A}{\beta} \cdot y \right] \quad \dots \quad (\text{A.16})$$

## A.2. Noise Bandwidth :

Noise bandwidth can be defined as

$$B_n = \int_0^\infty |G(\omega)|^2 df \quad \dots \quad (\text{A.17})$$

where  $G(\omega)$  is the normalised closed loop transfer function. (A.17) can also be written as

$$B_n = \frac{1}{2\pi j} \int_0^\infty G(p) G(-p) dp \quad (\text{A.18})$$

Now for the lag network, we have

$$f(p) = \frac{1+xpT}{1+(1+x)pT} \quad \dots \quad (\text{A.19})$$

$$\text{and} \quad G(p) = \frac{Kf(p)}{p + Kf(p)} \quad \dots \quad (\text{A.20})$$

$$\text{Hence} \quad B_n = \frac{K}{4} \cdot \frac{(\alpha + xKT)}{\alpha(1 + xKT)} \quad \dots \quad (\text{A.21})$$

$$\text{where} \quad \alpha = (1 + 1/x). \quad \dots \quad (\text{A.22})$$

#### REFERENCES

- Byard, S. and Eccles, W. H. 1941, *Wireless Eng.*, **18**, 2.  
 Byrne, C. J. 1962, *B. S. T. J.* **41**, 559.  
 Carnahan, C. W. and Kalmus, H. P. Aug. 1944, *Electronics*, 108.  
 Clerk, E. G. "Oscillators" 1954, Convention record of I.R.E., National convention, pp. 31.  
 Goldstein, A. J. 1962, *B. S. T. J.*, **41**, 603.  
 Gruen, W. J. 1953, *Proc. I.E.E. Aug.*, **41**, 1043.  
 Jelonek, Z., Celinski, O. and Syski, R. 1953, *Proc. I.E.E.* **79**,  
 Jelonek, Z. J. and Cowan, C. I. 1957, *Proc. I.E.E.*, **229** R.,  
 Labin, E., 1949, *Phillips Res. Rep.* **4**, 291.  
 Leek, R. 1957, *Elec. and Radio Eng.* **34**, 114, and 177.  
 Mc Aleer, H. T. 1959, *Proc. I.R.E.* **46**, 1137.  
 Minorsky, N. "Introduction to Non-linear Mechanics" (J. W. Edwards 1947 Ann Arbor)  
 Preston, G. W. and Tellier, J. C. 1953. *Proc. I.R.E.*, **41**,  
 Rey, T. J. 1960, *Proc. I.R.E.* **48**, 1760.  
 Richman, D. "Color Television" 1954, *Proc. I.R.E.*, **42**, 106.  
 Richman, D. 1954, *Proc. I.R.E. Vol.* **42**, 288.  
 Salmel, G. 1956, *Proc. I.R.E.*, **44**, 1582.  
 Spence, R. and Boothroyd, A. R. June, 1958, *Proc. I.E.E.* paper no. 307 R.  
 "Theory of Servo-mechanism"—Radiation Laboratory series. Vol. 25.  
 Tucker, D. G. and Jamieson, G. G. March, 1956, *Proc. I.E.E.*, paper no. **146** R.  
 Tucker, D. G. *Wireless Eng.* **24**, 178.  
 Tucker, D. G. 1943, *Elect. Engineering*, **15**, 412-457; 1943, **16**, 26 and 114.  
 Tucker, D. G. 1945, *Jour. I.E.E.* **92**, Part III, 226.  
 Van der Pol, B. 1927. *Phil. Mag.*, **3**, 65.

# *Letters to the Editor*

*The Board of Editors does not hold itself responsible for opinions expressed in the letters published in this section. The notes containing short reports of original investigations communicated to this section should not contain many figures and should not exceed 500 words in length. The contributions reaching the Secretary by the 15th of any month may be expected to appear in the issue for the next month. No proof will be sent to the author.*

## 8

### ULTRAVIOLET ABSORPTION OF CARBONATE AND BICARBONATE IONS

A. MOOKHERJI AND S. P. TANDON\*

PHYSICAL LABORATORIES, BURDWAN UNIVERSITY,

BURDWAN, W. B., INDIA.

*(Received January 15, 1964; Resubmitted, April 4, 1964)*

Carbonate and bicarbonate ions have planar structure and  $D_{3h}$  symmetry (Mooney, 1932) similar to that of nitrate ion and hence are expected to give rise to absorption spectra similar to nitrate ion (Mookherji and Tandon, 1962; Tandon, 1961). However, a detailed study (Janz and Mikawa, 1960) of the correlation of 0-0 repulsion force constant and separation distances, reveals that though there is a close resemblance between the structures of nitrate and carbonate ions yet they differ in charge distribution. There is positive charge on nitrogen atom in close proximity to the negative charge on the nitrate ion (Tandon, 1962), while carbon atom in carbonate ion has no charge. Due to these differences in charge distribution and values of atomic orbitals the energies of the absorption bands of nitrate and carbonate ions should not be the same, though the general nature of the spectrum be similar as demanded by close resemblance in structure. Hence the authors with improved technique made a close study of the spectrum with a "Uvispek" spectrophotometer scanning the spectrum at an interval of  $2.5\text{\AA}$  in the region  $1850\text{\AA}$  to  $3600\text{\AA}$ . Aqueous solutions at different concentrations of several carbonates and bicarbonates showed one weak band at about  $2000\text{\AA}$  and the other, very weak compared to the first, at about  $2700\text{\AA}$ . The band at  $2000\text{\AA}$  was observed earlier by Ley and Arends (1932) but not the band at  $2700\text{\AA}$ .

X-ray (Mooney, 1932), infrared (Ramdas, 1953) and magnetic studies (Mookherji, 1951) showed that the presence of hydrogen bond in bicarbonate ion

\*Physics Department, University of Jodhpur, Jodhpur, India.



does not affect the carbonate group. Consequently, the absorption spectra of carbonates and bicarbonates should be similar. This is what has been observed.

The band width of both the bands is almost the same and  $\sim 10^3 \text{ cm}^{-1}$  which is nearly the same as that of the nitrate ion. Hence it is inferred that the excited states for both the bands may be antibonding (Jorgensen, 1962).

The oscillator strength  $P$  for 2000 Å band was calculated following Jorgensen (1954) which comes out  $\sim 10^{-4}$ . This compares well with that of 3000 Å band of nitrate ion, suggesting that the transition is not an allowed one. The other band at 2700 Å has an oscillator strength  $\sim 10^{-6}$ , characteristic of a highly forbidden transition. Transition probabilities calculated following Tanabe and Sugano (1954) and Mookherji and Tandon (1962) for both the bands also lead to the same conclusion.

The band at 2000 Å showed fine structure but could not be studied closely because of poor intensity. Work is in progress in that direction in our laboratory, with improved procedure.

The shift of this band towards shorter wavelengths (blue shift) with progressive dilution, the feeble intensity ( $P \sim 10^{-4}$ ) and the resemblance of the structure with nitrate ion suggest a  $n \rightarrow \pi^*$  transition. This is in conformity with the findings of the polar solvent's influences on the absorption frequency (McConnell, 1952).

Calculations by LCAO-MO treatment of carbonate ion similar to that of nitrate ion by McEwen (1961) show that  $n \rightarrow \sigma^*$  transition has energy smaller than  $n \rightarrow \pi^*$  one. Thus low energy and intensity of the band at 2700 Å suggest that the band may be assigned to the forbidden  $n \rightarrow \sigma^*$  transition. This is further supported by the large band width of the same order as that of 2000 Å band revealing the antibonding character of the orbital giving rise to the excited state.

#### REFERENCES

- Janz, G. J. and Mikawa, Y., 1960, *J. Mol. Spectroscopy*, **5**, 92.  
 Jorgensen, C. K., 1954, *Acta Chem. Scand.*, **8**, 1502.  
 —do— 1962, *Absorption Spectra and Chemical bonding in Complexes*—Pergamon Press.  
 Ley, H. and Arends, B., 1932, *Z. physik Chem.*, **B17**, 192.  
 McConnell, H., 1952, *J. Chem. Phys.*, **207**, 700.  
 McEwen, K. L., 1961, *J. Chem. Phys.*, **34**, 547.  
 Mooney, C. L., 1932, *Phys. Rev.*, **39**, 861.  
 Mookherji, A., 1951, *Raj. Univ. Studies*, **1A**, 5.  
 Mookherji, A. and Tandon, S. P., 1962, *Indian J. Phys.* **36**, 211, 344.  
 Ramdas, A. K., 1953, *Proc. Ind. Acad. Sci.*, **37**, 441.  
 Tanabe Y. and Sugano, S., 1954, *J. Phys. Soc., Japan*, **9**, 766.  
 Tandon, S. P., 1961, *Raj. Univ. Studies*, **7**, 69.  
 —do— , 1962, *Proc. Raj. Acad. Sci.*, **9**, 58.

# PRELIMINARY OBSERVATIONS ON A REVERSIBLE STRUCTURAL CHANGE IN COBALT FLUOSILICATE HEXAHYDRATE

SIDDHARTHA RAY

DEPARTMENT OF MAGNETISM,

INDIAN ASSOCIATION FOR THE CULTIVATION OF SCIENCE,  
CALCUTTA-32.

(Received March 1, 1964)

It has been recently observed in our laboratory (Majumder and Datta, communicated for publication) that rhombohedral crystals of cobalt fluosilicate hexahydrate, suspended along the trigonal axis, start showing magnetic anisotropy when cooled below 248°K. Further, this change in magnetic behaviour has been found to be reversible with temperature. This phenomenon evidently indicates some reversible structural change in the crystals at the said low temperature, hence X-ray investigation was taken up to find out the nature of the change.

From the magnetic observations it appears that whatever the change it undergoes, a single crystal remains a single crystal in the new phase. So, oscillation and Weissenberg photographs could be obtained with crystals cooled well below the reported transition point. For the preliminary observations reported here, all the photographs were taken with crystals oscillating about the trigonal axis, in a Weissenberg camera equipped with a gas-flow type cooling system.

The Weissenberg photograph thus obtained at low temperature shows that corresponding to each spot appearing in the similar photograph taken at room temperature, there is a pair of spots, one of which lies at a slightly different Bragg angle than the other. The photograph thus contains two distinct families of spots, indicating that the diffraction pattern obtained at a temperature below the magnetic transition point corresponds to two different coexisting phases.

Both the families of spots can be indexed by triply primitive hexagonal cells (as is the case for a rhombohedral structure referred to hexagonal axes), with parameters  $a = 9.68 \pm .01 \text{ \AA}$  and  $9.51 \pm .01 \text{ \AA}$  respectively for the two. It may be mentioned here that the value of the corresponding parameter for cobalt fluosilicate hexahydrate at room temperature is  $9.31 \text{ \AA}$  (Hassel and Salvesen, 1927).

Information regarding the cell dimensions along the *c*-axis are obtained from the oscillation photograph taken below transition temperature. Here also the splitting up of the spots into pairs is observed, but since the members of the

same pair are found to lie on the same layer line, it is evident that the  $c$ -axes of both the phase are identical in direction and repeat distance. Since the cooling attachment used permits recording of only half the diffraction pattern (lying on one side of the equatorial layer line), the repeat distance along the common  $c$ -axis of the two phases can only be determined very roughly, and is found to be  $9.8\text{\AA}$ . Corresponding value for the crystal at room temperature is  $9.695\text{\AA}$  (Hassel and Salvesen, loc. cit.).

The most interesting feature regarding the two low temperature phases is revealed on close observation of the intensities of the spots in the Weissenberg photograph. While the intensities of the spots corresponding to the phase with  $a = 9.68 \pm .01\text{\AA}$ , reveal a three-fold symmetry, no evidence of such a symmetry is observed in the intensities of those corresponding to the second phase. Hence the second phase is only pseudo-hexagonal, with  $a = b = 9.51 \pm .01\text{\AA}$  and  $\gamma = 120^\circ$ . This lack of three-fold symmetry explains the appearance of magnetic anisotropy below the transition temperature.

Another interesting feature of the transition is that even when a crystal was pre-cooled for one hour before starting the X-ray exposure (which extended for two hours in this particular case), the diffraction pattern showed the simultaneous existence of both the phases. However, it was not possible to decide at present whether the difference in cooling treatment made any difference in the relative concentration of the two phases.

Reversibility of the transition has also been tested by taking the photograph of a crystal brought back to room temperature after the low temperature exposure, when the same diffraction pattern as that recorded initially at room temperature is obtained.

Further detailed work on the structures of the phases and their relationship with the original structure of the crystal is in progress.

The author expresses his gratefulness to Prof. A. Bose, D.Sc., F.N.I., for suggesting the problem and his keen interest in the work and also to Dr. R. K. Sen, D.Sc., Reader, Central Scientific Services, for many helpful suggestions during the course of the work, and for kind permission to use the low temperature attachment set up by his pupils.

#### REFERENCES

- Majumder, M. and Datta, S. K., (1964), (*In Press*)  
Hassel, O. and Salvesen, J. R., 1927, *Zeit. Phys. Chem.*, **128**, 345.

# A SHORT NOTE ON LIGAND FIELD THEORY OF THE MAGNETIC ANISOTROPY AND SUSCEPTIBILITY OF $\text{Fe}^{2+}$ TUTTON SALTS

B. BHATTACHARYYA\*

DEPT. OF MAGNETISM, INDIAN ASSOCIATION FOR THE CULTIVATION  
OF SCIENCE, CALCUTTA-32.

(Received May 26, 1964)

Investigations on the magnetic susceptibility and anisotropy of  $\text{Fe}(\text{NH}_4\text{SO}_4)_2 \cdot 6\text{H}_2\text{O}$  (Bose *et al.*, 1961) by Pryce's method shows a 20% reduction of the spin-orbit coupling owing to covalency effects. We have therefore, applied here the more reasonable and general method of molecular orbitals (Van-Vleck 1932, Stevens 1953, and Bose *et al.*, 1960) assuming that the covalency overlap is anisotropic.

The theoretical calculations of principal ionic susceptibilities of  $\text{Fe}^{2+}$  are made and compared with the experimental data on anisotropy and mean susceptibility for the salt  $\text{Fe}(\text{KSO}_4)_2 \cdot 6\text{H}_2\text{O}$  (Table I) which is isomorphous to the ammonium double salt previously investigated. It is assumed here as in the previous case that the ligand field has a small tetragonal component superposed on the predominant cubic part.

As no paramagnetic resonance data for  $\text{Fe}^{2+}$  Tutton salts is available, we compare the  $g$ -values of  $\text{Fe}(\text{KSO}_4)_2 \cdot 6\text{H}_2\text{O}$  with those of Tinkham's (1955) on  $\text{FeF}_2$  diluted with  $\text{ZnF}_2$ . Since the crystalline fields in  $\text{FeF}_2$  is truly orthorhombic the  $g$ -values are somewhat different in magnitude from that in Tutton salts but the order of magnitudes are comparable within the limits of approximations involved.

In the case of  $\text{Fe}(\text{NH}_4\text{SO}_4)_2 \cdot 6\text{H}_2\text{O}$ , the tetragonal field coefficient  $\Delta$  increases with temperature from a value of  $270 \text{ cm}^{-1}$  at  $20^\circ\text{K}$  to  $650 \text{ cm}^{-1}$  at  $300^\circ\text{K}$ . In the case of  $\text{Fe}(\text{KSO}_4)_2 \cdot 6\text{H}_2\text{O}$ ,  $\Delta$  changes from  $240 \text{ cm}^{-1}$  at  $90^\circ\text{K}$  to  $640 \text{ cm}^{-1}$  at  $300^\circ\text{K}$ . Thus we see that the order of the anisotropic field and also their variations with temperature are almost the same in the two cases. The increase in  $\Delta$  with temperature is due to thermal expansion or relaxation effects in the salts. In the case of  $\text{Fe}(\text{NH}_4\text{SO}_4)_2 \cdot 6\text{H}_2\text{O}$  the spin-orbit coupling coefficient has been decreased by 20% from its free ion value of  $-103 \text{ cm}^{-1}$  (Owen 1955, Bose *et al.*,

---

\*Lecturer, St. Xavier's College, Calcutta and Honorary Research Scholar, Indian Association for the Cultivation of Science.

1961). In the case of  $\text{Fe}(\text{KSO}_4)_2 \cdot 6\text{H}_2\text{O}$  we find the spin orbit coupling  $\zeta_{||} = -80 \text{ cm}^{-1}$ ,  $\zeta_{\perp} = -83 \text{ cm}^{-1}$  instead of free ion value of  $-103 \text{ cm}^{-1}$ . This indicates again almost the same overlap between the 3d  $\text{Fe}^{2+}$  and  $s$ - and  $p$ - $0^2$ -charge clouds, except that the overlap here has been taken as anisotropic.

The details of the work will be published shortly elsewhere.

TABLE I

$\text{Fe}(\text{KSO}_4)_2 \cdot 6\text{H}_2\text{O}$ .

$$k_{||} = 0.95, \quad \zeta_{||} = 0.80 \text{ cm}^{-1}$$

$$k_{\perp} = -80, \quad \zeta_{\perp} = -88 \text{ cm}^{-1}$$

Temp. °K	$\text{cm}^{-1}$	$p^2$	$p_{  }^2 - p_{\perp}$	$g$ -values
300	640	28.57 (28.58)	10.31 (10.34)	..
220	416	28.13 (28.08)	12.87 (12.70)	..
90	240	26.00 (26.27)	22.10 (22.01)	$g = 8.48$ $(8.97 \pm .02)$ $g = 6$ (6)

The values in the parenthesis in the 3rd and 4th column indicate the experimental results of Bose (1948). The  $g$ -values within parenthesis in the 5th column are Tinkham's (1955).

## ACKNOWLEDGMENT

The author is grateful to Prof. A. Bose, D.Sc., F.N.I. for suggesting the problem and guidance in the work. He is also grateful to his colleagues Sri R. Chatterjee, D.Phil., Sri U.S. Ghosh and Sri R. Rai of the department for all help and discussions in working out the theory and calculations of the parameters. Finally, he is very thankful to the authorities of the St. Xavier's College, Calcutta and Indian Association for the Cultivation of Science for permitting him to carry out the research project.

## REFERENCES

- Bose, A., 1948, *Ind. J. Physics*. **22**, 483.  
 Bose, A. Chakravarti A. S. and Chatterjee R, 1961, *proc. Roy. Soc. A* **261**, 207.  
 Bose, A. Chakravarti A. S. and Chatterjee R, 1960, *Proc. Roy. Soc. A*. **255**, 145.  
 Owen, J., 1955, *Proc. Roy. Soc. A*. **227**, 193.  
 Stevens K. W. H. 1953, *Proc. Roy. Soc. A*. **219**, 542.  
 Tinkham M. 1955, *Proc. Roy. Soc. A*. **236**, 535.  
 Van-Vleck J. H. 1932, *Phys. Rev.* **41**, 208.



# RAMAN SPECTRA OF BENZENE AND CARBON-DISULPHIDE AT $-209^{\circ}\text{C}$

S. C. SIRKAR, D. K. MUKHERJEE and P. K. BISHUI

INDIAN ASSOCIATION FOR THE CULTIVATION OF SCIENCE,  
CALCUTTA-32.

(Received, May 5, 1964)

## Plate VI

**ABSTRACT.** The Raman spectra of crystals of benzene and carbon-disulphide at  $-209^{\circ}\text{C}$  have been investigated using liquid nitrogen boiling under reduced pressure as the refrigerant. At  $-209^{\circ}\text{C}$  benzene gives five low frequency lines at 62, 82, 91, 100 and  $134\text{ cm}^{-1}$  respectively. It has been pointed out that the heat capacities calculated for the crystal below  $70^{\circ}\text{K}$  upto  $4^{\circ}\text{K}$ , agree well with observed values by choosing three frequencies  $64\text{ cm}^{-1}$ ,  $100\text{ cm}^{-1}$  and  $134\text{ cm}^{-1}$  for three Einstein functions and taking into account a Debye function as pointed out earlier.

From a study of the structure of crystals of benzene at  $-3^{\circ}\text{C}$  it has been concluded that due to attraction between the  $\pi$ -electron of any ring and the hydrogen atom of the neighbouring molecule the planes of every pair of adjacent molecules in the (010) plane are almost perpendicular to each other and they are inclined to the b-axis. The low-frequency Raman lines have been attributed to the angular oscillations of such individual molecules attached to each other through hydrogen bonding.

In the case of carbon disulphide also, the two lines at  $73\text{ cm}^{-1}$  and  $81\text{ cm}^{-1}$  have been assigned to angular oscillations in molecules forming polymeric chains in the crystal through S...S bonding parallel to one of the diagonals of the (001) plane of the tetragonal unit cell.

## INTRODUCTION

The Raman spectrum of single crystal of benzene was first studied by Gross and Vuks (1935) and two new lines at  $63$  and  $108\text{ cm}^{-1}$  were observed by them. The lines were attributed to lattice oscillations. One of the present authors (Sirkar, 1936) observed three new lines at 81, 98 and  $124\text{ cm}^{-1}$  respectively in the Raman spectrum of frozen benzene at  $-180^{\circ}\text{C}$ . He concluded that the new lines shift away from the Rayleigh line and a new line appears when the crystals at a temperature just below the freezing point are cooled to  $-180^{\circ}\text{C}$ . He suggested that probably these lines were due to oscillations in groups of molecules formed by intermolecular association in the solid state. Sirkar and Gupta (1938) pointed out that the heat capacities of crystalline benzene at low temperatures observed by previous workers could be explained by assuming a Debye function with  $\theta'$  equal to  $121.5^{\circ}\text{K}$  and taking into account the three Einstein functions corresponding to the three Raman shifts 81, 98 and  $124\text{ cm}^{-1}$  respectively.

The Raman spectrum of single crystal of benzene at a temperature just below the freezing point of the liquid was next investigated by Kastler and Fruhling (1944). They observed four new lines at 35, 55, 65 and 100  $\text{cm}^{-1}$  respectively in place of the two lines reported by Gross and Vuks (1935). Rousset (1944) calculated the heat capacities of the crystal at low temperatures assuming the line 35  $\text{cm}^{-1}$  to be due to free rotation of the molecule about an axis perpendicular to the plane of the molecule and taking Einstein functions corresponding to the other three frequencies and also a Debye function with  $\theta'$  equal to 1150°K.

The Raman spectrum of a polycrystalline mass of benzene at  $-180^{\circ}\text{C}$  was re-investigated by Sirkar and Ray (1950) and they observed five new lines at 47, 53, 78, 95 and 134  $\text{cm}^{-1}$  respectively. Assuming these lines to be due to two molecules associated to each other and the line 95  $\text{cm}^{-1}$  to be a doublet, they calculated the heat capacities of the crystal upto 4°K taking Einstein functions corresponding to three Raman shifts 58, 90 and 135  $\text{cm}^{-1}$  respectively and a Debye function with  $\theta'$  equal to 121.5°K. They observed that although the calculated values of  $C_p$  were slightly less than the observed values of  $C_p$  reported by Ahlberg *et al.* (1937) in the ranges from 4°K upto 10°K and also above 50°K, the calculated values were larger than the observed values for temperatures from 20°K upto 40°K. They suggested that the lowest frequency corresponding to the line 53  $\text{cm}^{-1}$  observed for the crystal at  $-180^{\circ}\text{C}$  might shift to 64  $\text{cm}^{-1}$  at temperatures below 40°K and in that case the heat capacities calculated on the above assumptions would agree satisfactorily with the observed values.

The study of the Raman spectra of many other organic compounds in the solid state at different temperatures below their freezing points has shown that the new lines in the low frequency region undergo changes in their positions and intensities with lowering of temperature of the crystals upto about  $-180^{\circ}\text{C}$ .

The changes observed in the spectrum of crystals of para-dichlorobenzene by Ray (1951) with changes in temperature upto  $-180^{\circ}\text{C}$  indicate that some irreversible change in the spectrum takes place with lowering of temperature of the crystals upto  $-180^{\circ}\text{C}$ . It was not known, however, how the spectra would change with the lowering of temperature below  $-180^{\circ}\text{C}$ . An attempt was therefore, made to make an arrangement for studying the Raman spectra of frozen organic compounds at about 64°K and the results obtained in the case of benzene and carbon disulphide are discussed in the present paper.

#### EXPERIMENTAL

The refrigerant used for lowering the temperature upto 64°K was liquid nitrogen boiling under reduced pressure. The liquid nitrogen was supplied by Indian Oxygen Ltd. The arrangement for photographing the Raman spectra at 64°K is shown in Fig. 1 in which the sources of light used for illuminating the subs-



tance have been omitted. The mouth of the transparent Pyrex glass Dewar

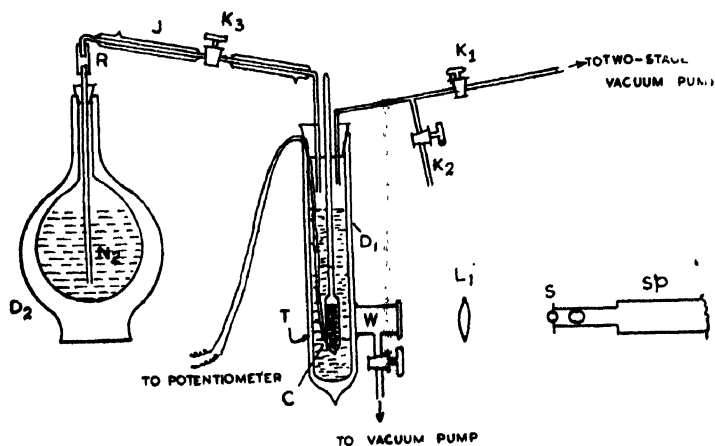


Fig. 1

vessel  $D_1$  is closed with a cork which is sealed with soft sealing wax. The vertical limb of the bent Pyrex glass tube provided with the stop cocks  $K_1$  and  $K_2$  enters into the vessel  $D_1$  through the cork upto a certain depth and the other end is connected to a high vacuum pump. The tube containing the sample is suspended inside the vessel so that its lower part rests in front of the window  $W$ . The open end of a wide and short glass tube with one of its ends closed with a glass plate is placed on the window and sealed with sealing wax. The tube thus closed at both ends is evacuated through a side tube connected to it so that no moisture can be deposited on the window when the Dewar vessel  $D_1$  is filled with liquid nitrogen. A third tube with its two ends bent as shown in the figure connects the Pyrex glass Dewar vessel  $D_1$  with the metallic Dewar vessel  $D_2$ . This tube is provided with a large stop cock  $K_3$  near its middle and the portions of the tube on both sides of  $K_3$  are double-walled, the regions between the two walls being evacuated. One of the short vertical limbs of the bent tube is connected through a rubber tube to a long narrow Pyrex tube which dips into liquid nitrogen contained in  $D_2$ . The other end enters into  $D_1$  through the cork. At first the stop cocks  $K_2$  and  $K_3$  were closed and the vessel  $D_1$  was evacuated. On opening  $K_3$  liquid nitrogen was drawn into  $D_1$  till the surface of the liquid rose upto a height below the lower ends of the two tubes which enter into  $D_1$  through the cork. The stop cock  $K_3$  was then closed and after some time the temperature measured with a copper-constantan couple was found to be almost constant. The constants of the thermocouple were determined by using the melting point of toluene, the boiling point of liquid oxygen and the boiling point of liquid nitrogen at atmospheric pressure as standard temperatures. When the crystals  $C$  formed inside the container attained this steady temperature the container was illuminated by light from two vertical mercury arcs which were focussed on the container

with the help of two wide glass tubes filled with distilled water. A fuess glass spectrograph giving a dispersion of about 12Å/mm in the 4047Å region was used to photograph the spectra. The exposure required varied from two to two and a half hours. When liquid nitrogen in D<sub>1</sub> was replenished the slit of the spectrograph was kept closed and it was opened again when the pressure in D<sub>1</sub> was sufficiently reduced by the pump. The lowest temperature attained was found to be  $-209^{\circ}\text{C}$ . The Raman spectra of benzene and carbon disulphide at this temperature were photographed using the arrangement mentioned above. The spectra of the compounds at  $-180^{\circ}\text{C}$  were also photographed using the same spectrograph in order to compare the results with those for the substances at  $-209^{\circ}\text{C}$ .

TABLE I  
Raman spectra of C<sub>6</sub>H<sub>6</sub> and CS<sub>2</sub>;  $\Delta\nu$  in  $\text{cm}^{-1}$

C <sub>6</sub> H <sub>6</sub> at $-180^{\circ}\text{C}$ Sirkar and Roy (1950)	C <sub>6</sub> H <sub>6</sub> at $-209^{\circ}\text{C}$ Present authors	CS <sub>2</sub> at $-183^{\circ}\text{C}$ Present authors	CS <sub>2</sub> at $-209^{\circ}\text{C}$ Present authors
47 (1)			
53 (2)	62 (3)		
		70 (15)	73 (10)
78 (5)	82 (5)	81 (3)	81 (2)
95 (1b)	91 (1)		
	100 (1)		
134 (3)	134 (3)		
603 (1)	605 (1)		
		656 (6)	658 (4)
		804 (2)	805 (1)
855 (2)	858 (2)		
989 (10)	992 (10)		
1174 (4)	1176 (4)		
1581 (3)	1584 (2)		
1602 (2)	1605 (2)		
3042 (2)	3046 (4)		
3046 (2)			
3063 (5)	3063 (4)		

## RESULTS AND DISCUSSION

The spectrograms for benzene and carbon disulphide are reproduced in Figs. 2, 3 and 4, Plate VI. The Raman shifts are given in Table I.

A comparison of the frequency shifts of benzene observed for the crystal at  $-180^{\circ}\text{C}$  and  $-209^{\circ}\text{C}$  shows that a significant change takes place in the positions of the lines in the low frequency region with the lowering of temperature from  $-180^{\circ}\text{C}$  to  $-209^{\circ}\text{C}$ . The lines 47 and  $53\text{ cm}^{-1}$  are replaced by a single line



Fig. 2. Benzene at  $-209^{\circ}\text{C}$ .  
Fig. 3. Carbondisulphide at  $-180^{\circ}\text{C}$ .  
Fig. 4. „ at  $-209^{\circ}\text{C}$ .



$62\text{ cm}^{-1}$  and also the line  $95\text{ cm}^{-1}$  splits up into two lines at  $91\text{ cm}^{-1}$  and  $100\text{ cm}^{-1}$  respectively with the lowering of temperature. Thus the predictions made by Sirkar and Ray (1950) that at temperatures below  $40^\circ\text{K}$  the lowest frequency of vibration might increase to  $64\text{ cm}^{-1}$  and the line  $95\text{ cm}^{-1}$  might split up into two lines are proved to be correct by the results. The results also support the conclusion that Einstein functions corresponding to three of the low frequency lines together with a suitable Debye function explain the heat capacities of the crystals of benzene from  $70^\circ\text{K}$  upto about  $4^\circ\text{K}$  quite satisfactorily.

In order to understand how three new modes of vibration of the molecule with such low frequencies arise in the crystal it is necessary to take into consideration the orientation of the molecules in the lattice given by Cox and Smith (1954) in the case of the crystal at  $-3^\circ\text{C}$ . The photograph of a model of the upper half of the unit cell made in accordance with the structure reported by them is shown in Fig. 5. The normal to the molecule at each corner of the ortho-

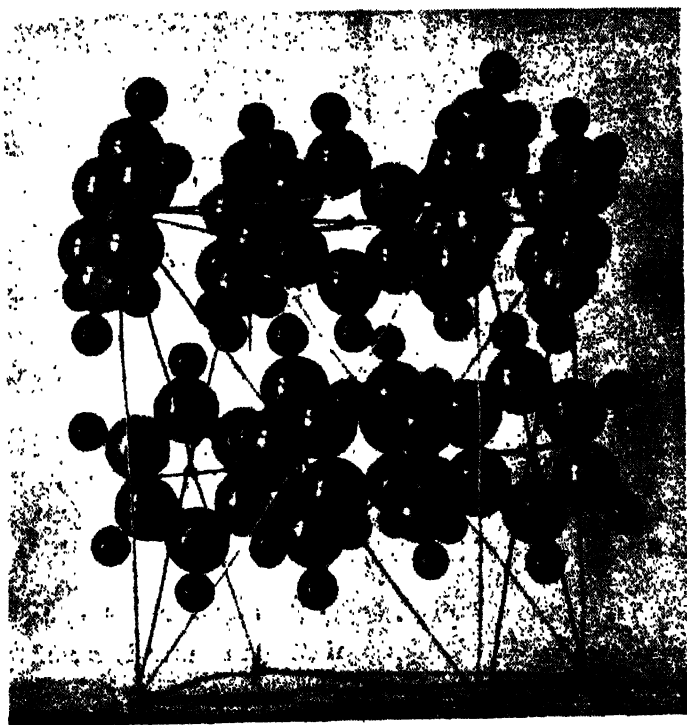


Fig. 5

rhombic unit cell is inclined at  $48^\circ$  to  $c$ -axis and at  $77^\circ$  to  $b$ -axis. The latter axis is vertical in Fig. 5. The other three molecules in the unit cell are derived by the two-fold screw axes parallel to  $b$ -axis at distance  $a/4$  in the  $(001)$  plane and also similar axes in the  $(010)$  and  $(100)$  faces parallel to  $a$ -axis at a distance  $c/4$

and to  $b$ -axis at a distance  $c/4$  respectively. The cell is a pseudo-face-centred one, the molecules at the centre of faces being turned with respect to those at the corners of the unit cell. It can be seen from the model that the planes of all the molecules are only slightly inclined to the  $b$ -axis, the angle of inclination being  $13^\circ$ , but no two adjacent molecules in the (010) plane are parallel to each other. In fact, every molecule in this plane is surrounded by its four nearest neighbours oriented in such a way that the angle between the normal to the plane of the molecule and that to any of its four neighbours is either about  $82^\circ$  or about  $92^\circ$ . The density of the crystal at  $-3^\circ\text{C}$  is about 1.08 g/cc.

It is a significant fact that the adjacent molecules in the (010) plane are not parallel to each other and also they are not parallel to  $b$ -axis so as to form a tetragonal lattice. The orientation shown in Fig. 5 indicates an attraction between the hydrogen atom of a molecule at the corner of the unit cell and the nearest carbon atom of the molecule at the centre of the (010) face. Probably the  $\pi$ -electrons of the carbon atoms are responsible for such an attraction. The small tilt about a diagonal of the (010) face diminishes the distance between the two such atoms lying below the (010) face on one side of the centre of the face and that between two such atoms lying above the (010) plane on the other side. The shortest distance between the centres of the hydrogen atom and the carbon atom mentioned above is about 2.72Å. It appears that whenever two benzene molecules try to approach each other their planes become almost mutually perpendicular to each other due to the attraction between the hydrogen atom of one of the molecules and a carbon atom of the other molecule. If this process is repeated in two almost mutually perpendicular directions a sheet of molecules form the (010) plane. It is evident from the structure that when the other such sheets parallel to (010) plane are arranged one above the other the shortest distances between the carbon atoms in the upper half of the molecule at the centre of the (010) face and the hydrogen atoms of the neighbouring molecules at the centres of the other two faces and at the corner of the unit cell are the same and have a value about 2.72Å. Similar distances occur also in the case of the lower half of the molecule at the centre of the (010) face.

Since there is a centre of symmetry at the centre of each molecule any translational oscillation of the molecules against each other is forbidden in Raman effect. The four lines at 35, 55, 65 and  $100\text{ cm}^{-1}$  observed by Kastler and Fruhling (1944) are therefore due to angular oscillations of the molecule. The first line may be due to such an oscillation about an axis perpendicular to the plane of the molecule. This axis almost coincides with a diagonal of the (010) face of the unit cell. The lines 55 and  $65\text{ cm}^{-1}$  are probably due to angular oscillation of the molecule about the other diagonal of the (010) face, the splitting arising from the slight difference between the molecule at the corner of the unit cell and that at the centre of the (010) face introduced by the deviation of the unit cell from the

tetragonal form and by the inclinations of the molecule to the *b*-axis. The line  $100\text{ cm}^{-1}$  may be due to an oscillation about the *b*-axis of the crystal.

The crystal structure of benzene at  $-180^{\circ}\text{C}$  or at still lower temperatures is not known. The lines 62, 82, 91, 100 and  $134\text{ cm}^{-1}$  given by the crystal at  $-209^{\circ}\text{C}$  are also due to such oscillations. It appears that frequencies of these oscillations increase and some of them are split up into two frequencies at the lower temperature. The angles between the normal to the molecule and the *c*-axis and *b*-axis may be greater than  $48^{\circ}$  and less than  $77^{\circ}$  respectively at  $-209^{\circ}\text{C}$ . In that case the primitive translation along *c*-axis may be much less than  $7.05\text{\AA}$  found for the crystal at  $-3^{\circ}\text{C}$ . The contraction of the lattice at the low temperature is expected to make the shortest C...H distance less than  $2.72\text{\AA}$ , and therefore, the strength of the C...H bond is expected to increase at the lower temperature. The increase in the tilt of the molecule about the horizontal axis may increase the difference in the environment of the molecule at the corner of the unit cell and that of the molecule at the centre of the (010) face and thus there may be at most six frequencies of angular oscillation. If two of them be very near to each other only five frequencies can be observed and the five Raman lines given in Table I for the crystal at  $-180^{\circ}\text{C}$  or  $-209^{\circ}\text{C}$  can be accounted for on these assumptions.

It may be pointed out here that Bhagavantam (1941) and independently Kastler and Rousset (1941) proposed that the low frequency lines in the Raman spectra of naphthalene and benzene might be due to angular oscillations of the molecules, pivoted in the lattice, about their three axes. The above discussions show that formation of weak intermolecular linkage is responsible for the restoring forces required for such oscillations in the crystals of benzene, as pointed out by Sirkar (1951). Table I shows that the frequencies of some of the other modes of oscillation of the benzene molecule also tend to increase at lower temperatures. The frequency shift  $858\text{ cm}^{-1}$  diminishes to  $849\text{ cm}^{-1}$  when the crystals are melted. As this line is due to a mode involving bending of the C-H bond in a plane perpendicular to the plane of the ring the increase in the frequency at low temperatures indicates formation of hydrogen bond. The slight increase in the frequencies of some of the modes of vibration of the ring may be due to slight increase in the strength of the C-C bond at lower temperatures.

The density of benzene at  $20^{\circ}\text{C}$  is about  $0.879\text{ g/cc}$  and that of the crystal at  $-3^{\circ}\text{C}$  is  $1.08\text{ g/cc}$ . So, the volume increases by about 22% when the crystals are melted and brought to a temperature of  $20^{\circ}\text{C}$ , and therefore, each of the diagonals of the (010) plane of length  $10.25\text{\AA}$  is represented by a distance  $10.97\text{\AA}$  in the liquid. If the arrangement of the molecules in the crystal is assumed to persist to some extent in the liquid the molecules will generally be free to rotate about an axis perpendicular to the plane of the ring, but it may be possible for some adjacent molecules to be still linked to each other through C...H bonding

# ON RUMER'S INVARIANT THEORY OF GRAVITATIONAL WAVES

K. D. KRORI

DEPARTMENT OF PHYSICS, COTTON COLLEGE, GAUHATI (ASSAM)

(Received, July 7, 1963 ; Resubmitted, April 22, 1964)

**ABSTRACT.** Propagation of gravitational potential and gravitational field-strength has been considered here on the basis of Rumer's Invariant Theory of Gravitational Waves. Finally some special cases of weak field have been discussed.

## INTRODUCTION

Rumer (1962) has constructed a theory of gravitation by breaking up the fourth-rank Riemann tensor  $R_{\mu\nu\alpha\beta}$  into a sum of two 10-component tensors  $M_{\mu\nu\alpha\beta}$  and  $F_{\mu\nu\alpha\beta}$ , both of which have the symmetry of Riemann tensor (anti-symmetrical in  $\mu$  and  $\nu$  as well as in  $\alpha$  and  $\beta$ ) :

$$R_{\mu\nu\alpha\beta} = M_{\mu\nu\alpha\beta} + F_{\mu\nu\alpha\beta} \quad \dots (1)$$

$M_{\mu\nu\alpha\beta}$  is called the matter-tensor and  $F_{\mu\nu\alpha\beta}$  the gravitational field-strength tensor. The expression for  $F_{\mu\nu}^{\alpha\beta}$  can be written as

$$\begin{aligned} F_{\mu\nu}^{\alpha\beta} &= R_{\mu\nu}^{\alpha\beta} - M_{\mu\nu}^{\alpha\beta} \\ &= R_{\mu\nu}^{\alpha\beta} + \frac{1}{2}[g_{\mu}^{\beta}T_{\nu}^{\alpha} + g_{\nu}^{\alpha}T_{\mu}^{\beta} - g_{\mu}^{\alpha}T_{\nu}^{\beta} - g_{\nu}^{\beta}T_{\mu}^{\alpha}] \\ &\quad - \frac{1}{8}(g_{\mu}^{\beta}g_{\nu}^{\alpha} - g_{\mu}^{\alpha}g_{\nu}^{\beta})T \end{aligned} \quad \dots (2)$$

where  $T_{\nu}^{\alpha}$  is the source-tensor. The field equations can be expressed as

$$(F_{\mu\nu}^{\alpha\beta})_{\beta} = \frac{1}{2}[(T_{\nu}^{\alpha})_{\mu} - (T_{\mu}^{\alpha})_{\nu}] - \frac{1}{8}(g_{\nu}^{\alpha}T_{,\mu} - g_{\mu}^{\alpha}T_{,\nu}) \quad \dots (3)$$

which consists of 20 independent equations.  $[(\ )_{\beta}]$  indicates covariant differentiation.]

The purpose of this paper is to discuss the propagation of the gravitational potential  $\phi_{\mu\alpha}$  (defined below) and of the gravitational field-strength  $F_{\mu\nu\alpha\beta}$  on the basis of Rumer's theory

## PROPAGATION OF GRAVITATIONAL POTENTIAL $\phi_{\mu\alpha}$

Considering the anti-symmetry of  $F_{\mu\nu\alpha\beta}$  in  $\alpha$  and  $\beta$ , it can be written as

$$F_{\mu\nu\alpha\beta} = (\psi_{\mu\nu\alpha})_{\beta} - (\psi_{\mu\nu\beta})_{\alpha} \quad \dots (4)$$



Again, because of anti-symmetry in  $\mu$  and  $\nu$ ,  $\psi_{\mu\nu\alpha}$  can be expressed as

$$\psi_{\mu\nu\alpha} = (\phi_{\mu\alpha})_{\nu} - (\phi_{\nu\alpha})_{\mu} \quad \dots (4a)$$

so that

$$F_{\mu\nu\alpha\beta} = (\phi_{\mu\alpha})_{\nu\beta} - (\phi_{\nu\alpha})_{\mu\beta} - (\phi_{\mu\beta})_{\nu\alpha} + (\phi_{\nu\beta})_{\mu\alpha} \quad \dots (5)$$

We consider that  $\phi_{\mu\alpha}$  is a traceless symmetric tensor of rank 2, obeying the divergence condition :

$$(\phi_{\mu}^{\alpha})_{\alpha} = 0 \quad \dots (6)$$

Now, from (2) and (5), we have

$$\begin{aligned} g^{\nu\beta}(\phi_{\mu\alpha})_{\nu\beta} - (\phi_{\alpha}^{\beta})_{\mu\beta} - (\phi_{\mu}^{\nu})_{\nu\alpha} + (\phi)_{\mu\alpha} &= g^{\nu\beta}F_{\mu\nu\alpha\beta} \\ &= R_{\mu\alpha} - (T_{\mu\alpha} - \frac{1}{2}g_{\mu\alpha}T) = 0 \end{aligned}$$

or (Eddington 1957)

$$g^{\nu\beta}(\phi_{\mu\alpha})_{\nu\beta} - (\phi_{\alpha}^{\beta})_{\mu\beta} - g^{\nu\beta}R_{\nu\mu\beta}^{\epsilon}\phi_{\epsilon\alpha} - g^{\nu\beta}R_{\alpha\mu\beta}^{\epsilon}\phi_{\nu\epsilon} - (\phi^{\nu}_{\mu})_{\nu\alpha} + (\phi)_{\mu\alpha} = 0 \quad \dots (7)$$

$$\square \phi_{\mu\alpha} = G_{\mu}^{\epsilon}\phi_{\epsilon\alpha} + g^{\nu\beta}R_{\alpha\mu\beta}^{\epsilon}\phi_{\nu\epsilon} \quad \dots (8)$$

remembering the properties attributed to  $\phi_{\mu\alpha}$  in (6), (8) gives the propagation of gravitational potential in matter.

#### PROPAGATION OF GRAVITATIONAL FIELD-STRENGTH $F_{\mu\nu\alpha\beta}$

From (3), we have, by covariant differentiation,

$$\begin{aligned} \frac{1}{2} [(T_{\alpha\nu})_{\mu\delta} - (T_{\alpha\mu})_{\nu\delta}] - \frac{1}{6} [g_{\alpha\nu}T_{\mu\delta} - g_{\alpha\mu}T_{\nu\delta}] &= g^{\gamma\beta}(F_{\mu\nu\alpha\beta})_{\gamma\delta} \\ &= g^{\gamma\beta}\{(F_{\mu\nu\alpha\beta})_{\delta\gamma} + R_{\mu\gamma\delta}^{\epsilon}F_{\epsilon\nu\alpha\beta} + R_{\nu\gamma\delta}^{\epsilon}F_{\mu\epsilon\alpha\beta} + R_{\alpha\gamma\delta}^{\epsilon}F_{\mu\nu\epsilon\beta} + R_{\beta\gamma\delta}^{\epsilon}F_{\mu\nu\alpha\epsilon}\} \\ &= g^{\gamma\beta}(F_{\mu\nu\alpha\delta})_{\beta\gamma} + g^{\gamma\beta}(F_{\mu\nu\delta\beta})_{\alpha\gamma} + g^{\gamma\beta}\{R_{\mu\gamma\delta}^{\epsilon}F_{\epsilon\nu\alpha\beta} + R_{\nu\gamma\delta}^{\epsilon}F_{\mu\epsilon\alpha\beta} + R_{\alpha\gamma\delta}^{\epsilon}F_{\mu\nu\epsilon\beta} \\ &+ R_{\beta\gamma\delta}^{\epsilon}F_{\mu\nu\alpha\epsilon} + (R_{\mu\beta\delta}^{\epsilon}\psi_{\epsilon\nu\alpha} + R_{\alpha\beta\delta}^{\epsilon}\psi_{\mu\nu\epsilon} + R_{\nu\beta\delta}^{\epsilon}\psi_{\mu\epsilon\alpha} - R_{\mu\alpha\delta}^{\epsilon}\psi_{\epsilon\nu\beta} - R_{\beta\alpha\delta}^{\epsilon}\psi_{\mu\nu\epsilon} \\ &- R_{\nu\alpha\delta}^{\epsilon}\psi_{\mu\epsilon\beta} + R_{\mu\alpha\beta}^{\epsilon}\psi_{\epsilon\nu\delta} + R_{\delta\alpha\beta}^{\epsilon}\psi_{\mu\nu\epsilon} + R_{\nu\alpha\beta}^{\epsilon}\psi_{\mu\epsilon\delta})_{\gamma}\} \quad \dots (9) \end{aligned}$$

Also, we have

$$\begin{aligned} \frac{1}{2} [(T_{\delta\nu})_{\mu\alpha} - (T_{\delta\mu})_{\nu\alpha}] - \frac{1}{6} [g_{\delta\nu}T_{\mu\alpha} - g_{\delta\mu}T_{\nu\alpha}] &= g^{\gamma\beta}(F_{\mu\nu\delta\beta})_{\gamma\alpha} \\ &= g^{\gamma\beta}\{(F_{\mu\nu\delta\beta})_{\alpha\gamma} + R_{\mu\gamma\alpha}^{\epsilon}F_{\epsilon\nu\delta\beta} + R_{\nu\gamma\alpha}^{\epsilon}F_{\mu\epsilon\delta\beta} + R_{\delta\gamma\alpha}^{\epsilon}F_{\mu\nu\epsilon\beta} + R_{\beta\gamma\alpha}^{\epsilon}F_{\mu\nu\delta\epsilon}\} \quad \dots (10) \end{aligned}$$

Subtracting (10) from (9)

$$\begin{aligned} \{\frac{1}{2} [(T_{\alpha\nu})_{\mu\delta} - (T_{\alpha\mu})_{\nu\delta}] - \frac{1}{6} [g_{\alpha\nu}T_{\mu\delta} - g_{\alpha\mu}T_{\nu\delta}]\} - \frac{1}{2} [(T_{\delta\nu})_{\mu\alpha} - (T_{\delta\mu})_{\nu\alpha}] - \frac{1}{6} [g_{\delta\nu}T_{\mu\alpha} \\ - g_{\delta\mu}T_{\nu\alpha}] &= g^{\gamma\beta}(F_{\mu\nu\alpha\beta})_{\gamma\delta} - g^{\gamma\beta}(F_{\mu\nu\delta\beta})_{\gamma\alpha} = \square F_{\mu\nu\alpha\delta} + g^{\gamma\beta}\{R_{\mu\gamma\delta}^{\epsilon}F_{\epsilon\nu\alpha\beta} \\ &+ R_{\nu\gamma\delta}^{\epsilon}F_{\mu\epsilon\alpha\beta} + R_{\alpha\gamma\delta}^{\epsilon}F_{\mu\nu\epsilon\beta} + R_{\beta\gamma\delta}^{\epsilon}F_{\mu\nu\alpha\epsilon}\} - (R_{\mu\gamma\alpha}^{\epsilon}F_{\epsilon\nu\delta\beta} + R_{\nu\gamma\alpha}^{\epsilon}F_{\mu\epsilon\delta\beta} + R_{\delta\gamma\alpha}^{\epsilon}F_{\mu\nu\epsilon\beta} \\ &+ R_{\beta\gamma\alpha}^{\epsilon}F_{\mu\nu\delta\epsilon}) + (R_{\mu\beta\delta}^{\epsilon}\psi_{\epsilon\nu\alpha} + R_{\alpha\beta\delta}^{\epsilon}\psi_{\mu\nu\epsilon} + R_{\nu\beta\delta}^{\epsilon}\psi_{\mu\epsilon\alpha} - R_{\mu\alpha\delta}^{\epsilon}\psi_{\epsilon\nu\beta} - R_{\beta\alpha\delta}^{\epsilon}\psi_{\mu\nu\epsilon} \\ &- R_{\nu\alpha\delta}^{\epsilon}\psi_{\mu\epsilon\beta} + R_{\mu\alpha\beta}^{\epsilon}\psi_{\epsilon\nu\delta} + R_{\delta\alpha\beta}^{\epsilon}\psi_{\mu\nu\epsilon} + R_{\nu\alpha\beta}^{\epsilon}\psi_{\mu\epsilon\delta})_{\gamma}\} \quad \dots (11) \end{aligned}$$

writing

$$\square F_{\mu\nu\alpha\delta} = g^{\gamma\beta}(F_{\mu\nu\alpha\delta})_{\beta\gamma}]$$

(11) gives the propagation of field-strength in matter.

#### WEAK FIELD APPROXIMATIONS: SOME SPECIAL CASES

If we consider the field to be weak, then we may write (8) in the following form :

(replacing  $g^{\nu\beta}$  by  $\delta^{\nu\beta}$ )

$$\square \phi_{\mu\alpha} = G^\epsilon_\mu \phi_{\epsilon\alpha} + \delta^{\nu\beta} M^\epsilon_{\alpha\mu\beta} \phi_{\nu\epsilon} \quad \dots (12)$$

Considering a thin distribution of matter or free space, (12) takes the simple form :

$$\square \phi_{\mu\alpha} = 0 \quad \dots (13)$$

This shows that gravitational potential travels with fundamental velocity through a very thin distribution of matter or free space.

Under the weak field condition, (11) comes to (replacing covariant differentiation by ordinary differentiation)

$$\begin{aligned} & \{ \tfrac{1}{2} [T_{\alpha\nu, \mu\delta} - T_{\alpha\mu, \nu\delta}] - \tfrac{1}{6} [\delta_{\alpha\nu} T_{, \mu\delta} - \delta_{\alpha\mu} T_{, \nu\delta}] \} \\ & - \{ \tfrac{1}{2} [T_{\delta\nu, \mu\alpha} - T_{\delta\mu, \nu\alpha}] - \tfrac{1}{6} [\delta_{\delta\nu} T_{, \mu\alpha} - \delta_{\delta\mu} T_{, \nu\alpha}] \} \\ & = \square F_{\mu\nu\alpha\delta} + \delta^{\gamma\beta} \{ (M^\epsilon_{\mu\gamma\delta} F_{\epsilon\nu\alpha\beta} + M^\epsilon_{\nu\gamma\delta} F_{\mu\epsilon\alpha\beta} + M^\epsilon_{\alpha\gamma\delta} F_{\mu\nu\epsilon\beta} + M^\epsilon_{\beta\gamma\delta} F_{\mu\nu\alpha\epsilon}) \\ & - (M^\epsilon_{\mu\gamma\alpha} F_{\epsilon\nu\delta\beta} + M^\epsilon_{\nu\gamma\alpha} F_{\mu\epsilon\delta\beta} + M^\epsilon_{\delta\gamma\alpha} F_{\mu\nu\epsilon\beta} + M^\epsilon_{\beta\gamma\alpha} F_{\mu\nu\delta\epsilon}) + (M^\epsilon_{\mu\beta\delta} \psi_{\epsilon\nu\alpha} \\ & + M^\epsilon_{\alpha\beta\delta} \psi_{\mu\nu\epsilon} + M^\epsilon_{\nu\beta\delta} \psi_{\mu\epsilon\alpha} - M^\epsilon_{\mu\alpha\delta} \psi_{\epsilon\nu\beta} - M^\epsilon_{\beta\alpha\delta} \psi_{\mu\nu\epsilon} - M^\epsilon_{\nu\alpha\delta} \psi_{\mu\epsilon\beta} \\ & + M^\epsilon_{\mu\alpha\beta} \psi_{\epsilon\nu\delta} + M^\epsilon_{\delta\alpha\beta} \psi_{\mu\nu\epsilon} + M^\epsilon_{\nu\alpha\beta} \psi_{\mu\epsilon\delta}), \gamma \} \quad \dots (14) \end{aligned}$$

Further simplification can be made by considering vacuum. In that case, we get from (14)

$$\square F_{\mu\nu\alpha\delta} = 0 \quad \dots (15)$$

This means that gravitational field strength also travels with fundamental velocity in vacuum.

#### PLANE GRAVITATIONAL WAVE: ANOTHER SPECIAL CASE

Following the idea of Weber (1961), we now consider the case of propagation of plane gravitational wave. In such a case the field changes only along one direction in space; we choose for this direction the axis  $x_1$ . Now we have from (5)

$$F_{\mu\nu\alpha\beta} = (\phi_{\mu\alpha})_{\nu\beta} - (\phi_{\nu\alpha})_{\mu\beta} - (\phi_{\mu\beta})_{\nu\alpha} + (\phi_{\nu\beta})_{\mu\alpha} \quad \dots (5)$$

It is evident for the case under consideration that the derivatives of  $\phi_{\mu\alpha}$  and  $\phi_{\mu\alpha,\nu}$  with respect to  $x_2$  and  $x_3$  vanish.

The 21 components of  $F_{\mu\nu\alpha\beta}$  may be written down as follows from (5) :

$$\left. \begin{aligned} F_{2424} &= \phi_{22,44} & F_{1224} &= -\phi_{22,14} & F_{1212} &= \phi_{22,11} \\ F_{2434} &= \phi_{23,44} & F_{1234} &= -\phi_{23,14} & F_{1213} &= \phi_{23,11} \\ F_{2434} &= \phi_{33,44} & F_{1324} &= -\phi_{23,14} & F_{1313} &= \phi_{33,11} \\ & & F_{1334} &= -\phi_{33,14} & & \end{aligned} \right\} \dots (16)$$

$$\left. \begin{aligned} F_{1223} &= 0 & F_{2323} &= 0 \\ F_{1323} &= 0 & F_{2324} &= 0 \\ F_{1423} &= 0 & F_{2334} &= 0 \end{aligned} \right\} \dots (17)$$

$$\left. \begin{aligned} F_{1434} &= \phi_{13,44} - \phi_{34,14} & F_{1424} &= \phi_{12,44} - \phi_{24,14} \\ F_{1314} &= \phi_{34,11} - \phi_{13,14} & F_{1214} &= \phi_{24,11} - \phi_{12,14} \\ & & F_{1414} &= \phi_{11,44} - \phi_{14,14} + \phi_{44,11} \end{aligned} \right\} \dots (18)$$

In vacuum,  $F_{\mu\nu} = 0$ . So, since we are considering weak field, we have from (16), (17) and (18) :

$$\left. \begin{aligned} F_{12} &= F_{1424} = 0 & F_{13} &= F_{1434} = 0 \\ F_{24} &= F_{1214} = 0 & F_{34} &= F_{1314} = 0 \\ F_{11} &= F_{1414} - F_{1313} - F_{1212} = 0 & F_{14} &= F_{1224} + F_{1334} = 0 \\ F_{22} &= F_{2424} - F_{1212} = 0 & F_{23} &= F_{2434} - F_{1213} = 0 \\ F_{33} &= F_{3434} - F_{1313} = 0 & F_{44} &= F_{3434} + F_{2424} + F_{1414} = 0 \end{aligned} \right\} \dots (19)$$

It is easily seen from (19) that  $F_{1431}$ ,  $F_{1314}$ ,  $F_{1424}$ ,  $F_{1214}$  and  $F_{1414}$  of (18) are all zero. Then the components of  $F_{\mu\nu\alpha\beta}$  that remain are the ten components of (16) which are expressed in terms of only three potential components  $\phi_{22}$ ,  $\phi_{23}$  and  $\phi_{33}$ . It is evident from (16), (18) and (19) that

$$\begin{aligned} \phi_{22,44} + \phi_{33,44} &= 0 \\ \text{or (on integration),} & \phi_{22} + \phi_{33} = 0 \end{aligned} \dots (20)$$

Here we have put the integration constants equal to zero since we are interested in the varying part of the field. Thus, a plane gravitational wave is determined by only two quantities  $\phi_{23}$  and  $\phi_{22} = -\phi_{33}$  and is transverse since it is determined by the potential tensor in  $x_2$ - $x_3$  plane only (Landau and Lifshitz, 1962).

#### REFERENCES

- Eddington, A. S., 1957, *The Mathematical Theory of Relativity*, Eq. (34.8), P-73.  
 Landau, L. D., and Lifshitz, E. M., 1962, *The Classical Theory of Fields*, P. 349-352.  
 Rumer, Yu. B., 1962, *Soviet Physics, JETP*, **15**, 402.  
 Weber, J., 1961, *General Relativity and Gravitational Waves*, P. 90-92.

# DIELECTRIC ABSORPTION AT 3 cm. IN SOME HIGHER ALKYL PHENOLS

G. C. HIREMATH and K. SURYANARAYANA RAO

DEPARTMENT OF PHYSICS, KARNATAK UNIVERSITY, DHARWAR

(Received December, 13, 1963)

**ABSTRACT.** Dielectric measurements have been carried out on para-octyl, -nonyl and -dodecyl phenols in solution in benzene at 3.22 cm. and at a radio frequency of 1 mc/sec. From the measurements at 3.22 cm. using a single frequency method, the relaxation time and the dipole moment have been determined for these molecules and from the radio frequency measurements, dipole moments have been deduced for the same molecules. The results are reported and discussed.

## INTRODUCTION

A programme of work on quantitative determinations of dielectric absorption, in particular, at microwave frequencies, of some molecules has been undertaken in this laboratory with a view to studying dielectric dispersion in these molecules and testing the existing theories of electric polarization and molecular structure from such studies. As a first step in this programme, a study of dielectric absorption in some alkyl phenols has been taken up, since for these molecules no studies of dielectric absorption particularly at microwave frequencies seem to have been carried out so far, as far as the authors are aware. The present investigation reports the results of dielectric measurements in solution in benzene at 3.22 cm and at a radio frequency of 1 mc/sec. carried out under this programme, on three higher alkyl phenols, namely, para-octyl, -nonyl and -dodecyl phenols, and the values of relaxation times and dipole moments determined for these molecules.

## METHOD

### *Dielectric measurements at 3 cm.*

In the wave-guide standing wave method (Roberts and Von Hippel, 1946; Dakin and Works, 1947; Surber Jr. and Crouch Jr, 1948; Heston Jr, and others, 1950) the inverse voltage standing wave ratio (VSWR)  $E_{min}/E_{max}$  exhibits (Von Hippel, 1954) maxima for sample lengths of odd multiples of  $\lambda_d/4$  with short circuit termination,  $\lambda_d$  being the guide wavelength in the dielectric filled section of the guide and for low loss media such as dilute solutions of a polar substance in a non-polar solvent, the magnitudes of these maxima increase with the number of the odd multiple. This makes the other losses small compared

to the dielectric loss of the sample, and therefore it is possible to determine the dielectric loss more accurately. As the rate of shift of the first minimum point in air with sample length is maximum in this region, it will be fairly easy to locate the positions of these maxima rather precisely. Another advantage of taking measurements on odd multiples of sample lengths is that computations of  $\epsilon'$  and  $\epsilon''$ , the dielectric constant and loss factor respectively, become much simplified.

The real part of the dielectric constant,  $\epsilon'$  is given by the equation

$$\epsilon' = \left(\frac{\lambda_0}{\lambda_c}\right)^2 + \left(\frac{\lambda_0}{\lambda_d}\right)^2 \left[1 - \left(\frac{\alpha_d \lambda_d}{2\pi}\right)^2\right] \quad \dots \quad (1)$$

where

$\alpha_d$  = attenuation resulting from dielectric power loss.

$\lambda_c$  = cut-off wave-length.

and  $\lambda_0$  = free space wave-length.

For low-loss media, such as dilute solutions of a polar substance in a non-polar solvent, this equation reduces to

$$\epsilon' = \left(\frac{\lambda_0}{\lambda_c}\right)^2 + \left(\frac{\lambda_0}{\lambda_d}\right)^2 \quad \dots \quad (2)$$

An experimental determination of  $\lambda_d$ , together with a knowledge of  $\lambda_0$  and  $\lambda_c$  will yield  $\epsilon'$  from the above equation for low-loss media.

The loss factor,  $\epsilon''$  is given by the relation

$$\epsilon'' = \frac{1}{\pi} \left(\frac{\lambda_0}{\lambda_d}\right)^2 \alpha_d \lambda_d \quad \dots \quad (3)$$

The inverse VSWR,  $\rho_n$  at the  $n$ -th maximum produced by a short circuited low-loss dielectric filled section, may be expressed as

$$\rho_n = \left(\frac{\lambda_g}{\lambda_d}\right) \cdot n \cdot (\alpha_d + \alpha_c) \frac{\lambda_d}{4} + R_{sc} \left(\frac{\lambda_g}{\lambda_d}\right)^2 \quad \dots \quad (4)$$

where  $\alpha_c$  = attenuation resulting from power loss in the walls of the dielectric section of the wave-guide,

$R_{sc}$  = the per unit resistance of the terminating plunger referred to the air-filled guide,

$\lambda_g$  = guide wave-length in the air-filled section

and  $n$  = an odd integer.

$R_{sc}$  may be determined either from calculated power loss or from the characteristic impedance of the metal. Using this value of  $R_{sc}$  and experimentally determined

value of  $\rho_n$  and the equation given above, the total attenuation ( $\alpha_d + \alpha_c$ ) can be determined. From this and a preliminary determination of  $\alpha_c$ ,  $\alpha_d$  can be obtained which when substituted into equation (3) will yield  $\epsilon''$ . However, in the present work, the total attenuation ( $\alpha_d + \alpha_c$ ) is obtained from the slope of the plot of  $\rho_n$  versus ' $n$ ', as this procedure eliminates the resistance of the plunger,  $R_{sc}$ .

#### *Determination of relaxation time and dipole moment*

A single frequency method for solutions due to Gopalkrishna (1957) has been used for the determination of the relaxation time ' $\tau$ ' and the dipole moment ' $\mu$ '. In this method, for determining ' $\tau$ ', a plot is made between

$$x = \frac{\epsilon' + \epsilon'^2 + \epsilon''^2 - 2}{(\epsilon' + 2)^2 + \epsilon''^2}$$

and

$$y = \frac{3\epsilon''}{(\epsilon' + 2)^2 + \epsilon''^2}$$

the slope of which yields  $\frac{1}{\omega\tau}$ ,  $\omega$  being the angular frequency. For the determination of ' $\mu$ ', a graph between  $x$  and  $W$ , the weight fraction, is plotted, the slope of which would be equal to

$$\frac{4\pi N\mu^2}{9kTM} \cdot \frac{1}{1 + \omega^2\tau^2} \cdot d_0$$

where  $N$  is the Avagadro's number

$k$  = the Boltzman constant

$T$  = absolute temperature

$M$  = Molecular weight of the solute

and  $d_0$  = density of the solvent.

#### *Determination of ' $\mu$ ' from Radio Frequency Measurements.*

Guggenheim's modified method (Guggenheim, 1949; 1951) is used for the determination of the dipole moment. In this method

$$\mu = 0.0128\sqrt{P_0 T}$$

where

$$P_0 = \frac{3}{(\epsilon_1 + 2)^2} \cdot \frac{M_2}{d_1} \cdot \Delta$$

where

$$\Delta = \left( \frac{\epsilon_{12} - \epsilon_1}{W_2} \right)_{W_2 \rightarrow 0} - \left( \frac{n_{12}^2 - n_1^2}{W_2} \right)_{W_2 \rightarrow 0}$$

$\epsilon_1$  = dielectric constant of the solvent

$\epsilon_{12}$  = dielectric constant of the solution

$M_2$  = Molecular weight of the solute

$d_1$  = density of the solvent

$W_2$  = weight fraction of the solute

$n_{12}$  = refractive index of the solution

$n_1$  = refractive index of the solvent.

$\Delta$  is determined from the difference of the intercepts of the plots  $\left( \frac{\epsilon_{12} - \epsilon_1}{W_2} \right)$  and  $\left( \frac{n_{12}^2 - n_1^2}{W_2} \right)$  against  $W_2$ .

# EXPERIMENTAL

*3 cm. equipment*: A block diagram of the experimental set-up for dielectric measurements at 3 cm. is shown in Fig. (1). All the components in the unit except the *E*-plane 90° bend, liquid absorption cell and galvanometer, are of

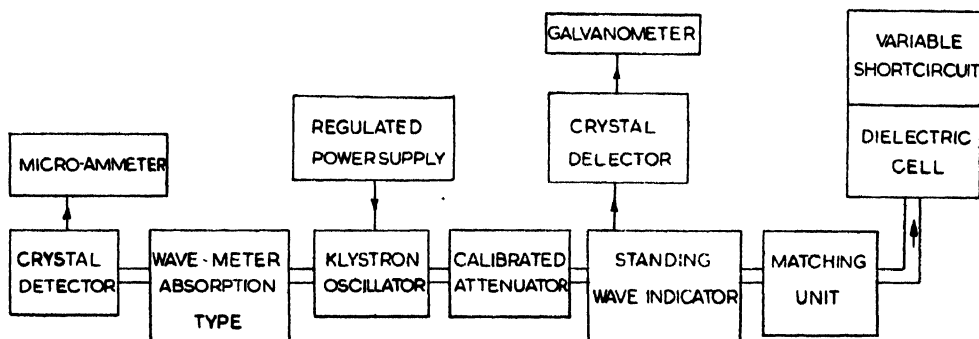


Fig. 1. Block diagram of the 3 cm. set-up

Scanners Ltd., London. *E*-plane 90° bend was fabricated by us and was found to have an inverse VSWR of 0.96 at 9295 mc/sec., the frequency at which the measurements were carried out. The dielectric absorption cell, also fabricated by us, consisted of a standard 1" × 1/2" O.D. × 0.050" wall, rectangular brass waveguide of length 6" silvered inside and was provided with a non-contact shorting plunger driven by a micrometer screw of traverse 4" and of least count (1/2000)". The galvanometer used was a low period one with a resistance of 450 ohms and had a sensitivity 2,000 m. per microampere at 2 meters scale distance. The accuracy of the probe displacement along the slotted line of the standing wave indicator used was 0.002 cm.

The unit was operated in the  $H_{01}$  mode. To provide adequate decoupling of the klystron, attenuator was set at a value greater than 10db. The standing

wave-indicator crystal was calibrated and found to obey the square law. A matching unit was used in between the slotted section and the cell to match out any possible reflections from the bend and the mica window and it was adjusted for the standing wave ratio to be very nearly equal to unity with a dummy load.

*Radio frequency set-up*: This set-up consisted of a Franklin oscillator (Le Fevre and others, 1950) oscillating at 1 mc/sec., which was coupled to a crystal controlled wave meter. The oscillatory circuit of the former included a dielectric cell and a precision condenser of Muirhead Co., England, with a total capacity of 250 pf and with a precision of 0.025 pf, all arranged in parallel. Grid tuned circuit of the wavemeter consisted of a stable 500 pf, variable condenser and a one-megacycle quartz crystal, all connected in parallel. The operation of the set-up was as described in the literature.

The experimental cell used is similar to that designed by Sayce and Briscoe (1925) and modified by Sugden (1933) and is described in the literature. The cell was silvered using the method recommended by Sugden. The deposition was found to be satisfactory only when the two solutions used in the silvering process were cooled to a temperature of about 10°C or lower, mixed and then transferred to the cell, instead of mixing and transferring them at the room temperature 27°C $\pm$ 1°C. The capacity of the cell was 52.56 pf.

*Measurements*. The three phenols *p*-octyl, -nonyl and -dodecyl were supplied by Rohm and Hass Co., U.S.A. They were distilled twice at low pressure (*p*-octyl phenol 146-47°C/8 mm. Hg; *p*-nonylphenol—165–67°C/4 mm.Hg, and *p*-dodecylphenol -186-87°C/4 mm.Hg) and rejecting the initial fractions, the fractions that distilled at the temperatures given above were collected. *p*-octyl phenol was a white flaked solid and the other two phenols were clear liquids. Analar benzene was used as the solvent. Before use it was dried over sodium wire and distilled under anhydrous conditions. Five to six solutions of each of the phenols after double distillation were prepared in conical flasks of 50 c.c. with ground glass stoppers and were studied immediately.

*At 3 cm*: The dielectric constant and the loss of the solvent benzene were measured at a frequency of 9295 mc/sec. ( $\lambda_0 = 3.22$  cm) and at the room temperature 27°C $\pm$ 1°C. They were respectively 2.270 and <0.001. For each solution six to seven successive maxima of inverse VSWR ' $\rho_n$ ' at the frequency and at the temperature mentioned just above, were located and measured. The maximum VSWR occurs for an electrical length very close to an exact resonant length. This would be the case for an electrically long low loss sample. Therefore, although six to seven maxima of VSWR ' $\rho_n$ ' were measured,  $\lambda_d$  was actually determined from the measurements on the higher resonant lengths only, namely, the 15th, 13th and 11th. From each of these higher resonant lengths  $\lambda_d/4$  was determined and from these a mean value for  $\lambda_d$  was obtained. This procedure adopted in evaluating  $\lambda_d$  enables changes of the order of 0.002 cm. in  $\lambda_d$  (this amounted to



a change of 0.004 in the value of  $\epsilon'$ ) to be determined. Using this average value of  $\lambda_d$ ,  $\epsilon'$  was determined from equation (2) given earlier. As for  $\epsilon''$  it can be seen from equation (4) the graph between ' $\rho_n$ ' and  $n$  (odd integer) is a straight-line whose slope will yield  $(\alpha_d + \alpha_c)$  and whose intercept on the  $\rho_n$  axis will give the plunger resistance. Such plots are shown in fig. 2 for the different solutions

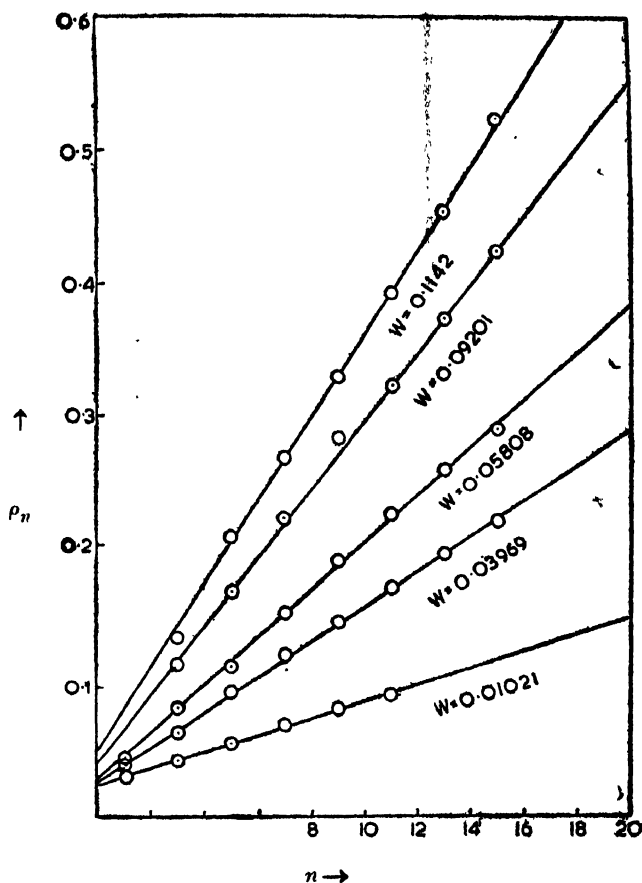


Fig. 2. Plots of  $\rho_n$  (inverse voltage standing wave ratio) versus  $n$  (odd integer) for different weight fractions of dodecyl phenol.

of dodecyl phenol.  $\alpha_c$  was found to be very small. Therefore, in the actual determination of  $\epsilon''$  using equation (3) total attenuation was used instead of  $\alpha_d$  and this did not introduce any significant error.

**At Radio frequency:** Dielectric constant  $\epsilon_1$  of benzene and that for the various solutions  $\epsilon_{12}$  was determined using the radio frequency set-up already described by finding the capacity of the cell with and without the substance. The dielectric constant of benzene at  $27^\circ\text{C} \pm 1^\circ\text{C}$  was 2.264. Refractive indices for the various solutions and for the solvent benzene were determined for the sodium D lines using a Pulfrich refractometer. The refractive index of benzene at  $27^\circ\text{C} \pm 1^\circ\text{C}$  was measured to be 1.49412.

## RESULTS

The  $\epsilon'$  and  $\epsilon''$  values determined at 3 cm. for the different solutions of each of the three phenols are given in tables. I, II and III. In these tables, the first column gives the weight fraction of the solute the second  $\epsilon'$  and the third  $\epsilon''$  while in the fourth and the fifth columns are given values of  $x$  and  $y$  needed in the determinations of  $\tau$  and  $\mu$ . The values of  $\epsilon'$  are estimated to be accurate to within 0.5% and those of  $\epsilon''$  to within 2%. From these  $\epsilon'$  and  $\epsilon''$  values,  $\tau$  and  $\mu$  were determined for the three phenols as indicated earlier and are given in table IV. The density of the solvent, benzene was taken to be 0.87901 gm/c.c.

TABLE I  
*p*-Octyl phenol

<i>W</i>	$\epsilon'$	$\epsilon''$	<i>x</i>	<i>y</i>
0.02298	2.286	0.01345	0.3002	0.002197
0.03897	2.297	0.01874	0.3018	0.003039
0.05788	2.313	0.02879	0.3045	0.004647
0.06766	2.320	0.03599	0.3057	0.005786
0.08855	2.332	0.04262	0.3077	0.006797
0.1298	2.353	0.06610	0.3112	0.010440

TABLE II  
*p*-Nonyl phenol

<i>W</i>	$\epsilon'$	$\epsilon''$	<i>x</i>	<i>y</i>
0.009279	2.286	0.008245	0.3002	0.001347
0.02773	2.301	0.01408	0.3022	0.002279
0.04444	2.309	0.02136	0.3039	0.003449
0.06270	2.320	0.02590	0.3056	0.004882
0.08095	2.320	0.03683	0.3056	0.005928
0.11400	2.332	0.04682	0.3077	0.007484

TABLE III  
*p*-Dodecyl phenol

<i>W</i>	$\epsilon'$	$\epsilon''$	<i>x</i>	<i>y</i>
0.01021	2.282	0.007457	0.2994	0.001220
0.03969	2.290	0.01569	0.3007	0.002556
0.05808	2.295	0.02218	0.3015	0.003606
0.09201	2.304	0.03157	0.3030	0.005112
0.1142	2.309	0.03904	0.3041	0.006303

TABLE IV

Molecule	$\mu$ in Debye units	$\tau$ in $\mu\mu$ sec.
<i>p</i> -Octyl phenol	$1.37 \pm 0.10$	$11.0 \pm 2.0$
<i>p</i> -Nonyl phenol	$1.37 \pm 0.10$	$12.4 \pm 2.0$
<i>p</i> -Dodecyl phenol	$1.19 \pm 0.10$	$18.4 \pm 2.0$

Plots of  $x$  against  $y$  and  $x$  against  $w$  are shown for dodecyl phenol in fig. 3 for the purpose of illustration.

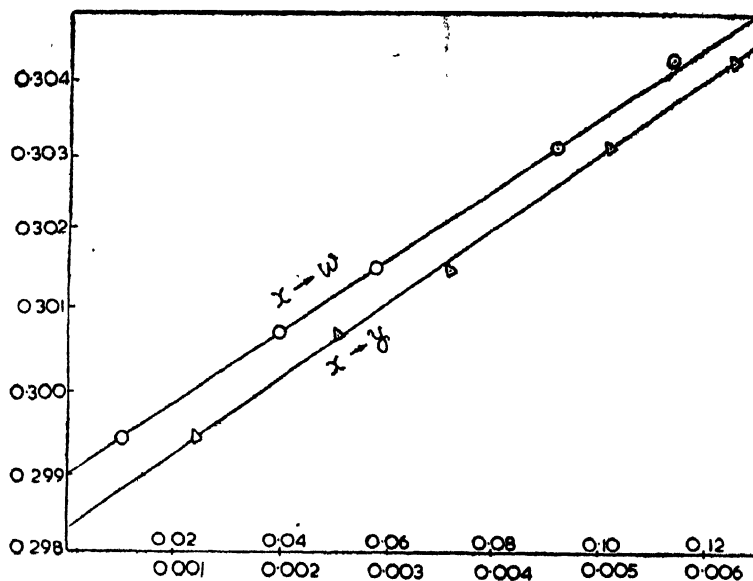


Fig. 3. Plots of  $x$  versus  $y$  and  $x$  versus  $W$  the weight fraction.

Tables V, VI and VII give the radio frequency values of  $\epsilon_{12}$  and  $n_{12}$  for different solutions of each of the three phenols together with the value of  $\mu$  of each molecule determined as outlined earlier.

TABLE V  
*p*-Octyl phenol

Wt. fraction $W_2$	Dielectric const. of the solution $\epsilon_{12}$	Refractive index of the solution $n_{12}$
0.008050	2.277	1.49459
0.01414	2.287	1.49459
0.02708	2.306	1.49483
0.03926	2.320	1.49493
0.05893	2.348	1.49511
0.08166	2.380	1.49535
$\mu = 1.53 \pm 0.03 D$		

TABLE VI  
*p*-Nonyl phenol

Wt. fraction $W_2$	Dielectric const. of the solution $\epsilon_{12}$	Refractive index of the solution $n_{12}$
0.01414	2.283	1.49445
0.02516	2.297	1.49459
0.04982	2.335	1.49487
0.06671	2.354	1.49501
0.08971	2.382	1.49516
$\mu = 1.59 \pm 0.03 D$		

TABLE VII  
*p*-Dodecyl phenol

Wt. fraction $W_2$	Dielectric const. of the solution $\epsilon_{12}$	Refractive index of the solution $n_{12}$
0.01504	2.281	1.49421
0.04182	2.308	1.49418
0.05478	2.323	1.49459
0.07394	2.342	1.49489
0.09574	2.373	1.49510
$\mu = 1.58 \pm 0.03 D$		

Plots of  $\frac{\epsilon_{12} - \epsilon_1}{W_2}$  versus  $W_2$  and  $\frac{n_{12}^2 - n_1^2}{W_2}$  versus  $W_2$  are given in fig. 4 for dodecyl phenol for the sake of illustration.

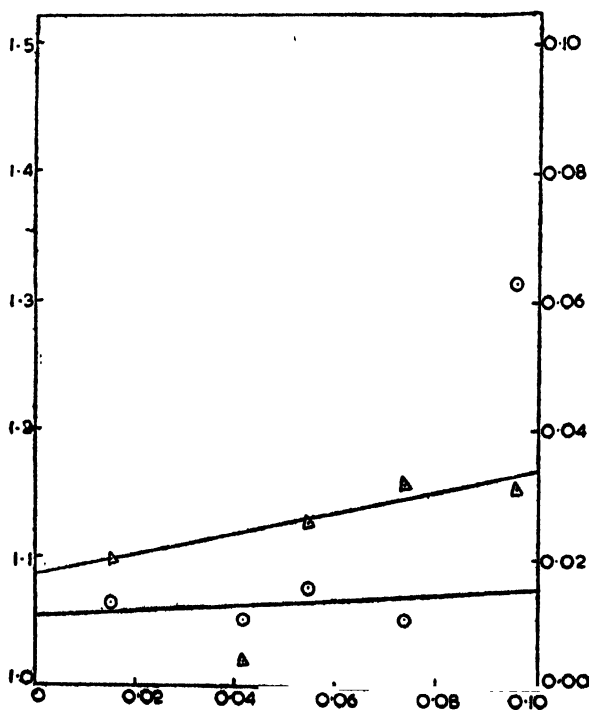


Fig. 4. Plots of  $\frac{\epsilon_{12} - \epsilon_1}{W_2}$  and  $\frac{n_{12}^2 - n_1^2}{W_2}$  versus  $W_2$  the weight fraction shown by O and Δ respectively.

The limits of accuracy of both the relaxation times and the dipole moments of these molecules have been arrived at from the results of several independent sets of measurements on each molecule.

#### DISCUSSION

The three molecules studied in this investigation are members of a homologous series. The dipole moments of these molecules determined in this work indicate that they are approximately equal. Two values for the dipole moment of phenol in benzene solution have been reported in the literature; one of them is around 1.45D (Boud, and others, 1955; Lombroso and Dumas, 1955; Katagiri, 1950) and the other around 1.6D (Donle and Gehreken, 1932; Bottcher 1952; Smyth, 1955; Kimura and Fujishiro, 1959, and Goode and Ibbitson, 1960). The radio frequency values determined by us for these molecules in benzene solution are close to one another and to the literature value for phenol, 1.6D. We have carried out dielectric measurements at 1 cm. too, on these three phenols in benzene solution (unpublished) and have evaluated both  $\tau$  and  $\mu$  for them, using the data at 3 cm., and 1 cm. and using a double frequency method of Whiffen and Thompson (1946). These values are in fair agreement with those at 3 cm., determined using a single frequency method already described. Both the microwave value of  $\mu$  are rather close to the other literature value for phenol in benzene solution, namely, 1.45D. Whatever may be the true value of the dipole moment of phenol in benzene solution, that is whether it is close to 1.6D or to 1.45D, the fact that the dipole moments of these molecules are approximately equal, whether we consider our radio frequency values or our microwave values, may indicate that the dipole moments of these phenols depend mainly on that of the OH group and little on that of the alkyl group.

There is, however, some divergence between the microwave values of  $\mu$  and the radio frequency values, reported in this investigation. It may be partly accounted for as follows: The accuracy we have attained in our measurements of  $\epsilon'$  and  $\epsilon''$  is of the order of magnitude that is normally employed for dielectric measurements at 3 cm. Values of  $\epsilon'$  of a solution determined for different lengths of the solution in the cell have been found to agree to within 0.5% and those of the loss factor,  $\epsilon''$  to within 2%. For these molecules which are higher members of a series with rather high molecular weights, the variation in  $\epsilon'$  with concentration has been found to be so small that, although detectable, it almost lies within the limits of error of measurements. That this reason may partly explain the discrepancy between the microwave and the radio frequency value of the dipole moment seems to be confirmed by our preliminary results on the same isomer of the lower phenols of the series, namely *p*-ethyl, -propyl and -butyl phenols. For these molecules the variation of  $\epsilon'$  with concentration has been found to be comparatively larger and the same degree of accuracy in the dielectric measurements

at 3 cm., has led to values of  $\mu$  for these lower phenols in fair agreement with the radio frequency values. However, we feel that the divergence between the radio frequency and microwave values in these higher phenols are more than could be attributed to this factor only. Further it may also be mentioned that similar discrepancies between the radio frequency values and those determined at microwave frequencies have also been reported in the literature in the case of a few other molecules.

With regard to the relaxation times of these molecules, it has not been possible to determine them more accurately for reasons mentioned above. But, yet the values seem to be of the right order of magnitude. It may be noted that they increase from octyl to dodecyl phenol as they should, in accordance with theory, because the relaxation time of a molecule depends upon the size of the molecule. To test this point further, a study of temperature variation of dielectric absorption of para-dodecyl phenol at 3 cm., has been undertaken and our preliminary results indicate that this molecule has a relaxation time in benzene solution at room temperature, around the value at 3 cm., reported above. Similar studies of temperature variation of dielectric absorption on the other two phenols also are in progress.

Investigations of dielectric absorption at microwave frequencies on some other phenols are in progress.

#### ACKNOWLEDGEMENT

One of the authors (G.C.H.) wishes to express his grateful thanks to the Ministry of Scientific Research and Cultural Affairs, Government of India, for the award of a Scientific Research Training Scholarship, during the tenure of which this work was mostly carried out. We are also thankful to Dr. S. Munavalli for having made available to us the samples of phenols used in this work.

#### REFERENCES

- Boud, A. H., Cleverdon, D., Collins, G. B. and Smith, J. W., 1955, *J. Chem. Soc.*, 3793.  
 Bottcher, C. J. F., 1952, "Theory of Electric Polarization", Elsevier Publishing Co., p. 312.  
 Dakin, T. W. and Works, N. C., 1947, *J. App. Phys.*, **18**, 799.  
 Donle H. L. and Gehrckens, K. A., 1932, *Z. physik chem. B.*, **18**, 316.  
 Gopalkrishna, K. V., 1957, *Trans. Faraday Soc.*, **53**, 767.  
 Goode, E. V. and Ibbitson, D. A., 1960, *J. Chem. Soc.*, 4265.  
 Guggenheim, E. A., 1949, *Trans. Faraday Soc.*, **45**, 714.  
 " 1951, " 47, 573.  
 Heston Jr. W. M., Franklin, A. D., Hennelly, E. S. and Smyth, C. P., 1950, *J. Am. Chem. Soc.*, **72**, 3443.  
 Katagiri, S., 1960, Tohoku Imperial University Science Reports, 1 Ser., **44**, 165-76.  
 Kimura, K. and Fujishiro, R., 1959, *Bull. Chem. Soc. Japan*, **32**, 433-38.  
 LeFevre, R. J. W., Ross, I. G. and Smythe, B. M., 1950, *J. Chem. Soc.*, 276.  
 Lumbroso, H. and Dumas, G., 1955, *Bull. Soc. Chem. France*, 651-59.  
 Roberts, S. and Von Hippel, A., 1946, *J. App. Phys.*, **17**, 610.  
 Sayce, L. A. and Briscoe, H. V. A., 1925, *J. Chem. Soc.*, 315.  
 Smyth, C. P., 1955, "Dielectric behaviour and structure, McGraw-Hill Book Co., p.314.  
 Sugden, S., 1933, *J. Chem. Soc.*, 770.  
 Surber, Jr., W. H. and Gronch, Jr, G. E., 1948, *J. App. Phys.*, **19**, 1130.  
 Von Hippel, Arther R., 1954, Editor "Dielectric materials and applications", The Technology Press of M. I. T. and John Wiley & Sons Inc., New York, p. 80.  
 Whiffen, D. H. and Thompson, H. W., 1946, *Trans. Faraday Soc.*, **42 A**, 114.

# APPLICATION OF ELECTROSTATIC MODEL OF HYDROGEN BOND TO HYDROGEN BONDING IN SOME ALIPHATIC ALCOHOLS AND PHENOL COMPOUNDS IN SOLUTIONS OF POLAR SOLVENTS

G. S. KASTHA and K. C. MEDHI

OPTICS DEPARTMENT,

INDIAN ASSOCIATION FOR THE CULTIVATION OF SCIENCE,  
CALCUTTA-32.

(Received April 3, 1964).

**ABSTRACT.** Coggeshall's method of treatment of electrostatic model of hydrogen bond as developed in an earlier paper (Kastha and Medhi, 1960) for investigating hydrogen bonding in aniline and substituted anilines in solutions in polar solvents, has been applied to the case where such hydrogen bridges are formed in very dilute solution between the solute molecules of some aliphatic alcohols, phenol and substituted phenols and the solvent molecules of ether, tetrahydrofuran and pyridine. The validity of the method has been discussed and it has been concluded that the method may be used to explain qualitatively certain features of hydrogen bonding in such cases.

## INTRODUCTION

Recently, Kastha and Medhi (1963) have applied Coggeshall's method of treatment of the electrostatic model of hydrogen bond to the case of hydrogen bonding in aniline and substituted anilines in different environments and have, under certain simplifying assumptions, been able to explain qualitatively certain experimental results previously obtained by them (Medhi and Kastha, 1963). It has been found, on the basis of this model, that in the series of phenyl amines investigated, the ratio of the values of the total solvent shifts in the frequencies of symmetric and asymmetric N-H stretching vibrations in the  $\text{NH}_2$  group in the molecule of any of the compounds in solutions in two polar solvents is a constant for the pair of solvents and is almost independent of the nature of the compound. However, in this case the investigation was limited to hydrogen bonds involving N-H bonds. In order to see whether such a model of hydrogen bond is also applicable when the hydrogen bridges are formed in solution between the hydrogen atom in the molecule of compounds containing other type of X-H bonds and molecules of polar solvents, the investigation has been extended to the case of solutions in polar solvents of compounds whose molecules contain hydroxyl groups.

*Application of Coggeshall's model to O-H...X hydrogen bonds*

Following Coggeshall (1950) and the method of application of his model as developed in a previous paper (Kastha and Medhi, 1963) it is easily found that the ratio of the values of the solvent shifts ( $\Delta\nu$ ) in the frequency of O-H stretching vibration in the molecule of a certain compound due to formation of linear O-H...X bridge in very dilute solutions of the compound in two polar solvents whose molecules contain atoms  $X_1$  and  $X_2$  respectively is given by

$$\frac{\Delta\nu_1}{\Delta\nu_2} = \left( \frac{q_{X_1}}{q_{X_2}} \frac{R_{H...X_2}}{R_{H...X_1}} \right)^2 \quad \dots (1)$$

where  $q_{X_1}$  and  $q_{X_2}$  are the unbalanced charges on atoms  $X_1$  and  $X_2$  respectively and  $R_{H...X_1}$  and  $R_{H...X_2}$  respectively denote the distances between the hydrogen atom in the O-H bond in a molecule of the compound used as the solute and the atoms  $X_1$  and  $X_2$  of the two polar solvent molecules forming the hydrogen bridges O-H... $X_1$  and O-H... $X_2$  respectively. It is seen from equation (1) that the ratio  $\Delta\nu_1/\Delta\nu_2$  should be approximately a constant for a particular pair of solvents and be almost independent of the nature of the compound containing the hydroxyl group. This would strictly hold in the case of structurally similar compounds provided that the distribution of unbalanced charges on the atoms of the solvent molecules taking part in the formation of hydrogen bridges is not affected to a

TABLE I

Compound	$\frac{\Delta\nu \text{ tetrahydrofuran}}{\Delta\nu \text{ ether}}$	$\frac{\Delta\nu \text{ pyridine}}{\Delta\nu \text{ ether}}$
Isopropyl alcohol	1.17	1.99
Tertiarybutyl alcohol	1.12	1.96
Ethyl alcohol	1.11	1.96
Methyl alcohol	1.10	2.01
Propargyl alcohol	1.08	1.98
Phenol	0.99	1.70
<i>p</i> -Cresol	1.04	1.77
<i>m</i> -Cresol	1.44	1.73
<i>p</i> -Chlorophenol	1.05	..
<i>p</i> -Nitrophenol	1.05	..
<i>m</i> -Nitrophenol	1.04	..



significant extent by the charges on the atoms of the solute molecules. Moreover, if  $X_1$  and  $X_2$  represent the same atom,  $q_{x_1} \approx q_{x_2}$  and  $R_{H...X_1} \approx R_{H...X_2}$  we have from Eqn. (1)  $\Delta\nu_1/\Delta\nu_2 \approx 1$ . In order to verify how far such conclusions are true, the values of the ratio of the solvent shifts ( $\Delta\nu_1/\Delta\nu_2$ ) in the vibrational frequency of the hydroxyl group in the molecules of compounds, calculated from the results reported by Henry (1959) in the case of very dilute solutions of some aliphatic alcohols, phenol and substituted phenols in ether, tetrahydrofuran and pyridine, are given in Table I

## DISCUSSION

It is seen from Table I that the values of  $\Delta\nu_1/\Delta\nu_2$  for the pair of solvents, tetrahydrofuran and ether (for which  $X_1$  and  $X_2$  both represent atoms of oxygen) are almost constant and independent of the nature of the solute molecules even though the molecules of the two series of solute compounds of aliphatic alcohols and aromatic phenols are different. Also the values of  $\Delta\nu_1/\Delta\nu_2$  are almost equal to unity in each case. In the case of the two solvents, pyridine and ether the ratio of the solvent shifts  $\Delta\nu_1/\Delta\nu_2$  is constant for the series of aliphatic alcohols and for the phenols. However, in this case the two values are different. This may be due to the difference in the nature of the molecules of the two series of compounds. It would, therefore, be interesting to compare the values of the ratio  $\Delta\nu_1/\Delta\nu_2$  in the case of two structurally similar type of molecules, viz., the phenols and the phenyl amines, in solutions in pyridine and in ether. If the geometry of the hydrogen bridges formed in the two cases of substituted benzenes in solutions in the same pair of polar solvents is not much different it is easily seen that

$$\frac{(\Delta\nu_1/\Delta\nu_2)_{\text{phenyl amines}}^{\text{phenyl}}}{(\Delta\nu_1/\Delta\nu_2)_{\text{phenols}}^{\text{phenyl}}} = \left\{ \left( \frac{R_{H...X_2}}{R_{H...X_1}} \right)_{\text{amines}}^{\text{phenyl}} \middle/ \left( \frac{R_{H...X_2}}{R_{H...X_1}} \right)_{\text{phenols}}^{\text{phenyl}} \right\}^2 \quad \dots (2)$$

A rough estimate of the value of the above ratio may be obtained from the values of the various interatomic distances involved in the hydrogen bond in the case of the phenyl amines and the phenol compounds. If the N-H and O-H bond lengths are taken as 1.09 Å and 0.96 Å respectively, and the values of the interatomic distances N-H...N, N-H...O, O-H...N and O-H...O involved in the various hydrogen bridges, as given by Pimental (1960), are used we get, for phenyl amines  $R_{H...N} \approx 2.01$  Å and  $R_{H...O} \approx 1.95$  Å and for the phenol compounds,  $R_{H...N} \approx 1.88$  Å and  $R_{O...H} \approx 1.71$  Å. Substituting these values on the right hand side expression of equation (2), we obtain,

$$\left( \frac{\Delta\nu_{\text{pyridine}}}{\Delta\nu_{\text{ether}}} \right)_{\text{amines}}^{\text{phenyl}} \middle/ \left( \frac{\Delta\nu_{\text{pyridine}}}{\Delta\nu_{\text{ether}}} \right)_{\text{phenols}}^{\text{phenyl}} = \left\{ \left( \frac{R_{H...O}}{R_{H...N}} \right)_{\text{amines}}^{\text{phenyl}} \middle/ \left( \frac{R_{H...O}}{R_{H...N}} \right)_{\text{phenols}}^{\text{phenyl}} \right\}^2 \approx 1.14$$

The experimental value for the left hand side expression of equation (2) obtained by substituting the average of  $\Delta\nu_1/\Delta\nu_2$  for phenyl amines [taken from the results of Kastha and Medhi (1963)] and that for the phenol compounds [taken from Table I] in solutions in pyridine and in ether, is found to be 1.09 and this agrees fairly well with the calculated value 1.14.

From the foregoing discussions it is concluded that the simple electrostatic model of hydrogen bonds investigated by Coggeshall in the case of hydrogen bonding between similar molecules may also be applied under certain restrictions to the case of formation of hydrogen bridges in solution between two dissimilar molecules of solute and solvent.

#### REFERENCES

- Coggeshall, N. S., 1950, *J. Chem. Phys.*, **18**, 978.  
Henry, L., 1959, *Hydrogen Bonding*, Pergamon Press.  
Kastha, G. S. and Medhi, K. C., 1963, *Ind. J. Phys.*, **37**, 568.  
Medhi, K. C. and Kastha, G. S., 1963, *Ind. J. Phys.*, **37**, 275.  
Pimentel, G. C. and McClellan, A. L., 1960, *The Hydrogen Bond*, W. H. Freeman and Company.

# THE EMISSION BAND SPECTRUM OF AsO

M. VENKATARAMANAIH AND S. V. J. LAKSHMAN

SPECTROSCOPIC LABORATORIES, DEPARTMENT OF PHYSICS,

SRI VENKATESWARA UNIVERSITY, TIRUPATI.

(Received January 24, 1964; Resubmitted, April 6, 1964).

## Plate VII

**ABSTRACT.** The band spectrum of AsO excited in a heavy current discharge run on a 2000 volt, 1 ampere transformer, revealed a large number of new bands in the region  $\lambda$  4100– $\lambda$ 3400Å. They have been analysed into two systems. The lower state frequency for both these systems has been found to be equal to the ground state frequency of the molecule. The molecular constants found for these two systems are summarised below:

$$E-X^2\Pi_r: \nu_e = \frac{27095.5 \text{ cm}^{-1}}{26802.5 \text{ cm}^{-1}}; \omega_e' = 714 \text{ cm}^{-1}$$

$$x_e' \omega_e' = 2.5 \text{ cm}^{-1}; \omega_e'' = 963 \text{ cm}^{-1} \quad x_e'' \omega_e'' = 4.5 \text{ cm}^{-1}$$

$$F-X^2\Pi_r: \omega_e'' \simeq 964 \text{ cm}^{-1}; \omega_e' \simeq 689 \text{ cm}^{-1}$$

## INTRODUCTION

In an earlier publication on this molecule, Lakshman and Rao (1960) reported two new doublet band systems designated as  $C^2\Delta-X^2\Pi_r$  and  $D(^3\Pi ?)-X^2\Pi_r$  in the region  $\lambda$ 3100– $\lambda$ 2400Å. Prior to this, Connelly (1934), Jenkins and Strait (1935), Shawhan and Morgan (1935), all about the same time reported independently two doublet systems  $A^2\Sigma-X^2\Pi$  and  $B^2\Sigma-X^2\Pi$  of AsO, in emission, in various sources of excitation in the region  $\lambda$  3450– $\lambda$ 2350Å. All these four systems reported namely,  $A-X$ ,  $B-X$ ,  $C-X$ , and  $D-X$ , have a common lower  $^2\Pi_r$  state, with a doublet splitting of  $1026 \text{ cm}^{-1}$ . Connelly's absorption experiments proved this lower  $^2\Pi$  system as the normal ground state of the AsO molecule.

The investigations on this molecule have been continued in order to obtain a band system analogous to the  $A^2\Pi-X^2\Pi$  system, earlier found in SbO by Mukherji (1931), Sen Gupta (1939), Lakshman and Rao (1960), and Shimauchi (1960). This work has led to the analysis and identification of two new systems designated as  $E-X^2\Pi_r$  and  $F-X^2\Pi_r$  in the band spectrum of the AsO molecule. The present paper deals with a detailed analysis of the bands of this system.

## E X P E R I M E N T A L

Experimental procedure adopted in the present investigations was the same as reported earlier by Lakshman and Rao (1960), except that a 2kv transformer had been used instead of a 4kv transformer. The bands are so very feeble in intensity, that exposures varying from 20 to 45 minutes were found necessary to photograph them on Ilford Special Rapid, Ilford Panchromatic and Agfa Isopan Superspecial plates using a Hilger Medium Quartz Spectrograph. Wavelengths of the band heads were made using iron arc lines as standards. The vacuum wave numbers were obtained from Kayser's tables.

## R E S U L T S

New bands obtained in the region  $\lambda 4100\text{--}\lambda 3400\text{\AA}$  are reproduced in plate VII. Though the bands are sharp they are so very feeble in intensity that all our attempts failed to photograph them with reasonable intensity on a large Littrow Spectrograph.

The new red degraded bands start from the long wave length side of the  $A-X$  system, i.e. about  $\lambda 3400\text{\AA}$  and extend upto nearly  $\lambda 4100\text{\AA}$ . It was at first thought that they could be the extension of the  $A-X$  system. Our attempts to fit them into the vibrational scheme of the  $A-X$  system were not successful. Therefore, it was concluded that they might fall into one or more separate systems. The wave length, wave number, intensity and classification of these band heads are all given in table I.

*F-X  $^2\pi$  system :*

Bands with heads at  $\lambda 3628.8$ ,  $\lambda 3659.8$ ,  $\lambda 3690.5\text{\AA}$  appear to form one sequence with a wave number interval approximately equal to  $235\text{ cm}^{-1}$ . Similarly another sequence of bands could be picked up with heads at  $\lambda 3510.2$ ,  $\lambda 3541.1$ , and  $\lambda 3570.9\text{\AA}$ , giving almost the same wave number interval. Further a wave number interval equal to  $931\text{ cm}^{-1}$  is found between the bands at  $\lambda 3510.2$  and  $\lambda 3628.8\text{\AA}$ . This is close to the  $\Delta G_{5/2}$  value of the lower  $X\ ^2\Pi$  state of the AsO molecule. Taking this as a clue, the other bands as far as they could, have been picked up to fit into a vibrational scheme as shown in Table II.

The rest of the bands could very well be fitted into two components of a doublet system, with a doublet interval of  $733\text{ cm}^{-1}$  in the upper state. Therefore it is quite propable to assume that the other component of this  $F-X\ ^2\Pi$  system has not been excited in the mode of excitation adopted by the authors. The approximate vibrational constants of this system are given hereunder :

$$\omega'_e \approx 689\text{ cm}^{-1}; \omega''_e \approx 964\text{ cm}^{-1}$$

TABLE I

Wave length, Wave number, Intensity and Vibrational assignments of the bands of  $E-X\ ^2\Pi$  and  $F-X\ ^2\Pi$  systems

$\lambda$ A	$\nu$ cm <sup>-1</sup>	Intensity Assignment	
E-X <sup>2</sup> $\Pi_{3/2}$			
3521.8	28386	1	2,0
3551.4	28148	2	3,1
3611.4	27682	1	1,0
3706.3	26973	1	0,0
3740.6	26726	1	1, 1
3842.1	26020	4	0,1
3987.1	25074	1	0,2
E-X <sup>2</sup> $\Pi_{3/2}$			
3650.5	27386	2	1,0
3682.3	27149	2	2,1
3747.1	26680	1	0,0
3920.8	25498	1	1,2
4032.7	24790	1	0,2
F-X <sup>2</sup> $\Pi$			
3428.0	29163	2	(V'+2,2)
3479.0	28736	2	V', 1
3510.2	28480	5	V'+1, 2
3541.1	28232	3	V'+2, 3
3570.9	27996	4	V'+3,4
3596.9	27794	4	V', 2
3628.8	27549	4	V'+1, 3
3659.8	27316	3	V'+2, 4
3690.5	27089	2	V'+3, 5

TABLE II

Vibrational Scheme of the band heads of the  $F-X^2\Pi$  system of AsO

$V'$ \ $V''$	0	1	2	3	4	5
$V'$	28736	942	27794			
			686			
$V'+1$			28480	931	27549	
			683		683	
$V'+2$			29163	931	28232	916 27316
					680	
$V'+3$					27996	907 27089

$E-X^2\Pi$  system

Table III gives the Deslandre's scheme for the two components of this system. The band heads of the two components of this system could be represented by the quantum formula :

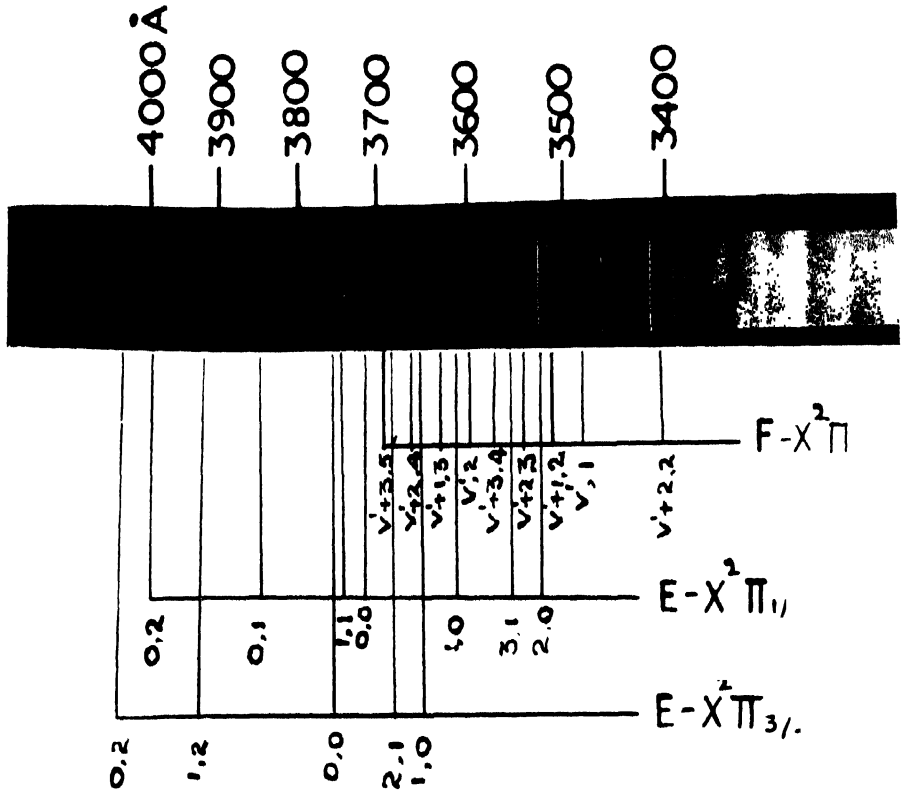
$$\nu = \frac{27095.5}{26802.5} + 714(V' + \frac{1}{2}) - 2.5(V' + \frac{1}{2})^2 - 963(V'' + \frac{1}{2}) + 4.5(V'' + \frac{1}{2})^2$$

to within an accuracy of 3 cm<sup>-1</sup>.

TABLE III

Vibrational scheme of the band heads of the  $E-X^2\Pi$  system of AsO

$V'$ \ $V''$	0	1	2
0	26973	953	26020 946 25074
	26680	—	— 24790
	709	—	706 — —
	706	—	— 708
7	27682	956	26726 — —
	27386	—	— 25498
	704	—	— —
	—	—	— —
2	28386	—	— — —
	—	—	27149 — —
3	—	—	28148 — —
	—	—	— — —



Medium Quartz Spectrogram  
The new E-X & F-X Systems of AsO





# DISCUSSION

The ground state electron configuration for the AsO molecule can be written in Mulliken's notation as

$$(Z\sigma)^2 (Y\sigma)^2 (x\sigma)^2 (\omega\Pi)^2 (V\Pi) \dots {}^2\Pi,$$

A study of the ionised spectra of molecules gives us a clue to know which of the two bonding orbitals ( $x\sigma$ ) or ( $\omega\Pi$ ) is possessing higher energy than the other. As  $\Pi$  state has been observed as the first excited state in the case of  $\text{NO}^+$  and  $\text{NS}^+$  we may expect for molecules with small internuclear distance  $\omega\Pi$  orbital to lie inside the  $x\sigma$  orbital. As  ${}^1\Sigma$  state has been observed as the first excited state in the case of  $\text{PO}^+$ ,  $\text{PS}^+$  and  $\text{AsO}^+$ , we may expect for molecules with large internuclear distance  $x\sigma$  orbital to lie inside the  $\omega\Pi$  orbital.

The states  $E$  and  $F$  may then be expected to belong to the following configuration.

$$(Z\sigma)^2 (Y\sigma)^2 (x\sigma)^2 (\omega\Pi)^3 (V\Pi)^2 \dots 2\Pi_i, {}^2\Pi_r, {}^2\Pi, {}^4\Pi_i$$

The  $E-X$  system may belong to a  $E^2\Pi_r-X^2\Pi_r$  transition with a splitting of  $733\text{ cm}^{-1}$  in the upper  $E$  state. Similarly the  $F-X$  system may belong to a  $F^2\Pi-X^2\Pi_r$  transition with upper  ${}^2\Pi$  state belonging to Hund's case (b). The nature of the states can however be only confirmed on the basis of a detailed rotational analysis.

# ACKNOWLEDGEMENT

The authors wish to express their grateful thanks to Professors P. Tiruvenganna Rao and K. R. Rao both of the Andhra University for their interest in this work. The authors thanks are also due to the authorities of this University for placing all the equipments necessary for this work, at their disposal. One of the authors (M.V.R.) is grateful to the C.S.I.R. (Delhi) for a Junior Research Fellowship.

# REFERENCES

- Connelly, F. C., 1934, *Proc. Phy. Soc., London A*, **46**, 790.  
 Jenkins, F. A., and Strait, L. A., 1935, *P. R.*, **47**, 136.  
 Lakshman, S. V. J., and Tiruvenganna Rao, P., 1960, *Ind. J. Phy.* **34**, 278.  
 Morgan, F., and Shawhay, E. N., 1935, *P. R.*, **47**, 192.  
 Morgan, F., and Shawhay, E. N., 1935, *P. R.*, **47**, 199.  
 Shimauchi, Midori, 1960, *Science of Light (Japan)*, **9**, 109.

# THE REFRACTIVE INDEX AND THE ABSORPTION INDEX FOR THE PROPAGATION OF RADIO WAVE IN THE IONOSPHERE IN SOME SPECIAL CASES

Y. S. N. MURTY

DEFENCE ELECTRONICS RESEARCH LABORATORY, HYDERABAD

and

S. R. KHASTGIR

BOSE INSTITUTE, CALCUTTA.

(Received May 2, 1964)

**ABSTRACT.** The analytical expressions for the refractive index and the absorption index of the ionosphere, obtained by Murty and Khastgir (1963) have been considered for the special cases, when (i)  $H=0$ , (ii)  $\nu=0$ , (iii)  $N=0$  and (iv)  $p_0^2=p^2$ . The longitudinal case, the transverse case, the *quasi*-transverse case and the case when  $\nu \ll p'$  have also been discussed. In the case when  $H=0$ , the expressions are reduced to those obtained by Mitra (1952) following Appleton and Chapman (1932). In the case when  $\nu=0$ , the expressions are the same as those corresponding to the limiting case discussed by Ratcliffe (1933). In the *quasi*-transverse case and in the case, when  $\nu \ll p'$ , it has been shown that the analytical expressions are reduced to those given earlier by Whitehead (1952, 1956).

It has been shown that the effect of the earth's magnetic field is not only to cause birefringence but also to change the values of the refractive index and the absorption index for both the ordinary and the extraordinary modes. Taking collisions into account, Ratcliffe's conclusion that the refractive index in the absence of the earth's magnetic field is minimum, when  $p_0^2/p^2=2$  and that it is zero when  $p_0^2/p^2=1$  for  $\nu=0$  has been confirmed.

## INTRODUCTION

Murty and Khastgir (1963) deduced general analytical expressions for the refractive index and the absorption index of the ionosphere from the Appleton-Hartree magneto-ionic formulae. In the present paper, some special cases have been considered. Some of these formulae obtained from the general analytical expressions under specified conditions have been found to agree with the formulae given by previous workers. The applications of the analytical expressions for the refractive index and the absorption index have also been discussed.

EXPRESSIONS FOR REFRACTIVE INDEX AND  
ABSORPTION INDEX IN SOME SPECIAL CASES

The general expressions for the refractive index  $\mu$  and the absorption index  $\chi$ , as given by Murty and Khastgir (1963) are :

$$\mu^2 = \frac{1}{2} \left[ \sqrt{1 + \frac{1+2a}{a^2+b^2}} + \left( 1 + \frac{a}{a^2+b^2} \right) \right] \quad \dots (1)$$

and 
$$\chi^2 = \frac{1}{2} \left[ \sqrt{1 + \frac{1+2a}{a^2+b^2}} - \left( 1 + \frac{a}{a^2+b^2} \right) \right] \quad \dots (2)$$

where

$$a = \alpha - s\gamma_L \quad \dots (3)$$

$$b = \beta + r\gamma_L \quad \dots (4)$$

$$r = \rho \sin \phi \quad \dots (5)$$

$$s = \rho \cos \phi \quad \dots (6)$$

$\rho$  = ratio of the amplitudes of the normal and the abnormal components of the magnetic vector of the radio-waves\*

$\phi$  = phase-difference between the two components

$$\cos 2\phi = a' - \sqrt{(1+a')^2 - 4a'b'} \quad (7)$$

$$a' = \frac{v_c^2}{v^2 + p'^2} \quad \dots (8)$$

$$b' = \frac{v^2}{v^2 + p'^2} \quad \dots (9)$$

$v$  = electron collisional frequency

$v_c$  = critical collisional frequency =  $p_H \cdot \frac{\sin^2 \theta}{2 \cos \theta}$

$$p' = p \left( 1 - \frac{p_0^2}{p^2} \right), \quad p_H = \frac{eH}{mc}, \quad p_0^2 = \frac{4\pi Ne^2}{m}$$

$p$  = angular frequency of the radio-wave

$H$  = earth's magnetic field

$N$  = electron number density

\*It has been shown by Murty & Khastgir (1959) that

$$\rho = \frac{a'}{r_0} \left[ \frac{r}{\cos \phi} - \frac{P'}{\sin \phi} \right] \text{ and } \rho^{-1} = \frac{a'}{r_0} \left[ \frac{r}{\cos \phi} + \frac{P'}{\sin \phi} \right]$$

$\theta$  angle between the positive direction of the magnetic field and the direction of wave propagation

$e, m$  = charge and mass of an electron

and  $c$  = velocity of light.

When  $\frac{1+2a}{a^2+b^2} \ll 1$ , the expressions (1) and (2) are reduced to

$$\mu^2 = 1 + \frac{1+4a}{4(a^2+b^2)} \quad \dots (1a)$$

$$\text{and} \quad \chi^2 = \frac{1}{4(a^2+b^2)} \quad (2a)$$

When  $a$  is negative, (1a) can be written as

$$\mu^2 = 1 - \frac{4|a| - 1}{4(a^2+b^2)} \quad (1b)$$

We shall now consider certain special cases :

*Case I—When the earth's magnetic field  $H$  is zero*

In this case, we find from (3) and (4) that

$a = \alpha$  and  $b = \beta$ , so that we can write

$$\mu_{H=0}^2 = \frac{1}{2} \left[ \sqrt{1 + \frac{1+2\alpha}{\alpha^2+\beta^2}} + \left( 1 + \frac{\alpha}{\alpha^2+\beta^2} \right) \right] \quad (10)$$

$$\text{and} \quad \chi_{H=0}^2 = \frac{1}{2} \left[ \sqrt{1 + \frac{1+2\alpha}{\alpha^2+\beta^2}} - \left( 1 + \frac{\alpha}{\alpha^2+\beta^2} \right) \right] \quad \dots (11)$$

These expressions for  $\mu_{H=0}^2$  and  $\chi_{H=0}^2$  are the same as those obtained by Mitra (1952) from the expressions for the electrical conductivity of an absorbing medium given by Appleton and Chapman (1932).

When, however,  $\frac{1+2\alpha}{\alpha^2+\beta^2} \ll 1$ , we have

$$\mu_{H=0}^2 = 1 + \frac{1+4\alpha}{4(\alpha^2+\beta^2)} \quad \dots (10a)$$

$$\text{and} \quad \chi_{H=0}^2 = \frac{1}{4(\alpha^2+\beta^2)} \quad \dots (11a)$$

Since  $\alpha$  is negative, (10a) can be written as :

$$\mu_{H=0}^2 = 1 - \frac{4|\alpha| - 1}{4(\alpha^2 + \beta^2)} \quad \dots (10b)$$

*Case II—When the electron collisional frequency  $\nu$  is zero*

In this case, we have  $\beta = 0$  and  $b' = 0$ , so that from (7)  $\phi = \frac{\pi}{2}$  and hence  $r = 0$  and  $b = 0$ . We can therefore write equations (1) and (2) as :

$$\mu_{\nu=0}^2 = \left( 1 + \frac{1}{\alpha} \right) = 1 + \frac{1}{\alpha - s\gamma} \quad \dots (12)$$

$$\text{and} \quad \chi_{\nu=0}^2 = 0 \quad \dots (13)$$

The wave-polarization has been taken as  $R = r + is = \rho e^{i\phi}$ , where  $r$  and  $s$  are defined by (5) and (6),  $\rho$  is the ratio of the amplitudes of the normal and the abnormal components of the magnetic vector of the wave and  $\phi$  the phase-difference between them. Since for  $\nu = 0$ ,  $r = 0$ , the Appleton-Hartree formula for the wave-polarization can be written as :

$$R = is = \frac{1}{i\gamma_L} \left[ -\frac{\gamma_T^2}{2(1+\alpha+i\beta)} \pm \sqrt{\frac{\gamma_T^4}{4(1+\alpha+i\beta)^2} + \gamma_L^2} \right] \quad \dots (14)$$

In (14) the negative sign of the electronic charge is taken into account.

Thus from (12) and (14), we get

$$\mu_{\nu=0}^2 = 1 + \frac{1}{\alpha - \frac{\gamma_T^2}{2(1+\alpha)} \pm \sqrt{\frac{\gamma_T^4}{4(1+\alpha)^2} + \gamma_L^2}} \quad \dots (12a)$$

This was discussed by Ratcliffe (1933).

From equations (1) and (12), it is found that the value of the refractive index in the absence of collisions is greater than the value in the presence of collisions.

*Case III—When the electron number density  $N$  is zero*

In this case  $\alpha \rightarrow \infty$  and  $\beta \rightarrow \infty$

and hence  $\alpha \rightarrow \infty$  and  $b \rightarrow \infty$

Thus we get

$$\mu_{N=0}^2 = 1 \quad \dots (15)$$

$$\chi_{N=0}^2 = 0 \quad \dots (16)$$

*Case IV—When  $p^2_0 = p^2$*

In this case, we have  $p' = 0$  and  $b' = 1$ , so that from (7)  $\phi = 0$  and hence

$s = 0$ ,  $\gamma = \rho$  and  $a = \alpha$ . Further  $\alpha = -1$  and  $\beta = \frac{\nu}{p}$ . Hence the equations (1) and (2) are reduced to

$$\mu^2_{p_0^2=p^2} = \frac{1}{2} \left[ \sqrt{1 - \frac{1}{1+b^2}} + \left(1 - \frac{1}{1+b^2}\right) \right] \quad \dots (17)$$

$$\text{and } \chi^2_{p_0^2=p^2} = \frac{1}{2} \left[ \sqrt{1 - \frac{1}{1+b^2}} - \left(1 - \frac{1}{1+b^2}\right) \right] \quad \dots (18)$$

It is seen from (17) that the value of  $\mu^2_{p_0^2=p^2}$  does not become zero at the point  $p_0^2 = p^2$ , when the collisional effects are predominant.

*Case V—Longitudinal Case (i.e. when  $\theta = 0$ ,  $\gamma_T = 0$  and  $\gamma_L = \gamma$ )*

In this case, we have  $\nu_e = 0$ ,  $a' = 0$ ,  $\phi = \frac{\pi}{2}$ . Hence  $r = 0$ ,  $b = \beta$  and  $R = is$ . Further with the help of (14), we get  $s = \pm 1$ , so that  $a = \alpha \pm \gamma$ . The equations (1) and (2) can therefore be written as :

$$\mu^2_{\theta=0} = \frac{1}{2} \left[ \sqrt{1 + \frac{2a}{a^2 + \beta^2}} + \left(1 + \frac{a}{a^2 + \beta^2}\right) \right] \quad \dots (19)$$

$$\text{and } \chi^2_{\theta=0} = \frac{1}{2} \left[ \sqrt{1 + \frac{2a}{a^2 + \beta^2}} - \left(1 + \frac{a}{a^2 + \beta^2}\right) \right] \quad \dots (20)$$

In this case the values of  $\mu$  and  $\chi$  are predominantly affected by the earth's magnetic field.

*Case VI—Transverse Case (i.e., when  $\theta = 90^\circ$ ,  $\gamma_L = 0$  and  $\gamma_T = \gamma$ )*

When  $\theta = 90^\circ$ , we have :

$$(a) \quad s\gamma = 0, \quad r\gamma_L = 0$$

$$(b) \quad s\gamma_L = \frac{\gamma^2(1+\alpha)}{(1+\alpha)^2 + \beta^2}, \quad r\gamma_L = \frac{\gamma^2\beta}{(1+\alpha)^2 + \beta^2}$$

Therefore we get

$$(a) \quad a = \alpha, \quad b = \beta$$

$$(b) \quad a = \alpha - \frac{\gamma^2(1+\alpha)}{(1+\alpha)^2 + \beta^2}, \quad b = \beta \left[ 1 + \frac{\gamma^2}{(1+\alpha)^2 + \beta^2} \right]$$

Using the values of  $a_{\theta=90^\circ}$  and  $b_{\theta=90^\circ}$  in equations (1) and (2) we get the expressions for  $\mu^2_{\theta=90^\circ}$  and  $\chi^2_{\theta=90^\circ}$ . In the transverse case, when  $\theta = 90^\circ$ , we find that one set of the values of  $\mu^2_{\theta=90^\circ}$  and  $\chi^2_{\theta=90^\circ}$ , are the same as  $\mu^2_{H=0}$  and  $\chi^2_{H=0}$  discussed earlier in Case I.

Case VII—Quasi-transverse Case

In the quasi-transverse case,  $\frac{\gamma_T^4}{4(1+\alpha+i\beta)^2} \gg \gamma_L^2$ , so that from (14), we get

$$\begin{aligned} i\gamma_L R_{QT} &= -\frac{\gamma_T^2}{2(1+\alpha+i\beta)} \pm \sqrt{\frac{\gamma_T^4}{4(1+\alpha+i\beta)^2} + \gamma_L^2} \\ &= -\frac{\gamma_T^2}{2(1+\alpha+i\beta)} \pm \left| \frac{\gamma_T^2}{2(1+\alpha+i\beta)} \right| \sqrt{1 + \frac{4\gamma_L^2(1+\alpha+i\beta)^2}{\gamma_T^4}} \\ &= -\frac{\gamma_T^2}{2(1+\alpha+i\beta)} \pm \left| \frac{\gamma_T^2}{2(1+\alpha+i\beta)} \right| \left[ 1 + \frac{2\gamma_L^2(1+\alpha+i\beta)^2}{\gamma_T^4} \right] \quad \dots (21) \end{aligned}$$

Now  $\frac{1}{1+\alpha+i\beta} = \frac{(1+\alpha)-i\beta}{(1+\alpha)^2+\beta^2}$ . Below the reflection level,  $p_0^2 = p^2$ ,  $(1+\alpha)$  is negative. Hence  $\left( \frac{1}{1+\alpha+i\beta} \right)$  is also negative in that region. Thus for the ordinary mode, below the level,  $p_0^2 = p^2$ , we have from (21) :

$$\begin{aligned} i\gamma_L R_{QT} &= i\gamma_L (r_{QT} + s_{QT}) \\ &= -\frac{\gamma_T^2}{2(1+\alpha+i\beta)} - \left| \frac{\gamma_T^2}{2(1+\alpha+i\beta)} \right| \left[ 1 + \frac{2\gamma_L^2(1+\alpha+i\beta)^2}{\gamma_T^4} \right] \\ &= \left| \frac{\gamma_T^2}{2(1+\alpha+i\beta)} \right| - \left| \frac{\gamma_T^2}{2(1+\alpha+i\beta)} \right| + \frac{\gamma_L^2}{\gamma_T^2} |(1+\alpha+i\beta)| \\ &= \frac{\gamma_L^2}{\gamma_T^2} |(1+\alpha+i\beta)| \quad \dots (22) \end{aligned}$$

Hence from (22), we get

$$\gamma_L r_{QT} = \beta \cot^2 \theta \text{ and } \gamma_L s_{QT} = -(1+\alpha) \cot^2 \theta \quad \dots (23)$$

Therefore we get

$$a_{QT} = \alpha + (1+\alpha) \cot^2 \theta \text{ and } b_{QT} = \beta \operatorname{cosec}^2 \theta \quad \dots (24)$$

The Appleton-Hartree formula for the square of the complex refractive index can be written as :

$$m^2 = (\mu - i\chi)^2 = 1 + \frac{1}{(\alpha + i\beta) + i\gamma_L(r + is)} = 1 + \frac{a - ib}{a^2 + b^2} \quad \dots (25)$$

Hence we get 
$$\mu^2 - \chi^2 = 1 + \frac{a}{a^2 + b^2} \quad \dots (26a)$$

and 
$$2\mu\chi = a^2 + b^2 \quad \dots (26b)$$

Thus when  $\chi^2 \ll \mu^2$  and  $\frac{v}{p} \ll 1$ , we can write from equations (24) and (26a)

$$\mu_{OT}^2 \approx 1 + \frac{1}{\alpha + (1+\alpha) \cot^2 \theta} \quad (\text{since } \beta = 0) \quad \dots (27)$$

$$\approx (1-x) \operatorname{cosec}^2 \theta$$

where

$$x = -\frac{1}{\dots}$$

Similarly, the expression for  $\chi_{OT}$  can be written from (24) and (26b)

$$\chi_{OT} = \frac{1}{2\mu_{OT}} \cdot \frac{\beta \operatorname{cosec}^2 \theta}{\{1 + (1+\alpha) \cot^2 \theta\}^2 + \beta^2 \operatorname{cosec}^4 \theta}$$

$$\frac{x^2 \beta \operatorname{cosec} \theta}{2\sqrt{1-x}} \quad \dots (28)$$

The expressions (27) and (28) are the same as those given earlier by Whitehead (1952).

*Case VIII—When  $v \ll p'$*

In this case, we can write equation (14) for the ordinary wave as :

$$iR \approx \frac{v_c(p' + iv)}{p'^2} - \sqrt{\frac{v_c^2(p' + iv)^2}{p'^4}} + 1$$

$$\approx \frac{v_c(p' + iv)}{p'^2} - \sqrt{(1+a')} + \frac{2iva'}{p'}$$

i.e., 
$$i(r + is) \approx \frac{a'(p' + iv)}{v_c} - \sqrt{1+a'} \left\{ 1 + \frac{iva'}{p'(1+a')} \right\}$$

i.e., 
$$r_{v \ll p'} \approx \frac{v \sqrt{a'}}{p'} - \frac{a'v}{p' \sqrt{1+a'}} \quad \dots (29)$$

and 
$$s_{v \ll p'} \approx \sqrt{1+a'} - \sqrt{a'} \quad \dots (30)$$



Therefore we get,

$$\alpha_{\nu < p'} = \alpha - \{\sqrt{1+a'} - \sqrt{a'}\}\gamma_L \quad \dots (31)$$

and 
$$b_{\nu < p'} = \beta + \frac{\nu \sqrt{a'}}{p'} \left\{ 1 - \frac{\sqrt{a'}}{\sqrt{1+a'}} \right\} \gamma_L \quad \dots (32)$$

Hence the expression for  $\mu_{\nu < p'}$  can be written from equation (1) as :

$$\mu_{\nu < p'}^2 \approx 1 + \frac{1}{a} \approx 1 + \frac{1}{\alpha - \{\sqrt{1+a'} - \sqrt{a'}\}\gamma_L} \quad \dots (33)$$

and from equation (2) we have :

$$\begin{aligned} \chi_{\nu < p'} &\approx \frac{1}{2\mu_{\nu < p'}} \cdot \frac{b_{\nu < p'}}{a_{\nu < p'}^2} \\ &\approx \frac{\beta + \frac{\nu \sqrt{a'}}{p'} \left\{ 1 - \frac{\sqrt{a'}}{\sqrt{1+a'}} \right\} \gamma_L}{2[\alpha - \{\sqrt{1+a'} - \sqrt{a'}\}\gamma_L]^2 \sqrt{1 + \frac{1}{\alpha - \{\sqrt{1+a'} - \sqrt{a'}\}\gamma_L}}} \quad \dots (34) \end{aligned}$$

The expressions for  $\mu_{\nu < p'}$ , and  $\chi_{\nu < p'}$  are the same as those obtained earlier by Whitehead (1956) (*vide* Appendix).

#### APPLICATIONS OF THE EXPRESSIONS FOR $\mu$ AND $\chi$

##### (i) Computation of the dispersion and absorption curves :

The dispersion and absorption curves showing the variation of  $\mu$  and  $\chi$  as function of the electron number density, for some assumed values of collisional frequency and earth's magnetic field conditions can be easily computed for different wave frequencies for both ordinary and extraordinary modes of propagation by using the expressions for  $\mu$  and  $\chi$  given in equations (1) and (2). The values of  $\rho$  and  $\phi$  are first computed by using the expressions given earlier by Murty and Khastgir (1959, 1960a). Then the values of  $r$  and  $s$ , corresponding to either ordinary or extraordinary mode are evaluated using equations (5) and (6). From equation (3) and (4) we can then get the values of  $a_0$ ,  $b_0$  or  $a_x$ ,  $b_x$  which can be used in equations (1) and (2) to get the value of  $\mu_0$ ,  $\chi_0$  or  $\mu_x$ ,  $\chi_x$ .

##### (ii) Evaluation of the group-refractive index of the ionospheric medium

The group refractive index  $\mu'$  can be written as,

$$\mu' = \mu + p \frac{\partial \mu}{\partial p} \quad \dots (35)$$

Equation (35) can also be written as :

$$\mu \mu' = \frac{1}{2p} (p^2 \mu^2) \quad \dots (36)$$

Using the general expression for  $\mu^2$  given in equation (1), the expression for  $\frac{d}{dp}$  ( $p^2\mu^2$ ) can be obtained. Hence by using equation (36), the general expression for the group refractive index  $\mu'$  can be deduced. The general expression for  $\mu'$  has already been obtained by Murty and Khastgir (1960c, 1961).

(iii) *Effect of earth's magnetic field on the refractive index and the absorption index of the ionosphere :*

As the negative sign of the electronic charge has already been taken into account,  $\gamma_L$  should be taken as positive. Considering now the negative sign of  $\alpha$ , we get from (3), (4), (5) and (6)

$$a^2 + b^2 = \alpha^2 + \beta^2 + \rho\gamma_L[2(\alpha \sin \phi + \beta \cos \phi) + \rho\gamma_L] \quad \dots (37)$$

We shall now discuss the cases of the ordinary and the extraordinary modes of propagation separately.

#### Ordinary Mode

Let us consider the ordinary mode in the northern hemisphere below the ionospheric reflection level,  $p_0^2 = p^2$ . We then have  $\rho < 1$  and  $\phi$  is in the first

quadrant  $\left[0 < \phi < \frac{\pi}{2}\right]^*$ , so that  $\sin \phi$  and  $\cos \phi$  (also  $s$  and  $r$ ) are positive.

Accordingly for the ordinary mode, under the conditions, we get from (37)

$$a_0^2 + b_0^2 > \alpha^2 + \beta^2$$

We have put:  $a = \alpha - s\gamma_L$ . Here  $\alpha$  is negative and  $s$  positive so that  $a = -|\alpha| - |s\gamma_L|$ . Hence  $a$  is negative and the approximate value of the refractive index would be given by (1b). Taking a 100 m-wave at the reflection level  $p_0^2 = p^2$ , the scalar magnitude of  $\alpha$  is unity and is very much greater than  $\rho\gamma_L$  or  $s\gamma_L$ . Comparing now (1b) with (10b), it is found that for the ordinary mode under the specified conditions, the effect of the earth's magnetic field would be to increase the refractive index. From (2a) and (11a) it is evident that the effect of the earth's magnetic field would be to decrease the absorption index for the ordinary mode.

#### Extraordinary mode

In the northern hemisphere for the extraordinary mode, below the ionospheric reflection level,  $\rho > 1$  and  $\phi$  is in the fourth quadrant  $\left(\frac{3\pi}{2} < \phi < 2\pi\right)^*$  so that  $\sin \phi$  and  $s$  are negative and  $\cos \phi$  and  $r$  positive. Accordingly for the extraordinary mode under the conditions we get from (37) :

$$a_x^2 + b_x^2 = \alpha^2 + \beta^2 - \rho\gamma_L[2(\alpha \sin \phi - \beta \cos \phi) - \rho\gamma_L] \quad \dots (38)$$

Thus  $a_x^2 + b_x^2 < \alpha^2 + \beta^2$ , provided  $\rho\gamma_L < 2(\alpha \sin \phi - \beta \cos \phi)$ . We have put  $a = \alpha - s\gamma_L$ . Here  $\alpha$  and  $s$  are negative, so that  $a = |s\gamma_L| - |\alpha|$ . When  $|s\gamma_L| < |\alpha|$ ,  $a$  is negative and the refractive index would then be given by (1b). Taking a

---

\*Vide Table I of the paper by Murty & Kastgir (1960b).

100  $m$ -wave at the reflection level,  $p_0^2 = p^2$ , as before, and comparing (1b) with (10b), it is found that for the extraordinary mode under the conditions, the effect of the earth's magnetic field would be to decrease the refractive index, since  $a_x^2 + b_x^2 < \alpha^2 + \beta^2$  for  $p\gamma_L < 2(\alpha \sin \phi - \beta \cos \phi)$ . From (2a) and (11a) it is evident that the effect of the earth's magnetic field would be to increase the absorption index for the extraordinary mode.

(iv) *Conditions of reflection from the ionosphere in the absence of the earth's magnetic field :*

Since  $\beta = \frac{p\nu}{p_0^2}$ ,  $\alpha\nu$ , the expression for  $\mu_{H=0}^2$  as given in (10) can be written as :

$$\mu_{H=0}^2 = \frac{1}{\nu} \left[ \sqrt{\frac{1+2\alpha}{\alpha^2 \left(1 + \frac{\nu^2}{p^2}\right)}} + \left\{ 1 + \frac{\alpha}{\alpha^2 \left(1 + \frac{\nu^2}{p^2}\right)} \right\} \right] \quad (39)$$

The condition of reflection of a wave of frequency  $\frac{p}{2\pi}$  from the ionosphere, where the electron collisional frequency is  $\nu$ , is then obtained by differentiating (39) with respect to  $\alpha$  and equating it to zero. It is easy to find that  $\mu_{H=0}^2$  would be minimum, when  $\frac{p_0^2}{p^2} = 2$ . When  $\nu = 0$ , the value of  $\mu_{H=0}^2$  is zero at  $p_0^2 = 1$ . This has been discussed by Ratcliffe (1959).

## CONCLUSION

From an analysis of the expressions for the refractive index and absorption index, obtained for the different special cases, it is concluded that :

(i) The effect of earth's magnetic field on the propagation of radio-waves in the ionosphere is not only to cause bi-refringence but also to change the values of the refractive index and the absorption index of the ionospheric medium.

(ii) The value of refractive index does not become zero at the point  $\frac{p_0^2}{p^2} = 1$ , when the collisional effects are taken into account.

(iii) The value of refractive index ( $\mu_{H=0}$ ) is minimum at  $\frac{p_0^2}{p^2} = 2$ , when the collisional effects are taken into account and is zero at  $\frac{p_0^2}{p^2} = 1$ , when  $\nu = 0$ .

(iv) In the longitudinal case, both the values of refractive index and the absorption index are predominantly affected by the earth's magnetic field.

(v) In the transverse case, one set of values of  $\mu_{\theta=30^\circ}$  and  $\chi_{\theta=90^\circ}$  are the same as those of  $\mu_{H=0}$  and  $\chi_{H=0}$ .

## REFERENCES

- Appleton, E. V. and Chapman, F. W., 1932, *Proc. Phys. Soc.*, **44**, 246.  
 Mitra, S. K., 1952, *The Upper Atmosphere*, 2nd Edition, p. 183.  
 Murty, Y. S. N., 1959, *Science & Culture*, **25**, 161.  
 Murty, Y. S. N. and Khastgir, S. R., 1959, *Proc. Nat. Inst. Sci. (India)*, **A25**, 255.  
 Murty, Y. S. N. and Khastgir, S. R., 1960(a) *J. Sci. and Ind. Res.*, **19B**, 281.  
 Murty, Y. S. N. and Khastgir, S. R., 1960(b) *J. Geophys. Res.*, **65**, 1449.  
 Murty, Y. S. N. and Khastgir, S. R., 1960(c) *J. Atmos. and Terr. Phys.*, **17**, 309.  
 Murty, Y. S. N. and Khastgir, S. R., 1961, *J. Atmos. and Terr. Phys.*, **21**, 65.  
 Murty, Y. S. N. and Khastgir, S. R., 1963, *J. Atmos. and Terr. Phys.*, **25**, 103.  
 Ratcliffe, J. A., 1959, *The magneto-ionic theory and its application to the ionosphere*, Sec. 9.4, p. 87.  
 Whitehead, J. D., 1952, *J. Atmos. and Terr. Phys.*, **2**, 361.  
 Whitehead, J. D., 1956, *J. Atmos. and Terr. Phys.*, **9**, 276.

## APPENDIX

Whitehead (1956) obtained the following expressions for  $\mu^2_{\nu < \nu'}$  and  $\chi_{\nu < \nu'}$

$$\mu^2_{\nu < \nu'} = 1 - \frac{X}{1 + Q_1 Y_L} \quad \dots \quad (40)$$

$$\text{and } \chi_{\nu < \nu'} = \frac{1}{2} \frac{XZ(1 + 2Q_2 \cot^2 \theta)}{(1 + Q_1 Y_L) \sqrt{1 - \frac{X}{1 + Q_1 Y_L}}} \quad \dots \quad (41)$$

where

$$Q_1 = \sqrt{1 + a'} - \sqrt{a'}$$

$$Q_2 = \frac{a'}{\sqrt{1 + a'}} (\sqrt{1 + a'} - \sqrt{a'})$$

$$\cot \theta = \frac{p_L}{p_L}, \quad Z = \beta X$$

$$Y_L = \frac{p_L}{p_T}, \quad X = \frac{p_0^2}{p^2}$$

Equation (40) can be rewritten as

$$\mu^2_{\nu < \nu'} = 1 + \frac{1}{\alpha - \{\sqrt{1 + a'} - \sqrt{a'}\} \gamma_L}$$

This is the same as given in equation (33). Equation (41) can be rewritten as

$$\chi_{\nu < \nu'} = \frac{1}{2} \frac{\beta + \frac{\gamma \sqrt{a'}}{p'} \left\{ 1 - \frac{\sqrt{a'}}{\sqrt{1 + a'}} \right\} \gamma_L}{\left[ \{\alpha - (\sqrt{1 + a'} - \sqrt{a'}) \gamma_L\}^2 \sqrt{1 + \frac{1}{\alpha - \{\sqrt{1 + a'} - \sqrt{a'}\} \gamma_L}} \right]}$$

This is the same as shown in equation (34).

# Letters to the Editor

*The Board of Editors does not hold itself responsible for opinions expressed in the letters published in this section. The notes containing short reports of original investigations communicated to this section should not contain many figures and should not exceed 500 words in length. The contributions reaching the Secretary by the 15th of any month may be expected to appear in the issue for the next month. No proof will be sent to the author.*

11

## ESTIMATION OF THE CRYSTALLINE ELECTRIC FIELD AND EVALUATION OF $g$ -FACTORS IN $\text{CuSO}_4 \cdot 5\text{H}_2\text{O}$

A. NARASIMHAMURTHY AND D. PREMASWARUP

MICROWAVE LABORATORY, ANDHRA UNIVERSITY, WALTAIR

(Received March 8, 1963 ; Resubmitted August 2, 1963, and October 9, 1963).

In  $\text{Cu}(\text{KSO}_4)_2 \cdot 6\text{H}_2\text{O}$  where the  $\text{Cu}^{++}$  ion is surrounded by six water molecules arranged with tetragonal symmetry, Polder (1942) calculated the induced and hence effective dipole moments of the two types of water molecules corresponding to the two different distances from the  $\text{Cu}^{++}$  ion. However, in the absence of any data on  $\text{Cu}(\text{KSO}_4)_2 \cdot 6\text{H}_2\text{O}$ , Polder took the distance parameters the same as in  $\text{CuSO}_4 \cdot 5\text{H}_2\text{O}$  in which the nearest neighbours of the  $\text{Cu}^{++}$  ion are established as four equidistant water molecule and two equidistant oxygen atoms (of the  $\text{SO}_4$  groups) distributed with tetragonal symmetry about the axis joining the two oxygen atoms according to the X-ray diffraction analysis of Lipson and Beevers (1934). These values are then utilised to calculate the strength of the crystalline electric field at the copper ion and the Stark energy splitting of the ground state. Results of this calculation were later used by Spence and Kikuchi (1950) to evaluate the principal  $g$ -values of the  $\text{Cu}^{++}$  ion in the  $\text{CuSO}_4 \cdot 5\text{H}_2\text{O}$  crystal. However, the effect of the very considerable differences in the values of the permanent dipole moments of water molecules and oxygen atoms (1.87D and 0 respectively) makes the calculation for this salt different from that of Polder. We have undertaken such calculations for  $\text{CuSO}_4 \cdot 5\text{H}_2\text{O}$  employing the method described in an earlier communication by us (1963) taking the oxygens as neutral atoms instead of  $(\text{SO}_4)^{2-}$  groups in view of the large size of this group compared to the  $\text{Cu}-\text{O}$  distance.

Both the water molecules and oxygen atoms are regarded as point dipoles placed at the corresponding lattice points with distances  $a = 2.0 \text{ \AA}$  and  $b = 2.3 \text{ \AA}$

respectively from the copper ion. Polarisabilities and permanent dipole moments of water and oxygen respectively are

$$\begin{aligned}\alpha_{\text{H}_2\text{O}} &= 1.48 \times 10^{-24} \text{cc} & \alpha_{\text{O}} &= 1.57 \times 10^{-24} \text{cc} \\ \alpha_{\text{H}_2\text{O}} &= 1.87 \text{D} & \mu_{\text{O}} &= 0\end{aligned}$$

Representing the effective dipole moments of the water molecule and oxygen atoms by  $\mu_a$  and  $\mu_b$  respectively, so oriented that their negative ends are towards  $\text{Cu}^{++}$ , one can write down from the fields at the different lattice points due to the surrounding charges and dipoles, the following equations.

$$\mu_a = \mu_{\text{H}_2\text{O}} + \alpha_{\text{H}_2\text{O}} \left[ \frac{Ze}{a^2} - \frac{\mu_a}{4a^3} - \frac{3\mu_a}{2\sqrt{2}a^3} - \frac{6ab\mu_b}{(a^2+b^2)^{5/2}} \right]$$

$$\mu_b = \mu_{\text{O}} + \alpha_{\text{O}} \left[ \frac{Ze}{b^2} - \frac{12ab\mu_a}{(a^2+b^2)^{5/2}} - \frac{\mu_b}{4b^3} \right]$$

The field in the immediate neighbourhood of the paramagnetic ion can be represented as usual by

$$V_{\text{cryst}} = A_2^0 r^2 Y_2^0 + A_4^0 r^4 Y_4^0 - A_4^{\pm 4} r^4 Y_4^{\pm 4}$$

Numerical values of the dipole moments and expressions and values for the field parameters are given in Table I.

TABLE I

	Authors	Polder
$\mu_a$	4.19D	4.00D
$\mu_b$	1.42D	3.33D
$A_2^0 \overline{r^2} = 12 \sqrt{\frac{\pi}{5}} \left[ \frac{\mu_a}{a^4} - \frac{\mu_b}{b^4} \right] r^2$	39200 $\text{cm}^{-1}$	24600 $\text{cm}^{-1}$
$A_4^0 \overline{r^4} = -20 \sqrt{\frac{\pi}{3}} \left[ \frac{3\mu_a}{a^6} + \frac{\mu_b}{b^6} \right] r^4$	-28300 "	-33300 "
$A_4^{\pm 4} \overline{r^4} = -\frac{5}{3} \sqrt{\frac{35\pi}{2}} \frac{\mu_a}{a^6} r^4$	-33000 "	31400 "

In the two different models, the relative magnitudes of  $A_4^0$  and  $A_4^{\pm 4}$  get reversed. As the crystal field parameters are directly related to the matrix elements of the potential energy, their sign and magnitude essentially determine the ultimate energy levels.

Under the tetragonal field the  $^2D$  state of the  $Cu^{++}$  free ion splits into three singlet and one doublet levels. Numerical values of the energies are as follows.

State	Level	Authors	Polder
$\phi_{1a}, \phi_{1b}$	$E_{1ab}$	7440 $cm^{-1}$	6606 $cm^{-1}$
$\phi_0$	$E_0$	2529 „	-1363 „
$\phi_{2b}$	$E_{2b}$	172 „	2224 „
$\phi_{2a}$	$E_{2a}$	-17298 „	-14143 „

In terms of the energy levels the principal  $g$ -factors are given by

$$g_i = 2 - 2\lambda \sum_{n \neq 0} \frac{\langle 0 | L_i | n \rangle \langle n | L_i | 0 \rangle}{E_n - E_0} \quad i = x, y, z$$

Under the present conditions the equations for  $g$  reduce to

$$g_z = g_{||} = 2 - 8\lambda / (E_{2b} - E_{2a})$$

$$g_x = g_y = g_{\perp} = 2 - 2\lambda / (E_{1ab} - E_{2a})$$

The spin-orbit coupling constant  $\lambda$  is taken as  $828 \text{ cm}^{-1}$ . Calculated values of  $g_{||}$  and  $g_{\perp}$  are indicated in Table II along with those obtained by Spence and Kikuchi using Polder's energy values. Experimental values obtained by various investigators are also included in the Table.

TABLE II

Calculated values				Experimental values		
	Authors	Spence and Kikuchi	Bagguley and Griffiths	Wheatley and Halliday	Arnold and Kip	Authors
$g_{  }$	2.38	2.43	2.40	2.39	2.38	2.41
$g_{\perp}$	2.07	2.08	2.08	2.07	2.05	2.07

In view of the large splittings of the ground state in both the models, the change in the calculated  $g$ -values is not very significant. However, a more significant change is obtained in regard to the energies of the various levels. In addition to an overall increase in the splittings due to the crystal field an actual crossing over of the levels  $\phi_0$  and  $\phi_{2b}$  occurs as one goes from Polder's model to the authors' model owing to a comparatively higher magnitude of the tetragonal parameter.

In conclusion certain approximations which had to be made to make the calculations simple may be clearly stated. The polarisation of the oxygen atoms by the sulphur and other oxygens of the  $SO_4$  group may slightly change its dipole

moment value. The values of  $\bar{r}^2$  and  $\bar{r}^4$  used in the calculations refer to the values corresponding to the 3d electrons only, any overlap between the Cu-3d and O-2p orbitals being neglected. Finally such an overlap may also introduce a small change in the value of  $\lambda$  the spin-orbit coupling constant.

The authors wish to express their deep indebtedness to Prof. K. R. Rao for his valuable guidance and kind encouragement throughout the progress of this work. One of us (A.N.) is grateful to the Council of Scientific and Industrial Research for the award of a Junior Research Fellowship.

#### REFERENCES

- Arnold, R. D., and Kip, A. F. 1949, *Phys. Rev.*, **75**, 1199.  
Bagguley, D. M. S., and Griffiths, J. H. E. 1947, *Nature*, **160**, 532.  
Lipson, H., and Beevers, C. A. 1934, *Proc. Roy. Soc.*, **A146**, 570.  
Narasimhamurthy, A., and Premaswarup, D. 1963, *Ind. J. of Pure Appl. Phys.*, **1**, 100.  
Polder, D. 1942, *Physica*, **9**, 709.  
Spence, R. D., and Kikuchi, C. 1950. *Am. Jour. Phys.*, **18**, 165.  
Wheatley, J., and Halliday, D. 1949, *Phys. Rev.*, **75**, 1412.



# IONOSPHERIC DISTURBANCES ACCOMPANYING NON-CROCHET AND CROCHET ASSOCIATED FLARES

S. D. DESHPANDE

DEPARTMENT OF PHYSICS, GOVT. POLYTECHNIC, KHAMGAON.

(Received March 2, 1964 ; Resubmitted April 1, 1964).

From the systematic comparison and study of data on Ionospheric flare effects reported by Indian Ionospheric Stations for 1957-58, two distinct groups of disturbances were selected. One group consisted of flares accompanying Sudden Cosmic Noise Absorption on 25 mc/s (Bhonsle 1960), a short wave fade out on about 6 mc/s and sometimes SEA at 27 and 100 kc/s but not a crochet or a geomagnetic disturbance. In second group flares were associated with crochet in addition to all the above ionospheric flare effects. This group can be termed as crochet associated flares after Dodson and Hedeman (1958). 12 cases of the events in first group and 14 in second were noted.

In all these events belonging to both the groups, except one or two, flare, associated ionospheric effects and crochet, if present, all start with almost simultaneous occurrence prevailing for a certain duration. Additional fade out or SEA on low frequency either precede or what is more likely follow this main disturbance in many events.

SCNA is the predominant of all flare effects as regards intensity and also duration in all the cases belonging to both the groups. Applying Shain and Mitra's (1954) criterion to classify flares on the basis of maximum absorption during associated SCNA, it is possible to compare the relative intensities of flares and the associated ionospheric disturbances. Table I gives such a classification for both the groups together with the values of maximum absorption during associated SCNAs. Similar classification of fade outs in two groups with importance estimated by their duration, as no record of the field strength was available, is given in Table II.

Dodson and Hedeman (1958) reported that no major SID's are associated with crochet flares though these are ordinarily important flares. Present analysis shows that, though crochet flares are ordinarily important flares, there is a proportional increase in the intensity of ionospheric flare effects also as evident from the tables. The minimum ionization, that will produce maximum absorption of cosmic noise to about 1.4db, seems to be essential to have a crochet associated with a flare.

One interesting fact observed is that the end of the simultaneously occurring disturbances is marked with the end of SCNA on 25 mc/s in almost all the

TABLE I

Flares Optically determined Class	Non-crochet Flare events		Crochet Flare events	
	Flare intensity by max. absorp- of SCNA Class	Value of max. absorption during SCNAs db	Flare intensity by max. absorp- of SCNA Class	Value of max. absorption during SCNAs db
1-	3	3.2	--	--
1	2	0.7	2	0.8
1+	2	0.7, 0.8, 1.1, 1.8	2	1.8
1+	--	--	3	4.3
2	2	0.9, 1.0, 1.1, 1.1	2	1.4
2	--	--	3	2.4, 2.6, 3.0, 3.5, 3.6, 4.47
2+	2	1.1	3	6.0
3	--	--	3	3.01, 10.0
3+	--	--	3	20.00

TABLE II

Duration	Non-crochet Flare disturbances Number of F.O.s	Crochet Flare disturbances Number of F.O.s
Below 30 min.	7	2
Between 30-50 min.	2	5
Above 50 min.	2	6

cases of non-crochet flare disturbances and in some of the crochet flare events if the end of the crochet is disregarded. This delay in the end of SCNA on higher frequency over that of a fade out on lower frequency is minimum of 10 min. in some cases and as large as 50 min. in others.

*D*-region absorption is inversely proportional to the square of the frequency and in cosmic noise single passage is involved. However total ionospheric ionization is responsible for cosmic noise absorption while only the *D*-region ionization is effective in case of communication fade out. Hence this delay in the recovery of SCNA, when much appreciable, may possibly be explained by the probable excess ionization present at higher levels (Mitra *et al.* 1958) rather more favourably during non-crochet flare disturbances.

## REFERENCES

- Bhonale, R. V., 1960, *Proc. Ind. Acad. Sci.*, **51A**, 189.  
 Dodson, Helen W., and Hedeman, E. Ruth., 1958, *Astrophys. J.*, **128**, 636.  
 Mitra, A. P., Sarada, K. A., Sarma, N. V. G., and Joshi, M. N., 1958, *J. Sci. Industr. Res.*, **17A**, Supplement 74.  
 Shain, C. A., and Mitra, A. P., 1954, *J. Atmos. Terr. Phys.*, **5**, 316.

# COHESIVE ENERGIES AND OTHER PROPERTIES OF IONIC CRYSTALS—I. ALKALI HALIDES\*

M. N. SHARMA AND M. P. MADAN

DEPARTMENT OF PHYSICS, LUCKNOW UNIVERSITY, INDIA

(Received February 6, 1964; Resubmitted May 14, 1964)

**ABSTRACT.** The lattice energies and other properties of ionic crystals have been studied on the basis of a Lennard-Jones (12:6) potential form and the necessary equations derived. Experimental data for the interionic distances and lattice energies for such crystal have been used to give the values of the repulsive force parameter B and the van der Waals Parameter C, which in turn have been utilised to obtain lattice energies, compressibilities and the coefficient of linear expansion. Satisfactory agreement is found between the experimental values and those calculated theoretically.

## INTRODUCTION

The treatment of lattice energy and other properties of ionic crystals was initially given by Born and later developed by Born and Mayer (1932) and others and has been summarised by Born and Huang (1954). The interaction energy of an ionic crystal, in addition to Coulomb energy, consists of an attractive and a repulsive term. The most widely used forms for the repulsive potential have been either the exponential variation of repulsion interaction with distance or simply an inverse power variation. Although the results obtained by considering the Born theory were consistent, there always seemed to be the uncertainty in the magnitude of the force index in the inverse form or the exponent in the exponential form.

In an ionic crystal, the degree of ionization of the constituent atoms is often such that the electronic configuration of all ions correspond to closed electronic shells, as in the case of inert gas atoms. The inert gas atoms have closed shells and the charge distributions are spherically symmetric. We may also expect that the charge distribution on each ion in an ionic crystal may have approximately spherical symmetry and that they interact according to central force law. Thus, it seems reasonable to assume that ions of an ionic crystal are of the same electronic structure as an inert gas, possess overlap energy (and van der Waals energy), following a law with the same interionic distance variation as for two-inert gas atoms, that is, with the same force indices but with different potential parameters.

Many of the properties of gases and liquids have been calculated and explained in terms of a commonly used interaction energy function, such as Lennard-Jones

---

\*A preliminary note on the subject has appeared in *Ind. J. Phys.* 1961, **35**, 596.

(12 : 6) potential. This potential is strictly true for the interaction of spherically symmetric atoms and molecules. It is therefore possible to describe a number of properties of ionic crystals on a common basis with the help of this potential in conjunction with the term for Coulomb energy. This, thus affords a unified approach for evaluating and interpreting the properties of ionic crystals as well as the knowledge about the interaction forces and it is reasonable to assume that such an analysis will achieve considerable success. In the present paper, we have used the Lennard-Jones (12 : 6) form representing the van der Waals energy and the overlap energy. The inclusion of van der Waals energy makes the law applicable more satisfactorily for heavier compounds.

The interionic energies in salt crystals of heavier elements may be assumed to be of the form

$$\phi(r) = A(r) + B(r) \quad \dots (1)$$

in which

$A(r)$  = attractive potential

$B(r)$  = repulsive potential

If we take Lennard-Jones (12 : 6) form in conjunction with the electrostatic energy term, we get the value of  $A(r)$  and  $B(r)$  as

$$A(r) = - \frac{\alpha e^2}{r} - \frac{C}{r^6} \quad (2)$$

$$B(r) = \frac{B}{r^{12}} \quad \dots (3)$$

where  $\alpha$  is Madelung's constant (1.7476 for NaCl type, and 1.7626 for the CsCl type) which is characteristic of the type of crystal structure and is independent of the dimensions of the lattice,  $e$  is the electronic charge ( $e = 4.803 \times 10^{-10}$  e.s.u.),  $r$  is the interionic distance,  $C$  is the van der Waals constant and  $B$  is the repulsive parameter which is calculable.

We have taken no account of the overlap potentials between other than nearest neighbours. Born and Huang (1954) have shown that the theoretical estimates are altered on this account by well under 1 per cent.

Cohesive energies for the ionic crystals are between a hundred and thousand times higher than the rare gas crystals and so the zero point energy is comparatively very unimportant for the ionic crystals, still one might take this into account.

If  $\epsilon_0$  is the zero point vibrational energy then the energy per cell in an ionic crystal may be represented as

$$\phi(r) = - \frac{\alpha e^2}{r} + \frac{B}{r^{12}} - \frac{C}{r^6} + \epsilon_0 \quad \dots (4)$$

In this equation we have not considered the dipole-quadrupole van der Waals term  $Dr^{-8}$ . However for a check we calculated the effect of this term on lattice energy and the compressibility and found that for lighter alkali halides, contribution due to this term is negligibly small. For higher alkali halides, the deviation is noticeable only in the expression for compressibility, but still is in neighbourhood of 1—2 percent. Therefore estimates of various properties based on (4) should be quite accurate. Equation (4) and the associated expressions can now be used to compute the interionic distances, the lattice energies, the repulsive force constant, the linear expansions and the compressibilities and compare them with experimental determinations as well as with those derived theoretically from other methods.

#### CALCULATION OF POTENTIAL PARAMETERS

The constants in potentials could be assigned values so as to give the best fit for various crystal properties of all the alkali halide lattices in static equilibrium. But, as these quantities for the static lattices are not directly observable, we can assume that at finite temperatures the energy of a lattice consists of two parts, (Hildebrand 1931) one dependent on its volume and the other only on temperature and express the first and second derivatives of the interaction energy in terms of the directly observable quantities. Thus, at equilibrium at zero pressure and at the absolute temperature  $T$ , Huggins (1937),

$$\frac{d\phi(r)}{dr} = \frac{3vT}{r\beta} \left( \frac{1}{V} \frac{\partial V}{\partial T} \right)_P \quad \dots (5)$$

and

$$\frac{d^2\phi(r)}{dr^2} = \frac{9v}{r^2\beta} F_{T,P} \quad \dots (6)$$

where

$$F_{T,P} = 1 + \frac{T}{\beta} \left( \frac{\partial \beta}{\partial T} \right) + \frac{T}{\beta^2 v} \left( \frac{\partial V}{\partial T} \right)_P \left( \frac{\partial \beta}{\partial P} \right)_T + \frac{2T}{3V} \left( \frac{\partial V}{\partial T} \right)_P$$

where  $\beta$  is compressibility,  $\left( \frac{1}{V} \right) \left( \frac{\partial V}{\partial T} \right)_P$  is thermal expansion coefficient and  $v$  is the volume of the lattice cell. If  $v$  is the molar volume, then  $v = \frac{V}{N} = Kr^3$  in which  $K$  is a constant that is characteristic of the type of the lattice.

##### (a) Repulsive parameter $B$

The potential parameters can be evaluated by using the experimental data for different crystal properties. Using equations (4) and (5), we get

$$B = r^{12} \left[ \left( \frac{\alpha e^2}{12r} + \frac{C}{2r^6} \right) - \frac{3Tv}{12} \left( \frac{1}{V} \right) \left( \frac{\partial V}{\partial T} \right)_P \right] \quad (7)$$

and also from equation (4)

$$B = -r^{12} \left[ \frac{5}{6} \frac{\alpha e^2}{r} + \phi(r) + \frac{3Tv}{6} \left( \frac{1}{V} \right) \left( \frac{\partial V}{\partial T} \right)_P - \epsilon_0 \right]. \quad \dots (8)$$

From an analysis of the experimental crystal structure data accurate values for the lattice constant are available, from which using the appropriate structure relationships for cubic lattices, nearest neighbour distance  $r$  can be obtained. These observed values of  $r$  (Huggins 1937) can be substituted in equation (7) to determine the constant  $B$ , if we have a knowledge of  $C$  from other means. The second term in the square bracket is only in the nature of a corresponding term in which experimental values may be used for any selected temperature. If the experimental data for another crystal property, viz, the lattice energy is used in conjunction with the data for  $r$ ,  $B$  could also be computed from equation (8). The values of  $B$  so obtained from both the methods are tabulated in Table I. Mayer's

TABLE I  
Values of the repulsive parameter  $B$

Crystal	$B \times 10^{104}$ (From eqn. 7)	$B \times 10^{104}$ (From eqn. 8)
CsF	72.74	—
CsCl	510.70	531.6
CsBr	817.70	864.6
CsI	1628.00	1496.0
RbCl	184.10	147.8
RbBr	309.20	275.4
RbI	643.60	627.2
KBr	189.90	141.5
KI	404.60	342.7
NaI	163.50	130.6

(1933) estimates of  $C$  obtained from an analysis of optical data were employed while using equation (7). For the sake of comparison few crystals of lighter alkali halides have also been included. It is seen that there is a good agreement in the values of the parameter  $B$ , obtained by using the value of  $C$  from optical data and that obtained by using the experimental values of the lattice energies.

(b) *The van der Waals attraction parameter  $C$*

Values of the lattice energy in conjunction with the experimental values of  $r$ , may be used to determine the attractive parameter  $C$  in a similar manner. The

van der Waal energy increases with the size of the ions and is quite appreciable for crystals of heavier elements. Equations (4) and (5) yield

$$C = -2r^6 \left[ \frac{11}{12} \frac{ae^2}{r} + \phi(r) + \frac{3vT}{12} \left( \frac{1}{\bar{V}} \right) \left( \frac{\partial V}{\partial T} \right)_P - \epsilon_0 \right]. \quad \dots (9)$$

The calculated  $C$  values from this equation are given in Table II, where they

TABLE II  
Values of the van der Waals parameter  $C$

Crystal	$C \times 10^{60}$ (From optical data)*	$C \times 10^{60}$ (From equ. 9)
CsF	495	—
CsCl	1590	1766.00
CsBr	2070	2410.00
CsI	2970	2279.00
RbCl	691	97.74
RbBr	898	485.90
RbI	1330	1201.00
KBr	605	—
KI	924	287.90
NaI	482	159.20

\*Mayer (1933)

have been compared with the values estimated by Mayer (1933) from a careful analysis of optical data. The table shows that there is a fair agreement between the two values and can be termed satisfactory, especially as the values of the lattice energies are subject to the possible experimental errors of the order of a few per cent. However, as expected, it may be noticed that the deviations are larger than those in the case of repulsive parameter  $B$ . These deviations are due to the relatively smaller contribution of van der Waals term to the total energy. The experimental lattice energies are tabulated in Table III.

TABLE III  
Calculated and observed values of crystal energies

Crystal	Experimental	Cohesive Energy $E$ in K Cal/mole.			
		Calculated (Present Work)	Calculated (Fowler, 1955)	Calculated (Cubicciotti, 1959)	Calculated (Huggins, 1937)
CsF	—	182.4	176.9	179.2	175.7
CsCl	157.8	156.8	157.3	155.9	153.1
CsBr	152.3	151.6	153.5	151.1	149.6
CsI	145.4 (141.5) <sup>H</sup>	142.9	147.7	143.6	142.5
RbCl	163.6	167.0	165.7	164.3	162.0
RbBr	158.0	162.6	160.6	157.6	156.1
RbI	149.7	150.1	153.5	149.1	148.0
KBr	161.2	165.5	166.3	162.7	161.3
KI	152.8	155.1	158.8	153.4	152.4
NaI	166.3	166.8	170.8	165.9	164.3

(H) Huggins (1937)

Thus, both the potential parameters, repulsive constant  $B$  and the attractive constant  $C$  can be estimated purely from the experimental data and can be used to compute other properties. If we also wish to calculate  $r$  theoretically, this can be done easily from equations (4) and (5) using the values of the potential parameters and solving the equations for  $r$  by any convenient method of successive approximation.

#### CALCULATION OF CRYSTAL PROPERTIES

##### (a) *Lattice energies :*

Evaluation of the potential parameters from the selected crystal properties, affords a means of calculating other properties of the crystals. As both the distance  $r$  and the energy  $\phi(r)$  have been used to obtain  $B$  and  $C$ , it would be preferable to calculate other properties than these to check the suitability of equation (1). Fortunately, as mentioned earlier,  $C$  can also be obtained separately from the optical data. Therefore, we can determine theoretically, if we use  $B$  as obtained from equation (7), and the experimental values of the constant  $C$  as obtained from the optical data. In Table IV, we have given values of the calculated cohesive energy  $E$  where  $E = -N\phi(r)$  along with the experimental values. In the table are also given values calculated by Fowler (1955) using an inverse ninth power term for the repulsive energy and by Huggins (1937) using an energy function



taking into consideration an exponential expression for the repulsive term along with an additional term for the dipole-quadrupole interaction term. It will be

TABLE IV  
Calculated and observed values of crystal compressibilities

Crystal	$\beta \times 10^{12}$ (bar)		
	Experimental	Calculated (Present work)	Calculated (Present Work)
	(a)	(b)	(c)
CaF	4.25 (4.25)	3.97	—
CsCl	5.95 (5.55)	5.53	5.43
CsBr	7.06 (6.28)	6.39	6.16
CsI	8.57 (7.83)	7.44	8.08
RbCl	6.65 (6.16)	5.45	6.15
RbBr	7.94 (7.38)	6.60	7.05
RbI	9.57 (9.00)	8.57	7.39
KBr	6.70 (6.45)	5.45	—
KI	8.54 (8.07)	7.13	7.82
NaI	7.07 (6.21)	4.68	5.49

(a) Cubicciotti (1959).

(b) Using  $B$  from equation (7).

(c) Using  $B$  and  $C$  from equations (8) and (9) respectively.

seen that the results obtained by us differ very slightly from those obtained by Huggins (1937) and in some cases are even better. Thus, the estimates of the cohesive energy based on equation (1) should be quite adequate.

#### (b) Crystal compressibilities

From the knowledge of  $B$  and  $C$ , we can derive crystal compressibilities which can be compared with observed values. Equation (6) can be written as

$$\beta = \frac{9vF_{T,p}}{\left( -\frac{2\alpha e^2}{r} + 12.13 \frac{B}{r^{13}} - 6.7 \frac{C}{r^7} \right)}. \quad \dots (10)$$

The term  $F_{T,p}$  is of the order of a small correcting term which vanishes at 0°K. Using experimental values for this term equation (10) enable to be computed utilizing  $B$  and  $C$  from equation (8) and (9) and also  $B$  from (7) and  $C$  from optical data. In equation (1), the slope of the repulsive term  $Br^{-n}$  ( $n = 12$ ), increases

rapidly as  $r$  diminishes. The effect of this distortion can be corrected, if we replace in  $\frac{d^2\phi(r)}{dr^2}$ , the expression  $n(n+1)$  by  $n^2$  to conform better with the realistic overlap energy (Fowler 1955). The values of  $\beta$  thus obtained are given in Table IV, where they have compared with experimentally observed values of the crystal compressibilities. The agreement is satisfactory.

TABLE V

Calculated and observed values of Coefficient of thermal expansion of crystals

Crystal	$\alpha^1 \times 10^6$		
	Experimental	Calculated (Present Work)	Calculated (Born Model)
NaI	48.3	47.99	42.87
KBr	40.0	37.44	43.08
RbCl	36.0	31.52	41.05
RbBr	38.0	42.61	41.90
CsCl	56.0	55.27	56.18

#### OTHER PROPERTIES OF CRYSTAL

Besides the properties discussed in preceding section, many other crystalline properties can be investigated on the basis of the interaction energy form of equation (1), and their calculated values compared with observation. However, we consider here only the coefficient of linear expansion.

The thermal expansion of solids can be qualitatively explained as the result of displacement of the equilibrium positions of the ions due to increase of the amplitude of vibration (Hummel 1950). In view of the influence of the ionic vibration on thermal expansion of solids attempts were made by several workers to correlate this property with vibration characteristics of the ions. An approximate thermodynamic equation for thermal expansion of ionic crystals can be derived and the calculated values of thermal expansion can be compared with the experimental results.

The potential energy at a distance  $r$  can be written as

$$\phi(r) = \phi_0(r) + a(r - r_0)^2 \quad \dots \quad (11)$$

where  $\phi_0(r)$  is the energy at the equilibrium distance  $r_0$ , and

$$a = \frac{1}{2} \left[ \frac{d^2\phi(r)}{dr^2} \right]. \quad \dots \quad (12)$$

Now if  $\alpha^1$  be the thermal expansion,  $C_v$  be the specific heat at constant volume, and  $\nu$  be the frequency of vibration then it can be shown that (Kumar 1959)

$$\alpha^1 = - \frac{C_v}{2ar_0} \left( \frac{1}{\nu} \frac{d\nu}{dr} \right). \quad \dots (13)$$

We know that the frequency of vibration of a simple harmonic oscillator is expressed as

$$\nu = \left( \frac{d^2\phi(r)/dr^2}{4\pi^2m} \right)^{1/2}, \quad \dots (14)$$

where  $m$  is the reduced mass of the oscillating ions.

At equilibrium position,  $r = r_0$ ,  $\frac{d\phi(r)}{dr} = 0$  and

$$\frac{d\nu}{dr} = \frac{1}{2\pi\sqrt{m}} \frac{1}{2} \left( \frac{d^2\phi(r)}{dr^2} \right)^{-1/2}_{r \sim r_0} \left( \frac{d^3\phi(r)}{dr^3} \right)_{r \sim r_0} \quad \dots (15)$$

We immediately find out, using  $\phi$  and its derivatives obtained from eqn. (4) in (13), that

$$\alpha^1 = \frac{C_v}{2r_0} \frac{\left( 176 \frac{\alpha e^2}{r_0} + 756 \frac{C}{r_0^3} \right)}{\left( 11 \frac{\alpha e^2}{r_0^3} + 36 \frac{C}{r_0^3} \right)^2}. \quad \dots (16)$$

Equation (16), thus derived is nevertheless, subject to certain simplifying assumptions (Kumar 1959). Further, the effect of the polarization of ions has not been considered. Certain empirical changes can be made to account for this effect. Increase in thermal expansion due to polarizability of the ion can be partially accounted for by replacing  $C_v$  with  $C_p$ . Also, on account of polarization, there is an arrangement of charge distributions, and there is some sort of distortion which accompanies the charge. Empirically the effect of this distortion can be taken care of if we rewrite our equation (16) as

$$\alpha^1 = \frac{C_p}{2r_0} S \frac{\left( 176 \frac{\alpha e^2}{r_0^4} + 756 \frac{C}{r_0^3} \right)}{\left( 11 \frac{\alpha e^2}{r_0^3} + 36 \frac{C}{r_0^3} \right)^2} \quad \dots (17)$$

the correction factor  $S$  is taken to be proportional to polarization  $P$  such that

$$S = (f \times P)$$

where  $P$  is related to the atomic polarizabilities of positive and negative ions in the usual way.  $f$  is given value 0.033 for NaCl type crystals and 0.045 for CsCl type crystals. The results are given in Table V, where they have also been compared with the experimental values. A fair agreement is seen between the two values.

The results of the calculation described above show that the use of the Lennard-Jones (12 : 6) potential form for the ionic crystals is not in conflict with the findings from the use of the original Born equations or its later modifications and describes the crystal properties to practically same degree as the latter, and there is very slight discrepancy between the results from different determinations. The discrepancies become more pronounced as we proceed towards lighter alkali halides. And hence as, for the inert gases and simple near-spherical molecules, different properties can be explained in terms of a single potential in inverse powers of the distance (i.e. L-J 12: 6 potential), it is possible to describe the various properties of ionic crystals, particularly of heavier compounds (high polarizability) by the use of the same simplified potential, even though the absolute computations of properties cannot be termed as better than the previous determinations. The deviation is further reduced if we also consider the dipole-quadrupole term  $D^r$ -8, for these crystals of heavier compounds.

#### ACKNOWLEDGMENT

The authors are thankful to Prof. P. N. Sharma, for his keen interest in this problem.

#### REFERENCES

- Born, M. and Mayer, J. E., 1932, *Zeit. f. Physik*, **75**, 1.  
Born, M. and Huang, K., 1954, *Dynamical Theory of Crystal Lattices*, Clarendon Press, Oxford.  
Cubicecotti, D., 1959, *J. Chem. Phys.*, **31**, 1646.  
Fowler, R. H., 1955, *Statistical Mechanics*, Oxford University Press.  
Hilderbrand, J. H., 1931, *Zeit. f. Phys.*, **67**, 127.  
Huggins, M. L., 1937, *J. Chem. Phys.* **5**, 143.  
Huggins, M. L., and Mayer, J. E., 1933, *J. Chem. Phys.*, **1**, 643.  
Hummel, F. A., 1950, *J. Amer. Ceram. Soc.*, **33**, 102.  
Kumar, S., 1959, *Proc. Nat. Inst. Sci. India.*, **25**, 364.  
Mayer, J. E., 1933, *J. Chem. Phys.*, **1**, 270.

# A NEW MULTIPLIER USING DEAD-BAND TYPE NONLINEARITY

A. K. NATH, N. G. NATH AND A. K. CHOUDHURY

INSTITUTE OF RADIO PHYSICS AND ELECTRONICS,  
CALCUTTA UNIVERSITY

(Received May 3, 1963)

**ABSTRACT.** An electronic analogue multiplier using dead-band type nonlinearity has been described. The multiplier can be readily set up by using standard operational amplifiers and a triangular wave generator. The static and dynamic accuracies of the multiplier are very high.

## INTRODUCTION

In analogue computers the product of two machine variables  $X$  and  $Y$  is obtained using mainly two different types of electronic multipliers. These are either time-division or quarter-square multipliers. In the latter case mostly diode function generators are used for approximating the square-law characteristics.

The static accuracy in a multiplier using diode square law function generator is limited by the total number of straight line segments approximating the square characteristics in any quadrant. In order to increase the accuracy the number of straight line segments have to be increased, with a consequent increase in the number of diodes. The upper limit in static accuracy in such multipliers can be obtained only after careful adjustment of the circuit.

The static and dynamic accuracies of a time-division multiplier are comparable to those of other linear computing elements used in an electronic analogue computer. The performance of such multipliers has been much improved by using the excellent switching properties of transistors (E. Kettel and W. Schneider, 1961; W. R. Seegmiller, 1962). These features have made time-division multiplier very popular.

In the present paper, we shall describe a multiplier in which basically the principle of Quarter-square multiplication is used. In the circuit described, the squaring of the input signals  $X$  and  $Y$  is obtained by feeding a symmetrical triangular wave of high repetition frequency along with the signals  $X$  and  $Y$  into a symmetrical dead-band type nonlinearity. (Norsworthy, K. H., 1954; Mayer, R. A., Davis, H. B., 1956; Bengt, Jiewertz, 1958; Gomperts, R. J., Righton, D. W., Readshaw, D., 1957; and Philbrick Triangular Wave Multiplier). The multiplier has the advantage of extreme simplicity in its circuit arrangement and

it overcomes many of the major disadvantages associated with diode multipliers using quarter-square principle. The only additional equipment required, besides the other computing elements available in an analogue computer, is a symmetrical triangular wave generator of high repetition frequency.

#### OPERATING PRINCIPLES OF MULTIPLIER

The transmission characteristics of a dead-band type nonlinearity is shown in Fig. 1.,

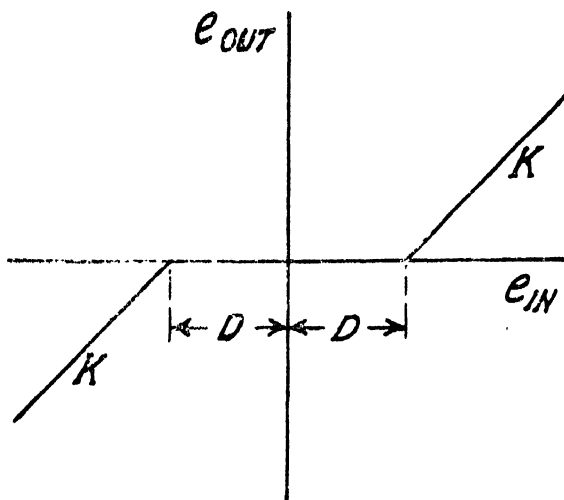


Fig. 1. Transmission characteristics of dead-band type nonlinearity.

$$\begin{aligned}
 e_{out} &= 0 & -D < e_{in} < D \\
 &= K(e_{in} - D) & D < e_{in} \\
 &= K(e_{in} + D) & -D > e_{in}
 \end{aligned}$$

where  $D$  is the dead-band width,

$K$  is the slope of the dead-band.

If the input is a symmetrical triangular wave of amplitude  $B(< D)$  mixed with a d.c. signal  $X$ , and the outputs from the positive and negative halves of the dead-band element are added, then the average value of the output is given by

$$V_1 = K \left( 1 - \frac{D}{B} \right) X \quad (1)$$

If the dead-band width is increased or decreased symmetrically by another d.c. signal  $Y$ , the average value of the output from the positive half of the nonlinearity will be given by

$$V_p = \frac{K}{4} \left[ B - 2(D \pm Y - X) + \frac{(D \pm Y - X)^2}{B} \right] \quad \dots (2)$$

and that from the negative half by

$$V_N = \frac{K}{4} \left[ B - 2(D \pm Y + X) + \frac{D \pm Y + X}{B} \right] \quad \dots (3)$$

and the average value of the added output is given by

$$\begin{aligned} V_2 &= \left( 1 - \frac{D \pm Y}{B} \right) KX \\ &= V_1 \mp \frac{XY}{B} K \end{aligned} \quad \dots (4)$$

Here  $V_1$  is proportional to  $X$  and  $K \frac{XY}{B}$  is the product term. Thus by adding a constant fraction  $\left( 1 - \frac{D}{B} \right) K$  of  $X$  in proper phase with  $V_2$ , the product  $\mp \frac{XY}{B} K$  is obtained. The scale factor of the multiplier is  $\frac{K}{B}$ .

From the right hand side of equations (2) and (3), it is obvious that the product term  $\frac{XY}{B} K$  is obtained because  $V_p$  and  $V_n$  contains terms proportional to  $(\pm Y - X)^2$  and  $(\pm Y + X)^2$  respectively. Evidently the output from the positive half or negative half of the dead-band element can be used for the generation of a square-law function.

### *The Multiplier Circuit*

Figure 2(a) shows the general circuit arrangement of the multiplier in schematic form. The transmission characteristics of the dead-band elements  $N_1$  and  $N_2$  are shown in Fig. 2(b) and (c) respectively. The output from the dead-band

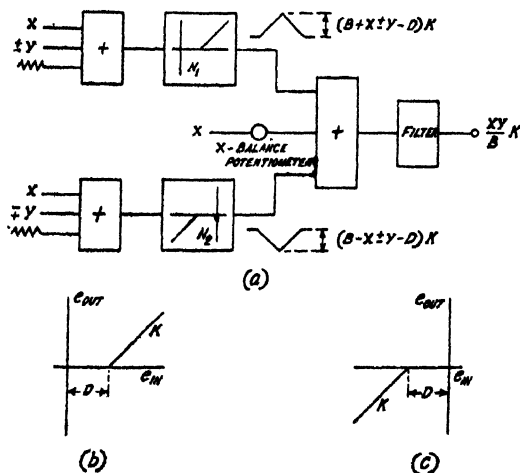


Fig. 2. (a) Block diagram of the multiplier.

(b) Transmission characteristics of  $N_1$ . (c) Transmission characteristics of  $N_2$ .

element  $N_1$  will be obtained only when input signal is more positive than  $D$ . Therefore if  $B$  be the amplitude of the triangular wave, peak output will be equal to  $(B \pm Y + X - D)K$ . Similarly, the output from the dead-band element  $N_2$  will be obtained only when the input signal is more negative than  $D$ . The magnitude of the peak output from  $N_2$  will be  $(B \pm Y - X - D)K$ . These two outputs along with a fraction  $-(1-D/B)$  of  $X$  is fed into a low-pass filter. The product term is obtained from the output of the filter.

### *Dead-band Circuits*

Figures 3(a) and (b) show the negative and positive halves of the conventional dead-band circuit (Jackson).  $A$  is a high gain drift stabilised d.c. amplifier. Voltages  $+V_1$  and  $-V_2$  are taken from stabilised sources and connected to the input terminals of resistances  $R_{V_1}$  and  $R_{V_2}$  respectively. The input signals  $X$ ,  $\pm Y$  and the triangular wave are connected to the resistances  $R_{V_1}$ ,  $R_{Y_1}$  and  $R_{T_1}$  of the negative half of the dead-band circuit and the signals  $X$ ,  $\pm Y$  and the triangular wave are connected to  $R_{X_2}$ ,  $R_{Y_2}$  and  $R_{T_2}$  respectively of the other half of dead-band circuit.

### *Static Adjustment of the Multiplier*

The equation (1) has been derived under assumption that the triangular wave is fed to an ideal dead-band element. This, in other words, means that in the circuit of Figs. 3(a) and (b) if  $V_1$  and  $V_2$  are equal in magnitude then

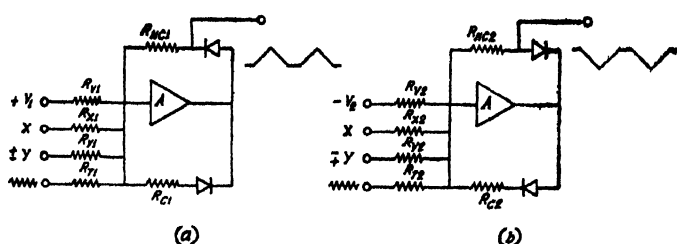


Fig. 3. (a) Positive half of the dead-band circuit.  
(b) Negative half of the dead-band circuit.

Resistances

$R_{V_1}$	be equal to	$R_{V_2}$
$R_{X_1}$	" "	$R_{X_2}$
$R_{Y_1}$	" "	$R_{Y_2}$
$R_{T_1}$	" "	$R_{T_2}$
$R_{nc_1}$	" "	$R_{nc_2}$
$R_{c_1}$	" "	$R_{c_2}$

and the gain of the adding circuit where the outputs from 3(a) and (b) are added



should be identical. But in actual practice it is very difficult to adjust so many resistances accurately.

The average value of the output from an adder, when signals from the circuit 3(a) and (b) are fed to its input points having gains  $K_a$  and  $K_b$  respectively, is given by

$$E_{out} = K_a \frac{R_{nc1}}{RT_1} \left[ \frac{B}{4} - \frac{\left( V_1 + \frac{RV_1}{RX_1} X \pm \frac{RV_1}{RY_1} Y \right) \frac{RT_1}{RV_1}}{2} + \frac{\left( V_1 + \frac{RV_1}{RX_1} X \pm \frac{RV_1}{RY_1} Y \right)^2}{4} \left( \frac{RT_1}{RV_1} \right)^2 \right] \\ - K_b \frac{R_{nc2}}{RT_2} \left[ \frac{B}{4} - \frac{\left( V_2 - \frac{RV_2}{RX_2} X \pm \frac{RV_2}{RY_2} Y \right) \frac{RT_2}{RV_2}}{2} + \frac{\left( V_2 - \frac{RV_2}{RX_2} X \pm \frac{RV_2}{RY_2} Y \right)^2}{4} \left( \frac{RT_2}{RV_2} \right)^2 \right] \quad \dots (5)$$

Equation (5) can be written in the form,

$$E_{out} = \alpha_0 + \alpha_X X + \alpha_Y Y + \alpha_{XY} XY + \alpha_1 X^2 + \alpha_2 Y^2 \quad \dots (6)$$

The coefficients  $\alpha_0, \alpha_X, \alpha_Y, \alpha_{XY}, \alpha_1$  and  $\alpha_2$  are related to the circuit parameters. If we adjust the circuit such that the co-efficients  $\alpha_1$  and  $\alpha_2$  are zero then average value of the output is given by

$$E_{out} = \alpha'_0 + \alpha'_X X + \alpha'_Y Y + \alpha'_{XY} XY$$

where  $\alpha'_0, \alpha'_X, \alpha'_Y$  and  $\alpha'_{XY}$  are the coefficients when the circuit has been adjusted for the condition  $\alpha_1 = \alpha_2 = 0$ . The terms  $\alpha'_0, \alpha'_X X$  and  $\alpha'_Y Y$  can be balanced out at the output by feeding a constant term and terms proportional to  $X$  and  $Y$  in proper phase at the input of the filter. From expression (5) we find that

$$\alpha_1 = \left[ \frac{RV_1}{RX_1} \right]^2 \left[ \frac{RT_1}{RV_1} \right]^2 \cdot \frac{R_{nc1}}{RT_1} K_a - \left[ \frac{RV_2}{RX_2} \right]^2 \left[ \frac{RT_2}{RV_2} \right]^2 \frac{R_{nc2}}{RT_2} K_b \quad (7)$$

and

$$\alpha_2 = \left[ \frac{RV_1}{RY_1} \right]^2 \left[ \frac{RT_1}{RV_1} \right]^2 \frac{R_{nc1}}{RT_1} K_a - \left[ \frac{RV_2}{RY_2} \right]^2 \left[ \frac{RT_2}{RV_2} \right]^2 \frac{R_{nc2}}{RT_2} K_b \quad (8)$$

$\alpha_1$  can be made zero if

$$\frac{K_a R_{w1} R T_1}{R X_1^2} = \frac{K_b R_{nc2} R T_2}{R X_2^2} \quad (9)$$

and  $\alpha_2$  can be adjusted to zero by satisfying the condition

$$\frac{K_a R_{nc1} R T_1}{R Y_1^2} = \frac{K_b R_{nc2} R T_2}{R Y_2^2} \quad (10)$$

The coefficients  $\alpha_1$  and  $\alpha_2$  can be adjusted to zero independently of one another by controlling any two different resistances in the circuit. This method of adjustment has been found to be very convenient in actual practice.

#### EXPERIMENTAL METHOD OF ADJUSTMENT OF STATIC AND LINEARITY CHARACTERISTICS OF THE MULTIPLIER

The simplified circuit arrangement of the multiplier is shown in Fig. 4. For adjusting the coefficient  $\alpha_1$  of the  $X^2$  term to zero, a low frequency signal is applied to  $R X_1$  and  $R X_2$  of the dead-band elements and the inputs to the terminals of  $R Y_1$

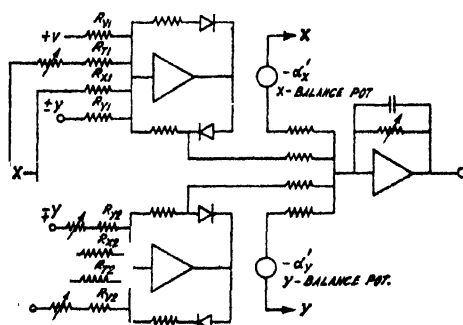


Fig. 4. Arrangement of the multiplier circuit.

and  $R Y_2$  are made zero. The  $X$ -balance potentiometer is adjusted to make the fundamental component of the output zero. If with this adjustment there is a second harmonic component of the  $X$ -signal at the output the variable resistance in series with  $R T_1$  is adjusted to minimise the second harmonic component. With the variation of  $R T_1$  there will appear some fundamental component at the output. This fundamental component is adjusted to zero for each adjustment of  $R T_1$ . By simultaneous adjustment of  $R T_1$  and  $X$ -balance potentiometer the output from the system is brought below the minimum detection level. Now if the  $X$ -signal is varied between zero and full value, the output should remain below the minimum detection level. Any variation in the output with the variation of  $X$ -signal indicates the departure from linearity of the  $X$  channel. The departure will be mainly due to the nonlinearity of the triangular wave.

TABLE  
 $X = 45$  volts peak.  $Y = 45$  volts d.c.  
 $X$ -balance potentiometer reading for balancing the product output

$Y \backslash X$	1.0	.9	.8	.7	.6	.5	.4	.3	.2	.1	0	.1	.2	.3	.4	.5	.6	.7	.8	.9	1.0
.1	.498	.5181	.539	.560	.581	.602	.6225	.6431	.6642	.685	.7057	.7261	.7469	.7679	.7882	.809	.8293	.850	.8705	.891	.911
.2	.498	.5181	.539	.560	.581	.602	.6225	.6431	.6642	.685	.7057	.7261	.7469	.7679	.7882	.809	.8293	.850	.8705	.891	.911
.3	.498	.5181	.539	.560	.581	.602	.6225	.6431	.6642	.685	.7057	.7261	.7469	.7679	.7882	.809	.8293	.850	.8705	.891	.911
.4	.498	.5181	.539	.560	.581	.602	.6225	.6431	.6642	.685	.7057	.7261	.7469	.7679	.7882	.809	.8293	.850	.8705	.891	.911
.5	.498	.5181	.539	.560	.581	.602	.6225	.6431	.6642	.685	.7057	.7261	.7469	.7679	.7882	.809	.8293	.850	.8705	.891	.911
.6	.498	.5181	.539	.560	.581	.602	.6225	.6431	.6642	.685	.7057	.7261	.7469	.7679	.7882	.809	.8293	.850	.8705	.891	.911
.7	.498	.5181	.539	.560	.581	.602	.6225	.6431	.6642	.685	.7057	.7261	.7469	.7679	.7882	.809	.8293	.850	.8705	.891	.911
.8	.498	.5181	.539	.560	.581	.602	.6225	.6431	.6642	.685	.7057	.7261	.7469	.7679	.7882	.809	.8293	.850	.8705	.891	.911
.9	.498	.5181	.539	.560	.581	.602	.6225	.6431	.6642	.685	.7057	.7261	.7469	.7679	.7882	.809	.8293	.850	.8705	.891	.911
1.0	.498	.5181	.539	.560	.581	.602	.6225	.6431	.6642	.685	.7057	.7261	.7469	.7679	.7882	.809	.8293	.850	.8705	.891	.911
For positive values of $Y$											For negative values of $Y$										

The coefficient  $\alpha_2$  associated with  $Y^2$  term in expression (6) is similarly adjusted to zero by feeding an a.c. signal at the  $Y$  inputs and simultaneously adjusting the  $Y$ -balance potentiometer and  $RY_1$ . After  $\alpha_2$  has been adjusted to zero at a particular frequency, and output from the system with the variation of  $Y$ -signal frequency will indicate that the phase difference between the two  $Y$  input signals is different from  $180^\circ$ . In the circuit designed, the variation with the adjustment in  $X$  or  $Y$  could easily be kept below 2 millivolts.

For measuring the linearity characteristics of the multiplier a low frequency signal is applied to the  $X$  channel and a d.c. signal is applied into  $Y$  channel. The  $Y$ -signal is adjusted to different values. For each adjustment of  $Y$  inputs, the output is balanced out by adjusting the  $X$  balance potentiometer. For fixed values of  $Y$  input the fraction of  $X$ -input required to balance the output is constant for all values of  $X$  input for a perfectly linear multiplier. The Table I below gives the reading of the  $X$ -balance potentiometer for different values of  $Y$  signal for the multiplier designed on the basis of this principle. The linearity characteristic is not given in the conventional four quadrant figure. Since it has been found that with  $\pm 2$  mv accuracy of the measuring instrument, there is negligible amount deviation from its linearity characteristics. Hence the linearity characteristic is given by potentiometer readings, required for balancing the product output.

#### *Dynamic Characteristics of the Multiplier*

If a d.c. signal is applied into one of the two inputs and a sine wave to the other input, the bandwidth (3db. point of the output sine wave) of the multiplier using 1 Kc/s triangular wave is found to be 30 c/s. Further studies are being made to increase the bandwidth of this type of multipliers.

#### CONCLUSION

The operation of the multiplier depends upon the square-law functions generated in the two halves of the dead-band element. These square-law function generators using the dead-band element with a triangular wave require least number of components and their static and dynamic accuracies will be much superior to those of biased diode type of square-law function generators. Obviously the static and dynamic accuracies of the multiplier are better. The linearity of the multiplier, particularly in the lower signal range is good. The bandwidth of the multiplier can be increased by using very high frequency triangular wave and using improved filters.

The multiplier is very easy to construct. In a standard analogue computer laboratory, having a single master triangular wave generator, a series of such multipliers can be constructed with usual analogue computer elements.

#### ACKNOWLEDGMENT

The authors wish to express their indebtedness to Prof. J. N. Bhar, D.Sc., F.N.J., M. Brit., I.R.E., for his guidance and keen interest in the work. One of

the authors ((N. G. Nath) also thankfully acknowledges the award of a Junior Research Fellowship by the CSIR, Government of India.

#### REFERENCES

- Bengt Jiewertz, 1958, Second International Analogue Computation Meeting, p. 103.  
Comperis, R. J., Ritton, D. W. and Readshaw, D., 1957, *Electronics Engineering*, **29**, 380.  
Kettel, E. and Schneider, W., 1961, *I.R.E. Transactions, EC-10*, 269.  
Jackson, A. S., 1960, *Analog Computation*, McGraw-Hill Book Company.  
Meyer, R. A. and Davis, H. B., 1956, *Electronics*, **24**, 182.  
Norsworthy, K. H., 1954, *Electronics Engineering*, **26**, 72.  
Stanley, Fifer, 1961, *Analog Computation*, McGraw-Hill Book Company.  
Seegmiller, W. R., 1962, *Electronics*, **30**, 54.

# A TRANSISTOR SAWTOOTH GENERATOR

R. R. DUTTA GUPTA

INSTITUTE OF RADIOPHYSICS AND ELECTRONICS,  
UNIVERSITY COLLEGE OF TECHNOLOGY,  
CALCUTTA 9.

(Received August, 24 1963)

**ABSTRACT.** Principal methods employed in improving the linearity of the output of a sawtooth generator are briefly described. The non-linearity caused by loading is also critically examined. A technique developed to compensate for the non-linearity is then presented. It is shown that the technique also enables one to obtain a reverse curvature which may be of importance in case the sawtooth output needs to be amplified before it can be of practical use.

## INTRODUCTION

Sawtooth waveforms having a high degree of linearity are required for a variety of purposes in electronic circuit applications. In current practice the Miller Integrator and the Bootstrap circuit have become standard methods for the production of such a linear waveform. (Chance *et al.*, 1949 and Bedford and Stevens, B.P. 474623). Neither of these devices can however either preserve a good linearity of waveform in the presence of loading or give a waveform having a reverse curvature. In the present paper we shall describe a fully transistorized arrangement that not only gives a linearity approaching that obtainable with any of the above circuits but is also capable of preserving the linearity even in the presence of resistive loading. An additional feature of this arrangement is that it permits one to obtain a wave form having a reverse curvature that can be adjusted smoothly to any assigned degree.

The paper starts with a brief reference to the existing arrangements for obtaining good linearity and their basic limitations. The theory of operation of the proposed new arrangement is then outlined. Results obtained with a practical circuit based on the theory are given and discussed briefly in the concluding Section.

## A BRIEF RESUME OF THE EXISTING METHODS OF IMPROVING LINEARITY

Normally, pentode charging gives a reasonably good linear waveform for all practical purposes. For precision work requiring a much higher degree of linearity, use is generally made of any one of the following :

- (i) inverse curvature of a valve characteristic,
- (ii) auxiliary time constant circuit and
- (iii) feedback.

A typical example using inverse curvature of a valve characteristic is the Bedford and Stevens' method of linearization. In this method the condenser is charged through a resistance to obtain an exponential waveform first. A portion of this is then fed at the input of an amplifier whose characteristic is shaped and the input and anode load so proportioned that at each point on the dynamic characteristic, the anode potential is equal to the difference between the p.d. across the condenser and the potential required to produce a linear characteristic. Obviously, then the resultant potential difference between the condenser and the anode of the amplifier gives a sweep that is linear.

A circuit involving the use of an auxiliary time constant is due to Hawkins (B.P. 511600) and is shown in Fig. 1. In this the product  $C_3R_2$  is made very large

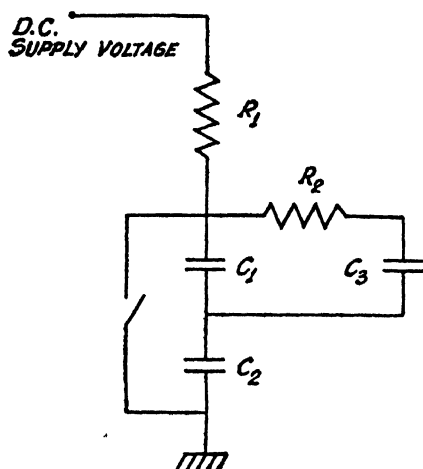


Fig. 1. Sawtooth generator with auxiliary time constant circuit.

so that when the condensers  $C_1$  and  $C_2$  are charged in series,  $C_3$  acquires a voltage that is smaller than that across  $C_1$ . Again, when  $C_1$  and  $C_2$  are completely discharged by the switch,  $C_3$  still retains a charge owing to the large time constant  $C_3R_2$ . Therefore, at the beginning of the charging period,  $C_1$  is charged both from the supply voltage and from  $C_3$ . This continues till the potential across  $C_3$  stops drooping and begins to rise again due to increased potential across  $C_1$ . The actual nature of voltage waveform across  $C_3$  is thus approximately parabolic while that across  $C_1$  and  $C_2$  exponential. The two may be made to cancel each other's curvature so that upon taking the sum one gets a waveform which is linear to a very high degree.

A highly linear sawtooth generator utilising feedback is due to Blumlein (BP. 400976) and is called the Miller Integrator after the name of J. M. Miller who first observed the effect of grid-anode capacitance on the input impedance of a valve amplifier (Miller). The integrator is shown schematically in Fig. 2. If the amplifier be supposed to have a voltage gain of  $-A$  from grid to anode, the effective capacitance between grid and cathode becomes  $(1+A)C$  where  $C$  is the

capacitance between grid and anode. Thus, the integrating circuit at the input, consisting of  $R$  and  $(1+A)C$ , effectively becomes a circuit of very large time constant.

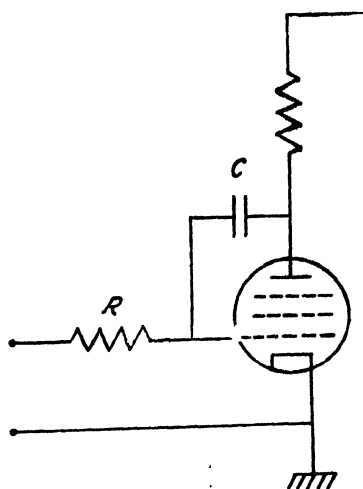


Fig. 2. Miller Integrator.

tant. As such, with a square wave drive the voltage swing obtainable at the grid of the amplifier is a very small fraction of the total supply voltage and hence the output waveform is extremely linear.

Another form of a precision sawtooth generator using feedback, known as Bootstrap Circuit, is shown in Fig. 3. The operation of the circuit may be described as follows.

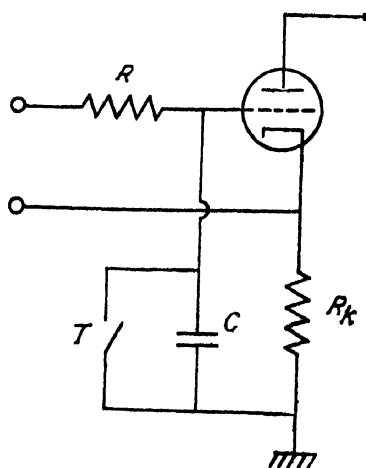


Fig. 3. Bootstrap circuit.

cribed as follows. If the cathode follower be supposed to possess unity gain, the voltage appearing across  $C$  also appears across  $R_k$  undiminished and in the same polarity so that the voltage across the resistance  $R$  remains constant. The cur-



rent through  $R$  therefore remains constant, charging the condenser  $C$  linearly with time until it is discharged by the switch  $T$ .

Considering both the Miller and the Bootstrap Circuits, it is implicit that the loading across the condensers must be completely absent as otherwise the exponential curvature would tend to appear. Neither of these is capable of giving a waveform having a reverse curvature. As such with these it is not possible, by any simple means to compensate for the exponential response of the amplifier stages which might have to be used subsequently under certain circumstances.

#### THE PROPOSED LINEARISING CIRCUIT AND ITS THEORY OF OPERATION

*Current and voltage in a shunt  $RC$  network :*

The relevance of examining the action of current through a parallel combination of  $R$  and  $C$  is obvious from the preceding section. Denoting current and voltage as functions of time  $t$ , viz.  $i(t)$  and  $v(t)$  respectively as shown in Fig. 4, the relation between them is found to be given by

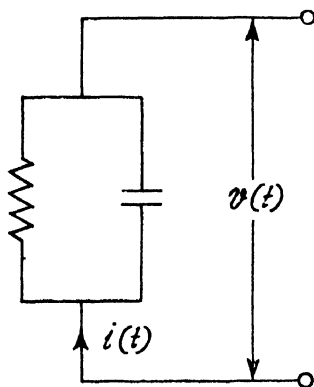


Fig. 4. Shunt  $RC$  network.

$$v(t) = Ke^{-\frac{t}{RC}} + e^{-\frac{t}{RC}} \int e^{\frac{t}{RC}} \cdot \frac{i(t)}{C} \cdot dt \quad (1)$$

where  $K$  is a constant of integration to be fixed by initial conditions.

It is easy to see from eqn. (1) that even if the charging current ( $i(t)$ ) be kept constant the voltage waveform across the combination of Fig. 4 does not increase linearly with time. As such, in order to obtain a linear sawtooth voltage across the combination, it is necessary that the current  $i(t)$  should vary in such a manner that  $v(t)$  in eqn. (1) becomes linearly related with time. We discuss below a practical arrangement for obtaining the required functional dependence of  $i(t)$ .

*Schematic description of the circuit :*

The suggested method for linearising the waveform through charging a shunt  $R$ - $C$  combination is shown schematically in Fig. 5. This utilises a pair

of transistors, one  $n-p-n$  and the other  $p-n-p$ .  $C$  and  $R$  in parallel with the admittance arising out of the loading effect of  $T_2$  form the circuit

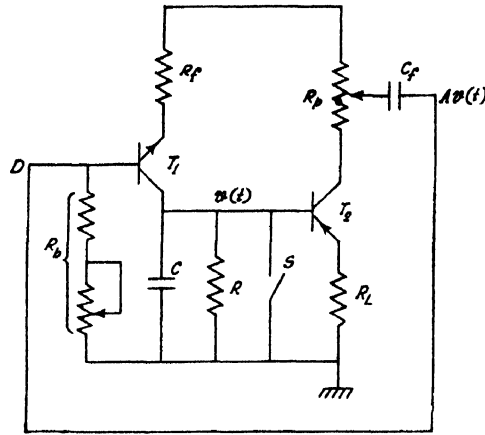


Fig. 5. Schematic arrangement for Transistor Sawtooth Generator.

being charged by  $T_1$ . In the absence of the feedback link marked  $D$ ,  $T_1$  delivers a constant charging current. As was mentioned before, this does not produce a linear waveform across  $C$ . With the feedback link, however,  $T_2$  acts as an amplifier and provides a feedback current to  $T_1$  which is dependant upon time in such a manner that the voltage across  $C$  becomes a linear function of time. As is evident, the arrangement under consideration belongs to the same family as that of Miller Integrator or Bootstrap Circuit. In contrast to these latter devices, however, this utilises a feedback, the magnitude of which can be controlled smoothly over a wide range. It is then possible with proper increase in feedback to even turn round the waveform giving a curvature in the reverse direction.

#### *Analysis of the linearising circuit :*

We adopt the following notation in the analysis.

$\beta_1$  : grounded-emitter current gain of  $T_1$ .

$R_b$  : resistance in the base circuit of  $T_1$  controlling the collector bias current.

$C$  : capacitance to be charged.

$R$  : load resistance across  $C$ .

$\beta_2$  : grounded-emitter current gain of  $T_2$ .

$R_L$  : resistance in the emitter circuit of  $T_2$ .

$R_p$  : potentiometer on the collector of  $T_2$  giving variable feedback to  $T_1$ .

$v(t)$  : instantaneous voltage across  $C$ .

$A$  : effective voltage amplification of  $T_2$  from base to the variable point of  $R_p$ .

On the basis of the plausible assumption that the loading effect of  $R_f$  and  $R_b$  on the amplification factor  $A$  is negligible, the collector current of  $T_1$  may be

written as given by  $Av(t)/R_f$ ,  $-Av(t)$  being the voltage feedback to  $T_1$  from the output of  $T_2$ . Thus at any instant  $t$ , the total collector current in  $T_1$  is given by

$$i(t) = I_0 + \frac{Av(t)}{R_f} \quad \dots (2)$$

where  $I_0$  is the quiescent current in the collector of  $T_1$  and this is the net current charging the combination of the condenser  $C$  and the effective resistance across it, viz,  $R$  and  $\beta_2 R_L$  in parallel. Denoting this effective resistance by  $R'$  and replacing  $R$  by  $R'$  in eqn. (1) we write,

$$v(t) = Ke^{-\frac{t}{R'C}} + e^{-\frac{t}{R'C}} \int e^{\frac{t}{R'C}} \left[ I_0 + \frac{Av(t)}{R_f} \right] dt.$$

$$\text{or,} \quad v(t) = Ke^{-\frac{t}{R'C}} + I_0 R' + \frac{A}{R_f C} e^{-\frac{t}{R'C}} \int e^{\frac{t}{R'C}} v(t) dt. \quad \dots (3)$$

It would be convenient to consider the solution of eqn.(3) under two separate heads viz (a) solution for the special case when we have an ideal sawtooth waveform and (b) the general solution.

*Condition for generation of sawtooth waveform :*

For  $v(t)$  in eqn. (3) to be linear,  $v(t) = \theta t$ , where  $\theta$  is a constant determining the slope of the voltage swing. Thus eqn(3) becomes,

$$\theta t = Ke^{-\frac{t}{R'C}} + I_0 R' + \frac{A}{R_f C} e^{-\frac{t}{R'C}} \int v(t) \cdot dt. \quad \dots (4)$$

It can be shown from eqn. (4) (see Appendix) that the conditions for generation of sawtooth waveform is given by.

$$\frac{AR'}{R_f} = 1, \quad \dots (5)$$

$$\text{and} \quad I_0 = \frac{A\theta R'C}{R_f} \quad \dots (6)$$

Inserting (5) in (6), we get,

$$I_0 = \theta C \quad \dots (7)$$

Eqn.(7) reveals that the slope of the linear sweep is the same as would be obtained due to the charging of  $C$  by a constant current  $I_0$  only. The feedback voltage at  $D$  appears just to have compensated for the loading across  $C$ .

*General solution :*

In order to obtain the general solution of eqn. (3) we put

$$\tau = R'C, \quad \dots (8)$$

and get upon differentiation

$$\frac{dv(t)}{dt} + v(t) \left( \frac{1}{\tau} - \frac{A}{R_f C} \right) = \frac{I_0}{C}. \quad \dots (9)$$

The solution of this equation is obtained as

$$v(t) = Be^{-\left(\frac{1}{\tau} - \frac{A}{R_f C}\right)t} + e^{-\left(\frac{1}{\tau} - \frac{A}{R_f C}\right)t} \int e^{\left(\frac{1}{\tau} - \frac{A}{R_f C}\right)t} \cdot \frac{I_0}{C} \cdot dt$$

$$\text{or,} \quad v(t) = Be^{-\left(\frac{1}{\tau} - \frac{A}{R_f C}\right)t} + \frac{I_0}{C \left(\frac{1}{\tau} - \frac{A}{R_f C}\right)}, \quad \dots (10)$$

where  $B$  is a constant of integration. As  $v(t) = 0$  at  $t = 0$ , eqn. (10) becomes,

$$v(t) = \frac{I_0}{C \left(\frac{1}{\tau} - \frac{A}{R_f C}\right)} \left[ 1 - e^{-\left(\frac{1}{\tau} - \frac{A}{R_f C}\right)t} \right]. \quad \dots (11)$$

Using (8), eqn. (11) becomes,

$$v(t) = \frac{I_0}{\left(\frac{1}{R'} - \frac{A}{R_f}\right)} \left[ 1 - e^{-\left(\frac{1}{R'} - \frac{A}{R_f}\right)t} \right], \quad \dots (12)$$

which is the general solution required. The constant  $\left(\frac{1}{R'} - \frac{A}{R_f}\right)$  may be adjusted to have a value positive, negative or approaching zero. This enables generation of waveform as mentioned below.

*Case I : Undercompensated :*

When

$$\frac{1}{R'} > \frac{A}{R_f}, \quad \dots (13)$$

eqn(12) gives an exponential waveform with a slope falling with time, the maximum value being given by  $\frac{I_0}{\left(\frac{1}{R'} - \frac{A}{R_f}\right)}$  for  $t$  approaching infinity.

*Case II. Critically compensated :*

In the limiting case when

$$\frac{1}{R'} \rightarrow \frac{A}{R_f}, \quad \dots (14)$$

eqn. (12) may be expanded retaining only the linear term in  $t$ . This gives

$$v(t) = \frac{I_0}{C} \cdot t, \quad \dots (15)$$

ensuring a linear waveform having a constant slope equal to  $\frac{I_0}{C}$  as deduced before in eqn. (7).

*Case III. Overcompensated :*

When

$$\frac{1}{R'} < \frac{A}{R_f}, \quad \dots (16)$$

eqn. (12) on being differentiated twice gives,

$$\frac{d^2v(t)}{dt^2} = + \frac{I_0}{C} \left( \frac{A}{R_f} - \frac{1}{R'} \right) e^{\left( \frac{A}{R_f} - \frac{1}{R'} \right) \cdot \frac{t}{C}} \quad \dots (17)$$

Inserting the condition of (16) in eqn. (17) we see that  $\frac{d^2v(t)}{dt^2}$  is positive implying thereby that the slope increases with time as shown in Fig. 6. The

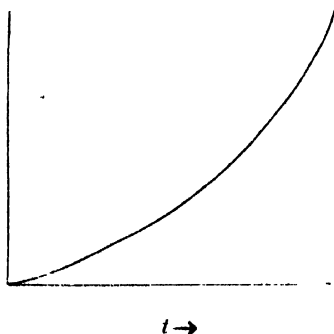


Fig. 6. Increasing slope with time.

amplitude of the waveform will be limited by the time interval in between switching across the condenser, i.e., by the switching frequency.

We now proceed to describe some experimental results in support of the relations deduced above.

#### EXPERIMENTAL RESULTS

The complete circuit diagram of the experimental set up is shown in Fig. 7 where  $T_1$  (OC139) is the charging transistor,  $T_2$  (OC72), the amplifier and  $T_3$  (OC44) the blocking oscillator for switching the condenser  $C$ , the waveform being observed across it. The experimental results demonstrating the validity of the

relationship derived earlier for the linear case viz, eqns. (5) and (7) are now outlined first.

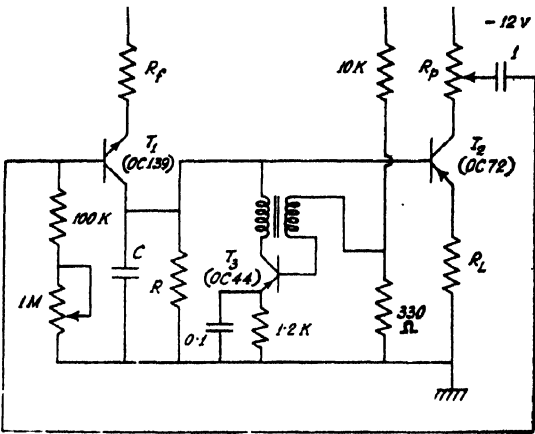


Fig. 7. Experimental arrangement for the Transistor Sawtooth Generator.

Table I gives the observed slope as a function of the capacity  $C$  for  $I_0 = 0.32$  ma. as well as the theoretical values of the slope as given by the equation,

$$I_0 = 0C. \qquad \qquad \qquad \dots \quad (7)$$

TABLE I

Charging current $I_0$ (ma)	Capacitance $C$ ( $\mu$ f)	Experimental slope (mv/ $\mu$ sec)	Theoretical slope (mv/ $\mu$ sec)
0.32	0.05	6.2	6.4
	0.10	3.2	3.2
	0.20	1.5	1.6
	0.52	0.6	0.6
	1.00	0.3	0.32

Columns 3 and 4 reveal satisfactory agreement between the experimental and calculated values of the slope.

Table II gives the observed slope as a function of the current  $I_0$  for  $C = 0.1\mu$ f as well as the theoretical value obtained from eqn. (7). In this case also the agreement between the experimental and calculated values is found to be excellent.

In order to seek experimental support for eqn. (5) it is necessary to express  $R'$  and  $A$  in explicit form relevant to the circuit configuration as shown in Fig. 7. The effective resistance  $R'$  in this latter case is a shunt combination of  $R$  and  $\beta_2 R_L$  and is given by

$$R' = \frac{\beta_2 R_L R}{(\beta_2 R_L + R)}. \qquad \qquad \qquad \dots \quad (18)$$

TABLE II

Capacitance $C(\mu f)$	Charging current $I_0(\text{ma})$	Experimental slope $(\text{mv}/\mu\text{sec})$	Theoretical slope $(\text{mv}/\mu\text{sec})$
0.1	0.67	6.4	6.7
	0.58	5.8	5.8
	0.50	5.0	5.0
	0.42	4.4	4.2
	0.33	3.3	3.3
	0.25	2.4	2.5

Also from Fig. 7, since the currents in the emitter and collector circuits of  $T_2$  are nearly equal and so also the emitter and base voltages, the gain at the collector of  $T_2$  would be given by the ratio of the collector to emitter resistances,  $\frac{R_p}{R_L}$ . If  $R_p$  be tapped for a fraction  $\gamma$  of the total output voltage, the effective gain  $A$  would be given by,

$$A = \frac{R_p}{R_L} \cdot \gamma. \quad \dots (19)$$

Using (5), (18) and (19) and rearranging one gets,

$$R_p \gamma = \frac{R_f(R + \beta_2 R_L)}{\beta_2 R}. \quad \dots (20)$$

Eqn. (20) shows that for a fixed value of  $R_f$ ,  $R$ ,  $R_L$  and  $\beta_2$ , the product  $R_p \gamma$  should be a constant for linear waveform. Table III confirms this result for  $R_f = 600$  ohms,  $R = 30\text{K}\Omega$ ,  $R_L = 50$  ohms and  $\beta_2 = 100$ . Columns 3 and 4 show satisfactory agreement between the experimental and calculated values of  $R_p \gamma$ .

Referring to Fig. 7 and rearranging eqn. (20)

$$\frac{\gamma}{R_f} = \frac{R + \beta_2 R_L}{\beta_2 R R_p}. \quad \dots (20a)$$

TABLE III

$R_p$ (ohms)	$\gamma$	$R_p \gamma$ (experimental)	$R_p \gamma$ (calculated)
500	0.013	6.50	7.00
325	0.021	6.82	
260	0.026	6.80	
180	0.037	6.66	
135	0.048	6.50	

Columns 3 and 4, Table IV again show agreement between the experimental and calculated values of  $\frac{\gamma}{R_f}$  based on (20a) with the following values of the various

parameters :

$$R = 30K\Omega, \beta_2 = 100, R_L = 50 \text{ ohms and } R_L = 325 \text{ ohms.}$$

TABLE IV

$R_f$ (ohms)	$\gamma$	$\frac{\gamma}{R_f}$ (experimental)	$\frac{\gamma}{R_f}$ (calculated)
130	0.004	$0.31 \times 10^{-4}$	$0.35 \times 10^{-4}$
300	0.010	$0.33 \times 10^{-4}$	
600	0.018	$0.30 \times 10^{-4}$	
1200	0.037	$0.31 \times 10^{-4}$	
2400	0.081	$0.34 \times 10^{-4}$	
4700	0.155	$0.33 \times 10^{-4}$	

TABLE V

$R_L$ (ohms)	$R$ ( $K\Omega$ )	$\gamma \times 10^3$ (experimental)	$\gamma \times 10^3$ (calculated)
50	30	21	22
	14.2	25	25
	10	27	28
	7.5	28	30
	4.3	37	40

TABLE VI

$R$ ( $k\Omega$ )	$R_L$ (ohms)	$\gamma \times 10^3$ (experimental)	$\gamma \times 10^3$ (calculated)
30	10	19	18.6
	30	20	19.6
	50	21	21.0
	100	25	24.0
	200	30	30.0
	300	35	36.0



Tables V and VI show the experimental and calculated values of  $\gamma$  for various values of  $R$  and  $R_L$  respectively. The agreements on the basis of calculations, according to eqn. (20) are again seen to be good.

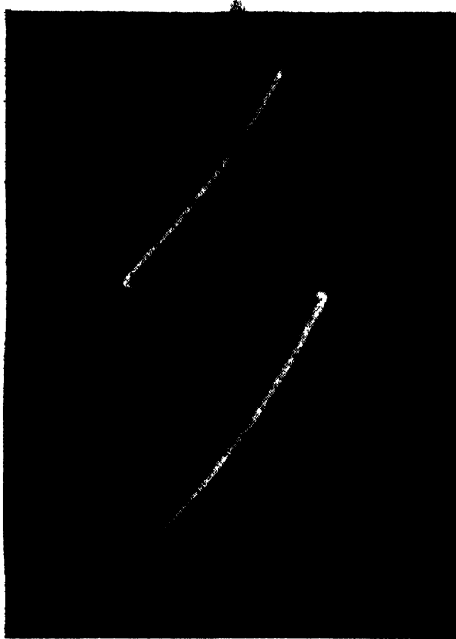


Fig. 8. Undercompensation.



Fig. 9. Critical compensation.

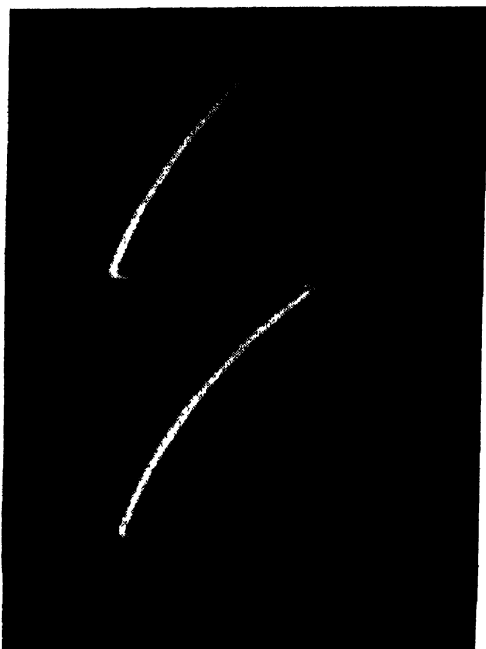


Fig. 10. Overcompensation.

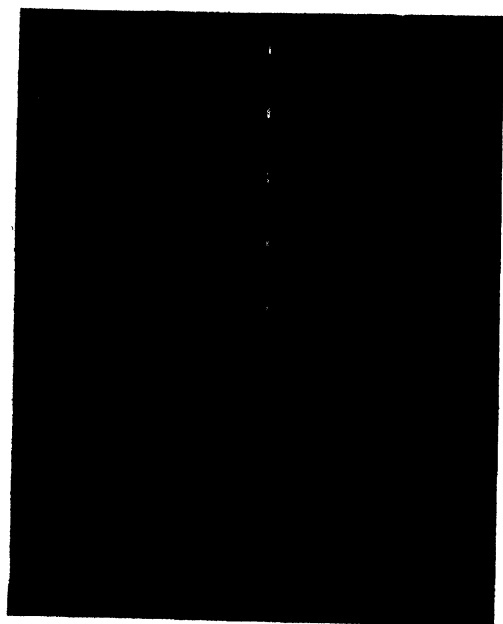


Fig. 11. Linear sawtooth with markers.

It has been shown earlier that three cases corresponding to under, critical and overcompensation are possible. The photographs representing them are presented in Figs. 8, 9 and 10 respectively. The linear sweep of Fig. 9 is also displayed in Fig. 11 with markers in order to illustrate its linearity.

# DISCUSSIONS

It has been seen with the proposed circuit that three possible types of waveform may be generated. Though surperfluous at first sight, the overcompensated case may be of considerable importance in linearising the ultimate waveform. For even supposing that a perfectly linear waveform is generated, it often needs amplification before adequate amplitude is obtained.

If the amplifier includes a coupling network, as shown in Fig. 12, then for a linear current driving through the network,

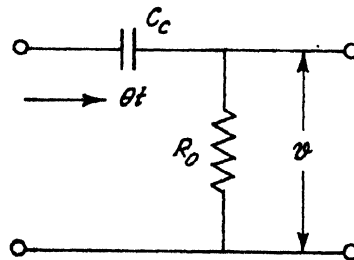


Fig. 12. Coupling network.

$$\partial(p) = \frac{\theta}{p^2} \cdot \frac{pC_oR_o}{(C + pC_oR_o)} \quad \dots (21)$$

in transform notations where  $\theta t$  has been assumed to be the driving current whose transform is  $\frac{\theta}{p^2}$ . Taking the inverse transform of (21),

$$v(t) = \theta R_o C_o \left( 1 - e^{-\frac{t}{R_o C_o}} \right). \quad \dots (22)$$

Thus (22) shows that even for a strictly linear drive the output voltage becomes exponential. Therefore if the drive  $\theta t$  is given an initial reverse curvature (Fig. 10), the amplifier output will tend to compensate for this and deliver an output waveform having reasonably good linearity.

# ACKNOWLEDGMENT

The author intends to thank Prof. J. N. Bhar for his kind interest in the work. He is particularly indebted to Prof. S. Deb for constant advice and helpful discus-

sions throughout the course of the work. Thanks are also extended to the Council of Scientific and Industrial Research for appointing him as Pool Officer.

#### REFERENCES

- Starr, A. T., 1953, Radio and Radar Technique, Sir Isaac Pitman & Sons, Ltd., London, p. 491.  
 Chance B., (*et. al*), 1949, Waveforms, Radiation Laboratory Series, No. 19, McGraw-Hill Book Co., Inc., p. 31-37.  
 Bedford, L. H. and Stevens, W. H., British Patent 474623.  
 Hawkins, G. F., British Patent 511600.  
 Blumlein, A. D., British Patent 400976.  
 Miller, J. M., Dependence of the Input Impedance of a 3-element Vacuum Tube upon the Load in the Plate Circuit, Nat. Bur. Standards Sci., Paper 351.

#### APPENDIX

We rewrite eqn. (4) from the text for the sake of convenience.

$$\theta t = K e^{-\frac{t}{R'C}} + I_0 R' + \frac{A}{R_f C} e^{-\frac{t}{R'C}} \int e^{\frac{t}{R'C}} v(t) dt. \quad (1)$$

Noting that,

$$\int e^{\frac{t}{R'C}} \cdot \theta t \cdot dt = (\theta t R'C - \theta R'^2 C^2) e^{\frac{t}{R'C}}$$

eqn. (1) becomes,

$$\dots \quad \theta t = K e^{-\frac{t}{R'C}} + I_0 R' + \frac{A}{R_f C} (\theta t R'C - \theta R'^2 C^2). \quad (2)$$

Putting  $t = 0$  in eqn. (2) one gets,

$$K = - \left( I_0 R' - \frac{A}{R_f C} \cdot \theta \cdot R'^2 C^2 \right). \quad (3)$$

From (2) and (3),

$$\theta t = \theta \cdot \frac{AR'}{R_f} \cdot t + R' \left( I_0 - \frac{A\theta R'C}{R_f} \right) (1 - e^{-\frac{t}{R'C}}). \quad (4)$$

Thus identity (4) gives the conditions for linear sweep as

$$\frac{AR'}{R_f} = 1, \quad (5)$$

and

$$I_0 = \frac{A\theta R'C}{R_f}. \quad (6)$$

# A SIMPLE COMPUTER FOR FOURIER ANALYSIS AND SYNTHESIS

J. DAS AND P. DASGUPTA

I.I.T., KANPUR

(Received February 7, 1964)

**ABSTRACT.** Three methods of computing Fourier coefficients by simple circuitry have been investigated. In the two Digital Schemes for evaluating  $\sum f_j \cos \theta_j$  or  $\sum f_j \sin \theta_j$  the Sine/Cosine translator is a selecting-cum-marker circuit using either two-motion electro-mechanical switches or diode matrices. The translated digits  $\cos \theta_j / \sin \theta_j$  are read out in the form of pulses, each of which again generates  $f_j$  pulses by triggering preset multivibrators. The sum is then obtained by counting all the serial pulses in a reversible counter. The translator is further simplified in a Hybrid computer, where analogue voltages proportional to  $\cos \theta_j / \sin \theta_j$  and  $f_j$  are multiplied in a semi-digital form, and the output is again in the form of a number of pulses proportional to the product. These methods are easily extended to two- and three-dimensional problems. An accuracy of 1% or better is easily obtained in the Hybrid computer, and the speed of operation, normally about 500 per hour, depends on the input circuits feeding  $\theta_j$  and  $f_j$ .

## INTRODUCTION

Many applications of Fourier Series and Fourier integrals are found in all branches of science and engineering, and in most practical cases, numerical methods have to be used to evaluate the Fourier coefficients. A periodic function  $f(\theta)$  may be represented as,

$$f(\theta) = a_0 + \sum a_n \cos n\theta + \sum b_n \sin n\theta$$

where, 
$$a_0 = \frac{1}{2\pi} \int_0^{2\pi} f(\theta) \cdot d\theta; \quad a_n = \frac{1}{\pi} \int_0^{2\pi} f(\theta) \cdot \cos n\theta \cdot d\theta;$$

and 
$$b_n = \frac{1}{\pi} \int_0^{2\pi} f(\theta) \cdot \sin n\theta \cdot d\theta.$$

When  $f(\theta)$  cannot be expressed in an analytic form, the above integrals are replaced by equivalent summations for numerical computation. Thus, either the synthesis of  $f(\theta)$  from the given  $a$ 's and  $b$ 's, or the analysis of  $f(\theta)$  in terms of the  $a$ 's and  $b$ 's require the determination of the sum of a series of the form  $\sum f_j \cos \theta_j$  or  $\sum f_j \sin \theta_j$ .

Many mechanical, electromechanical and electrical instruments, viz., Harvey Harmonic Analyser, Cathode ray tube, Wave analyser, Spectrum analyser etc. (Manley, 1945), have been developed to aid this numerical computation. The problem may also be solved very accurately in a general purpose Digital computer,

but such a machine is not available to all workers. It has been the purpose of the work, reported here, to solve the problem with much simpler circuits, but at the same time retaining some of the advantages of modern digital and analogue techniques.

### PRINCIPLES OF COMPUTATION

The main problem in Fourier analysis or synthesis is to numerically determine the summation  $\sum f_j \cos \theta_j$  or  $\sum f_j \sin \theta_j$  for various values of  $f_j$  and  $\theta_j$ . The problem, then, consists of three parts, viz., (a) Determination of  $\cos \theta_j/\sin \theta_j$  by some method of translation, (b) Multiplication of  $\cos \theta_j/\sin \theta_j$  by  $f_j$ , (c) Summation of the series, as indicated in Fig. 1. These functions may be done either by digital

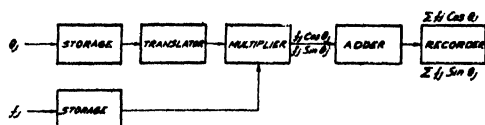


Fig. 1. Block Schematic of the Computer.

or analogue devices. The digital translator may be of electromechanical or electronic type. The input to the system may be stored by positioning some two-motion switches, and the translated digits may be retransmitted by impulse senders according to preset codes as is used in the Directors of a large automatic exchange. (Atkinson, 1955). The preset code may be changed, when required, by some rearrangements in the Translation field only. Using 3-digit values of  $\theta_j$ , the translated 3-digit values of  $\cos \theta_j/\sin \theta_j$  are transmitted to the multiplier in a serial order as shown in Fig. 2. To make the translator faster, electronic

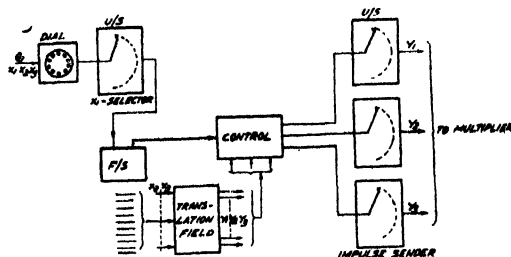


Fig. 2. Translator using Electro-mechanical switches.

circuits analogous to the above may also be used. Fig. 3 shows such a circuit, where the digits of  $\theta$  are stored either in a bank of decade counters using dekatron



Fig. 3. Digital translator using electronic devices.

tubes or in flip-flops. The marked leads of the counters operate a selecting circuit and one output lead is energised. This in turn will mark the corresponding out-

put leads of the marker matrix equivalent to the translator, and the marked leads will indicate the value of  $\cos \theta_j / \sin \theta_j$ . The selecting and marker matrices may be designed with either cold-cathode gas-discharge tubes or diodes (Flowers, 1952), and the impulse senders may be preset triggered-multivibrators giving a set number of pulses corresponding to  $\cos \theta_j / \sin \theta_j$ .

The analogue translator may be a Diode-function generator or a servosystem using sine/cosine potentiometers. A simpler analogue sine/cosine function generator has been developed using the sampling technique, as seen in Fig. 4. Here  $\theta_j$  is represented by a variable voltage which in turn varies the position of a

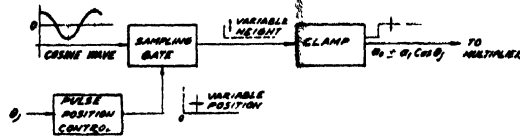


Fig. 4. Analogue translator using Sampling techniques.

sampling pulse with reference to the zero of a sinusoidal wave fed to the sampling gate. The sampled value will correspond to  $\sin \theta_j / \cos \theta_j$  and is transferred to the multiplier through a suitable clamp.

Since in simple calculations, a 2-digit or 3-digit accuracy in  $\cos \theta_j / \sin \theta_j$  and  $f_j$  would be sufficient, it is not necessary to use the complicated multiplying circuits required in standard digital computers. The serial pulses obtained from the translator-sender may be multiplied sequentially by generating a preset number of pulses corresponding to  $f_j$  for each pulse of  $\cos \theta_j / \sin \theta_j$ . The total number of pulses, if counted, would represent  $f_j \cos \theta_j / f_j \sin \theta_j$ . This may be accomplished by prosetting the triggered multivibrators with  $f_j$  and by allowing the MV's to be triggered once for each input pulse representing  $\cos \theta_j / \sin \theta_j$ , as shown in Fig. 5.

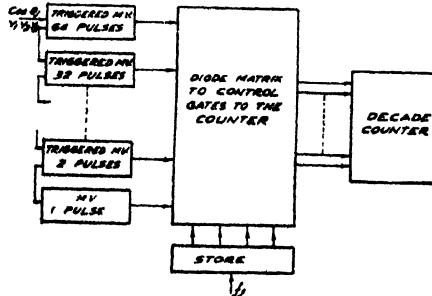


Fig. 5. Digital multiplier.

Here the inputs  $y_1 y_2 y_3$  trigger a series of  $MV$ 's which are controlled by auxiliary counters to produce a predetermined number of pulses according to the Binary code. The output from the  $MV$ 's are then controlled by a diode matrix preset by the codes of  $f_j$  and only those  $MV$ 's which combine to form the number in  $f_j$  are allowed to transmit their pulses to the final counter. Thus each pulse in  $y_1 y_2 y_3$  will send  $f_j$  pulses to the counter. Instead of using Binary-coded triggered

$MV$ 's, we may also use auxiliary decade counters in the feedback loop of the  $MV$ 's so as to control the number of pulses given by them and the counters would be preset by the digits in  $f_j$ .

Many types of analogue multipliers are in use, e.g., the multiplier using simultaneous amplitude and width modulation of sampling pulses, the multiplier using amplitude and frequency modulation of a sinusoidal carrier (Aiken and Susskind, 1961). The latter method is quite simple in circuitry and the  $FM$ -discriminator may be either a special network having the required slope-frequency characteristic (Tuttle, 1953) or a standard Foster-Seely circuit. The circuit may be further simplified by using a frequency-controlled  $MV$  as the carrier to the  $AM$ -modulator and the output simply detected by a diode and an  $RC$ -filter. This method, shown in Fig. 6., has the defect that the output is not simply  $e_1 e_2$ ; but has some constants

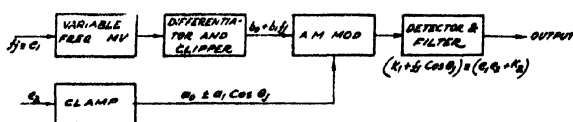


Fig. 6. Analogue multiplier.

$K_1$  and  $K_2$  varying with  $f_j$  and  $\cos \theta_j$ , and would require cancellation by suitable variable voltages. The problem has been effectively and simply solved by the Frequency-Counting multiplier shown in Fig. 7. where  $f_j$  controls a gate circuit with

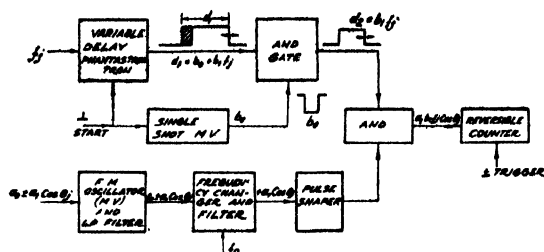


Fig. 7. Frequency counting multiplier.

a pulse of variable width  $= b_1 f_j$  and pulses corresponding to  $a_1 \cos \theta_j$  are passed through the gate. The number of the output pulses is then proportional to  $a_1 b_1 f_j \cos \theta_j$ , which are finally counted. The method has the added advantage that by using reversible counters (Churchill, 1952),  $\pm$  sign of  $\cos \theta_j$  may be taken care of by making the counter to add or to subtract in response to a trigger from the translator. The summation of the series  $\sum f_j \cos \theta_j$  is done most conveniently by digital methods using either a Binary or a Decade counter, and standard circuits are used for the purpose (Lesslie and Narin, 1962).

## DIGITAL SCHEMES

Based on the principles of Figs. 2 and 5, an electromechanical digital computer is shown in Fig. 8, where the values of  $\theta_j$  and  $f_j$  are assumed to be of two digits each. The circuits may be easily extended for more digits in  $\theta_j$  and  $f_j$ . The dialled



digit  $X_1 X_2$  of  $\theta_j$  drive a two-motion selector switch, similar to a Final selector in an auto-exchange (Atkinson, 1955), and mark a particular contact on the  $P$ -bank with full earth. All the contacts of the  $P$ -bank are connected to the

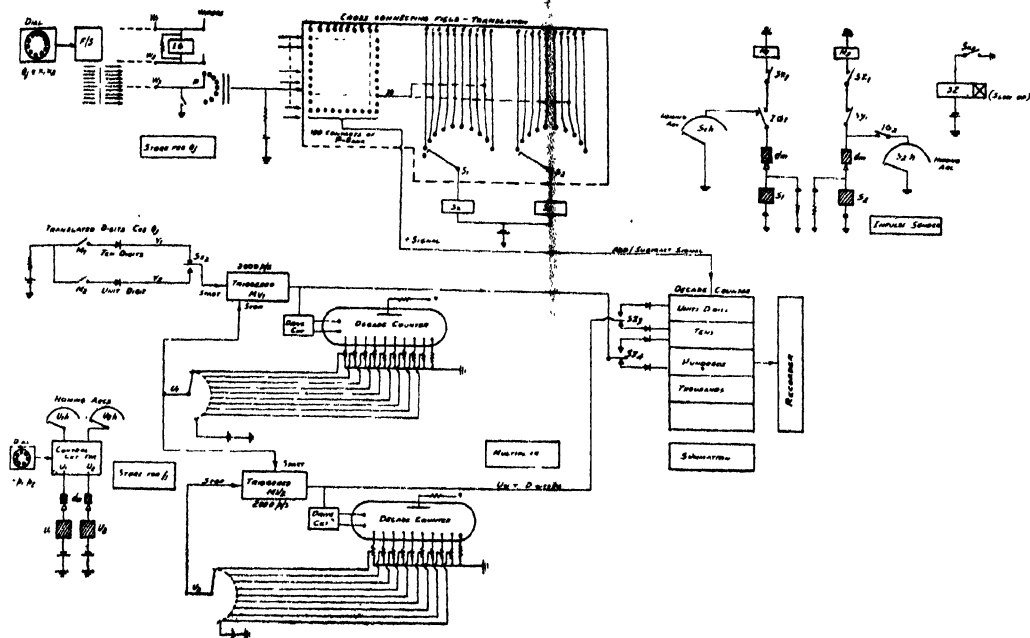


Fig. 8. A Complete Electro-mechanical Computer. (Translator correction shown for  $\cos 30^\circ = 0.87$ ).

Translation field such that  $X_1 X_2$  ultimately earth a pair of predetermined vertical wires connected to the outlets of  $S_1$  and  $S_2$  (e.g., for  $\theta_j = 30^\circ$ , the wires 8 and 7 are earthed as shown in the figure)). Along with the selection of  $\cos \theta_j$ , the other wipers of the selector operate the relay  $IG$  and  $IG_1$  starts the uniselector magnet  $S_1$ , which hunts through its own interrupter contact for the earthed wire (say, no. 8 in the Fig.). When the wiper  $S_1$  reaches the marked wire, the  $U/SS_1$  stops due to the operation of  $SX$  and  $U/S S_2$  starts hunting due to the operation  $SZ$ .  $S_2$  in its turn stops when the marked wire is encountered by the wiper  $S_2$ . The uniselectors are brought back to normal by the homing arcs  $S_{1h}$  and  $S_{2h}$  when  $IG$  is released. During the impulsing of  $S_1$  and  $S_2$ , the relays  $M_1$  and  $M_2$  send the translated digits  $Y_1 Y_2$  in a sequence and the pulses actuate the triggered multi-vibrator  $MV_1$  repeatedly. The multivibrators  $MV_1$  and  $MV_2$  are preset by the dialled digits  $p_1 p_2$  corresponding to  $f_j$  so that each pulse due to  $M_1$  and  $M_2$  produces  $(p_1 + p_2)$  pulses at the output of the  $MV$ 's, and the final decade counter counts and stores them. The dialled pulses  $p_1 p_2$  actuate two  $U/S$ 's  $U_1$  and  $U_2$  and position their wipers accordingly to control the number of pulses sent out by  $MV_1$  and  $MV_2$  each time they are excited by  $Y_1$  or  $Y_2$ . This is done by counting the output pulses by an auxiliary decade counter using Dekatron tubes (or flip-flops), and stopping the  $MV$  when the marked cathode sends a stop pulse

back to the  $MV$ . The stop pulse via  $U_1$  for  $MV_1$  starts  $MV_2$  and finally  $MV_2$  stops due to a stop pulse via  $U_2$  from its own counter. Due to the controlling contacts  $SZ_2$ ,  $SZ_3$  and  $SZ_4$ , the pulses  $Y_1 p_1$  are fed to the Hundreds' position and the pulses  $Y_1 p_2$  to the Tens' position of the counter. Similarly the pulses  $Y_2 p_1$  and  $Y_2 p_2$  are fed to the Ten's and Unit's positions respectively. The ambiguity of  $\pm Y_1 Y_2$  for  $\cos \theta_j$ ; may be taken care of by using a reversible counter (Churchill, 1952) for the final summation. In Dekatrons, reversing the drive changes the direction of rotation of the glow and addition or subtraction may be done by simply changing the drive circuit. To affect this addition or subtraction, a control signal is obtained from the translation field and either the direct or reverse drive circuit is used to store the digits  $Y_1 p_1$ ,  $Y_2 p_1$ ,  $Y_1 p_2$  and  $Y_2 p_2$ . Thus  $(\pm Y_1 Y_2 \times f_j) = f_j \cos \theta_j$ ; pulses are effectively stored in the final counter. The selector circuits may be released by an auxiliary contact in the dial and the operations repeated in a serial manner.

For an accuracy of two decimal places for  $\theta_j$  and  $f_j$ , one two-motion selector, four uniselectors along with the auxiliary circuits and final counters would be required. Since the  $U/S$ 's normally can give about 50 pulses per second and dialling requires about 2 seconds per digit, it will be possible to do about 350 summing operations in an hour if one can dial that quickly. The speed of  $MV$ 's would be about 2000 pulses/second as it is necessary to send at most 20 pulses to the counter for each pulse due to  $M_1$  or  $M_2$ . For three digit values of  $\theta_j$  and  $f_j$ , ten two-motion selectors and seven  $U/S$ 's would be necessary. The values of  $\Sigma f_j \cos \theta_j$  may be recorded (Das, 1959) if required by a 'readout' circuit and an electrical typewriter at the output of the final counter.

#### *All-electronic digital computer*

It is possible to replace the electromechanical storage and the selecting circuits of the above scheme with all-electronic circuits, as shown in Figs. 3 and 9. Here the dialled digits  $X_1 X_2$  for  $\theta_j$  are stored in a sequence in the ring counter  $M_1$  and  $M_2$  which are sequentially gated by the cold-cathode trigger tubes  $T_1$  and  $T_2$  (Flowers, 1951). The outputs of  $M_1$  and  $M_2$  control a diode-matrix  $D_1$  so that a single output of the matrix is energised and the translated  $\cos \theta_j$ ; is represented by an output  $Y_1 Y_2$  of the cross-connecting field. This output, in conjunction with the feed-back from the auxiliary counters  $M_3$  and  $M_4$ , causes the marker matrix  $D_2$  to send stop pulses to multivibrators  $MV_1$  and  $MV_2$ , which are initially triggered by a start signal from  $T_3$  synchronised with the translation of  $X_1 X_2$  to  $Y_1 Y_2$ . Thus  $MV_1$  and  $MV_2$ , controlled by these start-stop signals, transmit the translated digits  $Y_1 Y_2$  in a serial form to the multiplier unit. The ring counters  $M_1$ ,  $M_2$ ,  $M_3$  and  $M_4$  are reset before the new values of  $X_1 X_2$  are fed to the translator.

The multiplier unit is similar to that of Fig. 8, and the ring counters  $M_5$  and  $M_6$  are preset by the dialled digits  $p_1 p_2$  corresponding to  $f_j$ . The pulses of  $Y_1 Y_2$  repeatedly triggers  $MV_3$  (p.r.f. approx. 20 times that of  $MV_1$ ) which sends

out  $(p_1 + p_2)$  pulses to the counter for each input pulse. It is possible to use the same  $MV_3$  to send out  $p_1$  and  $p_2$  pulses if the reversible ring counters (Dekatron)  $M_5$  and  $M_6$  are preset by  $p_1$  and  $p_2$  through direct drive circuits (equivalent to addition) and are reset by the pulses from  $MV_3$  through reverse drive circuits

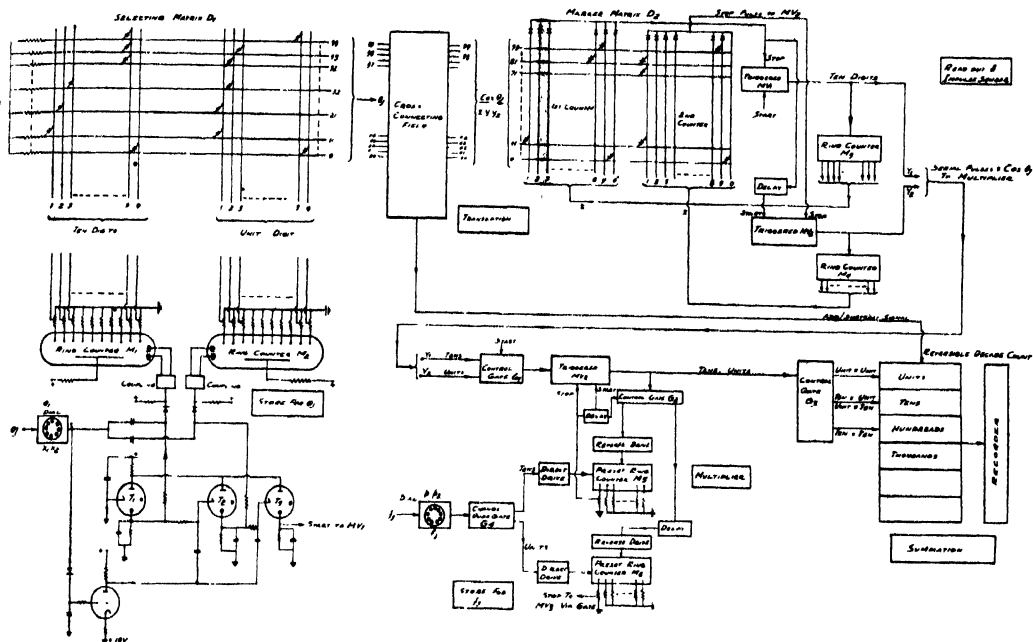


Fig. 9. An all-electronic Digital Computer.

(equivalent to subtraction) so that the stop pulses are always generated at the first cathodes of  $M_5$  and  $M_6$ . The counters  $M_5$  and  $M_6$  are controlled by the gate  $G_2$  to allow their operation in a sequence, and the gates  $G_1$ ,  $G_2$  and  $G_3$  are synchronised so that proper inputs are fed to the final counter in proper sequences i.e.  $Y_1 p_1$  to the Hundreds' position,  $Y_1 p_2$  to the Ten's position etc. The final counter is a reversible one, as explained in section 3, and the addition/subtraction is controlled by a signal from the translation field.

The circuit of Fig. 9 is for two-digit values of  $\theta_j$  and  $f_j$  and may be extended to three or four digit-values by using additional counters and larger diode matrices. For two-digit values, approximately ten decade counters and 500 diodes with their associated control circuits would be required. For 3-digit values, 13 counters and 700 diodes would be necessary. For Dekatron counters, the speed of counting is about 4-20 thousand pulses per second, but using hard valve circuits, higher speed of counting may be obtained. Thus the number of summing operations that can be performed in an hour mainly depends on the input circuits feeding the values of  $\theta_j$  and  $f_j$ . With dialled inputs, about 8 seconds would be required to feed the digits and not more than 500 operations can be done in an hour. The

speed of operations may be improved by feeding the digits through punched tapes or such other faster devices.

### A HYBRID COMPUTER

The principles of a hybrid computer has been shown in Figs. 4 and 7. A complete block schematic of the computer, along with the different timing waveforms, is shown in Fig. 10. The inputs  $\theta_j$  and  $f_j$  are in the form of calibrated voltages

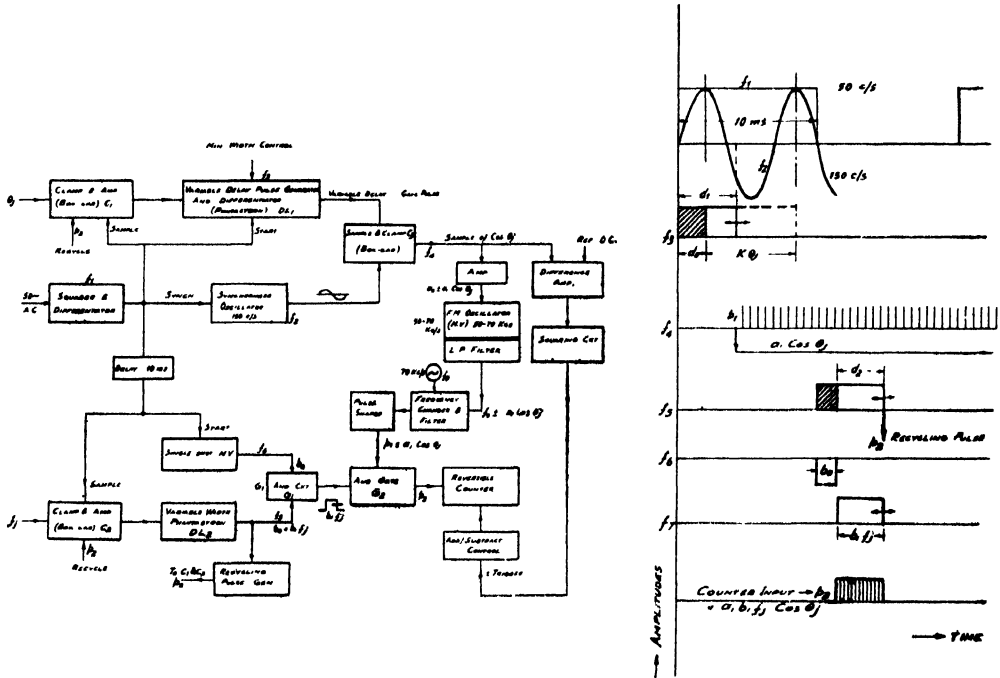


Fig. 10. An all-electronic Hybrid computer.

(a) Block Schematic of the equipment.

(b) The Timing waveforms of different circuits.

which are clamped by the 'Boxcar' circuits  $C_1$  and  $C_2$ . The variable delay generators  $DL_1$  and  $DL_2$  are Phantastrons with controllable mean delay so that the Sine/Cosine wave form  $f_2$  and the delayed pulses  $f_3$ ,  $f_4$  and  $f_5$  are properly synchronised. The translation of  $\theta_j$  to  $\cos \theta_j$  is obtained by the combined operations of the 'Boxcar'  $C_3$ , FM oscillator and frequency changer, and the pulses  $p_1$  is proportional to  $\cos \theta_j$ . The width of the gate pulse  $f_7$  is controlled by  $f_j$  and the output of the gate  $G_2$  is  $a_1 b_1 f_j \cos \theta_j = p_3$  pulses which are counted and stored in the final reversible counter.

The characteristics of the laboratory model of this computer have been quite satisfactory, as is seen in Fig. 11, where the linearity of the component circuits are shown. The 'Boxcar' and the phantastron circuits are quite linear and the maximum error in them is within  $\pm 2\%$ . The FM output  $p_1$  varies from 0–20 Kc/s with  $f_0 = 70$  Kc/s and is suitable to obtain 100 pulses for a gating pulse  $f_7 = 5$  msec and  $\cos \theta_j = \pm 1$ . Assuming that 5 msec. corresponds

to  $f_j = 100$ , there will be a single pulse output for  $\cos \theta_j = \pm .01$ ; and for  $f_j = 50\mu$  sec., corresponding to  $f_j = 1$ , there will be only one pulse for  $\cos \theta_j = \pm 1$ . Thus the accuracy in the multiplier would be about  $\pm 1\%$ ; but this may be

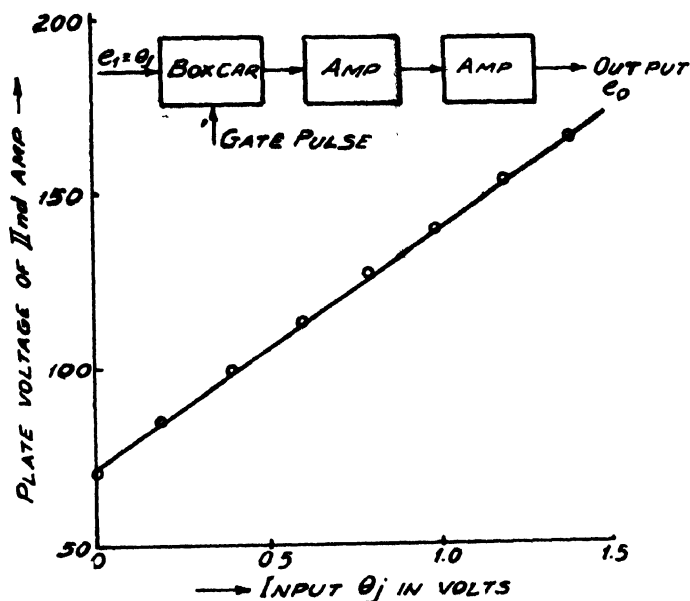


Fig. 11. Linearity characteristics of the Component circuits in the Hybrid Computer.  
(a) Input  $\theta_j$  vs. output voltages  $e_o$  of the Boxcar and the associated amplifiers.

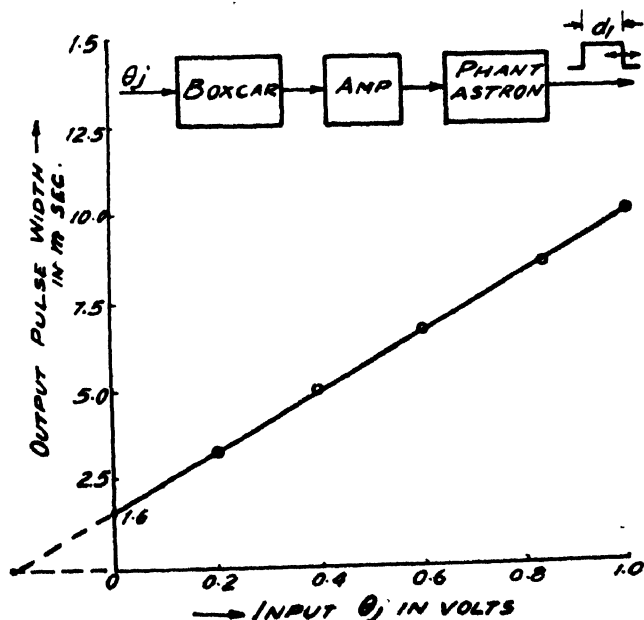


Fig. 11. (b) Variable of pulse width  $d_1$  of the phantastron with  $\theta_j$   
(minimum  $d_1 = 1.6$  ms. for  $\theta_j = 0$ ).

further improved if  $p_1$  varies in a higher frequency range, say, from 0 200 Kc/s. The overall translator-multiplier characteristics are shown in Fig. 12 for some

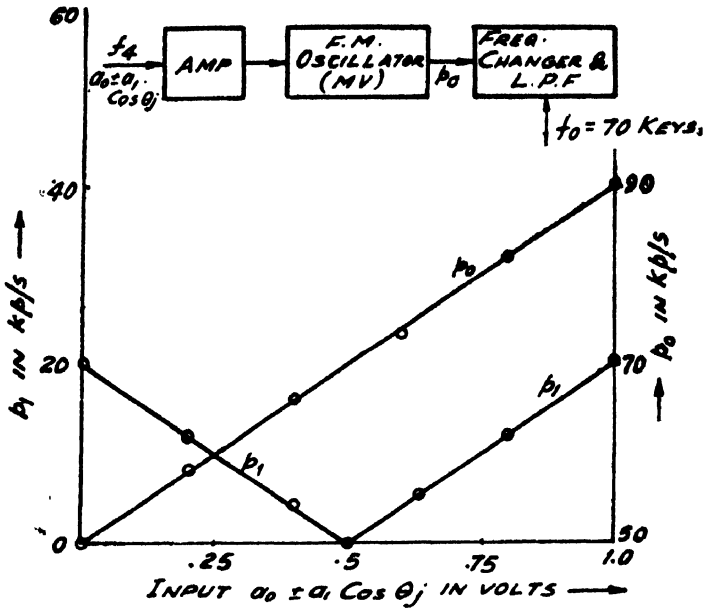


Fig. 11 (c) Variation of the frequency  $p_0$  of the FM oscillator and the beat freq.  $p_1 = (p_0 - f_0)$ , with input  $= (a_0 \pm a_1 \cos \theta_j)$ .

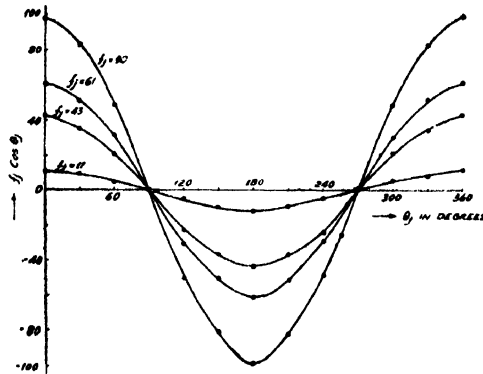


Fig. 12. Overall characteristics of the Hybrid Computer shown in Fig. 10. The counter outputs are for different  $\theta_j$  in degrees for  $f_j = 98, 61, 43$ , and 11. Errors is  $\pm 1$ .

values of  $f_j$ , and it is seen that the products  $f_j \cos \theta_j$  are within  $\pm 1$  of their correct values.

The calibrated voltage inputs  $\theta_j$  and  $f_j$  may be fed through push-button keys connected to a potential-divider chain. Two rows of keys, one for each digit in  $\theta_j/f_j$ , may be coupled through an adding circuit to give the two-digit values of the inputs. It is also possible to feed the inputs through two dials and the digits

stored in ring counters as is done in Fig. 9. The cathodes of the ring counters in Fig. 13 are connected to the adder through a suitable weighting network such

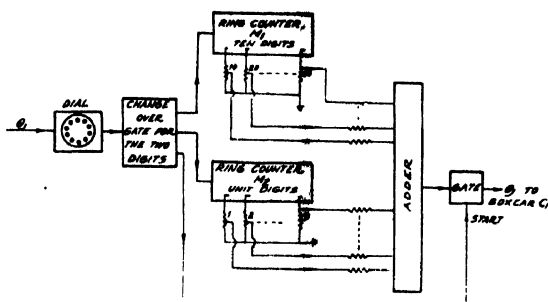


Fig. 13. Method of dialling the input  $\theta_j$  to the Translation of Fig. 10.

that the added output is proportional to the dialled input  $\theta_j$ . On completion of the storage (Flowers, 1951), a third gate feeds this added voltage  $\theta_j$  to the translator in Fig. 10. At the end of each summing operation, it would be necessary to discharge the clamps  $C_1$  and  $C_2$ ; this is done by using a recycling pulse generated from the trailing edge of the gate pulse  $f_5$  or  $f_7$ . If the whole system is synchronised with 50 c/s mains, then a single operation would be complete within 20 msec. Thus it would be possible to perform about 3000 operations per minute if the inputs can be fed at such speeds. The speed is then mainly controlled by the input circuit and would be restricted to about 500 operations per hour using common telephone dials.

#### *An extension to the two- and three- dimensional problems.*

In many physical problems, it is necessary to evaluate the summation  $\sum f_j \cos 2\pi (hx_j + ky_j + lz_j)$  or  $\sum f_j \cos 2\pi (hx_j + ky_j)$  and the input  $\theta_j$  to above computer has to be predetermined in terms of two or three-dimensional functions  $(hx_j + ky_j + lz_j)$ . If required, this may also be instrumented with circuits similar to those already discussed. Two such circuits for the two-dimensional case are shown in Fig. 14, which may be connected ahead of the relevant computers. The digital circuit of Fig. 14(a) is dial-controlled and uses the multiplier and adder similar to

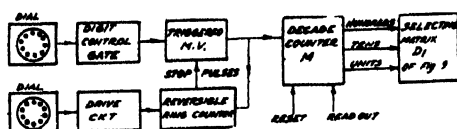


Fig. 14. Extension of the technique to two-dimensional problems.

(a) Digital multiplier—adder for functions  $(hx + ky)$ .

those of Fig. 9. The adder-counter  $M$  can now replace the digit-store  $M_1$  and  $M_2$  of Fig. 9. and the different digit signals (positive or zero voltages) may be directly

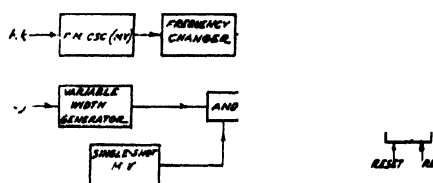


Fig. 14(b) Hybrid multiplier-adder for  $(hx+ky)$ .

fed to the selecting matrix  $D_1$ . The readout gate is operated after the required addition is completed in a manner similar to the generation of the start signal to  $MV_1$  from  $T_3$  of Fig. 9.

The hybrid circuit of Fig 14(b) uses the multiplier and adder of Fig. 10 and  $(hx_j+ky_j)$  is stored in the counter  $M$ . Since the input  $\theta_j$  to the translator is an analogue voltage, the counter output is taken through a digital-to-analogue converter similar to that shown in Fig. 13. The dialling arrangement of Fig. 13 may now be used to feed  $h, k, x, y$  to the above auxiliary multiplier-adder.

### CONCLUSIONS

Three simple and practical computing schemes for determining the Fourier coefficients have been studied, and the hybrid computer has been found to be sufficiently accurate (within about 1%) for general calculations. For higher accuracy and speed, the simplified digital computer may be used, although the speed is mainly dependent on the input circuit. The scheme with electromechanical switches is quite attractive and cheap, but careful maintenance of the equipment would be required for continuous operation. The electronic digital scheme uses about 700 diodes, 13 decade counters and associated control circuits for 3-digit values of  $\theta_j$  and  $f_j$ , whereas for 2-digit values of the variables, 500 diodes and 10 counters are necessary. The hybrid scheme, using 5 gates, FM and Width-modulation circuits and controls, would require about 40 tubes, and a summing operation will be completed in 20msec. The values of  $\theta_j$  and  $f_j$  may be fed through punched tapes or by simple dialling, and it will be possible to have about 500 operations per hour by using ordinary dials.

### ACKNOWLEDGMENT

The authors record their thanks to Dr. G. B. Mitra for suggesting the problem and for valuable discussions; and also to Prof. H. Rakshit, D.Sc., F.N.I., for his kind interest in the work.



REFERENCES

- Aiken, W. R. and Susskind, C., 1961, *Proc. Inst. Radio Engrs.*, **49**, 1550.  
Atkinson, J., 1955, "Automatic Telephony," Pitman and Sons.  
Churchill, J. L. W., 1952, *Jour. Brit. I.R.E.*, **12**, 447.  
Das, J., 1959, *Electronic Engineering*, **31**, 156.  
Flowers, T. H., 1951, *Post Office Elec. Engrs. Jour.* **43**, 177.  
Flowers, T. H., 1952, *Proc. Inst. Elec. Engrs.*, **99**, pt. I., 181.  
Leslie, W. H. P. and Nairn, D., 1962, *Electronic Engineering*, **34**, 227.  
Manley, R. G., 1945, "Waveform Analysis", Chapman and Hall.  
Tuttle, D. F. Jr., 1953, *Trans. Inst. Radio, Engrs. OT-2*, 6.

# Letters to the Editor

*The Board of Editors does not hold itself responsible for opinions expressed in the letters published in this section. The notes containing short reports of original investigations communicated to this section should not contain many figures and should not exceed 500 words in length. The contributions reaching the Secretary by the 15th of any month may be expected to appear in the issue for the next month. No proof will be sent to the author.*

13

## ULTRAVIOLET ABSORPTION OF CHLORATE BROMATE AND IODATE IONS

A. MOOKHERJI AND S. P. TANDON\*

PHYSICAL LABORATORIES, BURDWAN UNIVERSITY,

BURDWAN, W.B., INDIA,

(Received May 15, 1964)

Chlorate, bromate and iodate ions are known to have pyramidal structure with  $C_{3v}$  symmetry (Herzberg, 1960) in contrast to planar structure with  $D_{3h}$  symmetry of nitrate and carbonate ions (Tandon, 1962). Study of electronic structure (Pauling, 1960) of chlorate ion reveals the presence of charge on the chlorine atom, similar to that on nitrogen in nitrate ion (Janz and Mikawa, 1960). The difference in symmetry, structure and charge distribution, demands that the absorption spectrum of chlorate and carbonate ions should not be similar. The ultraviolet absorption spectrum of chlorate bromate and iodate ions has not been studied in details. Consequently, the authors with improved technique (Tandon, 1961) made a close study of the absorption spectrum of these ions in about ten salts with a UVISPEK spectrophotometer, scanning the spectrum at an interval of  $3.5 \text{ \AA}$  in the region  $1850 \text{ \AA}$  to  $3600 \text{ \AA}$ . Aqueous solutions at different concentrations of the chlorates, bromates and iodates, studied, showed one intense band at about  $2000 \text{ \AA}$ .

The band-width of the band is almost the same for all the three ions and is  $10^3 \text{ cm}^{-1}$ , which is nearly the same as that of the nitrate ion (Mookherji and Tandon, 1962). Hence it may be inferred that the excited state of the transition giving rise to the band is due to an antibonding orbital. (Jorgensen, 1962).

\* Now in Physics Department, University of Jodhpur, Jodhpur, Rajasthan, India.

The oscillator strength  $P$ , which is a measure of the intensity of the band, was calculated following Jorgensen (1954) and Jaffé and Orchin (1962), which comes out  $10^{-1}$  suggesting the band to be due to an allowed transition.

Following Tanabe and Sugano (1954) the transition probabilities were calculated from the  $P$  values, which also indicate the transition to be an allowed electronic one.

Constructing molecular orbitals of 26 valence electrons as LCAO appropriate to the  $C_{3v}$  point group by the method suggested by McGlynn and Kasha (1956), this may be assigned to the transition which raises an electron from weakly antibonding orbital on oxygen atoms to a strongly antibonding orbital on chlorine, bromine and iodine atoms in chlorate, bromate and iodate ions respectively. The shift of the band towards shorter wavelength (blue shift) coupled with increase with intensity and decrease in band-width with progressive dilution of the aqueous solution exhibits electron transfer spectra characteristics.

#### REFERENCES

- Herzberg, G. 1960, *Molecular Spectra and Molecular Structure*, Part II, (D. Van Nostrand Company, Inc., New York), 302.
- Jaffé, H. H. and Orchin, M. 1962, *Theory and Applications of Ultraviolet Spectroscopy* (John Wiley and Sons, Inc., New York), 111.
- Janz, G. J. and Mikawa, Y. : 1960, *J. Mol. Spectrosc.*, **5**, 92.
- Jorgensen, C. K. : 1954, *Acta Chem. Scand.*, **8**, 1502.
- Jorgensen, C. K. 1962, *Absorption Spectra and Chemical Bonding in Complexes*. (Addison Wesley Publishing Company, Inc. Reading Massachusetts) Ed. 1, 85.
- McGlynn, S. P. and Kasha, M., 1956, *J. Chem. Phys.*, **24**, 481.
- Mookherji, A. and Tandon, S. P., 1962, *Indian J. Phys.*, **36**, 211, 344.
- Pauling, L. 1960, *Nature of the Chemical Bond and the Structure of the Molecules and Crystals* (Cornell University Press) Ed. 3rd., 323.
- Tanabe, Y. and Sugano, S. 1954, *J. Phys. Soc. Japan*, **9**, 766.
- Tandon, S. P. 1961, *Raj. Univ. Studies*, **9**, 69.
- Tandon, S. P. 1962, *Proc. Raj. Acad. Sci.*, **9**(2), 3.

# MOLECULAR ORBITAL THEORY OF THE MAGNETIC PROPERTIES OF THE TETRAHEDRAL COPPER COMPLEX, $\text{Cs}_2\text{CuCl}_4$

R. CHATTERJEE, S. LAHIRY, U. S. GHOSH and S. MITRA

DEPARTMENT OF MAGNETISM,

INDIAN ASSOCIATION FOR THE CULTIVATION OF SCIENCES, JADAVPUR, CALCUTTA-32.

It has occurred to us that studies of the magnetic behaviour of tetrahedral complexes of the first transition series elements, which have received very little attention compared to the corresponding octahedral ones, would be of interest. And, in this direction, we have derived the theory of magnetic susceptibility and anisotropy of a tetrahedral Copper (II) complex,  $\text{Cs}_2\text{CuCl}_4$ , on the basis of molecular orbital theory of Van Vleck (1939), Stevens (1953) and Bose *et al* (1960). The X-ray determination of this complex by Helmholz and Kruh (1952), and of Morosin and Lingafelter (1961) indicate that the tetrahedron has a tetragonal distortion along the line joining the middle points of the opposite edges of the tetrahedron.

The  $3d^9\ ^2D$  ground state of the free  $\text{Cu}^{2+}$  ion is split under the cubic field into a lower lying orbital triplet,  $^2T_2$  and an upper orbital doublet  $^2E$  separated by  $10Dq$ , since the works of Gorter (1932), Van Vleck (1932) and Ballhausen have shown that the stark pattern for a tetrahedral complex is inverted with respect to an octahedral one. Further, the overall cubic separation is  $4/9$  times less which makes it necessary to consider the effect of upper orbital doublets through the second order spin-orbit coupling. Now operating on the appropriate orbital states

$$1+> = \frac{i}{\sqrt{2}} [ |xz> + i|yz> ]$$

$$1-> = -\frac{i}{\sqrt{2}} [ |xz> - i|yz> ]$$

$$|0> = |xy>$$

following Stevens (1953)

where

$$|yz> = N[d_{yz} + \lambda \frac{1}{4} \{ (\pi x_4 + \pi x_2 - \pi x_1 - \pi x_3) + \sqrt{3}(\pi y_4 + \pi y_2 - \pi y_1 - \pi y_3) \}]$$

$$|xz> = N[d_{xz} + \lambda \frac{1}{2} \{ \pi x_1 + \pi x_2 - \pi x_3 - \pi x_4 \}]$$

$$|xy> = N[d_{xy} + \lambda \frac{1}{4} \{ (\pi x_3 + \pi x_2 - \pi x_1 - \pi x_4) \sqrt{3}(\pi y_4 + \pi y_1 - \pi y_2 - \pi y_3) \}]$$

are taken from Wolfsberg and Helmholz (1952) in which  $N$  is the normalizing factor and  $\lambda$  is a measure of the amount of mixture of ligand  $p$ -orbitals with the central  $\text{Cu}^{2+}$   $d$ -orbitals, with the appropriate Hamiltonian

$$H = V_{\text{tetragonal}} + u_z s_z + \frac{1}{2}(u_+ s_- + u_- s_+)$$

where  $u.s$  is the spin-orbit interaction term and for a  $d$ -hole  $u$  is identical with  $\zeta L$ , we get three kramers doublets and their energies where,

$$\begin{aligned} \langle + | u_z | + \rangle &= - \langle - | u_z | - \rangle = \zeta \\ \langle + | u_- | 0 \rangle &= - \langle - | u_- | 0 \rangle = \sqrt{2}\zeta_1 \end{aligned}$$

and, also

$$\begin{aligned} \langle + | L_z | + \rangle &= - \langle - | L_z | - \rangle = k_1 \\ \langle + | L_- | 0 \rangle &= - \langle - | L_- | 0 \rangle = \sqrt{2}k_1 \end{aligned}$$

Operating on these Kramers doublets with the magnetic perturbation, the expression for ionic susceptibility ( $K_i$ ,  $i =$  or  $\perp$  to the tetragonal axis) has been derived which is a complicated one. The experimental values of susceptibility and anisotropy as measured between 300°K and 90°K could be fitted with the theoretical expression with the parameters given in the table. The value of  $\Delta$  is to be changed from 145 to 100  $\text{cm}^{-1}$  with temperature which has also been observed with many other octahedral complexes too (Bose *et al* 1960, 1961, 1963). The orbital reduction factor  $k$ , which takes into account the effect of the admixture of metal  $d$ -orbitals with ligand  $p$ -orbitals and the spin orbit coupling coefficient  $\xi_i$  which is to be reduced from the free ion value of 828  $\text{cm}^{-1}$ , partake the asymmetry of the ligand field.

TABLE

$\xi_{  } = 800 \text{ cm}^{-1}$	$k = 0.97$	$10Dq = 6000 \text{ cm}^{-1}$
$\xi_{\perp} = 550 \text{ cm}^{-1}$	$k_{\perp} = .89$	(Pappalardo, 1961)

---

Temp. °K	Angular parameter	$\Delta \text{cm}^{-1}$	$(k - k_{\perp}) \times 10^3$	$k \times 10^6$ Mean susc.
300	$\gamma^2 = .6487$	145	532	1695
	$\alpha^2 = .3517$		(526)	(1680)
200	$\gamma^2 = .6576$	120	701	2387
	$\alpha^2 = .3382$		(699)	(2420)
90	$\gamma^2 = .6745$	100	1184	5267
	$\alpha^2 = .3268$		(1176)	(5321)

$\Delta$  = tetragonal field separation of the lowest cubic level  $^2T_2$ .

The values in parentheses are the experimental values.

Details of the theory and evaluation of the experimental data will be published elsewhere in due course. The authors record their gratitude to Prof. A. Bose, D.Sc., F.N.I. for criticism and a many valuable discussions. Of the authors (S.L.) is grateful to the authorities of this institute for permitting him to work as an honorary worker and (S.M.) is thankful to the C.S.I.R. Govt. of India for the award of a Junior Fellowship.

## REFERENCES

- Ballhausen, C. J. 1954, Kg. Danske Videnskab, Selskab, *Mat-Phys-Med* **29**, 4.  
Bose, A., Chakravarty, A. S., and Chatterjee, R. *Proc. Roy. Soc. A*, **255**, 145.  
" " " 1961, *ibid.*, **261**, 207.  
Bose, A., and Chatterjee, R., 1963, *Proc. Phys. Soc.* **82**, 23.  
Gorter, C. J. 1932, *Phys. Rev.* **42**, 427.  
Helmholz, L. and Kruh, R. F., 1952, *J. Amer. Chem. Soc.* **74**, 1176.  
Morosin, B., and Lingafelter, E. C. 1961, *J. Phys. Chem.* **65**, 50.  
Pappalardo, R., 1961, *Mol. Spectroscopy*, **6**, 554.  
Stevens, K. W. H. 1953, *Proc. Roy. Soc. A*, **219**, 542.  
Van Vleck J. H., 1932, *Phys. Rev.* **41**, 208.  
" 1939, *J. Chem. Phys.* **7**, 61.  
Wolfsberg, M., and Helmholtz, L., 1952, *J. Chem. Phys.* **20**, 837

# ON THE ANGLE OF INCLINATION OF THE EQUIVALENT LIGHTNING CHANNEL

H. BHATTACHARYA and MANORANJAN RAO

DEPARTMENT OF PURE PHYSICS, CALCUTTA UNIVERSITY

(Received May 2, 1964)

**ABSTRACT.** It is shown that in the case of waveforms of reflected type of comparatively near origin, an estimate of the angle of inclination of the equivalent lightning channel can be made by measuring the relative amplitudes of the successive orders of reflection. The calculations have been carried out for four typical reflected types of the waveforms. Some of the characteristics of these waveforms like the phase-reversal, have been accounted for.

## INTRODUCTION

The relative amplitudes of the sky pulses successively reflected from the ionosphere have been shown to give an estimate of the ionospheric reflection coefficient (Schonland, *et al.*, 1940). Since the radiation from the return-stroke channel can be regarded as emitted from a series of linear channel elements, one above the other, each inclined to the horizontal at a different angle, the observed pulse will be the resultant of the pulses from these elements. The contribution of each of the pulses will depend upon its angle of emission. Thus, in principle, it should be possible to calculate the angle of inclination of the equivalent lightning channel from an analysis of the observed waveforms.

## THEORETICAL CONSIDERATIONS

If  $\theta$  is the angle made by the channel element with the horizontal (Fig. 1A),  $\phi$  the angle with the horizontal at which the radiation is emitted and  $\gamma$  be the amplitude of the elementary ground-pulse emitted by it at an angle  $\phi = 0$  then the corresponding amplitude  $\sigma_n$ , of its contribution to the  $n$ -th sky-pulse would be given by

$$\sigma_n = \frac{\sin \theta - \phi_n}{\sin \theta} \cdot \gamma \quad (1)$$

where  $\phi_n$  is the value of  $\phi$  for the  $n$ -th sky-pulse. Equation (1) may pass from positive to negative as  $\phi_n$  passes through the angle  $\theta$ , at which point  $\sigma_n = 0$ .

If  $\theta > \pi/2$  the ratio  $\frac{\sin \theta - \phi_n}{\sin \theta}$  is always positive. It can be seen from equation

(1) that when a sum of all such elementary pulses is made we may expect to find considerable variation in the resultant form of the pulse with the order of reflection  $n$ . However, such variations will not be prominent in the low-order reflected

pulses from distant sources since the lightning channel is usually vertical and since  $\phi_n$  in such cases is small. Figure 2 shows that the low-order pulses are very similar

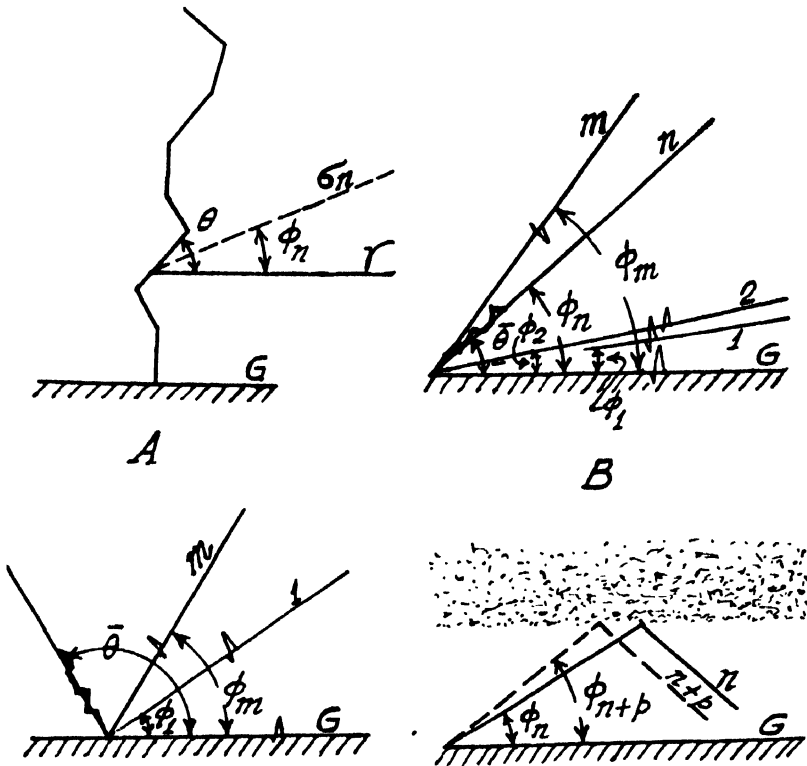


Fig. 1. (Taken from Schonland *et al*, 1940).



Fig. 2. May 27, 1963. 1800 IST.

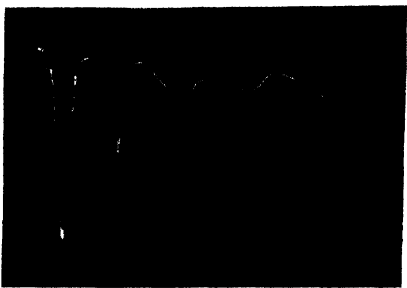


Fig. 3. June 6, 1963. 1620 IST.

in form to the ground pulse. With nearer sources or with pulses of higher order at any distance, there may be a considerable change in the final form of the pulse. A typical oscillogram showing the variation of pulse form with the order of reflection is shown in Fig. 3.



If now the actual channel, made up of a series of elementary channels, one above the other, and making different angles with the horizontal, be replaced by an equivalent channel making an angle  $\bar{\theta}$  with the horizontal, then, for  $\bar{\theta} < \pi/2$ , a reversal in phase will occur for a value of  $\phi_n \geq \bar{\theta}$  and the amplitude of the sky pulse will pass through a minimum at  $\phi_n = \bar{\theta}$  (Fig. 1B). Figure 4 is a typical example of such type. For  $\bar{\theta} > \pi/2$  the radiation of the channel, as a whole, may be greater in the direction of the sky pulses than along the ground (Fig. 1C). A typical illustration of such type is Fig. 5.



Fig. 4. June 6, 1963. 1620 IST.

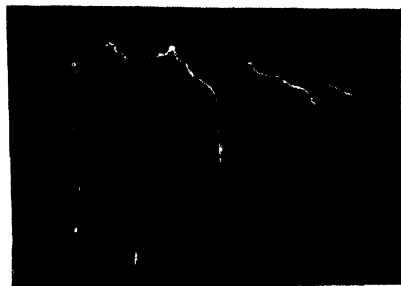


Fig. 5. June 26, 1963. 1650 IST.

In what follows is given a possible method of estimation of  $\bar{\theta}$  depending upon the relative amplitudes of the sky pulses and also the distance of the source and ionospheric reflection height.

Following Schonland *et al.* (1940) if  $s_{n+p}$  and  $s_n$  are the amplitudes of the  $(n+p)$ th and  $n$ -th sky pulses, produced by the summation of  $\sigma_{n+p}$  and  $\sigma_n$ , the ratio of the recorded amplitudes  $S_{n+p}$  and  $S_n$  will be given by

$$\frac{S_{n+p}}{S_n} = \frac{(s_{n+p}/D_{n+p}) \cdot (r_i)^{n+p} \cdot (r_g)^{n+p-1} \cdot \cos \phi_{n+p}}{(s_n/D_n) \cdot (r_i)^n \cdot (r_g)^{n-1} \cdot \cos \phi_n}$$

or 
$$\frac{S_{n+p}}{S_n} = \frac{s_{n+p}}{s_n} \cdot \frac{D_n}{D_{n+p}} \cdot \frac{\cos \phi_{n+p}}{\cos \phi_n} \cdot (r_i \cdot r_g)^p \quad \dots (2)$$

where  $D_{n+p}$  and  $D_n$  are the group paths for the  $(n+p)$ th and  $n$ -th resultant sky pulses and  $r_i$  and  $r_g$  are respectively the reflection coefficients of the ionosphere and the earth. If  $\phi_{n+p}$  and  $\phi_n$  be the angle made by  $(n+p)$ th and  $n$ -th pulses with the horizontal, then it can be shown (Fig. 1D) that

$$\frac{D_n}{D_{n+p}} = \frac{\cos \phi_{n+p}}{\cos \phi_n}$$

Therefore,

$$\frac{S_{n+p}}{S_n} = \frac{s_{n+p}}{s_n} \cdot \frac{\cos^2 \phi_{n+p}}{\cos^2 \phi_n} \cdot (r_i \cdot r_g)^p \quad \dots (3)$$

Following equation (1) we have for the equivalent channel inclined to the horizontal at an angle  $\bar{\theta}$  :

$$\frac{s_{n+p}}{s_n} = \frac{\sin \bar{\theta} - \phi_{n+p}}{\sin \bar{\theta} - \phi_n} \quad \dots \quad (4)$$

From equations (3) and (4) we have

$$\frac{S_{n+p}}{S_n} = \frac{\sin(\bar{\theta} - \phi_{n+p})}{\sin(\bar{\theta} - \phi_n)} \cdot \frac{\cos^2 \phi_{n+p}}{\cos^2 \phi_n} \cdot (r_i \cdot r_g)^p \quad \dots \quad (5)$$

$$\text{or} \quad \frac{S_{n+p}}{S_n} = \frac{\tan \bar{\theta} - \tan \phi_{n+p}}{\tan \bar{\theta} - \tan \phi_n} \cdot \frac{\cos^3 \phi_{n+p}}{\cos^3 \phi_n} \cdot (r_i r_g)^p \quad \dots \quad (6)$$

However, if the channel is nearly vertical ( $\bar{\theta} \simeq \pi/2$ ) and both the order of reflection  $n$  and the distance of the source  $D$  are large, then physically speaking,  $S_{n+p}/S_n$  will not be far from unity. Further, under such circumstances  $\cos \phi_{n+p}/\cos \phi_n$  will approximate to unity. If then we take  $r_g = 1$ , as is the case for long radio waves, equation (5) reduces to

$$r_i \geq \sqrt[p]{S_{n+p}/S_n} \quad \dots \quad (7)$$

This equation should give a lower limit to  $r_i$  which is not very far from its true value. Evidently  $\bar{\theta}$  can be calculated from equation (6) taking  $r_g = 1$ .

#### CALCULATIONS

For the evaluation of the angles  $\phi_{n+p}$  and  $\phi_n$ , the height  $h$  at which the atmospheric pulses are reflected from the ionosphere and the distance  $D$  of the lightning discharge are approximately calculated graphically, following Caton and Pierce (1952), from the equation given by :

$$ct_n = \sqrt{D^2 + 4n^2 h^2} \quad \dots \quad (8)$$

where  $t_n$  = time interval between the emission of the primary pulse and the arrival at the receiver of the pulse that has undergone  $n$  reflections at the ionosphere,

$D \approx$  distance between the source and the receiver,

$n$  = order of reflection,

$h$  = ionospheric reflection height,

$c$  = velocity of light.

Two sets of graphs, based on expression (8) have been drawn : (1) showing time-intervals between the first sky pulse and successive sky pulses, against  $D$  for a constant value of  $h$  and (2) showing similar time intervals against  $h$  for a constant value of  $D$  (see Figs. 6 and 7). A reference pulse is selected on the waveform and

the time-interval between this and the succeeding pulses of the same sign are measured. Trial values are then adopted for  $h$  and the reference pulse order, these being varied until a constant distance corresponding to all the measured

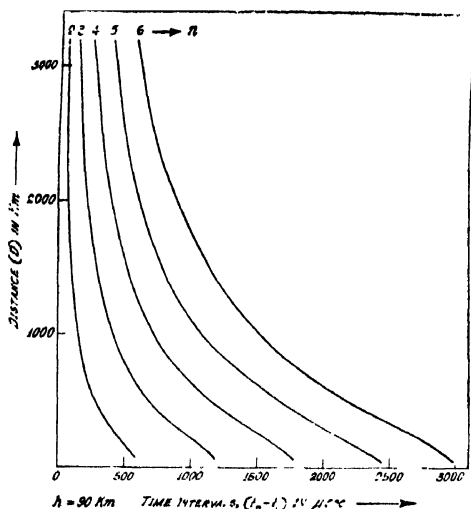


Fig- 6

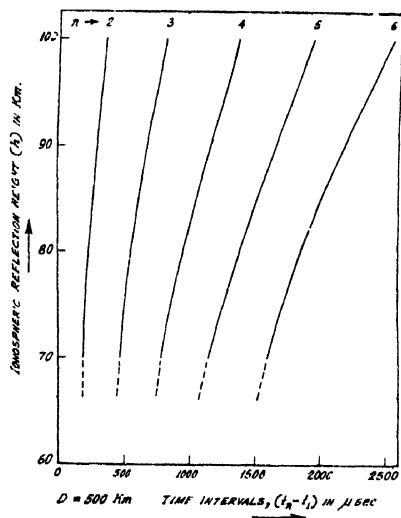


Fig 7

time-intervals is derived from set (1). Then a check is made on the obtained values of  $h$  and  $D$  by means of the set of graphs (2) by following a similar procedure. This then represents a mean determination over the waveform of the distance  $D$  and ionospheric reflection height  $h$ .

The values of  $D$  and  $h$  for the four oscillograms shown in figures 2 to 5 are as follows.

TABLE

Fig. No.	Distance $D$ in km	Height $h$ in km	$\bar{\theta}$
2	300	88	$112^\circ$
3	180	93	$109^\circ$
4	480	80	$59^\circ 36'$
5	375	92	$148^\circ$

The values of  $r_i$  have been calculated taking  $p = 2$  from equation (7) for each of the oscillograms. Taking  $r_0$  as unity and  $r_i$  as 0.8,  $\bar{\theta}$  is calculated from the equation (6). The values of  $\phi_{n+p}(\phi_{n+2}$  in the present case) and  $\phi_n$  have been obtained from the computed values of  $D$  and  $h$  for each of the waveforms.

The calculated values of the inclination  $\theta$  of the equivalent lightning channel are shown below the respective oscillograms and are also listed in last column of Table I.

#### DISCUSSION OF THE RESULTS

Referring to Figs. 2 and 3 it can be readily seen that though, both of the waveforms give nearly same values for  $\bar{\theta}$  and have the same order of reflection, the change in shape of the latter is more pronounced, as it originated in a nearer source. This, thus, is in accordance with what has already been discussed earlier. The value of  $\bar{\theta}$  in the case of Fig. 4 is  $59^{\circ}36'$  which by being less than  $90^{\circ}$ , causes a reversal in the phase of the pulse after certain orders of reflection. Thus the amplitude of the pulse undergoes a minimum at  $n = 5$  in the waveform of the Fig. 4 and a reversal of phase is obvious at  $n = 6$ . Finally, the waveform in Fig. 5 shows a ground pulse height smaller than the first order of reflection. The calculated value of  $\bar{\theta}$ , in this case, is  $148^{\circ}$ . Considering the group paths for the ground pulse and the first order of reflection and also the value of  $\phi_1$ , calculated from  $D$  and  $h$ , it can be shown that the ratio of the amplitudes of the first order pulse to the ground pulse is greater than unity, the value of  $r_1$  being taken as 0.8. Thus the observed nature of the waveform can be accounted for.

An additional check can be made on the calculations in the case of the waveform given in Fig. 4. As already explained above, the minimum of the amplitude occurs when  $\phi_n = \theta$ . Here the minimum occurs when  $n = 5$  and if  $\phi_5$  be evaluated, it should be of the same order as  $\theta$ . In fact, taking the distance of the lightning source as 480 km and the ionospheric reflection height as 80 km,  $\phi_5$  comes out to be between  $59^{\circ}$  and  $59^{\circ}6'$  which agrees fairly well with the calculated value of  $\bar{\theta} = 59^{\circ}36'$ .

#### CONCLUSION

The angle of inclination of the equivalent lightning channel can be obtained from the measurement of successive amplitudes of the reflected-type of waveform except in the case of the smooth sinusoidal type (Budden, 1951, 1952) which can explained on the basis of the mode theory of propagation.

#### ACKNOWLEDGMENT

The authors wish to express their grateful thanks to Prof. S. R. Khastgir, D.Sc., F.N.I., for his valuable guidance throughout the progress of the work. They also thank the C.S.I.R. for sponsoring the research scheme on Atmospherics.

#### REFERENCES

- Budden, K. G. (1951), *Phil. Mag.*, **42**, 833.
- „ „ (1952), *Phil. Mag.*, **43**, 1179.
- Caton, P. F. and Pierce, E. T. (1952), *Phil. Mag.*, **43**, 393.
- Schonland, B. F. J., Elder, J. S., Hodges, D. B., Phillips, W. E. and van Wyk, J. W. (1940), *Proc. Roy. Soc.* **A176**, 180.

# MEAN AMPLITUDES OF VIBRATION OF SOME TRIGONAL BIPYRAMIDAL PENTACHLORIDES

G. NAGARAJAN\*

DEPARTMENT OF CHEMISTRY, OKLAHOMA STATE UNIVERSITY,  
STILLWATER, OKLAHOMA, U.S.A.

(Received January, 1963; Resubmitted February, 27 1964)

**ABSTRACT.** For the determination of the mean-square amplitudes of vibration of trigonal bipyramidal pentahalides a method has been developed by giving the symmetry coordinates properly constructed and oriented, kinetic energy matrices, mean-square amplitude matrices, analytical expressions for all the possible mean-square amplitude quantities and secular equations for the normal frequencies. This method has been applied to determine the mean amplitudes of vibration for the pentachlorides of phosphorous, antimony and molybdenum at the temperatures  $T = 0$  and  $T = 298^\circ\text{K}$  respectively.

## INTRODUCTION

In the solid, liquid and vapour phase the Raman spectrum of phosphorous pentachloride was obtained by Krishnamurthi (1930) and Moureu, Magat and Wetroff (1937). Rouault (1940) and Sargent and Schomaker (1941) by their electron diffraction investigations and Pauling (1942) by his theoretical explanation established that phosphorous pentachloride has a trigonal bipyramidal structure with the symmetry point group  $D_{3h}$ . Using the then available Raman data, Siebert (1951) made a vibrational assignment on the basis of the above structure. Haarhoff and Pistorius (1959), on the basis of Wilson's group theoretical method (1939 and 1941) calculated the force constants without the two fundamental frequencies coming under the  $A_2''$  species in addition to other similar molecules. Recently Wilshurst and Bernstein (1957) have studied the Raman as well as infrared spectra of  $\text{PCl}_5$  in the liquid and gaseous states, assigned all the fundamental frequencies with a simple normal coordinate treatment and calculated the molar thermodynamic functions.

The Raman spectrum of antimony pentachloride was studied by Keirz and Stricks (1937), Moureu, Magat and Wetroff (1938) and Moureu, Sue and Magat (1947-1948). Rouault (1940) by his electron diffraction data in the gaseous state and Ohlberg (1954) by his X-ray diffraction measurements in the solid state confirmed the  $D_{3h}$  symmetry for  $\text{SbCl}_5$ . With the help of the existing Raman data, Siebert (1951) attempted a vibrational assignment on the basis of  $D_{3h}$  symmetry. Recently, Wilshurst (1960) has studied the infrared absorption

---

\* At present Department of Chemistry, University of Maryland, U. S. A.

spectrum in the gaseous state, assigned all the fundamental frequencies and then calculated the thermodynamic functions by the statistical method.

The Raman spectrum of niobium pentachloride was studied by Moureu, Magat and Wetroff (1938) and Moureu, Magat and Sue (1947-1948). Skinner and Sutton (1940) carried out an electron diffraction study and confirmed the trigonal bipyramidal structure for  $\text{NbCl}_5$ . Recently, Gaunt, and Ainscough (1957) have studied the Raman and infrared absorption spectra of this molecule and assigned all the fundamental frequencies on the basis of  $D_{3h}$  symmetry. Nagarajan (1962) has calculated the molar thermodynamic functions of this molecule after giving a detailed procedure for the calculation of these functions.

It is the aim of the present investigation to give a method for the determination of the mean-square amplitudes of vibration of trigonal bipyramidal  $\text{XY}_5$  type molecules following the principle outlined by Cyvin (1959) and then to apply for the computation of the mean-square amplitudes of vibration of  $\text{PCl}_5$ ,  $\text{SbCl}_5$  and  $\text{NbCl}_5$  from their vibrational spectral data at the temperatures  $T = 0$  and  $T = 298^\circ\text{K}$  respectively.

#### SYMMETRY COORDINATES

The trigonal bipyramidal pentahalides with the symmetry point group  $D_{3h}$  give rise to the following fundamental frequencies under the various irreducible representations:  $2A_1'(R, \rho) + 2A_2''(I, \perp) + 3E'(R, dp; I, \perp) + E''(R, dp)$  where  $R$ ,  $I$ ,  $\rho$ ,  $dp$ ,  $\perp$  and  $\perp$  stand for Raman active, infrared active, polarized, depolarized parallel and perpendicular respectively. Two normal modes of vibration under the  $A_1'$  species, one under the  $A_2''$  species and one under the  $E'$  species have been

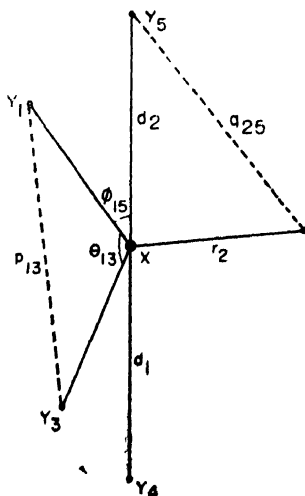


Fig. 1. The internal coordinates for the trigonal bipyramidal  $\text{XY}_5$  type molecule. The symbols denote deviations from the equilibrium distances and angles.

associated with essentially valency vibrations and the remaining with essentially deformation vibrations. The harmonic vibrations of the  $XY_6$  type molecule have been described by fourteen internal coordinates (Fig. 1). With the help of these internal coordinates the following set of symmetry coordinates satisfying the conditions of normalization, orthogonality and transformations of the concerned vibration species has been constructed :

$$S_1(A_1') = (3)^{-1/2}(r_1 + r_2 + r_3)$$

$$S_2(A_1') = (2)^{-1/2}(d_1 + d_2)$$

$$S_3(A_2'') = (2)^{-1/2}(d_1 - d_2)$$

$$S_4(A_2'') = (RD)^{1/2}(6)^{-1/2}(\phi_{14} + \phi_{24} + \phi_{34} - \phi_{15} - \phi_{25} - \phi_{35})$$

$$S_{5a}(E') = (6)^{-1/2}(2r_1 - r_2 - r_3)$$

$$S_{5b}(E') = (2)^{-1/2}(r_2 - r_3)$$

$$S_{6a}(E') = R(6)^{-1/2}(2\theta_{23} - \theta_{12} - \theta_{13})$$

$$S_{6b}(E') = R(2)^{-1/2}(\theta_{12} - \theta_{13})$$

$$S_{7a}(E'') = (RD)^{1/2}(12)^{-1/2}(2\phi_{11} - \phi_{24} - \phi_{34} + 2\phi_{15} - \phi_{25} - \phi_{35})$$

$$S_{7b}(E'') = (RD)^{1/2}(\phi_{24} + \phi_{34} + \phi_{25} - \phi_{35})/2$$

$$S_{8a}(E'') = (RD)^{1/2}(12)^{-1/2}(2\phi_{14} - \phi_{24} - \phi_{34} - 2\phi_{15} + \phi_{25} + \phi_{35})$$

$$S_{8b}(E'') = (RD)^{1/2}(\phi_{24} - \phi_{34} - \phi_{25} + \phi_{35})/2$$

$$S_{r1} = R(3)^{-1/2}(\theta_{12} + \theta_{23} + \theta_{13}) = 0 \text{ (Redundant)}$$

$$S_{r2} = (RD)^{1/2}(6)^{-1/2}(\phi_{14} + \phi_{24} + \phi_{34} + \phi_{15} + \phi_{25} + \phi_{35}) = 0 \text{ (Redundant)}$$

It should be noticed that the angle displacements have been multiplied by the equilibrium bond lengths  $R$  and  $D$  in order to maintain the same dimensions for the various mean-square amplitude quantities.

# KINETIC ENERGY MATRICES

Following the methods outlined by Wilson (1939, 1941), the symmetrized  $G$  and  $G^{-1}$  matrices have been obtained for the various irreducible representations as follows :

$$G_{11}(A_1') = \mu_y$$

$$G_{22}(A_1') = \mu_y$$

$$G_{12}(A_1') = G_{21}(A_1') = 0$$

$$G_{33}(A_2'') = 2\mu_x + \mu_y$$

$$G_{44}(A_2'') = 6\mu_x + 2\mu_y$$

$$G_{34}(A_2'') = G_{43}(A_2'') = (12)^{1/2}\mu_x$$

$$G_{55}(E') = (3/2)\mu_x + \mu_y$$

$$G_{11}^{-1}(A_1') = \mu_y^{-1}$$

$$G_{22}^{-1}(A_1') = \mu_y^{-1}$$

$$G_{12}^{-1}(A_1') = G_{21}^{-1}(A_1') = 0$$

$$G_{33}^{-1}(A_2'') = (3\mu_x + \mu_y)(5\mu_x + \mu_y)^{-1}\mu_y^{-1}$$

$$G_{44}^{-1}(A_2'') = \frac{1}{2}(2\mu_x + \mu_y)(5\mu_x + \mu_y)^{-1}\mu_y^{-1}$$

$$G_{34}^{-1}(A_2'') = G_{43}^{-1}(A_2'') \\ = 3^{1/2}\mu_x(5\mu_x + \mu_y)^{-1}\mu_y^{-1}$$

$$G_{55}^{-1}(E') = 3(\mu_x + \frac{1}{2}\mu_y)/K$$

$$\begin{aligned}
G_{66}(E') &= (9/2)\mu_x + 3\mu_y & G_{66}^{-1}(E') &= \{(\mu_x + \frac{1}{2}\mu_y) - \frac{1}{2}\mu_x^2\}/K \\
G_{77}(E') &= 3\mu_x + (3/2)\mu_y & G_{77}^{-1}(E') &= (3\mu_x + 2\mu_y)/2K \\
G_{56}(E') &= G_{65}(E') = 0 & G_{65}^{-1}(E') &= G_{56}^{-1}(E') = 0 \\
G_{57}(E') &= G_{75}(E') = -(3/2)^{\frac{1}{2}}\mu_x & G_{57}^{-1}(E') &= G_{75}^{-1}(E') = (3/2)^{\frac{1}{2}}\mu_x \\
G_{67}(E') &= G_{76}(E') = 0 & G_{67}^{-1}(E') &= G_{76}^{-1}(E') = 0 \\
G_{88}(E'') &= (7/2)\mu_y & G_{88}^{-1}(E'') &= (2/7)\mu_y^{-4}
\end{aligned}$$

Here  $K = (3/2)\{(3\mu_x + 2\mu_y)(\mu_x + \frac{1}{2}\mu_y) - \mu_x^2\}$

where  $\mu_x$  and  $\mu_y$  are the reciprocal masses of the X and Y atoms respectively.

#### MEAN-SQUARE AMPLITUDE MATRICES

Following the methods outlined by Cyvin (1959), the symmetrized mean-square amplitude matrices  $\Sigma$  have been obtained by introducing the symmetry coordinates as follows :

$$\begin{aligned}
\Sigma_{11}(A'_1) &= \langle S_1^2 \rangle = \sigma_r + 2\sigma_{rr} \\
\Sigma_{22}(A'_1) &= \langle S_2^2 \rangle = \sigma_d + \sigma_{dd} \\
\Sigma_{12}(A'_1) &= \Sigma_{21}(A'_1) = \langle S_1 S_2 \rangle = (6)^{\frac{1}{2}}\sigma_{rd} \\
\Sigma_{33}(A''_2) &= \langle S_3^2 \rangle = \sigma_d - \sigma_{dd} \\
\Sigma_{44}(A''_2) &= \langle S_4^2 \rangle = \sigma_\varphi - \sigma_{\varphi\varphi} + 2\sigma'_{\varphi\varphi} - 2\sigma''_{\varphi\varphi} \\
\Sigma_{34}(A''_2) &= \Sigma_{43}(A''_2) = \langle S_3 S_4 \rangle = (3)^{\frac{1}{2}}(\sigma_{d\varphi} - \sigma'_{\varphi\varphi}) \\
\Sigma_{55}(E') &= \langle S_{5a}^2 \rangle = \langle S_{5b}^2 \rangle = \sigma_r - \sigma_{rr} \\
\Sigma_{66}(E') &= \langle S_{6a}^2 \rangle = \langle S_{6b}^2 \rangle = \sigma_\theta - \sigma_{\theta\theta} \\
\Sigma_{77}(E') &= \langle S_{7a}^2 \rangle = \langle S_{7b}^2 \rangle = \sigma_\varphi + \sigma_{\varphi\varphi} - \sigma'_{\varphi\varphi} - \sigma''_{\varphi\varphi} \\
\Sigma_{56}(E') &= \Sigma_{65}(E') = \langle S_{5a} S_{6a} \rangle = \langle S_{5b} S_{6b} \rangle = \sigma_{r\theta} - \sigma'_{r\theta} \\
\Sigma_{57}(E') &= \Sigma_{75}(E') = \langle S_{57} S_{7a} \rangle = \langle S_{6b} S_{7b} \rangle = (2)^{\frac{1}{2}}(\sigma_{r\varphi} - \sigma'_{r\varphi}) \\
\Sigma_{67}(E') &= \Sigma_{76}(E') = \langle S_{6a} S_{7a} \rangle = \langle S_{6b} S_{7b} \rangle = (2)^{\frac{1}{2}}(\sigma_{\theta\varphi} - \sigma'_{\theta\varphi}) \\
\Sigma_{88}(E'') &= \langle S_{8a}^2 \rangle = \langle S_{8b}^2 \rangle = \sigma_\varphi - \sigma_{\varphi\varphi} - \sigma'_{\varphi\varphi} + \sigma''_{\varphi\varphi}
\end{aligned}$$

where the entering quantities have been defined by the mean values given in the following :

$$\begin{aligned}
\sigma_r &= \langle r_1^2 \rangle = \langle r_2^2 \rangle = \langle r_3^2 \rangle \\
\sigma_{rr} &= \langle r_1 r_2 \rangle = \langle r_1 r_3 \rangle = \langle r_2 r_3 \rangle \\
\sigma_d &= \langle d_1^2 \rangle = \langle d_2^2 \rangle \\
\sigma_{dd} &= \langle d_1 d_2 \rangle \\
\sigma_{rd} &= \langle r_1 d_1 \rangle = \langle r_2 d_1 \rangle = \langle r_3 d_1 \rangle = \langle r_1 d_2 \rangle = \langle r_2 d_2 \rangle = \langle r_3 d_2 \rangle \\
\sigma_\theta &= R^2 \langle \theta_{12}^2 \rangle = R^2 \langle \theta_{23}^2 \rangle = R^2 \langle \theta_{13}^2 \rangle
\end{aligned}$$



$$\begin{aligned}
 \sigma_{\theta\theta} &= R^2 \langle \theta_{12} \theta_{23} \rangle = R^2 \langle \theta_{12} \theta_{13} \rangle = R^2 \langle \theta_{23} \theta_{13} \rangle \\
 \sigma'_{\varphi} &= RD \langle \phi_{14}^2 \rangle = RD \langle \phi_{24}^2 \rangle = RD \langle \phi_{34}^2 \rangle = RD \langle \phi_{15}^2 \rangle = RD \langle \phi_{25}^2 \rangle \\
 &= RD \langle \phi_{35}^2 \rangle \\
 \sigma_{\varphi\varphi} &= RD \langle \phi_{14} \phi_{15} \rangle = RD \langle \phi_{24} \phi_{35} \rangle = RD \langle \phi_{34} \phi_{35} \rangle \\
 \sigma'_{\varphi\varphi} &= RD \langle \phi_{14} \phi_{24} \rangle = RD \langle \phi_{14} \phi_{34} \rangle = RD \langle \phi_{24} \phi_{34} \rangle = RD \langle \phi_{15} \phi_{25} \rangle \\
 &= RD \langle \phi_{15} \phi_{35} \rangle = RD \langle \phi_{25} \phi_{35} \rangle \\
 \sigma''_{\varphi\varphi} &= RD \langle \phi_{14} \phi_{25} \rangle = RD \langle \phi_{14} \phi_{25} \rangle = RD \langle \phi_{24} \phi_{15} \rangle = RD \langle \phi_{24} \phi_{35} \rangle \\
 &= RD \langle \phi_{34} \phi_{15} \rangle = RD \langle \phi_{34} \phi_{25} \rangle \\
 \sigma_{d\varphi} &= (RD)^{\frac{1}{2}} \langle d_1 \phi_{14} \rangle = (RD)^{\frac{1}{2}} \langle d_1 \phi_{24} \rangle = (RD)^{\frac{1}{2}} \langle d_1 \phi_{34} \rangle = (RD)^{\frac{1}{2}} \langle d_2 \phi_{15} \rangle \\
 &= (RD)^{\frac{1}{2}} \langle d_2 \phi_{25} \rangle = (RD)^{\frac{1}{2}} \langle d_2 \phi_{35} \rangle \\
 \sigma'_{d\varphi} &= (RD)^{\frac{1}{2}} \langle d_1 \phi_{15} \rangle = (RD)^{\frac{1}{2}} \langle d_1 \phi_{25} \rangle = (RD)^{\frac{1}{2}} \langle d_1 \phi_{35} \rangle = (RD)^{\frac{1}{2}} \langle d_2 \phi_{14} \rangle \\
 &= (RD)^{\frac{1}{2}} \langle d_2 \phi_{24} \rangle = (RD)^{\frac{1}{2}} \langle d_2 \phi_{34} \rangle \\
 \sigma_{r\theta} &= R \langle r_1 \theta_{12} \rangle = R \langle r_1 \theta_{13} \rangle = R \langle r_2 \theta_{12} \rangle = R \langle r_2 \theta_{23} \rangle = R \langle r_3 \theta_{23} \rangle \\
 &= R \langle r_3 \theta_{13} \rangle \\
 \sigma_{r\theta}' &= R \langle r_1 \theta_{23} \rangle = R \langle r_2 \theta_{13} \rangle = R \langle r_3 \theta_{12} \rangle \\
 \sigma_{r\varphi} &= (RD)^{\frac{1}{2}} \langle r_1 \phi_{14} \rangle = (RD)^{\frac{1}{2}} \langle r_1 \phi_{15} \rangle = (RD)^{\frac{1}{2}} \langle r_2 \phi_{24} \rangle = (RD)^{\frac{1}{2}} \langle r_2 \phi_{25} \rangle \\
 &= (RD)^{\frac{1}{2}} \langle r_3 \phi_{34} \rangle = (RD)^{\frac{1}{2}} \langle r_3 \phi_{35} \rangle \\
 \sigma'_{r\varphi} &= (RD)^{\frac{1}{2}} \langle r_1 \phi_{24} \rangle = (RD)^{\frac{1}{2}} \langle r_1 \phi_{34} \rangle = (RD)^{\frac{1}{2}} \langle r_1 \phi_{25} \rangle = (RD)^{\frac{1}{2}} \langle r_1 \phi_{35} \rangle \\
 &= (RD)^{\frac{1}{2}} \langle r_2 \phi_{14} \rangle = (RD)^{\frac{1}{2}} \langle r_2 \phi_{34} \rangle = (RD)^{\frac{1}{2}} \langle r_2 \phi_{15} \rangle = (RD)^{\frac{1}{2}} \langle r_2 \phi_{35} \rangle \\
 &= (RD)^{\frac{1}{2}} \langle r_3 \phi_{14} \rangle = (RD)^{\frac{1}{2}} \langle r_3 \phi_{24} \rangle = (RD)^{\frac{1}{2}} \langle r_3 \phi_{15} \rangle = (RD)^{\frac{1}{2}} \langle r_3 \phi_{25} \rangle \\
 \sigma_{\theta\varphi} &= (R^3 D)^{\frac{1}{2}} \langle \theta_{12} \theta_{14} \rangle = (R^3 D)^{\frac{1}{2}} \langle \theta_{12} \phi_{24} \rangle = (R^3 D)^{\frac{1}{2}} \langle \theta_{12} \phi_{15} \rangle \\
 &= (R^3 D)^{\frac{1}{2}} \langle \theta_{12} \phi_{25} \rangle = (R^3 D)^{\frac{1}{2}} \langle \theta_{23} \phi_{24} \rangle = (R^3 D)^{\frac{1}{2}} \langle \theta_{23} \phi_{34} \rangle \\
 &= (R^3 D)^{\frac{1}{2}} \langle \theta_{23} \phi_{35} \rangle = (R^3 D)^{\frac{1}{2}} \langle \theta_{23} \phi_{35} \rangle = (R^3 D)^{\frac{1}{2}} \langle \theta_{13} \phi_{14} \rangle \\
 &= (R^3 D)^{\frac{1}{2}} \langle \theta_{13} \phi_{34} \rangle = (R^3 D)^{\frac{1}{2}} \langle \theta_{13} \phi_{15} \rangle = (R^3 D)^{\frac{1}{2}} \langle \theta_{13} \phi_{35} \rangle \\
 \sigma'^{\theta}_{\varphi} &= (R^3 D)^{\frac{1}{2}} \langle \theta_{12} \phi_{34} \rangle = (R^3 D)^{\frac{1}{2}} \langle \theta_{12} \phi_{35} \rangle = (R^3 D)^{\frac{1}{2}} \langle \theta_{23} \phi_{14} \rangle \\
 &= (R^3 D)^{\frac{1}{2}} \langle \theta_{23} \phi_{15} \rangle \\
 &= (R^3 D)^{\frac{1}{2}} \langle \theta_{13} \phi_{24} \rangle = (R^3 D)^{\frac{1}{2}} \langle \theta_{13} \phi_{25} \rangle
 \end{aligned}$$

Some linear combinations of the above mean-square amplitude quantities have become zero due to the construction of two redundant coordinates in this case. From the well-known relations

$$\langle S_r^2 \rangle = 0; \quad \langle S_r S_i \rangle = 0$$

where  $S_r$  is the redundant coordinate and  $S_i$  an arbitrary coordinate, it has been found

$$\begin{aligned}
 \sigma_{\theta} + 2\sigma_{\theta\theta} &= 0 \\
 \sigma_{\varphi} + \sigma_{\varphi\varphi} + 2\sigma'_{\varphi\varphi} + 2\sigma''_{\varphi\varphi} &= 0
 \end{aligned}$$

$$2\sigma_{r\theta} + \sigma'_{r\theta} = 0$$

$$\sigma_{d\theta} = 0$$

$$\sigma_{r\varphi} + 2\sigma'_{r\varphi} = 0$$

$$\sigma_{d\varphi} + \sigma'_{d\varphi} = 0$$

$$2\sigma_{\theta\varphi} + \sigma'_{\theta\varphi} = 0$$

### NORMAL FREQUENCIES

From the secular equations  $|\Sigma G^{-1} - E\Delta| = 0$  set up by Cyvin (1959), the following set of equations for the normal frequencies containing the symmetrized mean-square amplitude matrix elements has been derived :

$$\Delta_1 + \Delta_2 = \Sigma_{11} G_{11}^{-1} + \Sigma_{22} G_{22}^{-1}$$

$$\Delta_1 \Delta_2 = (\Sigma_{11} \Sigma_{22} - \Sigma_{12}^2) (G_{11}^{-1} G_{22}^{-1})$$

$$\Delta_3 + \Delta_4 = \Sigma_{33} G_{33}^{-1} + \Sigma_{44} G_{44}^{-1} + 2\Sigma_{34} G_{34}^{-1}$$

$$\Delta_3 \Delta_4 = (\Sigma_{33} \Sigma_{44} - \Sigma_{34}^2) (G_{33}^{-1} G_{44}^{-1} - G_{34}^{-12})$$

$$\Delta_5 + \Delta_6 + \Delta_7 = \Sigma_{55} G_{55}^{-1} + \Sigma_{66} G_{66}^{-1} + \Sigma_{77} G_{77}^{-1} + 2\Sigma_{57} G_{57}^{-1}$$

$$\Delta_5 \Delta_6 + \Delta_5 \Delta_7 + \Delta_6 \Delta_7 = (\Sigma_{55} \Sigma_{66} - \Sigma_{56}^2) G_{55}^{-1} G_{66}^{-1} + (\Sigma_{55} \Sigma_{77} - \Sigma_{57}^2) (G_{55}^{-1} G_{66}^{-1} - G_{57}^{-12})$$

$$+ (\Sigma_{66} \Sigma_{77} - \Sigma_{67}^2) G_{66}^{-1} G_{77}^{-1} - 2(\Sigma_{56} \Sigma_{67} - \Sigma_{66} \Sigma_{57}) G_{66}^{-1} G_{57}^{-1}$$

$$\Delta_5 \Delta_6 \Delta_7 = (\Sigma_{55} \Sigma_{66} \Sigma_{77} - \Sigma_{55} \Sigma_{67}^2 - \Sigma_{66} \Sigma_{57}^2 - \Sigma_{77} \Sigma_{56}^2 + 2\Sigma_{56} \Sigma_{57} \Sigma_{67})$$

$$(G_{55}^{-1} G_{66}^{-1} - G_{77}^{-1} G_{66}^{-1} G_{57}^{-12})$$

$$\Delta_8 = \Sigma_{88} G_{88}^{-1}$$

$\Delta$  in the above equations has been related to the normal frequency  $\nu$  as

$$\Delta_i = (h/8\pi^2 r_i) \coth(h\nu_i/2KT)$$

where  $\kappa$  is the Boltzmann constant and  $T$  the temperature in degrees Kelvin.

### ADDITIONAL MEAN-SQUARE AMPLITUDE QUANTITIES

The interatomic distance displacements between the non-bonded atom pairs, instead of the angle derivations, have been taken into account and designated as  $p_{12}$ ,  $p_{23}$ ,  $p_{13}$ ,  $q_{15}$ ,  $q_{25}$  and  $q_{35}$  (Fig. 1). Then the following additional mean square amplitude quantities have been obtained :

$$\sigma_p = \langle p_{12}^2 \rangle = \langle p_{23}^2 \rangle = \langle p_{13}^2 \rangle$$

$$\sigma_{pp} = \langle p_{12} p_{23} \rangle = \langle p_{12} p_{13} \rangle = \langle p_{23} p_{13} \rangle$$

$$\sigma_q = \langle q_{14}^2 \rangle = \langle q_{24}^2 \rangle = \langle q_{34}^2 \rangle = \langle q_{15}^2 \rangle = \langle q_{25}^2 \rangle = \langle q_{35}^2 \rangle$$

$$\sigma_{qq} = \langle q_{14} q_{24} \rangle = \langle q_{14} q_{34} \rangle = \langle q_{24} q_{34} \rangle = \langle q_{15} q_{25} \rangle$$

$$= \langle q_{15} q_{35} \rangle = \langle q_{25} q_{35} \rangle$$

$$\sigma'_{qq} = \langle q_{14} q_{15} \rangle = \langle q_{24} q_{25} \rangle = \langle q_{34} q_{35} \rangle$$

$$\sigma''_{qq} = \langle q_{14} q_{25} \rangle = \langle q_{14} q_{35} \rangle = \langle q_{24} q_{35} \rangle = \langle q_{24} q_{15} \rangle - \langle q_{34} q_{15} \rangle \\ = \langle q_{34} q_{25} \rangle$$

$$\sigma_{pq} = \langle p_{12} q_{14} \rangle = \langle p_{12} q_{24} \rangle = \langle p_{12} q_{15} \rangle = \langle p_{12} q_{25} \rangle = \langle p_{23} q_{24} \rangle \\ = \langle p_{23} q_{34} \rangle = \langle p_{23} q_{25} \rangle = \langle p_{23} q_{35} \rangle = \langle p_{13} q_{34} \rangle = \langle p_{13} q_{14} \rangle \\ = \langle p_{13} q_{35} \rangle = \langle p_{13} q_{15} \rangle$$

$$\sigma'_{pq} = \langle p_{12} q_{34} \rangle = \langle p_{12} q_{35} \rangle = \langle p_{23} q_{14} \rangle = \langle p_{23} q_{15} \rangle = \langle p_{13} q_{14} \rangle \\ = \langle p_{13} q_{25} \rangle$$

The above additional mean-square amplitude quantities defined by the mean values of the deviations of the bonded as well as non-bonded distances are not independent of the mean-square amplitude quantities previously defined in one of the sections of this article by the mean values of the deviations of the interbond distances and interbond angles. All these quantities, in fact, may well be expressed analytically in terms of the symmetrized mean-square amplitude matrix elements  $\Sigma$ . If one of the introduced internal coordinates ( $\epsilon_1$ ) —  $r$ ,  $d$ ,  $R\theta$  or  $(RD)^{1/2}\phi$  has been given in terms of the symmetry coordinates by

$$\epsilon_i = \sum_k A_{ik} S_k$$

it has been found

$$\langle \epsilon_i \epsilon_j \rangle = \sum_k \sum_l A_{ik} A_{jl} \Sigma_{kl},$$

where  $\Sigma_{kl}$  denotes the elements of the  $\Sigma$  matrix. The mean-square amplitude quantities in terms of the symmetrized mean-square amplitude matrix elements  $\Sigma$  have been obtained as follows :

$$\sigma_r = (1/3)(\Sigma_{11} + 2\Sigma_{55})$$

$$\sigma_{rr} = (1/3)(\Sigma_{11} - \Sigma_{55})$$

$$\sigma_d = (1/2)(\Sigma_{22} + \Sigma_{33})$$

$$\sigma_{dd} = (1/2)(\Sigma_{22} - \Sigma_{33})$$

$$\sigma_{rd} = (6)^{-1}\Sigma_{12}$$

$$\sigma_\theta = (2/3)\Sigma_{66}$$

$$\sigma_{\theta\theta} = -(1/3)\Sigma_{66}$$

$$\sigma_\phi = (1/4)\Sigma_{44} + (5/12)\Sigma_{77} + (1/4)\Sigma_{88}$$

$$\sigma_{\phi\phi} = -(1/4)\Sigma_{44} + (1/4)\Sigma_{77} - (1/4)\Sigma_{88}$$

$$\sigma'_{\phi\phi} = (1/4)\Sigma_{44} - (1/12)\Sigma_{77} - (1/4)\Sigma_{88}$$

$$\sigma''_{\phi\phi} = -(1/4)\Sigma_{44} - (1/4)\Sigma_{77} + (1/4)\Sigma_{88}$$

$$\sigma_{R\theta} = (12)^{-1}\Sigma_{34}$$

$$\sigma'_{d\theta} = -(12)^{-1}\Sigma_{34}$$

$$\sigma_{r\theta} = (2/9)^{1/2}\Sigma_{57}$$

$$\sigma'_{r\theta} = -(18)^{-1}\Sigma_{57}$$

$$\sigma_{r\theta} = (1/3)\Sigma_{56}$$

$$\sigma'_{r\theta} = -(2/3)\Sigma_{56}$$

$$\sigma_p = \Sigma_{11} + (1/2)\Sigma_{55} + (1/6)\Sigma_{66} - (3)^{-1}\Sigma_{56}$$

$$\sigma_{pp} = \Sigma_{11} + (1/4)\Sigma_{55} - (1/12)\Sigma_{66} + (12)^{-1}\Sigma_{56}$$

$$\sigma_q = (1/6)\Sigma_{11} + (1/4)\Sigma_{22} + (1/4)\Sigma_{33} + (1/12)\Sigma_{44} + (1/3)\Sigma_{55} + (1/6)\Sigma_{77} \\ + (1/6)\Sigma_{88} + (6)^{-1}\Sigma_{12} + (12)^{-1}\Sigma_{34} + (2/9)^{1/2}\Sigma_{57}$$

$$\sigma_{qq} = (1/6)\Sigma_{11} + (1/4)\Sigma_{22} + (1/4)\Sigma_{33} + (1/12)\Sigma_{44} - (1/6)\Sigma_{55} - (1/12)\Sigma_{77} - (1/12)\Sigma_{88} \\ + (6)^{-1}\Sigma_{12} + (12)^{-1}\Sigma_{34} - (18)^{1/2}\Sigma_{57}$$

$$\sigma'_{qq} = (1/6)\Sigma_{11} + (1/4)\Sigma_{22} - (1/4)\Sigma_{33} - (1/12)\Sigma_{44} + (1/3)\Sigma_{55} + (1/6)\Sigma_{77} - (1/6)\Sigma_{88} \\ + (6)^{-1}\Sigma_{12} - (12)^{-1}\Sigma_{34} + (2/9)R\Sigma_{57}$$

$$\sigma''_{qq} = (1/6)\Sigma_{11} + (1/4)\Sigma_{22} - (1/4)\Sigma_{33} - (1/12)\Sigma_{44} - (1/6)\Sigma_{55} - (1/12)\Sigma_{77} \\ + (1/12)\Sigma_{88} + (6)^{-1}\Sigma_{12} - (12)^{-1}\Sigma_{34} - (18)^{-1}\Sigma_{57}$$

$$\sigma_{pq} = (6)^{-1}\Sigma_{11} + (24)^{-1}\Sigma_{55} + (1/2)\Sigma_{12} - (72)^{-1}\Sigma_{56} + (48)^{-1}\Sigma_{57} - (1/12)\Sigma_{67}$$

$$\sigma'_{pq} = (6)^{-1}\Sigma_{11} - (6)^{-1}\Sigma_{55} + (1/2)\Sigma_{12} + (18)^{-1}\Sigma_{56} - (12)^{-1}\Sigma_{57} + (1/6)\Sigma_{67}$$

It should be noticed that all of the mean-square amplitude quantities defined in the previous section appear in the symmetrized mean-square amplitude matrix elements except  $\sigma_{d\theta}$ . This becomes vanished by symmetry of the molecular system.

## RESULTS

The fundamental frequencies in  $\text{cm}^{-1}$  for  $\text{PCl}_5$  given by Wilmshurst and Bernstein (1957), for  $\text{SbCl}_5$  by Wilmshurst (1960) and for  $\text{NbCl}_5$  by Gaunt and Ainscough (1957) have been given in Table I. The secular equations giving the normal frequencies in terms of the mean-square amplitudes of vibration were constructed with the help of the fundamental frequencies  $\Sigma$  and  $G^{-1}$  matrices and then solved. Since it is not possible to solve all the symmetrized mean-square amplitude matrices uniquely, most of the non-diagonal terms were neglected for the sake of simplicity in the evaluation. In fact, the magnitude of many non-diagonal terms is effectively negligible in comparing that of the diagonal elements and the contribution of these toward the mean-square amplitude quantities is not much significant. The evaluated symmetrized mean-square amplitude matrices in  $\text{\AA}^2$  for the three molecules at the temperatures  $T = 0$  and  $T = 298^\circ\text{K}$  have been given in Tables II, III and IV respectively. The computed numerical

values of the mean-square amplitude quantities in  $\text{\AA}^2$  at these temperatures have been given in Tables V, VI and VII respectively where  $\sigma_r$  is the mean-square amplitude quantity due to the bonded atom pair  $X-Y$  in the girdle,  $\sigma_{rr}$  the quantity due to the interaction of two bonded atom pairs in the girdle,  $\sigma_d$  the quantity due to the bonded atom pair in the symmetry axis,  $\sigma_{dd}$  the interaction term due to two bonded atom pairs in the symmetry axis,  $\sigma_\theta$  the quantity due to the bending  $Y-X-Y$  in the equatorial plane,  $\sigma_\varphi$  the quantity due to the bending  $Y(\text{equatorial})-X-Y(\text{axial})$ ,  $\sigma_p$  the quantity due to the nonbonded atom pair  $Y-Y$  in the equatorial plane,  $\sigma_q$  the quantity due to the nonbonded atom pair  $Y(\text{equatorial})-Y(\text{axial})$  and  $\sigma_{\theta\theta}$ ,  $\sigma_{\varphi\varphi}$ ,  $\sigma'_{\varphi\varphi}$ ,  $\sigma''_{\varphi\varphi}$ ,  $\sigma_{dd}$ ,  $\sigma'_{rr}$ ,  $\sigma_{rr}$ ,  $\sigma'_{r\varphi}$ ,  $\sigma_{p\varphi}$ ,  $\sigma_{qq}$ ,  $\sigma'_{qq}$ ,  $\sigma''_{qq}$ ,  $\sigma_{pq}$  and  $\sigma'_{pq}$  are the respective interaction terms. The corresponding mean amplitudes of vibration in  $\text{\AA}$  for the bonded as well as nonbonded atom pairs have been reported in Table VIII for all the three molecules at the two temperatures.

It has been observed for all the three molecules that many of the interaction quantities due to the bonded distances, non-bonded distances and bendings of the molecule are significantly small (Tables V, VI and VII).

The mean-square amplitude quantity due to the bending  $Y-X-Y$  in the equatorial plane is always less than that of the bending  $Y(\text{equatorial})-X-Y(\text{axial})$  (Tables V, VI and VII).

The mean amplitudes of vibration for the bonded (axial) atom pairs are very similar to those of the bonded (equatorial) atom pairs. (Table VIII).

The mean amplitudes of vibration for the nonbonded (equatorial-axial) atom pairs are greater than those of the non bonded (equatorial-equatorial) atom pairs. (Table VIII).

The mean amplitudes of vibration for the nonbonded atom pairs are in general greater than those of the bonded atom pairs.

In general, for any molecule, if the fundamental frequencies in wave numbers are greater than  $1200\text{ cm}^{-1}$ , the hyperbolic cotangent differs very little from unity for the temperatures near  $298^\circ\text{K}$  i.e.  $\coth(h\nu/2KT) = 1$  and the consequent effect is that the mean-square amplitude of vibration is an independent function of temperature. If, on the other hand, the fundamental frequencies in wave numbers are less than  $200\text{ cm}^{-1}$ , the value of the coth function is not so accurate but merely approximate for the temperatures near  $298^\circ\text{K}$  and correspondingly the mean-square amplitude of vibration is a dependent function of temperature. In fact, in each molecule of the present investigation most of the fundamental frequencies fall between  $600\text{ cm}^{-1}$  and  $200\text{ cm}^{-1}$  except a few which may not seriously affect the calculations. Hence, the obtained values of the mean amplitudes of vibration for all the three molecules are the most probable and reliable ones.

TABLE I

Fundamental frequencies in  $\text{cm}^{-1}$  for some trigonal bipyramidal pentachlorides

Symmetry species	vibration	$\text{PCl}_5$	$\text{SbCl}_5$	$\text{NbCl}_5$
$A'_1$	$\nu_1$	394	356	412
	$\nu_2$	394	307	355
$A''_2$	$\nu_3$	465	384	315
	$\nu_4$	176	156	260
	$\nu_5$	592	398	497
$E'$	$\nu_6$	335	182	396
	$\nu_7$	100	74	106
$E''$	$\nu_8$	280	166	153

TABLE II

Symmetrized mean-square amplitude matrices in  $\text{\AA}^2$  for phosphorous pentachloride

Element	Symmetrized mean-square amplitude matrix	
	$T = 0$	$T = 298^\circ\text{K}$
$\Sigma_{11}$	0.0012071	0.0016876
$\Sigma_{22}$	0.0012071	0.0016876
$\Sigma_{33}$	0.0034016	0.0064436
$\Sigma_{44}$	0.0120245	0.0235547
$\Sigma_{31}$	-0.0019784	-0.0004759
$\Sigma_{55}$	0.0029865	0.0051924
$\Sigma_{66}$	0.0118936	0.0213646
$\Sigma_{77}$	0.0187428	0.0366932
$\Sigma_{57}$	0.0015374	0.0025835
$\Sigma_{88}$	0.0059449	0.0108410

TABLE III

Symmetrized mean-square amplitude matrices in  $\text{\AA}^2$  for antimony pentachloride

Element	Symmetrized mean-square amplitude matrix	
	T=0	T= 298°K
$\Sigma_{11}$	0.0015491	0.0026933
$\Sigma_{22}$	0.0013360	0.0020737
$\Sigma_{33}$	0.0024696	0.0106235
$\Sigma_{44}$	0.0075013	0.0128476
$\Sigma_{31}$	0	0
$\Sigma_{55}$	0.0023546	0.0084436
$\Sigma_{66}$	0.0092475	0.0167894
$\Sigma_{77}$	0.0140328	0.0279458
$\Sigma_{57}$	0.0011374	0.0023647
$\Sigma_{88}$	0.0100275	0.0414265

TABLE IV

Symmetrized mean-square amplitude matrices in  $\text{\AA}^2$  for niobium pentachloride

Element	Symmetrized mean-square amplitude matrix	
	T=0	T= 298°K
$\Sigma_{11}$	0.0013397	0.0020809
$\Sigma_{22}$	0.0011543	0.0015157
$\Sigma_{33}$	0.0024576	0.0043286
$\Sigma_{44}$	0.0069034	0.0129874
$\Sigma_{34}$	-0.0011565	-0.0016437
$\Sigma_{55}$	0.0023546	0.0036136
$\Sigma_{66}$	0.0064624	0.0119645
$\Sigma_{77}$	0.0092845	0.0194874
$\Sigma_{57}$	0.0009834	0.0018362
$\Sigma_{88}$	0.0108795	0.0449467

TABLE V

Mean-square amplitude quantities in Å<sup>2</sup> for phosphorous pentachloride

Symbol	Mean-square amplitude quantity	
	T = 0	T = 298°K
$\sigma_r$	0.0023934	0.0040241
$\sigma_{rr}$	-0.0005931	-0.0011683
$\sigma_d$	0.0023044	0.0040656
$\sigma_{dd}$	-0.0010973	-0.0023780
$\sigma_\theta$	0.0079291	0.0142431
$\sigma_{\theta\theta}$	-0.0039645	-0.0071215
$\sigma_\varphi$	0.0123018	0.0238880
$\sigma_{\varphi\varphi}$	0.0000934	0.0005743
$\sigma'_{\varphi\varphi}$	-0.0000420	0.0001206
$\sigma''_{\varphi\varphi}$	-0.0062050	-0.0123517
$\sigma_{d\varphi}$	-0.0005712	-0.0001374
$\sigma'_{d\varphi}$	0.0005712	0.0001374
$\sigma_{r\varphi}$	0.0007247	0.0012179
$\sigma'_{r\varphi}$	-0.0003624	-0.0006090
$\sigma_p$	0.0046827	0.0078446
$\sigma_{pp}$	-0.0005308	-0.0013909
$\sigma_q$	0.0076190	0.0150106
$\sigma_{qq}$	-0.0011333	-0.0012960
$\sigma'_{qq}$	0.0016256	0.0020884
$\sigma''_{qq}$	-0.0029137	-0.0058904
$\sigma_{pq}$	0.0013244	0.0021220
$\sigma'_{pq}$	-0.0011704	-0.0021769



TABLE VI

Mean-square amplitude quantities in  $\text{\AA}^2$  for antimony pentachloride

Symbol	Mean-square amplitude quantity	
	T = 0	T = 298°K
$\sigma_r$	0.0020861	0.0065268
$\sigma_{rr}$	-0.0002685	-0.0019168
$\sigma_d$	0.0019028	0.0063486
$\sigma_{dd}$	-0.0005668	-0.0042749
$\sigma_u$	0.0061650	0.0111929
$\sigma_{uu}$	-0.0030825	-0.0055965
$\sigma_\varphi$	0.0102292	0.0252125
$\sigma_{\varphi\varphi}$	-0.0008740	-0.0065820
$\sigma'_{\varphi\varphi}$	-0.0018610	-0.0094735
$\sigma''_{\varphi\varphi}$	-0.0028766	-0.0001582
$\sigma_{d\varphi}$	0	0.0011502
$\sigma'_{d\varphi}$	0	-0.0011502
$\sigma_{r\varphi}$	0.0005362	0.0011147
$\sigma'_{r\varphi}$	-0.0002681	-0.0005574
$\sigma_p$	0.0042677	0.0097133
$\sigma_{pp}$	0.0001897	-0.0008167
$\sigma_q$	0.0071659	0.0213352
$\sigma_{qq}$	-0.0008311	-0.0019017
$\sigma'_{qq}$	-0.0006617	-0.0022270
$\sigma''_{qq}$	-0.0016446	-0.0047507
$\sigma_{pq}$	0.0012773	0.0031645
$\sigma'_{pq}$	-0.0008651	-0.0034625

TABLE VII

Mean-square amplitude quantities in Å<sup>2</sup> for niobium pentachloride

Symbol	Mean-square amplitude quantity	
	T = 0	T = 298°K
$\sigma_r$	0.0020163	0.0031027
$\sigma_{rr}$	-0.0003383	-0.0005109
$\sigma_d$	0.0018060	0.0029222
$\sigma_{dd}$	-0.0006517	-0.0014065
$\sigma_{..}$	0.0043083	0.0119645
$\sigma_{..}$	-0.0021541	-0.0039882
$\sigma_\varphi$	0.0083143	0.0226038
$\sigma_{\varphi\varphi}$	-0.0021247	-0.0096117
$\sigma'_{\varphi\varphi}$	-0.0017677	-0.0096138
$\sigma''_{\varphi\varphi}$	-0.0013271	0.0031179
$\sigma_{d\varphi}$	-0.0003339	-0.0004745
$\sigma'_{d\varphi}$	0.0003339	0.0004745
$\sigma_{r\varphi}$	0.0004636	0.0008656
$\sigma'_{r\varphi}$	-0.0002378	-0.0004328
$\sigma_p$	0.0035941	0.0058818
$\sigma_{pp}$	0.0002124	0.0001804
$\sigma_q$	0.0059769	0.0152248
$\sigma_{qq}$	-0.0009370	-0.0039889
$\sigma'_{qq}$	-0.0001613	-0.0031374
$\sigma_{qq''}$	-0.0008352	0.0001223
$\sigma_{pq}$	0.0011695	0.0018523
$\sigma'_{pq}$	-0.0006983	-0.0011559

TABLE VIII

Mean amplitudes of vibration in Å for some trigonal bipyramidal pentachlorides

Molecule	Distance	Mean amplitude of vibration	
		T = 0	T = 298°K
PCl <sub>5</sub>	X—Y(equatorial)	0.0489	0.0634
	X—Y(axial)	0.0480	0.0638
	Y(equatorial)—Y(equatorial)	0.0684	0.0886
	Y(equatorial)—Y(axial)	0.0873	0.1225
SbCl <sub>5</sub>	X—Y(equatorial)	0.0458	0.0808
	X—Y(axial)	0.0436	0.0797
	Y(equatorial)—Y(equatorial)	0.0653	0.0986
	Y(equatorial)—Y(axial)	0.0847	0.1461
NbCl <sub>5</sub>	X—Y(equatorial)	0.0449	0.0557
	X—Y(axial)	0.0425	0.0541
	Y(equatorial)—Y(equatorial)	0.0600	0.0767
	Y(equatorial)—Y(axial)	0.0773	0.1234

## ACKNOWLEDGMENT

This work was supported by a grant from the Petroleum Research Fund administered by the American Chemical Society. Grateful acknowledgement is made to the donors of said Fund.

## REFERENCES

- Cyvin, S. J., 1959, *Spectrochimica Acta*. **15**, 828.  
 Gaunt, J. and Ainscough, J. B., 1957, *Spectrochimica Acta*. **10**, 52.  
 Haarhoff, P. C. and Pistorius, C. W. F. T., 1959, *Zeitschrift fuer Naturforschung*. **14**, 972.  
 Keirz, T. and Stricks, W., 1937, *Monatsh, Chem.* **71**, 1.  
 Krishnamurthi, P., 1930, *Ind. J. Phys.* **5**, 116.  
 Mourou, H., Magat, M. and Wetroff, G., 1937, *C. R. Acad. Sci. Paris*. **205**, 276.  
 Moureu, H. Magat, M. and Watroff, G., 1938, *Pro. Indian. Acad. Sci.* **8A**, 356.

- Moureu, H., Magat, M. and Sue, P., (1947-1948), Contributions a l'Etude de la structure Moléculaire, Victor Henri Commemorative Vol, P 125, Desoer, Liez.
- Nagarajan, G., 1962, *Bull. Soc. Chim. Belg.* **71**, 324.
- Ohlberg, S., 1954, *Acta Cryst.* **7**, 640.
- Pauling, L., "Nature of Chemical bond," (Cornell University Press, Ithaca), 1942, Second edition, Page 109.
- Ruault, M., 1940, *Ann. Phys.* **14**, 78.
- Sargent and Schomaker, V., 1941, *J. Chem. Phys.* **9**, 403.
- Siebert, G. 1962, H., 1951, *Z. anorg.u. allgem. Chem.* **265**, 303.
- Skinner, H. A. and Sutton, L. E., 1940, *Trans. Farad. Soc.* **36**, 668.
- Wilmschurst, J. K. and Bernstein, H. J., 1957, *J. Chem. Phys.* **27**, 661.
- Wilmschurst, J. K., 1960, *J. Mol. Spectroscopy.* **5**, 343.
- Wilson, E. B. Jr., 1939 and 1941, *J. Chem. Phys.* **7**, 1041; **9**, 76.

# COHESIVE ENERGIES AND OTHER PROPERTIES OF IONIC CRYSTALS—2. HALIDES OF COPPER, SILVER, THALLIUM AND AMMONIA

M. N. SHARMA and M. P. MADAN

DEPARTMENT OF PHYSICS, UNIVERSITY OF LUCKNOW, INDIA

(Received February 6, 1964)

**ABSTRACT.** Following the treatment employed in the case of alkali halides, the various crystal properties of other metal halides have been studied on the basis of a Lennard-Jones (12 : 6) potential energy form. Equations were modified to take into account the heavier metal halides such as of Copper, Silver, Thallium and Ammonia. The potential parameters were evaluated and the various properties computed. The agreement between the theoretical and experimental values served to justify the adequacy of the chosen potential form for these crystals also.

## INTRODUCTION

Cohesive energies and few other properties of some of the simple alkali halide crystals, representing both the lighter and heavier compounds were computed using the Lennard-Jones (12 : 6) potential form in conjunction with the expression for the Coulomb energy (Sharma and Madan, 1964). As for the inert gases and nearly spherical molecules, different properties can be explained in terms of a simple potential such as one used, it was also found possible to describe the various properties of alkali halides adequately with its help. It was found that  $n < 12$  is more suitable for lighter salts whereas  $n = 12$  is appropriate for heavier ones. The inclusion of the van der Waals term makes the potential form more suitable for heavier compounds. In the present paper we consider properties of crystals heavier than alkali halides, that is, metal halides of Silver, Thallium, Copper and Ammonia and compare them with the experimental results. The characteristics of these salts show definite variation from alkali halides crystals and thus have to be treated separately.

## COMPUTATION OF CRYSTAL PROPERTIES

Based on the Lennard-Jones (12: 6) potential form, the expression for the crystal energy can be written as

$$\phi(r) = \left( -\frac{\alpha e^2}{r} + \frac{B}{r^{12}} - \frac{C}{r^6} + \epsilon_0 \right) \quad \dots \quad (1)$$

where  $\alpha$  is the Madelung's constant,  $e$  is the electronic charge,  $\epsilon_0$  is the zero point energy,  $B$  and  $C$  are the repulsive and attractive parameters respectively and  $r$  is the interionic distance.

For alkali halide crystals, we had seen (Sharma and Madan, 1964) that the contribution of van der Waals energy term was small and therefore higher order terms such as dipole-quadrupole and others were not included in the expression for the crystal energy. However, van der Waals potentials show a systematic tendency to increase for salts of the heavier elements and as much the inclusion of the dipole-quadrupole term is important for these crystals. To consider the additional term ( $D/r^8$ ), we replace  $C$  of equation (1) by  $C_1$  where

$$C_1 = C \left( 1 + \frac{D}{Cr^2} \right) \quad \dots (2)$$

The introduction of dipole-quadrupole term slightly changes the expressions for the repulsive force parameter  $B$  and the compressibility  $\beta$ , and therefore expressions for  $B$  and  $\beta$  can now be written as,

$$B = \frac{r^{12}}{12} \left( \frac{\alpha e^2}{r} + \frac{6C_2}{r^6} - \frac{3}{\beta} \right) \quad \dots (3)$$

where

$$C_2 = C \left( 1 + \frac{8}{6} \frac{D}{Cr^2} \right)$$

and

$$\beta = \frac{9K_1 r^3}{\left( 2 \frac{\alpha e^2}{r} + 12.13 \frac{B}{r^{12}} - 6.7 \frac{C_3}{r^6} \right)} \quad \dots (4)$$

where

$$C_3 = C \left( 1 + \frac{72}{42} \frac{D}{Cr^2} \right).$$

Following Mayer (1933), Mayer and Levy (1933) and Bleick (1934), optical data could be utilised to estimate the values of  $C$  and  $D$ , from which using the experimental values for the interaction distance, we can easily evaluate  $C_1$ ,  $C_2$  and  $C_3$ . The values of these constants for metal halides are given in Table I. The repulsive force parameter  $B$ , is given in Table II and is computed from equation (3) using the experimental values of  $\beta$ ,  $T$  etc. as listed by Mayer *et al.*, (1933, 1934). From the knowledge of  $B$  and of  $C_1$ ,  $C_2$  and  $C_3$ , the lattice energies and the compressibilities for various salts can be calculated using equations (1) and (4). They are tabulated in Table III and IV respectively. In these

Tables, for the sake of comparison we have also reported values of  $E$  and  $\beta$  obtained by considering only the dipole dipole term.

TABLE I

Contribution of dipole-quadrupole term to lattice energy and compressibility

Crystal	$C \times 10^{10}$ (ergs $\times$ cm <sup>6</sup> )	$C_1 \times 10^{10}$ (ergs $\times$ cm <sup>6</sup> )	$C_2 \times 10^{10}$ (ergs $\times$ cm <sup>6</sup> )
TlCl	2270	2601.0	2837.0
TlBr	2785	3192.0	3483.0
TlI	3930	4524.0	4943.0
AgF	305	357.2	394.8
AgCl	767	360.2	399.6
AgBr	967	358.3	396.8
AgI	850	1035.0	1168.0
CuCl	146	173.5	193.1
CuBr	198	234.5	260.4
CuI	330	391.0	434.9
NH <sub>4</sub> F	217	251.8	276.7
NH <sub>4</sub> Cl	1251	1421.0	1543.0
NH <sub>4</sub> Br	1597	1814.0	1969.0
NH <sub>4</sub> I	2286	2595.0	2816.0

TABLE II

Calculation of Repulsive Force Parameter B

Crystal	$B \times 10^{104}$ (with C term)	$B \times 10^{104}$ (with D term) Equ. 3
TlCl	318.4000	347.9000
TlBr	462.1000	507.0000
TlI	840.9000	955.7000
AgF	9.4990	10.2800
AgCl	39.7500	44.1400
AgBr	60.5300	66.9400
AgI	45.1500	51.3500
CuCl	4.6120	4.8990
CuBr	8.1060	8.6282
CuI	16.7000	18.0300
NH <sub>4</sub> F	20.0700	20.9700
NH <sub>4</sub> Cl	265.3000	280.7000
NH <sub>4</sub> Br	449.9000	478.2000
NH <sub>4</sub> I	1018.0000	1081.0000

energy form. The assumptions of a greater van der Waals potential, particularly for the case of iodide (say, for silver and copper) will result in a better agreement with the experiment.

The calculated compressibilities as given in Table IV, need to be multiplied by a correction term  $F_{T,P}$  where

$$F_{T,P} = 1 + \frac{T}{\beta} (\partial\beta/\partial T)_P + \frac{T}{\beta^2 V} (\partial V/\partial T)_P (\partial\beta/\partial P)_T + \frac{2T}{3V} (\partial V/\partial T)_P$$

The experimental data for the terms appearing in this expression is not available in all cases and they can only be estimated in an indirect way. Therefore, this correction was not applied. However, the reported values of  $\beta$  are expected to change by about 7-8% on this account, as was seen by calculating this term for a few cases for which data were available. Keeping in mind, the effect of this correction, we can term the agreement between the theoretical and experimental values as satisfactory, except for thallium and ammonium salts, where the deviation are little more and cannot be accounted for successfully, due to uncertainty in experimental values.

The preceding treatment of the properties of metal halides shows that the Lennard-Jones (12 : 6) potential is quite adequate and practically equally successful for describing them as it is for molecular crystals and gaseous properties.

#### ACKNOWLEDGMENT

The authors are thankful to Prof. P. N. Sharma, for his keen interest in this problem.

#### REFERENCES

- Bleick, W. E., 1934, *J. Chem. Phys.*, **2**, 160.  
 Mayer, J. E., 1933, *J. Chem. Phys.*, **1**, 327.  
 Mayer, J. E., and Levy, B. B., 1933, *J. Chem. Phys.*, **1**, 647.  
 Sharma, M. N., and Madan, M. P., 1964, *Ind. J. Phys.* (Communicated)



# SOME APPROXIMATIONS OF SIGNALS AND INFORMATIONS

J. DAS

INDIAN INSTITUTE OF TECHNOLOGY, KHARAGPUR

(Received February 7, 1964)

**ABSTRACT.** Some methods for approximating time-varying signals and their information contents are discussed and the consequent reduction in the channel capacity for their efficient transmission is indicated. The graphical techniques used in Z-transform methods are mechanised electronically to approximate the waveform of a live signal, and sampling in the time-frequency plane, in time-plane or in frequency-plane alone approximates the information in a continuous semi-random process, e.g., in speech. The temporal and structural attributes of a signal may also be used in approximating the signal information. These lead to some new methods of modulation and band-compression, e.g. Slope-quantized PCM, Adaptive filter and Downward coding.

## INTRODUCTION

In analysis and synthesis of communication systems, in modulation processes, in control and servo systems and in various other applications, it becomes necessary to deal with complicated signals which may not be expressible in compact analytical forms. Even if some analytical forms are possible, the consequent difficulties in solving various integro-differential equations are formidable and hence successful attempts have been made to systematize the numerical calculations in the form of exponential series, time-series and Z-transform. However, these approximate methods, although convergent in processing, are applicable only to the time-limited signals, i.e., the exciting signal must be completely known for all time. For signals which are somewhat random function of time, such as speech, telemetering signals or any continuous information-bearing process, an approximate representation is possible by using their characteristics in the time-frequency plane. In a different class of applications, such as the reduction of the complexity of a signal, as is used in narrow-band coding schemes and the high-efficiency modulation systems, the redundancy of information in the signal is exploited to approximate it and then to economise on the required channel capacity. Here the temporal and structural characteristics of signals are used to determine the required approximation. Thus in all complicated applications, some sort of approximation is necessary to simplify the mechanism of representation and processing of signals and information. Along with a review of some existing approximation techniques, some new methods are proposed here

on the time and bandwidth necessary for the efficient transmission of information. Some schemes for such practical realization are discussed below. The methods in general fall under two classes of approximation, viz. (a) approximation of waveforms, (b) approximation of information. In problems of network representation and modulation, the approximation of waveforms has been widely used, whereas in problems of bandwidth compression, say in Television and Vocoders, the approximation of information has found many applications.

### Approximation of Waveforms

So far the use of the approximation of waveforms has been limited mostly to dead (time-limited) signals (except perhaps in  $\Delta$ -modulation). But it should be possible to use the same or similar techniques for live signals as well. Suppose we are required to design a function generator capable of giving a set of arbitrary repetitive waveforms. Without going into the existing methods of using diodes to make a broken-line approximation of the waveforms, we may first approximate the required  $f(t)$  with eqs.(6) or (7), and then, construct a set of delayed impulses whose heights are varied as required by the given  $f(t)$ . On double or triple integration of these impulse trains, we have the approximated  $f(t)$  which may be made repetitive also. The actual mechanisation of the process is shown

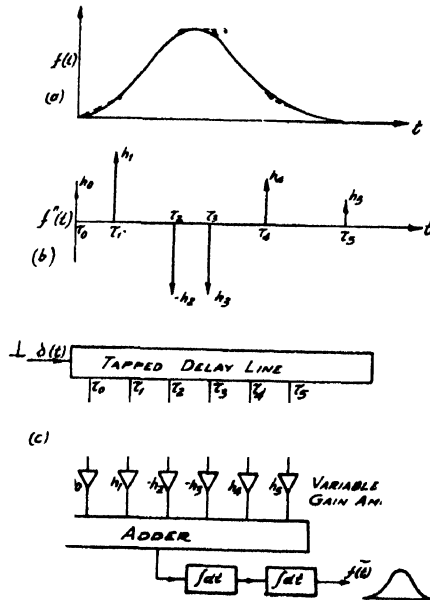


Fig. 3. A function generator and its waveform.

- (a) Linear segment approx. of the waveform.
- (b) Equivalent second derivative ( $\tau$ 's-time delays and  $h$ 's -heights of pulses).
- (c) Block schematic of the function generator.

in Fig. 3. From the estimation of error in this process and in the use of diodes, we find that this method yields better results with fewer components.

### Electronic delay line

It is generally difficult to obtain uniform and distortionless delay for a band of frequencies by using simple *LC*-networks. On the basis of the staircase approximation of  $f(t)$ , an electronic delay line, as shown in Fig. 4(a), may be used for many

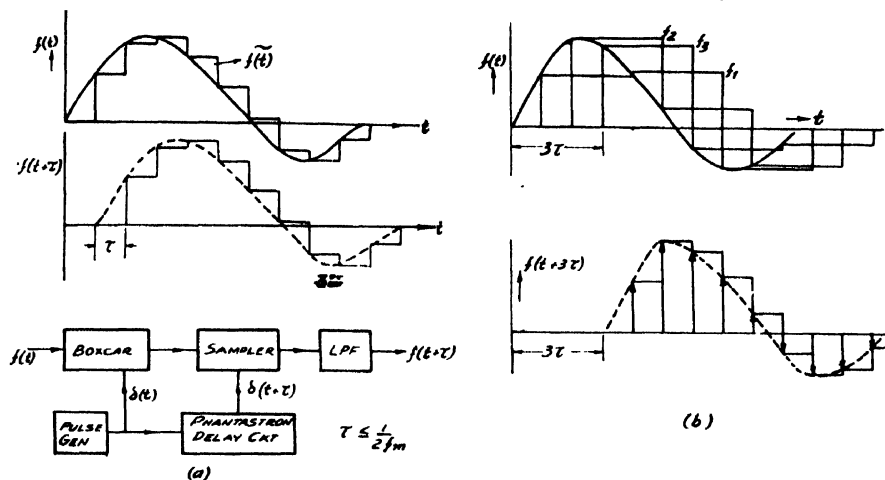


Fig. 4. An electronic delay line.

(a) Waveforms and the block schematic for  $\tau \leq \frac{1}{2f_m}$ .

(b) Waveforms for  $\tau > \frac{1}{2f_m}$  obtained by sampling in parallel.

applications. Here the staircase wave  $\tilde{f}(t)$  obtained through a Boxcar circuit is sampled again with delayed pulses, the delay  $\tau$  being less than  $\frac{1}{2f_m}$ , where  $f_m$  is the highest frequency in  $f(t)$ . Since the sample values remain constant for the time  $\tau \leq \frac{1}{2f_m}$ , the delayed samples, when filtered, will give a delayed  $f(t)$  without any distortion. To obtain a delay  $n\tau > \frac{1}{2f_m}$ , it will be necessary to use cascaded delay circuits, each giving a delay  $\tau$  less than  $\frac{1}{2f_m}$ .

Alternatively,  $f(t)$  may be sampled in parallel by  $n$  Boxcar circuits at time intervals of the required delay  $n\tau$ , each set of sampling pulses being delayed by  $\tau \leq \frac{1}{2f_m}$  in a sequence. The resultant staircase waveforms may now be sampled by the delayed sets of pulses, giving  $n$  sets of delayed impulses, as seen in Fig. 4(b). The sets are mixed and filtered to give an  $f(t)$  delayed by  $n\tau$ . The technique may also be used for any digitalized signal, e.g., the signal produced by  $\Delta$ -modulation or PCM.

### Orthogonal Filters

An alternative signal approximation, specially for speech, is obtained by using Huggin's (1956) method of signal analysis, as given by eqns.(10-12). Speech signals

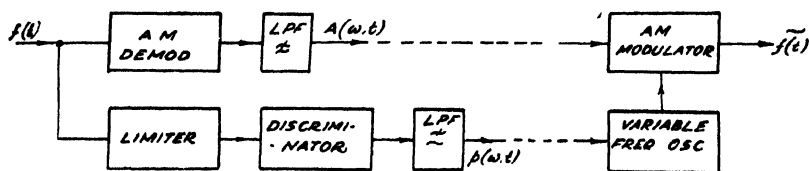


Fig. 11. Approx. of  $f(t)$  by AM-FM reduction.

of  $f(t)$  are made to modulate the narrow-band exciters in the receivers, the band exciters themselves being controlled by the pitch information obtained from the baseband of  $f(t)$ . The Vocoder may operate in a very small bandwidth of about 250 c/s under favourable conditions, but it is found that the narrow band filters produce appreciable phase distortions which have audible effects. To eliminate this and to be able to analyze and synthesize entirely in the time domain, cross-correlation Vocoder (David, 1956) have been designed. Here also the correlated amplitudes at fixed time intervals carry the signal information.

To avoid the use of many analyzing bandpass filter, an adaptive filter, shown in Fig. 12, may be used to select a particular formant of  $f(t)$ . If we assume that

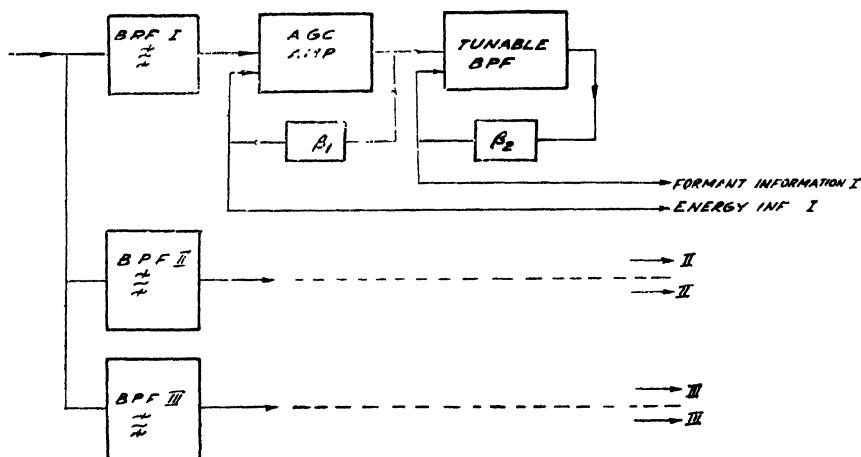


Fig. 12. An adaptive filter for synthesis of  $f(t)$ .

the signal energy is normally distributed in three or four concentrated bands of the total frequency spectrum (as it happens in speech signals), then each of the band may be automatically selected by an adaptive filter and the control signals, thus derived, may be used to transmit the necessary information to the receiver. For transmission of the six information signals of the process shown, a bandwidth of 300 c/s would generally be required.

Lawrence (1953) has shown that fully intelligible speech would be synthesized out of six slowly-varying parameters, viz. (a) the position of the three principal formants, (b) the intensity of the noise source for consonants, (c) the intensity and frequency of the exponentially decaying source with many harmonics for

vowels. The information signals for these synthesized speech require a bandwidth of 150 c/s. only. However the extraction of these basic signals is still a complex problem.

### Weighted Modulation

In most of the modulation systems, equal weightage is given to all values of the signal amplitude, and many binary digits are required in PCM to code the complete range of amplitude levels. It is, however, found that the probability of occurrence of all signal amplitudes is not same, e.g., the probability of the levels upto the r.m.s. value is 0.5 in speech. Hence there is some scope of increasing the channel capacity (Shannon, 1948) by giving suitable weightage to the different amplitudes corresponding to their probabilities, as is done in the Morse code for English letter. The optimum codes may be produced by using a translator after the Binary or Ternary codes and in the receiver, a complementary retranslation has to be used. However, the complete circuitry would be quite complex to be advantageous for simple applications.

One simple way to obtain some of the advantages of the optimum coding is to compress the signal before processing it for transmission. The compressed signal would contain most of the information of the original signal, and it has been shown that in highly compressed speech (Licklider *et al.*, 1947), the intelligibility is as good as 95% with the addition of a differentiator at the input. Basically the differentiator accentuates the high frequency components which are mostly responsible for the intelligibility. This result confirms the proposition that the processing of the slopes of  $f(t)$ , as done in SQ-PCM, will give beter approximation than that obtained from the processing of the sampled amplitudes of  $f(t)$ . It is expected, then, that many of our modulation methods will produce better results if differentiation and compression proceeds the modulator in the transmitter and the complementary equalization is done in the receiver.

A further possibility of reducing the effective bandwidth for transmission of  $\tilde{f}(t)$  lies in the fact that a digitalized signal may be coded downwards (Bell, 1953) for band-compression, of course at the cost of requiring higher  $S/N$  ratio in the transmission path. It has been found, with reference to Fig. 6, that the SQ-PCM gives a good quality speech (0.3 Kc/s band) with  $20,000 \pm$  pulses, and a 95%

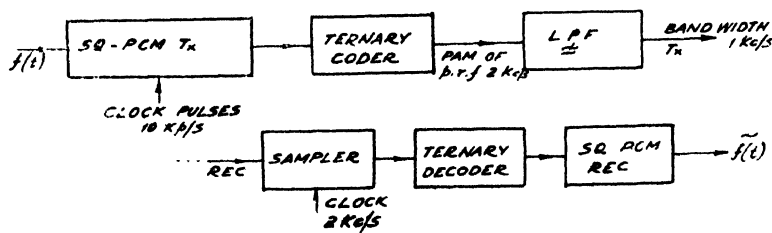


Fig. 13. Band-Compression by coding downwards.

intelligible speech may be obtained with as low as 10,000 pulses only. The groups of 5 (or more) pulses may be converted with a ternary code to PAM pulses of much lower p.r.f., as shown in Fig. 13. The filtered wave will then have a bandwidth of 1 Kc/s only for the original 10 Kc/s p.r.f. of the SQ-PCM. In the receiver if the complementary operations are performed, then the message signal would be of much better quality than that obtained by other methods for the same transmission bandwidth. Alternatively the multiplexed Binary PCM or SQ-PCM pulses may be grouped together to form the PAM pulses and transmitted in a reduced video bandwidth. The penalty for this compression by coding downwards would be that a  $S/N$  ratio of 40 db in the transmission medium would be required for the 100-level PAM pulses and 60 db for the 1000-level pulses.

#### DISCUSSION

Most of the schemes shown above aim at reducing the channel capacity or the required bandwidth for efficient transmission of signals. What remains to be decided is an appropriate error criterion so that  $\widetilde{f(t)}$  is a good approximation of  $f(t)$ . This, however, is an open question as the different error criteria, e.g., the r.m.s. error, average error, average differential error etc., are not equally applicable to all situations. If one aims at a good representation of the waveform only, then perhaps the r.m.s. error along with the average error in the derivative of  $\widetilde{f(t)}$  will indicate the goodness of the fit. If however, the information content of  $f(t)$  is to be approximated, then the cross-correlation between  $f(t)$  and  $\widetilde{f(t)}$  may give a better indication of the fitness. In speech synthesis, the integrated error in the spectrum along with the subjective intelligibility tests is considered sufficient.

In the existing narrow-band coding systems like Vocoders, a compression ratio of 10 : 1 or more has been obtained. It is estimated that for articulate speech, the channel capacity could be reduced from 60,000 bits/sec. to about 2000 bits/sec. only. But the necessary technique will surely be very much complicated. In television also, it may be possible to obtain a compression ratio of 20 : 1 as suggested by Gabor (1959), where the compression by "Contour interpolation" would give a factor of 4 to 8 and the equalization of information rate would provide a further factor of 3 to 4. In these systems, the effects of the transmission impairments like frequency and phase distortions, noise and nonlinearities in the transmission path, has not yet been fully determined. But it is expected that with the removal of redundant information in the signal, it will become more susceptible to the external distortion and noise. It is characteristic of the redundant signals, like speech, that they are immune to quite a lot of imperfections in their transmission and instrumentation; and some of these noise-resistant properties have to be sacrificed to gain the reduced transmission bandwidth.

In the methods discussed in earlier sections, only moderate saving in channel capacity is expected. Among the band compression schemes for speech, the sampl-

ing in the time domain or in the  $t-w$  plane would generally give a compression ratio of 3 : 1, while the sampling in the frequency domain may give a ratio of 5 : 1. The adaptive filter would similarly give a compression ratio of 5 : 1 or more, but the technique of coding downwards for a digitalized signal would give ratios higher than 3 : 1 depending upon the perfection obtained in the system instrumentation. In the SQ-PCM proposed here, it has been experimentally determined that for an acceptable speech quality, 20,000 pulses/sec. are sufficient, where as in PCM, a 4-digit code equivalent to a p.r.f. of 30 Kc/s and in  $\Delta$ -modulation, a p.r.f. of 40 Kc/s would be required. For a better  $S/N$  ratio, say, 30db approximately, SQ-PCM requires a p.r.f. of 30 Kc/s. but PCM requires a 5 unit code equivalent to 40 Kc/s and  $\Delta$ -modulation requires a p.r.f. of 50 Kc/s. Thus in these methods, some amount of compression and gain in channel capacity has no doubt been obtained; and this could be achieved with minimum complexity in instrumentation so that they may have wider application. Even this, if practically realized, would amount to more useful utilization of our existing transmission networks and systems.

#### ACKNOWLEDGMENT

The author wishes to thank Mr. S. K. Mullick and Mr. M. N. Faruqui for many helpful discussions and for working on some of these schemes. He also records his thanks to Prof. H. Rakshit, D.Sc., F.N.L., for his kind interest in the work.

#### REFERENCES

- Bell, D. A., 1953, "Information Theory", Pitman and Sons.  
Das, J., 1961, *Electronic Technology*, **38**, 298.  
David, E. E. Jr., 1956, *Trans. Inst. Radio Engrs.*, CT-3, 232.  
Dudley, H., 1955, *Jour. Audio Engg.*, **3**, 170.  
Gabor, D., 1959, *del Nuovo Cimento*, **13**, 467.  
Goodall, W. M., 1947, *Bell Sys. Tech. Jour.*, **26**, 395.  
Guillemin, E. A., 1953, *Proc. Nat. Electronics Conf. America*, **9**, 513.  
Huggins, W. H., 1956, *Trans. Inst. Radio Engrs.* CT-3, 210.  
Lawrence, W., 1953, "Communication Theory", Butterworths.  
Lerner, R. M., 1959, *Trans. Inst. Radio Engrs.*, CT-6, 197.  
Licklider, J. C. R. and Pollack, I., 1948, *Jour. Acoust. Soc. America*, **20**, 42.  
Miller, G. A. and Licklider, J. C. R., 1950, *Jour. Acoust. Soc. America*, **22**, 167.  
Schouten, J. F. et al, 1952, *Philips Tech. Rev.*, **13**, 237.  
Shannon, C. E., 1948, *Bell Sys., Tech. Jour.*, **27**, 397.  
Subrahmanyam, D. L. and Peterson, G. E., 1959, *Trans. Inst. Radio Engrs.*, AU-7, 148.  
Truxal, J. G., 1954, *Trans. Inst. Radio Engrs.*, CT-1, 49.  
Tustin, A., 1947, *Jour. Inst. Elec. Engrs.* **94** pt. 11-A, 130.

# ON THE DETERMINATION OF DISTORTION IN NUCLEAR EMULSIONS

PREM K. ADITYA

(Received December 3, 1963)

INDIAN INSTITUTE OF TECHNOLOGY, NEW DELHI-16, INDIA

**ABSTRACT.** A method is described by which extensive distortion present in emulsions can be measured and its influence on multiple Coulomb scattering measurements eliminated.

## INTRODUCTION

Nuclear emulsions have been known to have distortion, the presence of which severely affects the track contours. Distortion is understood to result from a shear between successive layers of emulsion which is produced by strain created during the processing schedule. Emulsions processed by different methods have been found to have different level and type of distortion.

The first quantitative estimate had been made by Cosyns and Vanderhaeghe (1950). In their method use is made of very steep tracks which acquire a C or S shape as a result of distortion. An elegant method for determination of distortion has been described by Major (1952) and later elaborated by Apostolakis and Major (1957).

The methods enumerated above have been widely used and give a fair indication on the level of distortion as it would affect the shape of tracks limited to a few mm length which is the situation in cosmic-ray exposed plates. With the advent of the machine-accelerated particles tracks of upto a few cm length, and confined to rather a single plane in emulsion, have been obtained. The distortion present in this case has been found to be of an extensive and different nature, (Aditya, 1962). The source of a considerable part of this distortion has been traced to another, namely the flexibility of the pellicle. The corresponding distortion is complicated and cannot be obtained by the methods known earlier.

In the earlier work (Aditya, 1962) the graphical plot method had been used to obtain distortion contours. The principle of the method is illustrated in Fig. 1. It appeared on further analysis that the method could be subjective in so far as the individual judgement on alignment and presence of large angle scatters has to be taken into account. In the present note we describe another method which is not subjective and gives the contour of distortion. The influence of this distortion, as on multiple Coulomb scattering measurements, can be easily taken care of, the procedure for which is described



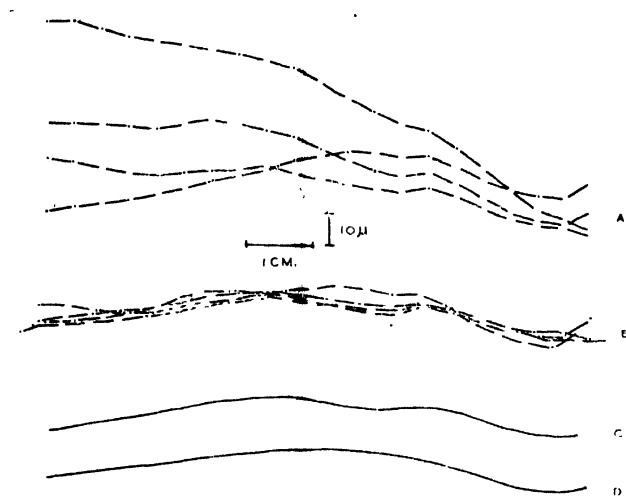


Fig. 1. Schematic explanation for the "graphic-plot" method. Four close tracks, as at (A), are superimposed, (B), from which the common contour (C), is extracted. An over-simplified version, as at (D), could possibly be derived from (C).

### THE METHOD

Coordinate measurements for a large number of close tracks are made and second differences,  $D$ , taking care of the sign formed, as is conventional. These

TABLE I

	Different tracks				Algebraic mean of rows
Different values along g each track.	$a_1$	$b_1$	$k_1$	$n_1$	$R_1$
	$a_2$	$b_2$	$k_2$	$n_2$	$R_2$
	$a_3$	$b_3$	$k_3$	$n_3$	
	$\vdots$	$\vdots$	$\vdots$	$\vdots$	
	$a_j$	$b_j$	$k_j$	$n_j$	$R_j$
	$\vdots$	$\vdots$	$\vdots$	$\vdots$	
	$a_x$	$b_x$	$k_x$	$n_x$	$R_x$
Algebraic mean of columns	$C_a$	$C_b$	$C_k$	$C_n$	

are entered in a table, as shown in Table I.  $a, b, \dots k, \dots n$ , refer to  $n$  close tracks, whereas  $1, 2, \dots j \dots x$ , refer to the  $x$ ,  $D$ -values on each track.  $x$  is evidently equal to  $(L/t - 1)$  where  $L$  is the length of each track and  $t$  is the cell length. For reasonable results  $x$  and  $n$  should be about 20, each.

If the values  $D$  were entirely true scattering, the magnitude and sign of the terms would be random so that the algebraic sum of both rows or columns should be zero. However, if all the tracks have some common contour of distortion, the magnitude of sagitta due to which is larger than the true sagitta, the algebraic sum of both the rows and columns will not be zero. The magnitude of the algebraic mean,  $R$ , along the row would be a direct function of the magnitude of correlation and the sign will indicate how the shape varies. The  $R$  values could thus vary rapidly both in magnitude and sign. Moreover, the algebraic sum,  $C$ , of the columns will have the same trend for all correlated tracks and would be zero if the distortion contour was equally distributed around a linear average, such as for an  $S$ -shape distortion of equal sagitta in the two halves or for a complicated contour. It would not be zero for a  $C$ -shaped distortion, for example. It is evident that the algebraic mean of the rows is the main quantity of interest.

The distortion contour can be obtained from the algebraic mean of the rows,  $R_1, R_2, \dots R_j \dots R_x$  by back integration, and twice, since this procedure is the reverse of the forming of second differences.\* A point need be made here of the influence of large angle scatters on the tracks. The presence of a large angle scatters will affect one or two values of  $D$ , and can be detected by subtracting

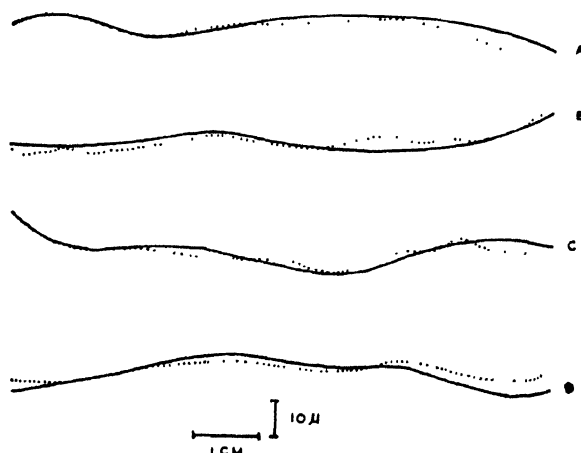


Fig. 2. Distortion contours of four samples as obtained by two methods : Graphical-plot method (solid line) and the method of Algebraic-mean (dotted line).

\* P. M. Sood, Chandigarh (private communication) has intimated that such a procedure had been suggested to him also by E. Dahl-Jensen, Copenhagen (private communication).

the algebraic mean from such suspected regions of scatter. A cut at the conventional 4 times the expected scattering sagitta will remove the large angle scatters. A modified algebraic mean may be found through successive steps, if required.

Some of the distortion contours (dotted lines) obtained by the method described above and those by the graphical-plot method (full lines) are shown in Fig. 2. The measurements had been made in  $600\mu$  (4.5 emulsions exposed to 27 GeV protons. Excellent agreement is found between the two methods. The contours are seen to be varying continuously in direction and magnitude.

#### ELIMINATION OF THE INFLUENCE OF DISTORTION

It is evident that the true scattering sagitta can be obtained by point to point subtraction of the distortion contour from the track coordinates. This procedure is not essential unless one is keen to look at the contour of distortion itself, because the algebraic mean along a row (corrected for large angle scatters) subtracted from the  $D$  values in the corresponding row directly gives the second differences for true scattering, perhaps with a little more noise.

In an earlier work, (Aditya *et al.* 1961, 1963) for samples having very large spurious scattering, the algebraic mean along the rows was found to be of very large magnitude and gradually changing sign. On the basis of the results of a later work (Aditya 1962), this behaviour can be attributed to presence of large

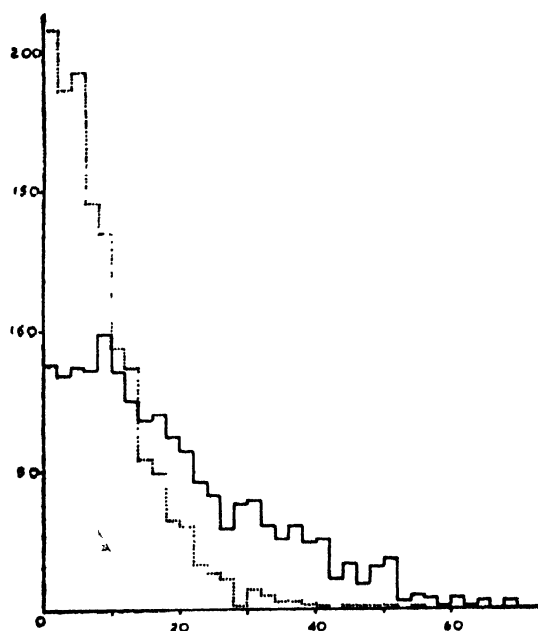


**Fig. 3.** Frequency histograms for 1285 scatters of 4 mm cell length over 27 GeV protons. Full line : observed data, excluding three scatters at 81, 83 and 95 respectively. Dotted line : corrected data, after distortion elimination.

distortion. We have found that by the process described above  $D_{observed}$  which was originally 2.5 times the  $D_{expected}$ , got reduced to 1.1 times, thereby eliminating almost the entire spurious scattering, see, for example, Fig. 3 for the observed and corrected frequency histograms. Whatever remains is due to the variation of distortion contour along depth. This, however, is not detrimental since this small spurious signal is expected to constitute a little increased noise level and can be quadratically subtracted.

In agreement with the findings of Aditya (1962) the magnitude and nature of spurious scattering has been recently shown (Aditya and Puri, (1964) to be a very close function of this distortion. Use of this method has also been made in another work (Aditya 1964) with great success.

#### ACKNOWLEDGMENT

This investigation forms part of a programme of work carried out with emulsions exposed at CERN. We express our thanks to the CERN Organisation for emulsion exposures.

For encouragement and laboratory facilities we are thankful to the Director of this Institute.

#### REFERENCES

- Aditya, P. K., Bhatia, V. S., and Sood, P. M., 1961.  
 "Minutes of Meeting on Nuclear Emulsion Technique with Special Reference to measurement of High Momenta," Bombay, pp. 34-47; and 1963, *Nuovo Cimento* **29**, 577.  
 Aditya, P. K., 1962, *Korpuskularphotographie*, IV, **513**.  
 Aditya, P. K., 1964, *Muovo Cimento* **31**, 477.  
 Aditya, P. K., and Puri R. K., 1964, *J. Sci. Inst.* (London), in Press.  
 Apostolakis, A. J., and Major, J. V., 1957, *Brit. J. Appl. Phys.*, **8**, **9**.  
 Cosyns, M., and Vanderhaeghe, G., 1950, *Bull. du Centre de Phys. Nucl.*, No. **15**.  
 Major, J. V., 1952, *Brit. J. Appl. Phys.*, **3**, 309.

# LIGAND FIELD THEORY OF MAGNETIC ANISOTROPY AND SUSCEPTIBILITY OF $\text{Fe}^{+2}$ TUTTON SALTS

B. D. BHATTACHARYYA\*

MAGNETISM DEPARTMENT, INDIAN ASSOCIATION FOR THE CULTIVATION OF SCIENCE,  
CALCUTTA-32.

(Received June 2, 1964)

**ABSTRACT.** The expression for the magnetic anisotropy and susceptibility of  $\text{Fe}^{2+}$  Tutton salts have been worked out on the basis of the more general molecular orbital method of Van-Vleck, Stevens and Bose et. al. Both the spin-orbit coupling coefficient and the effective orbital reduction factors along and perpendicular to the tetragonal axis of the complex are reduced anisotropically from their free ion value due to the anisotropic admixture of the central  $3d$ -charge cloud with the surrounding  $s$ - and  $p$ - charge clouds of the ligand oxygen atoms.

## INTRODUCTION

A detailed theory of the magnetic anisotropy and susceptibility of  $\text{Fe}^{2+}$  Tutton salts has been worked out on electrostatic approximations by Bose *et al* (1961). It is found that for the case of  $\text{Fe}(\text{NH}_4\text{SO}_4)_2 \cdot 6\text{H}_2\text{O}$  the value of the spin orbit coupling is reduced from its free ion value value of  $-103 \text{ cm}^{-1}$  by about 20%, owing to overlap of the central  $3d$  charge cloud with the surrounding  $s$ - and  $p$ - charge clouds of the ligand oxygen atoms. It appears therefore, more reasonable to apply to the problem, the more general method of molecular orbital approximations of Van-Vleck (1932), Stevens (1953) and Bose et. al (1960) so that the correct picture of the energy levels is obtained. It is also reasonable to assume that the overlap is anisotropic, the reduction in the spin-orbit coupling is also taken to be anisotropic in comparing the experimental results on  $\text{Fe}(\text{KSO}_4)_2 \cdot 6\text{H}_2\text{O}$  of Bose (1948) with our present theory. Since this salt is isomorphous to the ammonium salt (monoclinic, space group  $P2_1/a$ , 2 mols/cell) and no separate structural data is available, we thus assume for the present purpose, a tetragonal symmetry of the  $\text{Fe}^{2+} \cdot 6\text{H}_2\text{O}$  complex as in the other salt (Bose *et. al* 1961).

## MOLECULAR ORBITAL THEORY

The five fold orbital degeneracy of the ground state  $3d^6 \ ^5D$  of  $\text{Fe}^{2+}$  ion in the free state, is split up by the predominant cubic component of the crystal field into an orbital doublet  $E_{2g}$  and a triplet  $T_{2g}$ , the triplet lying lowest.

\* Dept. of Physics, St. Xavier's College, Calcutta and honorary research worker, Indian Association for the cultivation of Science, Calcutta-32.

For tetragonal symmetry of the ligand field, the wave functions of the lowest triplet are [Stevens (1953), Bose *et.al* (1961).]

$$\begin{aligned}
 | + > &= -\frac{1}{\sqrt{2}} [|yz> + i|zx>] \\
 | 0 > &= |xy> \quad \dots \quad (1) \\
 | - > &= \frac{1}{\sqrt{2}} [|yz> - i|zx>]
 \end{aligned}$$

where

$$\begin{aligned}
 |yz> &= N[|d, yz> + \lambda\{|p, z, 2> - |p, z, 5> + |p, y, 3> - |p, y, 6>\}] \\
 |xz> &= N[|d, xz> + \lambda\{|p, z, 1> - |p, z, 4> + |p, x, 3> - |p, x, 6>\}] \\
 |xy> &= N[|d, xy> + \lambda\{|p, y, 1> - |p, y, 4> + |p, x, 2> - |p, x, 5>\}] \quad (2)
 \end{aligned}$$

in which  $N$  is a normalizing factor and  $\lambda$  is a measure of the amount of mixture of the  $p$ -orbitals of the ligand oxygen with the central  $d$ -orbitals of the  $\text{Fe}^{2+}$  ion.

The appropriate Hamiltonian is

$$\mathbf{H} = \mathcal{H}_{\text{Tetragonal}} + u_z s_z + (u_x s_x + u_y s_y) \quad \dots \quad (3)$$

Since the effective orbital Lande splitting factors  $\alpha \simeq \alpha' \simeq 1$  very nearly for a  $D$ -state ion.

The effect of the tetragonal field is to split up the above triplet [eqn. (1)] by an amount  $\Delta$  into a doublet  $| + >, | - >$  and a singlet  $| 0 >$ . It will be seen later in connection with fitting the theory with experimental data, that unless the doublet is taken to lie lowest, no fitting with reasonable values of the parameters is possible.

The spin-orbit interaction takes the form  $\Sigma(u_i)s_i$  where  $u_i$  i.e. ( $u_x, u_y, u_z$ ) transform like  $T_1$  octahedral group (Bose *et. al* (1960) then inclusive of covalency, the non-zero matrix elements for  $u_x, u_y, u_z$  are given by

$$\begin{aligned}
 \langle + | u_z | + > &= - \langle - | u_z | - > = -\zeta_1 \\
 \langle + | u_x | 0 > &= \langle 0 | u_x | - > = -(\sqrt{2})\zeta_1 \\
 \langle - | u_y | 0 > &= \langle 0 | u_y | + > = i(\sqrt{2})\zeta_1 \quad \dots \quad (4)
 \end{aligned}$$

where  $\zeta_1, \zeta_1$  are the anisotropically reduced spin-orbit coupling coefficients of  $\text{Fe}^{2+}$  ion under the ligand field of the complex (Bose *et. al.* 1960). Here  $z$  axis is taken along the tetragonal axis of the ion and  $x, y$  axes give after orthonormal set with the axis.

Introducing with the five-fold degeneracy of each of the threeorbital states we obtain a secular determinant of the 15th. order which breaks up into two

quadratics, two singlets and a cubic. The eigen values for the  $|0\rangle$ ,  $|\pm 2\rangle$  and  $|\pm 3\rangle$  states are given as

$$\begin{aligned}
 E_0 &= \frac{1}{2}[(\zeta_{||} + \Delta) - \{(\zeta_{||} - \Delta)^2 + 24\zeta_{\perp}\}^{\frac{1}{2}}] \\
 E'_0 &= \frac{1}{2}[(\zeta_{||} + \Delta) + \{(\zeta_{||} - \Delta)^2 + 24\zeta_{\perp}\}^{\frac{1}{2}}] \\
 E''_0 &= \zeta_{||} \\
 E_2 &= \frac{1}{2}[(\Delta - \zeta_{||}) - \{(\Delta + \zeta_{||})^2 + 8\zeta_{\perp}\}^{\frac{1}{2}}] \quad \dots \quad (5) \\
 E'_2 &= \frac{1}{2}[(\Delta - \zeta_{||}) + \{(\Delta + \zeta_{||})^2 + 8\zeta_{\perp}\}^{\frac{1}{2}}] \\
 E_3 &= -2\zeta_{||}
 \end{aligned}$$

and the eigen values for the  $|\pm 1\rangle$  states are given by the roots of the cubic

$$x^3 - (2 + \eta)x^2 + (2\eta - 5\rho^2)x + 6\rho^2 = 0 \quad \dots \quad (6)$$

where  $x = E_i / \zeta_{||}$ ,  $E_i$  being the energy in  $\text{cm}^{-1}$ ,  $\eta = \Delta / \zeta_{||}$ ,  $\rho = \zeta_{\perp} / \zeta_{||}$  and  $E_i = E_1$ ,  $E''_1$  and  $E'_1$  respectively;

The corresponding eigenstates are given by

$$\begin{aligned}
 \psi_1 &= a_1|+, 0\rangle + b_1|0, 1\rangle + c_1|-, 2\rangle \\
 \psi_{-1} &= a_1|-, 0\rangle + b_1|0, -1\rangle + c_1|+, -2\rangle \\
 \psi_0 &= a_0|+, -1\rangle + b_0|0, 0\rangle + c_0|-, 1\rangle \\
 \psi''_0 &= a''_0|+, -1\rangle + b''_0|0, 0\rangle + c''_0|-, 1\rangle \\
 \psi''_1 &= a''_1|+, 0\rangle + b''_1|0, 1\rangle + c''_1|-, 2\rangle \\
 \psi''_{-1} &= a''_1|-, 0\rangle + b''_1|0, 1\rangle + c''_1|+, -2\rangle \\
 \psi_2 &= a_2|+, 1\rangle + b_2|0, 2\rangle \\
 \psi_{-2} &= a_2|-, -1\rangle + b_2|0, -2\rangle \\
 \psi_3 &= |+, 2\rangle \quad \dots \quad (7) \\
 \psi_{-3} &= |-, -2\rangle \\
 \psi'_2 &= b_2|+, 1\rangle - a_2|0, 2\rangle \\
 \psi'_{-2} &= b_2|-, -1\rangle - a_2|0, -2\rangle \\
 \psi'_1 &= \alpha'_1|+, 0\rangle + b'_1|0, 1\rangle + c'_1|-, 2\rangle \\
 \psi'_{-1} &= \alpha'_1|-, 0\rangle + b'_1|0, -1\rangle + c'_1|+, -2\rangle \\
 \psi'_0 &= a'_0|+, -1\rangle + b'_0|0, 0\rangle + c'_0|-, 1\rangle
 \end{aligned}$$

where

$$c_1 = \left[ \frac{3(2\zeta_{||} - E_1)^2}{2E_1^2} + \frac{(2\zeta_{||} - E_1)^2}{2\zeta_{\perp}^2} + 1 \right]^{-\frac{1}{2}},$$

$$b_1 = \frac{(2\zeta_{||} - E_1)}{(\sqrt{2}) \zeta_{\perp}} \cdot c_1$$

and 
$$a_1 = - \frac{(\sqrt{3})\zeta_1}{E_1} \cdot b_1$$

For  $a_1'$ ,  $b_1'$  and  $c_1'$  we are to replace  $E_1$  by  $E_1'$ . Also to get  $a_1''$ ,  $b_1''$  and  $c_1''$  we are to replace  $E_1$  by  $E_1''$ .

Further, 
$$b_0 = \left[ \frac{6\zeta_1^2}{(\zeta_1 - E_0)^2} + 1 \right]^{-1}$$

$$a_0 = c_0 = \frac{(\sqrt{3})\zeta_1}{(\zeta_1 - E_0)} b_0$$

To get  $a_0'$ ,  $b_0'$  we replace  $E_0$  by  $E_0'$  and to get  $a_0''$ ,  $b_0''$  we must replace  $E_0$  by  $E_0''$ . And finally

$$b_2 = \left[ - \frac{2\zeta_1^2}{(\Delta - E_2)^2} + 1 \right]^{-1}$$

$$a_2 = \frac{(\sqrt{2})\zeta_1}{(\Delta - E_2)} b_2$$

Similarly to obtain  $a_2'$ ,  $b_2'$  we replace  $E_2$  by  $E_2'$

### 3. The $g$ -values

The susceptibility and the  $g$ -values are calculated by the usual method of first and second order perturbations with the magnetic field Hamiltonian

$$\mathcal{H} = \beta \cdot (\mathbf{L} + 2\mathbf{S}) \cdot \mathbf{H} \quad \dots \quad (8)$$

The non-zero matrix elements for  $L$  being

$$\begin{aligned} \langle + | L_z | + \rangle &= - \langle - | L_z | - \rangle = -k_{\parallel} \\ \langle + | L_x | 0 \rangle &= \langle 0 | L_x | - \rangle = -(\sqrt{2})k_{\perp} \\ \langle - | L_y | 0 \rangle &= \langle 0 | L_y | + \rangle = i(\sqrt{2})k_{\perp} \end{aligned}$$

Where  $k_{11}$  and  $k_{\perp}$  are the orbital reduction factors (Stevens 1953, Bose *et.al* 1960). along and perpendicular to the tetragonal axis of the complex.

Thus we have

$$\begin{aligned} g_{\parallel} &= 2[(c_1^2 - a_1^2)k_{\parallel} + 2b_1^2 + 4c_1^2], \\ g_{\perp} &= 0 \end{aligned}$$

and the principal  $gm$ -ionic susceptibilities  $K_i$  ( $i = \parallel$  or  $\perp$ ) are

$$\begin{aligned} K_{\parallel} = \frac{N\beta^2}{kT} \left[ \frac{1}{T} \left\{ G_{1z} E_1 + G_{1z} E_1'' \exp \left( \frac{E_1 - E_1''}{kT} \right) + G_{1z} E_2 \exp \left\{ \frac{E_1 - E_2}{kT} \right\} \right. \right. \\ \left. \left. + G_{1z} E_3 \exp \left( \frac{E_1 - E_3}{kT} \right) + G_{1z} E_2' \exp \left( \frac{E_1 - E_2'}{kT} \right) + G_{1z} E_1' \exp \left( \frac{E_1 - E_1'}{kT} \right) \right\} \right] \end{aligned}$$



$$\begin{aligned}
 & + \left\{ G_{2z}E_1 + G_{2z}E_0 \exp \left( \frac{E_1 - E_0}{kT} \right) + G_{2z}E_0'' \exp \left( \frac{E_1 - E_0''}{kT} \right) \right. \\
 & + G_{2z}E_1'' \exp \left( \frac{E_1 - E_1''}{kT} \right) + G_{2z}E_2 \exp \left( \frac{E_1 - E_2}{kT} \right) + G_{2z}E_2' \exp \left( \frac{E_1 - E_2'}{kT} \right) \\
 & \left. + G_{2z}E_1' \exp \left( \frac{E_1 - E_1'}{kT} \right) + G_{2z}E_0' \exp \left( \frac{E_1 - E_0'}{kT} \right) \right\} \dots \quad (9)
 \end{aligned}$$

where

$$G_{1z}E_1 = 2[(4 + k_{11})c_1^2 + 2b_1^2 - k_{11}a_1^2]^2$$

$$G_{1z}E_1'' = 2[(4 + k_{11})c_1''^2 + 2b_1''^2 - k_{11}a_1''^2]^2$$

$$G_{1z}E_2 = 2[(2 - k_{11})a_2^2 + 4b_2^2]^2$$

$$G_{1z}E_3 = 2[4 - k_{11}]^2$$

$$G_{1z}E_2' = 2[(2 - k_{11})b_2^2 + 4a_2^2]^2$$

$$G_{1z}E_1' = 2[4 + k_{11})c_1'^2 + 2b_1'^2 - k_{11}a_1'^2]^2$$

$$G_{2z}E_1 = Y_1^1 + Y_1^2$$

$$G_{2z}E_0 = Y_0^0$$

$$G_{2z}E_0'' = Y_0^0 + Y_0^1$$

$$G_{2z}E_1'' = -Y_1^2 + Y_1^3$$

$$G_{2z}E_2 = Y_2^2 = G_{2z}E_2'$$

$$G_{2z}E_1' = -Y_1^1 - Y_1^3$$

$$G_{2z}E_0' = -Y_0^1$$

$$Y_0^0 = \frac{2a_0^2(k_{11} + 2)^2}{E_0'' - E_0}$$

$$Y_0^1 = \frac{2a_0'^2(k_{11} + 2)^2}{E_0' - E_0''}$$

$$Y_1^1 = \frac{2[(4 + k_{11})c_1c_1' + 2b_1b_1' - k_{11}a_1a_1'']^2}{E_1' - E_1}$$

$$Y_1^2 = \frac{2[4 + k_{11})c_1c_1'' + 2b_1b_1'' - k_{11}a_1a_1'']^2}{E_1'' - E_1}$$

$$Y_1^3 = \frac{2[(4 + k_{11})c_1c_1'' + 2b_1b_1'' - k_{11}a_1'a_1'']^2}{E_1' - E_1''}$$

$$Y_2^2 = \frac{2(2 + k_{11})^2a_2^2b_2^2}{E_2' - E_2}$$

and

$$\begin{aligned}
 K_1 = \frac{2N\beta^2}{kW} & \left[ G_{2x}E_1 + G_{2x}E_0 \exp\left(\frac{E_1-E_0}{kT}\right) + G_{2x}E_0'' \exp\left(\frac{E_1-E_0''}{kT}\right) \right. \\
 & + G_{2x}E_1'' \exp\left(\frac{E_1-E_1''}{kT}\right) + G_{2x}E_2 \exp\left(\frac{E_1-E_2}{kT}\right) + G_{2x}E_3 \exp\left(\frac{E_1-E_3}{kT}\right) \\
 & \left. + G_{2x}E_2' \exp\left(\frac{E_1-E_2'}{kT}\right) + G_{2x}E_1' \exp\left(\frac{E_1-E_1'}{kT}\right) + G_{2x}E_0' \exp\left(\frac{E_1-E_0'}{kT}\right) \right] \\
 & \dots \quad (10)
 \end{aligned}$$

where

$$\begin{aligned}
 W = 2 & + \exp\left(\frac{E_1-E_0}{kT}\right) + \exp\left(\frac{E_1-E_0''}{kT}\right) + 2 \exp\left(\frac{E_1-E_1''}{kT}\right) + 2 \exp\left(\frac{E_1-E_2}{kT}\right) \\
 & + 2 \exp\left(\frac{E_1-E_3}{kT}\right) + 2 \exp\left(\frac{E_1-E_2'}{kT}\right) + 2 \exp\left(\frac{E_1-E_1'}{kT}\right) + \exp\left(\frac{E_1-E_0'}{kT}\right)
 \end{aligned}$$

and

$$\begin{aligned}
 G_{2x}E_1 &= \frac{2A^2}{E_0-E_1} + \frac{2A_1^2}{E_0''-E_1} + \frac{2A_2^2}{E_2-E_1} + \frac{2A_3^2}{E_2'-E_1} + \frac{2A_{14}^2}{E_0'-E_1} \\
 G_{2x}E_0 &= \frac{2A^2}{E_1-E_0} + \frac{2A_4^2}{E_1''-E_0} + \frac{2A_5^2}{E_1'-E_0} \\
 G_{2x}E_0'' &= \frac{2A_1^2}{E_1-E_0''} + \frac{2A_6^2}{E_1''-E_0''} + \frac{2A_7^2}{E_1'-E_0''} \\
 G_{2x}E_1'' &= \frac{2A_4^2}{E_0-E_1''} + \frac{2A_6^2}{E_0''-E_1''} + \frac{2A_8^2}{E_2-E_1''} + \frac{2A_9^2}{E_2'-E_1''} + \frac{2A_{15}^2}{E_0'-E_1''} \\
 G_{2x}E_2 &= \frac{2A_2^2}{E_1-E_2} + \frac{2A_8^2}{E_1''-E_2} + \frac{2A_{10}^2}{E_3-E_2} + \frac{2A_{11}^2}{E_1'-E_2} \\
 G_{2x}E_3 &= \frac{2A_{10}^2}{E_2-E_3} + \frac{2A_{12}^2}{E_2'-E_3} \\
 G_{2x}E_2' &= \frac{2A_3^2}{E_1-E_2'} + \frac{2A_9^2}{E_1''-E_2'} + \frac{2A_{12}^2}{E_3-E_2'} + \frac{2A_{13}^2}{E_1'-E_2'} \\
 G_{2x}E_1' &= \frac{2A_6^2}{E_0-E_1'} + \frac{2A_7^2}{E_0''-E_1'} + \frac{2A_{11}^2}{E_2-E_1'} + \frac{2A_{13}^2}{E_2'-E_1'} + \frac{2A_{16}^2}{E_0'-E_1'} \\
 G_{2x}E_0' &= \frac{2A_{14}^2}{E_1-E_0'} + \frac{2A_{15}^2}{E_1''-E_0'} + \frac{2A_{16}^2}{E_1'-E_0'}
 \end{aligned}$$

where

$$A = \sqrt{6}(a_0a_1 + b_0b_1) - \frac{k_1}{\sqrt{2}} (a_0b_1 + b_0a_1) + 2a_0c_1$$

$$A_1 = \sqrt{6}a_1a_0'' - \frac{k_1}{\sqrt{2}} b_1 - 2c_1a_0''$$

$$A_2 = \sqrt{6}a_1a_2 - \frac{k_1}{\sqrt{2}} (a_2b_1 + b_2c_1) + 2b_1b_2$$

$$A_3 = \sqrt{6}a_1b_2 - \frac{k_1}{\sqrt{2}} (b_1b_2 - a_2c_1) - 2a_2b_1$$

$$A_4 = \sqrt{6}(a_0a_1'' + b_0b_1'') - \frac{k_1}{\sqrt{2}} (a_0b_1'' + b_0a_0'') + 2a_0c_1''$$

$$A_5 = \sqrt{6}(a_0a_1' + b_0b_1') - \frac{k_1}{\sqrt{2}} (a_0b_1' + b_0a_1') + 2a_0c_1'$$

$$A_6 = \sqrt{6}a_0''a_1'' - \frac{k_1}{\sqrt{2}} b_1'' - 2a_0''c_1''$$

$$A_7 = \sqrt{6}a_0''a_1' - \frac{k_1}{\sqrt{2}} b_1' - 2a_0''c_1'$$

$$A_8 = \sqrt{6}a_1''a_2 - \frac{k_1}{\sqrt{2}} (b_1''a_2 + b_2c_1'') + 2b_1''b_2$$

$$A_9 = \sqrt{6}a_1''b_2 - \frac{k_1}{\sqrt{2}} (b_1''b_2 - c_1''a_2) - 2b_1''a_2$$

$$A_{10} = 2a_0 - \frac{k_1}{\sqrt{2}} b_2$$

$$A_{11} = \sqrt{6}a_1'a_2 - \frac{k_1}{\sqrt{2}} (a_2b_1' + b_2c_1') + 2b_1'b_2$$

$$A_{12} = 2b_2 + \frac{k_1}{\sqrt{2}} a_2$$

$$A_{13} = \sqrt{6}a_1b_2 - \frac{k_1}{\sqrt{2}} (b_1'b_2 - a_2c_1') - 2b_1'a_2$$

$$A_{14} = \sqrt{6}(a_1a_0' + b_1'b_0') - \frac{k_1}{\sqrt{2}} (a_1b_0' + b_1a_0') + 2c_1a_0'$$

$$A_{15} = \sqrt{6}(a_1''a_0' + b_1''b_0') - \frac{k_1}{\sqrt{2}} (a_1''b_0' + b_1''a_0') + 2c_1''a_0'$$

$$A_{16} = \sqrt{6}(a_1'a_0' + b_1'b_0') - \frac{k_{\perp}}{\sqrt{2}}(a_1'a_0'b_0' + b_1'a_0') + 2c_1'a_0'$$

It is very reassuring that in the above formidable expressions quite a number of terms are negligible and several others having opposite signs cancel out each other in pairs, so that the final calculations are simplified. Nevertheless we have retained all the terms in the given expressions for the sake of completeness of the theoretical expressions.

#### EXPERIMENTAL DETAILS

The agreement of the theoretical anisotropy and susceptibility values with the experimental values of Bose (1948) on  $\text{Fe}(\text{KSO}_4)_2 \cdot 6\text{H}_2\text{O}$  is quite good as can be seen from Table I.

The values of the parameters  $\Delta$ ,  $\zeta_{\parallel}$ ,  $\zeta_{\perp}$ ,  $k_{\parallel}$  and  $k_{\perp}$  are obtained by trial and error to get the best fit. Our fitting with the experimental results is perfectly unique because even if we try to set the data only at two temperatures we have three unknown parameters  $\Delta$ ,  $\zeta_{\parallel}$  and  $\zeta_{\perp}$  whose values can be decided uniquely by fitting with the four observables viz. two mean susceptibilities and two anisotropy values at these two temperatures. However, in view of a large number of earlier experimental findings (Bose (Bose *et al.* 1960, 1961, 1961, 1963, 1964) it is very unlikely that  $\Delta$  should be constant. If we take temperature variation of  $\Delta$  into account we can get an unique fitting comparing the experimental results only at three different temperatures because in that case we have altogether five unknown parameters three  $\Delta$ 's,  $\zeta_{\parallel}$  and  $\zeta_{\perp}$  and six observables viz. three mean susceptibility values and three anisotropy values at the three temperatures under consideration.

In the case of  $\text{Fe}(\text{NH}_4\text{SO}_4)_2 \cdot 6\text{H}_2\text{O}$  the tetragonal field coefficient  $\Delta$  increases with temperature from a value of  $270 \text{ cm}^{-1}$  at  $20^\circ\text{K}$  to  $650 \text{ cm}^{-1}$  at  $300^\circ\text{K}$ . In the case of  $\text{Fe}(\text{KSO}_4)_2 \cdot 6\text{H}_2\text{O}$   $\Delta$  changes from  $240 \text{ cm}^{-1}$  at  $90^\circ\text{K}$  to  $640 \text{ cm}^{-1}$  at  $300^\circ\text{K}$ . Thus we see that the order of the anisotropic field and also their variations with temperature are almost the same in the two cases.

In the case of  $\text{Fe}(\text{NH}_4\text{SO}_4)_2 \cdot 6\text{H}_2\text{O}$  the spin-orbit coupling coefficient has been decreased by about 23% from its free ion value of  $-103 \text{ cm}^{-1}$  (Owen 1955, Bose *et.al* 1961). In the case of  $\text{Fe}(\text{KSO}_4)_2 \cdot 6\text{H}_2\text{O}$  the spin-orbit coupling coefficients are  $\zeta_{\parallel} = -80 \text{ cm}^{-1}$ ,  $\zeta_{\perp} = -88 \text{ cm}^{-1}$  instead of the free ion value of  $-103 \text{ cm}^{-1}$ . This indicates again almost the same overlap between the  $3d \text{ Fe}^{2+}$  and  $s$ - and  $p$ -  $\text{O}^{2-}$  charge clouds, except that the overlap here has been taken as anisotropic.

If the tetragonal field coefficient  $\Delta$  is negative, we have a singlet lying lowest after the tetragonal field and after introducing the spin-orbit coupling one magnetic singlet comes lowest with a doublet close to it. In this case  $K_{\perp}$  becomes greater than  $K_{\parallel}$  whereas when  $\Delta$  is positive we have a doublet ( $m = \pm 1$ ) lying lowest,

$K_{11}$  is necessarily greater than  $K_{\perp}$ . For the assumption that  $K_{\perp} > K_{11}$  i.e., for  $\Delta$  negative we could not fit the susceptibility and anisotropy both simultaneously for any reasonable values of the parameters. Hence we fit with our experimental results considering  $\Delta$  to be positive.

In the case of  $\text{Fe}(\text{NH}_4\text{SO}_4)_2 \cdot 6\text{H}_2\text{O}$  we have for  $\Delta = 270 \text{ cm}^{-1}$   $g_{11} = 8.989$ ,  $g_{11} = 0$ . In the case of the potassium salt  $g_{11} = 8.48$ ,  $g_{\perp} + 1 = 0$ ,  $\Delta = 240 \text{ cm}^{-1}$  which appear to agree well with the  $g$ -values given by Tinkham (1956) for  $\text{FeF}_2$  in  $\text{ZnF}_2$  at  $20^\circ\text{K}$ . Since the crystalline field in  $\text{FeF}_2$  has been found to be truly orthorhombic and also must be appreciably different in magnitude from that in Tutton salts owing to the difference in structure, the agreement is perhaps fortuitous, but nevertheless indicates that the order of magnitudes are comparable within the limits of approximation involved.

TABLE I

$\text{Fe}(\text{KSO}_4)_2 \cdot 6\text{H}_2\text{O}$				
		$k_{\parallel} = 0.95$	$\zeta_{\parallel} = -80 \text{ cm}^{-1}$	
		$k_{\perp} = 0.80$	$\zeta_{\perp} = -88 \text{ cm}^{-1}$	
temp $^\circ\text{K}$	$\text{cm}^{-1}$	$\rho^2$	$\rho^2 - \rho_1^2$	$g$ -values
300°K	640	28.57	10.31	
		(28.58)	(10.34)	—
220°K	416	28.13	12.87	
		(28.08)	(12.70)	—
90°K	240	26.00	22.10	
		(26.27)	(22.01)	—
				$g_{\parallel} = 8.48$
				(8.989)
				$g_{\perp} = 0$
				(0)

The values in the parenthesis in the 3rd. and 4th. column give the experimental results of Bose (1948). The  $g$ -values within parenthesis in the 5th. column are Tinkham's (1956) on  $\text{FeF}_2$  diluted with  $\text{ZnF}_2$  which have been discussed above.

#### ACKNOWLEDGMENT

The author is grateful to Prof. A. Bose for suggesting the problem and guidance in the work. He is also grateful to his colleagues Sri R. Chatterjee, D. Phil., U. S. Ghosh and Sri R. Rai. Finally, he is very thankful to the authorities of the St. Xavier's College, Calcutta, and Indian Association for the Cultivation of Science for permitting him to carry out the research work.

## REFERENCES

- Bose, A. 1918, *Ind. J. Physics* **22**, 484.  
Bose, A., Chakravarti, A. S. and Chatterjee, R. 1961, *Proc. Roy. Soc. A.* **216**, 207.  
Bose, A., Chakravarti, A. S. and Chatterjee, R., 1960, *Proc. Roy. Soc. A.* **255**, 145.  
Bleamy and Stevens 1953, *Reports on Prog. on Physics.* **16**, 108.  
Owen, J. 1955, *Proc. Roy. Soc. A.* **227**, 193.  
Stevens, K. W. H. 1953, *Proc. Roy. Soc. A.* **219**, 542.  
Tinkham, M., 1956, *Proc. Roy. Soc. A.* **23**, 535.  
Van-Vleck, J. H., 1932, *Phys. Rev.* **41**, 208.

ON THE THERMAL EXPANSION IN  $\text{Cu}_3\text{Au}$  ALLOY

B. N. DEY AND S. P. SEN GUPTA

INDIAN ASSOCIATION FOR THE CULTIVATION OF SCIENCE, CALCUTTA-32,

(Received, May 16, 1964)

**ABSTRACT.** Following Muto and Takagi's statistical treatment on  $\text{AB}_3$  type of binary ordered alloys, an expression for the thermal expansion coefficient  $\gamma$  as a function of long-range order parameter 's' has been obtained. For the alloy  $\text{Cu}_3\text{Au}$ , values of  $\gamma$  and compressibility  $\chi$  at temperatures 573°K, 623°K and 643°K have been evaluated and compared with the experimental data. The agreement is fairly satisfactory. The discontinuity of the thermal expansion at the transition temperature found experimentally has been also explained.

## INTRODUCTION

Order-disorder phenomena in binary alloy systems belong to the class of 'co-operative' phenomena of considerable intrinsic interest. Numerous metal alloy systems have substitutional solid solutions which exhibit superlattice formation near simple stoichiometric concentrations (Nix and Shockley, 1938). The theoretical investigations of the order-disorder transition in substitutional binary alloys mainly deal with the AB type of superlattice due to mathematical simplicity. The theory of the stability of superlattices as a function of temperature, was successfully developed by Bragg and Williams (1934, 35) by introducing the long-range order parameter and a reasonable refinement of Bragg-Williams approximation was made by Kirkwood (1938) in the AB type of superlattice. Following Kirkwood's method of solution, Hovi (1955) first obtained an expression for the thermal expansion coefficient for the AB type of superlattice and explained the discontinuity of expansion at the transition temperature in  $\beta$ -CuZn. In the same year (1955), Muto and Takagi extended the theoretical treatment for the AB type of superlattice to the  $\text{AB}_3$  type in a straight forward way. In the present investigation, an expression for the thermal expansion coefficient (as a function of the long-range order parameter) in  $\text{AB}_3$  type of binary alloys has been derived from the free energy expression as obtained by Muto and Takagi and the temperature variation of thermal expansion and also of compressibility in partly ordered alloy  $\text{Cu}_3\text{Au}$  have been explained on its basis.

## THEORY

Let us consider an alloy system consisting of two types of atoms A and B with N lattice points of which  $F_A N$  are  $\alpha$ -sites and  $F_B N$  are  $\beta$ -sites (here  $F_A$  and  $F_B$  denote fractions of A atoms and B atoms respectively). It is assumed that

each  $\alpha$ -site has  $z$  neighbours all  $\beta$ -sites and each  $\beta$ -site has  $z$  neighbours, of which  $z F_A/F_B$  are  $\alpha$ -sites and  $z (F_B - F_A)/F_B$  are  $\beta$ -sites.

In the state of perfect order, all  $\alpha$ -sites are occupied by A-atoms and all  $\beta$ -sites by B atoms. In the state of complete disorder, every lattice sites will be occupied on the average by A atoms and B atoms in proportion to their number  $F_A : F_B$ . In the intermediate order-states, the average distribution can be completely described by the Bragg-Williams order parameter or long-range order 's' defined by :

$$s = \frac{r_\alpha - F_A}{1 - F_A} = \frac{r_\beta - F_B}{1 - F_B}$$

where  $r_{\alpha(\beta)}$  is the fraction of  $\alpha(\beta)$  sites occupied by A(B) atoms and 's' is unity for perfect order and zero for the disordered state.

For  $AB_3$  type of superlattices, with  $F_A = 1/4$  and  $F_B = 3/4$ , Muto and Takagi (1955) considering Bragg-Williams approximation obtained the following expression for the 'configurational free energy' from a generalised statistical treatment :

$$F(s) - F(0) = \frac{NKT}{16} \left[ (1+3s) \log(1+3s) + 6(1-s) \log(1-s) + (9+3s) \log \left( 1 + \frac{s}{3} \right) - \frac{zu}{kT} s^2 \right] \quad \dots (1)$$

where  $u$  = ordering energy =  $u_{AB} - (u_{AA} + u_{BB})/2$  and  $u > 0$  for the formation of superlattice structure.

$k$  = Boltzmann constant.

$T$  = Temperature in  $^{\circ}\text{K}$ .

Now, minimizing the free energy by the condition :

$$\frac{\partial F}{\partial s} = 0$$

we obtain from the equation (1) :

$$K = \frac{u}{2kT} = \frac{3}{4sz} \log \frac{(1+3s) \left( 1 + \frac{s}{3} \right)}{(1-s)^2} \quad \dots (2)$$

which gives equilibrium values of 's' at different temperatures  $T$ .

On simplification :

$$K = \frac{4}{z} - \frac{8}{3z} s + \frac{196}{27z} s^2 - \frac{400}{27z} s^3 + \dots \quad \dots (2a)$$



Differentiating equation (1) with respect to volume  $v$  and taking into account that  $\frac{\partial F}{\partial s} = 0$ , we obtain for pressure :

$$p = -\frac{NkTz}{8} s^2 \frac{\partial K}{\partial v} \quad (3)$$

where  $s = s(v, T)$  and  $K = K(v, T)$ .

Using thermodynamic relations, it now follows from the above equation (3)

$$\frac{\gamma}{\chi} = \left[ \frac{\partial p}{\partial T} \right]_v = -\frac{Nkz}{8} \left[ s^2 \frac{\partial K}{\partial v} + T \left\{ 2s \frac{\partial s}{\partial T} \frac{\partial K}{\partial v} + s^2 \frac{\partial^2 K}{\partial T \partial v} \right\} \right] \quad \dots \quad (4)$$

and

$$\frac{1}{\chi} = -v \left[ \frac{\partial p}{\partial v} \right]_T = -v \frac{NkzT}{8} \left[ 2s \frac{\partial s}{\partial v} \frac{\partial K}{\partial v} + s^2 \frac{\partial^2 K}{\partial v^2} \right]$$

where  $\gamma =$  Thermal expansion coefficient, and  $\chi =$  compressibility. (5)

Hence, the thermal expansion coefficient :

$$\gamma = -\frac{s \frac{\partial K}{\partial v} + 2T \frac{\partial s}{\partial T} \frac{\partial K}{\partial v} + sT \frac{\partial^2 K}{\partial T \partial v}}{2vT \frac{\partial s}{\partial v} \frac{\partial K}{\partial v} + svT \frac{\partial^2 K}{\partial v^2}} \quad (6)$$

#### COMPARISON WITH RESULTS

Let us now apply the theory to the case of face-centred cubic  $\text{Cu}_3\text{Au}$  superlattice for a quantitative comparison between theory and experiment.

##### (i) Thermal expansion coefficient at different temperatures

In order to evaluate the thermal expansion coefficient  $\gamma$  at different temperatures from the expression (6), the derivatives  $\frac{\partial s}{\partial T}$ ,  $\frac{\partial s}{\partial v}$ ,  $\frac{\partial K}{\partial v}$ ,  $\frac{\partial^2 K}{\partial T \partial v}$  and  $\frac{\partial^2 K}{\partial v^2}$  are to be obtained.

Since  $s = s(v, T)$  and also  $K = K(v, T)$ , we have the following relations :

$$\left( \frac{\partial s}{\partial T} \right)_p = \left[ \frac{\partial s}{\partial T} \right]_v + \left[ \frac{\partial s}{\partial v} \right]_T \left[ \frac{\partial v}{\partial T} \right]_p$$

or, 
$$\left[ \frac{\partial s}{\partial v} \right]_T = \left[ \frac{\partial T}{\partial v} \right]_p \left[ \left[ \frac{\partial s}{\partial T} \right]_p - \left[ \frac{\partial s}{\partial T} \right]_v \right]$$

and similarly,  $\left[ \frac{\partial K}{\partial v} \right]_T = \left[ \frac{\partial K}{\partial v} \right]_p - \left[ \frac{\partial K}{\partial s} \right]_v \left[ \frac{\partial s}{\partial T} \right]_v \left[ \frac{\partial T}{\partial v} \right]_p$

Hence, using the above relations and the x-ray data reported by Keating and Warren (1951) and Owen and Liu (1947) of long-range order parameters and lattice parameters at different temperatures for the alloy  $\text{Cu}_3\text{Au}$ , we compute

the values of  $\left[ \frac{\partial s}{\partial v} \right]_T$  and  $\left[ \frac{\partial K}{\partial v} \right]_T$ . For the higher derivative  $\frac{\partial^2 K}{\partial v^2}$ , we have to

make the approximation  $\frac{\partial}{\partial v} \left[ \left[ \frac{\partial K}{\partial v} \right]_T \right]_T \approx - \frac{\partial}{\partial v} \left[ \left[ \frac{\partial K}{\partial v} \right]_T \right]_p$  (neglecting the

higher order terms), since lack of suitable data does not permit us to obtain the exact derivative. The validity of this approximation is tested from the evaluation of the compressibility factor  $\chi$  from the expression (4) using the theoretically determined values of the expansion coefficient  $\gamma$ . The values of all the parameters of expression (6) are tabulated in Table I while the theoretical and experimental values of the expansion coefficient and compressibility are given in Table II. The experimental values of  $\chi$ , according to Siegel (1940), do not have high precision. It now appears from the observation of Table II that the present approximation is quite justified and the theory satisfactorily explains the temperature variation of the thermal expansion coefficient for the  $\text{Cu}_3\text{Au}$  superlattice. The temperature variation of compressibility reveals that there is a dependence of  $\chi$  on order.

TABLE I

Values of the parameters required for the evaluation of  $\gamma$

T°K	s	$\frac{v^{(1)}}{(\text{in } \text{\AA}^3)}$	$\frac{\partial s}{\partial T}$	$\frac{\partial s}{\partial v}$	$\frac{\partial K}{\partial v}$	$\frac{\partial^2 K}{\partial T \partial v}$	$\frac{\partial^2 K}{\partial v^2}$
573	0.765	53.28	-0.001819	0.2063	-0.3910	0.002000	-0.6636
623	0.647	53.46	-0.003353	0.1731	-0.2456	0.003143	-1.0220
643	0.568	53.53	-0.004392	0.1169	-0.1756	0.006255	-1.3160

(1) Owen and Liu (1947)

TABLE II

Theoretical and experimental values of  $\gamma$  and  $\chi$  at different temperatures

T°K	$\gamma$ theor. $\times 10^6$ (per °K)	$\gamma$ expt. $\times 10^6$ (per °K) <sup>1</sup>	$\chi$ theor. $\times 10^{11}$ (cm <sup>2</sup> /dyne)	$\chi$ expt. $\times 10^{11}$ (cm <sup>2</sup> /dyne) <sup>2</sup>
573	68.5	54.1	0.409	0.660
623	86.2	71.8	0.402	0.666
643	118.0	113.5	0.422	0.678

(1) Owen and Liu (1947)

(2) Siegel (1940)

## (ii) Thermal expansion coefficient at the 'Transition-temperature'

Since  $K = K(s)$  as seen from the equation (2), the expression (6) for the thermal expansion coefficient can also be written in the alternative form :

$$s \frac{\partial K}{\partial s} \frac{\partial s}{\partial v} + T \left[ 2 \frac{\partial s}{\partial T} \frac{\partial K}{\partial s} \frac{\partial s}{\partial v} + s \left[ \frac{\partial^2 K}{\partial s^2} \frac{\partial s}{\partial v} \frac{\partial s}{\partial T} + \frac{\partial K}{\partial s} \frac{\partial^2 s}{\partial v \partial T} \right] \right. \\ \left. + vT \left[ 2 \left[ \frac{\partial s}{\partial v} \right]^2 \frac{\partial K}{\partial s} + s \left\{ \frac{\partial^2 K}{\partial s^2} \left[ \frac{\partial s}{\partial v} \right]^2 + \frac{\partial K}{\partial s} \frac{\partial^2 s}{\partial v^2} \right\} \right] \right] \quad \dots \quad (6a)$$

Let us examine this case at the 'Transition Temperature'. Now, as the transition temperature is approached from lower temperatures ( $s \rightarrow 0$ ,  $T \rightarrow T_{c-0}$ ), it follows from (2a) :

$$\lim_{s \rightarrow 0} \frac{\partial K}{\partial s} \neq 0 \quad \text{and} \quad \lim_{s \rightarrow 0} \frac{\partial^2 K}{\partial s^2}$$

Again, from the nature of the theoretical curve as predicted by Muto and Takagi (1955) and from the x-ray measurements of long-range order on  $\text{Cu}_3\text{Au}$  (Keating and Warren), we find that :

$$\lim_{s \rightarrow 0} \frac{\partial s}{\partial T} = \infty$$

Also, from the experimental observations of Owen and Liu (1947), we may write :

$$\lim_{s \rightarrow 0} \frac{\partial s}{\partial v} = \text{finite, as it appears that volume is not discontinuous at } T_c.$$

With the assumption that the higher derivatives  $\frac{\partial^2 s}{\partial v^2}$  and  $\frac{\partial^2 s}{\partial v \partial T}$  remain finite when  $s \rightarrow 0$ , we obtain from the above expression (6a), considering all the conditions :

$\lim_{s \rightarrow 0} \gamma$  is not finite which suggests that the thermal expansion coefficient is discontinuous at the 'Transition Temperature'.

Now, from the dilatometric observations of Nix and MacNair (1941) on  $\text{Cu}_3\text{Au}$ , we find that the thermal expansion coefficient shows a sharp peak at the transition temperature. It is also found from x-ray measurements of Owen and Liu (1947) that the rate of expansion increases as the transition temperature is approached and the value of the coefficient immediately after the transformation is about half its value immediately before the transformation.

Thus, we may conclude that the theory based on Bragg-Williams approximation is in fair agreement with the experimental observations. But the theory suffers from the limitation that it is not possible to derive the values of expansion coefficient  $\gamma$  in the low temperature region where the order-parameter ' $s$ ' is almost

$$\left. \begin{aligned}
 G = -\cot 2\phi &= \frac{K_1 - K_2}{2L} = \frac{\omega_x^2}{2\omega_z(r - \beta')} \\
 K_1 &= 1 - \frac{\beta'^2 - r\beta' - \omega_x^2}{c'} r, \quad K_2 = 1 - \frac{r(\beta'^2 - r\beta')}{c'}, \quad L = \frac{r(r - \beta')\omega_z}{c'} \\
 c' &= \beta'(\beta'^2 - \omega^2) - r(\beta'^2 - \omega_x^2), \quad \omega_x = \omega \sin \theta, \quad \omega_z = \omega \cos \theta \\
 \beta' &= 1 - j \frac{\nu}{p}, \quad \omega = \frac{p\pi}{p}, \quad p_H = \frac{eH}{mc}, \quad r = \frac{p_0^2}{p^2} = \frac{4\pi Ne^2}{mp^2} \\
 \dot{V} &= \frac{dV}{du}, \quad \dot{W} = \frac{dW}{du}, \quad \dot{\phi} = \frac{d\rho/du}{1 + \rho^2}
 \end{aligned} \right\} \dots (7)$$

#### COMPLEX REFRACTIVE INDEX

The well-known Appleton-Hartree formula (1927, 1929) for the square of complex refractive index  $q$  is given by

$$q^2 = 1 - \frac{1}{(\alpha + j\beta) - \frac{\gamma_T^2}{2(1 + \alpha + j\beta)} \pm \sqrt{4(1 + \alpha + j\beta)^2 + \gamma_L^2}} \dots (8)$$

The upper positive sign before the radical in eq. (8) refers to the extraordinary mode and the lower negative sign to the ordinary mode.

The notations in (8) are :

$$\alpha = -p^2/p_0^2, \quad p_0^2 = 4\pi Ne^2/m, \quad \beta = p\nu/p_0^2$$

$$\gamma = pp_H/p_0^2, \quad p_H = eH/mc, \quad \gamma_L = \gamma \cos \theta, \quad \gamma_T = \gamma \sin \theta$$

where

$\nu$  = electron collisional frequency

$H$  = intensity of the earth's magnetic field

$e, m$  = charge and mass of an electron

$c$  = velocity of light in vacuum,

$p$  = angular frequency of the wave,

$N$  = electron number density

and  $\theta$  = angle between the direction of propagation of the radio-wave and the positive direction of the earth's magnetic field.

In terms of the U.R.S.I. notations, Eq. (8) corresponds to :

$$q^2 = 1 - \frac{X}{1 - jZ - \frac{Y_T^2}{2(1 - X - jZ)} \pm \sqrt{4(1 - X - jZ)^2 + Y_L^2}} \dots (8.1)$$

The notations in Eq. (8.1) are :

$$X = \frac{4\pi N e^2}{m\omega^2} \quad , \quad Y_{L,T} = \frac{eH_{L,T}}{\omega mc} \quad , \quad Z = \frac{v}{\omega}$$

The angular frequency  $\omega$  of radio-wave is the same as  $p$  in the old notation. Associating the *plus* sign before the radical in Eq. (8.1) with the ordinary mode and the *minus* sign with the *extraordinary* mode (Ratcliffe, 1962), it can be easily shown that the minus sign before the radical in Eq. (8) corresponds to the ordinary mode and the plus sign to the extraordinary mode, so that, following the old notations we get for the 0-mode :

$$q_0^2 = 1 + \frac{1}{\alpha + j\beta - \frac{\gamma_T^2}{2(1+\alpha+j\beta)} - \sqrt{\left[ \frac{\gamma_T^4}{4(1+\alpha+j\beta)^2} + \gamma_L^2 \right]}} \quad \dots \quad (8.2)$$

and for the X-mode :

$$q_x^2 = 1 + \frac{1}{\alpha + j\beta - \frac{\gamma_T^2}{2(1+\alpha+j\beta)} + \sqrt{\left[ \frac{\gamma_T^4}{4(1+\alpha+j\beta)^2} + \gamma_L^2 \right]}} \quad \dots \quad (8.3)$$

We next compare these two formulae (8.2), (8.3) with equations (4) and (5) deduced from the coupled wave-equations of Saha, Banerjee and Guha (1951). From (7) it can be easily shown :

$$G = \frac{\gamma_T^2}{2\gamma_L(1+\alpha+j\beta)} \quad \dots \quad (7.1)$$

Since  $\omega_z = \frac{p_H}{p} \cos \theta$ , we get :

$$\begin{aligned} \rho_1 \omega_z &= (G + \sqrt{1+G^2}) \frac{p_H \cos \theta}{p} \\ &= \frac{p_0^2}{p^2} \left[ \frac{\gamma_T^2}{2(1+\alpha+j\beta)} - \sqrt{\frac{\gamma_T^4}{4(1+\alpha+j\beta)^2} + \gamma_L^2} \right] \end{aligned}$$

Hence putting the value of  $\rho_1 \omega_z$  in Eq. (4), we have

$$q_0^2 = 1 + \frac{1}{\alpha + j\beta - \frac{\gamma_T^2}{2(1+\alpha+j\beta)} + \sqrt{\frac{\gamma_T^4}{4(1+\alpha+j\beta)^2} + \gamma_L^2}}$$

It is seen that the last expression for the square of complex refractive index agrees with Eq. (8.3). Similarly, it can be shown that Eq. (5) agrees with (8.2). Hence Eqs. (4) and (5) should be interchanged as follows :

$$q_x^2 = 1 - \frac{r}{\beta' + \rho_1 \omega_z}$$

and

$$q_0^2 = 1 - \frac{r}{\beta' + \rho_2 \omega_z}$$

### COUPLED WAVE-EQUATIONS AND PROPAGATION VECTORS

Saha *et al* (1951) deduced the coupled wave-equations (1) and (1.1) by starting from the following equations :

$$\frac{d^2 E_x}{du^2} + K_1 E_x - j L E_y = 0 \quad \dots \quad (9)$$

$$\frac{d^2 E_y}{du^2} + K_2 E_y + j L E_x = 0 \quad \dots \quad (9.1)$$

and putting :

$$\begin{pmatrix} E_x \\ j E_y \end{pmatrix} = \begin{pmatrix} \cos \phi & -\sin \phi \\ \sin \phi & \cos \phi \end{pmatrix} \begin{pmatrix} V \\ W \end{pmatrix} \quad \dots \quad (10)$$

Using Eqs. (9), (9.1) and (10), it can be easily shown :

$$\begin{aligned} V'' + [K_1 \cos^2 \phi + K_2 \sin^2 \phi - 2L \sin \phi \cos \phi] V \\ - [(K_1 - K_2) \sin \phi \cos \phi + L(\cos^2 \phi - \sin^2 \phi)] W = 0 \end{aligned} \quad \dots \quad (1.2)$$

$$\begin{aligned} W'' + [K_1 \sin^2 \phi + K_2 \cos^2 \phi + 2L \cos \phi \sin \phi] W \\ - [(K_1 - K_2) \sin \phi \cos \phi + L(\cos^2 \phi - \sin^2 \phi)] V = 0 \end{aligned} \quad \dots \quad (1.3)$$

where

$$V'' = \ddot{V} - 2\dot{\phi}\dot{W} - \ddot{\phi}W - \dot{\phi}^2 V \quad \dots \quad (11)$$

$$W'' = \ddot{W} + 2\dot{\phi}\dot{V} + \ddot{\phi}V - \dot{\phi}^2 W \quad \dots \quad (11.1)$$

The coefficients of the cross-terms in Eqs. (1.2) and (1.3) may be made to disappear by writing  $\tan \phi = G \pm 1 + G^2$  as shown by Saha *et al*. Hence there are two values of  $\tan \phi$  given by  $G + \sqrt{1 + G^2}$  and  $G - \sqrt{1 + G^2}$ .

Let us write :

$$\tan \phi_1 = G - \sqrt{1+G^2} = \rho_1 \quad \dots \quad (12)$$

$$\tan \phi_2 = G + \sqrt{1+G^2} = \rho_2 \quad \dots \quad (12.1)$$

We next rotate the co-ordinate system through a complex angle  $\phi_1 = \tan^{-1}\rho_1$ . The equations (1.2) and (1.3) are then reduced to

$$V''_1 + [K_1 \cos^2 \phi_1 + K_2 \sin^2 \phi_1 - 2L \sin \phi_1 \cos \phi_1] V_1 = 0 \quad \dots \quad (1.4)$$

$$W''_1 + [K_1 \sin^2 \phi_1 + K_2 \cos^2 \phi_1 + 2L \sin \phi_1 \cos \phi_1] W_1 = 0 \quad \dots \quad (1.5)$$

where

$$V''_1 = \ddot{V}_1 - 2\dot{\phi}_1 \dot{W}_1 - \ddot{\phi}_1 W_1 - \dot{\phi}_1^2 V_1 \quad \dots \quad (11.2)$$

$$W''_1 = \ddot{W}_1 + 2\dot{\phi}_1 \dot{V}_1 + \ddot{\phi}_1 V_1 - \dot{\phi}_1^2 W_1 \quad \dots \quad (11.3)$$

$$V_1 = E_x \cos \phi_1 + jE_y \sin \phi_1 \quad \dots \quad (2.1)$$

$$W_1 = -E_x \sin \phi_1 + jE_y \cos \phi_1 \quad \dots \quad (3.1)$$

If we rotate the co-ordinate system through a complex angle  $\phi_2 = \tan^{-1}\rho_2$  then the equations (1.2) and (1.3) are reduced to

$$V''_2 + [K_1 \cos^2 \phi_2 + K_2 \sin^2 \phi_2 - 2L \sin \phi_2 \cos \phi_2] V_2 = 0 \quad \dots \quad (1.6)$$

$$W''_2 + [K_1 \sin^2 \phi_2 + K_2 \cos^2 \phi_2 + 2L \sin \phi_2 \cos \phi_2] W_2 = 0 \quad \dots \quad (1.7)$$

where

$$V''_2 = \ddot{V}_2 - 2\dot{\phi}_2 \dot{W}_2 - \ddot{\phi}_2 W_2 - \dot{\phi}_2^2 V_2 \quad (11.4)$$

$$W''_2 = \ddot{W}_2 + 2\dot{\phi}_2 \dot{V}_2 + \ddot{\phi}_2 V_2 - \dot{\phi}_2^2 W_2 \quad \dots \quad (11.5)$$

$$V_2 = E_x \cos \phi_2 + jE_y \sin \phi_2 \quad \dots \quad (2.2)$$

$$W_2 = -E_x \sin \phi_2 + jE_y \cos \phi_2 \quad \dots \quad (3.2)$$

It is shown in the Appendix that the following relations hold good :

$$K_1 \cos^2 \phi_1 + K_2 \sin^2 \phi_1 - 2L \sin \phi_1 \cos \phi_1 = 1 - \frac{r}{\beta' + \rho_1 \omega_z} = q_x^2 \quad \dots \quad (4.1)$$

$$K_1 \cos^2 \phi_2 + K_2 \sin^2 \phi_2 - 2L \sin \phi_2 \cos \phi_2 = 1 - \frac{r}{\beta' + \rho_2 \omega_z} = q_0^2 \quad \dots \quad (5.1)$$

$$K_1 \sin^2 \phi_1 + K_2 \cos^2 \phi_1 + 2L \sin \phi_1 \cos \phi_1 = 1 - \frac{r}{\beta' + \rho_2 \omega_z} = q_0^2 \quad \dots \quad (5.2)$$

$$K_1 \sin^2 \phi_2 + K_2 \cos^2 \phi_2 + 2L \sin \phi_2 \cos \phi_2 = 1 - \frac{r}{\beta' + \rho_1 \omega_z} = q_x^2 \quad \dots \quad (4.2)$$

Hence equations (1.4) and (1.5) should be called the coupled wave-equations for the  $X$ - and  $0$ -modes respectively and can be written as :

$$\ddot{V}_1 + (q_x^2 - \dot{\phi}_1^2) V_1 - 2\dot{\phi}_1 \dot{W}_1 + \ddot{\phi}_1 W_1 \text{ (for the } X\text{-mode)} \quad \dots \quad (1.8)$$

$$\ddot{W}_1 + (q_0^2 - \dot{\phi}_2^2) W_1 - 2\dot{\phi}_1 \dot{V}_1 - \ddot{\phi}_1 V_1 \text{ (for the } 0\text{-mode)} \quad \dots \quad (1.9)$$

where,

$$V_1 = \frac{E_x + j\rho_1 E_y}{\sqrt{1 + \rho_1^2}} \text{ (for the } X\text{-mode)} \quad \dots \quad (2.3)$$

$$W_1 = \frac{-\rho_1 E_x + jE_y}{\sqrt{1 + \rho_1^2}} \text{ (for the } 0\text{-mode)} \quad \dots \quad (3.3)$$

Similarly Eqs. (1.6) and (1.7) can be rewritten as :

$$\ddot{V}_2 + (q_0^2 - \dot{\phi}_2^2) V_2 - 2\dot{\phi}_2 \dot{W}_2 + \ddot{\phi}_2 W_2 \text{ (for the } 0\text{-mode)} \quad \dots \quad (1.10)$$

$$\ddot{W}_2 + (q_x^2 - \dot{\phi}_2^2) W_2 - 2\dot{\phi}_2 \dot{V}_2 - \ddot{\phi}_2 V_2 \text{ (for the } X\text{-mode)} \quad \dots \quad (1.11)$$

where

$$V_2 = \frac{E_x + j\rho_2 E_y}{\sqrt{1 + \rho_2^2}} \text{ (for the } 0\text{-mode)} \quad \dots \quad (2.4)$$

$$W_2 = \frac{-\rho_2 E_x + jE_y}{\sqrt{1 + \rho_2^2}} \text{ (for the } X\text{-mode)} \quad \dots \quad (3.4)$$

It has been shown in the Appendix

$$W_1 = V_2, W_2 = -V_1, \dot{\phi}_1 = \dot{\phi}_2 = \dot{\phi} \text{ (say)} \quad \dots \quad (13)$$

Hence, using (13), the equations (1.8) (1.9), (1.10) and (1.11) can be combined into two coupled equations : -

$$\ddot{V}_x + (q_x^2 - \dot{\phi}^2) V_x = 2\dot{\phi} \dot{V}_0 + \ddot{\phi} V_0 \text{ (for the } X\text{-mode)} \quad \dots \quad (1.12)$$

$$\ddot{V}_0 + (q_0^2 - \dot{\phi}^2) V_0 = -2\dot{\phi} \dot{V}_x - \ddot{\phi} V_x \text{ (for the } 0\text{-mode)} \quad \dots \quad (1.13)$$

where,

$$V_x = V_1 = -W_2 = \frac{E_x^{(x)} + j\rho_1 E_y^{(x)}}{\sqrt{1 + \rho_1^2}} = \text{Propagation vector for the } X\text{-mode} \quad (2.5)$$



$$V_0 = V_2 = W_1 = \frac{E_x^{(0)} + j\rho_2 E_y^{(0)}}{\sqrt{1 + \rho_2^2}} = \text{Propagation vector for the 0-mode ...} \quad (3.5)$$

$$\dot{\phi}_1 = \frac{d\rho_1/du}{1 + \rho_1^2} = \frac{d\rho_2/du}{1 + \rho_2^2} = \dot{\phi}_2 = \dot{\phi}$$

$$q_x^2 = 1 - \frac{r}{\beta' + \rho_1 \omega_z}, \quad q_0^2 = 1 - \frac{r}{\beta' + \rho_2 \omega_z}$$

Thus it is evident that the equations (1) and (1.1) were *incorrectly* labelled as the coupled wave-equations for the 0-mode and the X-mode respectively. It is shown in the next section that the equations (1) and (1.1) lose all their significance, if they are called the coupled wave-equations for the 0- and X-modes respectively.

#### WAVE-POLARIZATION

We start from the relations :

$$\begin{aligned} D_x &= q^2 E_x \\ D_y &= q^2 E_y \end{aligned} \quad \dots \quad (14)$$

The following expressions for the displacement vector were deduced by Saha *et al* (1951).

$$\begin{aligned} D_x &= K_1 E_x - jL E_y \\ D_y &= K_2 E_y + jL E_x \end{aligned} \quad \dots \quad (15)$$

From (14) and (15)

$$\frac{E_x}{E_y} = \frac{K_2 - q^2 - jL}{q^2 - K_1 - jL} = \frac{q^2 - jL - K_2}{q^2 - K_1 + jL} \quad \dots \quad (16)$$

Hence from (16)

$$q^2 = \frac{(K_1 + K_2) + \sqrt{(K_1 + K_2)^2 - 4(K_1 K_2 - L^2)}}{2} \quad \dots \quad (17)$$

From (16) and (17)

$$\frac{E_y - E_x}{E_y + E_x} = \pm \frac{\sqrt{(K_2 - K_1)^2 + 4L^2}}{(K_2 - K_1) - 2jL} \quad \dots \quad (16.1)$$

Taking the positive sign of Ea. (16.1)

$$\frac{E_y - E_x}{E_y + E_x} = \sqrt{\frac{(K_2 - K_1) + 2jL}{(K_2 - K_1) - 2jL}} \quad \dots \quad (16.2)$$

Since  $G = (K_1 - K_2)/2L$  we get :

$$\frac{E_y - E_x}{E_y + E_x} = \sqrt{\frac{G-j}{G+j}} \quad \dots (16.3)$$

Putting  $G = A \cos \psi$ ,  $1 = A \sin \psi$  where  $A = \sqrt{1 + G^2}$  we get from (16.3)

$$\frac{E_x}{E_y} = \tanh j\psi/2 \quad \dots (16.4)$$

Since  $\tan \psi = \frac{1}{G} = -\tan 2\phi$ , we have

$$\frac{E_x}{E_y} = -j \tan \phi = -j\rho \quad \dots (16.5)$$

The same Eq. (16.5) can be deduced by using the negative sign of Eq.(16.1).

There are two different values of  $\rho$ , viz.  $\rho_1 = G - \sqrt{1 + G^2}$  and  $\rho_2 = G + \sqrt{1 + G^2}$  and we have

$$\frac{E_x}{E_y} = -j\rho_1 \quad \dots (16.6)$$

$$\frac{E_x}{E_y} = j\rho_2 \quad \dots (16.7)$$

Let us now compare these equations (16.6) and (16.7) with the well-known Appleton-Hartree formula (1927-29) for the wave polarization in order to associate eqs. (16.6) and (16.7) with the so-called  $\theta$ - and  $X$ - modes.

Using the right-handed co-ordinate system (Fig. 1) the Appleton-Hartree formula for the wave-polarization in terms of magnetic vector components can be written as :

$$\frac{H_z}{H_y} = \frac{j}{\gamma_L} \left[ -\frac{\gamma_T^2}{2(1+\alpha+j\beta)} \pm \sqrt{\frac{\gamma_T^4}{4(1+\alpha+j\beta)^2} + \gamma_L^2} \right] \quad \dots (18)$$

where the direction of propagation of the radio wave is along the  $X$ -axis. In Eqs. (18), (16.6) and (16.7) the sign of the charge has not been taken into consideration.

In deriving the equations (16.6) and (16.7) the co-ordinate system of Fig. 2 has been used. When eq. (18) is referred to the co-ordinate system of Fig. 2, we have :

$$\frac{H_x}{H_y} = -\frac{j}{\gamma_L} \left[ -\frac{\gamma_T^2}{2(1+\alpha+j\beta)} + \sqrt{\frac{\gamma_T^4}{4(1+\alpha+j\beta)^2} + \gamma_L^2} \right] \quad \dots (18.1)$$

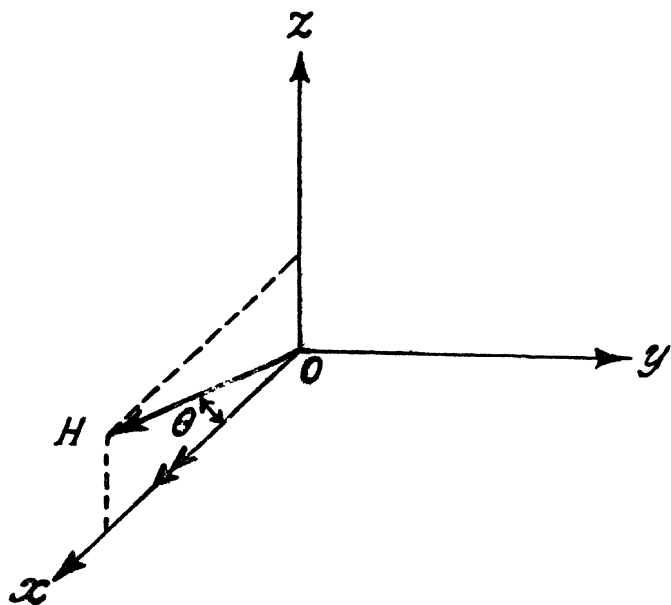


Fig. 1. Co-ordinate system (Saha *et al*).  
 $OH \rightarrow$  direction of the earth's magnetic field.  
 $OZ \rightarrow$  direction of the radio wave propagation.

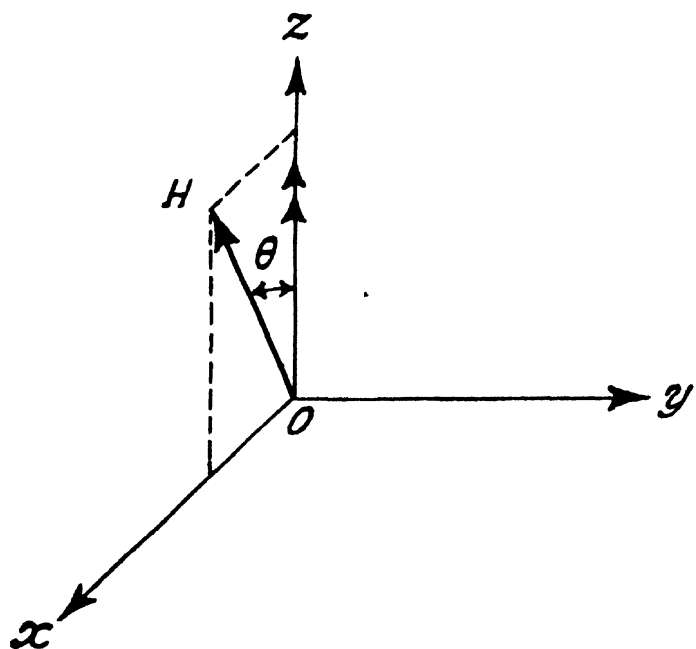


Fig. 2. Co-ordinate system (Appleton)  
 $OH \rightarrow$  direction of the earth's magnetic field.  
 $OX \rightarrow$  direction of the radio wave propagation.

where the direction of propagation of radio-wave is along  $Z$ -axis. Hence for the 0-mode :

$$\left( \frac{H_x}{H_y} \right)_0 = -\frac{j}{\gamma_L} \left[ -\frac{\gamma_T^2}{2(1+\alpha+j\beta)} - \sqrt{\frac{\gamma_T^4}{4(1+\alpha+j\beta)^2}} + \gamma_L^2 \right] \quad \dots \quad (18.2)$$

and for the  $X$ -mode :

$$\left( \frac{H_x}{H_y} \right)_x = -\frac{j}{\gamma_L} \left[ -\frac{\gamma_T^2}{2(1+\alpha+j\beta)} + \sqrt{\frac{\gamma_T^4}{4(1+\alpha+j\beta)^2}} + \gamma_L^2 \right] \quad \dots \quad (18.3)$$

Since  $E_x/E_y = -H_y/H_x$  we get from (18.2) and (18.3)

$$\left( \frac{E_x}{E_y} \right)_0 = -\frac{j}{\gamma_L} \left[ \frac{\gamma_T^2}{2(1+\alpha+j\beta)} - \sqrt{\frac{\gamma_T^4}{4(1+\alpha+j\beta)^2}} + \gamma_L^2 \right] \quad \dots \quad (18.4)$$

$$\left( \frac{E_x}{E_y} \right)_x = -\frac{j}{\gamma_L} \left[ \frac{\gamma_T^2}{2(1+\alpha+j\beta)} + \sqrt{\frac{\gamma_T^4}{4(1+\alpha+j\beta)^2}} + \gamma_L^2 \right] \quad \dots \quad (18.5)$$

From (7.1) and (12)

$$-j\rho_1 = -\frac{j}{\gamma_L} \left[ \frac{\gamma_T^2}{2(1+\alpha+j\beta)} - \sqrt{\frac{\gamma_T^4}{4(1+\alpha+j\beta)^2}} + \gamma_L^2 \right]$$

Since the above expression for  $-j\rho_1$  agrees with (18.4) we have for the 0-mode :

$$\left( \frac{E_x}{E_y} \right)_0 = -j\rho_1 \quad \dots \quad (16.8)$$

Similarly for the  $X$ -mode :

$$\left( \frac{E_x}{E_y} \right)_x = -j\rho_2 \quad \dots \quad (16.9)$$

In view of Eqs. (16.8) and (16.9) it is seen from (2) and (3) that  $V$  and  $W$  are reduced to zero; hence the equations (1) and (1.1) lose all their significance, if these wave equations (1) and (1.1) are associated with the 0- and  $X$ -mode respectively.

#### RELATION BETWEEN THE ELECTRIC AND MAGNETIC FIELDS

We start from the eqs. of propagation of the magnetic vector (1947) :

$$\begin{aligned} \frac{d^2 H_x}{du^2} + K_2 H_x - jLH_y &= 0 \\ \frac{d^2 H_y}{du^2} + K_1 H_y + jLH_x &= 0 \end{aligned} \quad \dots \quad (19)$$

and rotate the co-ordinate system (Fig. 2) through a complex angle  $\phi'$  and put

$$\begin{pmatrix} jH_y \\ H_x \end{pmatrix} = \begin{pmatrix} \cos \phi' & -\sin \phi' \\ \sin \phi' & \cos \phi' \end{pmatrix} \begin{pmatrix} V_H \\ W_H \end{pmatrix} \quad \dots \quad (20)$$

Using (19) and (20) it can be easily shown :

$$\begin{aligned} \ddot{V}_H + [K_1 \cos^2 \phi' + K_2 \sin^2 \phi' - 2L \sin \phi' \cos \phi' - \dot{\phi}'^2] V_H \\ - [L(\cos^2 \phi' - \sin^2 \phi') + (K_1 - K_2) \sin \phi' \cos \phi'] W_H = 2\dot{\phi}' \dot{W}_H + \ddot{\phi}' W_H \dots \quad (19.1) \end{aligned}$$

and

$$\begin{aligned} \ddot{W}_H + [K_1 \sin^2 \phi' + K_2 \cos^2 \phi' + 2L \sin \phi' \cos \phi' - \dot{\phi}'^2] W_H \\ - [(K_1 - K_2) \cos \phi' \sin \phi' + L(\cos^2 \phi' - \sin^2 \phi')] V_H = -2\dot{\phi}' \dot{V}_H - \ddot{\phi}' V_H \dots \quad (19.2) \end{aligned}$$

Putting  $\frac{K_1 - K_2}{2L} = G = -\cot 2\phi'$  Eqs. (19.1) and (19.2) are reduced to

$$\begin{aligned} \ddot{V}_H + [K_1 \cos^2 \phi' + K_2 \sin^2 \phi' - 2L \sin \phi' \cos \phi' - \dot{\phi}'^2] V_H \\ = 2\dot{\phi}' \dot{W}_H + \ddot{\phi}' W_H \dots \quad (19.3) \end{aligned}$$

and,

$$\begin{aligned} \ddot{W}_H + [K_1 \sin^2 \phi' + K_2 \cos^2 \phi' + 2L \sin \phi' \cos \phi' - \dot{\phi}'^2] W_H \\ = -2\dot{\phi}' \dot{V}_H - \ddot{\phi}' V_H \dots \quad (19.4) \end{aligned}$$

where,

$$V_H = jH_y \cos \phi' + H_x \sin \phi' \quad \dots \quad (2.6)$$

$$W_H = -jH_y \sin \phi' + H_x \cos \phi' \quad \dots \quad (3.6)$$

Putting  $\frac{K_1 - K_2}{2L} = G = -\cot 2\phi'$  Eqs (1.2) and (1.3) can be written as :

$$\ddot{V} + [K_1 \cos^2 \phi + K_2 \sin^2 \phi - 2L \sin \phi \cos \phi - \dot{\phi}^2] V = 2\dot{\phi} \dot{W} + \ddot{\phi} W \dots \quad (1.12)$$

and

$$\ddot{W} + [K_1 \sin^2 \phi + K_2 \cos^2 \phi + 2L \sin \phi \cos \phi - \dot{\phi}^2] W = -2\dot{\phi} \dot{V} - \ddot{\phi} V \dots \quad (1.13)$$

Since  $\phi = \phi'$ , we get from (1.12), (1.13) and (19.3), (19.4)

$$V = V_H \quad \text{and} \quad W = W_H$$

i.e.,

$$\begin{aligned} E_x \cos \phi + jH_y \sin \phi &= jH_y \cos \phi + H_x \sin \phi \\ -E_x \sin \phi + jE_y \cos \phi &= -jH_y \sin \phi + H_x \cos \phi \end{aligned} \quad \dots (21)$$

From (21)

$$\frac{H_x}{H_y} = -\frac{E_y}{E_x}$$

#### A P P E N D I X

$$\tan \phi_1 = \rho_1 = G - \sqrt{1+G^2} \quad \dots (i)$$

$$\dots \quad \cos 2\phi_1 = -\frac{\rho_1^2 - 1}{\rho_1^2 + 1} = -\frac{G}{\sqrt{1+G^2}} \quad \dots (ii)$$

$$\tan \phi_2 = \rho_2 = G + \sqrt{1+G^2} \quad \dots (iii)$$

$$\cos 2\phi_2 = -\frac{\rho_2^2 - 1}{\rho_2^2 + 1} = -\frac{G}{\sqrt{1+G^2}} \quad \dots (iv)$$

Now,

$$\begin{aligned} q^2 &= K_1 \cos^2 \phi_2 + K_2 \sin^2 \phi_2 - 2L \sin \phi_2 \cos \phi_2 \\ &= \frac{K_1 + K_2}{2} + \frac{1}{2} (K_1 - K_2) \cos 2\phi_2 - L \sin 2\phi_2 \end{aligned}$$

Since,  $(K_1 - K_2)/2L = G = -\cot 2\phi_2$

$$q^2 = \frac{K_1}{2} \left( 1 + \frac{1}{\cos 2\phi_2} \right) + \frac{K_2}{2} \left( 1 - \frac{1}{\cos 2\phi_2} \right)$$

Using (iv), (i) and (iii)

$$q^2 = \frac{K_1 \rho_1 + K_2 \rho_2}{2G} = \frac{K_1 \rho_1 + K_2 \rho_2}{\rho_1 + \rho_2}$$

Now putting

$$\left. \begin{aligned} K_1 &= 1 - A_1 \quad \text{where} \quad A_1 = \frac{r}{c'} [(\beta'^2 - r\beta') - \omega_x^2] \\ \text{and} \\ K_2 &= 1 - A_2 \quad \text{where} \quad A_2 = \frac{r}{c'} (\beta'^2 - r\beta') \end{aligned} \right] \quad \dots (v)$$

We get

$$q^2 = 1 - \frac{A_1 \rho_1 + A_2 \rho_2}{\rho_1 + \rho_2} \quad \dots \quad \text{(vi)}$$

We have also :

$$L = \frac{r}{C''} (\beta' - \beta'') \omega_z \quad \dots \quad \text{(vii)}$$

$$C'' = (\beta' - r)(\beta' + \rho_1 \omega_z)(\beta' + \rho_2 \omega_z) \quad \dots \quad \text{(viii)}$$

Using (v) and (vii)

$$\rho_1 + \rho_2 = 2G = \frac{K_1}{2L} \frac{K_2}{\omega_z} = \frac{r \omega_z^2}{L C''} = \frac{\omega_x^2}{\omega_z (r - \beta'')} \quad \dots \quad \text{(ix)}$$

Using (ix), (v), (i), (ii)

$$\frac{A_1 \rho_1 + A_2 \rho_2}{\rho_1 + \rho_2} = \frac{L}{\omega_z} (\beta' + \rho_1 \omega_z) \quad \dots \quad \text{(x)}$$

Using (x), (vii), (viii)

$$\frac{A_1 \rho_1 + A_2 \rho_2}{\rho_1 + \rho_2} = \frac{r}{\beta' + \rho_2 \omega_z}$$

Hence

$$\begin{aligned} q^2 &= K_1 \cos^2 \phi_2 + K_2 \sin^2 \phi_2 + 2L \sin \phi_2 \cos \phi_2 \\ &= 1 - \frac{r}{\beta' + \rho_2 \omega_z} = \text{square of the complex Refractive Index} \end{aligned}$$

for the O-mode.

This is the same as Eqn. (5.1).

Similarly Eqs. (4.1), (4.2) and (5.2) can be deduced.

From Eqs. (i) and (iii), we get ... (xi)

$$\phi_2 - \phi_1 = \pi/2$$

Hence using (xi), (3.1) and (2.2)

$$W_1 = V_2$$

and using (xi), (3.2) and (2.1)

$$W_2 = -V_1$$

Using (12) and (12.1)

$$\dot{\phi}_1 = \dot{\phi}_2$$

#### REFERENCES

- Appleton, E. v. 1927, U.R.S.I. paper (Washington).  
Hartree, E. R. 1929, *Proc. Camb. Phil. Soc.*, **25**, 47.  
Ratcliffe, J. A. 1962, *The Magneto-ionic Theory And Its Application To The Ionosphere* (Cambridge University Press), p.69.  
Saha, M. N., Banerjee, B. K. and Guha, U. C. 1947, *Ind. Jour. Phys.* **21**, 181.  
Saha, M. N., Banerjee, B. K. and Guha, U. C. 1951 *Proc. Nat. Inst. Sci. (India)*, **17**,



# ORIENTATIONS OF THE ORTHORHOMBIC $g$ -TENSORS AND THEIR MAGNITUDES IN $\text{Cu}(\text{KSO}_4)_2 \cdot 6\text{H}_2\text{O}$ AND $\text{Cu}(\text{NH}_4\text{SO}_4)_2 \cdot 6\text{H}_2\text{O}$ CRYSTALS

A. BOSE, U. S. GHOSH, R. N. BAGCHI\* AND A. K. PAL

DEPARTMENT OF MAGNETISM,

INDIAN ASSOCIATION FOR THE CULTIVATION OF SCIENCE,

JADAVPUR, CALCUTTA-32, INDIA

(Received July, 9, 1964)

**ABSTRACT.** The principal  $g$ -values of the magnetic complex  $\text{Cu}^{2+} \cdot 6\text{H}_2\text{O}$  and their orientations in the unit cells of the two copper tutton salts  $\text{CuK}_2(\text{SO}_4)_2 \cdot 6\text{H}_2\text{O}$  and  $\text{Cu}(\text{NH}_4)_2(\text{SO}_4)_2 \cdot 6\text{H}_2\text{O}$  have been determined at room temperature with the help of a 1.2 cm e.p.r. spectrometer. The measurement clearly shows an orthorhombic distortion of the paramagnetic complex in both the salts. A direct and convenient method has been devised to find the orthorhombic  $g$ -values and their orientations.

## INTRODUCTION

Paramagnetic resonance experiment in octahedral  $\text{Cu}^{2+}$  complexes has the special advantage of a very simple resonance condition given by  $h\nu = g\beta H$  where the symbols have their usual significance. In general, the  $g$ -values are different for different directions of the applied magnetic field except in the rare case of a complex having cubic symmetry. Earlier work of Bleaney, Penrose and Plumptre (1949) on the *undiluted* copper tutton salts at 90°K considered in the main a tetragonal symmetry of the  $\text{Cu}^{2+} \cdot 6\text{H}_2\text{O}$  complexes and tetragonal ionic  $g$ -values  $g_{\parallel}$  and  $g_{\perp}$  were determined, although some of their more detailed results indicated small but appreciable departure from tetragonality. In the case of  $\text{CuK}_2(\text{SO}_4)_2 \cdot 6\text{H}_2\text{O}$  they calculated indirectly by trial the ortho-rhombic  $g$ -values and their orientations at 90°K.

Bleaney *et al* used straight galvanometric detection of resonance absorption and a fluxmeter for the measurement of magnetic field. Moreover some of the planes in which they carried their measurements were not natural faces of the crystals, which were therefore experimentally difficult to orient horizontally in the magnetic field. There has been very little further work to determine accurately by the e.p.r. method the location of the principal ionic  $g$ -axes in crystals, though this should provide the most fruitful complement to X-ray structural work and magnetic susceptibility data. We have, therefore, developed a direct, convenient

\*Bangabasi College, Calcutta.

and elegant theoretical method of finding the ortho-rhombic  $g$ -values and their orientations working in simple planes of the crystals (all natural faces or planes normal to natural edges) with the help of a refined, low noise-to-signal ratio c.p.r. experimental arrangement.

#### EXPERIMENTAL ARRANGEMENTS

The experimental arrangements will be described briefly in this paper; the details have been discussed in a previous communication (Ghosh *et al.*, 1963).

The spectrometer is of transmission type and employs a 2K33 klystron as the source of microwaves (1.28 cm wave length). The  $H_{10}$  mode is excited in the rectangular  $K$ -band waveguide. Microwaves are fed into and out of a cylindrical cavity resonator excited in the dominant mode  $H_{11}$ , placed between the parallel pole faces of a strong electromagnet (Newport type) through two small coupling holes at the top face of the cavity. The transmitted microwave power is detected by silicon tungsten crystal IN 26.

Any natural face of a single crystal sample on which a measurement is to be taken is attached flat upon the end face of a microwave choke, co-axial with it and flush with the inner top surface, passing into the cavity through a hole at the top of it. For measurement in a plane normal to a natural edge, the edge is set normal to the face of the choke. By rotating the microwave choke from above the sample can be turned through any desired angle with respect to the magnetic field. The cavity is tuned by means of a shorting plunger at its bottom running in a fine screw thread and accurately operated from above with a gear arrangement, even when the cavity is surrounded by a cryostat.

The actual measurement is made with a phase sensitive detection device in which a  $d$ -c derivative response of the absorption signal is ultimately obtained in a centre-zero micro-ammeter ( $50\text{-}0\text{-}50\mu A$ ) as the static magnetic field, modulated sinusodially at 33 c/s and at a suitable low amplitude, slowly sweeps the absorption line. The position of an absorption peak is indicated when the centre-zero micro-ammeter needle just attains the null position after reaching one extremity as we slowly increase the static field. In this condition of the magnetic field the frequency of a transitron oscillator (Knoeble and Hahn; 1948) is adjusted to show proton resonance signal in one of the two beams of a double beam Cossor 1049, oscilloscope, the proton probe being placed very near the cavity in the central region of the pole gap. The second beam of the C.R.O. is utilized in detecting the narrow paramagnetic resonance signal of a standard sample of the free radical D.P.P.H placed at the centre of the tuning plunger of the cavity. Differences in the magnetic field for the small differences in position in these cases are found to be inappreciable. The  $g$ -value is obtained from the relation

$$g = g_D \frac{v_N'}{v_N}$$

where  $g_D$  is the  $g$ -value for D.P.P.H ( $g_D = 2.0036$ ) and  $\nu_N'$  and  $\nu_A$  are the radio frequencies at which proton resonance occurs in the magnetic fields corresponding to the e.p.r signals of D.P.P.H and the experimental sample respectively. These proton resonance frequencies are measured with the help of an accurate frequency meter having crystal check points, Type 3010, Funkwerk Erfurt.

#### THEORY OF THE METHOD OF LOCATING AND MEASURING PRINCIPAL IONIC $g$ -VALUES

Each of the  $N$  identical but nonparallel magnetic complexes in the unit cell of the crystal, will in general, give its own separate resonance line. It may easily be shown that if  $G_1$ ,  $G_2$  and  $G_3$  be the principal  $g$ -values along the three orthorhombic symmetry axes of an ion the spectroscopic splitting factor  $g$ , when the field is applied in a general direction whose direction cosines relative to  $G_1$ ,  $G_2$ ,  $G_3$  axes are  $l$ ,  $m$  and  $n$  respectively, is given by

$$g^2 = G_1^2 l^2 + G_2^2 m^2 + G_3^2 n^2 \quad \dots (1)$$

From the X-ray structural analysis (Hoffmann, 1931) the Tutton salts (belonging to monoclinic class, space group  $P2/m$ ) are known to contain two crystallographically equivalent but magnetically inequivalent (i.e. nonparallel) ions in the unit cell, orientation of one being derived from that of the other by reflection in the  $a-c$  (010) plane. This is corroborated by the paramagnetic resonance experiment (Bleaney *et al*, loc. cit) which shows in general two absorption signals corresponding to the two ions, for a given direction of the applied magnetic field, the separation of the signals depending upon relative orientations of the ions with respect to the magnetic field. Thus, the  $g^2$ -ellipsoids given by relation (1) for the two ions are oriented arbitrarily with respect to each other, consistent with the symmetry of the unit cell.

Calling the  $a$  and  $b$  axes of the monoclinic crystal  $X$  and  $Y$  axes of our co-ordinate system and a line perpendicular to them the  $Z$  axis, its positive direction being taken to lie within the obtuse monoclinic angle, the direction cosines of the  $G_1$ ,  $G_2$  and  $G_3$  axes of the two ions relative to  $X$ ,  $Y$  and  $Z$  axes respectively are written in the usual matrix form as

	$X$	$Y$	$Z$
$G_1$	$\alpha_1$	$\pm\beta$	$\gamma_1$
$G_2$	$\alpha_2$	$\pm\beta_2$	$\gamma_2$
$G_3$	$\alpha_3$	$\pm\beta_3$	$\gamma_3$

The positive and negative signs of  $\beta$ 's refer to the first and second ion respectively, the labelling of the ions as first and second being quite arbitrary. The general equation of each of the  $g^2$ -ellipsoids in  $X$ ,  $Y$ ,  $Z$  system can be written as

$$\zeta_{11}X^2 + \zeta_{22}Y^2 + \zeta_{33}Z^2 + 2\zeta_{12}XY + 2\zeta_{23}YZ + 2\zeta_{13}XZ = 1 \quad \dots (3)$$

where

$$\left. \begin{aligned} \zeta_{11} &= \sum_{i=1}^3 G_i^2 \alpha_i^2 \\ \zeta_{22} &= \sum_{i=1}^3 G_i^2 \beta_i^2 \\ \zeta_{33} &= \sum_{i=1}^3 G_i^2 \gamma_i^2 \end{aligned} \right\} \dots \quad (4)$$

$$\left. \begin{aligned} \zeta_{12} &= \pm \sum_{i=1}^3 G_i^2 \alpha_i \beta_i \\ \zeta_{23} &= \pm \sum_{i=1}^3 G_i^2 \beta_i \gamma_i \\ \zeta_{13} &= \sum_{i=1}^3 G_i^2 \alpha_i \gamma_i \end{aligned} \right\} \dots \quad (5)$$

The positive sign of  $\zeta_{12}$  and  $\zeta_{23}$  corresponds to the 1st ion and the negative sign to the second ion.

If the values of the six co-efficients  $\zeta_{11}$ ,  $\zeta_{22}$ ,  $\zeta_{33}$ ,  $\zeta_{12}$ ,  $\zeta_{23}$  and  $\zeta_{13}$  are found experimentally, the three principal values  $G_1$ ,  $G_2$  and  $G_3$  and the direction cosines of  $G_1$ ,  $G_2$ ,  $G_3$  axes relative to  $X$ ,  $Y$  and  $Z$  axes, respectively, can be obtained by diagonalizing the matrix :

$$\begin{pmatrix} \zeta_{11} & \zeta_{12} & \zeta_{13} \\ \zeta_{12} & \zeta_{22} & \zeta_{23} \\ \zeta_{13} & \zeta_{23} & \zeta_{33} \end{pmatrix} \quad (6)$$

Paramagnetic resonance experiments may be performed to give the values of the above six co-efficients. Suppose for the *first* ion, we denote the  $g$ -values along any two mutually perpendicular directions in the  $(hkl)$  plane of the crystal by  $g_\theta^{(1)}$  and  $g^{(1)}_{90^\circ + \theta}$ . Let the direction cosines of the normal to this plane relative to  $X$ ,  $Y$ ,  $Z$  axes be  $\mu_1$ ,  $\mu_2$  and  $\mu_3$  respectively and the  $g$ -value along the normal be denoted by  $g_N^{(1)}$ . We then have from (3)

$$g_N^{2(1)} = \zeta_{11}\mu_1^2 + \zeta_{22}\mu_2^2 + \zeta_{33}\mu_3^2 + 2\zeta_{12}\mu_1\mu_2 + 2\zeta_{23}\mu_2\mu_3 + 2\zeta_{13}\mu_1\mu_3 \quad (7)$$

Now, the directions of  $g_\theta^{(1)}$ ,  $g^{(1)}_{90^\circ + \theta}$  and  $g_N^{(1)}$  form an orthogonal set and considering the  $g^2$ -ellipsoid for the first ion, it can be shown that

$$g_\theta^{2(1)} + g^{2(1)}_{90^\circ + \theta} + g_N^{2(1)} = \zeta_{11} + \zeta_{22} + \zeta_{33} \quad (8)$$

Hence

$$g_{\theta}^{2(1)} + g_{90^{\circ} + \theta}^{2(1)} = \zeta_{11}(1 - \mu_1^2) + \zeta_{22}(1 - \mu_2^2) + \zeta_{33}(1 - \mu_3^2) - 2\zeta_{12}\mu_1\mu_2 - 2\zeta_{23}\mu_2\mu_3 - 2\zeta_{13}\mu_1\mu_3 \quad (9)$$

Similarly for the *second* ion (using the minus sign before  $\zeta_{12}$  and  $\zeta_{23}$ )

$$g_{\theta}^{2(2)} + g_{90^{\circ} + \theta}^{2(2)} = \zeta_{11}(1 - \mu_1^2) + \zeta_{22}(1 - \mu_2^2) + \zeta_{33}(1 - \mu_3^2) + 2\zeta_{12}\mu_1\mu_2 + 2\zeta_{23}\mu_2\mu_3 - 2\zeta_{13}\mu_1\mu_3 \quad (10)$$

From (9) and (10), we have

$$\left[ \frac{1}{2}(g_{\theta}^{2(1)} + g_{90^{\circ} + \theta}^{2(1)}) + (g_{\theta}^{2(2)} + g_{90^{\circ} + \theta}^{2(2)}) \right] = \zeta_{11}(1 - \mu_1^2) + \zeta_{22}(1 - \mu_2^2) + \zeta_{33}(1 - \mu_3^2) - 2\zeta_{13}\mu_1\mu_3 \quad (11)$$

and

$$\left[ (g_{\theta}^{2(2)} + g_{90^{\circ} + \theta}^{2(2)}) - (g_{\theta}^{2(1)} + g_{90^{\circ} + \theta}^{2(1)}) \right] = 4\mu_2[\zeta_{12}\mu_1 + \zeta_{23}\mu_3] \dots \quad (12)$$

The expressions for  $\mu_1$ ,  $\mu_2$  and  $\mu_3$  are given by

$$\mu_1 = \frac{a}{c} \sin \beta, \quad \mu_2 = \frac{a}{b} \sin \beta, \quad \mu_3 = \frac{1}{a \tan \beta}$$

where

$$p = \left[ \left( \frac{h}{a} \right)^2 + \left( \frac{1}{c \sin \beta} - \frac{h}{a \tan \beta} \right)^2 \right]^{\frac{1}{2}}$$

$\beta$  is the obtuse monoclinic angle and  $a : b : c$  are the axial length ratios which are enough to evaluate the direction cosines.

In practice the  $g$ -values are measured along different directions in a plane at intervals of  $5^{\circ}$  say and  $g^2$ -values are plotted against the angular rotation of the sample starting from any arbitrary direction. For each direction there will be two  $g^2$ -values corresponding to the two ions in the unit cell, but the graph for each individual ion is easily recognised by noting that maximum and minimum occurs at  $90^{\circ}$  interval since they correspond to the minimum and maximum semidiameter of the elliptical section of the ellipsoid by the working plane, and the sum of  $g^2$  values at  $90^{\circ}$  apart is constant as may be seen from equations (9) and (10).

Working with four different planes we shall have four different equations of the type (11) and the four co-efficients  $\zeta_{11}$ ,  $\zeta_{22}$ ,  $\zeta_{33}$  and  $\zeta_{13}$  can be easily found. Out of the measurements in the above four different planes those in two can be

utilized to get the values of the remaining two co-efficients  $\zeta_{12}$  and  $\zeta_{23}$  with the help of two different equations of the type (12). But in this case a difficulty arises for a possible ambiguity of labelling of the two ions in the L.H.S. of equation (12) while going from one crystal plane to the other and two sets of values of  $\zeta_{12}$  and  $\zeta_{23}$  will be obtained for one ion. For a unique solution we proceed as follows :

Instead of four general planes chosen for measurement one of them is selected to be the  $a-b$  (001) face or a plane normal to  $a$ -axis. When we work in the (001) face the equations of the two ellipses resulting from the intersection of the ellipsoids for the two ions by (001) face are obtained from equations (3) and (5) by putting  $Z = 0$ , as :

$\zeta_{11}X^2 + \zeta_{22}Y^2 + 2\zeta_{12}XY = 1$  for the first ion

and  $\zeta_{11}X^2 + \zeta_{22}Y^2 + 2\zeta_{12}XY = 1$  for the second ion.

If  $\phi$  be the angle that a chosen direction in this plane makes with the  $X$ -axis (i.e.  $a$ -axis) and  $r^{(1)}$  and  $r^{(2)}$  be the semidiameters of the two ellipses in this direction for the first and second ion respectively we have,

$$\zeta_{11} \cos^2 \phi + \zeta_{22} \sin^2 \phi + 2\zeta_{12} \cos \phi \sin \phi = \frac{1}{r^{2(1)}} = g_{\phi}^{(1)2}$$

and

$$\zeta_{11} \cos^2 \phi + \zeta_{22} \sin^2 \phi - 2\zeta_{12} \cos \phi \sin \phi = \frac{1}{r^{2(2)}} = g_{\phi}^{(2)2}$$

Hence

$$2\zeta_{12} \sin 2\phi = g_{\phi}^{(1)2} - g_{\phi}^{(2)2}$$

At  $\pm 45^\circ$  apart from this direction we shall have

$$2\zeta_{12} \sin 2(\phi \pm 45^\circ) = g_{\phi \pm 45^\circ}^{(1)2} - g_{\phi \pm 45^\circ}^{(2)2}$$

Therefore,

$$\zeta_{12} = + \frac{1}{2} \left[ (g_{\phi}^{(1)2} \sim g_{\phi}^{(2)2}) + (g_{\phi \pm 45^\circ}^{(1)2} \sim g_{\phi \pm 45^\circ}^{(2)2}) \right]^{\frac{1}{2}} \quad \dots (13)$$

From a similar measurement in the plane with  $a$ -axis vertical (plane normal to  $a$ -axis) we get a similar equation for  $\zeta_{23}$ . The constancy of the value of  $\zeta_{12}$  and  $\zeta_{23}$  thus obtained from different pairs of measurement at  $45^\circ$  apart provides a check on our measurement in these two planes.

Thus, measuring the  $g$ -values for the two ions at  $45^\circ$  apart in the (001) plane or the plane normal to  $a$ -axis and using equations of the type (13) we shall get unambiguous magnitudes of  $\zeta_{12}$  or  $\zeta_{23}$  but with an ambiguity of sign. Then of the two possible sets of solution of  $\zeta_{12}$  and  $\zeta_{23}$  obtained from the two equations of the

type (12) the set for which the magnitude of  $\zeta_{12}$  or  $\zeta_{23}$  agrees with that obtained from the equation of the type (13) is to be considered as the correct one in sign and magnitude. At the same time this procedure provides a check on the magnitudes of  $\zeta_{12}$  or  $\zeta_{23}$  and hence on the measurements concerned.

It should be noted that the sign of  $\zeta_{12}$  and  $\zeta_{23}$  becomes reversed while going from one ion to the other as seen from equation (5). If they are determined with an ambiguity of sign such as  $\zeta_{12} = \pm \delta$  and  $\zeta_{23} = \pm \sigma$ , we can uniquely find their values as follows. We start with the following two possible sets from one of the two ions

$$\begin{aligned} & \zeta_{12} = \delta \quad , \quad \zeta_{23} = \sigma \\ \text{or} \quad & \zeta_{12} = \delta \quad , \quad \zeta_{23} = -\sigma \end{aligned} \quad \dots (14)$$

The correct set will be decided from measurement in another plane and equation (12) so that the absolute magnitudes of the L.H.S and R.H.S. of equation (12) are equal. The correct set for the other ion corresponding to  $\zeta_{12} = -\delta$  immediately follows

In some planes of the tutton salts depending upon the nature of the crystal the absorption signals for the two ions are not well resolved and these faces are generally not chosen for our measurement. In the  $a-c$  (010) plane, the signals for the two ions will coincide. This is because the two ellipses resulting from the intersection of the two  $g^2$ -ellipsoids by the (010) plane coincide with each other. The equations of the two ellipses are found to be the same and given by

$$\zeta_{11}X^2 + \zeta_{33}Z^2 + 2\zeta_{13}XZ = 1 \quad \dots (15)$$

Measurement in this plane will not only simplify the equation (11) which becomes  $g_\theta^2 + g_{90^\circ+\theta}^2 = \zeta_{11} + \zeta_{33}$  but also serves as a check on the value of  $\zeta_{13}$  obtained otherwise. From (15),  $g_{max}^2$  and  $g_{min}^2$  in this plane is given by the two roots of  $\lambda$  of the following determinantal equation

$$\begin{vmatrix} \zeta_{11}-\lambda & \zeta_{13} \\ \zeta_{13} & \zeta_{33}-\lambda \end{vmatrix} = 0$$

$$\text{or} \quad \lambda = \frac{1}{2} [(\zeta_{11} + \zeta_{33}) \pm \sqrt{(\zeta_{11} - \zeta_{33})^2 + 4\zeta_{13}^2}]$$

$$\text{Hence} \quad (g_{max}^2 - g_{min}^2)^2 = (\zeta_{11} - \zeta_{33})^2 + 4\zeta_{13}^2 \quad \dots (16)$$

$$\text{Also} \quad g_\theta^2 + g_{90^\circ+\theta}^2 = g_{max}^2 + g_{min}^2 = \zeta_{11} + \zeta_{33} \quad \dots (17)$$

Thus check on the magnitude of  $\zeta_{13}$  can be made with the help of equation (16.)

With the general methods discussed above all the six co-efficients  $\zeta_{ij}$ 's can be determined, and the matrix (7) is then diagonalized to give the principal  $g^2$ -values and their direction cosines. Instead of solving a third order secular equation

which involves solution of a cubic equation which in turn often introduces a large error in the final result and sometimes leads to imaginary roots due to small errors in the experiment the matrix (7) is diagonalized by the matrix method of successive approximation (Nye 1957) which is found to be the most suitable in such calculations.

In practice special planes are chosen depending upon the type of salt under investigation, such that while solving for the six co-efficients  $\zeta_{ij}$  calculations are made simplified and the number of working planes is reduced to a minimum. In the case of  $\text{CuK}_2(\text{SO}_4)_2 \cdot 6\text{H}_2\text{O}$  it has been shown in the course of the following discussion that measurements in three appropriately chosen planes will suffice to give the six co-efficients with a procedure slightly different from that outlined in the general method.

## RESULTS

### (1) $\text{CuK}_2(\text{SO}_4)_2 \cdot 6\text{H}_2\text{O}$

In this case measurements have been made in the following three natural faces of the crystal (1) 'c' i.e. (001) plane (2) 'q' i.e. (0 $\bar{1}$ 1) or (011) plane (3) 'p' i.e. (110) or (1 $\bar{1}$ 0) plane. A check on our results has been made with an additional measurement in the (010) plane. As indicated above there are two possible values of the Miller indices for the 'p' and 'q' faces and hence  $\mu_2$  has equal magnitude but opposite signs for the two possible values of the Miller indices of each of these planes. But equation (10) does not depend on the sign of  $\mu_2$  and the ambiguity

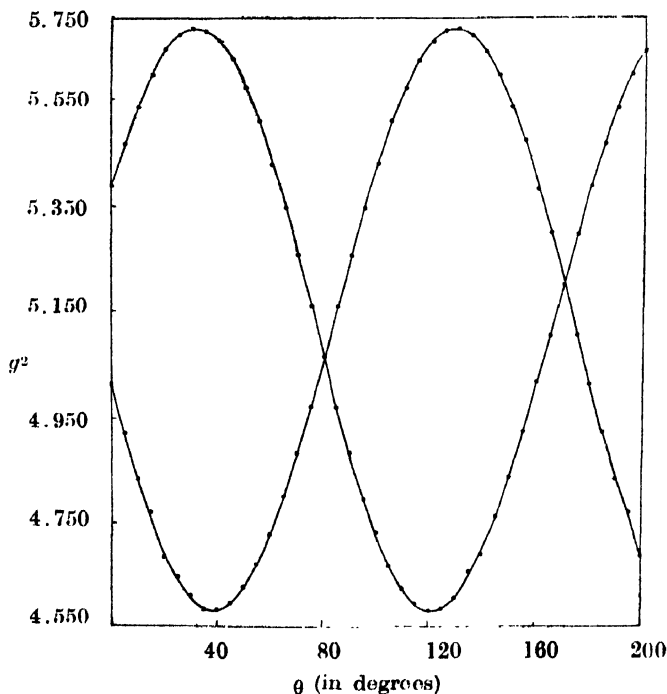


Fig. 1, 'ab' face  $\text{Cu}(\text{KSO}_4)_2 \cdot 6\text{H}_2\text{O}$ .



of its sign adds no further complication to equation (11) since the ambiguity of the sign already present in the L.H.S. of equation (11) is removed by the procedure described earlier.

$g^2$ -values are plotted against angular rotation of the sample in each of the above three planes (Figs. 1, 2, 3). The  $g^2-\theta$  graphs show common  $g$ -values for both the ions in two directions in each plane. From equation (3) we find that for both the ions the value of the  $g^2$  along 'a' and 'b' (i.e.  $X$  and  $Y$ ) axes are  $\zeta_{11}$  and  $\zeta_{22}$  respectively which indicates the common  $g$ -values for the two ions in these directions. Since only the  $a$ -axis lies in both 'c' and 'q' planes we can find the value of  $\zeta_{11}$  from the graphs for these two planes (Figs. 1 and 2).

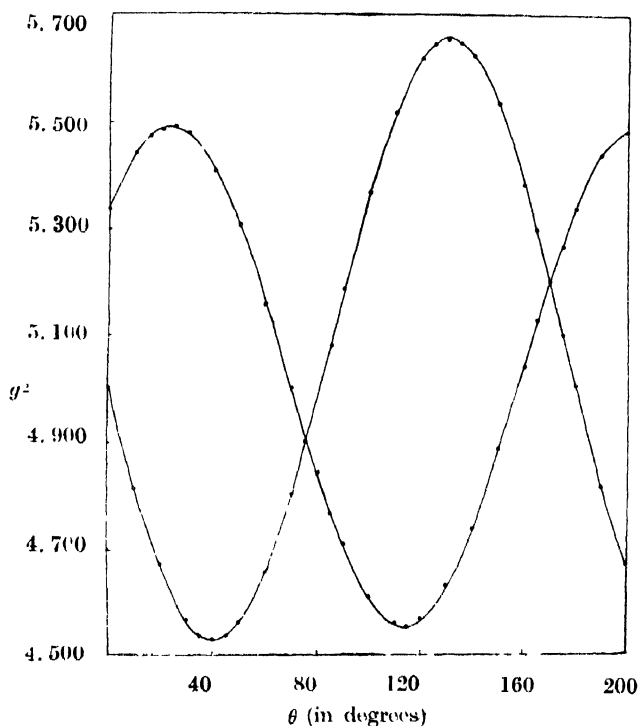


Fig. 2. 'q' face,  $\text{Cu}(\text{KSO}_4)_2 \cdot 6\text{H}_2\text{O}$ .

Having found the value of  $\zeta_{11}$ , the remaining five co-efficients are obtained from the measurements in the above three planes and equations (11), (12) and (13), and removing the ambiguity of the sign of  $\zeta_{12}$  and  $\zeta_{23}$  in a manner stated earlier; no measurements in extra planes are necessary. However, the measurement in the (010) plane (Fig. 4) is used as a check on these values. The matrix (7) is thus found to be

$$\begin{array}{ccc} 5.201(3) & - & .545(8) & - & .140(0) \\ - & .545(8) & 5.061(6) & & .091(0) \\ - & .140(0) & .091(0) & & 4.302(8) \end{array}$$

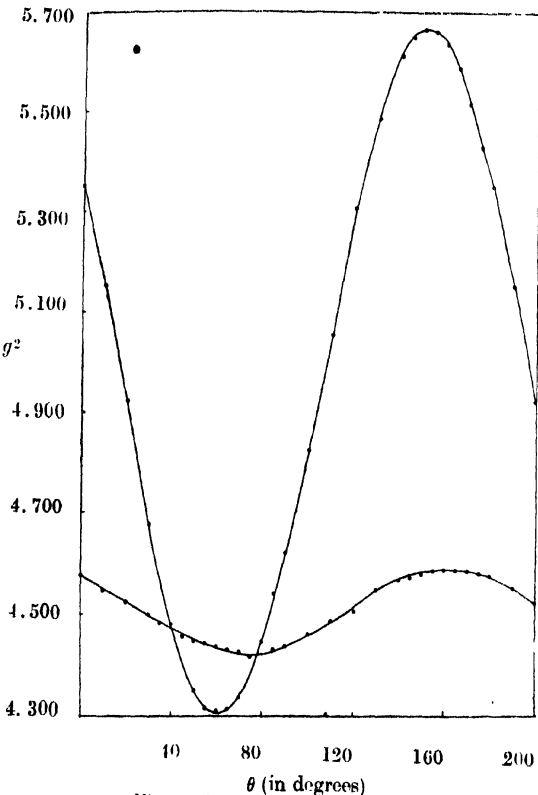


Fig. 3. 'p'-face,  $\text{Cu}(\text{KSO}_4)_2 \cdot 6\text{H}_2\text{O}$ .

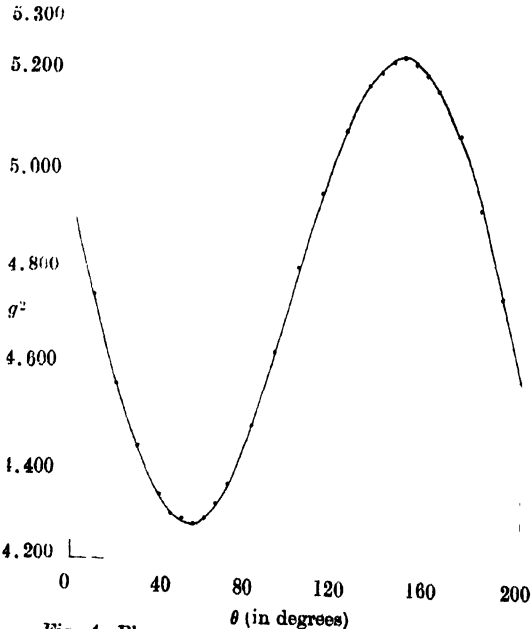


Fig. 4. Plane normal to 'b'-axes,  $\text{Cu}(\text{KSO}_4)_2 \cdot 6\text{H}_2\text{O}$ .

This matrix has been diagonalised by the matrix method of successive approximation and leads to the principal  $g^2$ -values and direction cosines as follows:

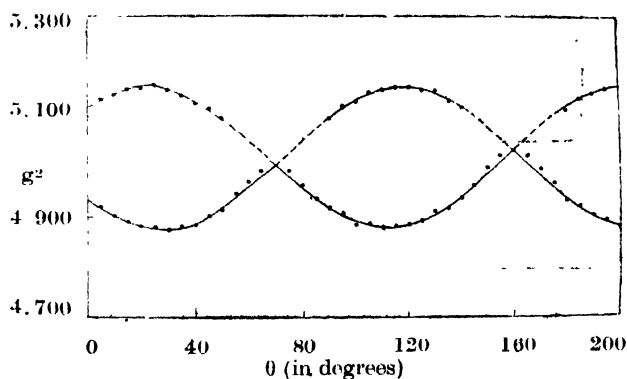
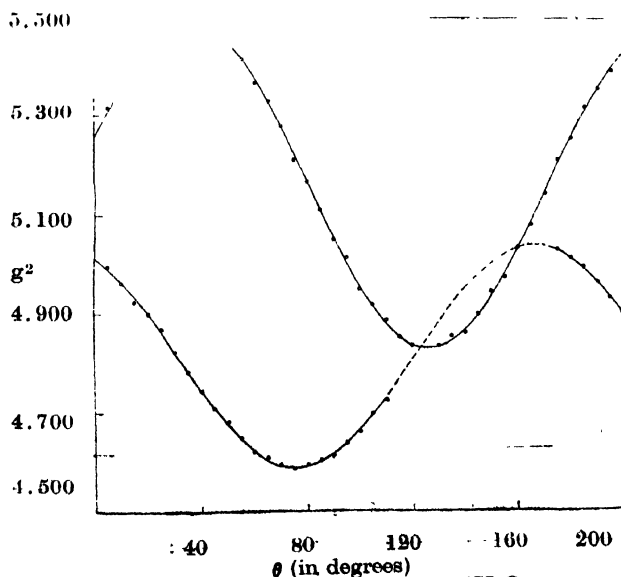
$$\begin{array}{llll}
 G_1^2 = 4.225(4) & \alpha_1 = .295(0) & \beta_1 = -.291(3) & \gamma_1 = .910(0) \\
 G_2^2 = 4.656(1) & \alpha_2 = .586(6) & \beta_2 = -.695(9) & \gamma_2 = -.413(1) \\
 G_3^2 = 5.685(4) & \alpha_3 = .753(6) & \beta_3 = .656(4) & \gamma_3 = -.034(9)
 \end{array}$$

The principal  $g$ -values and their angular orientations relative to the crystallographic axes are given in table I.

TABLE I

	$a(X)$	$b(Y \equiv X_3)$	$c'(Z)$	$X_1$	$X_2$
$(K_1)G_1 = 2.05_5$ (2.04)	72°50'	106°56'	24°30'	70°5'	153°22'
$(K_2)G_2 = 2.15_7$ (2.14)	74°20'	104°54'	21°57'		
	54°5'	134°8'	114°24'	55°36'	63°45'
	(53°12')	(135°10')	(111°49')		
$(K_3)G_3 = 2.38_1$ (2.36)	41°6'	48°59'	92°	41°20'	85°48'
	(41°5')	(49°)	(92°6')		

(values within parentheses are obtained from the approximate results of Bleaney *et al* at 90°K)


 Fig. 5. 'ab' face  $\text{Cu}(\text{NH}_4\text{SO}_4)_2 \cdot 6\text{H}_2\text{O}$ 

 Fig. 6. 'q' face  $\text{Cu}(\text{NH}_4\text{SO}_4)_2 \cdot 6\text{H}_2\text{O}$

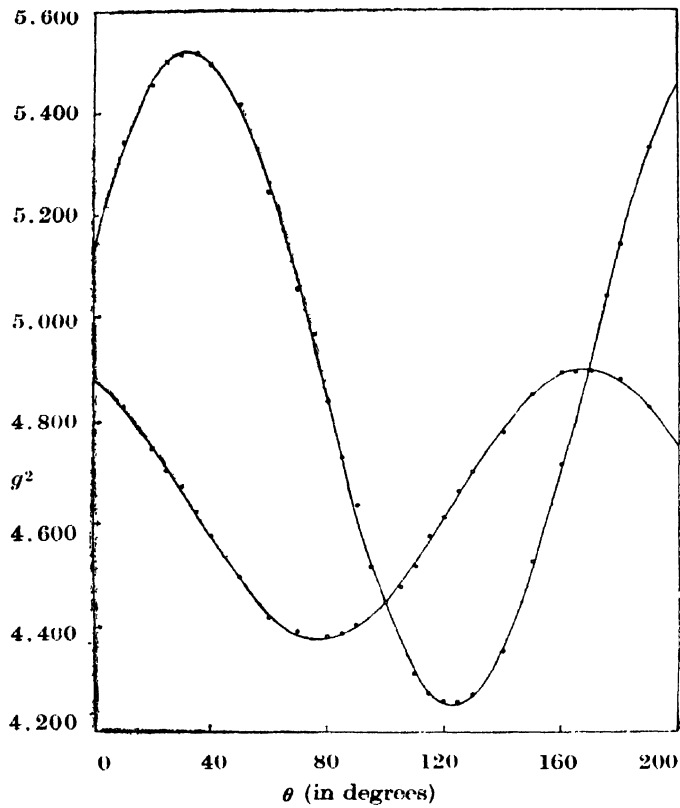


Fig. 7. 'P' face  $\text{Cu}(\text{NH}_4\text{SO}_4)_2 \cdot 6\text{H}_2\text{O}$

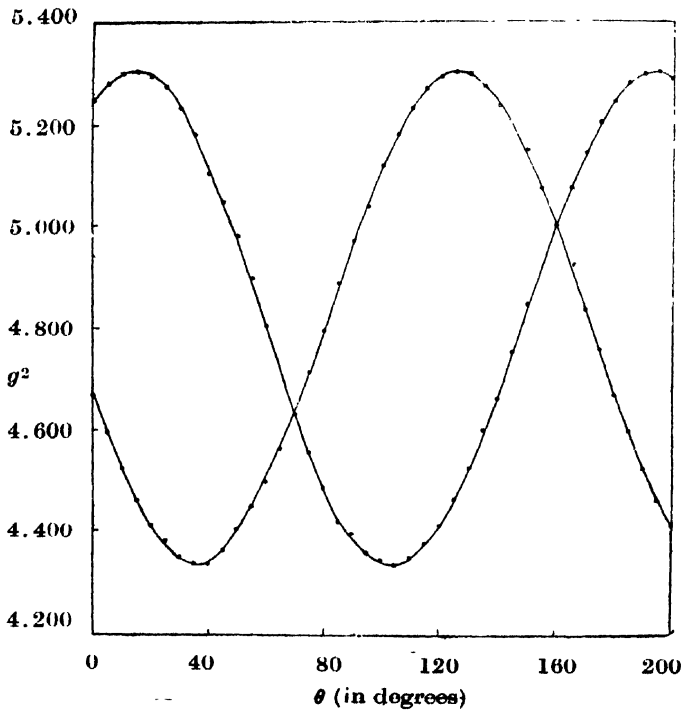
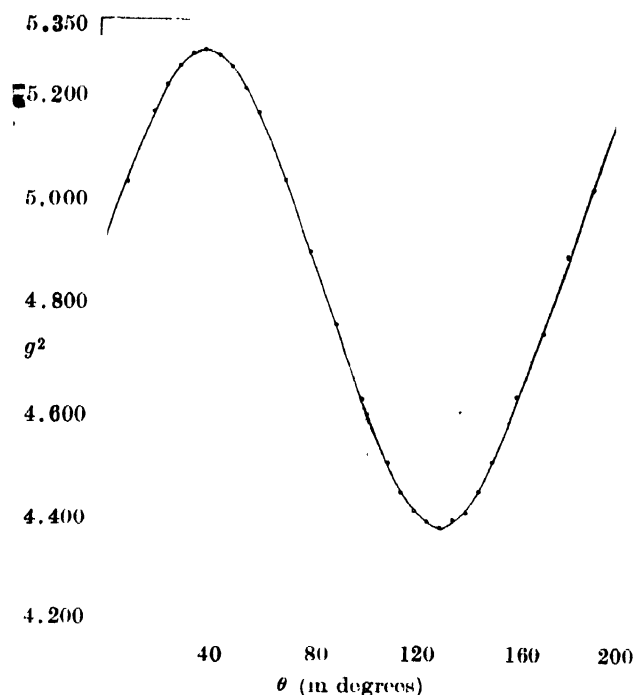


Fig. 8. Plane normal to  $a$ -axis,  $\text{Cu}(\text{NH}_4\text{SO}_4)_2 \cdot 6\text{H}_2\text{O}$

Fig. 9. Plane normal to b-axis  $\text{Cu}(\text{NH}_4\text{SO}_4)_2, 6\text{H}_2\text{O}$ (2)  $\text{Cu}(\text{NH}_4)_2(\text{SO}_4)_2, 6\text{H}_2\text{O}$ 

In this crystal from measurement in the 'q' i.e. (011) or (0 $\bar{1}$ 1) plane, it was found that the  $g^2$  vs.  $\theta$  curves for the two ions are not well resolved over a comparatively large region (Fig. 6) and hence one of the intersecting points could not be accurately decided, so that the results in this plane could not be used. This made it necessary to take measurements in four different planes, viz., (1) 'c' (001) plane; (2) 'p' i.e. (1 $\bar{1}$ 0) or (110) plane; (3) plane normal to the  $a$ -axis (4) (010) plane (Figs. 5, 7, 8 and 9).

From the measurements in the above four planes and equations (11), (12) and (13) and removing the ambiguity of signs of  $\zeta_{12}$  and  $\zeta_{23}$  in a manner stated earlier, all the six co-efficients  $\zeta_{ij}$  have been determined and the matrix (7) is found to be

$$\begin{array}{ccc} 5.032(1) & .140(0) & .411(8) \\ .140(0) & 5.002(0) & .447(3) \\ .411(8) & .447(3) & 4.641(6) \end{array}$$

Diagonalization of this matrix leads to the principal  $g$ -values and their orientations given in table II.

TABLE II

	$a(X)$	$b(Y \perp X_3)$	$c'(Z)$	$\chi_1$	$\chi_2$
$(K_1)G_1 = 2.05_8$	109°54'	115°45'	33°30'	77°3'	150°44'
$(K_2)G_2 = 2.20_8$	41°52'	131°51'	92°14'	54°58'	61°40'
$(K_3)G_3 = 2.35_8$	54°54'	52°45'	56°36'	37°50'	95°41'

## DISCUSSION OF THE RESULTS

It will be seen from the results that the  $g^2$ -ellipsoids are of definitely orthorhombic symmetry at 300°K for both the salts and the departure from tetragonality is greater for the ammonium salt. The inclination of the  $G_3$  axis to the  $\chi_1$ -axis, maximum principal crystalline susceptibility axis in the plane (010), is in fair agreement with the angle which the corresponding  $K_3$  axis (principal ionic susceptibility) makes with  $\chi_1$ -axis, calculated from magnetic anisotropy data on the assumption of approximate tetragonal symmetry about the  $K_3$  axis. The orientations of the  $\chi_1$  and  $\chi_2$  axes in crystals are obtained from magnetic anisotropy

experiments ((Bose *et al.* 1957). It will be seen that the angle  $\widehat{G_3\chi_1}$  from Table I for the potassium salt is 41° 20' as against the angle  $\widehat{K_3\chi_1} = 41^\circ 24'$  calculated from magnetic anisotropy data. The angles made by  $G_3$  and  $K_1$  with  $\chi_3$  are 48° 59' and 48° 36', respectively. Similarly, for the ammonium salt the angles with reference to  $\chi_1$  are 37° 50', 40° 24', and with reference to  $\chi_3$ , 52° 45' and 49° 36'. The angles made by  $G_3$  and  $K_1$  with the  $\chi_3$  and  $\chi_1$  directions in this salt are somewhat different. It is also to be noted that though the two salts are isomorphous the orientations of  $G_i$  axes are very different in the two.

In the case of the potassium salt, our values of the angles and also the  $G_i$  values at 300°K are somewhat different from those of Bleaney *et al.*, from measurements at 90°K given in parenthesis in Table I; this is to be expected, since calculations from magtic anisotropy data (Bose *et al.* loc. cit.) do show small variation of the angles between 300°K and 90°K. No similar data for the ammonium salt are available, but in this case magnetic anisotropy calculations show large variation of some of the angular parameters with temperature, and these are being currently investigated by us in greater details.

The importance of above investigations for X-ray structure analysis is obvious. Moreover, when we have extended these measurements to high and low temperatures, the large amount of magnetic anisotropy data for paramagnetic crystals accumulated by us, will be amenable to accurate and unique interpretation in terms of the anisotropic ligand field theories developed by us in recent years (Bose *et al.*, 1960, 1961, 1963) ,

## REFERENCES

- Bleaney, B., Penrose, R. P., and Plumpton, Betty I., 1949, *Proc. Roy. Soc., A*, **198**, 406.  
Bleaney, B., Penrose, R. P., and Plumpton, Betty I., 1949, *Proc. Roy. Soc., A*, **198**, 4406.  
Bose, A., Mitra, S. C. and Sunil K. Datta, 1957, *Proc. Roy. Soc., A*, **239**, 165.  
Bose, A., Chakraborty, A. S. and Chatterjee, R., 1960, *Proc. Roy. Soc., A*, **255**, 145.  
Bose, A., Chakraborty, A. S. and Chatterjee, R., 1960, *Proc. Roy. Soc., A*, **255**, 145.  
-do- 1961, " " " A, **261**, 43.  
-do- 1961, " " " A, **261**, 207.  
-do- 1963, *Proc. Phys. Soc.* **82**, 23.  
  
(Ghosh, U. S., Bagchi, R. N. and Pal, A. K., 1963, *Ind. Jour. Phys.*, **37**, 555.  
Hofmann, W., 1931, *Z. Kryshallogr.*, **78**, 279.  
Knoeble, H. W. and Hahn, E. L., 1951, *Rev. Sci. Instrum.*, **22**, No. 12, 904.  
Nye, J. F., 1957, *Physical Properties of crystals*, (Oxford Univ. Press), 165.

# Letters to the Editor

The Board of Editors does not hold itself responsible for opinions expressed in the letters published in this section. The notes containing short reports of original investigations communicated to this section should not contain many figures and should not exceed 500 words in length. The contributions reaching the Secretary by the 15th of any month may be expected to appear in the issue for the next month. No proof will be sent to the author.

15

## X-RAY ANALYSIS OF RADIOACTIVE FALLOUT OVER CALCUTTA

PRABIR K. SANDELL, J. MUKHERJEE AND SUSHIL K. DAS

DEPARTMENT OF PHYSICS, JADAVPUR UNIVERSITY, CALCUTTA-32

(Received, September 9, 1963)

Since 1961, the radioactive fallout over Calcutta has been systematically collected and studied in our laboratory. The samples were generally classified

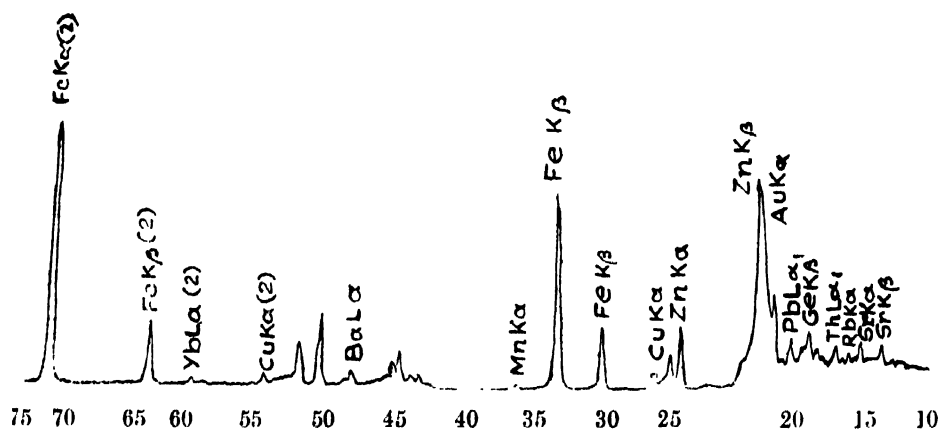


Fig. 1. X-ray Spectrum of Sample —A, at 36Kv, 24mA.

Scale factor —

$\times 8$  between  $9^\circ$  to  $24^\circ$

$\times 64$  between  $24^\circ$  to  $43^\circ$

$\times 8$  between  $43^\circ$  to  $75^\circ$

20 Scans. Time constant—4.



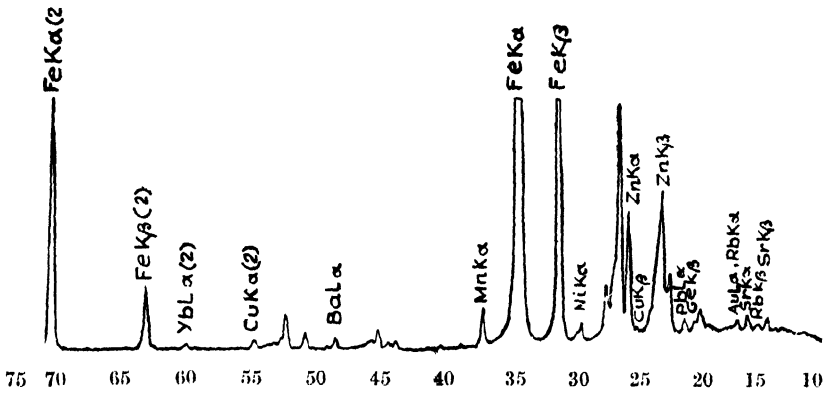


Fig. 2. X-ray Spectrum of Sample—B, at 36Kv, 24mA.

Scale factor :—

× 8 between 10° to 75°

20 Scan. Time constant—4.

into three groups. The first Group 1 (sample A) consisted of air-borne particles deposited in an enamelled tray smeared with glycerine, on dry rainless days. During rainy days, however, the rainborne dust was collected along with rain-water in an empty tray. The water was filtered, the insoluble residue forming the material for Group 2 (Sample B). The filtrate was finally evaporated to dryness, yielding working material for Group 3 (sample C). The samples were separately powdered in an agate mortar and pressed into pills of appropriate sizes.

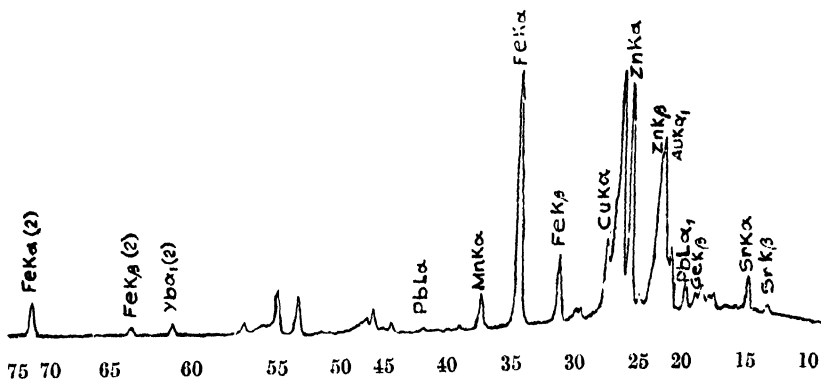


Fig. 3. X-ray Spectrum of Sample—C, at 36Kv, 24mA.

Scale factor :— × 8 between 10° to 75°

20 Scan.

Time constant—4.

The X-ray spectrographic analyses were carried out with a plane crystal quartz X-ray spectrophotograph whose analytical range extends from Ti (At. No. 22) upwards. An appropriate idea of the distribution of the heavy and light elements was obtained by varying the high tension applied to the X-ray tube. The X-ray

spectra of the samples A, B, and C, so obtained, were compared with standard curves of the following elements, Ni, Cu, Fe, Mn, Bi and Au, under the same parametric conditions for 26 calibration. To detect the presence of recognisable quantities of Uranium, all the spectra were compared to the spectrum of a uraninite mineral sample.

The graphs A, B and C represent the spectra of the respective group samples taken at 36KV and 24MA. The spectra have been crosschecked in every case with those taken at 20 KV, 24MA. The elements identified are tabulated sample-wise in Table I.

It may be noted that Pb and W peaks are present in all the graphs. Presumably the W lines owe their origin to the  $W^{181}$  of Hardtack test or scatterings of the incident beam, while the Pb lines could also be due to the presence of lead lining of the sample holder.

TABLE I

Sample A : dry fallout	Zn, Fe, Cu, Th, Mn, Ni, Au, Bi, Rb, Sr, Yb, Ba.
Sample B : Residue from rain- borne fallout.	Zn, Fe, Cu, Mn, Sr, Ni, Au, Bi, Rb, Ba, Yb.
Sample C : Water soluble salts from rainborne fall-out.	Zn, Fe, Cu, Sr, Ni, Mn, Bi, Au, Yb.

In sample 'A' (dry fallout), Zn, Cu, Fe, and Sn are present in much greater quantities than in sample 'B', filtered as rain-borne fall-out. Th is present only in sample A. It may be noted that Zn predominates as a water soluble salt, while Ba and Fe predominate in insoluble form. The presence of large quantities of Fe, Zn and Mn have also been corroborated by chemical analysis.

We are indebted to Prof. S. D. Chatterjee for his active interest and guidance in the work.

## THE CRYSTAL STRUCTURE OF PYROCATECHOL

S. K. TALAPATRA\*

INDIAN ASSOCIATION FOR THE CULTIVATION OF SCIENCE, JADAVPUR, CALCUTTA-32.

(Received June 22, 1964)

The structural formula of pyrocatechol is shown in Fig. 1.

Caspari (1926) obtained the space group of pyrocatechol as  $C2/m$  with  $a = 17.46 \text{ \AA}$ ,  $b = 10.74 \text{ \AA}$ ,  $c = 5.4 \text{ \AA}$ ,  $\beta = 94^\circ 15'$  and  $n = 8$ . Kitaigorodskii (1948) found this data incompatible on the basis of the theory of close packing of organic molecules, and redetermined the space group as  $P2_1/c$  with  $a = 10.15 \text{ \AA}$ ,  $b = 5.48 \text{ \AA}$ ,  $c = 11.00 \text{ \AA}$ ,  $\beta = 118^\circ$  and  $n = 4$ . Infrared absorption spectra of pyrocatechol in solution show two sharp and nearly equal peaks in the region of O-H fundamental (Davies, 1938) indicating thereby the presence of a weak intramolecular hydrogen bond. Pauling accounted for the two peaks by assuming that one of the two O—H bonds in the molecule is in the *cis* position and the other in the *trans* position. It was, therefore, of interest to determine the crystal structure and study the nature of hydrogen bonding in the solid state of pyrocatechol.

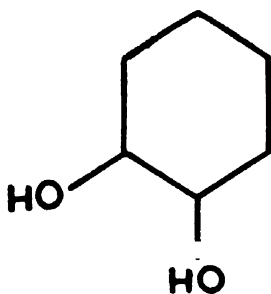


Fig. 1.

The substance is highly hygroscopic and gradually sublimates at room temperature and as such a small single crystal was sealed in a thin-walled glass capillary of .4mm diameter for taking the X-ray photographs. Preliminary investigations confirmed the space group and cell dimensions obtained by Kitaigorodskii. This cell could also be obtained by suitable reduction of the arbitrary unit cell suggested by Caspari.

The short  $b$  axis indicated that the (010) projection was likely to be most informative, and thus zero layer Weissenberg photographs about [010] axis using  $\text{CuK}\alpha$  radiation were taken with different times of exposure, and the relative

\* Lecturer in Physics, Jadavpur University, Calcutta-32.

integrated intensities of the spots were estimated visually. The relative intensity data were then placed on the absolute scale by Wilson's statistical method (1942). The atomic scattering factors of carbon and oxygen were taken from Berghuis *et al* (1955) an average isotropic B factor of  $3.0 \text{ \AA}^2$  was used.

In deducing the trial structure, the pyrocatechol molecule was assumed to be planar with C—OH bond length equal to that of  $\alpha$ -resorcinol (Robertson, 1936). Since pyrocatechol contains atoms of nearly the same scattering factors (Carbon and Oxygen), and the (010) projection gives the plane group P2 with only two molecules per effective unit cell, it was considered convenient to make direct use of the Fourier-transform principle (Hanson *et al.*, 1953). The hol weighted reciprocal-lattice section (Fig. 2) shows four prominent peaks on the

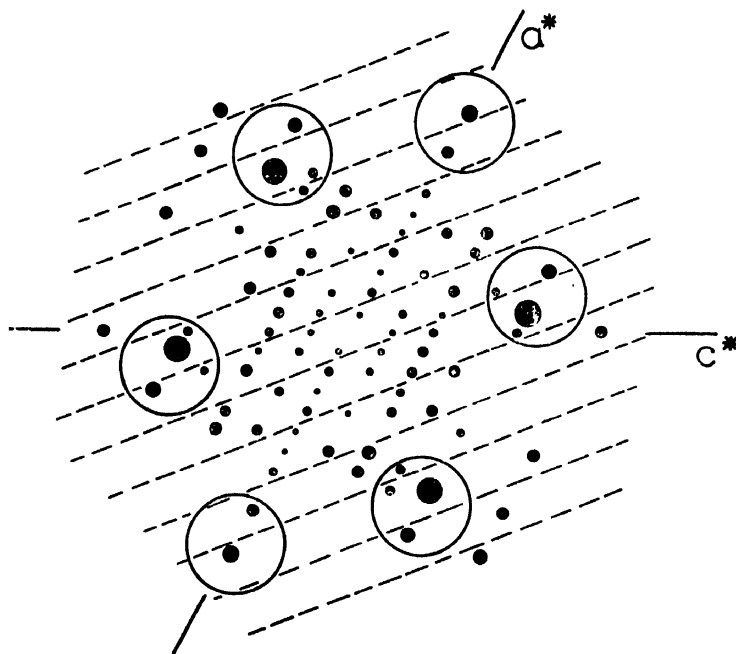


Fig. 2. Hol-section of the weighted reciprocal-lattice of pyrocatechol with broken lines representing the nodal lines of the fringe system. The benzene peaks are indicated by small circles (weight proportional to the unitary structure factors).

'benzene circle' (Taylor, 1952) and two less prominent ones extended beyond it; when joined together by straight lines they make a clear hexagon.

These peaks are, evidently, due to the benzene ring, which forms the nucleus of the molecule, and are less effected by the OH groups, as the centrosymmetrical portion of a molecule has always a stronger influence on its transform than the non-centrosymmetrical portion. The projected shape of the benzene ring was, therefore, obtained from the positions of the peaks, and the tilt of the molecule to the (010) plane was calculated to be approximately  $33^\circ$ . Careful search of the weighted section also indicates the presence of straight nodal lines of a fringe

system presumably produced by the two centrosymmetric benzene rings in the effective unit cell. From their positions, the coordinates of the centres of the molecules were deduced as  $z = 0.9\text{\AA}$  and  $x = 1.6\text{\AA}$ . The positions of the OH groups were then fixed by trial-and-error method. Taking the coordinates of carbon and oxygen atoms thus obtained the structure factors of all the observed (hol) reflections were calculated. This showed a residual of 40% (approx.). The (010) electron density projection was computed after assigning the calculated phases (signs) to the respective observed structure amplitudes (Fig. 3).

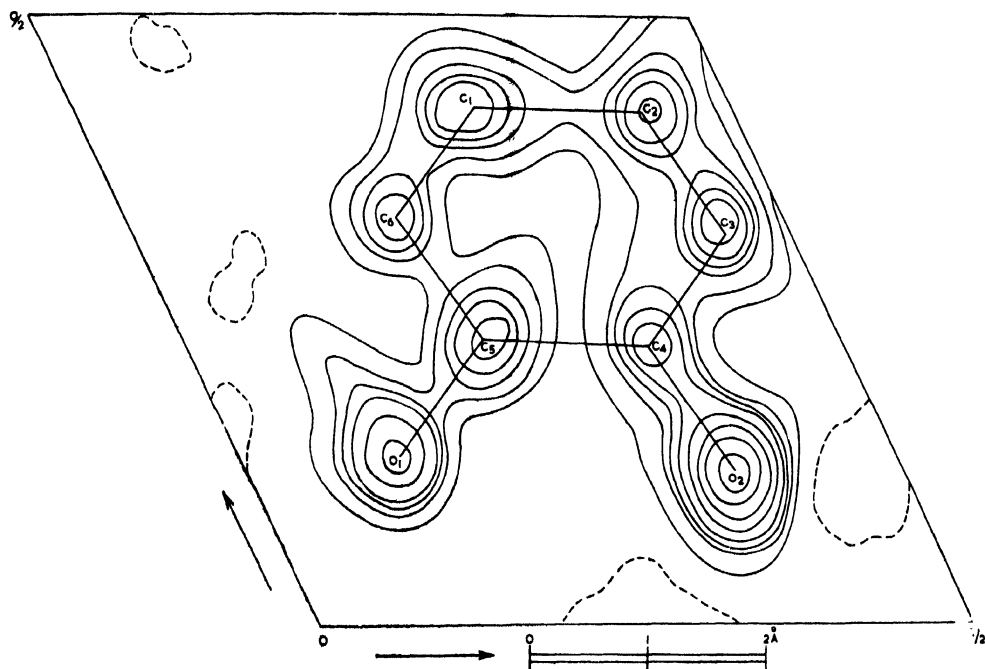


Fig. 3. First (010) electron density projection with contours drawn at arbitrary intervals. Zero-electron contours are shown by broken lines.

TABLE I

Atom	$x/a$	$z/c$	Atom	$x/a$	$z/c$
C <sub>1</sub>	+0.426	+0.302	C <sub>5</sub>	+0.230	+0.226
C <sub>2</sub>	+0.425	+0.433	C <sub>6</sub>	+0.331	+0.203
C <sub>3</sub>	+0.328	+0.453	O <sub>1</sub>	+0.140	+0.118
C <sub>4</sub>	+0.225	+0.356	O <sub>2</sub>	+0.125	+0.370

In the electron density map the atoms are well resolved, and the carbon and oxygen peaks are distinguishable. The  $x$  and  $z$  coordinates (Table I) obtained from the map gave better agreement between the observed and calculated struc-

ture factors, and the  $R$  value dropped to 30%. Further refinement is in progress. Details of the investigation will be published shortly.

## ACKNOWLEDGEMENT

The author is highly indebted to Dr. R. K. Sen, D.Sc., for guidance and to Prof. K. Banerjee, D.Sc., F.N.I., for his keen interest and encouragement during the progress of the work. He also places on record his deep sense of gratitude to Prof. H. Lipson, F.R.S., of the Manchester College of Science and Technology for helpful suggestions while the latter was in Calcutta as a visiting Professor.

## REFERENCES

- Berghuis, J., Haanappel, I. J. M., Potters, M., Loopstra, B. O., Mac Gillavry, C. H., and Veenendaal, A. L., (1955), *Acta Cryst.*, **8**, 478.  
Caspari, W. A., 1926, *J. Chem. Soc.*, 573.  
Hanson, A. W., Lipson, H., Taylor, C. A., 1953 *Proc. Roy. Soc. A*, **218**, 371.  
Kitaigorodskii, A. I., 1948, *Izvest. Akad. Nauk., U.S.S.R., Otdel. Khim. Nauk* 278-89.  
Lipson, H., Taylor, C. A., 1951, *Acta Cryst.*, **4**, 458.  
Pauling, L., 1936, *JACS.*, **58**, 94.  
Taylor, C. A., 1952, *Nature, Lond.*, **169**, 1088.  
Wilson, A. J. C., 1942, *Nature, London*, **150**, 152.

## ELECTRON MOBILITY IN A MAGNETIC FIELD

S. N. SEN AND R. N. GUPTA

DEPARTMENT OF PHYSICS, UNIVERSITY OF NORTH BENGAL,  
SILIGURI, WEST BENGAL

(Received May 2, 1964)

**ABSTRACT.** The values of electron mobility in air in presence of a magnetic field varying from 0 to 200 Gauss and over a wide range of pressure have been computed from breakdown measurements. The validity of the expression  $\mu/\mu_H = (1 + C_1 H^2/P^2)$  deduced by Townsend and Gill (1938) and also by Blevin and Haydon (1958) has been tested by plotting  $\mu/\mu_H$  against  $1/P^2$  and the curve is a straight line for a limited range of pressure above .125 m.m. of Hg. The constant  $C_1$  is found to decrease with the increase of the magnetic field and the curve of  $C_1$  against  $H$  is parabolic in nature. An analytical expression has been deduced which explains the observed variation to a first approximation.

## INTRODUCTION

It was shown by Townsend and Gill (1938) that the mobility of the electrons in the direction of the field in presence of a magnetic field is reduced and is given by

$$\mu_H = \frac{\mu}{1 + \omega_H^2 \tau^2} \quad \dots (1)$$

where  $\tau$  is the time between two successive collisions and  $\omega_H = eH/mc$ . Blevin and Haydon (1958) considering the bulk properties of electron avalanches have deduced that

$$\mu_H = \frac{\mu}{1 + C_1 H^2/P^2} \quad \dots (2)$$

where  $C_1 = \left[ \frac{e}{m} \cdot \frac{L}{u} \right]^2$ ,  $L$  denoting the mean free path of the electron in the gas at a pressure of 1 m.m. of Hg and  $u$  denotes the random velocity of the electrons in the gas. It can easily be shown that equation (1) reduces to equation (2) if a simple calculation be carried out; from equation (2) it is seen that

$$\mu/\mu_H = 1 + C_1 H^2/P^2.$$

and if the values of  $\mu/\mu_H$  be plotted against  $1/P^2$ , for a constant value of the magnetic field then the curve should be a straight line and the intercept of the curve with the axis along which  $\mu/\mu_H$  has been plotted should be numerically equal to unity

while the slope of the curve should provide the value of the constant  $C_1$ . The object of this note is to verify equation (1) or (2) so as to determine the range of pressure over which it is valid and to see whether  $C_1$  is a constant over the range of magnetic field investigated.

#### METHOD OF COMPUTATION OF MOBILITY

In our preliminary note we have not made any experimental measurement of mobility which we propose to undertake very soon. Unfortunately we have not come across in the literature any data for the measurement of mobility in a magnetic field. Sen and Ghosh (1962) determined the breakdown potential in air in presence of a magnetic field varying from 0 to 200 gauss and over a wide range of pressure. If  $E$  denotes the breakdown potential per unit length then the random velocity  $u$  can be calculated from the relation

$$\frac{1}{2} mu^2 = eE$$

and the drift velocity of the electrons can be determined from the relation

$$v = (K)^{\frac{1}{2}}/u.$$

where

$$K = (2m/M)$$

where  $m$  is the mass of the electron and  $M$  is the mass of the positive ion. (Von Engel (1959). That this method of calculating the drift velocity of electrons is reasonably accurate is evident because the same order of drift velocity has been obtained as is found in the literature. In presence of magnetic field also the same procedure of calculating the drift velocity from breakdown potentials has been adopted.

#### DISCUSSION AND RESULTS

The values of  $\mu/\mu_H$  have been plotted against  $1/P^2$  in fig. 1 for different values of the magnetic field. The curve is a straight line for pressures above .125 mm of Hg and below this value it bends down in each case with a negative slope. The

TABLE I

Magnetic field in Gauss	$C_1 \times 10^7$
20	6.02
30	3.80
50	1.60
100	.66
150	.41
200	.52



intercepts made by the curves are different for different values of the magnetic field and lies between 1.0 to 1.1. The values of  $C_1$  as calculated for different curves are entered into Table I.

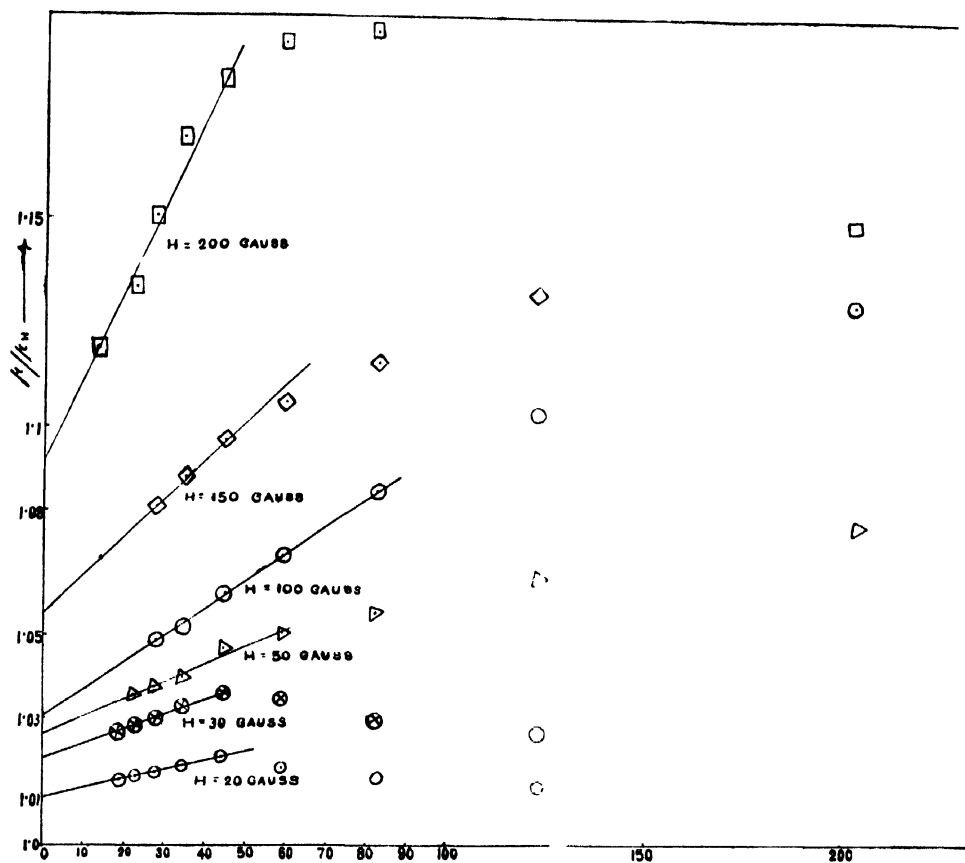


Fig. 1.  $1/\rho^2 \rightarrow$

From Table I it is evident that  $C_1$  as deduced from the curves is not a constant but decreases with the increase of the magnetic field and the average value as deduced by Sen and Ghosh (1962) namely  $7.464 \times 10^7$  is greater than the highest value obtained here. The values of  $C_1$  calculated from different curves have been plotted against the corresponding values of the magnetic field and the curve is parabolic in nature. Haydon (1961) has also reported different values of  $C_1$  for Hydrogen by plotting  $\alpha_H/\alpha_0$  where  $\alpha$  is the first Townsend coefficient against values of  $(H/E)$  varying from 0 to 2.5. From this result he has concluded that possibly drift velocity is a linear function of  $(E/P)$  for small  $(E/P)$  values but varies as  $(E/P)^n$  where  $n > 1$  for larger values of  $(E/P)$ . An attempt has been made here to explain the variation of  $C_1$  with  $H$ . We have

$$C_1 = \left[ \frac{e}{m} \cdot \frac{L}{u_H} \right]^2 = A/u_H^2$$

where  $A$  is a constant, and  $u_H$  is the random velocity of electrons in presence of a magnetic field. That the random velocity of electrons varies in presence of magnetic field is evident from the fact that the electron temperature which is a measure of the random velocity varies in a magnetic field also. Hence

$$C_1 = \frac{AK}{v_H^2} \text{ where } K = (2m/M)$$

$$= \frac{a'}{v_H^2} \text{ where } a' \text{ is another constant.}$$

and it has been pointed out by Blevin and Haydon

$$v_0/v_H = [1 + C_1 H^2/P^2].$$

$$\therefore C_1 = \frac{a'[1 + C_1 H^2/P^2]^2}{v_0^2} = a[1 + C_1 H^2/P^2]^2 \text{ where } a = a'/v$$

$$\therefore C_1 = \frac{[1 - 2a \cdot H^2/P^2] \pm \sqrt{(2a \cdot H^2/P^2 - 1)^2 - 4a^2 H^4/P^4}}{2aH^4/P^4}$$

$$= \frac{[1 - 2a \cdot H^2/P^2] \pm \sqrt{1 - 4aH^2/P^2}}{2aH^4/P^4}$$

$$\approx \frac{P^2}{H^2} \left\{ \frac{P^2}{aH^2} - 2 \right\}$$

which shows that the value of  $C_1$  should decrease with the increase in magnetic field. The nature of the curve in Fig. 2 shows that for values of magnetic field

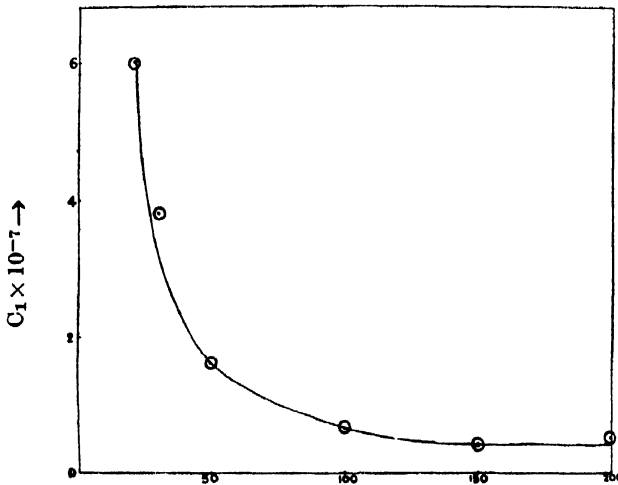


Fig. 2.  $H$  in gauss  $\rightarrow$

greater than 100 gauss, the value of  $C_1$  tends to assume a constant value where as for smaller values of magnetic field it is very susceptible to change for small changes in the magnetic field.

In conclusion it may be stated that the expression for mobility of electrons in a magnetic field as deduced either by Townsend and Gill or by Blevin and Haydon is valid for a limited range of pressure above .125 mm of Hg and the constant  $C_1$  becomes a function of the magnetic field, but practically becomes a constant for values of magnetic field greater than 100 gauss. At the same time, it must be borne in mind that the conclusions reached above are derived from computed values of mobility from breakdown measurements, which the authors think are liable to error. A systematic investigation of mobility measurements in presence of a magnetic field has therefore been undertaken and the results will be reported in future.

#### ACKNOWLEDGMENT

The present work forms part of a programme of work in the C.S.I.R. scheme entitled "Electrical discharge Phenomena in Gases and its investigation by Microwave probe and optical methods" and the authors are indebted to Council of Scientific and Industrial Research Government of India for financing the Project.

#### REFERENCES

- Blevin, H. A. and Haydon, S. C., 1958, *Aust. J. Phys.* **11**, 18.  
Haydon, S. C., 1961, *Proc. Fifth. Int. Conf. on Ionization Phenomena in Gases. Munich*, **1**, 7, 63.  
Sen, S. N. and Ghosh, A. K., 1962, *Proc. Phys. Soc. (London)* **80**, 909.  
Townsend, J. J. and Gill, E. W. B., 1938, *Phil Mag.*, **26**, 290.  
Von Engel A 1955, *Ionised Gases*. (Clarendon Press Oxford).

# COHESIVE ENERGY, COMPRESSIBILITY AND THERMAL EXPANSION OF DIATOMIC CRYSTALS

C. M. KACHHAVA AND S. C. SAXENA

PHYSICS DEPARTMENT, RAJASTHAN UNIVERSITY, JAIPUR, INDIA.

(Received December 13, 1963 ; Resubmitted May 25, 1964)

**ABSTRACT.** In this paper we suggest various methods of calculating cohesive energy, compressibility and thermal expansion of diatomic crystals, and apply them for the particular case of alkali halides. The procedure suggested by us recently for evaluating one parameter of the potential energy function by using the molecular constants is upheld and confirmed, as the results, thus obtained, favourably compare with those based on crystal constants only.

## INTRODUCTION

If the interaction potential energy between atoms of a crystal lattice be known several macroscopic properties can be predicted. However, even to fix the two unknown parameters of the simplest potential energy expression one needs the knowledge of equilibrium interionic separation in the lattice  $r_0$ , the compressibility  $\beta$ , its temperature and pressure derivatives, and the coefficient of thermal expansion  $\alpha$ , Born and Huang (1956). Usually such data are not available and therefore alternative procedures which may not require the knowledge of so many crystal properties will be useful. A somewhat limited success only has been achieved in this direction by assigning a finite size to the ions or atoms constituting the lattice, Kettel (1956), Pauling (1960), and Kachhava and Saxena (1963a).

Recently we (1963b) have suggested to fix one of the parameters of the potential energy function of the diatomic crystals by considering the equilibrium internuclear separation and the force constant. This procedure therefore requires the knowledge of a comparatively smaller number of crystal properties and hence can be used for their determination. We in this paper propose to investigate in particular the diatomic alkali halide crystals and will consider the three simple properties viz., cohesive energy ( $W$ ),  $\beta$  and  $\alpha$ .

## POTENTIALS AND DETERMINATION OF PARAMETERS

We will consider in our calculations the following three forms for the mutual potential energy per ion-pair in a crystal lattice,  $\phi(r)$ , :

$$\phi(r) = -\frac{\alpha e^2}{r} - \frac{C}{r^6} - \frac{D}{r^8} + \frac{A_1}{r^n}, \quad \dots \quad (1)$$

$$\phi(r) = -\frac{\alpha e^2}{r} - \frac{C}{r^6} - \frac{D}{r^8} + A_3 e^{-r/\rho}, \quad \dots (2)$$

and

$$\phi(r) = -\frac{\alpha e^2}{r} - \frac{C}{r^6} - \frac{D}{r^8} + A_3 e^{-\sigma r^2}. \quad \dots (3)$$

Here  $\phi(r)$  is the potential energy of an ion-pair interacting with the rest of the lattice and with each other,  $r$  is the interionic separation,  $\alpha$  the Madelung constant,  $C$  and  $D$  are the van der Waals constants,  $A_1, A_2, A_3, n, \rho$  and  $\sigma$  are the potential parameters. The first two are the familiar Born and Born-Mayer potentials respectively, while the third one is usually referred as the Gaussian potential and is due to Varshni and Shukla (1961). It will be noted that all the three potentials differ only in assuming the different forms for the overlap energy, and this form will be used to characterise the potential. The constants  $C$  and  $D$  have already been evaluated by Mayer (1933) and we have used the values given by him.

One constant of each potential i.e.  $n, \rho$  or  $\sigma$  can be determined using the molecular constants and adopting the procedure given by Kachhava and Saxena (1963*b*) except we have used potentials similar to those given by Eqs. (1) to (3). The other constant is evaluated from the condition,

$$\frac{\partial \phi(r)}{\partial r} = 0, \quad \text{at } r = r_0. \quad \dots (4)$$

A more general form of Eq. (4) is

$$r \frac{\partial \phi(r)}{\partial r} = \frac{3rT}{\beta} \left( \frac{1}{V} \frac{\partial V}{\partial T} \right)_P. \quad \dots (5)$$

In Eq. (5)  $v$  is the volume of the molecule,  $V$  and  $P$  represent the volume and pressure respectively, and  $\left( \frac{1}{V} \frac{\partial V}{\partial T} \right)_P$  stands for  $\alpha$ .

Born and Mayer (1932) have also derived the relation

$$r^2 \frac{d^2 \phi(r)}{dr^2} = \frac{9v}{\beta} \left[ 1 + \frac{T}{\beta} \left\{ \left( \frac{\partial \beta}{\partial T} \right)_P + \left( \frac{1}{V} \frac{\partial V}{\partial T} \right)_P \left( \frac{1}{\beta} \frac{\partial \beta}{\partial P} \right)_T \right\} + \frac{2}{3} T \left( \frac{1}{V} \frac{\partial V}{\partial T} \right)_P \right]. \quad \dots (6)$$

The quantity within square brackets in Eq. (6) is usually not much different from unity around room temperature and is equal to unity at absolute zero. Equation (6) is therefore very often used in the following simple form and specially when the various derivatives of  $\beta$ , and  $\alpha$  are not known :

$$r^2 \frac{d^2 \phi(r)}{dr^2} = \frac{9v}{\beta}. \quad (7)$$

Equations (5) and (6) may be combined to eliminate  $\alpha$  yielding the relation

$$r^2 \frac{d^2\phi(r)}{dr^2} = \frac{9v}{\beta} \left[ 1 + \frac{T}{\beta} \left\{ \left( \frac{\partial\beta}{\partial T} \right)_P + \frac{\beta r}{3vT} \left( \frac{\partial\phi(r)}{\partial r} \right) \left( \frac{1}{\beta} \frac{\partial\beta}{\partial P} \right)_T \right\} + \frac{2\beta r}{9v} \left( \frac{\partial\phi(r)}{\partial r} \right) \right] \dots (8)$$

Equation (8) can also be used to evaluate the second potential parameter if  $\beta$  and its temperature and pressure derivatives be known.

One can also eliminate  $\beta$  from Eqs. (5) and (7) so that

$$\frac{d\phi(r)}{dr} = \frac{\alpha r T}{3} \frac{d^2\phi(r)}{dr^2} \dots (9)$$

Equation (9) can also be used to determine the second potential parameter when  $\alpha$  is known.

#### COHESIVE ENERGY

Thus, knowing the potential parameters,  $\phi(r_0)$  and hence the cohesive energy per mole,  $W$ , is computed by the following relation :

$$W = -[N\phi(r_0) + \epsilon_0], \dots (10)$$

Where  $N$  is the Avogadro's number and  $\epsilon_0$  is the zero-point energy per mole. We have used the  $\epsilon_0$  values given by Cubicciotti (1959).

Computed values of the cohesive energy for all the alkali halide crystals according to the various procedures outlined in the previous section are reported in Table I along with the experimental values. Columns 3, 5 and 7 list the calculated values according to the potentials of Eqs. (1), (2) and (3) respectively. The two potential parameters were determined in each case by using the molecular constants and the approximate condition given by Eq. (4). The agreement between theory and experiment is not satisfactory for the inverse potential but is good for the exponential and gaussian potentials with a preference for the former. To see the effect of using the approximate Eq. (4) we have also evaluated the potential parameters of the exponential potential in conjunction with the molecular constants and Eq. (5) and the values of cohesive energy so obtained are given in Col. 9 of Table 1. These values are in very much agreement with the values of Col. 5 thereby indicating that the use of Eq. (4) instead of Eq. (5) will not vitiate the values of  $W$  appreciably and is important, for Eq. (5) involves the knowledge of both  $\alpha$  and  $\beta$ .

Evaluation of potential parameters from molecular constants and Eq.(9) yields values for  $W$  which are listed in Col. 11 of Table 1. These values refer to

the exponential potential and are also in good agreement with the experimental values. In an analogous fashion Eq. (8) can also be used instead of Eq. (9) to fix the second parameter of the potential energy function. The calculated values of cohesive energy obtained in this manner and on the exponential potential are reported in Col. 13 of Table 1. This approach, however, does not always lead to satisfactory results and in Table 1 we list only those cases where agreement with the experimental values is reasonable. The reason for the failure of this method can be easily understood if we look into the following expression used for the determination of the potential parameter  $A_2$ :

$$A_2 = \frac{\left( \frac{2\alpha e^2}{r_0} + \frac{42C}{r_0^6} + \frac{72D}{r_0^8} \right) + \frac{9v}{\beta} \left\{ 1 + T \left( \frac{1}{\beta} \frac{\partial \beta}{\partial T} \right)_P \right\} + \left\{ \frac{3}{\beta} \left( \frac{1}{\beta} \frac{\partial \beta}{\partial P} \right)_T + 2 \right\}}{\frac{r_0}{\rho} \left[ \frac{r_0}{\rho} + 2 + \frac{3}{\beta} \left( \frac{1}{\beta} \frac{\partial \beta}{\partial P} \right)_T \right]} \left\{ \frac{\alpha e^2}{r_0} + \frac{6C}{r_0^6} + \frac{8D}{r_0^8} \right\} \quad \dots \quad (11)$$

For all those substances where enhanced discrepancies are found it turns out that the value of  $A_2$  is sensitively controlled by the terms containing  $\frac{\partial \beta}{\partial P}$ . It so happens that both numerator and denominator effectively become the difference of two almost equal quantities and as the accuracy with which  $\frac{\partial \beta}{\partial P}$  is known is rather small we get absurd values for  $A_2$  from Eq. (11).

We (1963c) have also recently computed the cohesive energies of all these compounds on these three potentials using the crystal properties only viz., Eqs. (5) and (6). The average absolute deviations for the inverse, exponential and gaussian potentials are 1.1, 0.97 and 0.95 per cent respectively. The results of Table 1 are thus of comparable accuracy and confirm the approach adopted in their calculation. This procedure has the advantage of unifying the molecular and crystal properties on the basis of one common parameter and also for determining the parameters, knowledge of  $\alpha$  and  $\beta$  is not required and therefore these properties can be predicted. We will consider this possibility in the next two sections.

#### COMPRESSIBILITY

The potential determined from the knowledge of molecular constants and Eq. (4) can be used to calculate  $\beta$  from Eq. (7). This method is rigorous but for the fact that  $r_0$  values used in computation refer to room temperature instead of 0°K. Actual calculations reveal that this approximation does not affect the

values of  $\beta$  very much and can be taken as an approximate method for evaluating it. Calculated values of  $\beta$  according to this procedure and for all the three potentials are given in Table 2. The direct experimental values at 25°C as well as those reduced to 0°A in conjunction with the data of Cubicciotti (1959) are also listed in this table for comparison. The values obtained on the basis of the inverse and gaussian potentials are inadequate while the exponential potential yields better results. The calculated values of  $\beta$  are also given for the exponential potential leaving van der Waals terms with a view to see the relative contributions of the latter. It will be noted that for better accuracy dispersion terms should be considered.

The two parameters of the potential energy function can also be determined by the use of molecular constants and the experimental value of the cohesive energy. This may, however, be not a very suitable approach as in ionic crystals the contribution of the overlap part to the total potential energy is only about 10%. Actual calculated values of  $\beta$  according to this procedure and Eq. (7) confirm this for the percentage deviations between theory and experiment usually increase as one considers the various halides of the same element from fluoride to iodide and also as the element is changed from Li to Cs.

Instead of using the molecular constants we can use Eq. (4) and the cohesive energy values to determine the two parameters of the potential energy function and then  $\beta$  is calculated from Eq. (7). Two sets of values of  $\beta$  obtained in this fashion, one for the exponential potential without dispersion terms and the other with dispersion terms, are given in Table II. The latter set of values are in better agreement with the experimental values and does emphasize the importance of dispersion terms in evaluating  $\beta$ . In these calculations of  $\beta$  we have made use of only the crystal properties and the fact that these are in good agreement with the values where molecular constants have been used to evaluate the common parameter, substantiates the latter approach.

We can also determine the potential completely by the knowledge of molecular constants and Eq. (9) and then  $\beta$  can be evaluated from Eq. (7). Values obtained in this way are also recorded in Table II and these are in good agreement with the experimental values at 25°C.

#### THERMAL EXPANSION

Theoretically speaking the two parameters of the potential can be determined using the molecular constants and either the cohesive energy or Eq. (8) and then  $\alpha$  is calculated from Eq. (5). We could also employ the combination of cohesive energy and Eq. (8) and then in conjunction with Eq. (5)  $\alpha$  can be calculated. In actual practice none of these methods yields satisfactory results the reason being the insensitivity of the cohesive energy for the purpose of evaluating the potential parameters and the small accuracy with which  $\beta$  and its derivatives are usually known.



TABLE I  
Cohesive energy of alkali halide crystals in K cal/mole.

Sub- stance	Exptl. Potential c	Inverse Potential c	%dev. c	Expo- nential potential c	% dev. c	Gaussian potential c	% dev. c	Expo- nential potential d	% dev. d	Expo- nential potential e	% dev. e	Expo- nential potential f	% dev. f
LiF	246.0a	240.3	-2.3	248.8	+1.1	262.7	+6.8	250.6	+1.9	250.7	+1.9	248.2	+0.8
LiCl	201.5b	189.0	-6.2	201.9	+0.2	210.3	+4.8	203.6	+1.0	203.9	+1.2	198.1	-1.5
LiBr	191.5b	176.9	-7.6	189.2	+1.2	197.3	+3.0	191.2	-0.2	191.3	-0.1	187.1	-2.3
LiI	180.0b	163.6	-9.1	174.6	-3.0	182.0	+1.1	176.9	-1.7	177.0	-1.7	172.1	-4.4
NaF	218.0a	—	—	—	—	—	—	—	—	—	—	—	—
NaCl	184.7b	176.6	-4.4	185.5	+0.4	190.0	+2.9	187.1	+1.3	189.2	+2.4	186.2	+0.8
NaBr	175.9b	167.9	-4.7	176.0	+0.1	181.8	+3.4	177.8	+1.1	179.0	+1.8	174.8	-0.6
NaI	166.3b	155.6	-6.4	163.3	-1.8	168.7	+1.4	165.1	-0.7	165.1	-0.7	165.7	-0.4
KF	193.0b	181.5	-6.0	193.8	+0.4	202.0	+4.7	195.4	+1.2	195.4	+1.2	194.5	+0.8
KCl	167.8b	161.7	-3.6	168.9	+0.7	174.1	+3.8	170.3	+1.5	170.4	+1.7	166.3	-0.9
KBr	161.2b	153.5	-4.8	159.6	-1.0	165.4	+2.6	162.2	+0.6	162.1	+0.6	164.4	+2.0
KI	152.8b	141.0	-7.7	149.2	-2.4	154.2	+0.9	151.1	-1.1	150.8	-1.3	—	—
RbF	—	180.0	—	189.7	—	195.9	—	191.1	—	191.3	—	—	—
RbCl	163.6b	155.3	-5.0	162.5	-0.7	167.6	+2.4	163.9	+0.2	163.9	+0.2	163.8	+0.1
RbBr	158.0b	149.2	-5.6	155.7	-1.5	159.0	+0.6	157.1	-0.6	157.2	-0.5	156.5	-1.0
RbI	149.7b	138.5	-7.5	145.1	-3.2	150.0	+0.2	146.8	-2.0	146.6	-2.1	141.2	-5.7
CsF	—	172.4	—	181.6	—	187.8	—	182.9	—	183.2	—	—	—
CsCl	157.8b	146.6	-7.1	154.5	-2.1	160.1	+1.5	156.7	-0.7	156.7	-1.0	—	—
CsBr	152.3b	139.5	-8.4	147.5	-3.2	153.2	+0.6	149.6	-1.8	149.5	-1.8	—	—
CsI	145.4b	122.8	-15.0	136.7	-6.0	142.2	+2.2	139.1	-4.3	138.4	-5.0	—	—
Avg. Abs. % dev.	6.6	1.7	2.5	1.3	1.5	1.6							

a. Plendl, J. N., 1961, *Phys. Rev.*, **123**, 1174.

b. Born, M., and Huang, K., 1956, *Dynamical Theory of Crystal Lattices*, (Oxford: Clarendon Press).

c. Potential parameters determined using the molecular constants and Eq. (4).

d. Potential parameters determined using the molecular constants and Eq. (5).

e. Potential parameters determined using the molecular constants and Eq. (9).

f. Potential parameters determined using the molecular constants and Eq. (8).

TABLE II  
Compressibility ( $\beta$ ) of alkali halide crystals in  $10^{-12}$  cm<sup>2</sup> dyne<sup>-1</sup>

Substance	Exptl.		Inverse		Simple*		Exponential		Exponential		Gaussian	
	298°A	0°A	Potential	% Dev.	Potential	% Dev.	Potential	% Dev.	Potential	% dev.	Potential	% dev.
LiF	1.43a	1.34	1.90	+41.8	1.28	-4.5	1.26	-6.0	0.71	-47.0		
LiCl	3.17a	3.04	3.53	+16.1	2.61	-14.1	2.49	-18.1	1.54	-50.0		
LiBr	3.90a	3.44	4.59	+33.4	3.56	+3.6	3.20	-7.0	1.97	-42.7		
LiI	5.30a	4.52	6.16	+35.8	4.67	+3.1	4.32	-4.4	2.68	-40.7		
NaF	2.06a	1.94	—	—	—	—	—	—	—	—		
NaCl	3.97a	3.24	4.42	+36.4	3.58	+10.5	3.42	+5.5	2.32	-28.4		
NaBr	4.75a	4.17	5.32	+27.6	4.37	+10.0	3.79	-9.1	2.80	-32.9		
NaI	6.21a	5.29	7.17	+35.5	5.94	+13.0	5.52	+4.3	3.75	-29.1		
KF	3.14a	2.95	4.25	+44.1	3.25	+10.2	3.07	+4.1	1.93	-34.6		
KCl	5.50a	4.93	5.96	+20.9	5.00	+1.4	4.68	-6.1	3.25	-10.2		
KBr	6.45a	5.53	7.54	+36.4	6.36	+15.0	5.96	+7.8	4.14	-24.8		
KI	8.07a	7.25	10.11	+39.4	8.91	+23.0	8.28	+15.0	5.74	-20.8		
RbF	3.66a	3.44	3.81	+10.8	3.05	-11.3	2.83	-17.7	1.84	-46.5		
RbCl	6.16a	5.61	7.01	+25.0	5.91	+5.3	5.45	-2.7	3.76	-33.0		
RbBr	7.38a	6.14	8.10	+31.9	6.98	+13.7	6.41	+14.3	5.07	-17.4		
RbI	9.00a	7.98	11.35	+42.2	9.86	+23.7	9.01	+13.0	6.25	-21.7		
CsF	4.25a	4.00	4.34	+8.5	3.32	-17.0	3.02	-24.5	2.00	-50.0		
CsCl	5.55a	4.64	6.77	+46.0	5.62	-21.1	4.91	+5.8	3.20	-31.0		
CsBr	6.28a	5.61	7.63	+36.0	7.20	+28.4	5.75	+2.5	3.85	-31.4		
CsI	7.83a	6.62	12.98	+96.4	10.80	+63.1	9.48	+43.2	6.04	-8.8		
Avg.	Obs.	% dev.		35.4		15.4		10.9		31.6		

TABLE II—(contd.)

Substance	Exptl.		Simple*		Exponential potential $e$	% dev.	Exponential potential $f$		% dev.	Exponential potential $g$		% dev.
	298°A	0°A	Exponential	potential								
LiF	1.43a	1.34	1.52	1.39	1.39	+ 3.7	1.14	1.14	-14.9	1.34	1.34	- 6.3
LiCl	3.17a	3.04	2.67	2.53	2.53	-13.9	2.45	2.45	-19.4	2.77	2.77	-12.6
LiBr	3.90a	3.44	2.88	2.83	2.83	-16.3	3.66	3.66	- 6.3	3.63	3.63	- 6.9
LiI	5.30a	4.52	2.91	3.08	3.08	-35.6	6.30	6.30	+39.4	5.02	5.02	- 5.3
NaF	2.06a	1.94	2.18	2.13	2.13	-12.4	—	—	—	—	—	—
NaCl	3.97a	3.24	3.63	3.58	3.58	+12.0	3.27	3.27	+ 1.0	4.35	4.35	+ 9.6
NaBr	4.75a	4.17	3.69	4.16	4.16	-11.5	5.68	5.68	+36.2	4.60	4.60	+ 3.2
NaI	6.21a	5.29	4.16	6.93	6.93	-21.4	4.16	4.16	-21.4	6.27	6.27	+ 1.0
KF	3.14a	2.95	3.24	3.19	3.19	-10.2	2.95	2.95	0.0	3.34	3.34	- 6.4
KCl	5.50a	4.93	4.79	5.03	5.03	- 2.8	4.36	4.36	-11.5	5.12	5.12	- 6.9
KBr	6.45a	5.53	5.31	5.74	5.74	- 3.8	6.20	6.20	-12.1	6.62	6.62	+ 2.6
KI	8.07a	7.25	5.61	6.42	6.42	-22.6	10.94	10.94	+50.9	8.31	8.31	+ 3.0
RbF	3.66a	3.44	—	—	—	—	—	—	—	3.12	3.12	-12.0
RbCl	6.16a	5.61	4.41	5.05	5.05	-21.4	5.90	5.90	+ 5.2	6.02	6.02	- 2.3
RbBr	7.38a	6.14	4.44	5.51	5.51	-27.6	7.51	7.51	+22.3	7.11	7.11	- 3.7
RbI	9.00a	7.98	4.79	6.40	6.40	-40.0	13.31	13.31	-66.8	10.08	10.08	+12.0
CsF	4.25b	4.00	—	—	—	—	—	—	—	3.37	3.37	-20.7
CsCl	5.55c	4.64	2.22	3.86	3.86	-52.2	6.37	6.37	+37.3	5.67	5.67	+ 2.2
CsBr	6.28c	5.61	2.22	4.13	4.13	-60.5	8.29	8.29	+47.8	6.60	6.60	+ 5.1
CsI	7.83c	6.62	1.47	4.80	4.80	-77.8	24.62	24.62	+272.0	10.80	10.80	+37.8
Avg.	abs.	% dev.	25.2	14.3	—	—	—	—	—	—	—	8.2

a. Spangenberg, K., 1956, *Naturwissenschaften*, **43**, 394; Spangenberg, K., and Haussühl, S., 1957, *Z. Krist.*, **109**, 422.b. Huggins, M. L., 1937, *J. Chem. Phys.*, **5**, 143; 1947, *Ibid.*, **15**, 212.c. Bridgman, P., 1940, *Proc. Amer. Acad. Arts. Sci.*, **74**, 21.d. Potential parameters evaluated using molecular constants and Eq. (4) and  $\beta$  calculated from Eq. (7).e. Potential parameters evaluated using cohesive energy and Eq. (4) and  $\beta$  calculated from Eq. (7).

f. Potential parameters evaluated using molecular constants and cohesive energy.

g. Potential parameters evaluated using molecular constants and Eq. (9).

\*Exponential potential without dispersion terms.

TABLE III

Thermal expansion ( $\alpha$ ) of alkali halide crystals in  $10^{-5}/^{\circ}\text{C}$ .

Substance	Exptl. <i>a</i>	Exponential potential	
		<i>b</i>	<i>c</i>
LiF	9.2	17.9	—
LiCl	12.2	36.4	14.10
LiBr	14.0	23.1	— 8.72
LiI	16.7	22.8	27.83
NaF	9.8	—	—
NaCl	11.0	16.5	—60.25
NaBr	11.9	15.5	7.34
NaI	13.5	12.3	— 5.96
KF	10.0	13.8	— 0.965
KCl	10.1	16.8	4.76
KBr	11.0	8.1	6.11
KI	12.5	7.9	16.48
RbF	9.5	45.7	—
RbCl	9.85	13.3	10.22
RbBr	10.4	14.3	8.42
RbI	11.9	—0.13	17.03
CsF	9.5	33.3	—
CsCl	13.65	11.5	17.23
CsBr	13.9	8.7	20.57
CsI	14.6	—18.7	22.64

*a.* Huggings, M. L., 1937, *J. Chem. Phys.*, **5**, 143.

*b.* Potential parameters evaluated using molecular constants and Eq. (7) and then  $\alpha$  is calculated from Eq. (5).

*c.* Potential parameters evaluated using molecular constant and cohesive energy and then  $\alpha$  is calculated from Eq. (5).

However, for the approximate estimation of  $\alpha$  we found two methods fairly satisfactory and dependable. The two parameters can be determined with the use of Eq. (7) and either the molecular constants or the cohesive energy and subsequently  $\alpha$  is calculated from Eq. (5). Computed values of  $\alpha$  according to both these procedures for the exponential potential are given in Table 3 along with the experimental values. The agreement between theory and experiment is only approximate and is obvious because of the use of Eq. (7) which is not rigorous. Nevertheless, these methods can be used with reliance for estimating the values of  $\alpha$ . The listings of Table III further confirm the approach of evaluating the common parameter of the potential from the use of molecular constants instead of crystal constants.

REFERENCES

- Born, M., and Huang, K., 1956, *Dynamical Theory of Crystal Lattices*, (Oxford : Clarendon Press).
- Born, M., and Mayer, J. E., 1932, *Zeit. f.* **1**, 75.
- Cubieciotti, D., 1959, *J. Chem. Phys.*, **31**, 1964 ; *Ibid.*, 1961, **34**, 2189.
- Kachhava, C. M., and Saxena, S. C., 1963a, *Molecular Phys.*, **7**, 465 (1964).
- Kachhava, C. M. and Saxena, S. C., 1963b, *Phil. Mag.* **8**, 1429.
- Kachhava, C. M., and Saxena, S. C., 1963c, to be published.
- Kittel, C., 1956, *Introduction to Solid State Physics*, (New York : Wiley).
- Mayer, J. E., 1933, *J. Chem. Phys.*, **1**, 270.
- Pauling, L., 1960, *The Nature of the Chemical Bond*, (Cornell : University Press).
- Varshni, Y. P., and Shukla, R. C., 1961, *J. Chem. Phys.*, **35**, 582.

ON THE  $\beta \rightarrow \beta'$  TRANSFORMATION IN CU-SN ALLOY

B. N. DEY and M. A. QUADER

DEPARTMENT OF GENERAL PHYSICS AND X-RAYS,  
INDIAN ASSOCIATION FOR THE CULTIVATION OF SCIENCE, CALCUTTA-32.

(Received May 21, 1964)

**ABSTRACT.** The x-ray powder diffraction pattern of  $\beta'$  Cu-Sn alloy phase has been interpreted on the basis of a tetragonal unit cell with  $a = 3.726$  Å and  $c = 3.642$  Å. The probable space groups are  $P4/n$  and  $P4/nmm$ . There are four atoms in the unit cell.

## INTRODUCTION

According to the phase diagram of the Cu-Sn system (Lyman, 1948) the  $\beta$  phase forms peritectically at  $798^\circ\text{C}$  and decomposes at  $586^\circ\text{C}$  in the range of composition of 23.6 to 27 wt. % of tin. Earlier X-ray investigations of the  $\beta$  phase by Isawa (1936; 1937) revealed that the body-centred-cubic  $\beta$  phase alloy containing less than 25wt. % Sn transformed to  $\beta'$  phase on quenching from above  $600^\circ\text{C}$ ; and the phase thus formed transformed to  $\alpha + \delta$  phases on annealing. However, the  $\beta$  phase alloy containing 25 to 27 wt. % Sn gave the  $\beta$  phase itself on quenching. Isaichev (1939a and b) also reported that the  $\beta$  phase alloy containing 23.6 to 25wt% Sn transformed martensitically to  $\beta'$  phase on quenching. From the X-ray pattern he suggested that there did exist some orientation relationship between  $\beta$  and  $\beta'$  phases. However, the structure of the  $\beta'$  phase have not been determined in either of the above investigations. The metallographic study of the  $\beta$  phase Cu-Sn alloy by Greninger and Mooradian (1938) exhibited markings parallel to  $[133]_\beta$  in as-quenched metastable  $\beta$  phase. The markings had been shown to be due to lattice transformations with  $[133]_\beta$  as the habit plane; the reversal of this martensite was also observed. A preliminary crystallographic study of  $\beta'$  phase has been reported here.

## EXPERIMENTAL DETAILS

The  $\beta$  phase Cu-Sn alloy with 15.08 at.% Sn was prepared from spectroscopically pure Matthey copper and tin by melting accurately weighed quantities of the metals in evacuated and sealed silica tubes. The alloy thus prepared was homogenized at  $780^\circ\text{C}$  for one week and then quenched in water. Filings obtained from the homogenized alloy were taken in evacuated and sealed pyrex tubes, annealed for two hours between  $620$  to  $630^\circ\text{C}$  and then quenched in oil. Oil was used as the quenching medium for the use of water resulted in oxidation in some cases. In most of the cases of quenching either

$\beta$  phase or a mixture of  $\beta$  and other phases was obtained except in two occasions, when the transformation only to  $\beta'$  phase was obtained. X-ray diffraction photographs for the  $\beta$  and  $\beta'$  phases were obtained using copper  $K_{\alpha}$  radiations from a Philips x-ray generator. The diffraction patterns for the  $\beta$  and  $\beta'$  phases are represented schematically in the Fig. 1.

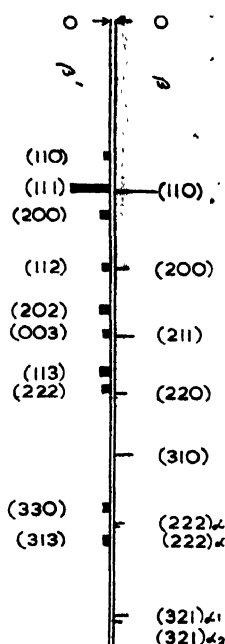


Fig. 1—Schematic representation of diffraction pattern of  $\beta$  and  $\beta'$  phases Cu-Sn alloy. The height of the lines represent relative intensity.

#### INTERPRETATION OF THE POWDER DIFFRACTION PATTERN

For the  $\beta$  phase alloy the diffraction lines are sharp and strong while those for the  $\beta'$  phase are all diffuse. The diffuseness of the diffraction lines shows that the structure of the  $\beta'$  phase is heavily faulted. However, the diffraction pattern for the  $\beta'$  phase could be interpreted, as given in Table I on the basis of a tetragonal unit cell with  $a = 3.726 \text{ \AA}$ ,  $c = 3.642 \text{ \AA}$  and  $c/a = .977$  (using for copper radiations  $\lambda K_{\alpha_1} = 1.54051$  and  $\lambda K_{\alpha_2} = 1.54433 \text{ \AA}$ ). For the  $\beta$  phase alloy with A2 structure the lattice parameter  $a = 2.9816 \text{ \AA}$  at  $35^\circ\text{C}$  (room temperature).

It is evident from Table I that reflections with  $(hkl)$  and  $(hko)$  when  $h+k = 2n+1$  are absent and the possible space groups of  $\beta'$  phase are therefore  $P4/n$  and  $P4/nmm$ . The  $\beta'$  phase has roughly twice the volume of the  $\beta$  phase and therefore the probable number of atoms per unit cell of the  $\beta'$  phase are four.

TABLE I  
Diffraction pattern for  $\beta'$  phase Alloy.

$\text{Sin}^2 \theta$ obs	$\text{Sin}^2 \theta$ cal.	(hkl)	Intensity
.0859	.0856	(110)	v.w.
.1306	.1304	(111)	s
.1717	.1712	(200)	w
.2650	.2648	(112)	v.w.
.3505	.3504	(202)	v.w.
.4002	.3996	(003)	w
.4851	.4852	(113)	w
.5213	.5216	(222)	v.w.
.7705	.7704	(330)	v.v.w
.8271	.8276	(313)	v.v.w

The crystallographic aspect of the  $\beta \rightarrow \beta'$  transformation could not be assessed at the present stage of investigation. Further X-ray and metallography work with single crystal grains of  $\beta$  phase alloy are included in our future programme.

#### ACKNOWLEDGMENT

The authors are indebted to Prof. B. N. Srivastava, D.Sc., F.N.I., for his continued interest and encouragement in this work. One of us (B.N.D.) wishes to acknowledge a research grant from C.S.I.R. (New Delhi).

#### REFERENCES

- Greninger, A. B., and Mooradian, V. G., 1938, *Trans. AIME*, **128**, 337.  
 Isaichev, I., 1939a, *J. Tech. Phys.* (U.S.S.R.), **9**, 1286; 1939b, *Ibid.*, **9**, 1867.  
 Isawa, T., 1936, *Tetsu to Hagane*, **22**, 960; 1937, *Mem. Royjun Col. Eng.*, **10**, 53.  
 Lyman, T., 1948, *Metals Handbook*, American Soc. Metals, Cleveland pp. 1204.



# DYNAMIC ELASTIC MODULUS AND DAMPING COEFFICIENT OF SOME INDIAN TIMBERS

W. J. JOHN AND M. M. LAL

DEFENCE RESEARCH LABORATORY (MATERIALS), KANPUR

(Received July 19, 1963)

**ABSTRACT.** The dynamic elastic modulus  $E_d$  and damping coefficient in terms of  $1/Q$ , which is also related to logarithmic decrement  $\delta$ , have been measured parallel to grain on thirteen kinds of Indian timber employing a flexural vibration method. The static elastic modulus  $E_s$  has also been determined on the same samples.

The dynamic modulus  $E_d$  varies from  $0.80 \times 10^{11}$  to  $1.61 \times 10^{11}$  dynes/cm<sup>2</sup> and  $E_s$  the static modulus from  $0.66 \times 10^{11}$  to  $1.42 \times 10^{11}$  dynes/cm<sup>2</sup>.  $E_d$  averages about 15 per cent higher than  $E_s$  while  $\delta$  ranges from 0.028 to 0.053. Results show that in general  $\delta$  increases with  $E_d/E_s$ .

## INTRODUCTION

Considerable amount of indigenous timbers is being used for the construction of aircrafts, automobiles, bridges and similar other structures which are subject to dynamic forces. But as yet no systematic information is available on the dynamic elastic and damping properties of these materials. A knowledge of the dynamic elastic and damping characteristics of timbers is helpful in making an intelligent and economic use of the materials in all technical applications where vibrations must be considered. From an engineering point of view, in structural components where vibration is a hazard, the use of materials which have a high damping capacity is preferred if other strength properties are satisfactory. The damping capacity of wood is greater than for most other structural materials particularly the metals (Brown, Panshin and Forsaith, 1952).

The present preliminary investigation relates to some indigenous timbers of common use. Only 13 kinds of timber were selected for study from those listed in IS 399-1952 "Indian Standard Classification of Commercial Timbers and their Zonal Distribution." The timber specimens were procured in the log form (about 3 ft. long) from the forest departments of the various states in India. Only one log of each type was obtained. No attempt was made to study the variations of the properties in different parts of the same tree, or from tree to tree of the same type grown in different regions, nor even the properties in different directions. No exhaustive statistical analysis of the data is, therefore, made; only the mean and standard errors are shown.

The dynamic elastic modulus and the damping coefficient were determined parallel to the grain at about 12% moisture content by a flexural vibration method. These were compared with the static modulus determined on the same samples by the loaded beam method.

## THEORETICAL CONSIDERATIONS

### *Dynamic Modulus of Elasticity (Young's)*

The method is based on the vibration of a rectangular bar in the free-free mode i.e. the ends of the bar are left free. It has been shown that in this mode of vibration at the fundamental resonance frequency the nodal points are situated at distances 0.224 times the length of the bar from either ends. The frequency of the vibration in such a mode has been worked out (Lord Rayleigh, 1926) as

$$f = \frac{kc m^2}{2\pi l^2}$$

where  $k$  = radius of gyration of the section about an axis perpendicular to the plane of bending.

$c$  = velocity of propagation of sound,

$m$  = a constant = 4.730 for the fundamental,

$l$  = length of the bar.

Since 
$$c = \left[ \frac{E_d}{\rho} \right]^{\frac{1}{2}}$$

where  $E_d$  = dynamic modulus of elasticity,

$\rho$  = density;

$$E_d = \frac{4\pi^2 l^4 f^2 \rho}{m^4 k^2}$$

For a bar of rectangular cross-section  $k = \frac{t}{(12)^{\frac{1}{4}}}$ , where  $t$  is the thickness, so that

$$E_d = \frac{48\pi^2 l^4 f^2 \rho}{m^4 t^2} T,$$

where  $T$  is a correction factor introduced (Timoshenko 1921, 1922) to account for the effect of rotary inertia and moment of shear.  $T$  has been shown to depend on  $\frac{k}{l}$  and Poisson's ratio  $\mu$ . Values of  $T$  have been computed for the fundamental frequency, assuming  $\mu = \frac{1}{3}$  using the equation (Pickett, 1945)

$$T = 1 + 88.12 \left( \frac{k}{l} \right)^2 - \frac{1572 \left( \frac{k}{l} \right)^4}{1 + 92.61 \left( \frac{k}{l} \right)^2} - 125 \left( \frac{k}{l} \right)^4$$

This can be made nearly equal to unity by making  $\frac{k}{l}$  small. In the actual samples chosen the thickness was small compared to the length that is  $\frac{t}{l} = 0.025$  so that  $T = 1.005$  for  $\mu = \frac{1}{2}$ . The value of  $\mu$  (longitudinal) for wood varies between  $\frac{1}{4}$  to  $\frac{1}{2}$  (Hearmon, 1953). The correction therefore amounts to only 0.5% and so has been neglected.

### *Damping Coefficient*

The energy required to maintain a bar in sustained vibration is dissipated in overcoming the internal friction of the bar in which case it is converted into heat and secondly, in transferring energy to the external surrounding. The damping capacity  $\Delta W$  is the energy per unit volume per cycle used in overcoming the internal friction. Following electrical analogy the  $Q$  of a specimen is given as (Obert and Duvall, 1941),

$$Q = \frac{2\pi W}{\Delta W}.$$

where  $W$  is the total energy of vibration per unit volume per cycle.  $Q$  can be measured from the sharpness of resonance curve; if  $f_0$  is the resonant frequency and  $\Delta f$  the width of the resonance curve in cycles/sec at  $\frac{1}{2}$  of the maximum amplitude then,

$$Q = \frac{f_0}{\Delta f}.$$

Similarly in terms of the logarithmic decrement  $\delta$  of a free vibration whose amplitude decreases exponentially

$$Q = \frac{\pi}{\delta}.$$

In the present investigation it has been found convenient to evaluate  $\frac{1}{Q} =$

$\frac{\Delta f}{f_0}$  and also the logarithmic decrement  $\delta = \frac{\pi}{Q}$ .

### *Static Modulus of Elasticity*

Under static bending in the case of a simple end-supported beam of a rectangular cross-section carrying a centre load, the modulus of elasticity  $E_s$  is given by (Brown etc., 1952)

$$E_s = \frac{PL^3}{48yI},$$

where  $P$  = Load applied at centre of beam,  
 $L$  = Span,  
 $y$  = Deflection due to load  $P$ ,  
 $I$  = Moment of inertia of the beam  
 $= b t^3/12$ , where  $b$  = breadth of beam, and  
 $t$  = thickness of beam.

Substituting the value of  $I$

$$E_s = \frac{P\Gamma^3}{4ybt^3}.$$

### EXPERIMENTAL

The logs of wood in air-dry condition were sawn into 2ft.  $\times$  2 ins  $\times$  2 ins sticks in accordance with the sectioning scheme shown in Fig. 1. About 20-25 samples having length 10 inches along the grain, breadth 0.5 inch and thickness 0.25 inch,

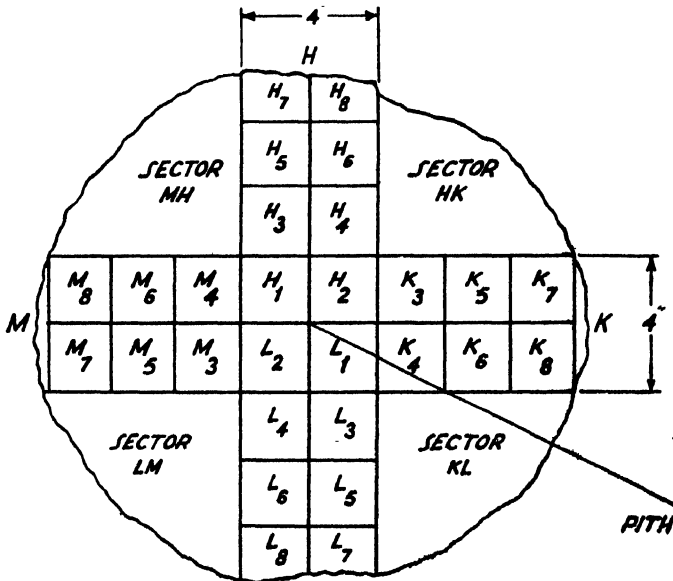


Fig. 1. Sectioning Scheme of Sawing and Sampling a Timber Log.

were prepared out of these sticks cut from a log. Prior to test these samples were conditioned to a moisture content of about 12 per cent by keeping them over a saturated solution of sodium chloride at room temperature for about two weeks till there was no change in weight.

The apparatus used is shown in Fig.-2.

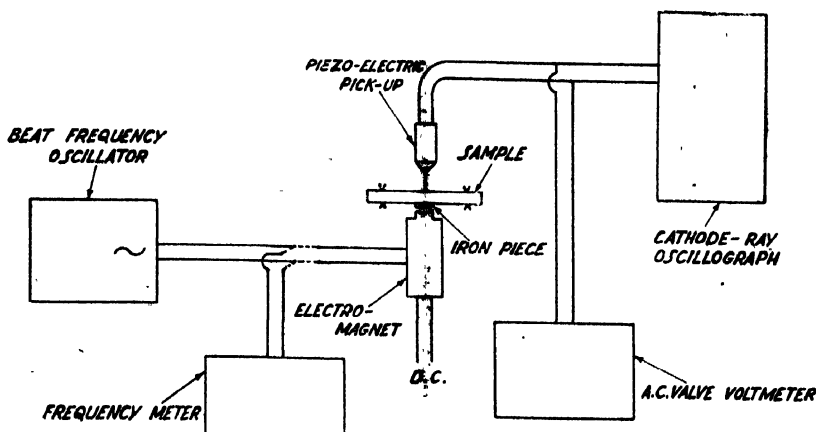


Fig. 2. Schematic Diagram of the Apparatus for the Measurement of Dynamic Young's Modulus and Damping Coefficient of Timber in Flexural Vibration.

A small rectangular piece of soft-iron sheet weighing about 0.27 gm. was tached firmly at the centre of the sample. The sample was mounted on two horizontal knife-edge supports at the nodal points, the two ends being left free. The knife-edges are embedded in heavy iron blocks previously adjusted for parallelism and separated by a distance equal to  $0.552l (= l - 2 \times 0.224l)$ . To ensure that the sample properly rested on the lower knife edges and was not bodily shifted while vibrating, masses of approximately 120 gms. each were suspended from two knife edges placed exactly above the lower knife edges at the nodal points. The effect of these masses on the vibration of the sample was found to be insignificant since they were suspended at the nodal points.

The electro-magnetic driver was positioned just below the centre of the sample under the soft-iron piece fixed to the sample. The distance between the electro-magnet and the iron piece fixed to the sample was about 1 mm. The electromagnet was energised by a beat frequency oscillator, and the sample was made to vibrate to resonance at the fundamental by varying the frequency of the oscillator.

The amplitude of vibration was observed by means of a piezoelectric pick-up connected to a valve voltmeter and to a cathode-ray oscillograph. At resonance the maximum wave-amplitude on the oscillograph screen as well as the voltage indicated on the valve voltmeter were noted. The resonance frequency  $f_0$  was measured on a frequency meter. All the samples were tested under conditions to give the same amplitude of vibration as measured on the valve voltmeter.

The two frequencies  $f_1$  and  $f_2$  at which the pick-up voltage falls to  $1/2^{1/2}$  of its maximum value were found. As  $f_1$  and  $f_2$  were near, the frequency scale of the oscillator was enlarged by arranging a condenser across the zero adjusting condenser of the beat frequency oscillator (Obert and Duvall, 1941). This gives  $\Delta f$ .

TABLE I  
Results of Measurement of Dynamic and Static Young's Moduli,  $1/Q$  &  $\delta$  of Indian Timbers (Parallel to Grain).

Sl. No.	Kind of timber Botanical Name (Common Name)	Moisture content %	No. of test pieces taken	Density $\rho$		Resonance Frequency of gms/cm <sup>3</sup> c.p.s. Range	Young's Moduli				Ratio $\gamma = \frac{E_d}{E_s}$ Mean	Damping Coefficient $\frac{1}{Q} = \frac{\Delta f}{f_0}$ Mean	Logarithmic Decrement $\delta = \pi \frac{1}{Q}$ Mean	S.E.
				Mass at test Vol. at test gms/cm <sup>3</sup> Mean	Mean		$E_d$ Dynamic (Adiabatic) 10 <sup>11</sup> dynes/cm <sup>2</sup>	$E_s$ Static (Isothermal) 10 <sup>11</sup> dynes/cm <sup>2</sup>	Mean	S.E.				
1.	<i>Tectona grandis</i> (Teak)	10.9	25	0.594		410-525	1.21 $\pm$ 0.03	1.09 $\pm$ 0.03	1.12	0.010	0.030 $\pm$ 0.001			
2.	<i>Shorea robusta</i> (Sal)	11.7	21	0.793		420-490	1.61 $\pm$ 0.03	1.42 $\pm$ 0.04	1.14	0.009	0.028 $\pm$ 0.002			
3.	<i>Albizia lebbek</i> (Kokko)	9.7	22	0.654		446-540	1.53 $\pm$ 0.04	1.38 $\pm$ 0.03	1.11	0.010	0.031 $\pm$ 0.002			
4.	<i>Terminalia tomentosa</i> (Laurel)	11.9	22	0.758		325-401	0.89 $\pm$ 0.03	0.71 $\pm$ 0.03	1.26	0.017	0.053 $\pm$ 0.001			
5.	<i>Adina cordifolia</i> (Haldu)	13.2	24	0.636		389-520	1.18 $\pm$ 0.03	1.04 $\pm$ 0.03	1.14	0.010	0.030 $\pm$ 0.002			
6.	<i>Pinus longifolia</i> (Chir)	13.3	24	0.614		483-560	1.54 $\pm$ 0.03	1.41 $\pm$ 0.03	1.09	0.014	0.045 $\pm$ 0.001			
7.	<i>Cedrus deodara</i> (Deodar)	13.8	24	0.601		350-524	1.08 $\pm$ 0.04	0.90 $\pm$ 0.04	1.20	0.014	0.045 $\pm$ 0.002			
8.	<i>Picea morinda</i> (Spruce)	12.4	24	0.461		427-571	1.09 $\pm$ 0.04	0.95 $\pm$ 0.04	1.16	0.011	0.036 $\pm$ 0.001			
9.	<i>Terminalia paniculata</i> (Kindal)	14.4	22	0.884		387-486	1.44 $\pm$ 0.05	1.26 $\pm$ 0.04	1.14	0.013	0.040 $\pm$ 0.002			
10.	<i>Langerstroemia lanceolata</i> (Benteak)	14.0	23	0.704		370-480	1.14 $\pm$ 0.04	0.93 $\pm$ 0.04	1.24	0.014	0.043 $\pm$ 0.001			
11.	<i>Dalbergia latifolia</i> (Rosewood)	10.7	21	0.788		385-441	1.26 $\pm$ 0.02	1.10 $\pm$ 0.02	1.15	0.011	0.035 $\pm$ 0.001			
12.	<i>Pinus excelsa</i> (Blue Pine)	11.7	25	0.427		373-559	0.81 $\pm$ 0.03	0.66 $\pm$ 0.03	1.23	0.014	0.043 $\pm$ 0.001			
13.	<i>Artocarpus integrifolius</i> (Kathal)	12.9	24	0.508		374.460	0.80 $\pm$ 0.02	0.67 $\pm$ 0.02	1.20	0.012	0.039 $\pm$ 0.001			

S.E. = Standard Error.

From the above observations the dynamic elastic modulus  $E_d$ , the damping coefficient in terms of  $1/Q$  and the logarithmic decrement  $\delta$  were calculated.

For the measurement of  $E_s$  by the static method, the sample was supported on two knife-edges with a span of 25.0 cm. and loaded at the centre. The load was increased to 2 Kgms in steps of 500 gms and the maximum deflections were noted by a gauge with a least count of 1 mil. (0.001"). The deflections were also noted while unloading. The mean deflection for 500 gms was found from which  $E_s$  was calculated.

Finally the moisture content was determined on six samples selected from the 20-25 samples, by the oven-dry method.

### RESULTS

The average values of the density  $\rho$ , dynamic and static Young's moduli  $E_d$  and  $E_s$ , their ratio  $\gamma = E_d/E_s$ , the damping coefficient  $1/Q$  and the logarithmic decrement  $\delta$  are entered in Table I. As an estimate of the dispersion of the observed  $E_d$  and  $E_s$ , their standard errors are also shown.

### DISCUSSION OF RESULTS

The results show that the dynamic elastic modulus is about 10-20% higher than the static value. This is in agreement with the findings of other workers quoted in literature (Brown, etc., 1952)(Kuenzi, 1952) and to be expected on theoretical considerations since the static value measures the isothermal modulus and the dynamic value at the frequencies involved (300-600 c/s) measures the adiabatic modulus (Mason, 1958).

The logarithmic decrement  $\delta$  varies between 0.028 to 0.053 which is of the same order as observed by other investigators quoted in literature (Brown, etc, 1952)(Hearmon, 1953). The  $\delta$  values plotted against  $\gamma = E_d/E_s$  shows a general trend of increase of  $\delta$  with  $\gamma$ . This is to be expected since both  $\delta$  and  $\gamma$  are concerned with the frictional heat losses within the sample.

### ACKNOWLEDGEMENTS

Grateful acknowledgements are due to Dr. P. S. Srinivasan for initiating this research problem and for his initial guidance in the work. We also acknowledge our thanks to Dr. J. N. Nanda, Director, Defence Research Laboratory (Materials), Kanpur for his keen interest and permission to publish this paper.

- Hearmon R. F. S., 1953, *Mechanical Properties of Wood and Paper* (Edited by R. Meredith), Part A, Ch. II, Interscience Publishers, Inc., New York, 19-47.
- Kuenzi E. W., Jan. 25, 1952, Symposium on Determination of Elastic Constants, 55th Annual Meeting, A. S. T. M., N. Y., 31.
- Lord Rayleigh, 1926, *Theory of Sound*, Second Ed., Vol. 1, The Macmillan Co., London, 242-306.
- Mason W. P., 1958, *Physical Acoustics and the Properties of Solids*, D. Van Nostrand Co. Inc., Princeton, New Jersey, 203.
- Obert L. and Duvall W. I., 1941, *A.S.T.M. Proc.*, **41**, 1053.
- Pickett Gerald, 1945, *A.S.T.M. Proc.*, **45**, 846.
- Timoshenko S., 1921, *Phil. Mag., Series 6*, **41**, 744.
- Timoshenko S., 1922, *Phil. Mag., Series 6*, **43**, 125.



## AN ANTIPROTON EVENT

G. C. DEKA

DEPT. OF PHYSICS, COTTON COLLEGE, GAUHATI.

AND

T. D. GOSWAMI

DEPARTMENT OF PHYSICS, GAUHATI UNIVERSITY

(Received January 2, 1964 ; Resubmitted July 2, 1964)

## Plate

**ABSTRACT.** During the systematic scanning for double stars in nuclear emulsions exposed to 3 Gev. pion beam an event was recorded and from analysis it can be interpreted as due to the annihilation of an antiproton produced in the emulsion. The details of the event along with a microphotograph are given below.

## INTRODUCTION

A G-5 emulsion stack was exposed to 3 Gev negative pion beam at the Berkeley Bevatron and it was developed at the T.I.F.R., Bombay. During the area scanning for hyperfragments a double star was observed; the parent star of size  $(7+0).0$  has all its tracks produced by slow particles and the total kinetic energy associated with the star is quite low. There is no minimum ionising track in the known direction of the primary pion beam. No energetic charged particle is associated with it except the suspected antiproton which after travelling a distance of  $1057\mu$  in the same emulsion plate apparently stops and gives rise to a second big star of size  $(9+1)\bar{p}$ . The inter-connecting track emitted from the parent star is quite flat and it is not difficult to know its direction of motion from the change of ionisation. The mass measurement by constant sagitta method is also possible. The second star is also carefully examined for any minimum ionising track in the known primary direction; but, there is no such track. All the particles except three coming out from the star stop in the same emulsion plate. The light track which goes out of the plate and is followed for a distance of 1.8 c.m. is indentified as due to a pion, the direction of its motion can also be determined.

The mass from the constant sagitta measurements on the inter connecting track—

$$\bar{D} = 0.8 \pm .2\mu, \text{—using the scheme } p(1, 0)$$

The Mass—value obtained is

$$= 1566 \pm 1212 \text{ Mev} \\ 628$$

The error shown is purely statistical.

TABLE I  
Details of the Second Star

Track No.	Identity of the particles	Ranges	Energy Mev.
1	$\alpha$	200 $\mu$	21.5
2	$\alpha$	277.3	26.5
3	p	86.6	8.2
4	p	182.5	5.1
5	$\alpha$	203	21.6
6	$\pi$	18000	34.0
7	p	400	8.2
8	p	150	4.5
9	p	487	9.2

The following equation is used by several workers to estimate the total energy involved in the annihilation process,

$$E_R(\text{Mev}) = 2.2\bar{T}_g N_g + \bar{T}_b(N_b + 4 \times 3N_b) + 8(N_b + N_g)$$

where,

$E_R(\text{Mev})$  = Total energy released among the charged heavy particles.

$\bar{T}_g$  = Average K.E. of the grey tracks where  $E > 35$  Mev.

$\bar{T}_b$  = — — — black tracks where  $E < 35$  Mev.

$N_b$  = No. of black tracks.

$N_g$  = — grey —

$8(N_b + N_g)$  = B.E. of the nucleons.

In this problem,

$$N_g = 0 \quad N_b = 8$$

$$\bar{T}_g = 0, \quad \bar{T}_b = 99.8/8 \text{ Mev},$$

$$E_R(\text{Mev}) = \bar{T}_b(N_b + 4 \times 3N_b) + 8 \times N_b$$

$$= \frac{99.8}{8} (8 + 12 \times 8) + 8 \times 8$$

$$= 99.8 \times 13 + 64$$

$$= 1361.4 \text{ Mev for heavy particles.}$$

For the pion the total energy is

$$E_\pi = (34 + 139.6)$$

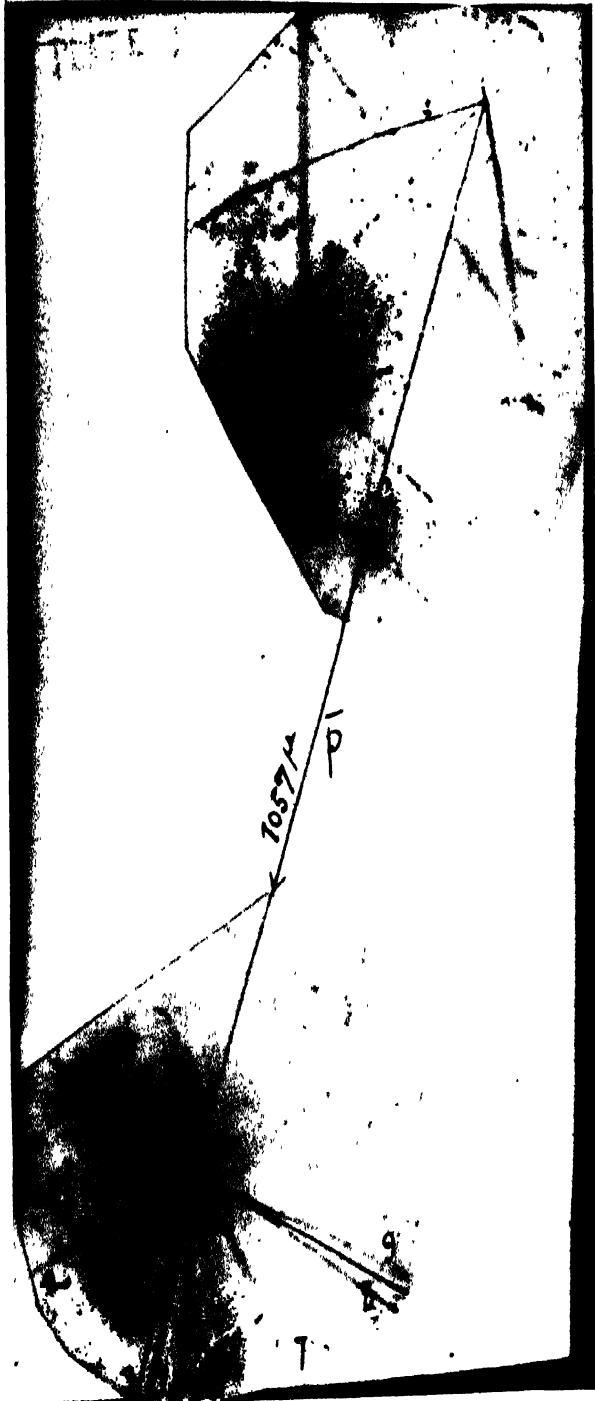
$$= 173.6 \text{ Mev.}$$

Hence the total energy involved in the disintegration is = 1535 Mev.

#### DISCUSSIONS

Possibility of the event being due to

- (i)  $\Pi^-K^-$  and  $\Sigma^-$ -capture in the emulsion,
- (ii) chance coincidence,
- (iii) 2 G.e.v. pion interaction,





## *An Antiproton Run*

could be eliminated from the following considerations :

The interconnecting track which is a flat and long one does not show the characteristic coulomb scatterings of a pion track. The larger kinetic energy released in the second star eliminates the possibility of a  $\Sigma^-$ -capture in which the energy-release does not exceed 100 Mev. The mass measurement on the track is more in favour of a proton rather than a  $k$ -meson, also the total K.E. involved is much higher than what we expect from  $K^-$ -capture star i.e. 475 Mev.

As both the stars are situated in a clean part of the emulsion, the details of the event can be examined quite closely and one can eliminate the possibility of chance coincidence from such observations. Further, the stars were examined in the similar way under high magnification for any minimum ionising tracks, but there was none. Such tracks in other directions were followed through to know the direction of motion thinking that the first star might be produced by some of them. From these observations we are led to a tentative conclusion as follows : the interconnecting track is due to an antiproton produced in the first star which is perhaps initiated by either an anti neutron or a very high energetic neutron; the antiproton so produced is then annihilated at rest by an emulsion nucleus which as a result is disintegrated.

### *Possible sources of production of the antiproton*

As the parent star which is a small one has not any visible primary track, so it must be produced by some electrically neutral particle. The incident pion of the kinetic energy 3 G.e.v. can by no means produce an antiproton because it requires K.E. in the laboratory system at least 7 Bev. one is then inclined to think of the event to be due to a cosmic ray neutron or antineutron. The results of the previous balloon flight experiments indicate that the existence of antiproton and antineutron in cosmic rays is very rare and the production cross-section of antiproton in such reactions is also believed to be extremely low.

Now one has to think of the neutron and antineutron directly coming from the target, such particles being least affected by the bending magnetic field of the accelerating machine. These neutrons could be produced by the 10 Bev proton beam of the Bevatron hitting the target, and then these can travel in any direction without losing any appreciable amount of energy; the magnetic field however can produce some spinning effect on these particle because of their magnetic moment.

Hence the following reactions are considered—



For these reactions we have to consider the following points,—similar to the case of electron—pair production by photon, an antinucleon is produced when

a nucleon in a Dirac's negative energy state is raised to a positive energy state leaving a hole i.e. an antinucleon. This means that the production of an anti-nucleon will simultaneously lead to the production of its counter part i.e. a proton and an antiproton, a neutron and an anti-neutron. The most promising mechanism for production of nucleon-antinucleon pair is the nucleon-nucleon collision, when such a pair is produced the final state consists of four particles each possessing the mass of the nucleon ( $M$ ). At the threshold the incident nucleon must possess a K.E. of at least  $6M = 938 \times 6 = 5.628$  Bev. in order to produce a nucleon-antinucleon pair with a target nucleus at rest. Again using the Fermi energy of 22 Mev for a nucleon and assuming the most favourable circumstances i.e. the nucleon moving in an equal and opposite direction to the incident nucleon, the threshold is reduced to 4.6 Bev. This means that the incident nucleon must possess K.E. at least 4.6 Bev.

So far the properties of anti-proton production have been studied by several workers, all reasonable estimate indicate extremely small cross-sections for nucleon-antinucleon pair production except at very high energy of the order of  $10^{13}$  ev. Antiproton production is therefore rather rare, although their detection is not so difficult.

Now assuming the second star to be an annihilation of the antiproton, we consider various possibilities. The annihilation of an antinucleon by a nucleon has some features in common with positron-electron annihilation, but there are some differences too. The nucleons have strong interactions with the pi-meson field much stronger than the electro-magnetic field and consequently the annihilation process should give rise to a pair of gamma-rays. Hence any of the following annihilation reactions may take place.

$$P + P^- \rightarrow \pi^+ + \pi^- \quad \dots (1)$$

$$\rightarrow 2\pi^0 \quad \dots (2)$$

$$N + P^- \rightarrow \pi^- + \pi^0 \quad \dots (3)$$

As our star possesses only one pion track any of these reactions are quite likely.

#### ACKNOWLEDGEMENT

We gratefully acknowledge the financial support of Department of Atomic Energy, Govt. of India. We also like to thank Dr. K. M. Pathak and Shri D. Kakoty, M.Sc., for some discussions. Our thanks go also to Shri S. Das for doing most of the scanning work.

#### REFERENCES

- Powell, C. F., Fowler P. M. and Perkins, D. H. "The Study of Elementary particles", 414.  
 Marshak, Robert E., "Meson physics", 338.

# ON THE DEPENDENCE OF THE TIME OF RELAXATION OF NITROBENZENE IN SOLUTIONS IN NON POLAR SOLVENTS ON THE VISCOSITY OF THE SOLUTIONS

J. BHATTACHARYYA, (Miss) B. SINHA, S. B. ROY AND  
G. S. KASTHA

OPTICS DEPARTMENT, INDIAN ASSOCIATION FOR THE CULTIVATION OF SCIENCE  
CALCUTTA-32

(Received July 7, 1964)

**ABSTRACT.** The dielectric loss due to absorption of microwaves of frequency 38.8 KMc/s in dilute solutions of  $\text{CCl}_4$ ,  $\text{C}_6\text{H}_6$ ,  $\text{C}_6\text{H}_{14}$  at different temperatures and in mixed solvents of paraffin +  $\text{CCl}_4$ , paraffin +  $\text{C}_6\text{H}_6$  and paraffin +  $\text{C}_6\text{H}_{14}$  at constant temperature but at different viscosities have been studied. It has been found that the values of  $\tan \delta$  or  $T \tan \delta$  at different viscosities in solutions in pure solvents or in mixed solvents lie on smooth curves. The values of  $\tan \delta$  for the same value of viscosity in solution in pure and in mixed solvents, agree with each other, so long the viscosity remains within 1.3 c.p. Within this limit the time of relaxation is proportional to viscosity of the solution. It is concluded that within certain limitations the dependence of  $\tan \delta$  on the viscosity in a dilute solution may be expressed by the Debye equation.

Incidentally, a method has been suggested for the determination of dipole moment of polar molecule in solution in nonpolar solvent when a maximum in the value of  $\tan \delta$  could not be obtained.

## INTRODUCTION

The dielectric loss accompanying absorption of microwaves of wavelength 3-cm and 1.25 cm in dilute solutions of nitrobenzene and of some other polar organic compounds in  $\text{C}_6\text{H}_6$  and  $\text{CCl}_4$  and in mixed solvents of high viscosity paraffin and a nonpolar solvent such as  $\text{CCl}_4$ ,  $\text{C}_6\text{H}_6$ ,  $\text{C}_6\text{H}_{14}$  and  $\text{CS}_2$  have been studied by many workers (Whiffen and Thompson, 1946; Hall *et al.*, 1946; Cripwell and Sutherland 1946; Chau *et al.*, 1957 and Rajan, 1957). From these results it was concluded that though the Debye expression for dielectric loss in dilute solutions of polar compounds in nonpolar solvents is fairly obeyed, the Debye relation connecting the time of relaxation with the macroscopic viscosity of the solution and the radius of the rotor does not hold good (Whiffen and Thompson, 1946; Jackson and Powles, 1946).

The effect of viscosity on the dielectric loss was studied by Jackson and Powles (1946) who found that in the case of solution of benzophenone in high viscosity paraffin the whole loss curve obtained by varying the frequency of microwave radiation becomes broader and also the frequency at which maximum loss

occurs is shifted towards lower frequency value in comparison with those obtained in the case of dilute solution of benzophenone in benzene.

Hall *et al.* (1946) studied the absorption of microwaves of wavelength 3-cm in solutions of nitrobenzene in mixed solvents of paraffin +  $\text{CCl}_4$ , paraffin +  $\text{C}_6\text{H}_6$  and paraffin +  $\text{C}_6\text{H}_{14}$  with variation of viscosity and found that in each case maximum attenuation occurs at such viscosity-value of the solution which increases as the viscosity of the low viscosity component in the mixed solvents decreases. Whiffen (1946) suggested that all these results might indicate that the Debye equation for loss tangent does not hold in the case of solution whose viscosity is greater than 1.5 c.p.

In order to determine how the value of loss tangent and the time of relaxation are related with the viscosity of the solution, it would be necessary to make a comparative study of the variation of dielectric loss with the variation of viscosity produced either by changing the temperature of the solution or by mixing with the solution high viscosity paraffin in different proportions. With this object, the absorption of microwaves in the frequency region 35 Kmc/s—39Kmc/s by dilute solutions of nitrobenzene in various nonpolar solvents at different temperatures and different viscosities has been studied and the results obtained have been discussed in the present paper.

#### EXPERIMENTAL

Experimental arrangements for studying the absorption of microwaves in solutions at different temperatures and at different viscosities are shown in the schematic diagram, figure I. Microwave power from the signal generator (Model E.H.F. G3540—1 of Polarad Electronics Corporation) is passed through a U-shaped absorption cell containing the solution, the temperature of which can

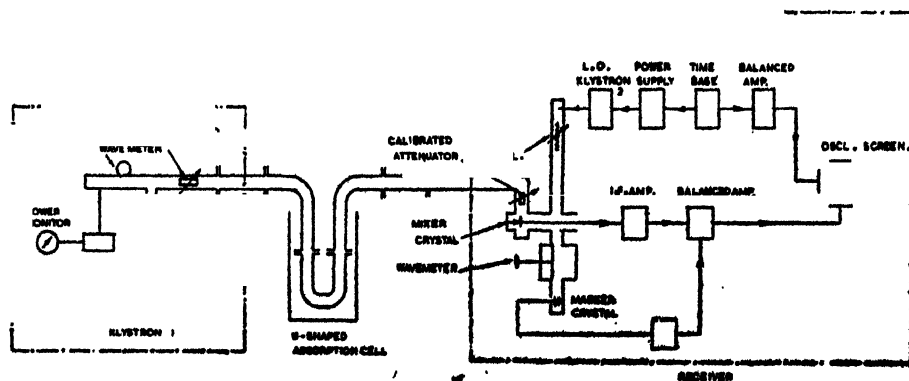


Fig. 1. Schematic diagram of the experimental arrangements for measuring dielectric loss.

be raised or lowered to any desired value by placing the cell in a suitable hot or cold bath. The signal after absorption in the cell is detected by a superheterodyne receiver having a sensitivity of 55 db. (Microwave spectrum analyzer model



SA40 of Applied Dynamics Corporation). The frequency of the local oscillator is swept by a 20c/s saw-tooth voltage so that it can follow the signal. The same saw-tooth voltage is used for the horizontal deflecting plates of the scope. After about half an hour of switching on the instruments the signal on the screen becomes steady. The constancy in the microwave power of the signal source is seen from the thermistor bridge power monitor. The frequency of the signal is measured with an accuracy of 0.1% by means of absorption type wavemeters incorporated in the signal generator as well as in the receiver. With the pure solvent (2 cc) in the absorption cell, the calibrated attenuator on the instruments are adjusted to give a full scale deflection on the scope. With the solution (2 c.c.) in the cell, the attenuators are again adjusted for the same full scale deflection. The difference in the readings of the attenuators gives directly the loss of microwave power in *db* due to absorption in solution with an accuracy of 0.25 *db*. The distance of the absorption cell is about 90 cm. either from the signal generator or from the receiver so that the temperature variations of the cell can not reach them. Mica windows are used in the absorption cell to prevent the vapour of the solution from entering the signal generator or the receiver. The validity of the Beer's Law is seen from the linear change in the amount of absorption either with variation of the concentration of the solution or of the path length. This also indicates that the formation of stationary waves, if any, is negligible.

Chemically pure nitrobenzene, used as solute and  $\text{CCl}_4$ ,  $\text{C}_6\text{H}_6$ ,  $\text{C}_6\text{H}_{14}$  used as solvents were distilled repeatedly and thoroughly dried before being used in the investigations. The dielectric loss of the solvents in a path length of 24 cm was measured and found to be negligible. Medical paraffin, which also showed negligible absorption in the same path length, was used to produce mixed solvents of variable viscosity. The values of dielectric constants and viscosities of the solvents were taken from the International Critical Tables. The viscosities of paraffin and of the mixed solvents at room temperature were determined experimentally.

## RESULTS

### *Calculation of loss tangent ( $\tan \delta$ )*

The observed loss of microwave power ( $\phi$ ) in *db* due to absorption of microwaves in dilute solutions of nitrobenzene in various solvents is related to the value of attenuation coefficient  $\psi$  (Whiffen, 1946) by the relation  $\psi = \frac{.2303}{L} \phi$  where  $L$  is the length of absorbing path in cm. The values were then converted into  $\tan \delta$ -values with the help of the relations given by Jackson (1946) and by Whiffen and Thompson (1946). In calculating the  $\tan \delta$ -values the value of real dielectric constant  $\epsilon$  of the solution was taken to be the same as that of the solvent and its variation with temperature was neglected. In the case of mixed solvents, Paraffin +  $\text{C}_6\text{H}_6$ , Paraffin +  $\text{CCl}_4$ , Paraffin +  $\text{C}_6\text{H}_{14}$ , the value of  $\epsilon$  was taken to be

2.2 because the dielectric constant of paraffin is 2.2 and those of pure solvents are about 2 in all cases. The estimated error in  $\tan \delta$ -values is about 5%. These values are given in Tables I, II and III.

TABLE IA

$1.95 \times 10^{-4}$  moles/cc of nitrobenzene in  $\text{CCl}_4$ . Volume of solution in the cell 2cc

Temp (abs)	$\tan \delta$	$T \tan \delta$	$\tau \times 10^{12}$ sec	$\tau \times 10^{12}$ sec (lit)	$\eta \times 10^3$ poise	$\frac{\tau}{\eta} \times 10^{10}$
262	.03	7.89	25.6		—	—
274	.036	9.86	20.05		13.3	15.0
283	.038	10.75	18.3		12.5	14.64
294	.041	12.05	16.1	15.2 <sup>a</sup>	9.52	16.9
				14.0 <sup>b</sup>		
303	.047	14.24	13.2		8.25	16
313	.05	15.65	11.8		7.50	15.73
323	.051	16.47	10.9		6.56	16.6
333	.053	17.65	9.8		5.75	17
343	.056	19.21	9.06		5.24	17.2

a. Whiffen (1950)

b. Chau, Fevre and Tardif (1957)

TABLE IB

$1.95 \times 10^{-4}$  moles/cc of nitrobenzene in  $\text{CCl}_4$ +paraffin

Volume = 2cc Temperature = 30°C

Percentage of paraffin	$\tan \delta$	$T \tan \delta$	$\tau \times 10^{12}$ sec	$\eta \times 10^3$ poise	$\frac{\tau}{\eta} \times 10^{10}$
0%	.0458	13.88	13.60	8.25	16.48
10%	.0413	12.51	15.40	10.10	15.24
20%	.0362	10.97	17.85	11.57	15.42
100%	.029	8.79	22.80	164.7	1.38

TABLE IIA

$1.95 \times 10^{-4}$  moles/cc of nitrobenzene in benzene  
Volume of solution in the cell = 2 cc

Temp (abs)	$\tan \delta$	T $\tan \delta$	$\tau \times 10^{12}$ sec	$\tau \times 10^{12}$ sec lit	$\eta \times 10^3$ poise	$\frac{\tau}{\eta} \times 10^{10}$
267	.0298	7.95	25			
274	.0397	10.82	17.9		9.00	19.9
285	.048	13.68	13.91		7.55	18
				11.5 <sup>a</sup>		
293	.0514	15.06	12.31	11.6 <sup>b</sup>	6.47	19
				13.0 <sup>c</sup>		
				11.0 <sup>d</sup>		
				12.3 <sup>e</sup>		
303	.054	16.36	11.13		5.60	19.9
314	.056	17.58	10.8		4.90	22
323	.0578	18.67	9.3		4.36	21.3
333	.0606	20.18	8.09		3.89	20.8
347	.0646	22.42	6.37		3.36	18.95

a—Jackson and Powles (1946)

b—Whiffen and Thompson (1946)

c—Cripwell and Sutherland (1946)

d—Chau, Fevre and Tardif (1957)

e—Gopala Krishna (1957)

TABLE IIB

$1.95 \times 10^{-4}$  moles/cc of nitrobenzene in benzene + paraffin  
Volume of solution in the cell 2cc. Temperature = 30°C

Percentage of paraffin	$\tan \delta$	T $\tan \delta$	$\tau \times 10^{12}$ sec	$\eta \times 10^3$ poise	$\frac{\tau}{\eta} \times 10^{10}$
0%	.0536	16.24	11.2	5.61	20
20%	.0493	14.94	12.5	7.69	16.25
40%	.041	12.42	15.52	12.05	12.88
60%	.035	10.61	18.5	19.57	9.45
100%	.029	8.79	22.8	164.7	1.38

TABLE IIIA

1.95  $\times 10^{-4}$  moles/cc of nitrobenzene in hexane  
Volume of solution in the cell = 2 cc

Temp (abs)	$\tan \delta$	$T \tan \eta$	$\tau \times 10^{12}$ sec	$\delta \times 10^{12}$ sec (lit)	$\tau \times 10^3$ poise	$\tau/\eta \times 10^{10}$
265	.062	16.43	9.70			
274	.072	19.73	7.17	6.8 <sup>a</sup>	3.89	18.43
303	.075	22.79	4.53		2.89	15.67

<sup>a</sup>Chau, Fevere and Tardif (1957)

TABLE IIIB

1.95  $\times 10^{-4}$  moles/cc of nitrobenzene in hexane + paraffin  
Volume of solution in the cell = 2cc Temperature = 30°C

Percentage of paraffin	$\tan \delta$	$T \tan \delta$	$\tau \times 10^{12}$ sec	$\eta \times 10^3$ poise	$\tau/\eta \times 10^{10}$
0. %	.075	21.57	4.53	2.89	15.67
20%	.064	19.39	8.7	5.25	16.5
40%	.0508	15.39	11.99	9.91	12.09
60%	.0469	14.21	13.23	16.93	7.8
80%	.0369	11.18	17.48	44.45	3.93
100%	.029	8.79	22.8	164.7	1.38

From the data given by Cripwell and Sutherland (1946) for  $\tan \delta$ -value (reduced to a theoretical concentration of 1 gm.mol/100 c.c.) in the case of solution of nitrobenzene in benzene at about 20°C for two wavelengths 3.25 cm and 1.25 cm, the value of  $\tan \delta$  for the same concentration at the wavelength 7.7 mm was calculated and found to be 2.50. This agrees well with the  $\tan \delta$ -value 2.63 obtained for the same theoretical concentration in the present investigation.

#### *Calculation of time of relaxation ( $\tau$ )*

The expression for loss tangent in the case of dilute solution of polar molecules in nonpolar solvent is given by the Debye equation

$$\tan \delta = \frac{(\epsilon + 2)^2}{\epsilon} \cdot \frac{4\pi N c \mu^2}{27kT} \cdot \frac{\omega \tau}{1 + \omega^2 \tau^2} \quad \dots (1)$$

where the various symbols have their usual meaning. For the calculation of  $\tau$  with the help of the above equation from the observed values of  $\tan \delta$ , the value of  $\mu$  is required. In the present case as the maximum value of  $\tan \delta$  was not obtained, the value of  $\mu$  could not be determined independently. So  $\mu$  was taken as 3.98D from the literature (c.f. Jackson and Powles, 1946; Cripwell and Sutherland, 1946). The calculated values of  $\tau$  along with the macroscopic viscosity  $\eta$  are given in Tables I, II and III. The  $\tau$ -values reported by other workers have been included in the Tables for comparison. The last column of each table contains the values of  $\tau/\eta$ .

## DISCUSSION

### (a) Variation of loss tangent with viscosity

The values of  $\tan \delta$  and  $T \tan \delta$  obtained in the case of each of the solutions have been plotted separately against the  $\log \eta$  values of the respective solutions and are shown in Figs. 2a, 2b and 2c. It can be seen that in all the cases points corresponding to the values of  $\tan \delta$  and  $T \tan \delta$  at different values of viscosity obtained either by changing the temperature of the solution or by varying the proportion of paraffin added to the solution lie on smooth curves. It is also seen that the values of  $T \tan \delta$  decreases almost exponentially with increase in the value of  $\log \eta$ . This is also evident from the near constancy in the values of  $T \tan \delta \cdot \eta$  given in Tables I and II. However, in the case of the solutions in mixed solvents,  $T \tan \delta$ -values do not decrease as rapidly with increase of viscosity

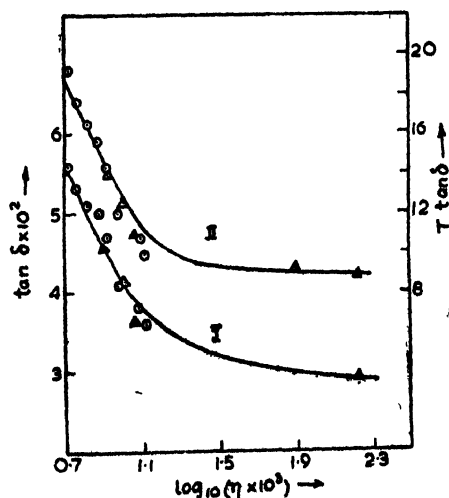


Fig. 2a. Curve I. Variation of loss tangent with logarithm of viscosity for solutions of nitrobenzene in  $\text{CCl}_4$  and in  $\text{CCl}_4$  + paraffin.

Curve II Dependence of  $T \tan \delta$  on  $\log \eta$  for the same solutions.

$\Delta$  Points for variation of temperature

O Points for variation of viscosity at constant temperature.

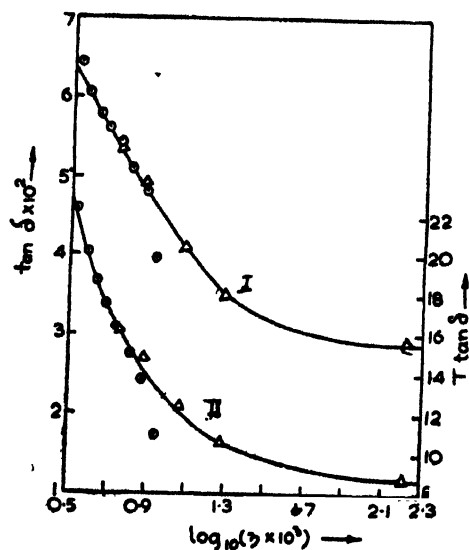


Fig. 2b. Curve I Variation of loss tangent with logarithm of viscosity for solutions of nitrobenzene in benzene and in benzene+paraffin.

Curve II Dependence of  $T \tan \delta$  on  $\log \eta$  for the same solutions.

$\Delta$  Points for variation of temperature.

O Points for variation of viscosity at constant temperature.

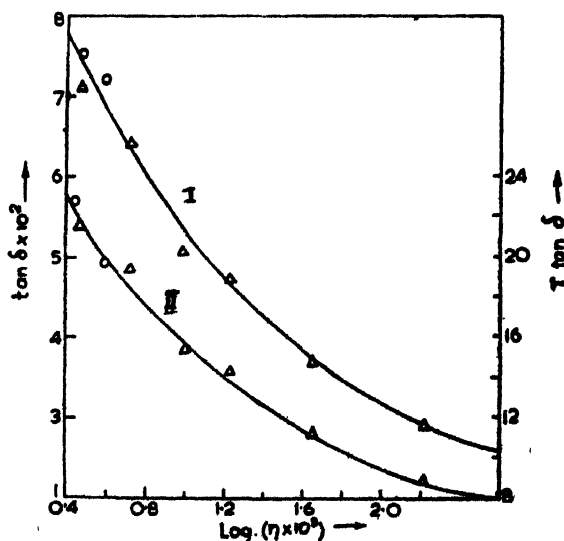


Fig. 2c. Curve I Variation of loss tangent with logarithm of viscosity for solutions of nitrobenzene in hexane and in hexane+paraffin.

Curve II Dependence of  $T \tan \delta$  on  $\log \eta$  for the same solutions.

O Points for variation of temperature.

$\Delta$  Points for variation of viscosity at constant temperature.

as would be expected if the same exponential law would hold, but instead, the values of  $T \tan \delta$  tend to reach constant limiting values. It may be noted that so long the viscosity of the solution remains within a certain value which is about 1.3 c.p. in the present case, the variation in the value of  $\tan \delta$  or  $T \tan \delta$  by varying the value of  $\eta$  does not depend on whether the change of  $\eta$  is effected by changing the temperature of the solution or the concentration of paraffin in the solution.

(b) *Relation between  $\tau$  and  $\eta$*

Whiffen and Thompson (1946) discussed the variation of  $\tau$  and  $\eta$  with temperature in terms of the expressions

$$\left. \begin{aligned} \tau &= A \cdot e^{E_r/RT} \\ \eta &= B \cdot e^{E_\eta/RT} \end{aligned} \right\} \dots (2)$$

where  $A$  and  $B$  are constants. Molar activation energy for dielectric relaxation  $E_r$  and that for viscous flow  $E_\eta$  have been measured from the inclinations of the straight line plots of  $\log \tau$  and  $\log \eta$  against  $1/T$  (Figs. 3a, 3b) in the case of solutions of nitrobenzene in  $\text{CCl}_4$  and  $\text{C}_6\text{H}_6$ . The values of  $E_r$  and  $E_\eta$  are given in Table IV.  $E_r$ -value in hexane solution was calculated from the  $\tau$ -values at two temperatures.

TABLE IV

Solution in	$E_r$ in K.Cal/mole	$E_\eta$ in K.Cal/mole	$E_r/E_\eta$
$\text{CCl}_4$	2.25	2.44	0.92
$\text{C}_6\text{H}_6$	2.56	2.53	1.01
$\text{C}_6\text{H}_{14}$	2.08	1.84	1.13

The closeness in the values of  $E_r$  and  $E_\eta$  in all cases suggests that there might be a simple relation between  $\tau$  and  $\eta$  which, with the help of the above two equations, may be expressed as

$$\tau/\eta = D \cdot e^{(E_r - E_\eta)/R\eta T} \text{ or } \tau = \alpha \cdot \eta^{E_r/E_\eta} \quad (3)$$

where  $D$  and  $\alpha$  are constants. The value of  $\tau$  will increase, remain constant or decrease with increase of temperature or decrease of viscosity according as  $E_r \lesseqgtr E_\eta$ . This is found to be approximately true from the  $\tau/\eta$ -values given in Tables I, II and III.

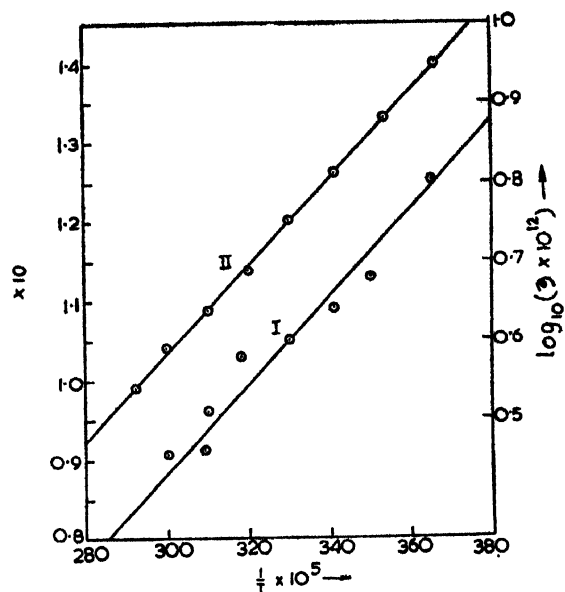


Fig. 3a. Curve I Plot of  $\log \tau$  vs  $1/T$  for solution of nitrobenzene in  $\text{CCl}_4$   
 Curve II Plot of  $\log \eta$  vs  $1/T$  for  $\text{CCl}_4$ .

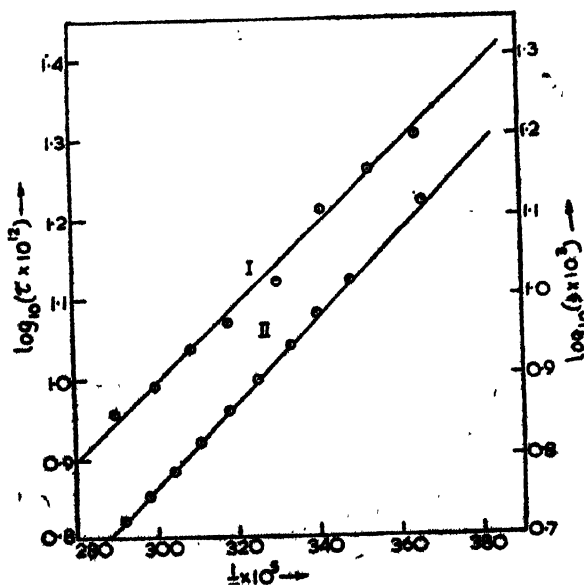


Fig. 3b. Curve I Plot of  $\log \tau$  vs  $1/T$  for solution of nitrobenzene in benzene.  
 Curve II Plot of  $\log \eta$  vs  $1/T$  for benzene.



If the relation (3) holds, the plot of  $\log \tau$  vs  $\log \eta$  would be a straight line with an inclination  $E_\tau/E_\eta$ . Actually, the plots of  $\log \tau$  vs  $\log \eta$  (Figs. 4a, 4b and 4c) are almost linear upto certain values of  $\eta$  and the values of the inclination  $E_\tau/E_\eta$  agree well with the ratios of  $E_\tau$  and  $E_\eta$  determined separately. Because of the

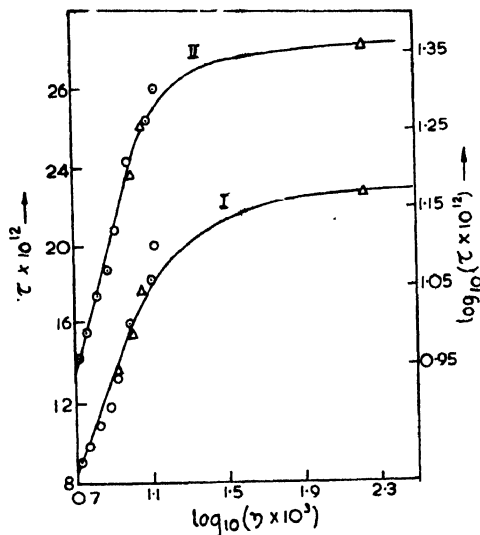


Fig. 4a Curve I Graph of  $\tau$  vs  $\log \eta$  for solutions of nitrobenzene in  $\text{CCl}_4$  and in  $\text{CCl}_4 + \text{paraffin}$ .

Curve II Graph of  $\log \tau$  vs  $\log \eta$  for the same solutions.

O Points for variation of temperature.

$\Delta$  Points for variation of viscosity at constant temperature.

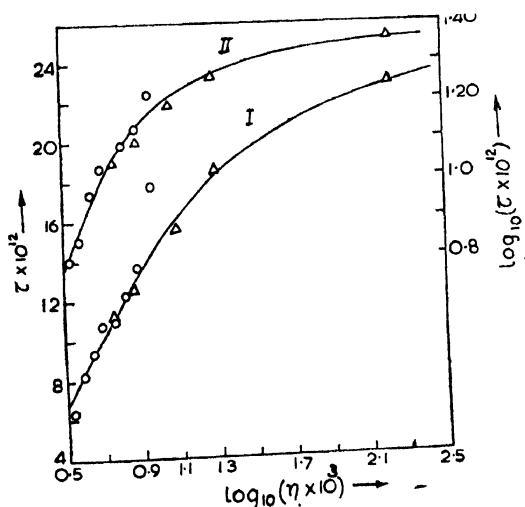


Fig. 4b. Curve I Graph of  $\tau$  vs  $\log \eta$  for solutions of nitrobenzene in benzene and in benzene + paraffin.

Curve II Graph of  $\log \tau$  vs  $\log \eta$  for the same solutions.

O Points for variation of temperature.

$\Delta$  Points for variation of viscosity at constant temperature.

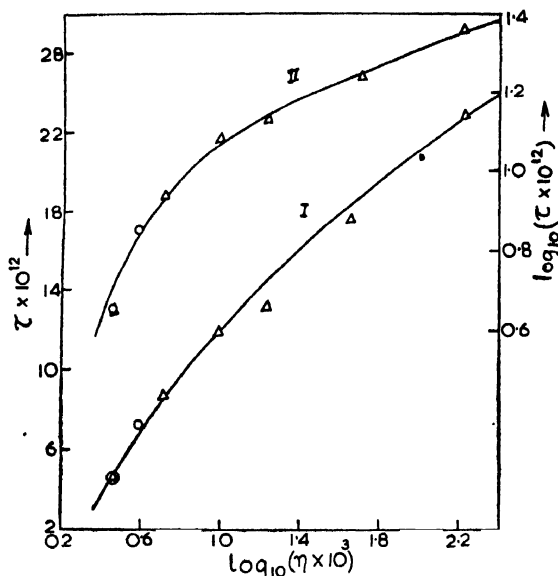


Fig. 4c. Curve I Graph of  $\tau$  vs  $\log \eta$  for solutions of nitrobenzene in hexane and in hexane + paraffin.

Curve II Graph of  $\log \tau$  vs  $\log \eta$  for the same solutions.

○ Points for variation of temperature.

Δ Points for variation of viscosity at constant temperature.

non-linearity of the curves  $\log \tau$  vs  $\log \eta$  at higher viscosity values, the value of the inclination of the tangent at any point on the curve which measures  $E_\tau/E_\eta$  decreases with increasing viscosity. All these considerations are applicable in the case of solutions in pure solvents when the viscosity is varied by changing the temperature.

It is thus seen that the equation (3) fairly represents the variation in  $\tau/\eta$  values over a wide range of temperature, whereas the values of  $\tau/\eta$  obtained from the Debye relation

$$\tau = \frac{4\pi\eta a^3}{kT} \quad (4)$$

should always decrease with increasing temperature, which is not observed. Moreover, according to equation (4), for the same polar molecule in two solutions of different viscosities,  $\tau_1/\tau_2$  should be equal to  $\eta_1/\eta_2$  at a constant temperature. The present experimental results and those of previous workers (Jackson and Powles, 1946; Whiffen and Thompson, 1946) show that for widely different viscosities of the solutions, the relation (4) does not hold good. These discrepancies probably arise from the fact that the macroscopic viscosity ( $\eta$ ) has been used in equation (4) in place of the internal viscosity.

(c) Calculation of the radius of the rotor

Using the value of  $\tau/\eta$  obtained experimentally, the values of radius of the rotor as calculated by using equation (4) are given in Table V.

TABLE V

Solution in	T°K	$a^3$ in Å <sup>3</sup>
CCl <sub>4</sub>	343	6.5
C <sub>6</sub> H <sub>6</sub>	333	7.6
C <sub>6</sub> H <sub>14</sub>	274	5.5

The value of  $a^3$  calculated from the density of nitrobenzene is 40.6 Å<sup>3</sup>. Even allowing for free space the reduced value would be much larger than the value of  $a^3$  given in Table V. As the radius of the spherical rotor comes out to be much smaller than the size of the actual molecule computed also from the chemical bond data, it is difficult to identify the rotor with the whole molecule. However, one may be tempted to identify the rotor with the NO<sub>2</sub> group in the phenyl ring. Though it is known that the NO<sub>2</sub> group is in the plane of the benzene ring, the NO<sub>2</sub> group may acquire a slight moment directed away from the plane in solutions in various solvents (Jenkins, 1936). But whether this may cause the NO<sub>2</sub> group to rotate is still to be seen and for this purpose investigations on the dielectric loss in a series of substituted nitrobenzenes in solutions in different nonpolar solvents have been undertaken.

(d) Debye expression for dielectric loss as a function of viscosity of the solution

The Debye expression given in equation (1) depends besides other quantities, on the value of the expression  $\omega\tau/1 + \omega^2\tau^2$ , which for  $\omega\tau > 2$  can be approximated

by  $\frac{1}{\omega\tau} e^{-\frac{1}{\omega^2\tau^2}}$  to a good degree of accuracy. Combining the equations (1), (3)

and (5) the following expression for  $\tan \delta$  as a function of  $\eta$  is obtained,

$$T \cdot \tan \delta = \frac{P}{\eta^\gamma} e^{\frac{1}{\omega^2\tau^2} - Q/\eta^{2\gamma}} \quad \dots (6)$$

where  $P = \frac{4\pi N c \mu^2}{27 k \alpha \omega} \cdot \frac{(\epsilon + 2)^2}{\epsilon}$ ,  $Q = \frac{1}{\alpha^2 \omega^2}$  and  $\gamma = E_\tau/E_\eta$ . When  $\gamma = 1$  and  $\eta$  is

large the equation (6) becomes  $T \tan \delta \approx P/\eta$  which may also be written as  $T \cdot \tan \delta \approx P \cdot e^{-2.303 \log 10 \eta}$ . The experimental results tally with the equation as discussed in Sec. (a). In the case of solutions with higher values of viscosity, since  $\gamma$  decreases with increase of viscosity, the value of  $T \cdot \tan \delta$  would not decrease as rapidly

as would have occurred if  $\gamma$  were equal to 1. This is also in accordance with experimental results. Thus it may be concluded that within certain limitations the dependence of  $\tan \delta$  on viscosity may be described by the Debye expression.

(c) *A method for the determination of the dipole moment ( $\mu$ ).*

Incidentally, the equation (6) provides a rough method for the determination of  $\mu$  of polar molecule. Equation (6) may be written in the form

$$\log_{10} (T \tan \delta \cdot \eta^\gamma) = \log_{10} P - \frac{Q}{\eta^{2\gamma}} \cdot \log_{10} e \quad (7)$$

For a constant value of  $\gamma$ , which generally lies between 0.9 and 1.0 within viscosity limit of 1.3c.p., the graph of  $\log (T \tan \delta \cdot \eta^\gamma)$  vs  $\frac{1}{\eta^{2\gamma}}$  would be a straight line from whose intercept and inclination the value of  $\mu$  can be calculated from relations given in equation (6). Such graphs have been shown in the case of solutions in  $C_6H_6$  and in  $CCl_4$  in Figs. 5a and 5b for  $\gamma$  values 1.0 and 0.9 respectively. The

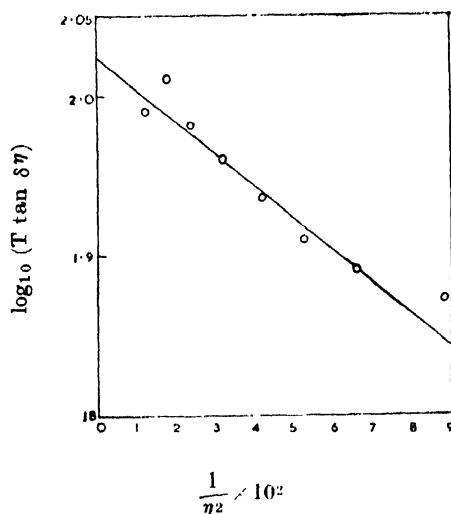


Fig. 5a. Graph of  $\log (T \tan \delta \cdot \eta^\gamma)$  vs  $\frac{1}{\eta^{2\gamma}}$  for solution in benzene with  $\gamma = 1.0$ .

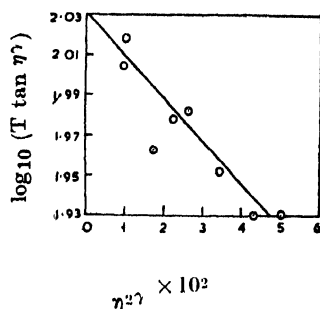


Fig. 5b. Graph of  $\log (T \tan \delta \cdot \eta^\gamma)$  vs  $1/\eta^{2\gamma}$  for solution in carbontetrachloride with  $\gamma = 0.9$ .

value of  $\mu$  calculated from the graphs are given in Table VI. The literature value is included for comparison.

TABLE VI

Solution in	$\mu$ in Debye Unit calculated	$\mu$ in Debye Unit Literature value
$\text{CCl}_4$	3.90	3.98
$\text{C}_6\text{H}_6$	3.92	

The value of  $\mu$  obtained by the above method is smaller than the value of  $\mu$  used in the present investigation by about 2%. Considering the various approximations involved, this may be regarded as satisfactory. If this method is applicable in general remains to be seen. For this purpose the investigations are being extended to a large number of polar organic compounds.

#### ACKNOWLEDGMENT

The authors express their grateful thanks to Mr. A. K. Sarkar, Workshop Superintendent, Indian Association for the Cultivation of Science, for help in fabricating the wave guide components used in the present experiment.

#### REFERENCES

- Chau, J. Y., Le Fevre, R. W. and Tardif, J., 1957, *J. Chem. Soc. Part II*, pp. 2293.  
 Crepwell, F. J. and Sutherland, G. B. B. M., 1946, *Trans. Farad. Soc.*, **42A**, 149.  
 Gopala Krishna, K. V., 1957, *Trans. Farad. Soc.*, **53**, 767.  
 Hall, H. W., Halliday, I. G., Johnson, W. A and Walker, S., 1946, *Trans. Farad. Soc.*, **42A**, 136.  
 Jackson, W., 1946, *Trans. Farad. Soc.*, **42A**, 15.  
 Jackson, W. and Powles, J. G., 1946, *Trans. Farad. Soc.*, **42A**, 136.  
 Jenkins, H. O., 1936, *J. Chem. Soc.*, p.862  
 Rajan, S., 1956, *Curr. Sc.*, **23**, 238.  
 Whiffen, D. H. 1946, *Trans. Farad. Soc.*, **42A**, 156.  
 Whiffen, D. H., 1950, *Trans. Farad. Soc.*, **46**, 13.  
 Whiffen, D. H. and Thompson, H. W., 1946, *Trans. Farad. Soc.*, **42A** 114, 122.

# Letters to the Editor

*The Board of Editors does not hold itself responsible for opinions expressed in the letters published in this section. The notes containing short reports of original investigations communicated to this section should not contain many figures and should not exceed 500 words in length. The contributions reaching the Secretary by the 15th of any month may be expected to appear in the issue for the next month. No proof will be sent to the author.*

17

## A NOTE ON THE FRANCK-CONDON FACTORS OF VO ( $A^2\Delta-X^2\Delta$ ) BAND SYSTEM

N. SREEDHARA MURTHY, T. K. SREERANGA SETTY  
AND MISS K. V. SUMATHI\*

SPECTROSCOPIC LABORATORY, DEPARTMENT OF PHYSICS, CENTRAL COLLEGE  
BANGALORE-1

(Received December 30, 1963)

The accurate data of Franck-Condon (FC) factors of the band system of  $VO(A^2\Delta-X^2\Delta)$  is important to the astrophysicist as some stars, for example R. Leonis, emit radiations fairly rich in VO bands (Merrill, 1940). Tawde and Murthy (1957) have reported the calculations of FC-factors of this system. These calculations needed revision in two respects. In the first place, it is necessary to use anharmonic wave functions of Morse type in place of harmonic ones used earlier. Secondly, the  $\Delta r_e$  value ( $-0.08\text{\AA}$ ), from the preliminary announcement by Lagerqvist and Selin (1955), used in the calculations is to be replaced by the exact value (Lagerqvist and Selin, 1957). The FC-factors of the VO band system have been computed according to the procedure given by Tawde and Murthy (1959) using the numerical integration method, involving the Morse functions. The same procedure has been employed later by Singh and Jain (1961) and Tawde and Korwar (1962), to compute the FC-factors of some other systems. The molecular constants given by Lagerqvist and Selin (1957) have been used for the computation and are entered in Table I. The values of the Morse constants  $\alpha_1$  and  $\alpha_2$  used for this computation are  $\alpha_1 = 2.1831_{16}A^{-1}$  and  $\alpha_2 = 1.8944_5A^{-1}$ .

The resulting FC-factors are entered in columns 2 and 4 of Table II

Similar values of FC-factors for the VO system have been reported by Prasad (1963) using an identical procedure but using  $\Delta r_e = 0.08\text{\AA}$  from the preliminary

\* Now at the Dept. of Physics, Govt. Arts and Science College, Bangalore.

TABLE I  
Molecular constants of  $VO(A^2\Delta - X^2\Delta)$  system

(i)	(ii)	(iii)	(iv)
$X^2\Delta$	1011.56	4.97	1.589
$A^2\Delta$	865.9	6.6	1.672

(i) Electronic state, (ii)  $\omega_e$  ( $\text{cm}^{-1}$ ), (iii)  $\omega_e x_e$  ( $\text{cm}^{-1}$ ),  
(iv)  $r_e$  ( $\text{\AA}$ )

TABLE II  
 $VO(A^2\Delta - X^2\Delta)$  band system

Bands $v', v''$	FC-factors	Bands $v', v''$	FC-factors
0,0	0.303	2,0	0.204
0,1	0.391	2,1	0.077
0,2	0.218	2,2	0.144
0,3	0.070	2,3	0.006
1,0	0.324	3,0	0.100
1,1	0.012	3,1	0.171
1,2	0.149	3,2	0.002
1,3	0.281	3,3	0.152

announcement by Lagerqvist and Selin (1955). As FC-factors are sensitive to change in molecular constants (McKellar and Tawde 1951), particularly  $\Delta r_e$ , the FC-factors given by Prasad indicate only the trend of values in the second decimal place. It is thought that the revised results, given here would be more useful in the interpretation of the  $VO$  band system of stellar and laboratory sources.

The authors are thankful to Prof. N. R. Tawde, Karnatak University, Dharwar, for his kind interest and advice in the work and help in the preparation of the manuscript, and to Dr. Syed Ziauddin, Head of the Dept. of Physics, Central College, Bangalore, for encouragement.

#### REFERENCES

- Lagerqvist, A. and Selin, L. E., 1955, *Naturwissenschaften*, **42**, 65.  
 Lagerqvist, A. and Selin, L. E., 1957, *Arkiv for Fysik*, **12**, 553.  
 McKellar, A. and Tawde, N. R., 1951, *Astrophys. J.*, **113**, 440.  
 Merrill, P. W., 1940, *Spectra of Long period variables*, University of Chicago Press.  
 Prasad, S. S., 1963, *Proc. Phys. Soc. (Lond.)*, **82**, 419.  
 Singh, N. L., and Jain, D. C., 1961, *Proc. phys. Soc. (Lond.)*, **77**, 817.  
 Tawde, N. R. and Murthy, N. Sreedhara, 1957, *Ind. J. Phys.*, **31**, 391.  
 Tawde, N. R. and Murthy, N. Sreedhara, 1959, *Physica*, **25**, 610.  
 Tawde, N. R. and Korwar, V. M., 1962, *Proc. Phys. Soc. (Lond.)*, **80**, 794.

## EXCHANGE NARROWING OF DPPH LINE SHAPE IN ESR

B. N. MISRA

DEPARTMENT OF PHYSICS, UNIVERSITY OF ALLAHABAD (INDIA)

(Received November 21, 1960 : Resubmitted July 28, 1964)

The line width of Paramagnetic resonance lines in solids and liquids is mostly controlled by : (i) dipole-dipole interaction, (ii) spin-lattice interaction and (iii) exchange interaction.

Van-Vleck (1948) discussed the broadening, taking in view the effect of dipole-dipole interactions and suggested that in the absence of exchange interaction which is true for dilute paramagnetic salts, the Gaussian function becomes a fair approximation to the line shape. The theory of VanVleck could not estimate the line width in substances showing large exchange phenomenon when the curve falls off rapidly. Anderson and Weiss (1953) discussed the line shape in paramagnetic resonance where large exchange interaction is present. Their theory showed Lorentzian line shape which have been verified experimentally by many workers for certain substances. Kubo and Tomita (1954) discussed the theory of Magnetic resonance on quantum mechanical basis and expressed that in presence of large exchange interaction the line shape is Lorentzian and the expression for half width between half maximum absorption points can be represented as.

$$\Delta\omega = \frac{4.18\omega_{10}^2}{\omega_{20}} \quad \dots (1)$$

where

$\omega_{10}^2$  is the width due to  $dd$  interactions and  $\omega_{20}$  is the narrowing due to exchange.

The expressions for  $\omega_{10}^2$  and  $\omega_{20}$  have been given by Chirkov and Kokin (1958), are as follows,

$$\omega_{10}^2 = 3.79g^4\beta^4\hbar^{-2}d^{-6} \quad (2)$$

and

$$\omega_{20} = 3.65 |J| \hbar \quad \dots (3)$$

where,

$d$  is mean spin distance,

and  $J$  is exchange integral,

Substituting the values of,  $g = 2.0036$ , Holden, Yager and Merritt (1951),  $\beta$  and  $\hbar$  in the expressions 2 and 3, it is found that,

$$\omega_{10}^2 = 40.62X d^{-6}X10^{-28} \text{ sec}^{-2}. \quad \dots (4)$$

and

$$\omega_{20} = 3.462 \times 10^{21} \times |J| \text{ sec.}^{-1} \quad \dots (5)$$



In the present paper the value of the exchange integral  $J$  for different mean spin distances for DPPH has been calculated with the help of expressions 1,4 and 5, using the measured values of  $\Delta\omega$ , Bruin and Bruin (1956) with varying mean spin distance from 9 Å to 14.5 Å and within the temperature range of 100°K to 400°K in powder DPPH. The values of  $\omega_{10}^2$  have been computed and taking these computed values of  $\omega_{10}^2$  and measured values of  $\Delta\omega$  for different mean spin distances  $d$  and the temperatures, the values of  $\omega_{20}$ , the width, due to narrowing have been calculated. These values of  $\omega_{20}$  have been used for obtaining the different values of  $J$ .

### RESULT

The value of the exchange integral  $J$  as found above lies between  $5.57 \times 10^{-24}$  Joules and  $0.07 \times 10^{-24}$  Joules for mean spin distances varying from 9 Å to 14.5 Å. In the case of powder DPPH with mean spin distance of 9 Å, and between the temperature range of 100°K to 400K, the value lies between  $3.32 \times 10^{-24}$  Joules and  $6.73 \times 10^{-24}$  Joules. The nature of variation of  $J$  values in these two cases is shown in figures 1 and 2.

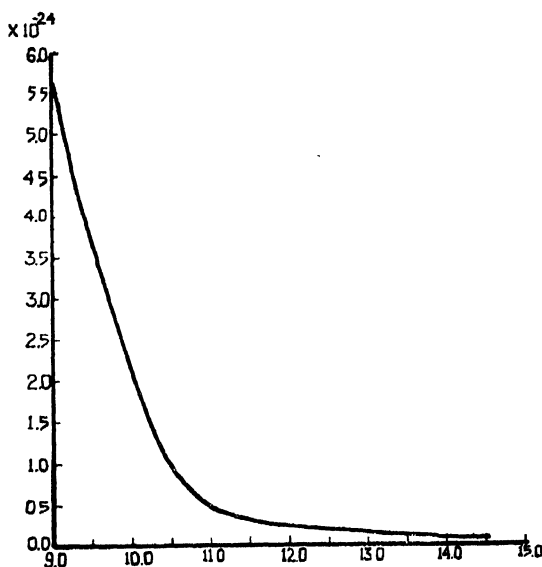


Fig. 1. Variation of exchange integral  $J$  with concentration in DPPH.

x axis. Mean spin distance in Angstroms.

y axis. Exchange Integral  $J$  in Joules.

### DISCUSSION

The first graph indicates that the variation of exchange integral  $J$  between mean spin distances of 11.5 Å and 14.5 Å is very slow but it starts increasing very rapidly as the mean spin distance is decreased below it. This shows that the nature of exchange interaction below 11.5 Å is different than above it. This kind of

behaviour of exchange interaction may be probably due to the contribution of some short range effect when the spins come closer together.

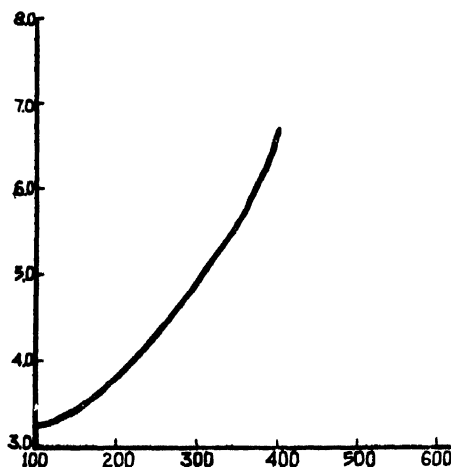


Fig. 2. "Variation of exchange integral  $J$  with temperature in Power DPPH."

x axis. Temperature in °K.

y axis. Exchange integral  $J$  in Joules.

The graph 2 which represents the variation of  $J$  with temperature shows that the value of  $J$  increases as the temperature rises. Walter et al. (1956) have found that it is not only the exchange interaction but there are other factors also which are responsible for the narrowing. They have discussed the motional narrowing due to the delocalization of the unpaired electrons in molecular orbitals. In free radicals the electrons will pass over several atoms in its orbitals and this motion at higher temperature may produce more averaging of the dipole dipole interaction and thus causing the narrowing of the lines. One may therefore say that at higher temperatures the more narrowing is due to the combined effect of exchange interaction and motional narrowing.

#### ACKNOWLEDGEMENT

The author is grateful to Sri Krishnaji for his kind interest in the work.

#### REFERENCE

- VanVleck, J. H. 1948, *Phys. Rev.* **74**, 1184.  
 Anderson, P. W. and Weiss, P. R. 1953, *Rev. Mod. Phys.* **25**, 269.  
 Kubo, R. and Tomita, A. 1954, *J. Phys. Soc. Japan*, **9**, 888.  
 Chirkov, A. K. and Kokin, A. A. 1958, *J.E.T.P. (USSR)*, **35**, 50-55.  
 Holden, A. N. Yager, W. A. and Merritt, F. R. 1951, *J. Chem. Phys.* **19**, 1319.  
 Bruin, F. and Bruin, M. 1956, *Physica*, **XXII**, 129.  
 Walter, R. I. et. al. 1956, *J. Chem. Phys.* **25**, 319.

# COBALT K X-RAY ABSORPTION SPECTRUM IN PINK AND BLUE SOLUTIONS OF COBALT (II) CHLORIDE

CHINTAMANI MANDE AND A. R. CHETAL

DEPARTMENT OF PHYSICS, UNIVERSITY OF POONA, POONA-7.

(Received September 23, 1963; Resubmitted June 12, 1964).

Van Nordstrand (1960a, b) has recently reported a large number of *K* absorption curves of transition metal ions in different types of compounds. He classifies these curves in four categories (see Sinha and Mande, 1963 for details). Of these, the type IV curves, that is the curves for the transition metal ions with tetrahedral surroundings, alone show the splitting of the principal absorption edge. Sinha and Mande (1963) have explained this splitting of the absorption discontinuity on the basis of the ligand field theory. It appears, that the tetrahedrally surrounded metal ion gives a very characteristic X-ray absorption spectrum. In this note we report the shape of the *K* X-ray absorption discontinuity of cobalt in pink and blue solutions of cobalt chloride.

A Cauchois type bent crystal X-ray spectrograph of diameter 40 cms, designed and constructed in our workshop, was used in this investigation. A well tried crystal of mica was used as analyser. The spectra were photographed using the (100) and (201) reflections of mica. A Philips sealed X-ray tube with tungsten target was employed. It was operated at 20KV, the current ranging from 20ma to 30 ma. Exposure times varied from 12 to 30 hours on Agfa ultraviolet plates. Microphotometer records of the plates were obtained with magnification 50 on a Moll microphotometer. The absorption cell containing the solution of cobalt chloride was placed in front of the X-ray tube window and was supported by means of two screws provided on the shield of the X-ray tube. The proper thickness of the absorbing solution was attained by placing the solution between two very thin films of celluloid separated by a stainless steel sheet of requisite thickness. Deep blue solutions were obtained by adding excess of concentrated HCl to the pink solutions.

The forms of Co K absorption edge in pink and blue solutions of  $\text{CoCl}_2$  respectively are shown in figures 1 and 2. These forms have been obtained from several microphotometer records taken in turn from several plates obtained under varying conditions of exposure. It is seen that these curves resemble very well with type I and type IV spectra respectively obtained by Van Nordstrand. However, it should be noted that the curves given by Van Nordstrand are absorption coefficient versus energy curves, where as our curves show the variation of transmitted intensity with energy. It will be seen that Fig. 1 shows a single *K*

discontinuity while Fig. 2 shows the splitting of the principal absorption edge into two successive components  $K_1$  and  $K_2$ . Both discontinuities show secondary fine structure near the absorption edge on the high energy side. However, for the blue solution, the curve somewhat flattens after the maximum of the secondary structure.

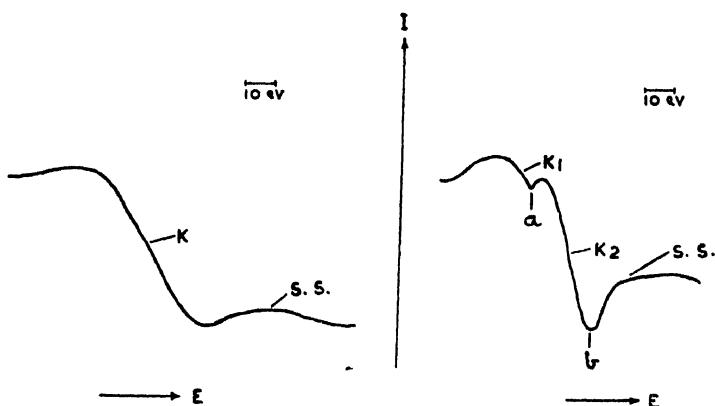


Fig. 1

Fig. 2

Figures 1 and 2 show the form of the Co K absorption edge in pink and blue solutions respectively of cobalt chloride. The markings S. S. stand for secondary structure.

The  $K$  absorption curves for the pink and blue solutions of cobalt chloride obtained in this investigation are characteristic of the transition metal ion associated with an octahedral co-ordination in the common salts and the ion associated with a tetrahedral configuration respectively. Hence we conclude that in the pink solution the  $\text{Co}^{++}$  ion is octahedrally surrounded and in the blue solution the coordination is a tetrahedral one. In the general interpretation given by Sinha and Mande, the minima at the markings 'a' and 'b' in Fig. 2 represent the X-ray absorption transitions  $1s \rightarrow 4p$  and  $1s \rightarrow p$  limit. The empty  $4p$  orbital of the  $\text{Co}^{++}$  ion is localised only in the tetrahedral configuration, thus making possible the  $1s \rightarrow 4p$  transition.

These results also establish that although in the solution state the lattice structure breaks down, the individual octahedral and tetrahedral units around the cobalt ion retain their identity. This work thus supports the assumptions made by Mookherji (1962) about the nature of the crystal fields in his recent magnetic studies of these solutions.

#### ACKNOWLEDGEMENT

Our thanks are due to the Council of Scientific and Industrial Research, New Delhi for sanctioning a research scheme under which this work has been done.

#### REFERENCES

- Sinha K. P. and Mande, C., 1963, *Ind. J. Phys.*, **37**, 257.  
 Van Nordstrand, R. A., 1960, *Conf. Non-crystalline solids*, John Wiley and Sons, New York.  
 Van Nordstrand, R. A., 1960, *Advances in Catalysis*, Vol. 12, Academic Press, New York.  
 Mookherji, T., 1962, *Ind. J. Phys.*, **36**, 215.

# REFLECTION AND TRANSMISSION PROPERTIES OF A STRATIFIED PLASMA\*

J. BASU.

INSTITUTE OF RADIO PHYSICS AND ELECTRONICS

UNIVERSITY OF CALCUTTA\*\*

(Received, May 14, 1964)

**ABSTRACT.** Equations are derived for the reflection and transmission coefficients of a plane electromagnetic wave incident normally on a plasma having a homogeneous layer in the middle and inhomogeneous layers on both sides. The equations are expressed in terms of parameters which can be calculated from the characteristic properties of the plasma by applying a numerical method and using a digital computer. It is found to be possible to simplify the calculations if the inhomogeneous layers are identical.

A plasma with a trapezoidal distribution of electron density along its thickness is discussed. The reflection and transmission coefficients for a number of such plasmas can be directly calculated from the results reported in the paper. The results refer to a few typical thicknesses of the inhomogeneous layers of the plasma, for which approximate methods that have been generally used in the past for determining the coefficients turn out to be unsatisfactory.

## INTRODUCTION

Over the last four or five decades the interaction of an electromagnetic wave and a gaseous plasma has attracted an appreciable amount of attention particularly as due to radio-wave exploration of the ionosphere,—which can be treated consisting of a few layers of plasma,—in connection with long distance radio-wave communication. In recent years the knowledge of the subject is finding wider application in various fields, such as the earth-to-satellite communication systems, microwave diagnostic methods for plasmas in thermo-nuclear experiments and in discharge and shock-wave tubes (Francis, 1960). The method for determining the reflection and transmission coefficients of a plane electromagnetic wave incident normally on a plasma with an arbitrary distribution of electron density has been described elsewhere (Nicol and Basu, 1962). However, in practice, the electron density in a plasma can be often assumed to be uniform except in the boundary regions, where the electron density gradually changes from zero to that of the uniform film. Such a plasma can be treated as a stratified one with a uniform film in the middle and inhomogeneous boundary layers on both sides. The reflection and transmission properties of the plasma can be expressed in terms of : (1) the thickness of and propagation coefficient for the

---

\*The abstract of the paper was published, in a slightly different form, in Part III of the Proceedings of the 50th Session of the Indian Science Congress.

\*\*Present address: Saha Institute of Nuclear Physics, 92, Acharya P. C. Road, Calcutta—9.

uniform film, and (2) the reflection and transmission coefficients for the inhomogeneous layers. This has the advantage that the calculation of the reflection and transmission coefficients for plasmas with a central uniform layer of variable thickness but with the same inhomogeneous layers becomes easy. Further simplifications in the calculations are possible if the inhomogeneous layers on either side are identical.

The distribution of electron density in plasmas obtained in discharge tubes is, in many cases, trapezoidal (Wharton and Slager, 1960). This paper reports numerical results in graphical form, which may be used to give the reflection and transmission coefficients for a wide range of plasmas with trapezoidal distribution of electron density. The thicknesses of the inhomogeneous layers of the plasmas are taken to be of the order of a wavelength of the incident wave, since it is in these cases that approximate treatments, such as the Wentzel-Kramers-Brillouin method, become unsatisfactory.

To make the calculations tractable several simplifying assumptions are made. The plasma layers which are of finite thickness are taken to be infinite in lateral directions so that diffraction effects can be neglected. The plasma is assumed to be free from any magnetic field except that of the incident electromagnetic radiation, and the variation of electron density in the plasma is assumed one-dimensional, viz., only along its thickness.

#### GENERAL EQUATIONS\*

In Fig. 1, the section  $AD$  represents a stratified medium, consisting of a uniform film  $BC$ , marked 2, and inhomogeneous boundary layers  $AB$  and  $CD$ . The inhomogeneous layers separate the uniform film from the homogeneous media 1 and 3.

#### \*LIST OF PRINCIPAL SYMBOLS

$e$  = Charge on an electron.

$l$  = Thickness of a uniform film.

$l'$  = Thickness of an inhomogeneous layer.

$m_e$  = Mass of an electron.

$N$  = Number density of electrons.

$N_c$  = Critical number density of electrons =  $\frac{\epsilon_0 m_e \omega^2}{e^2}$  in a rationalized system.

$N_u$  = Number density of electrons in a uniform plasma.

$n$  = Refractive index of a plasma.

$n_u$  = Refractive index of a uniform plasma.

$y$  = Wave admittance normalized with respect to that of free space.

$\gamma_0$  = Propagation coefficient in free space.

$\gamma$  = Propagation coefficient in a plasma.

$\gamma_u$  = Propagation coefficient in a uniform film.

$\epsilon_0$  = Absolute permittivity of free space.

$\lambda_0$  = Free-space wavelength.

$\nu$  = Frequency of collisions of electrons with heavy particles.

$\rho$  = Reflection coefficient for the electric field.

$\tau$  = Transmission coefficient for the electric field.

$\omega$  = Angular wave-frequency.

Let  $\gamma_u$  be the propagation coefficient in the uniform film and  $l$  be its thickness. Let  $\rho_{12}$  and  $\tau_{12}$  represent the reflection and transmission coefficients, for the layer  $AB$ , of a plane electromagnetic wave incident normally from the medium 1 under the condition that both the media 1 and 2 are semi-infinite, separated by the layer. Let  $\rho_{21}$  and  $\tau_{21}$  represent the coefficients of a wave incident normally from the medium 2 under the same condition as before. Similarly, for the layer  $BC$ , let  $\rho_{23}$  and  $\tau_{23}$  be the coefficients of a wave incident from the medium 2 under the condition that the media 2 and 3 are semi-infinite, separated by  $BC$ . If the propagation coefficients at all points in  $AB$  and  $CD$  are known, the above reflection and transmission coefficients can be calculated by a numerical method described elsewhere in detail (Nicol and Basu, 1962).

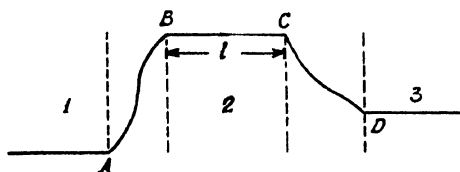


Fig. 1. Stratified medium consisting of a uniform film and inhomogeneous boundary layers.

BC, marked 2—Uniform film.

AB, CD—inhomogeneous boundary layers.

1, 3—homogeneous media.

Now, let a plane electromagnetic wave be incident normally on the whole stratified medium  $AD$  from the medium 1. The over-all reflection and transmission coefficients are given by the following equations (see Appendix 1 for the derivation of the equations).

$$\rho = \rho_{12} + \frac{\tau_{12}\tau_{21}\rho_{23}e^{-2\gamma_u l}}{1 - \rho_{21}\rho_{23}e^{-2\gamma_u l}} \quad \dots (1)$$

$$\tau = \frac{\tau_{12}\tau_{23}e^{-\gamma_u l}}{1 - \rho_{21}\rho_{23}e^{-2\gamma_u l}} \quad \dots (2)$$

Let us assume that  $AD$  in Fig. 1 represents a stratified plasma. The propagation coefficient in a plasma is given by (Ratcliffe, 1959)

$$\begin{aligned} \gamma &= \gamma_0 n \\ &= \gamma_0 \left[ 1 - \frac{N/N_c}{1 - i(\nu/\omega)} \right]^{1/2} \quad \dots (3)^* \end{aligned}$$

\*For definitions of quantities see the List of Principal Symbols.

Hence, if the electron density and collision frequency at all points in the plasma are known, the propagation coefficients for a wave of angular frequency  $\omega$  can be calculated from eqn. (3), and the over-all reflection and transmission coefficients can then be determined from eqns. (1) and (2).

#### INHOMOGENEOUS LAYERS OF ZERO THICKNESS

If the inhomogeneous layers  $AB$  and  $CD$  in Fig. 1 disappear, leaving the uniform film  $BC'$  between the media 1 and 3, the quantities  $\rho_{12}$ ,  $\tau_{12}$ ,  $\rho_{21}$ ,  $\tau_{21}$ ,  $\rho_{23}$  and  $\tau_{23}$  are all given by the Fresnel formulae. We find that eqns. (1) and (2) are now converted into the well-known formulae for the reflection and transmission coefficients for a uniform film (Born and Wolf, 1959).

$$\rho = \frac{\rho_{12} + \rho_{23}e^{-2\gamma ul}}{1 + \rho_{12}\rho_{23}e^{-2\gamma ul}} \quad \dots \quad (4)$$

$$\tau = \frac{\tau_{12}\tau_{23}e^{-\gamma ul}}{1 + \rho_{12}\rho_{23}e^{-2\gamma ul}} \quad \dots \quad (5)$$

In this trivial case the quantities  $\rho_{12}$ ,  $\tau_{12}$ , etc. are directly obtained from the refractive indices of the media 1, 2 and 3.

#### IDENTICAL INHOMOGENEOUS LAYERS

Let us assume that in Fig. 1, the media 1 and 3 are the same and that the inhomogeneous layers  $AB$  and  $DC'$  are identical. This can usually be taken as a valid assumption if  $AD$  represents a plasma bounded on either side by free space or air. The over-all reflection and transmission coefficients are, from eqns. (1) and (2),

$$\rho = \rho_{12} + \frac{\tau_{12}\tau_{21}\rho_{21}e^{-2\gamma ul}}{1 - (\rho_{21}e^{-\gamma ul})^2} \quad \dots \quad (6)$$

$$\tau = \frac{\tau_{12}\tau_{21}e^{-\gamma ul}}{1 - (\rho_{21}e^{-\gamma ul})^2} \quad \dots \quad (7)$$

Numerical calculations can be simplified by using the relations derived in Appendix 2 and enumerated below.

First we have

$$\tau_{12}/y_1 = \tau_{21}/y_2 \quad (8)$$

where  $y_1$  and  $y_2$  are the wave admittances of the media 1 and 2, normalized with respect to the wave admittance of free space. Hence, if either of  $\tau_{12}$  and  $\tau_{21}$  is known, the other one can be readily determined. It is to be noted here that if the permeability of a medium is unity, the normalized wave admittance is equal to its refractive index. In particular, a plasma is diamagnetic, but only weakly so, and its permeability can be assumed to be unity.



Let us next make a simplifying assumption that the wave admittance is real all throughout the media under consideration. For a plasma the assumption implies that the electron collision frequency is very small, compared to the frequency of the incident wave, and that nowhere in the plasma the electron density exceeds the so-called critical value for the particular wave-frequency. The following relations are now found to hold good.

$$|\rho_{12}| = |\rho_{21}| \quad \dots (9)$$

$$\angle \rho_{12} + \angle \rho_{21} = -\pi + 2\angle \tau_{12} \quad \dots (10)$$

$$|\tau_{12}|/y_1 = |\tau_{21}|/y_2 \quad \dots (11)$$

$$\angle \tau_{12} = \angle \tau_{21} \quad \dots (12)$$

If, therefore, numerical calculations are made for one of the pairs,  $(\rho_{12}, \tau_{12})$  or  $(\rho_{21}, \tau_{21})$ , the other pair can be determined from the above equations.

#### LINEAR DISTRIBUTION OF ELECTRON DENSITY IN INHOMOGENEOUS LAYERS

In many practical cases a plasma can be reasonably assumed to have a trapezoidal distribution of electron density, as shown in Fig. 2 (Wharton and Slager, 1960). Such a plasma can be thought of as having a uniform film in the middle and inhomogeneous layers with linear distribution of electron density on either side.

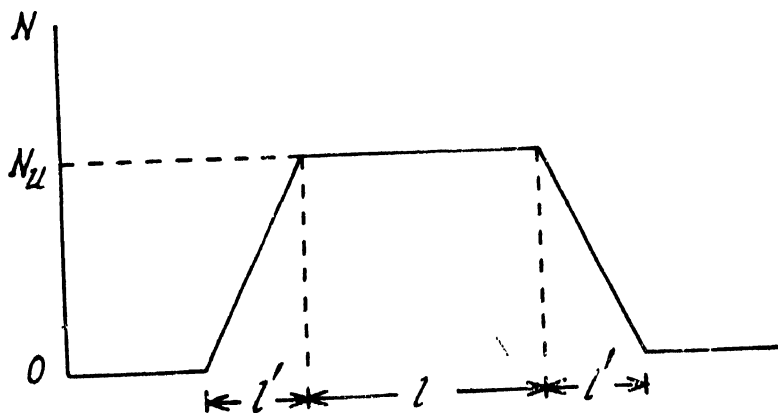


Fig. 2. Trapezoidal distribution of electron density.

Let us consider an inhomogeneous plasma layer  $A'B'$  of thickness  $l'$  and with linear density distribution, separating free space from a semi-infinite uniform plasma with electron density  $N_u$  (Fig. 3). The reflection and transmission coefficients for the layer are given below in graphical form, the thickness  $l'$  being taken as  $\lambda_0/2$ ,  $\lambda_0$  or  $2\lambda_0$  where  $\lambda_0$  represents the free-space wavelength of the incident elec-

tromagnetic radiation. The coefficients were obtained by a step-by-step integration process (Nicoll and Basu, 1962) carried out on the Mercury computer at Manchester University. For the sake of simplicity the collision frequency of electrons is assumed to be negligible, compared to the frequency of the incident wave. For plasmas with trapezoidal distribution of electron density and with inhomogeneous layers of thickness  $\lambda_0/2$ ,  $\lambda_0$  or  $2\lambda_0$ , the over-all reflection and transmission coefficients can be readily calculated from the given results by using eqns. (1) and (2).

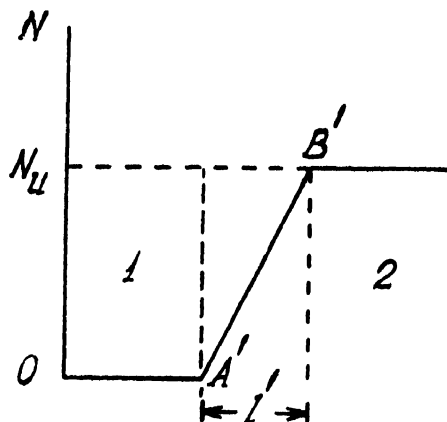


Fig. 3. Inhomogeneous plasma layer with linear distribution of electron density, separating free space from a uniform plasma.

$A'B'$ —inhomogeneous plasma layer.

1—free space.

2—uniform plasma.

It may be mentioned that the results which were calculated on the basis of a numerical method could also be obtained by the algebraic method devised by Hartree (1928-29) for determining the reflection coefficient and extended by the author (Basu, 1960) for determining the transmission coefficient as well.

#### (a) Wave incident from free space

Figures 4(a) and (b) show respectively the magnitude and phase angle of the reflection coefficient,  $|\rho_{12}|$  and  $\angle \rho_{12}$ , for different thicknesses of the inhomogeneous layer  $A'B'$  when a plane electromagnetic wave is incident normally on the layer from free space. The magnitude and phase angle of the transmission coefficient,  $|\tau_{12}|$  and  $\angle \tau_{12}$ , are shown in Figs. 4(c) and (d). A few salient features of the plots in Figs. 4(a) through (d) are discussed below.

Fig. 4(a) :  $|\rho_{12}|$  increases with the increase of  $N_u$  until  $N_u$  reaches  $N_c$ , the critical density. Once the critical density is reached, all the incident wave is reflected, and  $|\rho_{12}|$  remains at unity for further increase of  $N_u$ . The greater the thickness of the inhomogeneous layer, the smoother the transition from free

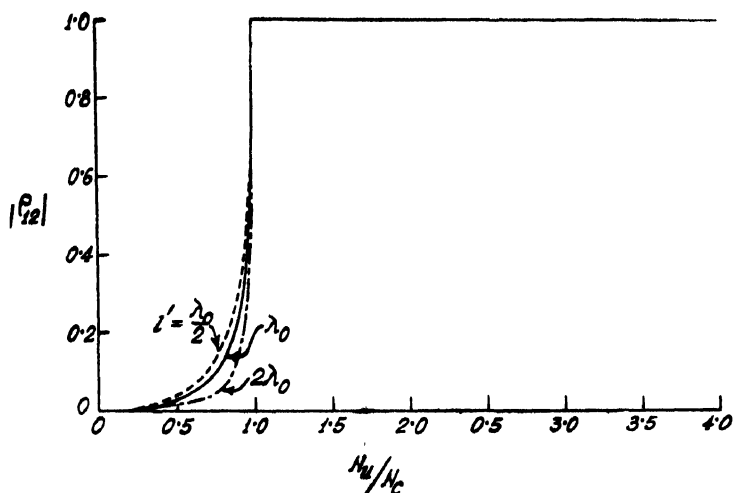
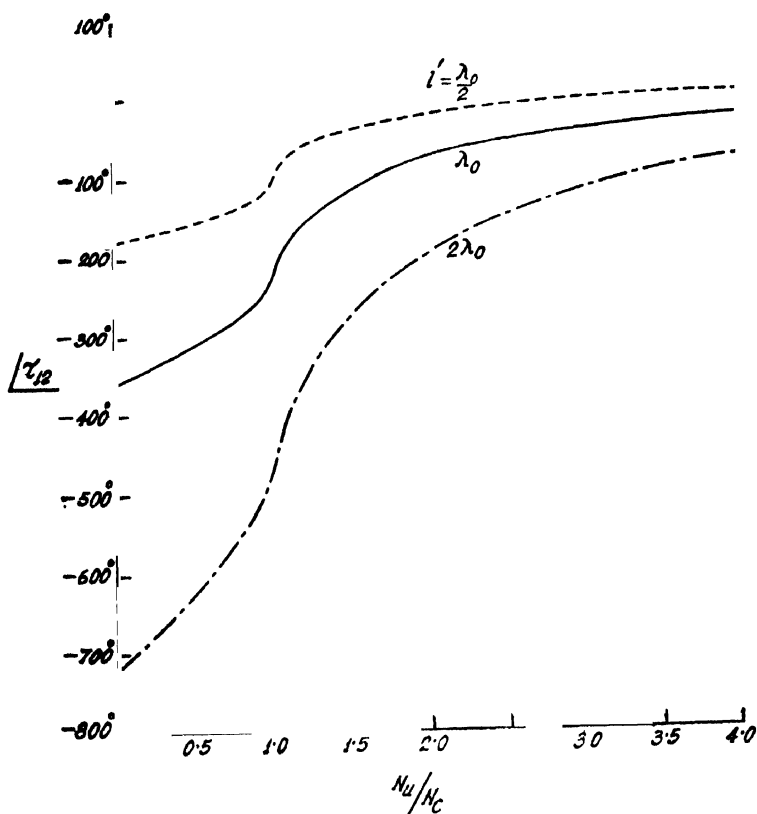


Fig. 4. Characteristics for the layer  $A'B'$  in Fig. 3 when a plane wave is incident normally from free space.

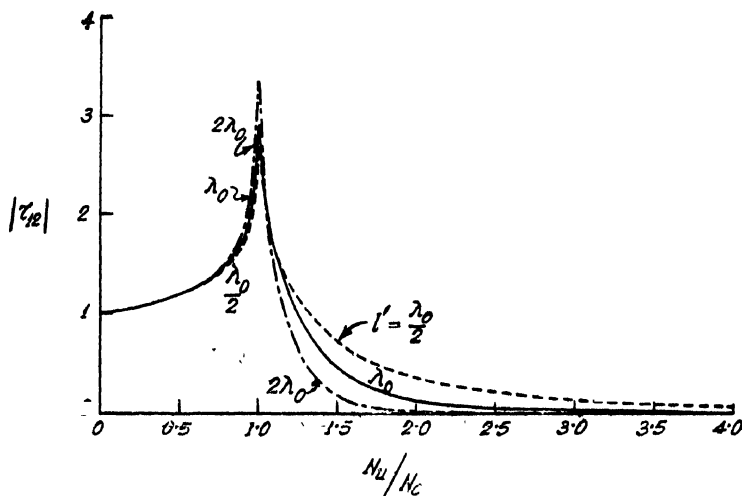
(a) Magnitude of the reflection coefficient.



(b) Phase angle of the reflection coefficient.

space to the uniform plasma and hence the less the value of  $|\rho_{12}|$  for the same electron density  $N_u$  when  $N_u < N_c$ .

Fig. 4(b) : The reflection takes place, in general, from all parts of the inhomogeneous layer, and the net reflected wave first lags behind the incident wave.

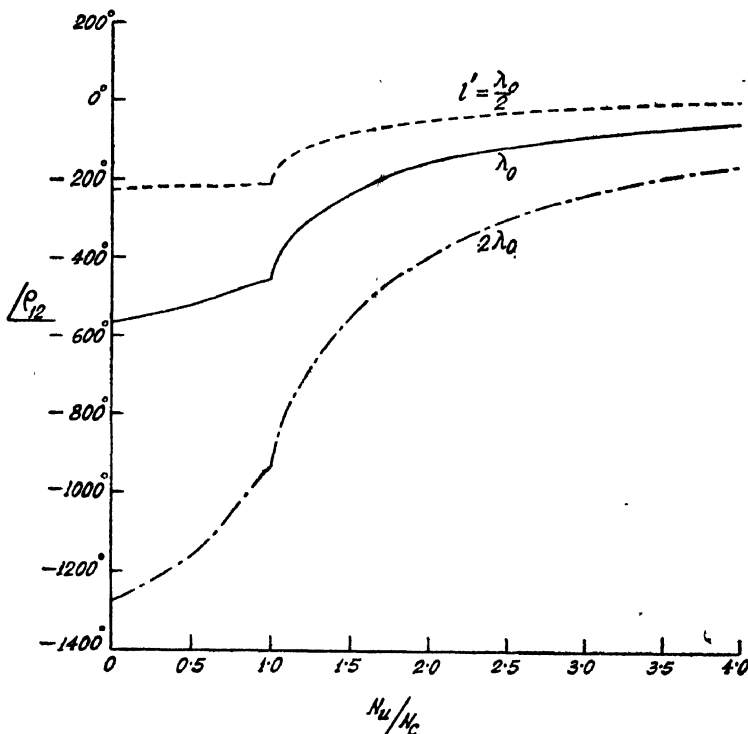


(c) Magnitude of the transmission coefficient.

The lagging angle, i.e.,  $-\angle\rho_{12}$  decreases as  $N_u$  increases. When  $N_u$  equals  $N_c$ , there is a discontinuity in the curvature of the plot for  $\angle\rho_{12}$ . This is the point after which the refractive index of a part of the plasma becomes imaginary. When  $N_u$  tends toward infinity, the electron density even at the input boundary is very high, and the wave is effectively reflected right at that boundary; now the reflection angle approaches  $180^\circ$  in the limit (cf. Nicoll and Basu, 1962). If  $N_u$  is kept fixed and the thickness  $l'$  is increased,  $-\angle\rho_{12}$  increases. However, the difference between the angles is reduced as  $N_u$  rises, the difference being zero when  $N_u = \infty$ .

Fig. 4(c) : When  $N_u < N_c$ , the magnitude of the transmitted electric vector is given by  $|\tau_{12}| = (p_t/n_u)^{1/2}$ , where  $p_t$  is the transmitted power normalized with respect to the incident power and  $n_u$  is the refractive index of the uniform plasma. With the increase of  $N_u$  from zero,  $p_t$  which is equal to  $1 - |\rho_{12}|^2$  is reduced, but  $n_u$  is reduced at a faster rate; as a result  $|\tau_{12}|$  increases. When, however,  $N_u$  exceeds  $N_c$ , the refractive index becomes imaginary in a part of the inhomogeneous layer, and the wave is attenuated; now with the increase of  $N_u$  the attenuation increases and  $|\tau_{12}|$  is reduced more and more. It is interesting to note that although the transmitted power  $p_t$  is zero in this region, the transmitted electric vector is not so; the vector is, in this case, associated with an evanescent wave in the uniform plasma. Let us next consider different thicknesses of the inhomogeneous layer, and let  $N_u < N_c$ . An increase in the thickness results in a decrease

in  $|\rho_{12}|^2$  and, therefore, in an increase in  $p_t$ . Hence for the same electron density  $N_u$ , i.e., for the same refractive index  $n_u$ , the greater the thickness  $l'$ , the higher the value of  $|\tau_{12}|$ . When  $N_u > N_c$ , the region over which the wave is attenuated increases with an increase in  $l'$ , and  $|\tau_{12}|$  decreases at a more rapid rate.



(d) Phase angle of the transmission coefficient.

Fig. 4(d) : Initially at  $N_u = 0$  the phase angle of the transmitted electric vector,  $\angle \tau_{12}$ , corresponds to the thickness of the inhomogeneous layer, this angle being negative as the transmitted vector lags behind the incident one. With the increase in  $N_u$  the electron density throughout the layer increases, and the refractive index is reduced. This results in a decrease in the effective path-length in the layer, and  $-\angle \tau_{12}$  is diminished. At  $N_u = N_c$  there is a noticeable change in the curvature of the plot of the phase angle. The greater the thickness  $l'$ , obviously the higher the initial value of  $-\angle \tau_{12}$ . The difference between the transmission angles, however, decreases with increase in  $N_u$ . All the plots approach  $90^\circ$  as  $N_u$  tends to infinity. This is due to the fact that the phase change occurs now mainly at the input boundary, where the limiting value is  $90^\circ$ .

#### (b) Wave incident from the uniform plasma

Referring to the model in Fig. 3, let us assume that a plane electromagnetic wave is incident normally on the inhomogeneous layer from the semi-infinite uniform plasma. The magnitude and phase angle of the reflection coefficient,

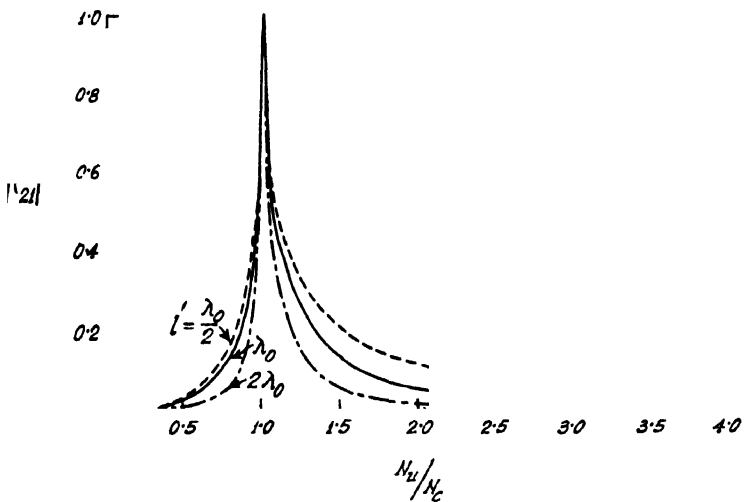
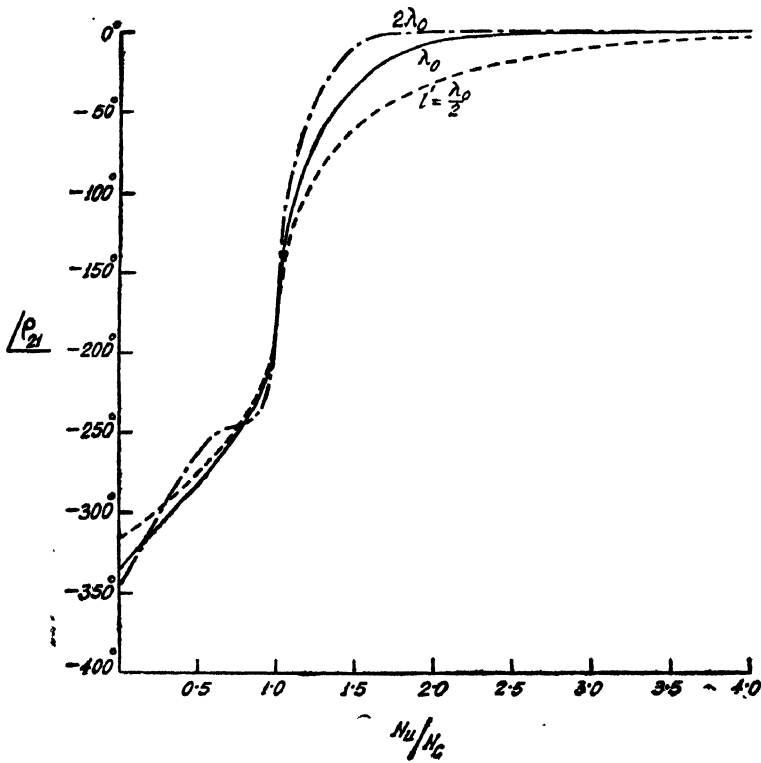


Fig. 5. (a) Characteristics for the layer A' B' in Fig. 3 when a plane wave is incident normally from the uniform plasma.



(b)—represent the same parameters as described below Fig. 4.

$|\rho_{21}|$  and  $\angle\rho_{21}$ , are plotted in Figs. 5(a) and (b). The corresponding quantities for the transmission coefficient,  $|\tau_{21}|$  and  $\angle\tau_{21}$ , are shown in Figs. 5(c) and (d).

The plots in Figs. 4 and 5 conform to the relation given in eqn. (8) in the general case and to those in eqns. (9) through (12) for  $N_u < N_c$ . The following additional points are worth noting in connection with the plots in Figs. 5(a) through (d).

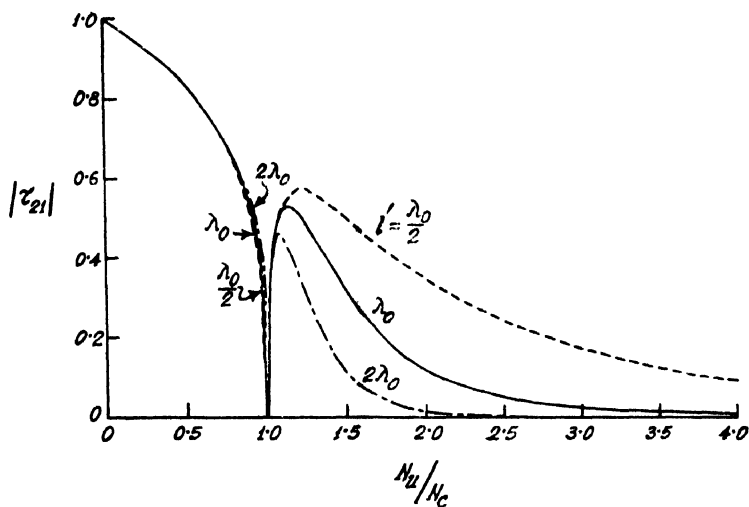


Fig. 5(c)

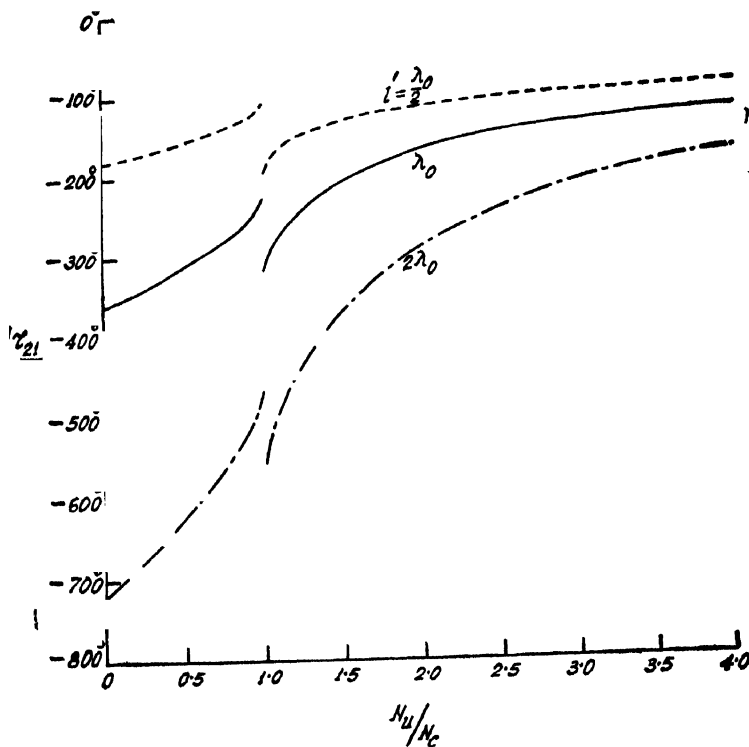


Fig. 5 (d)

(1) Consider the case :  $N_u = N_c$ .

$\rho_{21} = |1| \angle -180^\circ = -1$ , and  $\tau_{21} = 0$ . The uniform plasma is now perfectly short-circuited, as it were, at the input boundary of the inhomogeneous layer. Since the refractive index of the plasma is zero, there is no change of the electric field in the plasma, and the resultant electric field all throughout is zero. There is an abrupt change of  $90^\circ$  in each plot of  $\angle \tau_{21}$ , corresponding to the fact that the refractive index of the uniform plasma is real when  $N_u < N_c$  and imaginary when  $N_u > N_c$ .

(2) Consider the case :  $N_u > N_c$ .

The uniform plasma is reactive in nature, and the energy associated with electromagnetic waves inside the plasma is in the form of stored energy. However,  $\tau_{21}$  has a finite magnitude, indicating that it is still possible to transmit some power out. This can be explained by the presence of a 'reflected wave' in the plasma. A similar situation arises when a microwave piston attenuator is terminated by a resistive load (Barlow and Cullen, 1950).

If the thickness of the inhomogeneous layer were zero, i.e., if there were a sudden transition from the uniform plasma to free space,  $|\rho_{21}|$  would have remained constant at unity as  $N_u$  increased beyond  $N_c$ , and  $|\tau_{21}|$  would have simultaneously increased, reaching 2 at  $N_u = \infty$ . For a finite thickness of the inhomogeneous layer the net reflected wave can be thought of as the resultant of the waves reflected from all parts of the layer, and on account of the reactive attenuation of the waves in the layer,  $|\rho_{21}|$  is reduced with the increase of  $N_u$ , as shown in Fig. 5(a);  $|\tau_{21}|$  first increases as  $N_u$  increases, but as the attenuation becomes predominant,  $|\tau_{21}|$  gets reduced with further increase in  $N_u$  (Fig. 5c).

As  $N_u$  increases beyond  $N_c$ , the penetration becomes less and  $-\angle \rho_{21}$  decreases, the penetration tending to zero in the limit and  $-\angle \rho_{21}$  tending to  $0^\circ$  (Fig. 5b),  $-\angle \tau_{21}$  also approaches  $0^\circ$  at the same time (Fig. 5d), as there is, in the limit, no phase change in the whole plasma medium nor any at the output boundary.

### (c) *Triangular distribution of the electron density*

If the thickness of the uniform film in Fig. 2 is made equal to zero, the trapezoidal distribution of electron density becomes a triangular one. The overall reflection and transmission coefficients for a few models of the plasma with triangular density distribution have been previously reported by Nicoll and Basu (1962). The results obtained on the basis of eqns. (6) and (7) and the plots in Figs. 4 and 5 are found to be in conformity with the previous results.

## CONCLUSIONS

The reflection and transmission coefficients for the whole column  $AD$  in Fig. 1 can be obtained by the numerical method described by Nicoll and Basu (1962). However, if the inhomogeneous layers  $AB$  and  $CD$  remain the same and only



the thickness of the uniform film  $BC$  changes, it is not necessary to go through the numerical process every time; eqns. (1) and (2) can be, instead, utilized. The reflection and transmission coefficients for some models of plasmas with trapezoidal distribution of electron density can be directly calculated from the results reported in this paper; the inhomogeneous layers of the plasmas must, of course, correspond to those that have been discussed.

The method described in deriving eqns. (1) and (2) can be readily extended to yield the reflection and transmission properties of a system consisting of a number of homogeneous and inhomogeneous layers, e.g., a plasma with trapezoidal distribution of electron density, enclosed by the glass walls of the container.

#### ACKNOWLEDGMENT

The work described in this paper was initiated when the author was on the research staff of the Manchester College of Science and Technology, England, during the period 1960-61. He is indebted to Prof. C. Adamson and the late Prof. E. Bradshaw for providing research facilities in the Department of Electrical Engineering of the College. He is particularly indebted to the Director of the Computing Machine Laboratory, Manchester University, for the calculations performed on the Mercury computer.

The author wishes to acknowledge his gratitude to Prof. J. N. Bhar for his kind permission to continue the work in the Institute of Radio Physics and Electronics, University of Calcutta.

#### APPENDIX I

##### DERIVATION OF THE GENERAL EQUATIONS

Considering Fig. 1, let a plane electromagnetic wave be incident normally on the stratified medium  $AD$  from the medium 1. At the points  $A$ ,  $B$  and  $C$  there are now two resultant waves, one forward-moving and the other backward-moving. However, at  $D$  there is only the forward-moving wave in the medium 3, which corresponds to the wave transmitted out. We assume that at the point  $D$  the electric field corresponding to this wave is given by a vector of unit magnitude and zero phase. The reflection and transmission coefficients for the inhomogeneous layers  $AB$  and  $CD$  are given by  $\rho_{12}$ ,  $\tau_{12}$ , etc., as described in Sec. II.

The electric fields of the forward and backward waves in the medium 2 at the point  $C$  are :

$$E_{f(c)} = \frac{1}{\tau_{23}} \quad \dots \quad (\text{A.1})$$

$$E_{b(c)} = \frac{\rho_{23}}{\tau_{23}} \quad \dots \quad (\text{A.2})$$

The corresponding quantities in the same medium at the point  $B$  are :

$$E_{f(B)} = \frac{e\gamma u l}{\tau_{23}} \quad \dots \quad (\text{A.3})$$

$$E_{b(B)} = \frac{\rho_{23}e^{-\gamma u l}}{\tau_{23}} \quad \dots \quad (\text{A.4})$$

The forward wave at  $B$  can be divided into two parts, the electric field of the first part being  $\rho_{21}E_{b(B)}$  and that of the other being  $E_{f(B)} - \rho_{21}E_{b(B)}$ . The backward wave at  $B$  together with the first part of the forward wave corresponds to a backward wave in the medium 1; the electric field of this backward wave at the point  $A$  is  $\tau_{21}E_{b(B)}$ . The second part of the forward wave at  $B$  corresponds to a forward wave plus a backward wave in the medium 1; the electric fields of these waves at  $A$  are  $(\tau_{12})^{-1}(E_{f(B)} - \rho_{21}E_{b(B)})$  and  $\rho_{12}(\tau_{12})^{-1}(E_{f(B)} - \rho_{21}E_{b(B)})$  respectively.

Hence the electric fields of the total forward and backward waves in the medium 1 at the point  $A$  are :

$$\begin{aligned} E_{f(A)} &= \frac{1}{\tau_{12}} (E_{f(B)} - \rho_{21}E_{b(B)}) \\ &= \frac{e\gamma u l}{\tau_{12}\tau_{23}} (1 - \rho_{21}\rho_{23}e^{-2\gamma u l}) \quad \dots \quad (\text{A.5}) \end{aligned}$$

$$\begin{aligned} E_{b(A)} &= \tau_{21}E_{b(B)} + \frac{\rho_{12}}{\tau_{12}}(E_{f(B)} - \rho_{21}E_{b(B)}) \\ &= \frac{\tau_{21}\rho_{23}e^{-\gamma u l}}{\tau_{23}} + \frac{\rho_{12}e\gamma u l}{\tau_{12}\tau_{23}} (1 - \rho_{21}\rho_{23}e^{-2\gamma u l}) \quad \dots \quad (\text{A.6}) \end{aligned}$$

The over-all reflection coefficient for the stratified medium  $AD$  is given by

$$\rho = \frac{E_{b(A)}}{E_{f(A)}} \quad \dots \quad (\text{A.7})$$

Since the transmitted electric vector at  $D$  has been assumed to be of unit magnitude and zero phase, the over-all transmission coefficient is given by

$$\tau = \frac{1}{E_{f(A)}} \quad \dots \quad (\text{A.8})$$

The general equations (1) and (2) in Sec. II are derived from eqns. (A.5) through (A.8).

It should be noted that the equations can also be derived in two other ways, as mentioned by Montgomery (1947) in a different context.

## APPENDIX 2

### RELATIONS BETWEEN THE REFLECTION AND TRANSMISSION COEFFICIENTS FOR AN INHOMOGENEOUS LAYER

Let an inhomogeneous layer lie between two semi-infinite homogeneous media 1 and 2. Here we determine the relations between  $\rho_{12}$ ,  $\rho_{21}$ ,  $\tau_{12}$  and  $\tau_{21}$  where  $\rho_{12}$  and  $\tau_{12}$  represent the reflection and transmission coefficients, for the inhomogeneous layer, of a plane electromagnetic wave incident normally from the medium 1 while  $\rho_{21}$  and  $\tau_{21}$  represent the corresponding quantities if the wave is incident from the medium 2.

The inhomogeneous layer can be considered as a stratified medium consisting of a very large number of thin films. If the thicknesses of the films are sufficiently small, it is permissible to regard the refractive index to be constant throughout each film.

Now, Born and Wolf (1959) have derived expressions for the reflection and transmission coefficients for a stratified medium in terms of a matrix which is a characteristic property of the particular medium. Let  $M$  represent the characteristic matrix for the inhomogeneous layer under consideration. We can relate the electric and magnetic fields at the input and output boundaries,  $E_i$ ,  $H_i$ , and  $E_0$ ,  $H_0$ , in the following way.

$$\begin{bmatrix} E_i \\ H_i \end{bmatrix} = M \begin{bmatrix} E_0 \\ H_0 \end{bmatrix} = \begin{bmatrix} m_{11} & m_{12} \\ m_{21} & m_{22} \end{bmatrix} \begin{bmatrix} E_0 \\ H_0 \end{bmatrix} \quad \dots \quad (\text{A.9})$$

The reflection and transmission coefficients for the inhomogeneous layer,  $\rho_i$  and  $\tau_i$ , can be expressed in terms of the elements of the matrix  $M$ .

$$\rho_i = \frac{(m_{11}y_i - m_{22}y_0) + (m_{12}y_iy_0 - m_{21})}{(m_{11}y_i + m_{22}y_0) + (m_{12}y_iy_0 + m_{21})} \quad \dots \quad (\text{A.10})$$

$$\tau_i = \frac{2y_i}{(m_{11}y_i + m_{22}y_0) + (m_{12}y_iy_0 + m_{21})} \quad \dots \quad (\text{A.11})$$

In the above equations  $y_i$  and  $y_0$  are the wave admittances of the homogeneous media on the input and output sides of the inhomogeneous layer, normalized with respect to the wave admittance of free space.

Let us consider the thin films constituting the inhomogeneous layer. Let these films, starting from the input boundary, be designated as (1), (2), ... (n),

and let  $M^{(1)}, M^{(2)} \dots M^{(n)}$  be their characteristic matrices. It can be shown that

$$M = M^{(1)} M^{(2)} \dots M^{(n)} \quad \dots (A.12)$$

Let

$$M^{(1)} = \begin{bmatrix} m_{11}^{(1)} & m_{12}^{(1)} \\ m_{21}^{(1)} & m_{22}^{(1)} \end{bmatrix}, \quad M^{(2)} = \begin{bmatrix} m_{11}^{(2)} & m_{12}^{(2)} \\ m_{21}^{(2)} & m_{22}^{(2)} \end{bmatrix}, \text{ etc.}$$

Then, from eqn. (A.12),

$$\begin{aligned} & \begin{bmatrix} m_{11} & m_{12} \\ m_{21} & m_{22} \end{bmatrix} \\ &= \begin{bmatrix} m_{11}^{(1)} & m_{12}^{(1)} \\ m_{21}^{(1)} & m_{22}^{(1)} \end{bmatrix} \begin{bmatrix} m_{11}^{(2)} & m_{12}^{(2)} \\ m_{21}^{(2)} & m_{22}^{(2)} \end{bmatrix} \dots \begin{bmatrix} m_{11}^{(n)} & m_{12}^{(n)} \\ m_{21}^{(n)} & m_{22}^{(n)} \end{bmatrix} \\ &= \begin{bmatrix} \sum m_{1a_1}^{(1)} m_{a_1 a_2}^{(2)} m_{a_2 a_3}^{(3)} \dots m_{a_{n-2} a_{n-1}}^{(n-1)} m_{a_{n-1}}^{(n)} \\ \sum m_{2a_1}^{(1)} m_{a_1 a_2}^{(2)} m_{a_2 a_3}^{(3)} \dots m_{a_{n-2} a_{n-1}}^{(n-1)} m_{a_{n-1}}^{(n)} \\ \sum m_{1a_1}^{(1)} m_{a_1 a_2}^{(2)} m_{a_2 a_3}^{(3)} \dots m_{a_{n-2} a_{n-1}}^{(n-1)} m_{a_{n-1}}^{(n)} 2^{(n)} \\ \sum m_{2a_1}^{(1)} m_{a_1 a_2}^{(2)} m_{a_2 a_3}^{(3)} \dots m_{a_{n-2} a_{n-1}}^{(n-1)} m_{a_{n-1}}^{(n)} 2^{(n)} \end{bmatrix} \dots \quad (A.13) \end{aligned}$$

where each of  $a_1, a_2, a_3, \dots, a_{n-2}, a_{n-1}$  can be either 1 or 2.

From eqn. (A.13)

$$\left. \begin{aligned} m_{11} &= \sum m_{1a_1}^{(1)} m_{a_1 a_2}^{(2)} m_{a_2 a_3}^{(3)} \dots m_{a_{n-2} a_{n-1}}^{(n-1)} m_{a_{n-1}}^{(n)} \\ m_{12} &= \sum m_{1a_1}^{(1)} m_{a_1 a_2}^{(2)} m_{a_2 a_3}^{(3)} \dots m_{a_{n-2} a_{n-1}}^{(n-1)} m_{a_{n-1}}^{(n)} 2^{(n)} \\ m_{21} &= \sum m_{2a_1}^{(1)} m_{a_1 a_2}^{(2)} m_{a_2 a_3}^{(3)} \dots m_{a_{n-2} a_{n-1}}^{(n-1)} m_{a_{n-1}}^{(n)} \\ m_{22} &= \sum m_{2a_1}^{(1)} m_{a_1 a_2}^{(2)} m_{a_2 a_3}^{(3)} \dots m_{a_{n-2} a_{n-1}}^{(n-1)} m_{a_{n-1}}^{(n)} 2^{(n)} \end{aligned} \right\} \dots \quad (A.14)$$

Let us first imagine that an electromagnetic wave is incident on the inhomogeneous layer from the medium 1. Let the films extending from the medium 1 to 2 be designated as (1), (2) ... (n). Then the characteristic matrix of the whole layer is given by eqn. (A.12), and its elements are given by eqn. (A.14). The reflection coefficient  $\rho_{12}$  and the transmission coefficient  $\tau_{12}$  are obtained from eqns. (A.10) and (A.11).

$$\rho_{12} = \frac{(m_{11}y_1 - m_{22}y_2) - (m_{12}y_1y_2 - m_{21})}{(m_{11}y_1 + m_{22}y_2) + (m_{12}y_1y_2 + m_{21})} \quad \dots \quad (\text{A.15})$$

$$\tau_{12} = \frac{2y_1}{(m_{11}y_1 + m_{22}y_2) + (m_{12}y_1y_2 + m_{21})} \quad \dots \quad (\text{A.16})$$

where  $y_1$  and  $y_2$  are the normalized wave admittances of the media 1 and 2.

Let us next imagine that an electromagnetic wave is incident on the inhomogeneous layer from the medium 2. Starting from the input boundary, the thin films are now  $(n), (n-1), \dots (1)$ . Let  $M'$  be the characteristic matrix for the whole layer in this case. Then,

$$M' = M^{(n)} M^{(n-1)} \dots M^{(1)} \quad \dots \quad (\text{A.17})$$

If

$$M' = \begin{bmatrix} m'_{11} & m'_{12} \\ m'_{21} & m'_{22} \end{bmatrix} \quad \dots \quad (\text{A.18})$$

it can be easily shown that

$$\left. \begin{aligned} m'_{11} &= \Sigma m_{1a_1}^{(n)} m_{a_1a_2}^{(n-1)} m_{a_2a_3}^{(n-2)} \dots m_{a_{n-2}a_{n-1}}^{(2)} m_{a_{n-1}}^{1(1)} \\ m'_{12} &= \Sigma m_{1a_1}^{(n)} m_{a_1a_2}^{(n-1)} m_{a_2a_3}^{(n-2)} \dots m_{a_{n-2}a_{n-1}}^{(2)} m_{a_{n-1}}^{2(1)} \\ m'_{21} &= \Sigma m_{2a_1}^{(n)} m_{a_1a_2}^{(n-1)} m_{a_2a_3}^{(n-2)} \dots m_{a_{n-2}a_{n-1}}^{(2)} m_{a_{n-1}}^{1(1)} \\ m'_{22} &= \Sigma m_{2a_1}^{(n)} m_{a_1a_2}^{(n-1)} m_{a_2a_3}^{(n-2)} \dots m_{a_{n-2}a_{n-1}}^{(2)} m_{a_{n-1}}^{2(1)} \end{aligned} \right\} \dots \quad (\text{A.19})$$

where, as in eqn. (A.14), each of  $a_1, a_2, a_3, \dots a_{n-2}, a_{n-1}$  can be either 1 or 2.

Now, following Born and Wolf (1959), the characteristic matrix of the thin film  $(r)$  can be written

$$\begin{aligned} M^{(r)} &= \begin{bmatrix} m_{11}^{(r)} & m_{12}^{(r)} \\ m_{21}^{(r)} & m_{22}^{(r)} \end{bmatrix} \\ &= \begin{bmatrix} \cos(\gamma_0 n_r \delta l_r) & -\left(\frac{i}{y_r}\right) \sin(\gamma_0 n_r \delta l_r) \\ -i y_r \sin(\gamma_0 n_r \delta l_r) & \cos(\gamma_0 n_r \delta l_r) \end{bmatrix} \quad \dots \quad (\text{A.20}) \end{aligned}$$

where  $n_r$  and  $y_r$  are respectively the refractive index and normalized wave admittance of the film,  $\delta l_r$  is its thickness, and  $\gamma_0$  is the propagation coefficient of the incident wave in free space.

It is found from eqn. (A.20) that

$$m_{11}^{(r)} = m_{22}^{(r)} \quad \dots \quad (\text{A.21})$$

Since eqn. (A.21) is valid for all the thin films, i.e., for all values of  $(r)$  from (1) to  $(n)$ , it can be shown from eqns. (A.14) and (A.19) that

$$\left. \begin{aligned} m'_{11} &= m_{22} \\ m'_{12} &= m_{12} \\ m'_{21} &= m_{21} \\ m'_{22} &= m_{11} \end{aligned} \right\} \quad \dots \quad (\text{A.22})$$

Considering eqns. (A.10), (A.11) and (A.22), the reflection and transmission coefficients,  $\rho_{21}$  and  $\tau_{21}$ , are given by

$$\begin{aligned}\rho_{21} &= \frac{(m'_{11}y_2 - m'_{22}y_1) + (m'_{12}y_2y_1 - m'_{21})}{(m'_{11}y_2 + m'_{22}y_1) + (m'_{12}y_2y_1 + m'_{21})} \\ &= \frac{-(m_{11}y_1 - m_{22}y_2) + (m_{12}y_1y_2 - m_{21})}{(m_{11}y_1 + m_{22}y_2) + (m_{12}y_1y_2 + m_{21})} \quad \dots \quad (\text{A.23})\end{aligned}$$

$$\begin{aligned}\tau_{21} &= \frac{2y_2}{(m'_{11}y_1 + m'_{22}y_2) + (m'_{12}y_1y_2 + m'_{21})} \\ &= \frac{2y_2}{(m_{11}y_1 + m_{22}y_2) + (m_{12}y_1y_2 + m_{21})} \quad \dots \quad (\text{A.24})\end{aligned}$$

The relation given in eqn. (8) in Sec. IV is obtained from eqns. (A.16) and (A.24).

If the wave admittance is assumed to be real all throughout the media under consideration,  $y_1$  and  $y_2$  are real.  $m_{11}$  and  $m_{22}$  can also be shown to be real while  $m_{12}$  and  $m_{21}$  turn out to be imaginary. Under these conditions eqns. (A.15), (A.16), (A.23) and (A.24) give the relations expressed in eqns. (9), (11) and (12) in Sec. IV. It is also found that

$$\angle \rho_{12} + \angle \rho_{21} = k\pi + 2\angle \tau_{12} \quad (\text{A.25})$$

where  $k$  can be any integer. Since eqn. (A.15) is a general equation, it must be valid for the trivial case when the thickness of the inhomogeneous layer becomes zero; it is then found from Fresnel's formulae that  $k = -1$ . Hence we get the relation in eqn. (10).

#### REFERENCES

- Barlow, H. M. and Cullen, A. L., 1950, *Microwave Measurements*, Constable and Company, p. 242.
- Basu, J., 1960, Ph.D. Thesis, Manchester University, p. 28.
- Born, M. and Wolf, 1959, *Principles of Optics: Electromagnetic Theory of Propagation, Interference and Diffraction of Light*, Pergamon Press, p. 50.
- Francois, G., 1960, *Ionization Phenomena in Gases*, Butterworths Scientific Publications, p. 158.
- Hartree, D. R., 1928-29, *Proc. Camb. Phil. Soc.*, **25**, 97.
- Montgomery, C. G. (ed.), 1947, *Technique of Microwave Measurements*, McGraw-Hill Book Company, Inc., p. 562.
- Nicoll, G. R. and Basu, J., 1962, *Proc. I.E.E.*, **109**, C, 335.
- Ratcliffe, J. A., 1959, *The Magneto-Ionic Theory and its Applications to the Ionosphere*, Cambridge University Press, p. 81.
- Wharton, C. B. and Slager, D. M., 1960, *J. Appl. Phys.*, **31**, 428.

# X-RAY DIFFRACTION STUDY OF CELLULOSE DEGRADATION

W. J. JOHN, B. C. BISWAS and S. S. KRISHNAN

DEFENCE RESEARCH LABORATORY (MATERIALS), KANPUR, INDIA

(Received August 14, 1964)

## Plate IX

**ABSTRACT.** The changes in crystalline and amorphous portions of cotton fibres during deterioration by exposure to sunlight, to ultraviolet light and to fungal attack were studied by X-ray diffraction method. It was found in all these cases there was a small but statistically significant decrease in crystallinity during deterioration. In the case of micro-biological attack the change is not significant at the end of the first month but during the succeeding months the crystallinity significantly decreases showing thereby that the micro-organisms in the later stages attack crystalline portions as well without showing any preference to amorphous regions.

## INTRODUCTION

Considerable literature exists on X-ray investigation of the Crystalline structure of cellulose, their orientation and their change under chemical treatments (Mark *et al.*, 1954). But X-ray studies of the amorphous portion of cellulose are few. Hess (1941) and coworkers showed that crystalline interferences were destroyed by powdering cellulose in a vibrating ball mill giving place to broad amorphous ring similar to those produced by liquids. Hermans and Weidinger (1946) showed that the powder can be recrystallised on heating for a few minutes in the water wet condition and in the X-ray diagram the crystalline interferences reappeared on a diffuse back-ground of lower intensity but having the same shape and location. From the decrease in intensity of the background a quantitative estimate was made of crystallised portion. In 1948 Hermans and Weidinger made a quantitative investigation of the intensity of X-rays scattered by crystalline and amorphous portions in some native and regenerated cellulose fibres and estimated the crystalline and amorphous portions of the fibres. Similar techniques were employed by Kast and Flaschner (1948) and Krimm and Tobolsky (1951).

The present investigation is an attempt to follow the changes in crystalline and amorphous regions in cellulose during degradation by exposure to ultraviolet light, sunshine and microorganisms, by X-ray methods. The technique adopted was given by Hermans and Weidinger (1948).

## EXPERIMENTAL

*Preparation of Samples*

Cotton fabric dosootie (scoured, 7-7.5 oz/sq.yd.) the fabric of Indian Tentage was selected as the basic material since the degradation of this material has been studied extensively in this laboratory by chemical and biochemical methods. Fibres were drawn at random from this material for X-ray investigations. One yard pieces cut from different places on a roll were used as control samples.

Exposure to sunlight was carried out in the exposure yard of these laboratories only during hours of sunshine. 3 yards were exposed at about 4 ft. above ground at an angle of  $45^\circ$  facing South (Kanpur latitude and longitude being  $26^\circ 26'N$   $80^\circ 22'E$ ) and 1 yard pieces were drawn at the end of each month. Each month's exposure corresponds to approximately 100-125 hours of sunshine of intensity approximately 50-60 mw/cm<sup>2</sup>.

Exposure to ultra-violet radiation was carried out with a mercury arc lamp. Samples approximately 20" square were exposed to the radiation from a 'Hanovia' Alpine sun arc lamp at a distance of 30 cms away from the source on a curved surface specially prepared to ensure uniform radiation. In later models this uniformity was ensured by properly curved reflectors. The characteristics of this lamp were determined and the following values of intensities were obtained at 30 cms from the lamp where samples were exposed :

U.V. below	2900 Å = 88 mw/cm <sup>2</sup>
U.V. above	2900 Å = 192 mw/cm <sup>2</sup>
Visible	4000-7000 Å = 199 mw/cm <sup>2</sup>
Total radiation	= 479 mw/cm <sup>2</sup>

The rise in temperature of the samples was minimised by a blast of air from fan. The exposures were done during winter and the humidity was low. The fabric was in contact with air throughout. Samples were exposed for 24, 48, 72 and 96 hours.

A third set of 3 yard samples were exposed in the tropic room of the laboratories which is maintained at  $85 \pm 2^\circ F$  and  $90 \pm 2\% RH$ . One yard samples were drawn at the end of each month. The fungi responsible for the degradation were identified to be mainly *Curvularia*, *Fusarium*, *Alternaria*, *Helminthosporium* and *Penicillium* species. The samples exposed in the tropic room were cleaned by boiling in water for 2-3 minutes followed by repeated rinsing by fresh water.

The fibre samples for the X-ray were prepared as follows. Several threads were taken out at random from the fabric. Approximately 30 mgm of the fibres were separated out of these threads, laid at random on a glass plate and wetted with a 2% solution of gum arabic. This was made into a pellet by pressing in





Fig. 2. X-ray diffraction pattern of samples exposed to fungi for 1, 2 and 3 months.



a mould, an accurately drilled and polished hole in a brass cylinder and dried at 100°C.

### *X-Ray Technique*

The finished pellet was mounted on a specimen holder which can be fitted over a pinhole collimator. The X-ray used is Nickel filtered copper radiation from a tube operating at 33 KV and 18 ma. The diffraction pattern was photographed on a flat camera, the film (10cm x 8 cm) being at a distance of 5 cm from the specimen. The pattern was restricted to one quadrant of the film using lead sectors.

In order to estimate the intensity of the incident beam a Goppel cone of 1.5 cm larger diameter was mounted at the centre of the flat camera and served as a miniature second camera. Over the Goppel cone a Lindemann tube containing finely powdered aluminium stearate was mounted giving rise to a diffraction pattern consisting of Debye Scherrer circles on the small section of the film inside the Goppel cone. The intensity  $I_c$  of the comparison interference peak caused by aluminium stearate will bear a constant ratio to the incident intensity  $I$ . Hence the intensity values due to cellulose interference peaks ( $I_{hkl}$ ) on the film outside the Goppel cone was estimated in comparison to  $I_c$ . All the rings due to cellulose lie well outside the Goppel cone. The patterns were obtained by exposure of 2 hours each.

Similar pellets were prepared from fabrics after degradations and X-ray diffraction patterns were recorded in the other sectors. A typical pattern is recorded in Fig. 2.

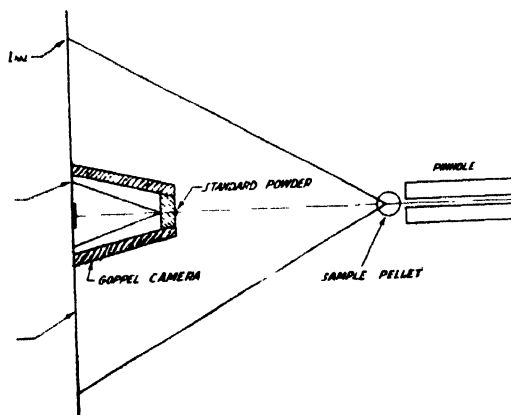


Fig. 1. Set up for X-ray exposures.

The intensities were measured by means of a microphotometer radially and plotted as in Fig. 3. The initial peak is inside the Goppel cone and is due to

aluminium stearate. The peaks outside the Goppel cones are due to cellulose. The boundary line between the crystalline peaks and the general background is traced by following the trend of the initial part of the curve and joining it to the second minimum of the cellulose interference rings by a smooth curve. As the separation between the first two peaks (101) and  $(10\bar{1}+002+021)$  overlap the first minimum lies above the general background.

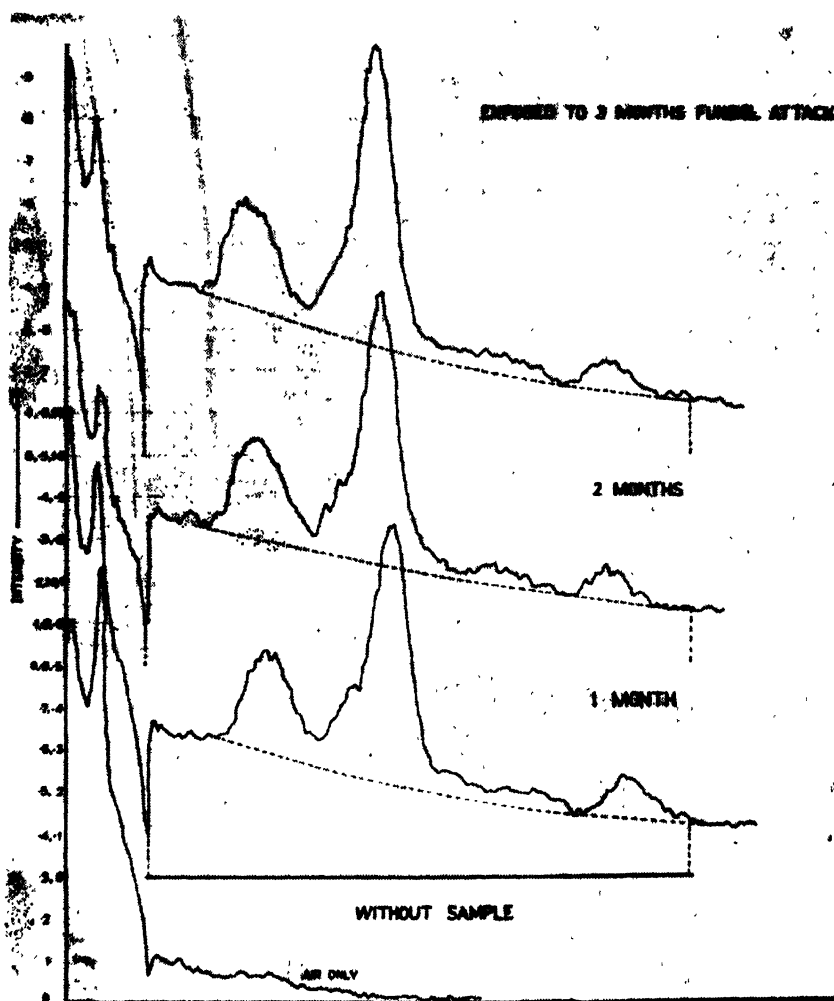


Fig. 3. Microphotometric intensity curves for X-ray diffraction patterns.

The integrated intensities of the crystalline and amorphous regions were calculated from the graph by determining the areas under the observed curve and the smooth line giving the general background. The background is due to : (1) scattering by air ; (2) scattering by amorphous portion of the cellulose ; (3) Compton

and thermal scattering contributed by both crystalline and amorphous portions and (4) errors due to nonmonochromatic nature of the X-rays used.

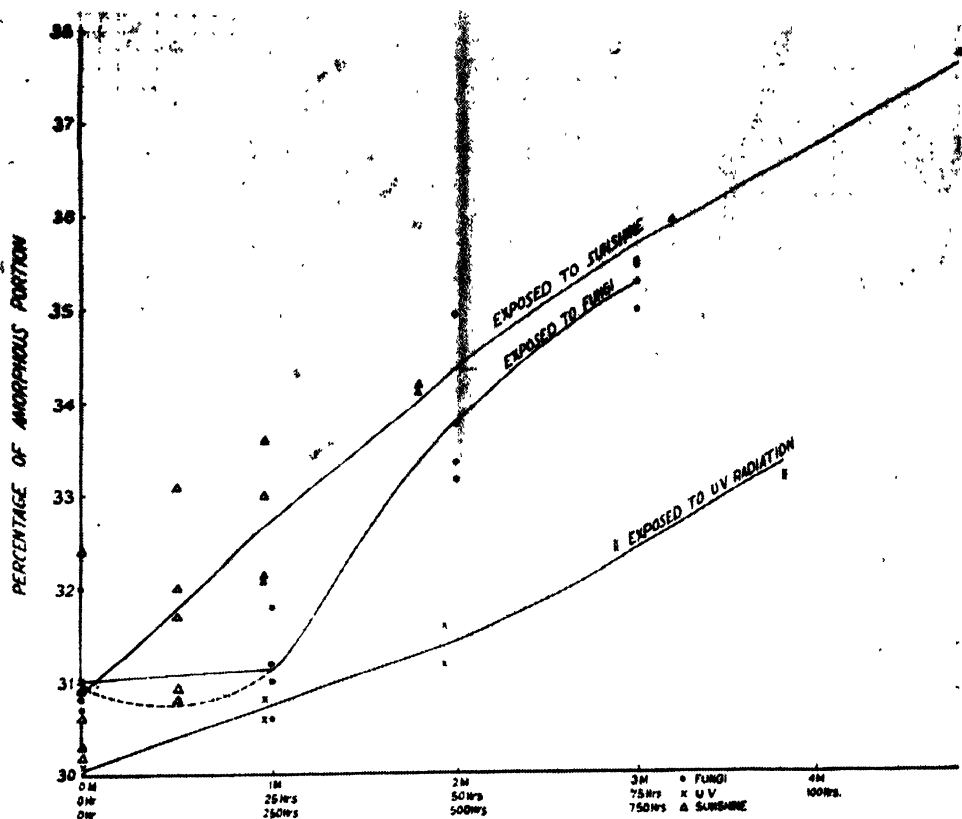


Fig. 4. Graphic representation of results.

As the object of the experiment was only to follow the changes occurring in the amorphous and crystalline portion, the background correction was determined by assuming the value of crystallinity in the first control sample to be 70% after Hermans and Weidinger (1948). The correction thus calculated was applied in subsequent samples. Control samples for exposures were repeated before examining each set of deteriorated samples. The control samples were thus repeated 10 times during the course of 3 years and the mean value of amorphous portion was found to be  $30.8 \pm 1.1\%$  using the same background correction for all as determined above.

## RESULTS

The percentage of amorphous portions of the deteriorated samples are shown in Table below. They are also graphically represented in Fig. 4.

# CORRELATION OF DISSOCIATION ENERGY AND MOLECULAR CONSTANTS OF DIATOMIC MOLECULES

S. P. TANDON and KAMALA TANDON\*

PHYSICS DEPARTMENT, UNIVERSITY OF JODHPUR, JODHPUR, INDIA

(Received April 4, 1964; Resubmitted July 16, 1964)

**ABSTRACT.** A new relation, connecting dissociation energy ( $D_0$ ), force constant of infinitesimal amplitude ( $k_e$ ) and internuclear equilibrium distance ( $r_e$ ) has been deduced from Sutherland's potential function. It is of the form  $D_0 - k_e(A + Br_e + Cr_e^2)$ , where A, B and C are constants and are same for a molecular group of similar diatomic molecules. The applicability of the relation has been shown in the case of about two hundred diatomic molecules forming nineteen molecular groups. Dissociation energy, hitherto unknown, of thirty diatomic molecules has also been predicted.

## INTRODUCTION

During last four decades, numerous potential functions (Rittner, 1951; Varshni, 1957 and 1958a, Varshni *et al*, 1961) and empirical or semiempirical relations connecting (Pauling, 1954; Varshni, 1958b, Somayajulu, 1960) the various molecular constants of diatomic molecules have been suggested.

Molecules having constant type of bonding are known to form a molecular group (Varshni, 1958b) or sequence (Somayajulu, 1960). For such a sequence the force constant for infinitesimal amplitude  $k_e$  is inversely proportional to the equilibrium internuclear distance  $r_e$  (Kratzer, 1920; Glasstone, 1936; Davies, 1949; Heath *et al*, 1950; Smyth, 1956), which in turn is inversely proportional to dissociation energy  $D_0$  (Pauling, 1954). Combination of these relations lead Somayajulu (1960) to calculate the dissociation energy of molecules assuming

$\frac{k_e r_e}{D_0}$  to be constant for a sequence and called it sequence constant  $S$ . Calculations show three main discrepancies: (1) values of  $S$  for different members of a sequence show much variation (Table, XII). (2) The estimated value of  $D_0$  for the first member of the sequence differs much from the observed one in nearly all the cases. (3) The potential functions so far proposed (Varshni, 1957) do not lead to this relation. For example, the Linnett's function (1940, 1942)

$$U = a r^{-m} - b e^{-nr} \quad \dots (1)$$

\*Chemistry Department, University of Jodhpur, India.

leads to the result (Somayajulu, 1960)

$$\frac{k_e r_e}{D_0} = mn \left[ 1 + \frac{1}{(m-n)r_e} \right] \quad \dots (2)$$

We shall deduce new relation connecting the three molecular constants,  $k_e$ ,  $r_e$  and  $D_0$  from the Sutherland's potential function (1940), which is well established (Varshni, 1958).

We shall also use this relation to estimate  $D_0$  values, hitherto unknown, in the case of many diatomic molecules.

#### NEW RELATIONS

A satisfactory potential function of a diatomic molecule satisfies the following conditions (Varshni, 1958a) :

$$U(r_e) - U(\infty) = -D_0 \quad \dots (3)$$

$$\frac{dU}{dr} \Big|_{r=r_e} = 0 \quad \dots (4)$$

and

$$\frac{d^2U}{dr^2} \Big|_{r=r_e} = k_e \quad \dots (5)$$

Applying these conditions on potential function

$$U(r) = \frac{a}{(r-d)^m} - \frac{b}{(r-d)^n} \quad \dots (6)$$

due to Sutherland (1940), we obtain

$$k_e = \frac{am(m-n)}{(r_e-d)^{m+2}} \quad \dots (7)$$

and

$$D_0 = \frac{a}{(r_e-d)^m} - \frac{b}{n} \quad \dots (8)$$

From Equations (7) and (8) we get

$$\frac{D_0}{k_e} = \frac{n}{m} (r_e-d)^2 \quad \dots (9)$$

where  $m$ ,  $n$  and  $d$  have been assumed to be constant for similar molecules. Equation (9) may be expressed in a general form

$$D_0 = k_e(A + Br_e + Cr_e^2) \quad \dots (10)$$

which is the new relation.  $A$ ,  $B$  and  $C$  are constants, which may be expected to be the same for the molecules having similar bonding. The relation (10) has been applied to about two hundred diatomic molecules.

#### DATA AND PROCEDURE

The equilibrium internuclear distance  $r_e$  values are expressed in Å and are taken from the "Tables of Interatomic distances and configuration of molecules and Ions" (The Chemical Society, London, England, 1958) except where indicated. The  $r_e$  values in paranthesis are roughly estimated ones.

The values of force constant for infinitesimal amplitude  $k_e$  expressed in  $md/A$  have been calculated from molecular data given by Herzberg (1950) unless stated otherwise.

The observed values of dissociation energy  $D_0^\circ$ , referred to  $0^\circ K$ , are expressed in electron volts. The values which are followed by  $H$  in paranthesis are taken from Herzberg's molecular data (1950). Similarly,  $G$  in paranthesis refers to data taken from Gaydon's book (1953) and that referred by Herzberg (1950) as Gaydon's data.  $D_0^0$  values in paranthesis are uncertain ones.

The procedure to estimate  $D_0$  values is very simple. Constants  $A$ ,  $B$  and  $C$  for a molecular group are determined using  $D_0^\circ$ ,  $r_e$  and  $k_e$  values for three molecules for which these are known accurately. Having determined  $A$ ,  $B$  and  $C$  mere substitution of  $k_e$  and  $r_e$  values in equation (10) yields  $D_0$  values for other molecules of the group.  $T$  and  $S$  in paranthesis in Tables I to XX, refer to these estimated  $D_0$  values and those estimated by Somayajulu (1960) respectively. 1a, 1b, 2a, ... etc. refer to the groups of the periodic table. 1a-7b refers to the molecular group of diatomic molecules formed by the combination of atoms belonging to 1a and 7b groups of the periodic table. Other symbols have similar meanings.

#### DISCUSSION

Study of the new relation connecting the dissociation energy  $D_0$ , force constant  $k_e$  and equilibrium internuclear distance  $r_e$  reveals that  $r_e$  values must be very accurately known, since higher powers of  $r_e$  appear in equation (10). While accurate  $k_e$  values, except in few cases, where they are estimated by Sheline method (1950) or method of Varshni and Majumdar (1955, 1956) or by any other method, are available for a large number of molecules, accurate  $r_e$  values are available only for few. Many unknown  $r_e$  values have been estimated by methods like Pauling's additivity of atomic radii, Schomaker-Stevenson equation (Gordy, 1946), Sheline method (1950), Varshni's relation (1958b) or Somayajulu's relation (1960). The use of these estimated  $r_e$  values is likely to produce divergence between



observed and estimated  $D_0$  values. In certain cases the observed  $D_0^\circ$  values are themselves uncertain where they are put in parenthesis. Large differences between observed and estimated  $D_0$  values are expected in such cases. It is important to note that often spectroscopic, photochemical, thermochemical and electron impact appearance potential methods yield conflicting  $D_0^\circ$  values. In most of the cases the convergence limit of bands with its adjoining continuum is not obtained. Birge and Spooner (1926) have suggested a method of extrapolation (Herzberg, 1950; Gaydon, 1953) to the convergence limit from the observed bands. In such cases  $D_0$  values estimated by equation (10) may be used to assign most probable  $D_0^\circ$  values. The unknown  $D_0^\circ$  values of thirty diatomic molecules have also been estimated by this relation.

To show the applicability of the new relation,  $D_0$  values estimated using this relation, indicated by (T) and those estimated by Somayajulu, indicated by (S), along with percentage errors in comparison with observed  $D_0^\circ$  values are collected in Tables I to XIX. Values of average errors for different molecular groups are presented in Table XX. Close study of these tables reveals that the new relation yields much better results than Somayajulu's relation, because for twelve out of fifteen molecular groups the percentage error for (T) is less than that for (S). However, the average error for (T) in the case of 1a-H, 1a-7b and 4b-6b molecular groups is only 0.016%, 0.18%, and 1% higher than that for (S) respectively. Average error for molecules for which estimates of  $D_0$  values have been made by new relation as well as by that of Somayajulu, are 1.76% and 2.78% for the former and latter respectively. This further confirms the superiority of the new relation. In the present study the scope of the applicability of the new relation is widened by including fifty more diatomic molecules belonging to 1b-7b, 2a-7b, 2b-7b and 4b-7b groups which have not been studied by Somayajulu.

TABLE I  
Hydrides of 1a group  
 $A = 2.829$ ,  $B = -1.533$ ,  $C = 0.7798$

Molecule	$r_e$	$k_e$	$D_0^\circ$ Observed	(S)		(T)	
				$D_0$ Cal.	Error %	$D_0$ Cal.	Error %
LiH	1.595	1.026	2.429 <sup>a</sup> , (2.5) (H)	2.429	0	2.427	-0.08
NaH	1.887	0.781	2.05 $\pm$ 0.2(G), 2.2(H)	2.187	0	2.140	0
KH	2.244	0.5614	1.86 $\pm$ 0.15(G), 1.86(H)	1.868	0	1.859	0
RbH	2.376	0.5148	1.7 $\pm$ 0.2(G), (1.9)(H)	1.809	0	1.837	0
CsH	2.494	0.467	1.8 $\pm$ 0.3(G), (1.9) (H)	1.728	0	1.800	-4
Average error %				0		0.016	

<sup>a</sup>. Valasee (1957)

TABLE II  
Hydrides of 1b group  
 $A = 4.030$ ,  $B = -4.201$ ,  $C = 1.583$

Molecule	$r_e$		$D_o^\circ$ Observed	(S)		(T)	
				$D_o$ Cal.	Error%	$D_o$ Cal.	Error%
CuH	1.4631	2.2	$2.7 \pm 0.3(\text{G}), < 2.89(\text{H})$	2.77	0	2.797	0
AgH	1.6174	1.817	$2.5(\text{H}), 2.3 \pm 0.1(\text{G})$	2.53	+1.2	2.502	+0.08
AuH	1.5237	3.138	$4.1a, 3.1(\text{H})$	4.12	+0.5	4.10	0
Average error %					0.57		0.03

The upper state is assumed to be  $\tilde{\Sigma}^+$ , then it correlates with normal products and gives  $D'' = 4.1$  ev.

TABLE III  
Hydrides of 2a group  
 $A = 1.071$ ,  $B = -1.002$ ,  $C = 0.6671$

Molecule	$r_e$	$k_e$	$D_o^\circ$ Observed	(S)		(T)	
				$D_o$ Cal.	Error %	$D_o$ cal.	Error %
BeH	1.343	2.263	$2.3 \pm 0.3(\text{G}), 2.2(\text{H})$	2.72	+4.6	2.041	0
MgH	1.731	1.275	$2.0 \pm 0.5(\text{G}), \leq 2.49(\text{H})$	1.97	0	1.704	0
CaH	2.002	0.977	$1.7(\text{G}), \leq 1.70(\text{H})$	1.75	+3.0	1.70	0
SrH	2.1456	0.854	$1.65 \pm 1(\text{G}), \leq 1.68(\text{H})$	1.64	0	1.702	0
BaH	2.232	0.809	$1.8 \pm 0.1(\text{G}), \leq 1.82(\text{H})$	1.61	-5.3	1.745	0
Average error %					2.6		0

TABLE IV  
Hydrides of 3b group  
 $A = -0.1279$ ,  $B = 1.095$ ,  $C = -0.0029$

Molecules	$r_e$	$k_e$	$D_o^\circ$ Obsrvod	(S)		(T)	
				$D_o$ Cal.	Error %	$D_o$ Cal.	Error %
BH	1.233	(2.789) <sup>a</sup>	$3.0 \pm 0.4(\text{G}), < 3.51(\text{H})$	3.8	11.8	3.4	0
AlH	1.646	1.62	$2.9 \pm 0.2(\text{G}), < 3.06(\text{H})$	2.72	0	2.7	0
GaH	1.72 <sup>b</sup>	1.42 <sup>b</sup>	Unknown	2.49	—	2.088	—
InH	1.838	1.28	$2.5 \pm 0.1(\text{G}), \leq 2.48(\text{H})$	2.4	0	2.40	0
TlH	1.87	1.143	$\leq 2.18(\text{H})$	2.18	0	2.18	0
Average errr %					3.0		0

a. Estimated using equation (10).

b.  $k_e$  recalculated by Sheline method (1950).

TABLE V

Hydrides of 4b group

$$A = -1.744, \quad B = 3.020, \quad C = -0.6891$$

Molecule	$r_e$	$k_e$	$D_0^\circ$ Observed	(S)		(T)	
				$D_0$ Cal.	Error %	$D_0$ Cal.	Error %
CH	1.12	4.484	3.47(G)(H)	3.86	+11.2	3.47	0
SiH	1.521 <sup>a</sup>	2.39 <sup>a</sup>	3.19 $\pm$ 0.25 <sup>a</sup>	2.79	-5.1	2.99	0
GeH	(1.66) <sup>b</sup> (1.591) <sup>c</sup>	1.87	unknown	2.28	—	2.56	—
SnH	1.785	(1.469) <sup>d</sup>	2.13 <sup>c</sup> , <3.2(H)	2.06	-3.3	2.13	0
PbH	1.839	1.445	$\leq$ 2.04(H)	2.04	0	2.14	+4.9
Average Error %				4.8		1.2	

a. Douglas (1957) b. Sheline (1950); c. Somayajulu (1960); d. Varshni (1958b); e. Assuming that the predissociation at 3.2 eV occurs into Sn(1D)+H(2S).

TABLE VI

Hydrides of 5b group

$$A = -0.8443, \quad B = 1.503, \quad C = -0.0937$$

Molecule	$r_e$	$k_e$	$D_0^\circ$ Observed	(S)		(T)	
				$D_0$ Cal.	Error %	$D_0$ Cal.	Error %
NH	1.038	6.02	3.7 $\pm$ 0.5(G), 3.8(H)	4.45	+6.0	3.70	0
PH	1.43	3.26	Unknown	3.32	—	3.63	—
AsH	1.58 <sup>a</sup>	2.43 <sup>a</sup>	Unknown	2.61	—	3.15	—
SbH	1.76 <sup>a</sup>	2.05 <sup>a</sup>	Unknown	2.5	—	3.10	—
BiH	1.809	1.708	2.5 $\pm$ 0.3(G), 2.7(H)	2.2	0	2.67	0
Average error %				3.0		0	

a. Sheline (1950)

TABLE VII

Hydrides of 6b group

$$A = 0.5779, \quad B = -0.4614, \quad C = 0.4608$$

Molecule	$r_e$	$k_e$	$D_0^\circ$ Observed	(S)		(T)	
				$D_0$ Cal.	Error %	$D_0$ Cal.	Error %
OH	0.971	7.791	0.393 $\pm$ 0.03 <sup>a</sup>	4.519	+2.6	4.395	0
SH	1.34 <sup>b</sup>	4.193 <sup>c</sup>	4.02 $>$ D <sup>c</sup> $>$ 2.88 <sup>b</sup>	3.59	0	3.300	0
SeH	1.50 <sup>d</sup>	3.18 <sup>a</sup>	Unknown	2.99	—	2.934	—
TeH	1.69 <sup>d</sup>	2.53 <sup>c</sup>	Unknown	2.70	—	2.820	—
PeH	1.77 <sup>d</sup>	2.1 <sup>d</sup>	Unknown	—	—	2.53	—
Average error %				1.3		0	

a. Barrow (1956); b. Ramsay (1952); c. Leach (1954); d. Sheline (1950)

TABLE VIII

Hydrides of 7b group

$$A = -0.8548 \quad B = 2.211, \quad C = -0.6788$$

Molecule	$r_e$	$k_e$	$D_0^\circ$ Observe	(S)		(T)	
				$D_0$ Cal.	Error:	$D_0$ Cal.	Error %
FH	0.9171	9.655	$5.8 \pm 0.1$ , $\leq 6.40$ (H)	5.713	0	5.81	0
TH	1.275	5.157	4.430(H), 4.431(G)	4.242	-4.2	4.43	0
BrH	1.4138	4.116	3.754(H)	3.754	0	3.756	+0.05
IH	1.604	3.141	$3.06 \pm 0.01$ (G), 3.056(H)	3.251	+5.9	2.971	-2.6
AtH	1.68 <sup>a</sup>	2.7 <sup>a</sup>	unknown	--	--	2.539	--
Average error %				2.5		0.66	

a. Recalculated by method of Sheline (1950).

TABLE IX

1a-1a group

$$A = 0.8501, \quad B = 1.200, \quad C = 0.0127$$

Molecule	$r_e$		$D_0^\circ$ Observed	(S)		(T)	
				$D_0$ Cal.	Error %	$D_0$ Cal.	Error %
LiLi	2.672	0.2552	$1.10 \pm 0.05$ (G), 1.03(H)	0.98	-4.9	1.059	0
NaNa	3.078	0.1717	$0.75 \pm 0.03$ (G), 0.73(H)	0.76	0	0.800	+2.6
KK	3.923	0.0985	$0.56 \pm 0.04$ <sup>a</sup> , $0.51 \pm$ $0.05$ (G), 0.514(H)	0.555	0	0.567	0
RbRb	(4.18) <sup>b</sup>	0.082	0.49(H), $0.47 \pm 0.05$ (G)	0.493	0	0.490	0
CsCs	(4.50) <sup>c</sup>	0.06901	0.45(H), $0.45 \pm 0.04$ (G)	0.453	0	0.449	0
KLi	(3.29) <sup>c</sup>	(0.1487) <sup>d</sup>	Unknown	—	—	0.734	—
RbLi	(3.53) <sup>c</sup>	(0.1294) <sup>d</sup>	Unknown	—	—	0.679	—
CsLi	(3.83) <sup>c</sup>	(0.1094) <sup>d</sup>	Unknown	—	—	0.616	—
KNa	(0.1296) <sup>c</sup>	0.1296	$0.62 \pm 0.03$ (G)	0.65	0	0.657	+1.0
CaNa	(3.75) <sup>c</sup>	0.108	Unknown	0.58	—	0.597	—
Average error %				0.8		0.6	

a. Loonis *et al* (1932), b. Guggenheimer (1946), c. Gordy (1946), d. Varshni (1958b).

TABLE X  
5b-5b group  
 $A = -0.4891$ ,  $B = 0.9770$ ,  $C = -0.1317$

Molecule	$r_e$	$k_e$	$D_0^\circ$ Observed	(S)		(T)	
				$D_0$	Cal. Error %	$D_0$	Cal. Error %
NN	1.0976	22.962	9.756(H)	11.0	+21.0	9.753	-0.3
PP	1.8943	5.556	5.03 or 4.12(H)	4.93	-2.0	4.938	+1.8
AsAs	2.08	4.069	$\leq 3.96$ (H)	3.96	0	3.96	0
SbSb	2.48	2.611	$3.0 \pm 0.5$ (G)	3.03	0	2.935	0
BiBi	2.68	1.836	2.2 or 1.7(H)	2.3	+4.5	2.172	+1.3
PN	1.491	10.16	$7.1 \pm 0.05^a$ , (6.3)(H)	7.09	0	6.86	-2.5
AsN	(1.59) <sup>b</sup>	7.926	$5.0 \pm 1.0$ (G)	5.9	0	5.795	0
SbN	(1.79) <sup>b</sup>	6.564	5.5 <sup>c</sup>	5.5	0	5.50	0
SbSb	(2.58) <sup>b</sup>	2.193	$3.0 \pm 2.0$ (G), (3.0)(H)	2.65	0	2.531	0
Average error %				3.05		0.65	

a. Huffman *et al*(1954); b. Somayajulu (1960), c. Assuming the limit of the upper state to correlate with  $Sb(^2D) + (^4S)$ .

TABLE XI  
6b-6b group  
 $A = -1.3191$ ,  $B = 1.943$ ,  $C = 0.4059$

Molecule	$r_e$	$k_e$	$D_0^\circ$ Observed	(S)		(T)	
				$D_0$	Cal. Error%	$D_0$	Cal. Error%
OO	1.2074	11.765	$5.1148 \pm 0.002^a$	6.436	+25.8	5.119	+0.4
SS	1.889	4.959	4.4(H), 4.6(G)	4.243	-3.6	4.474	+1.7
SeSe	2.152	3.612	$\leq 3.55$ (H)	3.52	0	3.548	0
TeTe	2.59	3.368	3.18(H)	2.78	-12.6	3.329	+4.7
SO	1.4933	3.921	5.358 or 4.212 <sup>b</sup>	5.358	0	5.361	+0.06
SeO	(1.62) <sup>c</sup>	6.44	(5.4)(H), $3.5 \pm 1.0$ (G)	4.725	+5.0	4.915	-9.0
TeO	(1.82) <sup>c</sup>	5.304	3.453(H)	4.372	+26.6	4.621	+34.1
Average error %				10.5		7.14	

a. Brix *et al* (1954); b. Norrish *et al* (1959); c. Somayajulu (1960).

TABLE XII

7b-7b group

$$A = -1.240, \quad B = 1.646, \quad C = -0.3241$$

Molecule	S*	$r_e$	$k_e$	$D_0^\circ$ Observed	(S)		(T)	
					$D_0$ Cal.	Error %	$D_0$ Cal.	Error %
FF	1.418	1.418	4.453	$2.17 \pm 0.2a, < 2.75(H)$	2.313	0	2.046	0
ClCl	1.488	1.988	3.286	$2.475(H)(G)$	2.393	-3.3	2.478	+0.1
BrBr	2.284	2.284	2.458	$1.971(H)$	2.056	+4.3	2.041	+3.5
II	2.729	2.667	1.721	$1.5417(H)$	1.681	+9.0	1.457	-5.5
FCI	1.629	1.628	4.483 <sup>b</sup>	$2.616$ or $2.557(H)$	2.719	+4.0	2.60	-0.6
FBr	1.756	1.755	4.095 <sup>c</sup>	$2.60$ or $2.19(H)$	2.637	+1.4	2.668	+2.6
FI	2.050	(2.05) <sup>d</sup>	3.64	$2.87(G)$	2.73	-4.9	2.81	-2.1
BrCl	2.141	2.138	2.717	$2.26(H)$	2.128	-5.8	2.173	3.8
ICI	2.321	2.321	(2.383) <sup>d</sup>	$1.52(H)o$	2.026	-5.8	1.993	-7.4
IBr	2.434	2.434	2.064	$1.817(H)$	1.84	+1.2	2.749	-3.7
Average error %					4.0		2.9	

Sequence constant  $S^* = (r_e k_e / D_0)$ a. Caunt and Barrow (1949), b. Nielsen *et al* (1951), c. Durie (1951), d. Somayajulu (1960)

TABLE XIII

1a-7b group

$$A = -0.3731, \quad B = 1.978, \quad C' = -0.0972$$

Molecule	$r_e$	$k_e$	$D_0^\circ$ Observed	(S)		(T)	
				$D_0$ Cal.	Error %	$D_0$ Cal.	Error %
LiF	(1.59) <sup>a</sup>	(2.36) <sup>b</sup>	$5.95 \pm 0.2(G), \leq 6.6(H)$	5.95	0	5.95	0
LiCl	(1.97) <sup>e</sup>	1.499 <sup>d</sup>	$5.0 \pm 0.3(G)$	4.8	0	4.72	0
LiBr	2.17 <sup>c</sup>	1.248 <sup>d</sup>	$4.35 \pm 0.3(G)$	4.3	0	4.32	0
LiI	2.392 <sup>e</sup>	0.9727 <sup>f</sup>	$3.5 \pm 0.2(G)$	3.69	0	3.70	0
NaF	(2.0) <sup>e</sup>	(1.465) <sup>b</sup>	$4.65 \pm 0.2(G), \leq 5.3(H)$	4.65	0	4.68	0
NaCl	2.3606 <sup>e</sup>	1.1 <sup>d</sup>	$4.24 \pm 0.05(G)$	4.15	-1.0	4.131	-1.4
NaBr	2.502 <sup>e</sup>	0.959 <sup>d</sup>	$3.80 \pm 0.1(G), 3.85(H)$	3.81	0	3.804	0
NaI	2.7115 <sup>e</sup>	0.7631 <sup>d</sup>	$3.07 \pm 0.1(G), 3.16(H)$	3.28	+3.5	3.18	+0.3
KF	2.55 <sup>d</sup>	1.205 <sup>a</sup>	$5.0 \pm 0.25(G)$	5.0	0	4.943	0
		1.24 <sup>a</sup>				5.087	0
KCl	2.667 <sup>e</sup>	1.02 <sup>a</sup>	$4.4 \pm 0.05(G), 4.42(H)$	4.32	-0.7	4.30	-1.1
KBr	2.821 <sup>e</sup>	0.83 <sup>a</sup>	$3.94 \pm 0.05(G), 3.96(H)$	3.72	-4.4	3.68	-5.7
KI	3.048 <sup>e</sup>	0.704 <sup>a</sup>	$3.32 \pm 0.05(G), 3.33(H)$	3.39	+0.6	3.35	0
RbF	(2.31) <sup>e</sup>	1.39 <sup>a</sup>	$5.35 \pm 0.2(G),$	5.1	-1.0	5.113	-0.7
RbCl	2.787 <sup>h</sup>	1.076	$4.50 \pm 0.2(G), > 3.96(H)$	4.76	+1.3	4.718	+0.4
RbBr	2.945 <sup>e</sup>	0.788 <sup>a</sup>	$4.0 \pm 0.25(G)$	3.74	-0.02	3.63	-3.2
RbI	3.177 <sup>e</sup>	0.633 <sup>a</sup>	$3.35 \pm 0.1(G), 3.29(H)$	3.33	0	3.122	-3.9
CsF	2.345 <sup>e</sup>	1.451	$5.5 \pm 0.2(G)$	5.4	0	5.38	0
CsCl	2.906 <sup>e</sup>	0.95 <sup>a</sup>	$4.6 \pm 0.2(G)$	4.38	-0.5	4.4	0
CsBr	3.072 <sup>e</sup>	0.86 <sup>a</sup>	$4.1 \pm 0.25(G), \geq 3.9(H)$	4.19	0	4.12	0
CsI	3.315 <sup>e</sup>	(0.665) <sup>b</sup>	$3.4 \pm 0.1(G), 3.3(H)$	3.5	0	3.40	0
Average error %				0.65		0.83	

a. Barrow *et al* (1953), b. Somayajulu (1960), c. Rittner (1951), d. Rice *et al* (1957), e. Henig *et al* (1954), f. Klemperer *et al* (1957), g. Grabner *et al* (1950), h. Tirschka *et al* (1954).

TABLE XIV

1b-7b group\*

$$A = 6.718, \quad B = -6.125, \quad C' = 1.599$$

Molecule	$r_e$	$k_e$	$D_0^\circ$ Observed	(T)	
				$D_0$ Cal.	Error %
CuF	1.743	3.32	(3.0)(H)	3.0	0
CuCl	(2.24) <sup>a</sup>	2.301	(3.0)(H)	2.4	-25.0
CuBr	(2.42) <sup>a</sup>	2.035	2.7 ± 0.5(G), (2.5)(H)	2.57	0
CuI	2.40 <sup>b</sup> (2.63) <sup>a</sup>	1.738	(3.0)(H), 1.9 ± 0.2(G)	2.14	+2.0
AgF	(1.998) <sup>c</sup>	(2.619) <sup>d</sup>	Unknown	2.91	-3.0
AgCl	(2.42) <sup>a</sup>	1.832	3.1(H)	2.26	—
AgBr	(2.59) <sup>a</sup>	1.637	2.6(H)	2.31	-25.5
AgI	(2.81) <sup>a</sup>	1.453	2.98(H)	2.60	0
AuCl	(2.48) <sup>a</sup>	2.564	3.5(H), 2.8 ± 0.5(G)	3.1	+4.0
				3.50	0
Average error %					6.6

\*  $D_0$  values have not been calculated by Somayajulu (1960)

a. Calculated by Schomaker-Stevenson rule (see Gerdy, 1946)

b. Guggenheimer (1946), C. Varshni (1958b)

d. Varshni *et al* (1955, 1956),

TABLE XV

2a-7b group\*

$$A = -1.5383, \quad B = 1.623, \quad C = -0.0825$$

Molecule	$r_e$	$k_e$	$D_0^\circ$ Observed	(T)	
				$D_0$ Cal.	Error %
BeF	1.361	5.768	4.0 ± 1.0(G)	3.0	0
BeCl	(1.7) <sup>a</sup>	3.025	3.0(G)	3.0	0
BeBr	(2.05) <sup>b</sup>	(2.145) <sup>c</sup>	Unknown	4.09	—
BeI	(2.33) <sup>b</sup>	(2.612) <sup>c</sup>	Unknown	4.69	—
MgF	(1.752) <sup>a</sup>	3.216	3.2 ± 0.7(G)	3.37	0
MgCl	(2.29) <sup>b</sup>	1.815	(3.2)(H)	3.2	0
MgBr	(2.44) <sup>b</sup>	1.514	≤ 3.35(H)	2.92	0
MgI	(2.72) <sup>b</sup>	(1.17) <sup>a</sup>	Unknown	2.65	—
CaF	(2.02) <sup>a</sup>	2.615	3.15(H)	3.67	+16.5
CaCl	1.86	1.504	≤ 2.76(H)	1.79	0
CaBr	(2.70) <sup>b</sup>	1.274	(2.9)(H)	2.9	0
CaI	(2.98) <sup>b</sup>	1.051	(2.8)(H)	2.7	-3.6
SrF	(2.13) <sup>b</sup>	2.30	2.7 ± 1.0(G), (3.5)(H)	3.55	0
SrCl	(2.68) <sup>b</sup>	1.345	(3.0)(H), 2.5 ± 1.0(G)	3.0	0
SrBr	(2.83) <sup>b</sup>	1.146	(2.8)(H)	2.8	0
SrI	(3.11) <sup>b</sup>	0.9231	2.2(H)	2.5	+13.6
BaF	(2.22) <sup>b</sup>	2.161	(3.8)(H)	3.62	-4.7
BaCl	(2.77) <sup>b</sup>	(1.162) <sup>d</sup>	(2.7)(H)	2.7	0
BaBr	(2.92) <sup>b</sup>	1.109	(2.8)(H)	2.8	0
BaI	(3.20) <sup>b</sup>	(0.874) <sup>c</sup>	Unknown	2.44	—
Average error %					2.9

\*  $D_0$  values have not been calculated by Somayajulu (1960).

a. Varshni (1958b),

b. Margrave (1954),

c. estimated by method of Varshni *et al* (1955, 1956)

d. estimated by equation (10).

TABLE XVI

2b-7b group\*

$$A = -0.9328, \quad B = 1.849, \quad C = -0.5073$$

Molecule	$r_e$	$k_e$	$D_0^\circ$ Observed	(T)	
				$D_0$ Cal.	Error %
ZnF	(1.59) <sup>a</sup>	(3.441) <sup>b</sup>	Unknown	2.496	—
ZnCl	(1.945) <sup>b</sup>	2.046	$2.5 \pm 1.0$ (G)	1.523	0
BnBr	(2.136) <sup>b</sup>	(1.661) <sup>c</sup>	Unknown	1.165	—
ZnI	(2.30) <sup>b</sup>	1.25	$1.8 \pm 0.6$ (G)	0.800	-33.3
CdF	(1.723) <sup>b</sup>	(2.74) <sup>b</sup>	Unknown	2.045	—
CdCl	(2.094) <sup>b</sup>	1.716	$2.2 \pm 1.0$ (G)	1.225	0
CdBr	(2.248) <sup>b</sup>	1.455	$2.8 \pm 1.0$ (G)	1.960	0
HgF	(1.74) <sup>a</sup>	2.406	(1.8)(H), $1.4 \pm 0.5$ (G)	1.798	0
HgCl	(2.23) <sup>b</sup>	1.502	1.0(H)	1.000	0
HgBr	2.44 <sup>a</sup>	1.180	0.7(H)	0.7	0
HgI	2.55 <sup>a</sup>	0.7223	$0.30 \pm 0.05$ (G), 0.36(H)	0.35	0
Average error %					4.2

\*  $D_0$  values have not been calculated by Somayajulu (1960),

a. Guggenheimer (1946),

b. Varshni (1958b),

c. estimated by method of Varshni *et al* (1955, 1956)

TABLE XVII

3b-7b group

$$A = -1.0879, \quad B = 2.279, \quad C = -0.4596 \text{ for 7b-B group}$$

$$A = -5.407, \quad B = 6.226, \quad C = -1.204 \text{ for the rest}$$

Molecule	$r_e$	$k_e$	$D_0^\circ$ Observed	(S)		(T)	
				$D_0$ Cal.	Error %	$D_0$ Cal.	Error %
BF	1.262	8.043	$8.5 \pm 0.5$ (G)	8.50	0	8.5	0
BCl	1.716	3.473	$5.1 \pm 0.4$ (G)	5.0	0	5.1	0
BBr	1.887	2.665	$4.2 \pm 0.2$ (G), (4.1)(H)	4.21	0	4.15	0
BI	(2.17) <sup>a</sup>	(1.86) <sup>b</sup>	Unknown	3.3	—	3.24	—
AlF	1.654 <sup>c</sup>	4.191 <sup>d</sup>	$6.7 \pm 0.3$ (G)	6.83	0	6.68	0
AlCl	2.138	2.078	$5.0 \pm 0.2$ (G)	4.38	-8.7	5.0	0
AlBr	2.295	1.692	$4.3 \pm 0.3$ (G)	3.83	-4.2	4.29	0
AlI	2.53 <sup>c</sup>	1.31	$3.7 \pm 0.7$	3.3	0	3.47	0
GaF	1.775 <sup>d</sup>	3.41 <sup>e</sup>	$6.2 \pm 0.03$ <sup>g</sup>	5.96	-3.4	6.32	+1.6
GaCl	2.208 <sup>d</sup>	1.821	$4.99 \pm 0.02$ (G)	3.96	-20.3	4.5	-9.4
GaBr	(2.35) <sup>a</sup>	1.516	$3.5 \pm 0.8$ (G)	3.5	0	3.9	0
GaI	(2.50) <sup>b</sup>	1.233	$2.9 \pm 0.2$ (G), 2.88(H)	3.0	0	3.25	+4.8
InE	1.985 <sup>c</sup>	2.74 <sup>e</sup>	5.41(G)	5.36	-0.9	6.05	+11.8
InCl	2.401 <sup>c</sup>	1.591	$4.5 \pm 0.1$ (G)	3.76	-14.5	4.15	-5.7
InBr	2.541 <sup>c</sup>	1.366	$3.4 \pm 0.2$ (G)	3.42	0	3.60	0
InI	(2.72) <sup>c</sup>	1.114	$2.8 \pm 0.2$ (G)	3.0	0	2.92	0
TlF	(1.93) <sup>a</sup>	2.31	$4.75 \pm 0.2$ (G)	4.74	0	4.91	0
TlCl	2.541 <sup>c</sup>	1.453	<3.19(H)	3.64	+14.1	2.16	0
TlBr	2.68	1.26	$3.2 \pm 1$ (G), 3.19(H)	3.25	0	3.32	+0.6
TlI	2.814	1.038	$2.8 \pm 0.23$ <sup>f</sup> , 2.64(H)	2.88	0	2.68	0
Average error %					3.5		1.8

a. Margrave (1954), b. Varshni (1958b), c. Barrow *et al* (1957), d. Naude *et al* (1955),e. Guggenheimer (1946), f. Brewer *et al* (1950), g. Barrow *et al* (1954), h. estimated by Schomaker-Stevenson rule (see Gerdy, 1956).



TABLE XVIII

4b-7b group\*

$$A = -3.346, \quad B = 3.768, \quad C = -0.6664$$

Molecule	$r_g$	$k_g$	$D_0^\circ$ Observed	(T)	
				$D_0$ Cal.	Error %
CF	1.271 <sup>a</sup>	7.406 <sup>a</sup>	Unknown	2.707	—
CCl	1.73 <sup>b</sup>	3.766	Unknown	4.440	—
CBr	(1.901) <sup>c</sup>	(2.925) <sup>c</sup>	Unknown	5.567	—
CI	(2.175) <sup>c</sup>	(2.175) <sup>c</sup>	Unknown	3.680	—
SiF	(1.603) <sup>c</sup>	4.892	4.8(H)	4.8	0
SiCl	2.00 <sup>b</sup>	2.624	4.0(H)	4.0	0
SiBr	2.15 <sup>b</sup>	2.213	3.7(H)	3.7	0
SiI	(2.459) <sup>c</sup>	(1.658) <sup>c</sup>	Unknown	3.14	—
GeF	(1.670) <sup>c</sup>	3.925	(4.9)(H)	4.3	-10.2
GeCl	(2.08) <sup>b</sup>	2.323	(4.0)(H)	3.74	-6.5
GeBr	(2.29) <sup>b</sup>	1.971	(3.0)(H)	3.5	+16.7
GeI	(2.558) <sup>c</sup>	(1.523) <sup>c</sup>	Unknown	2.94	—
SnF	(1.82) <sup>b</sup>	3.278	3.9(H)	4.28	+9.7
SnCl	2.32 <sup>b</sup>	1.976	3.6(H), 3.2±0.5(G)	3.6	0
SnBr	2.44	1.726	(3.0)(H)	3.247	+8.2
SnI	(2.682) <sup>c</sup>	(1.373) <sup>c</sup>	Unknown	2.7	—
PbF	(2.01) <sup>b</sup>	2.630	≤4.5, 3.47(H)	4.04	0
PbCl	2.43 <sup>b</sup>	1.627	2.6±0.4(G), 3.1(H)	3.05	-1.7
PbBr	2.60 <sup>b</sup>	1.449	2.9(H), 2.2+0.4(G)	2.82	-2.7
PbI	(2.86) <sup>c</sup>	1.194	2.8(H)	2.4	-14.3
Average error %					5.4

\* $D_0$  values have not been calculated by Somayajulu (1960).

a. Rosen (1951),

b. Guggenheimer (1946),

c. Varshni (1958b).

TABLE XIX  
4b-6b group  
 $A = -0.6803$ ,  $B = 1.317$ ,  $B = -0.1742$

Molecule	$r_e$	$k_e$	$D_0^\circ$ Observed	(S)		(T)	
				$D_0$ Cal.	Error %	$D_0$ Cal.	Error %
CO	1.1282	19.02	11.11(G)	11.11	0	11.115	+ 0.04
CS	1.534	8.488	7.9 <sup>a</sup> , 7.2 $\pm$ 1.0(G)	7.90	0	7.907	0
CSe	1.669	6.585	6.8(H)	6.67	-1.9	6.8	0
CTe	(1.949) <sup>b</sup>	4.945 <sup>c</sup>	Unknown	5.85	—	6.066	—
SiO	1.510	9.247	8.0 $\pm$ 1.0(G), 8.9 $\pm$ 0.27 <sup>d</sup>	8.09	0	8.436	0
SiS	1.9288	4.937	6.4 $\pm$ 0.5(G)	5.78	-2.0	5.983	0
SiSe	(2.14) <sup>e</sup>	4.094	5.3 $\pm$ 0.5(G), 5.8(H)	5.32	0	5.490	0
SiTe	(2.34) <sup>e</sup>	3.130	4.5 $\pm$ 0.3(G)	4.44	0	4.521	0
GeO	1.6507	7.525	6.75 $\pm$ 0.28 <sup>d</sup> , 6.9(H)	7.20	-3.1	7.677	+10.0
GeS	(2.06) <sup>e</sup>	4.358	5.66 $\pm$ 0.13(G), 5.6(H)	5.45	-1.4	5.643	0
GeSe	(2.19) <sup>e</sup>	3.743	4.98 $\pm$ 0.25(G)	5.02	0	5.128	0
GeTe	(2.39) <sup>e</sup>	2.902	4.1 $\pm$ 0.4(G)	4.13	0	4.278	0
SnO	1.838	5.615	5.9 <sup>a</sup>	5.98	+1.3	6.474	+ 9.7
SnS	(2.26) <sup>e</sup>	3.536	4.81 $\pm$ 0.28 <sup>f</sup>	4.85	0	4.979	0
SnSe	(2.37) <sup>e</sup>	3.066	5.54 <sup>g</sup> , 4.6(H)	4.45	-2.0	4.5	-0.9
SnTe	(2.57) <sup>e</sup>	2.439	4.1 <sup>g</sup>	3.81	-7.1	3.798	-7.3
PbO	1.922	4.557	(4.3)(H)	5.07	+17.9	5.508	+28.1
PbS	2.395	2.992	4.6 <sup>h</sup> , (4.7)(H)	4.35	-5.4	4.42	-3.9
PbSe	(2.53) <sup>e</sup>	2.595	3.5 $\pm$ 1.0(G), 4.27 <sup>h</sup>	3.98	0	3.992	0
PbTe	(2.73) <sup>e</sup>	2.086	3.5(H)	3.46	-1.1	3.378	-3.5
Average error				2.3		3.3	

a. Thermochemical values, b. Varshni (1958b), c. Rosen (1951), d. Barrow *et al* (1954), e. Guggenheimer (1946), f. Barrow *et al* (1953), g. Vago *et al* (1946), h. Vago *et al* (1948).

TABLE XX  
Average percentage errors

Molecular Group	(S)	(T)
1a-H	0	0.016
1b-H	0.57	0.03
2a-H	2.6	0
3b-H	3.0	0
4b-H	4.9	1.2
5b-H	3.0	0
6b-H	1.3	0
7b-H	2.5	0.66
1a-1a	0.8	0.6
5b-5b	3.05	0.65
6b-6b	10.5	7.14
7b-7b	4.0	2.9
1a-7b	0.65	0.83
1b-7b	—	6.6
2a-7b	—	2.9
2b-7b	—	4.2
3b-7b	3.5	1.8
4b-7b	—	5.4
4b-6b	2.3	3.3

## ACKNOWLEDGMENT

We wish to express our indebtedness to Dr. A. Mookherji, D.Sc., Professor of Physics, University of Burdwan and Dr. R. C. Kapoor, D. Phil., D. Sc., Professor of Chemistry, University of Jadhpur for helpful suggestions. Thanks are also due to Dr. G. P. Srivastava, Dr. G. V. Bakore, Dr. G. L. Gupta and Dr. M. N. Avasthi for reading the manuscript critically. Finally we wish to express heartfelt thanks to Mr. B. N. Jha, Vice-Chancellor, University of Jodhpur, for help and encouragement.

## REFERENCES

- Barrow, R. F., Drummond, G. and Rowlinson, H. C., 1953, *Proc. Phys. Soc.*, London, **A66**, 885.  
 Barrow, R. F. and Caunt, A. D., 1953, *Proc. Roy. Soc.*, London, **A219**, 120.  
 Barrow, R. F. and Rowlinson, H. C., 1954, *Proc. Roy. Soc.*, London, **A224**, 374.  
 Barrow, R. F., 1956, *Arkiv Fysik*, **11**, 281.  
 Barrow, R. F., Dodsworth, P. G., and Zeeman, P. B., 1957, *Proc. Phys. Soc.*, London, **A 70**, 34.  
 Birge, R. T. and Sponer, H., 1926, *Phys. Rev.*, **28**, 259.  
 Brewer, L., 1959, *J. Chem. Phys.*, **31**, 1143.  
 Brix, P. and Herzberg, G., 1954, *Can. J. Phys.*, **32**, 110.  
 Caunt, A. D. and Barrow, R. F., 1949, *Nature*, **164**, 753.

- Cottrell, T. L., 1958, *The Strengths of the Chemical bonds*, 2nd. ed. (Butterworths Scientific Publications Ltd., London)
- Davies, M., 1949, *J. Chem. Phys.*, **17**, 374.
- Douglas, A. E., 1957, *Can. J. Phys.*, **35**, 71.
- Durie, R. A., 1951, *Proc. Roy. Soc., London*, **A207**, 388.
- Gaydon, A. G., 1953, *Dissociation Energies*, (Chapman and Hall Ltd., London).
- Glasstone, S., 1936, *Recent Advances in Physical Chemistry*, 3rd. ed. (P. Blakiston's Son and Co. Inc., Philadelphia).
- Gordy, W., 1946, *J. Chem. Phys.*, **14**, 305
- Guggenheimer, K. M., 1946, *Proc. Phys. Soc.*, London, **58**, 456
- Grabner, L. and Hughes, V., 1950, *Phys. Rev.*, **79**, 819
- Health, D. F., Linnett, J. W., and Wheatley, P. J., 1950, *Trans. Faraday Soc.*, **46**, 137
- Herzberg, G., 1950, *Molecular Spectra and Molecular Structure I. Spectra of Diatomic Molecules*, 2nd ed (D. Van Nostrand Company, New York)
- Honig, A., Mandol, M., Stich, M. L., and Townes, C. H., 1954, *Phys. Rev.*, **96**, 629
- Huffman, E. O., 1954, *J. Am. Chem. Soc.*, **76**, 6239
- Klemperer, W. and Rice, S. A., 1957, *J. Chem. Phys.*, **26**, 618
- Kratzer, A., 1920, *Z. Physik*, **3**, 289
- Leach, S., 1954, *J. Chem. Phys.*, **22**, 1261
- Linnett, J. W., 1940, *Trans. Faraday Soc.*, **36**, 1123
- Linnett, J. W., 1942, *Trans. Faraday Soc.*, **38**, 1
- Loomis, F. W. and Nausbaum, R. E., 1932, *Phys. Rev.*, **39**, 89.
- Margrave, J. L., 1954, *J. Phys. Chem.*, **58**, 258.
- Naude, S. M., and Hulse, T. J., 1955, *Can. J. Phys.*, **33**, 573
- Nielsen, A. H., and Jones, E. A., 1951, *J. Chem. Phys.*, **19**, 1117.
- Norrish, R. G. W. and Oldershaw, G. A., 1959, *Proc. Roy. Soc.*, London, **A249**, 498
- Pauling, L., 1954, *J. Phys. Chem.*, **58**, 662.
- Ramsay, D. A., 1952, *J. Chem. Phys.*, **20**, 1920.
- Rice, S. A. and Klemperer, W., 1957, *J. Chem. Phys.*, **27**, 643.
- Rittner, E. S., 1951, *J. Chem. Phys.*, **19**, 1030.
- Rosen, B., 1951, *Donnees spectroscopiques Concernant les Molecules Diatomiques* (Hermann and Cie Depositaires, Paris.).
- Sheline, R. K., 1950, *J. Chem. Phys.*, **18**, 927.
- Smyth, R. P., 1956, *J. Phys. Chem.*, **60**, 1293.
- Somayajulu, G. R., 1960, *J. Chem. Phys.*, **33**, 1541.
- Sutherland, G. B. B. M., 1940, *J. Chem. Phys.*, **8**, 161.
- Trischka, J. W. and Braunstein, B., 1954, *Phys. Rev.*, **96**, 968.
- Vago, E. E., and Barrow, R. F., 1946, *Proc. Phys. Soc.*, London, **58**, 538.
- Vago, E. E. and Barrow, R. F., 1948, *Victor Henri Commemorative Volume* (Maison Desoeur, Liege, Belgium).
- Valasco, R., 1957, *Can. J. Phys.*, **35**, 1204.
- Varshni, Y. P., and Majumdar, K., 1955, *Indian J. Phys.*, **29**, 38, 285.
- Varshni, Y. P., and Majumdar, K., 1956, *Indian J. Phys.*, **30**, 303.
- Varshni, Y. P., 1957, *Revs. Mod. Phys.*, **29**, 664.
- Varshni, Y. P., 1958, *J. Chem. Phys.*, **28**, a. 1078, b. 1081.
- Varshni, Y. P. and Shukla, R. C., 1961, *J. Chem. Phys.*, **35**, 582.

# LOW ANGLE X-RAY MEASUREMENTS ON DENSELY PACKED COLLOIDAL SYSTEMS—WOOL

T. RATHO

REGIONAL ENGINEERING COLLEGE, ROURKELA

(Received May 18, 1964; Resubmitted July 17, 1964)

**ABSTRACT.** Low angle x-ray methods have been applied to determine the size of the scattering inhomogeneities in wool assuming it to belong to the densely packed colloidal system after Guinier methods of evaluation. The absence of particle scattering in such systems is made clear.

## INTRODUCTION

By using the low angle scattering camera of Kratky it has been possible to determine the size of the large sized particles. The difference between particle scattering as in the case of dilute colloidal systems and scattering by matter in densely packed colloidal systems as considered by Porod (1951) and Kratky (1952) becomes clear. It has been possible to determine the thickness of the layers assuming wool to be distributed in layers with free spaces in between.

## EXPERIMENT

A sample of wool of the type Greany Lincoln Ewes from England was the substance investigated. In order to remove any amount of impurity and fats the sample was washed with soap, cleaned in a stream of distilled water, cooked with 1:3 mixture of aether and alcohol for 25 hours, in cyclohexane for 8 hours and finally in benzene for 8 hours to attain high degree of purity. Cooking the sample for longer periods produced no effect on the x-ray diagram, as by the above process most of the fats were removed and the substance arranged itself in layers with free spaces in between. It was then stretched to avoid any curling, its density determined and an amount with a definite cross-section was introduced into a Mark capillary, the scattering due to the empty capillary container having been determined previously. The sample had the following constants :-

Length      35 mm.

Weight      31 mg.

Density     0.32gm/c.c.

Thickness   1.88 mm. (This was also the internal diameter of the Mark capillary.)

Exposures were taken with the empty capillaries, exposure time in each case being  $2/3$  of that for the corresponding sample. This is due to the difference in absorption between the container glass and the sample, the latter being a strong absorber exposure times were less therefore for empty containers. The capillary containing the sample was so placed that the length of the primary beam was parallel to the fibre axis. Therefore the diffraction pattern should correspond to the equator representation of the fibre diagram of "O" Kratky (1955) or Polanyi (1921).

The apparatus used is the well known small angle scattering camera of Kratky (1958) fitted with a photographic arrangement. As it is desired to photograph the scattered intensity from very small angles up to high angular values, in the small angle region, it is not possible to obtain the complete picture in a single photograph. When the time of exposure is large, the scattered intensity as registered by the photographic film at very small angles is so strong that it cannot be measured by densitometer. For too short exposures, intensity corresponding to larger angles being very weak, cannot be registered by a photographic film at all. Therefore it was decided to photograph the whole region in parts by keeping the primary beam shutter of the apparatus at various heights following the procedure of Kratky outlined in this paper. A series of photographs were obtained with different times of exposure by adjusting the primary beam shutter at different heights. The highest of the primary beam shutter and the corresponding exposure timings are given below.

Height of the primary beam shutter in 1/100 mm.	Exposure time in minutes
185	12
195	24
207	48
221	96
238	192
260	384

The time of exposure varied from 12 mins. to 384 mins., thus photographing a range corresponding to Bragg values of  $800\text{ \AA}$  to  $50\text{ \AA}$  for  $\lambda = 1.54\text{ \AA}$  in stages. After this the corresponding densitometer curves were obtained under identical conditions. Each partial curve represents a particular angular range of diffraction. They are plotted in parts in Fig. I. After this the total curve can be obtained by multiplying the partial curve intensities with their respective time factors. The experimental measurements and their relative transformations are given in Table I. A Siemens apparatus fitted with a copper target was

employed in the present investigation. The balanced filter method due to Kratky (1943) was utilized to obtain the above partial intensity curves due to  $\text{CuK}\alpha$  radiation. The entrance slit of the low angle camera was 0.11 mm. and the film sample distance was 135 mm.

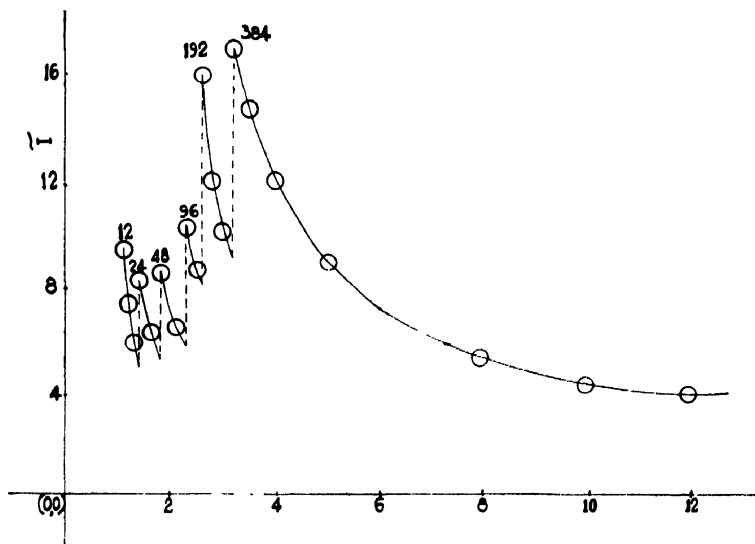


Fig. 1.  $ap = 13.5 \times 25.4$

#### DISCUSSION AND THEORY

As wool is an oriented substance one can proceed with the smeared-out curve and no slit correction is necessary. Moreover due to a very large difference in the scattered intensity of the innermost and the outermost portions of the curve, it is only convenient to plot  $\log \widetilde{I}$  versus  $m$  to know the exact nature of the scattering curve (Fig. 2). Here  $\widetilde{I}$  is the smeared-out intensity and  $m$  is the

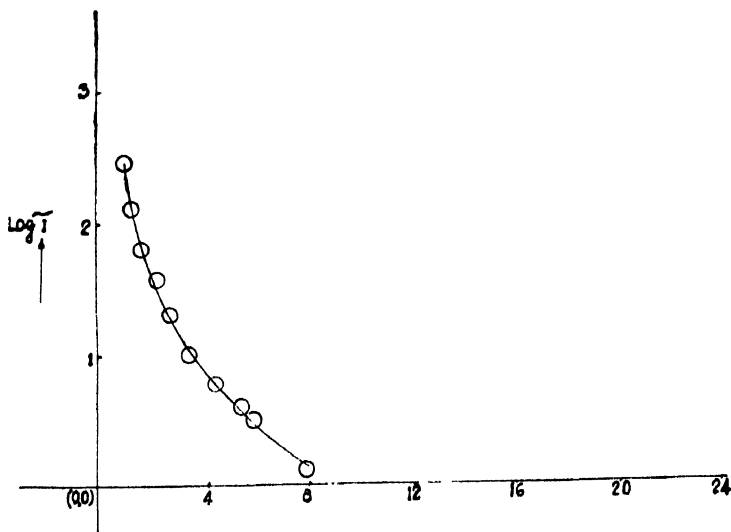


Fig. 2.  $\rightarrow m ap = 13.5 \times 25.4$

distance from the centre of the primary beam measured along the densitometer curve and is therefore a function of the scattering angle  $2\theta$ . The double logarithmic plot  $\log \widetilde{I}$  versus  $\log m$  is a straight line of slope  $-2.86$  (Fig. 3).

According to Porod (1953) the tail portion of the smeared-out scattering curve of a general two phase system decreases like  $k/m^3$  where  $k$  is a measure of the interface of the two phases. As usual  $m$  is given by

$$2\theta = m/ap$$

where  $2\theta$  is the angle of scattering, “ $a$ ”, the film sample distance and “ $p$ ” is the transformation factor. The intensity  $I$  can therefore be expressed as

$$\widetilde{I} = K/m^3$$

$$\therefore \log \widetilde{I} = \log (k/m^3)$$

$$\therefore \log \widetilde{I} = \log k - 3 \log m$$

$$\therefore \frac{d \log \widetilde{I}}{d \log m} \dots 3, \text{ since } \log k \text{ is a constant.}$$

As  $\tan \alpha$ , the slope of the straight line in the double logarithmic plot is about  $-3$ , (Fig. 3), this exactly represents the tail portion of such a smeared-out curve for accessible scattering angles. It is not possible therefore to determine the size of the scattering inhomogeneities as a whole. We can estimate that it must only be larger than the largest measurable Bragg-value of about

$$D = \frac{\lambda}{1} \quad ap \text{ \AA}$$

i.e.  $D = 1.54 \times 13.5 \times 25.4 = 520 \text{ \AA}$ ; for  $\lambda = 1.54 \text{ \AA}$ ,  $a = 13.5$  and  $P = 25.4$ .

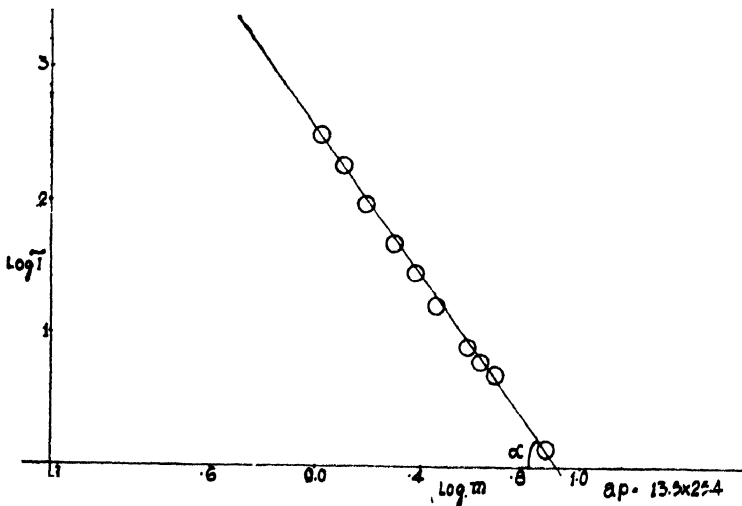


Fig. 3.  $\tan \alpha = -2.86$



Assuming micelles of variable thickness as model for the scattering system (Kratky and Porod, 1949), we can hope to obtain the mean thickness from the Guinier plot  $\log \tilde{I}m^2$  versus  $m^2$ . From such a curve one can easily get, on drawing two asymptotic tangents at the two extremities, two values of the thickness factor of about 60 Å and 125 Å respectively.

TABLE I  
Measurements on wool, filter difference method

1 <i>m</i>	2 <i>I</i>	3 <i>F</i>	4 $\frac{\tilde{I}}{I \times F}$
1.1	9.3		293.6
1.2	7.3	32	229.6
1.3	5.8		181.6
1.4	8.1		125.6
1.6	6.1	16	93.6
1.8	8.4		63.2
2.1	6.35	8	46.8
2.3	10.2		36.8
2.5	8.5	4	30.0
2.6	16.0		28.0
2.8	12.0		20.0
3.0	10.0	2	16.0
3.2	13.0		13.0
3.5	10.7		10.7
4.0	8.0		8.0
4.5	6.2	1	6.2

*I*—Intensity not corrected for time factor.

*F*—Time factor.

$\tilde{I}$ —Smeared-out intensity

×—Corrected for the background intensity.

A thorough theoretical handling of the problem of low angle scattering is due to Porod (1949) which applies to fully oriented systems like regenerated cellulose. The scattering of such a system treated after Babinet's reciprocal relation, after certain assumptions, leads to a scattering function  $\phi_2$  resulting out of interparticle interference. This effect is very important where the distance between neighbouring particles is much smaller than the dimensions of the particles themselves. The function  $\phi_2$  increases rapidly to very high values as the

scattering angle  $2\theta$  approaches zero. When  $2\theta = 0$  this intensity becomes infinite. That is why in the case of wool, irregular system not highly oriented, the scattering curve, (Fig. 2), is very steep and runs almost parallel to the  $Y$  axis for very small values of  $2\theta$ . In this case the particle scattering is practically absent due to the irregularity of the free space and the occupied space. While interparticular effects are predominant. The scattered intensity speaks about the spread or extension of the micelle system.

### CONCLUSION

The size of the scattering inhomogeneities in wool are larger than  $520 \text{ \AA}$ . Interparticular interference is predominant in the system.

### REFERENCES

- Kratky, O., 1942, *Naturwiss*, **30**, 542.  
" (1955), *Physik der Hochpolymeren*, **3**, 288.  
Kratky, O. and Scala, Z., 1958, *Z. Elektrochemie*, **62**(1), 66.  
Kratky, O. and Porod, G., 1949, *J. Colloid Sci.*, **4**, 36.  
Kratky, O. and Sekora, A., 1943, *Naturwissenschaften*, **31**, 46.  
Polanyi, M., 1921, *Z. Physik*, **7**, 149.  
Porod, G., 1951, *Kolloid, Z.*, **124**(2), 83.  
Porod, G., 1953, *Kolloid-Z.*, **133**, 16.  
Porod, G., 1949, *Acta Physica Aust.*, **3**(1), 66.

# Letters to the Editor

The Board of Editors does not hold itself responsible for opinions expressed in the letters published in this section. The notes containing short reports of original investigations communicated to this section should not contain many figures and should not exceed 500 words in length. The contributions reaching the Secretary by the 15th of any month may be expected to appear in the issue for the next month. No proof will be sent to the author.

20

## A PRELIMINARY NOTES ON MAGNETIC SUSCEPTIBILITY AND ANISOTROPY IN TETRAHEDRALLY CO-ORDINATED $\text{Co}^{++}$ ION †

S. KUMAR\*, S. MITRA and R. RAI

MAGNETISM DEPARTMENT, INDIAN ASSOCIATION FOR THE CULTIVATION  
OF SCIENCE, JADAVPUR, CALCUTTA-32

(Received August 14, 1964)

The double chlorides  $\text{CoCs}_2\text{Cl}_4$  and  $\text{CoCs}_3\text{Cl}_5$  both have a slightly distorted tetrahedron of four  $\text{Cl}^-$  ions with the  $\text{Co}^{2+}$  at the centre. The  $\text{Co}^{2+}$  may be considered to be under a predominantly cubic ligand field of the type  $T_d$ , which splits the  $3d^7\ ^4F$  ground state of  $\text{Co}^{++}$  into an orbital singlet  $^4A_2$  and two triplets  $^4T_2$  and  $^4T_1$  each with fourfold degeneracy due to spin so long as the small distortion is neglected. The  $^4A_2$  level lies lowest with  $^4T_2$  and  $^4T_1$  successively at energies  $3500\text{ cm}^{-1}$  and  $6300\text{ cm}^{-1}$  above it (Cotton *et al.* 1961). Spin-orbit coupling has non-vanishing matrix elements between  $^4T_2$  and  $^4A_2$  and in the presence of the small tetragonal field, caused by the abovementioned distortion taking place along a line joining the opposite edges of the tetrahedron (Powell and Wells, 1935), splits up the  $^4A_2$  level into two Kramer's doublets with separation of the order of  $9\text{ cm}^{-1}$ . (Bowers and Owen, 1955). No mixing of  $^4T_1(F)$  and  $^4T_1(P)$  levels with  $^4A_2$  comes directly except in a very high order through  $^4T_2$ , which can therefore be neglected.

Calculation upto second order of magnetic perturbation  $\beta H(L + 2S)$  yields the expression for principal magnetic susceptibility  $K_i$  ( $i = \parallel$  or  $\perp$  to the tetragonal axis of the ion) which explains well (Table I) the magnetic measurements of mean susceptibility and anisotropy in the range  $300^\circ\text{K}$  to  $90^\circ\text{K}$  by one of us (S.M.) on  $\text{CoCs}_3\text{Cl}_5$ . It is seen that the spin-orbit coupling parameters parallel

---

† A part of the work has been submitted for both reading and publication to the International Conference on magnetism—1964 Nottingham (U.K.) communicated on 8-2-64.

\*Present address—The Patent Office, Calcutta-17.

and perpendicular to the tetragonal axis of the ion ( $\zeta_{\parallel}$  and  $\zeta_{\perp}$ ) are reduced to  $-140 \text{ cm}^{-1}$  and  $-120 \text{ cm}^{-1}$  respectively, from the free ion value of  $-180 \text{ cm}^{-1}$  (Laporte, 1928). The corresponding values of orbital reduction factors are  $\kappa_{\parallel} = 0.92$  and  $\kappa_{\perp} = 0.98$ . The cubic field coefficient  $Dq$  is  $350 \text{ cm}^{-1}$ ;  $\Delta$ , the tetragonal field separation of the excited  ${}^4T_2$  level varies from  $322 \text{ cm}^{-1}$  at  $90^\circ\text{K}$  to  $980 \text{ cm}^{-1}$  at  $300^\circ\text{K}$ .

The values of the parameters taken here are consistent with the paramagnetic resonance measurements (Bowers and Owen, 1953) and spectroscopic fine structure results (Cotton *et al.*, 1961).

The anisotropic reduction in  $\zeta$  is (1) due to an anisotropic overlap of the surrounding ligands  $s$ - and  $p$ -charge clouds with the central  $d$ -charge clouds (Bose *et al.*, 1960) and also (2) due to the  $3d$ - $4p$  configurational interaction arising from the non-centrosymmetry of the complex (Bose *et al.*, 1964). The increase in  $\Delta$  from  $322 \text{ cm}^{-1}$  at  $90^\circ\text{K}$  to  $980 \text{ cm}^{-1}$  at  $300^\circ\text{K}$  is due to the thermal expansion or relaxation effects of the lattice. Details of the experimental and theoretical results will be published shortly along with those on  $\text{CoCs}_2\text{Cl}_4$  which have also been completed by us.

TABLE

$$Dq = 350 \text{ cm}^{-1} \quad \zeta = -140 \text{ cm}^{-1} \quad \zeta_{\perp} = 120 \text{ cm}^{-1}, \quad \kappa_{\parallel} = 0.92, \kappa_{\perp} = 0.98$$

Temp $^\circ\text{K}$	$\text{cm}^{-1}$	$p_1^2$	$(p_1^3 - p_1^2)$	$g$ values	zero field splitting $\text{cm}^{-1}$
300 $^\circ\text{K}$	980	21.84 (21.81)	1.55 (1.56)		
200 $^\circ$	630	21.16 (21.26)	1.73 (1.72)		
90 $^\circ\text{K}$	322	19.96 (20.00)	2.34 (2.34)	$g = 2.30$ $(2.32 \pm .04)$ $g_1 = 2.28$ $(2.27 \pm .04)$	8.5 (9.0)

Values in parantheses are the experimental values.

## ACKNOWLEDGMENT

The authors are grateful to Prof. A. Bose for his guidance and suggestions, and also to Mr. S. Ray for helpful discussions. One of us (S.K.) is grateful to the Controller-General of Patents, Designs & Trade Marks for permitting him to do part-time research work and to The Director of the Indian Association for the Cultivation of Science for providing laboratory facilities.

## REFERENCES

- Bowers, K. D. and Owen, J., *Rep. Progr. Phys.*, **18**, 304.  
 Bose, A., Chakravarty, A. S. and Chattrji, R., 1960, *Proc. Roy. Soc.*, **A255**, 145.  
 Bose, A., Rai, R. and Mitra, S., 1964, *Proc. Phys. Soc.*, (communicated)  
 Cotton, F. A., Goodgame, D. M. L. and Goodgame M., 1961, *J. Amer. Chem. Soc.*, **83**, 4690.  
 Laporte, O., 1928, *Z. f. Krist.*, **47**, 761.  
 Powel, H. and Wells A. P., 1935, *J. Chem. Soc.*, 359.

# A NOTE ON THE HYDROGEN BONDING IN ISOMERIC AMINOPYRIDINES IN RELATION TO THEIR BASICITIES

K. C. MEDHI and G. S. KASTHA

OPTICS DEPARTMENT, INDIAN ASSOCIATION FOR THE CULTIVATION OF SCIENCE,  
CALCUTTA-32

(Received August 3, 1964)

**ABSTRACT.** The infrared absorption spectra due to fundamental N-H stretching vibrations of 2-, 3- and 4-aminopyridines in different environments have been studied and the frequencies of the symmetric and asymmetric N-H stretching vibrations of these compounds in very dilute solutions in  $\text{CCl}_4$  have been compared with those of aniline in solution in the same solvent. It has been observed that the total solvent shifts in the N-H stretching vibrational frequencies of any of the aminopyridines in solutions in different solvents are linearly related to those of aniline in solutions in the corresponding solvents. The significance of the observed linearity and of the slopes of the straight line graphs in relation to the hydrogen bonding capacity and the basicities of the molecules of the aminopyridines has been discussed.

## INTRODUCTION

From a study of the infrared absorption bands due to N-H stretching vibrations of aniline and some substituted anilines, it has been shown (Medhi and Kastha, 1963) that the ratios of the total solvent shifts, due to hydrogen bonding, in the frequencies of symmetric and asymmetric stretching vibrations of the N-H bonds in the  $\text{NH}_2$  group in the molecule of any of these compounds in solutions in different solvents to those of aniline in solutions in the corresponding solvents are almost constant which is independent of the nature of the solvents. It was also shown that the constant values of these ratios, which are respectively greater or less than unity for compounds with electronegative or electropositive substituents, bear an almost linear relationship with the  $pK_a$ -values of the various phenyl amines and that they may be regarded as a measure of the proton donating power of these compounds with respect to aniline. In a subsequent paper (Kastha and Medhi, 1963) it was pointed out that in the series of phenyl amines investigated, under certain assumptions, the value of this constant for a particular compound is approximately equal to the ratio of the total charge on the nitrogen atom of the  $\text{NH}_2$  group in aniline molecule to that on the N-atom in a molecule of the compound.

All these considerations apply to the case of aniline and its derivatives where the basic character of any of these compounds is due to the N-atom of the  $\text{NH}_2$  group external to the benzene nucleus of its molecule. In order to see how far the conclusions mentioned in the previous paragraph are valid when the benzene

ring in the molecule of an amino-compound contains a nuclear N-atom in addition to the external  $\text{NH}_2$  group the infrared absorption bands due to fundamental N-H stretching vibrations of the three isomeric aminopyridines in different states and also in dilute solutions in a large number of polar and non-polar solvents have been investigated. The results obtained have been discussed in the following paragraphs.

#### EXPERIMENTAL

The samples of 2-, 3- and 4-aminopyridines were supplied by Light and Company of England, and these were purified by repeated fractionation under reduced pressure. The sample of aniline used was of E. Merck's G. R. quality. The solvents were of chemically pure quality which were purified and dried by standard methods.

The infrared absorption spectra of all the compounds in the region of fundamental N-H stretching vibrations in different states and in very dilute solutions in the various solvents were recorded on a Perkin-Elmer Model 21 spectrophotometer with NaCl optics. The standard atmospheric water vapour band at  $3740\text{ cm}^{-1}$  and the bands due to N-H stretching vibrations of aniline in very dilute solution in  $\text{CCl}_4$  were used to check the calibration of the instrument from time to time.

#### RESULTS AND DISCUSSION

The frequencies of the absorption bands due to symmetric ( $\nu_s$ ) and asymmetric ( $\nu_a$ ) N-H stretching vibrations in the pure aminopyridines and also in their solutions in different solvents are given in Table I in which are also included for comparison the N-H stretching vibrational frequencies of aniline in solutions in the same solvents. These frequencies of aniline in solutions in carbon disulphide, benzene, acetonitrile, nitromethane and dioxane have been recorded in the present investigation, while the remaining ones are taken from data reported earlier (Medhi and Kastha, 1963). The total solvent shifts ( $\Delta\nu_t = \Delta\nu_s + \Delta\nu_a$ ) in the N-H stretching vibrational frequencies of the isomeric aminopyridines and aniline in different environments have been tabulated in Table II. The  $pK_a$ -value of aniline taken from Whetsel's paper (1961) and those of the aminopyridines determined experimentally by Albert *et al.* (1948) are included in both Tables I and II.

It is seen from Table I that the symmetric and asymmetric N-H stretching vibrational frequencies of 2-aminopyridine in solution in  $\text{CCl}_4$  are almost identical with those of 4-aminopyridine in solution in the same solvent, while these frequencies of 3-aminopyridine in  $\text{CCl}_4$  solution are smaller than those of either of the two compounds. Both the frequencies of 2- and 4-aminopyridines in  $\text{CCl}_4$  solution are much higher than those of aniline in solution in the same solvent, but in the case of solution of 3-aminopyridine in  $\text{CCl}_4$ , these frequencies, though slightly higher, are very nearly the same as those of aniline. The higher values of these frequencies in the aminopyridines are to be expected, because the nuclear N-atom in the molecule of any of these compounds is more electron attracting than a corres-

ponding C—H group in the molecule of aniline. The consequent larger migration of charge from the NH<sub>2</sub> group to the ring would enhance the stretching vibrational frequencies of the N—H bonds.

The almost equality in the frequencies of N—H stretching vibrations in the molecules of 2- and 4-aminopyridines suggests that the values of the excess charge on the N-atoms in the 2-position and in the 4-position of the benzene ring with respect to the NH<sub>2</sub> group are almost equal while the higher values of these frequencies in comparison to those of aniline would indicate that magnitude of this excess charge is appreciable in both the molecules.

TABLE I  
N—H stretching frequencies  $\nu_s$  and  $\nu_n$  in cm<sup>-1</sup>

Compound and $pK_n$ Solvent	2-amino pyridine 6.86	3-amino pyridine 5.98	4-amino pyridine 9.17	Aniline 4.68
Carbon tetrachloride	3420 3508	3405 3480	3422 3508	3402 3476
Benzene	3413 3495	3395 3465		3393 3466
Carbon disulphide	3409 3402			3394 3470
Chloroform	3417 3509	3406 3481	3424 3521	3398 3460
Acetonitrile	3400 3483	3387 3456	3409 3489	3380 3457
Nitromethane	3410 3502	3400 3467	3419 3506	3393 3465
Acetone	3390 3472	3389 3441	3385 3462	3380 3450
Ether	3380 3464	3376 3448	3379 3448	3376 3448
Dioxane	3373 3464	3380 3442	3384 3452	3380 3451
Tetra hydrofuran	3370 3453	3377 3437	3383 3442	3364 3438
Pyridine	3340 3460	3352 3450	3369 3459	3340 3430
Pure liquid	3330 3455	3340 3430		3360 3420
Pure solid	3310 3452	3315 3391	3319 3445	

TABLE II

Total solvent shift in N-H stretching frequencies

$$\Delta\nu_t = \Delta\nu_s + \Delta\nu_a \text{ in cm}^{-1}$$

Compound and $pK_a$ Solvent	2-amino pyridine 6.86	3-amino pyridine 5.98	4-amino pyridine 9.17	Aniline 4.68
Benzene	20	25	—	19
Carbon disulphide	27	—	—	14
Chloroform	2	—2	—6	20
Acetonitrile	45	42	32	41
Nitromethane	16	18	5	20
Acetone	66	55	83	48
Ether	84	61	103	54
Dioxane	91	63	94	47
Tetrahydrofuran	105	71	105	76
Pyridine	128	83	102	108
Pure liquid	143	115	—	98
Pure solid	166	179	166	—

Similar arguments in the case of 3-aminopyridine would show that the excess  $\pi$ -electron density on the nuclear N-atom is very small. These conclusions are in agreement with the calculations of Longuet-Higgin's (1950) who showed that the values of excess  $\pi$ -electron density on the nuclear N-atoms in 2- and 4-aminopyridines are equal while that in the case of 3-aminopyridine is zero,



It is seen from Table I that in the case of all the isomeric aminopyridines the frequencies of both the N-H stretching vibrations in different environments are less than those observed for each of the compounds in solution in  $\text{CCl}_4$ . In order to find out whether the total solvent shifts ( $\Delta\nu_t$ ) of the three isomeric aminopyridines in solutions in different solvents show any correspondence with those of aniline in solutions in the same series of solvents (Table II), as observed previously in the case of other substituted anilines (Medhi and Kastha, 1963), the values of  $\Delta\nu_t$  for each of the compounds have been plotted against the corresponding  $\Delta\nu_t$  values of aniline in Figs. 1a, b and c.

It can be seen from the figures that the plots for all the three isomeric aminopyridines are straight lines with different slopes for different compounds. In the case of 4-aminopyridine, however, the points are widely scattered about the mean straight line and the value of the slope is not so certain as in the case of the other two compounds.

From this almost linear relation it may be concluded that the mechanism of hydrogen bond formation in the case of all the aminopyridines in different environments is similar to that occurring in the case of aniline under the same conditions.

The linear relation that has been shown to exist between the slopes of the straight lines for the various phenyl amines and their  $pK_a$ -values (Medhi and

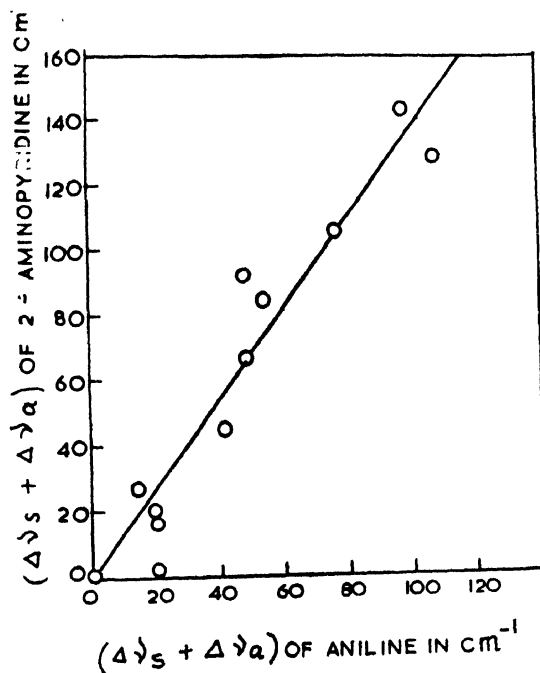


Fig. 1. Plot of total solvent shifts ( $\Delta\nu_s + \Delta\nu_a$ ) in  $\text{cm}^{-1}$  of the compounds against those of aniline (a) 2-Aminopyridine. (b) 3-Aminopyridine. (c) 4-Aminopyridine.

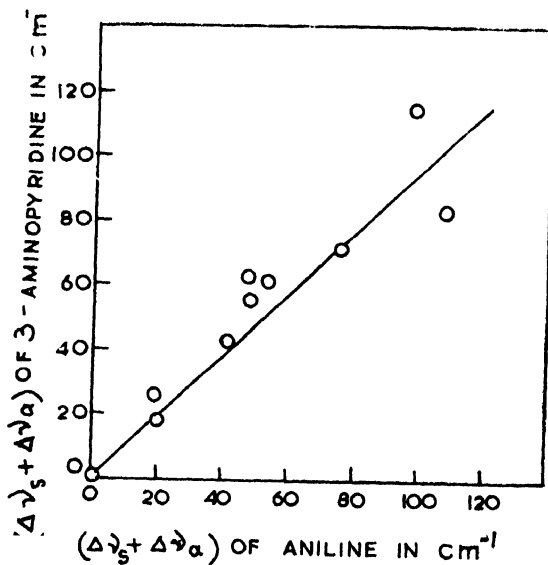


Fig. 1. (b)

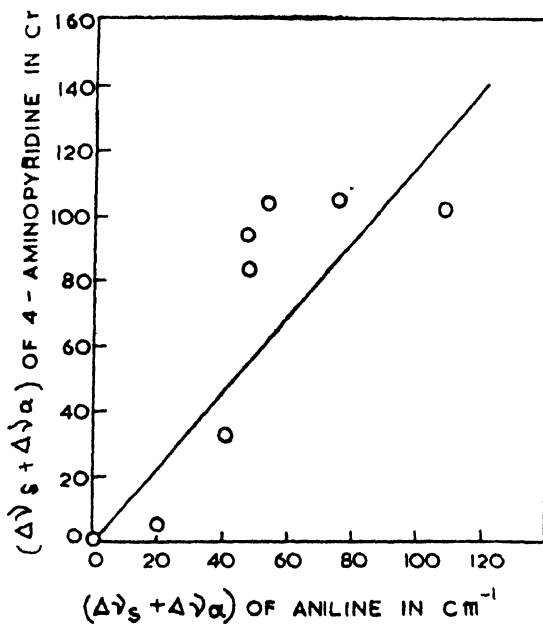


Fig. 1. (c)

Kastha, 1963) has been used in the case of the aminopyridines to obtain the  $pK_a$ -values of these compounds by interpolation from the slopes of the straight lines in Figs. 1a, b and c. These values are given in Table III. The experimental

values of  $pK_a$  for these compounds (Albert *et al.*, 1948) are also included in the Table for comparison

TABLE III

Compound	Interpolated $pK_a$ -value	Experimental $pK_a$ -value
2-aminopyridine	1.1	6.86
3-aminopyridine	4.8	5.98
4-aminopyridine	3.0	9.17

The interpolated  $pK_a$ -values are found to be smaller than the experimental  $pK_a$ -values. This may indicate that the two different values of basicity have their origins in different mechanisms. In the aminopyridines and similar N-heterocyclic amines the basicities of the compounds arise from the nuclear N-atoms in their molecules (Longuet-Higgins, 1950). However, in the case of aniline and its derivatives the N-atom in the  $NH_2$  group of the molecules is responsible for their basicities. In the molecules of the phenyl amines the charge on the N-atom of the  $NH_2$  group directly determines both the  $pK_a$ -value and the capacity for formation of hydrogen bonds (c.f. Kastha and Medhi, 1963). But in the case of the aminopyridines the excess  $\pi$ -electron density on the nuclear N-atom in the molecules of the compounds is responsible for their  $pK_a$ -values while the strength of the hydrogen bridges formed by the molecules of these compounds in different environments is governed by the charge on the N-atom of the amino-group. These facts may explain the difference between the interpolated  $pK_a$ -values and the experimental  $pK_a$ -values in the case of the aminopyridines.

#### REFERENCES

- Albert, A., Goldacre, R. and Phillips, J., 1948, *J. Chem. Soc.*, 2240.  
 Kastha, G. S. and Medhi, K. C., 1963, *Ind. J. Phys.*, **37**, 568.  
 Longuet-Higgins, H. C., 1950, *J. Chem. Phys.*, **18**, 274.  
 Medhi, K. C. and Kastha, G. S., 1963, *Ind. J. Phys.*, **37**, 139 ; 275.  
 Whetsel, K. B., 1961, *Spectrochim. Acta*, **17**, 614.

# STABILITY OF A GRAVITATING FLUID LAYER OF UNIFORM THICKNESS IN THE PRESENCE OF CORIOLIS FORCE AND A MAGNETIC FIELD

B. B. CHAKRABORTY

DEPARTMENT OF APPLIED MATHEMATICS, INDIAN INSTITUTE OF SCIENCE, BANGALORE 12

(Received December 7, 1963)

**ABSTRACT.** The stability of a gravitating fluid layer of finite thickness in the presence of a magnetic field and a Coriolis force is studied by the use of the normal mode method. The previous results obtained by Oganesyan are derived from the general result of the present case. It is found that suitably high values of angular velocity of rotation can stabilize the fluid layer completely for the symmetric perturbations in the absence of the magnetic field. But the presence of the magnetic field has a destabilizing influence.

## INTRODUCTION

Safranov (1960) has pointed out the importance of the study of gravitational and magneto-gravitational stability of fluid layers of finite thickness in the astronomical context. Oganesyan (1961) has recently studied the gravitational and magnetogravitational stability of a fluid layer of infinite extension but of finite thickness. He takes the conductivity of the fluid as infinite. In the present paper we have studied the corresponding problem in the presence of a Coriolis force arising due to the rotation of the fluid layer uniformly about an axis which is normal to the plane of the fluid surface in equilibrium.

Our conclusion is that rotation affects, in a very important way, the stability criterion in the absence of a magnetic field. We find that for the angular velocity of rotation and for the density appropriate for our galaxy, rotation can stabilize fully the fluid layer.

But the magnetic field is able to suppress this effect of rotation and it appears that stability criterion is unaffected by rotation in this case.

We employ the normal mode method in contrast with the energy method used by Oganesyan (1961). Oganesyan's all results follow as particular cases of our general result.

## BASIC EQUATIONS

The basic equations in the steady case holding in the infinitely conducting fluid layer are the following.

$$\rho \left\{ \frac{\partial \mathbf{V}}{\partial t} + \mathbf{V} \cdot \nabla \mathbf{V} + 2 \underline{\Omega} \times \mathbf{V} + \underline{\Omega} \times (\underline{\Omega} \times \mathbf{r}) \right\} = -\nabla p + \mu \operatorname{curl} \mathbf{H} \times \mathbf{H} - \rho \nabla U, \dots (1)$$

$$\operatorname{div} \mathbf{V} = 0, \quad \dots \quad (2)$$

$$\frac{\partial \mathbf{H}}{\partial t} = \operatorname{curl} (\mathbf{V} \times \mathbf{H}), \quad \dots \quad (3)$$

$$\operatorname{div} \mathbf{H} = 0, \quad \dots \quad (4)$$

$$\nabla^2 U = 4\pi G \rho. \quad \dots \quad (5)$$

In the above we have used the M.K.S. system of units. The symbols  $\Omega$ ,  $U$  and  $G$  represents the angular velocity of rotation of the fluid layer, the gravitational potential and the universal gravitational constant. The other symbols have the usual meanings.

We shall take  $\Omega$  to be along the  $z$ -axis. The fluid layer in steady state is confined within the planes  $z = \pm h$ ,  $2h$  being the thickness of the layer.

The equations holding in the surrounding non-conducting fluid, which is also assumed to be rotating in the steady state with angular velocity  $\Omega$ , are

$$\rho_0 \left\{ \frac{\partial \mathbf{V}}{\partial t} + \mathbf{V} \cdot \nabla \mathbf{V} + 2\Omega \times \mathbf{V} + \Omega (\Omega \cdot \mathbf{r}) \right\} = -\nabla p - \rho_0 \nabla U, \quad (6)$$

$$\operatorname{div} \mathbf{V} = 0, \quad \dots \quad (7)$$

$$\operatorname{curl} \mathbf{H} = 0, \quad \dots \quad (8)$$

$$\nabla^2 U = 4\pi G \rho_0 \quad \dots \quad (9)$$

where  $\rho_0$  is the density of the non-conducting fluid and  $U$  is the gravitational potential there.

The magnetic field in the steady (equilibrium) state is taken to be uniform and along  $x$ -axis. It is denoted by  $\mathbf{H}_0$ .

For small perturbations about the equilibrium state we have, after linearization, the following equations.

$$\rho \left( \frac{\partial \widetilde{\mathbf{V}}}{\partial t} + 2\Omega \times \widetilde{\mathbf{V}} \right) = -\nabla \bar{p} + \mu \operatorname{curl} \widetilde{\mathbf{H}} + \mathbf{H}_0 \cdot \nabla \widetilde{\mathbf{U}} \quad \dots \quad (10)$$

$$\operatorname{div} \widetilde{\mathbf{V}} = 0 \quad \dots \quad (11)$$

$$\frac{\partial \widetilde{\mathbf{H}}}{\partial t} = \operatorname{curl} (\widetilde{\mathbf{V}} \times \widetilde{\mathbf{H}}_0) \quad \dots \quad (12)$$

$$\operatorname{div} \widetilde{\mathbf{H}} = 0, \quad \dots \quad (13)$$

$$\nabla^2 \widetilde{\mathcal{U}} = 0, \quad \dots \quad (14)$$

holding in the conducting fluid. Similar equations for small perturbations are obtained from equations 6–9 which hold for the non-conducting fluid.

### *Solutions of the Perturbation Equations*

If  $q$  is any physical quantity the perturbation in it is denoted by  $\tilde{q}$ . We shall assume, in the further discussion,  $\tilde{q}$  to be of the form

$$\tilde{q} = \tilde{q}(z)k^{i(\sigma t + kx + ly)} \quad \dots \quad (15)$$

where  $\sigma$  is the frequency of oscillations and  $k$  and  $l$  are wave numbers in  $x$  and  $y$  directions.

### *Solutions in the Conducting Fluid Layer*

The equation (12) in view of (11) gives

$$\widetilde{\mathbf{H}} = -\frac{kH}{\sigma} \widetilde{\mathbf{v}}, \quad \dots \quad (16)$$

where

$$|\mathbf{H}_0| = H.$$

Taking the curl of (10), and using (11), (15) and the constancy of  $\mathbf{H}_0$  and  $\Omega$  we have

$$A\mathbf{w} = -2\Omega \frac{\partial \tilde{\mathbf{v}}}{\partial z}, \quad \dots \quad (17)$$

where

$$\mathbf{w} = \text{curl } \tilde{\mathbf{V}} \quad \dots \quad (18)$$

and

$$A = i\sigma - \frac{\nu k^2}{\rho\sigma} \quad \dots \quad (19)$$

Using (11), we have from the  $z$ -component of (17)

$$v_y = \frac{\tilde{v}_x(Al - 2\Omega k)}{2\Omega l + Ak} \quad \dots \quad (20)$$

In view of (11) and (20), we have from (17),

$$D^2 \tilde{v}_x = m^2 \tilde{v}_x, \quad \dots \quad (21)$$

where

$$m^2 = -\frac{A^2(k^2 + l^2)}{A^2 + 4\Omega^2} \quad \dots \quad (22)$$

We shall consider perturbations symmetrical about  $z = 0$  plane. Considering the distribution of  $\hat{v}_z$  about  $z = 0$ , it is clear that  $\hat{v}_z$  is an odd function of  $z$ . Using the above result we have from (11), (20) and (21)

$$\left. \begin{aligned} \hat{v}_x &= C \cosh mz \\ \hat{v}_y &= \frac{\{4l - 2\Omega k\}}{\{2\Omega l + Ak\}} C \cosh mz \\ \hat{v}_z &= -\frac{i\{4(k^2 + l^2)\}C \sinh mz}{m\{2\Omega l + Ak\}} \end{aligned} \right\} \dots \quad (23)$$

when  $C$  is an arbitrary constant.

From the symmetry of the configuration we have the condition

$$\frac{\partial \hat{U}}{\partial z} = 0 \text{ at } z = 0. \quad \text{In view of this condition we have from (14)}$$

$$\hat{U} = C' \cosh (k^2 + l^2)z. \quad \dots \quad (24)$$

Similarly, we can easily find

$$\hat{V} = C'' e^{-\sqrt{k^2 + l^2}z} \quad \dots \quad (25)$$

The velocity components for the non-conducting fluid are

$$\left. \begin{aligned} \hat{v}_x &= C_1 e^{-m'z} \\ \hat{v}_y &= \frac{(i\sigma l - 2\Omega k)}{2\Omega l + i\sigma k} \hat{v}_x, \\ \hat{v}_z &= -\frac{\sigma(k^2 + l^2)(C_1 e^{-m'z})}{m'(2\Omega l + i\sigma k)} \end{aligned} \right\} \dots \quad (26)$$

where  $C_1$  is an arbitrary constant and

$$m'^2 = \frac{\sigma^2(k^2 + l^2)}{\sigma^2 - 4\Omega^2}. \quad \dots \quad (27)$$

From the equations for the perturbations it is clear that  $\widetilde{H}$  is given by

$$\widetilde{H} = \text{grad } \widetilde{\phi}, \quad \nabla^2 \widetilde{\phi} = 0, \quad \dots \quad (28)$$

in the non-conducting fluid. In view of (15) we have

$$\widetilde{\phi} = L e^{-\sqrt{k^2 + l^2}z} \quad \dots \quad (29)$$

*Boundary Conditions and the Dispersion Relations*

$$\text{If} \quad z = h + \delta z e^{i(nt+kx+ly)} \quad \dots \quad (30)$$

is the equation of the upper interface between the conducting and the nonconducting fluids, the perturbation  $\tilde{\mathbf{n}}$  in the unit normal is given by

$$\tilde{\mathbf{n}} = (lk\delta z, il\delta z, 0)e^{i(nt+kx+ly)} \quad \dots \quad (31)$$

The gravitational potential satisfies the following boundary conditions at the interface of the two fluids :

- (i) Continuity of the gravitational potential;
- (ii) Continuity of the normal component of the gradient of the gravitational potentials.

The perturbations in the gravitational potentials, satisfying the above boundary conditions are

$$\begin{aligned} \hat{\psi} &= \frac{4\pi i G(\rho - \rho_0)\hat{v}_z(h) \cosh(k^2 + l^2)^{1/2} h e^{-\sqrt{k^2 + l^2} z}}{\sigma(k^2 + l^2)^{1/2}} \\ \hat{\psi} &= \frac{4\pi i G(\rho - \rho_0)\hat{v}_z(h) \cosh(k^2 + l^2)^{1/2} z}{\sigma(k^2 + l^2)^{1/2} e^{\sqrt{k^2 + l^2} h}} \end{aligned} \quad (32)$$

The other boundary conditions required may be written as follows (cf. Kruskal and Schwarzschild, 1954).

$$u = \mathbf{n} \cdot \mathbf{V}, \quad \mathbf{n} \cdot [\mathbf{B}] = \mu_0 \mathbf{j}^* \quad \dots \quad (33, 44)$$

$$\mathbf{n} \cdot [\mathbf{B}] = 0, \quad \mathbf{j}^* \cdot \mathbf{B} - \mathbf{n} \cdot [\mathbf{j}] = 0. \quad \dots \quad (35, 36)$$

In the above  $\mathbf{n}$  is the unit normal vector (directed in the conducting fluid) of surface.  $p$  and  $\mathbf{V}$  are the pressure and velocity on the interface. The brackets denote the jump in the enclosed quantities upon crossing the interface from the non-conducting to the conducting fluid.  $\mathbf{B}$  denotes the arithmetic mean of the magnetic induction just on each side of the interface.

The condition (35), in view of (33), implies  $\hat{H}_2 = 0$ , in the nonconducting fluid. Hence (28) and (29) show that the perturbations in the magnetic field vanish in the non-conducting fluid.

The boundary conditions satisfied by the perturbations are obtained from 33-36 in the usual manner by linearization. Eliminating  $\hat{\mathbf{j}}^*$  with the help of



(34), we find that the  $x$ - and  $y$ -components of (36) are identically satisfied. The  $z$ -component finally gives the dispersion relation

$$\left[ \frac{4\pi G(\rho - \rho_0)^2}{\sigma(k^2 + l^2)^{1/2} \{1 + \tanh(k^2 + l^2)^{1/2} h\}} - \frac{\rho_0(\sigma^2 - 4\Omega^2)^{1/2}}{(k^2 + l^2)^{1/2}} + \frac{4\pi G\rho h(\rho_0 - \rho)}{\sigma} \right] \\ \times \frac{\sqrt{k^2 + l^2} \sqrt{A^2 + 4\Omega^2}}{2\Omega l + Ak} \tanh \left\{ \frac{A\sqrt{k^2 + l^2}}{\sqrt{A^2 + 4\Omega^2}} h \right\} + \left\{ \frac{\rho}{k} \left[ \sigma + \frac{2i\Omega(Ah - 2\Omega k)}{2\Omega l + Ak} \right] \right. \\ \left. \frac{\mu H^2 k}{\sigma} \right\} = 0. \quad \dots (37)$$

# DISCUSSION

We shall first discuss the dispersion relation in special cases before considering it in the general case.

*Case I.*  $\Omega = 0, \rho_0 = 0, H = 0.$

In this case, in the absence of rotation, magnetic field and outside matter, the dispersion relation (37) reduces to

$$4\pi G\rho h \left[ 1 - \frac{1}{h\sqrt{k^2 + l^2} \{1 + \tanh(k^2 + l^2)^{1/2} h\}} \right. \\ \left. \times \sqrt{k^2 + l^2} \tanh \sqrt{k^2 + l^2} h - \sigma^2 \right] = 0. \quad \dots (38)$$

This is the result obtained by Oganessian (1961). He finds that the layer is unstable for all waves for which  $\sqrt{k^2 + l^2} h < g_0 = 0.64$  and it is stable when  $\sqrt{k^2 + l^2} h > g_0 = 0.64$ .

*Case II.*  $\Omega = 0, \rho_0 \neq 0.$

In this case, in the absence of rotation and outside fluid, the dispersion relation reduces to

$$4\pi G\rho \sqrt{k^2 + l^2} h \tanh(\sqrt{k^2 + l^2} h) \left\{ 1 - \frac{1}{h(k^2 + l^2)^{1/2} \{1 + \tanh \sqrt{k^2 + l^2} h\}} \right. \\ \left. + \frac{\mu H^2 k^2}{4\pi G\rho^2 h \sqrt{k^2 + l^2} \tanh(\sqrt{k^2 + l^2} h)} \right\} = \sigma^2. \quad \dots (39)$$

This result has been obtained by Oganessian (1961).

*Case III.*  $\rho_0 = 0, H = 0.$

The dispersion relation reduces to

$$\left\{ \frac{4\pi G\rho^2}{\sqrt{k^2 + l^2} \{1 + \tanh(k^2 + l^2)^{1/2} h\}} - 4\pi G\rho^2 h \right\}$$

$$\propto \sqrt{k^2 + l^2} \tan \left( \frac{\sqrt{k^2 + l^2} \sigma}{\sqrt{4\Omega^2 - \sigma^2}} \right) h - \rho \sigma (4\Omega^2 - \sigma^2)^{\frac{1}{2}} = 0. \quad \dots (40)$$

By investigating the nature of  $\sigma$  in the dispersion relation (40), it is possible to show that there is stability if

$$\frac{\pi G \rho}{\Omega^2} \left[ \frac{1}{h \sqrt{k^2 + l^2} \{1 + \tanh(k^2 + l^2)^{\frac{1}{2}} h\}} - 1 \right] h^2 (k^2 + l^2) < 1,$$

and instability if the left hand side of the inequality is greater than unity (see the Appendix). Thus the critical value of  $h \sqrt{k^2 + l^2}$  at which instability sets in is given by the equation

$$\frac{\pi G \rho}{\Omega^2} \left[ \frac{1}{h \sqrt{k^2 + l^2} \{1 + \tanh(k^2 + l^2)^{\frac{1}{2}} h\}} - 1 \right] h^2 (k^2 + l^2) = 1. \quad \dots (41)$$

We also note that the dispersion relation (40) reduces to (41) as  $\sigma \rightarrow 0$ , i.e. the principle of exchange of stability holds good (cf. Chandrasekhar 1952).

We have computed the value of

$$\left[ \frac{1}{h \sqrt{k^2 + l^2} \{1 + \tanh(k^2 + l^2)^{\frac{1}{2}} h\}} - 1 \right] h^2 (k^2 + l^2)$$

for different values of  $h \sqrt{k^2 + l^2}$ . We find that this has the maximum value 0.143 at  $h(k^2 + l^2)^{\frac{1}{2}} = 0.30$ . Thus the left hand side of (41) is always less than unity if

$$\frac{\pi G \rho}{\Omega^2} < 0.143 \quad \dots (42)$$

Hence if (42) is satisfied there is always stability. With  $\Omega \sim 10^{15}$  per sec. (42) suggests that for a density  $\rho = 10^{-21}$  gm/cc the system is stable. The values of  $\Omega$  and  $\rho$  noted above are obtained in our galaxy (Chandrasekhar, 1955).

It may be noted that the result (42) is independent of the thickness  $h$  of the fluid layer, and thus valid for all values of  $h$ .

*Case IV.*  $\rho_0 = 0$ .

In this case, when  $\sigma \rightarrow 0$ , the dispersion relation reduces to

$$4\pi G \rho \sqrt{k^2 + l^2} h \tanh(\sqrt{k^2 + l^2} h) \times \left[ 1 - \frac{1}{\sqrt{k^2 + l^2} h \{1 + \tanh(k^2 + l^2)^{\frac{1}{2}} h\}} + \frac{\mu k^2 h^2 n^2}{\sqrt{k^2 + l^2} h \tanh(h \sqrt{k^2 + l^2})} \right] = 0, \quad \dots (43)$$

where

$$\eta = \frac{H}{4\pi \sqrt{G \rho h}}. \quad \dots (44)$$

The equation (43) is the same as that obtained by Oganessian (1961) in the absence of rotation for the critical values of the wave numbers at which instability sets in. On examining the dispersion relation (37) for values of  $\sqrt{k^2+l^2}h$  and  $kh$  which are in a small neighbourhood of  $(g_1, g_2)$  where  $\sqrt{k^2+l^2}h = g_1$  and  $kh = g_2$  are roots of (43), it is clear that we can find  $\sqrt{k^2+l^2}h$  and  $kh$  for which there is instability whatever be the values of  $\rho$  and  $\Omega$ . Thus the magnetic field has a destabilizing effect.

# APPENDIX

We shall briefly prove that the principle of the exchange of stability holds in case III, i.e.  $\sigma = 0$  gives the critical wave-lengths at which instability sets in.

Let

$$\frac{\sigma}{\sqrt{4\Omega^2 - \sigma^2}} = X.$$

Then the dispersion relation in case III reduces to

$$\left[ \frac{4\pi G\rho^2}{(k^2+l^2)^{\frac{1}{2}}\{1+\tanh(k^2+l^2)^{\frac{1}{2}}h\}} - 4\pi G\rho^2h \right] (1+X^2)\sqrt{k^2+l^2} \\ \times \sin(\sqrt{k^2+l^2}hX) + 4\Omega^2X\rho \cos(\sqrt{k^2+l^2}hX) = 0. \quad \dots \quad (\text{A-1})$$

Let  $|X| = R$  be large so that  $R$  is the  $n$ -th root of  $\cos(\sqrt{k^2+l^2}hX) = 0$  where  $n$  is large. We note that for  $|X| \geq R$ ,

$|\cos(\sqrt{k^2+l^2}hX)|$  and  $|\sin(\sqrt{k^2+l^2}hX)|$  are of the same order of magnitude, except near  $X = \pm R$ , where  $\left| \frac{\sin(\sqrt{k^2+l^2}hX)}{\cos(\sqrt{k^2+l^2}hX)} \right|$  tends to an indefinitely large

quantity as  $X \rightarrow \pm R$ . Hence by Rouch's theorem the equation (A-1) has the same number of roots within  $|X| = R$  as the equation

$$(1+X^2)\sqrt{k^2+l^2} \sin(\sqrt{k^2+l^2}hX) = 0. \quad \dots \quad (\text{A-2})$$

Now,  $X = 0$  is a root of both (A-1) and (A-2). Writing (A-1) as

$$\left[ \frac{4\pi G\rho^2}{(k^2+l^2)^{\frac{1}{2}}\{1+\tanh(k^2+l^2)^{\frac{1}{2}}h\}} - 4\pi G\rho^2h \right] \\ \times \frac{\sqrt{k^2+l^2}}{4\Omega^2\rho} \tan(\sqrt{k^2+l^2}hX) = \frac{X}{1+X^2}, \quad \dots \quad (\text{A-3})$$

we draw the graphs of the right hand side as well as left hand side of (A-3) against real positive values of  $X$ . (The equation (A-1) or (A-3) has equal and opposite roots in pairs). It is clear that corresponding to the  $n$  roots of  $\cos(\sqrt{k^2+l^2}hX) = 0$  within the circle  $|X| = R$  there are  $n$  vertical asymptotes of the graph of

the left hand side of (A-3) and there will be  $n-1$  intersections of the graph of the left hand side with that of the right hand side between  $X = \beta_1$  and  $X = \beta_n$  where  $\beta_1$  and  $\beta_n$  are the first and the  $n$ -th roots of

$$\cos(\sqrt{k^2 + l^2} hX) = 0, \quad \left( \beta_1 = \frac{\pi}{2h\sqrt{k^2 + l^2}} \right).$$

Thus  $X = 0$  and  $n-1$  other roots between  $X = \beta_1$  and  $X = \beta_n$  for (A-3) are located corresponding to the  $n$  roots of  $\sin(\sqrt{k^2 + l^2} hX) = 0$  between  $X = 0$  and  $X = \beta_n$ . But the roots of (A-3) that correspond to the roots  $X = \pm i$  of (A-2) are still to be accounted for.

Considering the growth rates of the left hand side and the right hand side of (A-3) between  $X = 0$  and  $X = \beta_1$  it can be shown that there is one root between  $X = 0$  and  $X = \beta_1$  when

$$\alpha = \frac{\pi^2 \rho h^2 (k^2 + l^2)}{\Omega^2} \left[ \frac{1}{h(k^2 + l^2) \left\{ 1 + \tanh^2(k^2 + l^2)^2 h \right\}} - 1 \right]$$

lie between 0 and 1.

If  $\alpha > 1$ , then there is no root (real) between  $X = 0$  and  $X = \beta_1$ . In this case only possibility is that there will be a complex or a purely imaginary root  $X = iX_1$  (with real  $X_1$ ), such that

$$1 = X_1^2.$$

If  $\alpha < 0$ , there is a root  $X = iX_1$  such that  $X_1 > 1$ .

From the relation  $\frac{\sigma}{\sqrt{4\Omega^2 - \sigma^2}} = X$ , it is clear that when  $\alpha = 1$ ,  $\sigma$  is either imaginary or complex. From (A-1), it is clear that the dispersion relation is even in  $X$  and  $\sigma$ . Hence equal and opposite roots  $\sigma$  occur in pairs. Thus imaginary or complex  $\sigma$  indicates instability.

#### ACKNOWLEDGMENT

The author gratefully records his indebtedness to Prof. P. L. Bhatnagar for his kind encouragement and guidance in the preparation of the paper.

#### REFERENCES

- Chandrasekhar, S. (1952), *Philosophical Magazine*, **43**, 501.
- Chandrasekhar, S. (1955), *Vistas in Astronomy*.
- Oganesyan, R. S. (1961), *Soviet Astronomy*, **4**, 434.
- Oganesyan, R. S. (1961), *Soviet Astronomy*, **4**, 634.
- Safranov, V. S. (1960), *Annales D'Astrophysique*, **23**, 979.

# LOW ENERGY NUCLEAR BURSTS OF COSMIC RAYS AT SEA LEVEL

S. R. GANGULY AND S. D. CHATTERJEE

DEPARTMENT OF PHYSICS, JADAVPUR UNIVERSITY, CALCUTTA-32

(Received September 16, 1964)

## Plate X

**ABSTRACT.** Measurement of cosmic ray burst in a thin-walled unshielded ionization chamber at Calcutta (sea level) is described. Bursts due to nuclear interactions are isolated from those due to airshowers by counter coincidence method. The integral size-frequency distribution of nuclear bursts is found to be capable of being represented by a power law with exponent  $-3.4$ .

The energy of an incident particle initiating a nuclear burst of a given size is evaluated with the help of the results of energy measurements of star prongs in photographic emulsion by other workers. The energy spectrum of cosmic ray nuclear-active particles producing bursts at sea level is then constructed and it is found that this can be represented by an empirical relation as:  $N(E) = 240.E^{72-89 \log E}$  within the energy-range investigated viz., from 50 Mev to about 1 Bev.

## INTRODUCTION

Experiments on bursts in unshielded ionization chambers by various workers viz. Montgomery and Montgomery (1949), Carmichael (1948), (1955) and Bridge, Hazen, Rossi and Williams (1948) have established that such bursts are caused by two separate processes, i) extensive air showers and ii) nuclear interactions occurring in the wall or in the gas of the chamber. Different methods have been devised for isolating the latter from the former. Observation of bursts in unshielded chambers offers a convenient method for studying the low energy (below the energy at which meson production becomes important) nuclear interactions of cosmic rays with matter. This method has, indeed, been utilised by many workers, e.g., Coor (1951), Simpson *et al.* (1951), Rossi (1948), Montgomery *et al.* (1950), for the investigation of diverse characteristics such as the intensity variation with altitude and the absorption mean free path in air, the variation with latitude etc. of low energy nucleonic component of cosmic rays. The present experiment is designed to evaluate the energy distribution of cosmic ray particles producing bursts in an unshielded chamber at sea level.

## EXPERIMENTAL ARRANGEMENT

The apparatus consisted of a spherical ionization chamber made of steel, having a diameter of 10 cm. and wall thickness 3.2 mm. The gaseous volume of the chamber was 3.8 litres. Pure Argon (99% purity) was further purified by

passing it through a trap immersed in liquid oxygen. The chamber was filled with the gas to a pressure of about 20 atmospheres. The particulars of our ionization chamber are listed in Table I.

The chamber was used as a pulse ionization chamber employing positive-ion collection. The outer wall of the chamber was kept at a high potential of +1500 volts, while the central electrode was connected to an electrometer tube. In our experiment R.C.A. acorn tube type 959 was used instead of the conventional electrometer tube as suggested by Nielson (1947). The grid-leak of the tube was  $1 \times 10^{11}$  ohms. The electrometer tube was followed by a d.c. amplifier and a short period galvanometer. The trace of the galvanometer spot was recorded photographically on a continuously moving 35 mm. ciné film by means of a camera driven by a synchronous motor. The record was projected on a graduated screen and the pulse heights were measured. A diagram of the ionization chamber is shown in Fig. 1 and the arrangement of the associated equipments is shown schematically in Fig. 2.

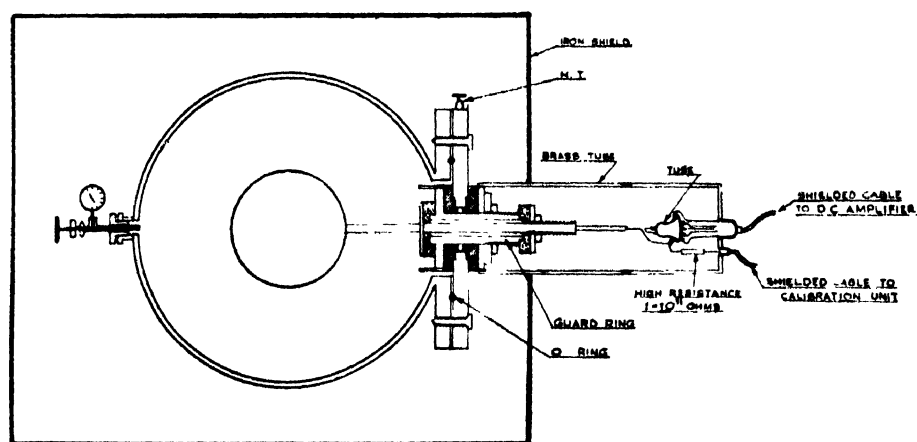


FIG. 1. THE IONIZATION CHAMBER

INSULATORS  POLYTHENE  
 EPOXYITE

The ionization chamber was calibrated by applying a calibration pulse of known potential to the collecting electrode. The capacity of the chamber connected to the input of the d.c. amplifier was measured with the help of a quadrant electrometer and a standard capacitor. These values enabled us to estimate the burst size in terms of the number of ion pairs produced.

In order to isolate bursts due to nuclear interactions from those due to air-showers, the following method was employed. Two G-M counter trays, each consisting of two G-M counters connected in parallel were placed on either side of the ion chamber and in the same horizontal plane with it. The separation between a counter tray and the chamber was  $\frac{1}{2}$  metre. A coincidence between

the discharges of the two counter trays was employed to ignite a lamp. This produced a 'dot' on the same photographic film on which the galvanometer trace was also recorded. The arrangement is shown in Fig. 2. A pulse in the ioni-

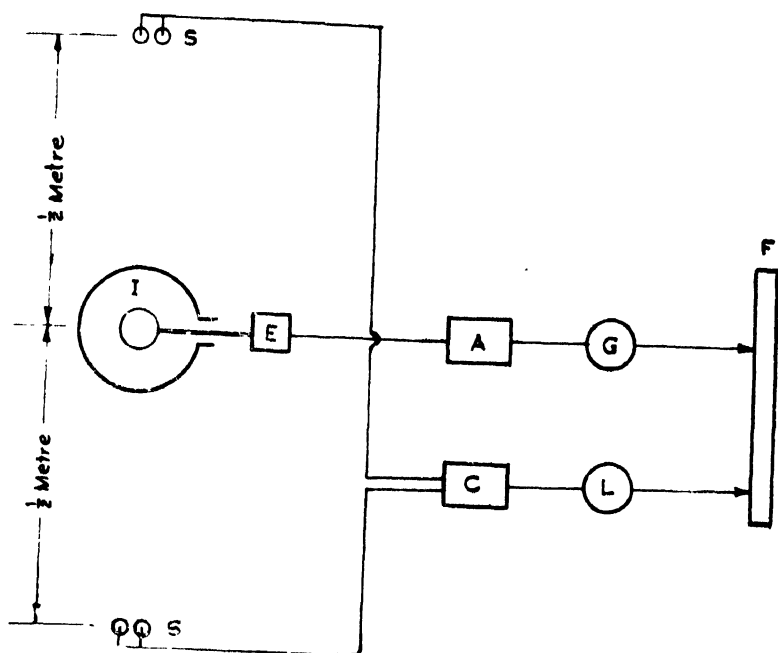


Fig. 2.

I— Ionization chamber  
E— Electrometer tube  
A—D. C. amplifier  
G— Galvanometer

F—Film  
S, S—Shower trays  
C— Coincidence circuit  
L— Lamp.

zation chamber coincident with a dot due to counter trays was recognised as a burst produced by air shower. A burst unaccompanied by such a simultaneous shower dot was taken to be a nuclear burst. Facsimiles of record are shown in Fig. 3.

## RESULTS AND DISCUSSIONS

### (A) *Size-frequency distribution of nuclear bursts*

The pulse height pertaining to a burst as measured by projecting the film on a screen was converted to the corresponding potential change of the central electrode by comparing with the calibration pulse. From the change of potential

( $V$ ) of the central electrode, the total number of ion pairs formed in the burst was obtained by the relation :

$$\text{Number of ion pairs} = \frac{Q}{e} = \frac{C.V}{e} \quad (1)$$

where  $Q$  = the charge collected by the central electrode,

$C$  = the capacity of the chamber and its attachments,

and  $e$  = the electronic charge.

The results of the measurements are represented by the integral size-frequency distribution of bursts shown in Fig. 4. The frequency of all bursts larger than a given size was plotted as a function of the size in curve  $A$ . The frequency of

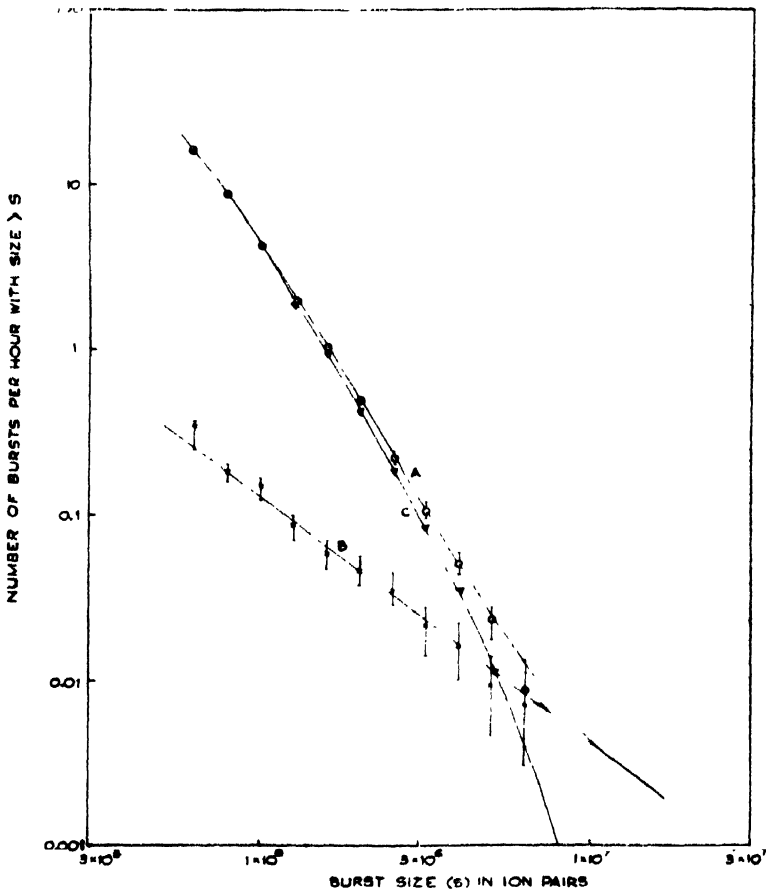
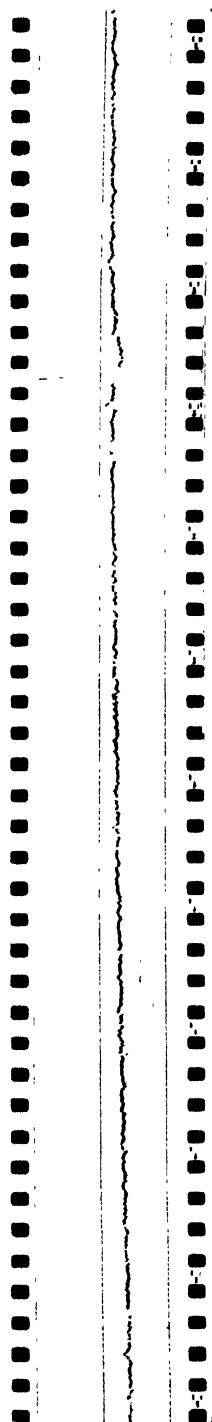


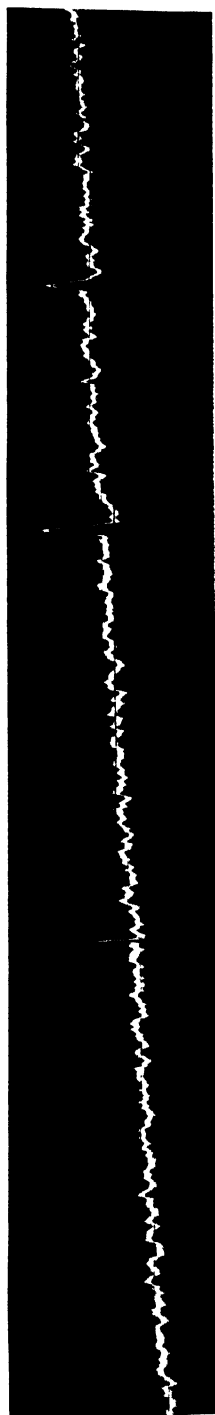
FIG. 4 INTEGRAL SIZE-FREQUENCY DISTRIBUTION OF BURSTS.  
(A) ALL BURSTS. (B) AIR SHOWERS (C) NUCLEAR BURSTS.

bursts due to air showers as obtained from the coincidence between the chamber and the shower trays was plotted against burst size in curve  $B$ . The frequency of air showers was then subtracted from the frequency of all bursts of the same size so that the remainder represented bursts due to nuclear interactions only.

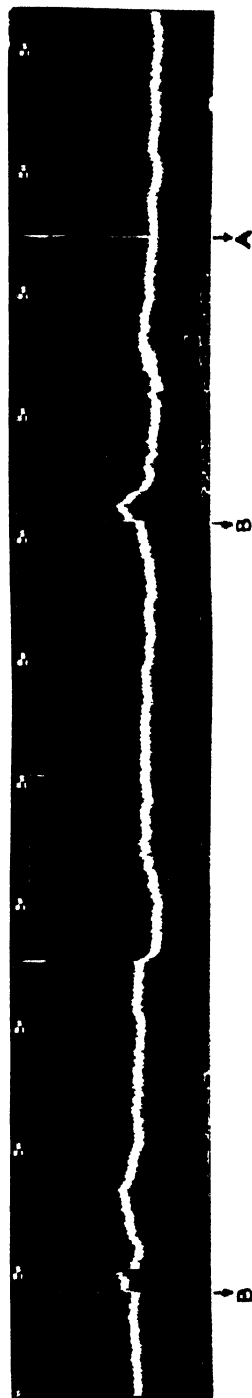




(a) Trace of a large burst as recorded by an Einthoven string galvanometer.



(b) A typical record of bursts using D'Arsonval galvanometer and fast film movement.



(c) A typical record of nuclear and air-shower bursts as recorded by a Ruhstrat Galvanometer, with slower film movement.

A = Burst due to air shower.

B = Nuclear bursts.

Fig. 3. Facsimiles of the record.



The size-frequency distribution of nuclear bursts, so obtained, is shown in curve C. This is also drawn separately in Fig. 5 (curve A).

The size-frequency curve shows that the frequency distribution of nuclear bursts can be approximately represented by a power law of the form :

$$N(>S) = A.S^{-\gamma} \quad \dots (2)$$

where  $N(>S)$  represents the number (frequency) of bursts larger than the given size  $S$ ,

$S$  is the burst size in ion pairs,

$A$  is a constant,

and the exponent  $\gamma$  has the value  $\gamma = -3.4$ .

This power law is seen to be valid within the range of burst size from  $8 \times 10^5$  to

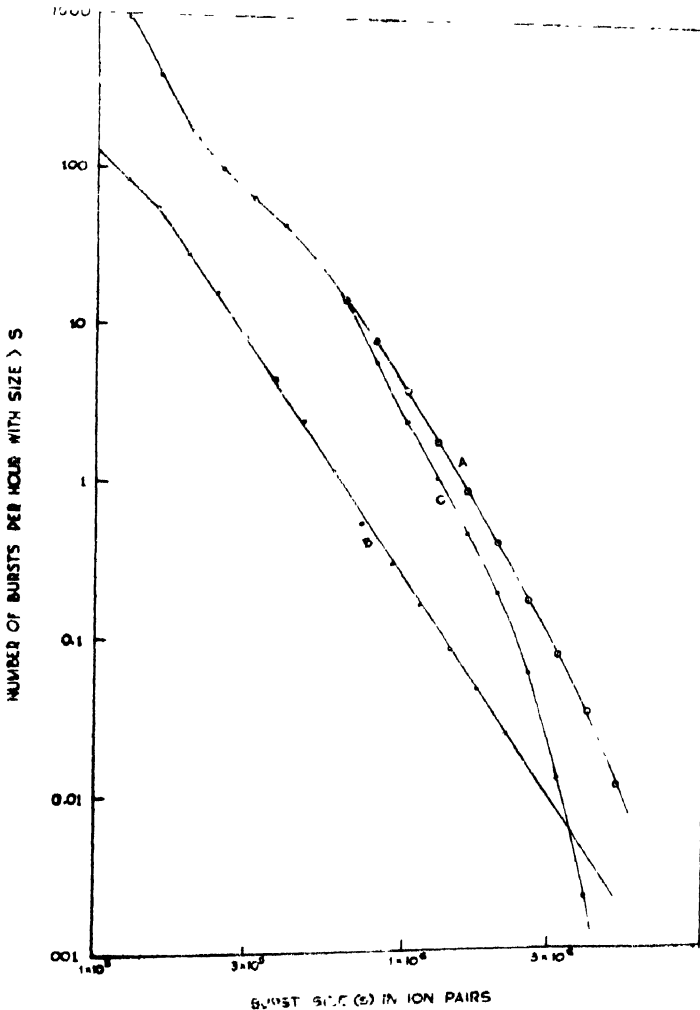


FIG. 5. SIZE-FREQUENCY DISTRIBUTION OF NUCLEAR BURSTS.

(A) - PRESENT AUTHORS (B) MONTGOMERY & MONTGOMERY (C) - CARMICHAEL

$3 \times 10^6$  ion pairs. For larger bursts, the frequency tends to decrease very rapidly with size.

In Fig. 5, are also plotted for comparison the size-frequency distribution curves of bursts in unshielded chamber obtained by Montgomery and Montgomery (1949) (curve B) and by Carmichael and Steljes (1955) (curve C). Certain relevant details regarding the apparatuses used by them are listed in Table I along with those of the present experiment.

TABLE I

Author	Altitude of Observation	Chamber geometry	Dimensions (outer dia)	Chamber wall	Gaseous volume (litres)	Gas	Pressure (atm.)	Exponent of Power law
Montgomery and Montgomery	3510m	Cylindrical	3"	1/32" brass	1	Argon	4.8	-3.2
Carmichael and Steljes	Sea level	Spherical	8"	1/16" Steel	4.4	"	50	
Present authors	"	"	8"	1/8" Steel	3.8	"	20	3.4

Montgomery and Montgomery's chamber was of smaller area and of smaller volume than ours. A change in these parameters would probably shift the curve vertically and laterally but the shape of the curve will not be altered. It is seen that Montgomery's distribution can be represented by a power law similar to equation (2) within a burst range from  $2 \times 10^5$  to  $2 \times 10^6$  ion pairs with an exponent  $\gamma = -3.2$ . The value of  $\gamma$  obtained in the present experiment is seen to be in agreement with that of Montgomery and Montgomery.

Curve (C), Fig. 5 was drawn by subtracting the frequency of air showers from the corresponding frequency of all bursts from the data given in the paper of Carmichael and Steljes. It is seen that Carmichael's frequency distribution cannot be represented by a power law for any considerable range of burst size.

#### (B) *Energy spectrum of the bursts*

A nuclear burst is produced when a nuclear interaction occurs between an incident cosmic ray nuclear-active particle (N-component) and a nucleus of the chamber wall or of the chamber gas. The heavily ionizing particles released in the interaction produce the ionization pulse inside the gaseous volume of the chamber. The number of ion pairs produced in a burst is, therefore, a measure of the kinetic energy of all the secondary ionizing particles of the interaction and this energy can be evaluated from the relation :

$$E = \omega.S \quad \dots(3)$$

where  $S$  is the size of the burst in ion pairs,

and  $\omega$  is the energy required to create an ion pair, which is 25.4 ev for Argon. (Rutherford, Chadwick and Ellis, 1930).

But there are both charged and neutral particles (neutrons) among the secondaries of the interaction, and the chamber fails to record these neutrons. Hence the energy calculated from relation (3) has to be corrected for the contribution of neutrons to the total kinetic energy of the particles emitted in the burst process, which can be done approximately in the following way. Most of the ionizing secondaries of the interaction are protons, as revealed in the observation of cosmic ray stars in photographic emulsion. Also the majority of nuclear interactions occur within the wall of the chamber rather than within its gaseous volume. We may, then, assume the neutron/proton ratio among the emitted particles to be equal to 1.15 corresponding to the ratio of neutrons to protons in iron nucleus. The energy obtained from equation (3) is, therefore, multiplied by 2.15 to get the the total kinetic energy-release in a burst. The resulting number-energy distribution is plotted in Fig. 6.

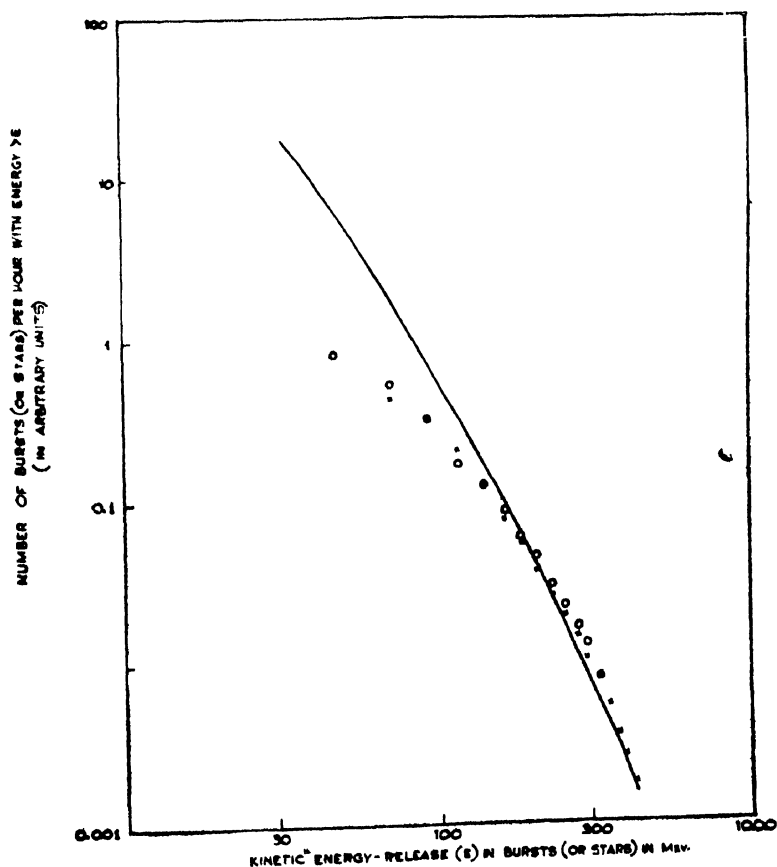


FIG. 6. NUMBER-ENERGY DISTRIBUTION OF BURSTS AND STARS.  
 — PRESENT AUTHORS.    ○ N. PAGA.    × BROWN ET AL.

Since a nuclear burst is a process similar to that of formation of stars in photographic emulsion, we may compare the results of the present experiment with the observation of cosmic ray stars. The number of heavy tracks in a star is a measure of the energy released in the process. Majority of the heavy tracks are due to protons (Brown *et al.* 1949) and we may take the number of neutron/proton emitted in a star to be equal to 1.3 corresponding to the ratio of neutrons to protons in silver bromide. The number of heavy prongs in a star is then multiplied by 2.3 to account for the missing neutrons. Now we may assume that average kinetic energy of a secondary particle is 10 Mev (as observed from measurements of Brown *et al.*, the average kinetic energy of a dense track is 10 Mev). The total number of prongs in a star should then be further multiplied by 10 to obtain the energy-release in a star. The variation of number of stars with energy is deduced in the above way from the observations of cosmic ray stars at mountain altitude by Page (1950) and by Brown *et al.* (1949). These are also plotted in Fig. 6. From Brown's data, we have neglected stars accompanied by meson production (stars with thin tracks). In any case the omission did not appreciably affect the shape of the distribution. It may be seen that the distributions obtained from the measurements of both the authors are roughly in agreement with that obtained from the burst measurement of

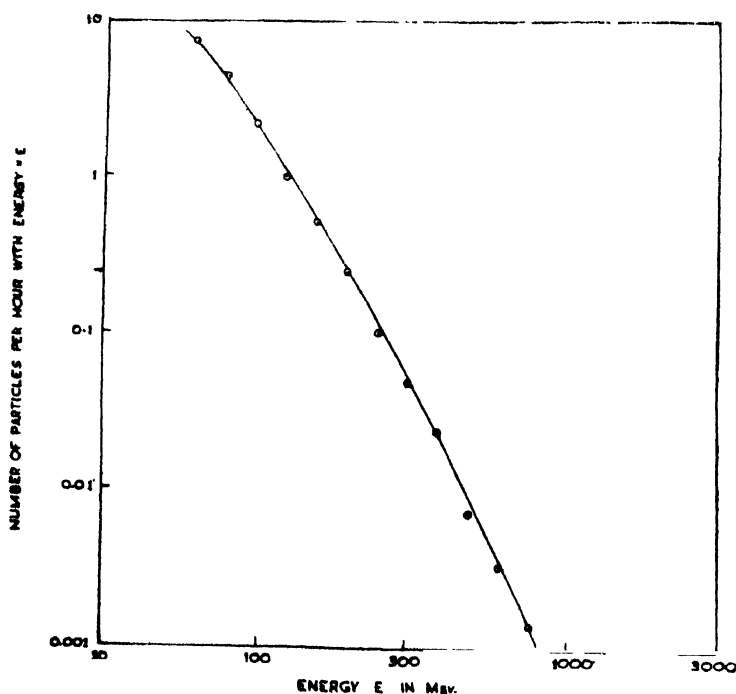


FIG. 7. ENERGY SPECTRUM OF BURST PRODUCING RADIATION

the present experiment, except in the region of low prong number. Taking into consideration the fact that the two measurements (that of bursts and of

tars) were taken at different altitudes and by completely different techniques, the agreement in Fig. 6 perhaps indicates that our approximate method of evaluating the kinetic energy cannot be very much in error.

The burst energy shown in Fig. 6 gives the total kinetic energy of the secondary particles emitted in the nuclear process leading to a burst. But this is not the total energy that is transferred by the incident cosmic ray particle to the struck nucleus; because, in addition to the kinetic energy, binding energy has also to be supplied in the process of emission of a particle. Since there is no way of directly recording the number of particles producing the ionization of a burst in an ionization chamber, we assume as we have done in case of stars in emulsion, that average kinetic energy ( $E$ ) of a particle emitted in a burst-process is 10 Mev. Then, the number of secondaries released in a burst is  $E/10$ , and assuming the binding energy per particle to be 8 Mev, we get the total energy (binding energy + kinetic energy) transferred in a burst to be equal to  $1.8E$ . Variation of number of bursts with this total energy is shown in Fig. 7. Assuming that the incident particle spends whole of its energy in producing the burst, Fig. 7 may be taken to represent the differential energy spectrum of the burst producing radiation. Within the energy-range under investigation, viz., from 50 Mev to about 1 Bev, this energy spectrum can be represented by a relation of the form :

$$N(E) = 240E^{(0.72-0.89 \log E)} \quad (4)$$

where  $N(E)$  is the number of particles with energy  $E$  Mev.

In this analysis we have made two assumptions. Firstly, we have assumed all the secondaries of a burst (or a star) process are protons. Actually, besides protons there will be  $\alpha$ -particles also. The presence of  $\alpha$ -particles may affect our calculations in two ways. (i) We have taken the kinetic energy of all the neutrons to be 1.15 times the measured kinetic energy of all the secondaries. Strictly speaking, we should have taken 1.15 times the kinetic energy of the protons only. (ii) We have assumed the binding energy of all the secondaries to be 8 Mev. This might lead to an overestimate of the total energy because the binding energy of  $\alpha$ -particles is of smaller value (about 4 Mev). Since  $\alpha$ -particles constitute only a small fraction of the total number of secondaries (in Brown's measurements, the ratio of the number of  $\alpha$ -particles to the total number of charged secondaries varies from 0.15 to a maximum of 0.3 only), the error involved is not perhaps serious. Secondly, we have taken the average kinetic energy of all secondaries to be equal to 10 Mev. But, as Brown *et al.* (1949) have shown, the average kinetic energy of a grey track is much greater than this; a grey track corresponds to a fast proton of energy greater than 30 Mev. In a burst, a fast secondary proton corresponding to a grey track in stars will have a range larger than the average path length of a particle (13 cm.) inside the gaseous volume of the chamber. Because of its higher energy, the fast protons will have low specific ionization so

that only a small fraction of its energy will be spent in producing ionization inside the chamber gas which may not be much different from 10 Mev. Thus we may conclude that in spite of the simplifications made, equation (4) (and the Fig. 7) represent the energy spectrum fairly well.

## REFERENCES

- Bridge, H. S., Hazen, W. E., Rossi, B. and Williams, R. W., 1948, *Phys. Rev.*, **74**, 1083.  
Brown, R. H., Camerini, U., Fowler, P., King, D. T. and Powel, C. F., 1949, *Phil. Mag.*, **40**, 862.  
Carmichael, H., 1948, *Phys. Rev.*, **74**, 1667.  
Carmichael H. and Steljes, J. F., 1955, *Phys. Rev.*, **99**, 1542.  
Coor, T., 1951, *Phys. Rev.*, **82**, 478.  
Montgomery, C. G. and Montgomery, D. D., 1949, *Phys. Rev.*, **76**, 1482.  
Montgomery, C. G., Montgomery, D. D. and Northrop, J. A., 1950, *Phys. Rev.*, **79**, 293.  
Nielsen, C. E., 1947, *Rev. Sci. Inst.*, **18**, 18.  
Page, N., 1950, *Proc. Phys. Soc.*, **A63**, 250.  
Rossi, B., 1948, *Rev. Mod. Phys.*, **20**, 537.  
Rutherford, E., Chadwick, J. and Ellis, C. D., 1930, *Radiations from radioactive substances*, Cambridge. p. 31.  
Simpson, J. A., Baldwin, H. W. and Uretz, R. B., 1951, *Phys. Rev.*, **84**, 332.



# EFFECT OF ELECTROLYTIC CURRENTS ON A CURRENT CARRYING CONDUCTOR

M. S. GAUR, G. P. BHATNAGAR, AND V. S. DUBEY

PHYSICS DEPARTMENT, MADHAV COLLEGE (VIKRAM UNIVERSITY) UJJAIN

(Received January 20, 1964)

**ABSTRACT.** Superimposition of electrolytic current on a current carrying conductor (Pt. Wire) is studied by keeping the heating currents constant. The effect has been found to be purely a change of potential difference across the two ends of the wire dipped in an electrolyte at constant temperature. This effect is not due to the change of resistance of the wire (i.e. due to change of temperature of the wire) but due to the point to point variation of current in the wire. The contention is supported by theoretical considerations, which are verified experimentally.

## INTRODUCTION

Effect of ionic currents (electrolytic bubbles) on heat-transfer was reported by Mixon and du pont (1959) to show that there is some lowering of the heat transfer at high electrolytic currents. Arjas and Legvold (1958) have studied a similar phenomenon in gases. Edkie, Rao and Gogate (1961) have reported in a note that at first there is a gradual rise in the heat transfer and then there is a sudden fall at high ionic currents. Bhand, Gaur and Gogate (1963) and Bhand, Patgaonkar and Gogate (1963) have investigated the effect in more details and have reported continuous curves of rise and then fall of the heat transfer coefficients with increase of electrolytic currents. In the curves for  $h/h_0$  against  $\log i$  ( $i$  being electrolytic current) using the same platinum wire at different temperatures, the maximas in all the cases seem to be present at about 100 mA. electrolytic current. In the other curves for different platinum wires also the maximas will be obtained at about 100 mA. of electrolytic current if current densities (currents per equal area of the surface) were considered. Due to these peculiar results and the reported analogy to the heat transfer in boiling liquids, in the present work these effects have been studied in greater details, the effect being reported upto 400 mA.

Using similar arrangements as by Bhand, Gaur and Gogate (1963) and taking a platinum wire of 0.015 cm. diameter; 15.2 cm. length and keeping  $\Delta\theta = 8.3^\circ\text{C}$  above the temperature of bath, the effect was observed upto 1000 mA. of electrolytic current. The effect is shown in Fig. 1.  $h/h_0$  reduces to almost zero at about 800 mA. of electrolytic current. If the electrolytic current is increased further the bridge remains unbalanced. In the observations reported by Bhand, *et al*, it is assumed that at lower electrolytic currents due to increase in the heat transfer the temperature and thus the resistance of the wire falls, which is then

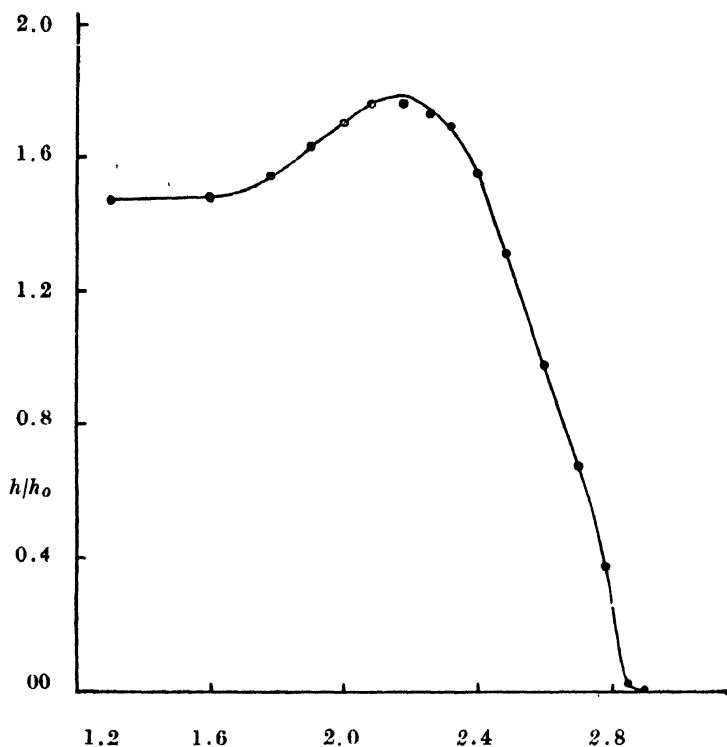


Fig. 1. Curve showing variation of  $h_1/h_0$  against  $\log i$  ( $i$  being the electrolytic current in mA)

brought back to its original value by increasing the heating current  $I$ . And that at higher electrolytic currents due to the presence of bubble formation on the platinum wire (Positive electrode) there is a blocked of heat flux and hence the temperature and thus the resistance of the platinum wire rises which is brought back to its original value again by decreasing the heating current  $I$ . In the observations (Fig. 1) the effect looks to be similar with a maxima at about 100 mA. of electrolytic current, but it is difficult to accommodate the increase in the resistance of the platinum wire to maintain its temperature at  $\Delta\theta = 8.3^\circ\text{C}$  above the bath temperature at nearly 800 mA. electrolytic current and on almost zero heating current. What kind of heat blockade could heat the wire when there is almost no heating current? These observations thus create a suspicion in the validity of the assumptions of the so-called fall or rise of the resistance of the platinum wire. Therefore, the problem has been restudied by keeping the heating currents constant and measuring the so-called actual fall or rise in the resistance of the platinum wire with the electrolytic currents.

#### EXPERIMENTAL

The experimental arrangement used is shown in Fig. 2 in which  $AB$  is the platinum wire dipped horizontally in a large tube full of an weak electrolyte and is surrounded by a co-axial cylinder; the weak electrolyte was just tap water

without adding any acid or alkali. The cylinder and the platinum wire form the two electrodes for the electrolytic circuit. The electrolytic current is fed

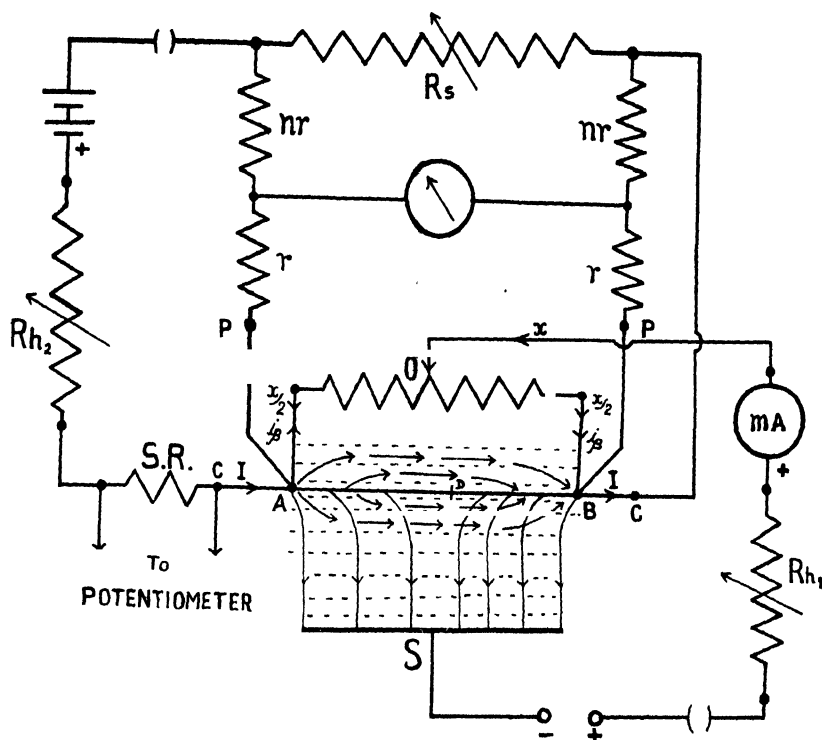


Fig. 2. Circuit diagram used for measurements.  $R_s$  is the calibrated resistance arm of the PYE Kelvin Bridge.

from a D.C. Generator through a certain tapping 0 of a high resistance of about 143 ohms put in parallel with the platinum wire. The D.C. Compound Generator used is G.E.C. F.2.A, which is run by a three phase A.C. motor and maintains constant voltage of 220V. upto 22.7 Amps. current. The required electrolytic current was adjusted and maintained constant with the help of a rheostat  $Rh_1$  in series with the generator. The platinum wire forms the unknown arm of the Kelvin's double bridge (Pye). The wire is heated by a current drawn from 12 volts Exide Batteries and is maintained constant with the help of a rheostat  $Rh_2$  in series. A standard resistance of 0.1 ohm in series measures the heating current flowing in the platinum wire by balancing the potential difference across its terminals on a crompton potentiometer. Thus, having the same experimental arrangement as used by previous workers (Bhand, Gaur and Gogate) the procedure adopted in this measurement was that the resistance of the heat transferring platinum wire was measured by keeping the heating acurrent constant.

For each measurement, firstly, for every electrolytic current and with no heating current, a balance was obtained in the bridge (no deflection in the galva-

nometer) by adjusting the tapping 0 of the shunting rheostats. This ensures that half of the electrolytic current enters at *A* and the other half at *B* each flowing on equal lengths of the platinum wire, keeping *A* and *B* at the same potential. Secondly, after removing the electrolytic current, heating current was adjusted to a particular value *I* and resistance *R* was measured. Lastly, the electrolytic current was put on and keeping the heating current constant the resistance *R<sub>i</sub>* was measured. Thus increase or decrease in the resistance  $\pm dR = (R_i - R)$  is known, the temperature of the bath was maintained at 20°C throughout the experiment. However by the end of the experiment in any set if there was a slight rise of temperature of the bath by 0.5°C or 1°C then *R* was corrected to  $R(1 + \alpha t)$  and thus *dR* was suitably corrected.

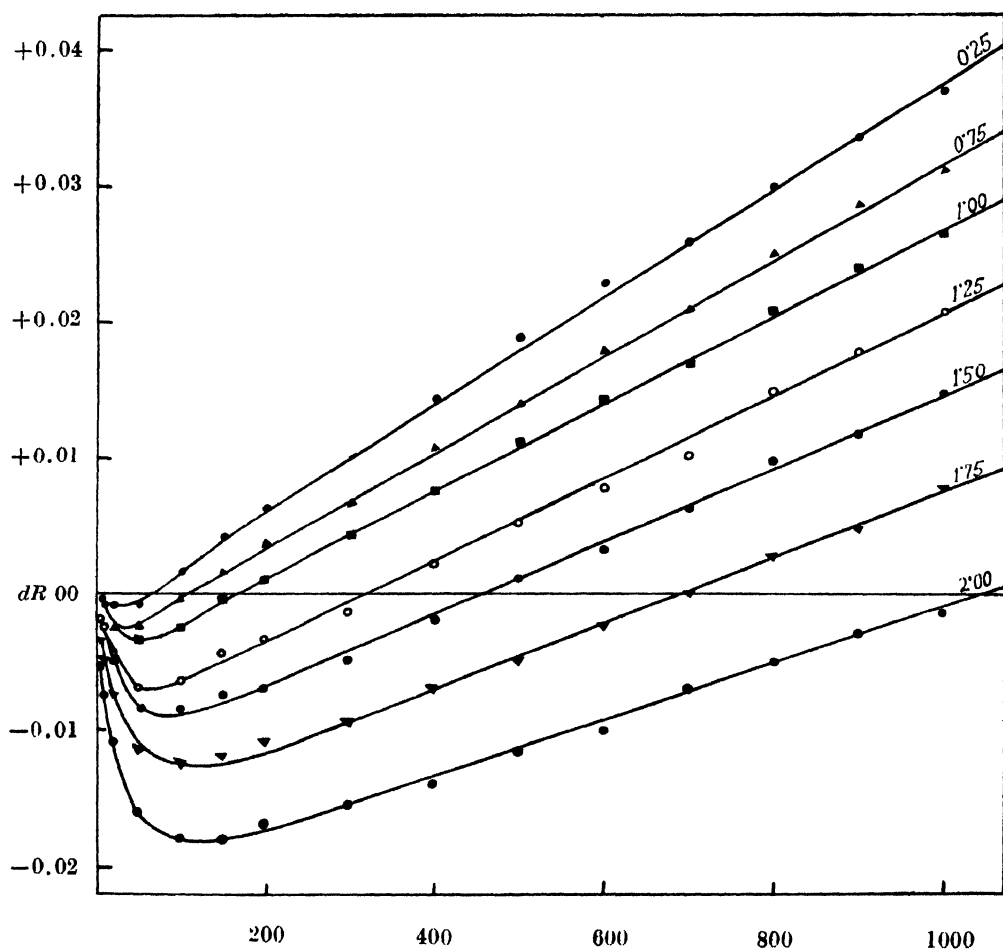


Fig. 3. Curves showing variation of  $dR$  in ohm with respect to electrolytic currents in mA. at different heating currents in amperes.

Fig. 3 shows the results obtained from these observations. The graph is a plot of  $dR$  with respect to different electrolytic currents (*x*) on each heating current from 0.25 amp. to 2.0 amp.

THEORETICAL CONSIDERATIONS AND  
INTERPRETATION OF RESULTS

From the simple considerations of the paths of heating currents  $I$  and electrolytic current  $x$  superimposed on it (see Fig. 2) it is quite clear that it is not the single current  $I$  which is flowing in the wire. Therefore, at any time to say that  $(R \pm Rd)$ , the measured value of the resistance from the bridge, is the resistance of the platinum wire, will not be true. It is of interest to note that  $I$  is the current entering at  $A$  and emerging at  $B$  the points at which the wire is connected to the Kelvin bridge. This is the necessary condition to obtain the balance in the bridge, that is, the bridge can be balanced if the currents in the known arm and in the leads of the unknown arm are equal. Hence it is clear that the balance of the bridge can be obtained for  $(R \pm dR)$ , the resistance in the known arm having a current  $I$ , when  $(R \pm dR)$ ,  $I$ , is the potential difference across  $AB$  even when the actual current flowing in the platinum wire may be distributed or different.

In the measurement of the resistance at a current  $I$  with no electrolytic current, it is assumed that the shunting resistance is large enough and hence the branching current  $i_\beta$  is negligible. However, for more accurate measurements if this need be considered, let  $r$  be the real resistance of the wire and  $R$  the measured value, then as  $(I - i_\beta)$  is the current flowing in the platinum wire, the potential difference across the wire  $AB$  will be

$$r(I - i_\beta) = RI$$

It may be further added that there will be some leakage of current in the electrolytic and, therefore, the whole current  $(I - i_\beta)$  will not be flowing in the platinum wire and hence there will be a further decrease of potential difference across  $AB$ . Let the leakage current with no electrolytic current be also included in  $i_\beta$  to raise it to  $i'_\beta$  then we have

$$r(I - i'_\beta) = RI;$$

or

$$r = R \left( \frac{I}{I - i'_\beta} \right) = R(1 + k)$$

where  $k = i'_\beta/I$  nearly constant for all values of  $I$ . Therefore a correction factor of  $(1 + k)$  will have to be applied to all the values of  $R$  for the determination of  $r$ .

To evaluate the potential difference across the platinum wire a point to point current will have to be considered in the wire due to superimposition of the electrolytic current on  $(I - i'_\beta)$  current in place of current  $I$ . Let  $x$  be the electrolytic current, then  $x/2$  will be the current entering at  $A$  and  $x/2$  at  $B$ . Because the potential of the  $A$  side of the wire will be higher than the potential of the  $B$  side due to the heating current it is evident that the  $A$  side length  $l_1$  along which half the electrolytic current  $x/2$  flows varying from  $x/2$  to 0 will be greater than the

$B$  side length  $l_2$  where it varies again from  $x/2$  to 0 from the end  $B$ . Thus there is a point to point variation of the current from  $\left(I - i'_\beta + \frac{x}{2}\right)$  to  $\left(I - i'_\beta - \frac{x}{2}\right)$ .

Therefore the total potential difference across  $AB$  due to this effect

$$= \sum_0^{l_1} \sum_{x/2}^0 d\rho i + \sum_0^{l_2} \sum_0^{-x/2} d\rho i \left[ \begin{array}{l} i = \text{current at any point on the wire} \\ \rho = \text{resistance per unit length of the wire} \end{array} \right]$$

$$= \sum_0^{l_1} \sum_{i'=-x/2}^{i'=0} d\rho (I - i'_\beta + i') + \sum_0^{l_2} \sum_{i'=0}^{i'=x/2} d\rho (I - i'_\beta + i')$$

$i' =$  the effective electrolytic current at any point in the wire]

$$= l_1 \rho (I - i'_\beta) + \frac{l_1 \rho}{2} \cdot \frac{x}{2} + l_2 \rho (I - i'_\beta) - \frac{l_2 \rho}{2} \cdot \frac{x}{2}$$

$$= (l_1 + l_2) \rho (I - i'_\beta) + \frac{l_1 - l_2}{2} \rho \cdot \frac{x}{2}$$

$$= \gamma (I - i' \rho) + \frac{l_1 - l_2}{2} \rho \cdot \frac{x}{2}$$

$$= RI + \frac{l_1 - l_2}{2} \rho \cdot \frac{x}{2}$$

In addition there will be a decrease of potential on application of electrolytic current due to increase in the leakage of the heating current through the electrolyte. Let it be a factor  $C$ , a function of heating current  $I$  and resistance of the wire. The factor  $C$  will increase with the increase of  $x$  due to increase in the conductivity and may become almost constant after attaining a maximum value at some value of the electrolytic current.

The overall potential difference across  $AB$  is

$$RI + \frac{l_1 - l_2}{2} \rho \cdot \frac{x}{2} - C(I).$$

To summarise the assumptions are :

1. No change in the resistance of the wire due to the introduction of electrolytic current.
2. Marked effect is due to the change of potential difference due to the variation of point to point current in the wire.
  - (a) Due to the superimposition of electrolytic current  $x/2$  to 0 along the length  $l_1$  and 0 to  $-x/2$  along the length  $l_2$ .
  - (b)  $l_1 > l_2$
  - (c) Increase in the leakage of current through the electrolyte will decrease the potential by a factor  $C(I)$ .

- (d) The factor  $C(I)$  will increase with the increase of  $x$  and may become almost constant after attaining a maximum value. Thus

$$(R+dR)I = RI + \frac{(l_1-l_2)}{2} \rho \frac{x}{2} - C(I);$$

or, 
$$dRI = \frac{l_1-l_2}{2} \rho \frac{x}{2} - C(I)$$

Let  $(l_1-l_2) = 2\Delta l$ ; [ $\Delta l$  being the distance of the bifurcating point  $D$ , from the middle point of the platinum wire.]

Then

$$dRI = \Delta l \frac{\gamma}{L} \frac{x}{2} - C'(I), \text{ where } \rho = \frac{\gamma}{L}, L \text{ being the length of the platinum wire;}$$

or, 
$$\frac{dR}{\gamma} = \frac{\Delta l}{2L} \cdot \frac{x}{I} - C''(I), \text{ where } C'(I) = \frac{C(I)}{\gamma I}$$

This deduction is very well demonstrated by the graphs drawn between  $dR$  and  $x$  (see Fig. 3) when

$$\frac{\Delta l}{2L} \cdot \frac{x}{I} < C''(I), \text{ } dR \text{ is negative;}$$

$$\frac{\Delta l}{2L} \cdot \frac{x}{I} = C''(I), \text{ } dR \text{ is zero;}$$

and when  $\frac{\Delta l}{2L} \cdot \frac{x}{I} > C''(I), dR$  is positive.

$\Delta l$  seems to be the property of the ratio of the potentials of points  $A$  and  $B$  with respect to the cathode cylinder and hence  $\Delta l$  will go on decreasing and may become nearly constant at higher electrolytic currents when potentials of  $A$  and  $B$  with respect to the cylinder are large.

The leakage fraction  $C''(I)$  increases with the increase of  $x$  due to the increase of the conductivity of the electrolyte and attains a maximum value (say at about 100 mA. of electrolytic current) and then becomes almost constant.

This effect is very clearly brought out in the experimental curves (Fig. 3) giving an increase of dip in the negative sector. and as soon as both the factors  $\Delta l$  and  $C''(I)$  become constant a straight line portion of the curve is obtained which satisfies the equation

$$\frac{dR}{r} = \frac{\Delta l}{2L} \cdot \frac{x}{I} - C''(I), \text{ for } dR \text{ and } x.$$

The values of  $\Delta l$  and  $C'(I)$  are calculated for different currents from the straight line portions of the curves and are shown in Table I.

TABLE I

Values of  $\Delta l/2L$  and  $C'(I)$  for different heating currents.

No.	Heating current $I$ in amperes	$\Delta l/2L$	$C'(I)$
1.	0.25	0.009	0.0024
2.	0.75	0.025	0.0038
3.	1.00	0.030	0.0056
4.	1.25	0.035	0.0090
5.	1.50	0.037	0.0116
6.	1.75	0.039	0.0159
7.	2.00	0.041	0.0215

Both the factors  $\Delta l/2L$  and  $C'(I)$  are found to be increasing with the increase of the heating current  $I$ . They do not give any simple relationship with the heating current or electrolytic current which shows that the relations are quite complex.

#### RESULTS AND CONCLUSIONS

(1) When an electrolytic current is applied on a heated platinum wire through a central tapping  $\theta$  in a shunt resistance there is no change in the resistance of the platinum wire.

(2) The effect is purely a change in the potential across the platinum wire. The change is due to the addition of two factors :

(a) Electrolytic current does not flow on equal portions from the two ends of the platinum wire, resulting in an increase of potential difference proportional to  $\Delta l$ . This factor  $\Delta l$  decreases with the increase of the electrolytic current and then becomes constant.

(b) Decrease of potential difference due to the leakage of current through the electrolyte by a factor  $C'(I)$ . This factor  $C'(I)$  increases with the increase of the electrolytic current and then becomes constant.

(3) The constant values of  $\Delta l$  and  $C'(I)$  both are found to be increasing with the increase of the heating current  $I$ .

These results, therefore, conclusively go to show that the superimposition of the electrolytic bubble formation causes no decrease and/or increase of the resistance of the platinum wire. Therefore, there is no adequate evidence to show that there is any marked effect of change in the heat transfer from the heated



platinum wire as reported by the previous authors (Bhand, Gaur and Gogate, 1963).

#### ACKNOWLEDGMENT

The authors wish to thank Dr. Shiv Mangal Singh 'Suman', Principal, Madhav College, Ujjain for providing all the facilities for carrying out the work. Thanks are also extended to Shri P. S. Kale, Asstt. Professor and in-charge of the department of Physics, Madhav College, Ujjain. They are grateful to Dr. G. L. Datta, Vice-Chancellor and Dr. D. V. Gogate, Prof. and Head of the Physics Department, Vikram University, Ujjain, for inspiration and constant encouragement in the work. The authors are also grateful to Prof. S. D. Chaubey, Principal K. P. College, Dewas for helpful discussions.

#### REFERENCES

- Arjas and Logvold, 1958, *Jour. Chem. Phys.*, **29**, 3.  
Bhand, S. C., Gaur, M. S. and Gogate, D. V., 1963, *Ind. Jour. Phys.*, **37**, 19, 185.  
Bhand, S. C., Patgaonkar, G. V. and Gogate, D. V., 1963, *Jr. Sci. and Industri. Res.*  
Edkie, R. G., Rao, R. D and Gogate, D. V., 1961, *Jr. Sci. and Industri. Res.* **20**3, 548.  
Mixon, F. O. and du Pont, E. L., 1959, *Chem. Engg. Progr.*, **55**, 49.

# Letters to the Editor

*The Board of Editors does not hold itself responsible for opinions expressed in the letters published in this section. The notes containing short reports of original investigations communicated to this section should not contain many figures and should not exceed 500 words in length. The contributions reaching the Secretary by the 15th of any month may be expected to appear in the issue for the next month. No proof will be sent to the author.*

21

## ON NUCLEAR EXCITATION AND FORMATION ENERGIES IV

A. K. DUTTA, B. PAL, P. GANGULY and D. BANERJEE

PALIT LABORATORY OF PHYSICS, CALCUTTA UNIVERSITY, 92 ACHARYYA PRAFULLA CHANDRA ROAD, CALCUTTA-9.

(Received September 2, 1964)

It has been shown in the previous communication-III (Dutta and others, 1964) that the binding energy of weakly bound nuclei is measured in terms of the deviation in energy from the isobaric nucleus, with optimum energy and neutron content, caused by one or more neutron proton exchanges, in accordance with the relation,

$$E = E_0 - \beta(N - N_0)^2 - E_0 - \beta\{N - N_0 + \eta(\Delta N)\}^2, \text{ where,} \\ E_0 = B(A) + F(I) + F(Z) = B(A) + a_z \cos \pi f(Z) + a_1 \cos \pi f(I).$$

The neutron proton exchange energy  $\beta$ , may be ascertained directly from the binding energy data (Konig *et al.* 1962) by relation (c), as shown in the previous communication III. It has also been found that the  $\beta$  values for different mass members are composed of two parts — one dependent on  $A$  only and the other dependent primarily on the periodically varying potential energy curve  $F(Z)$  and also on  $F(I)$ , to some extent. The strong enhancement of  $\beta$  values at the minima of the  $F(Z)$  potential curve and a decrease at the maxima, makes the behaviour of neutron proton exchange energy  $\beta$  similar to the expected change for the general process of excitation energy. As such it was considered worthwhile to compare the  $\beta$  values with the excitation energies of the nuclei. It was recognised that on account of the fundamental difference in odd mass and even mass nuclear structure, the excitation energies for them should be studied in separate groups. We have taken the 1st and 3rd excitation energies for the most strongly bound odd and even mass nuclei, (Nuclear data sheets, 1962), as a first step, and have plotted them alongside the  $\beta$  values, against a mass number scale,

The similarity of all the excitation energies with the  $\beta$  values, both in respect of their dependence on  $A$  as also in respect of their dependence on the periodic potential energy curves is evident from Fig. 1, and may be regarded to be of significance.

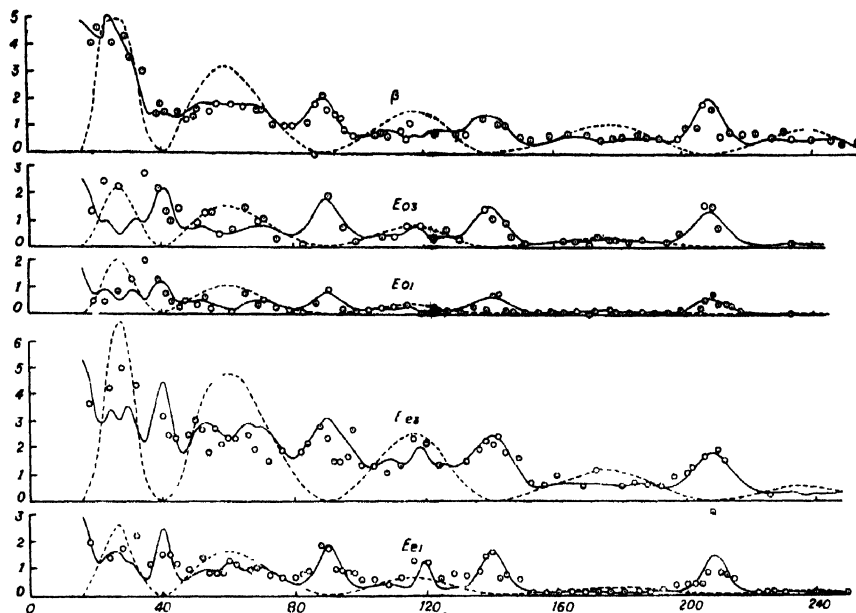


Fig. 1

In view of the close resemblance of the curves for the excitation energies and the neutron proton exchange energies against mass numbers, we may describe them by a general form of relationship, as

$$\begin{aligned}
 E_i &= \epsilon_i(A, f(Z)) + \epsilon_i(A, A_z, \min) - \epsilon_i(A, A_z, \max) + \epsilon_i(A, A_1, \min) \\
 &= (a_0 + b_0 e^{-\alpha_0 A})(1 + \cos \pi f(Z)) + (a_1 + b_1 e^{-\alpha_1 A})e^{-k_1 \alpha_z (A - A_{1, \min})^2} \\
 &\quad - (b_2 e^{-\alpha_z A})e^{-\alpha_z (A - A_{z \max})^2} + \sum_j c_j e^{-\gamma_j (A - A_j)^2}
 \end{aligned}$$

The values so calculated and the experimental values are shown in Fig. 1. Here, the suffix  $i$ , stands for the character of excitation, e.g., even 1, odd 3,  $\beta$  ( $\Delta N = 1$ ), etc.;  $A$ ,  $f(Z)$ ,  $A_z \min$  etc. in the paranthesis indicate the dependence of energy on  $A$ ,  $f(Z)$  and the maxima or minima positions of the  $f(Z)$  function in mass numbers. It also depends on  $\alpha_z$ , the amplitude of the  $F(Z)$  function at the minima positions, for the  $\beta$  values. In the case of  $\beta$  values for  $\Delta N$  different from 1, all components except  $(a_0 + b_0 e^{-\alpha_0 A})$ , the  $A$  dependent part, is to be multiplied by the factor  $\sigma$ , where

$$\sigma(\Delta N) = 0.6 + 0.6 \tanh(1.6 - 0.8 \Delta N),$$

the same relation as obtained before.

The constant  $a_0 = 0$ , except for  $\beta$ , where it obtains the magnitude 0.425, the constants  $b_1$  and  $\alpha_1$  are the same as  $b_0$  and  $\alpha_0$  except for  $\beta$ , where the factor  $(a_1 + b_1 e^{-\alpha_1 A})$  is replaced by  $0.125a_2$ ; the constant  $\alpha_2$ , determining the shape of the Gaussian distribution of energy at the maxima and the minima positions of the  $f(Z)$  function is of magnitude  $40/(\Delta T)^2$ , in all cases, where  $\Delta T$  is the complete period in mass number scale at the respective minima and maxima positions of the  $f(Z)$  function. The  $A_j$  values replacing  $A_{1, min}$  are contributing at some minima only and are slightly displaced from the minima positions. The remaining constants, which vary, are given in the tabulated form below:—

TABLE I  
Constants for  $\beta$  and excitation energies

$E_i$	$b_0$	$a_0 \times 10^2$	$a_1$	$k_1$	$b_2$	$a_2 \times 10^2$	$C_1$	$C_2$	$\gamma_i$	$A_1$	$A_2$
$E_{01}$	1.6	1.800	0.5	2.5	2.21	1.443	0.30	0.15	.074	115	176
$E_{03}$	1.5	1.171	1.3	2.0	2.44	1.421	0.50	0.2	.154	117	178
$E_{01}$	2.0	1.555	1.4	3.125	1.38	1.097	0.45	1.0	.167	61	119
$E_{03}$	4.7	1.138	1.4	1.25	4.78	1.180	0.0	0.92	.167	61	118
$\beta(\frac{\Delta N}{-1})$	3.64	1.950	0.0	2.0	2.16	0.723	4.53	0.0	.002	0	0

The expression for  $\beta$ , as stated now, changes the form of representation of its magnitude, used in communication III, before. Along with it, we also modify the analytical expressions for some of the components of  $E_0$ , namely  $f(Z)$ ,  $a_1$  and  $\phi$ , to obtain the different contributory parts of  $E_0$  in a more regular shape. The expressions for the components of  $E_0$  and thus of the binding energies of all nuclei, may be put as follows. The expression for  $N_0$  remains unaltered.

Relations :

$$B(A) = -9.828A + 8.877 \times 10^{-3} A^2 + C_{ij} \text{ mev.}$$

$$C(ee) = 32.2; C(e_o o_e) = 33.0; C(oo) = 34 + 80A^{-1} \quad \dots (1)$$

$$\begin{aligned} N_0^* &= 0.6302A - 0.1287A \exp(-7.95 \times 10^{-3} A) - .00155A \\ &\times \cos \pi \{0.794 \sinh .0372(A - 104)\} \{1 - \tanh .6(A - 45)\} \\ &\times \{1 - \tanh .6(A - 145)\} \end{aligned}$$

$$\eta(\Delta N) = 0.1 |N_0^* - N| - 0.1 \quad \dots (2)$$

$$\begin{aligned} f(Z) &= -.051 + 0.0339A - 2. \exp -1.18 \times 10^{-3} A^2 + 0.311 \exp -2.25 \times 10^{-3} \\ &\quad (A - 144)^2. \end{aligned}$$

$$a_z = 10.9 - 2.9 \{ \sin \pi 0.5 f(Z) - \sum_i \exp -\alpha_i (A - A_i(F_z \text{ min}))^2 \}; \left[ \alpha_i = \frac{200}{T^2} \right]$$

$$a_1 = 10 - 3 \sin \pi \{ \tanh \alpha_1 (A - 116) \}; \quad [\alpha = .013] \quad \dots (3)$$

$$\phi = 1.052 + .088 \sin \pi (\exp \gamma A);$$

$$\gamma_i = \begin{cases} 6.196 \times 10^{-3}, & A < 170 \\ 6.836 \times 10^{-3}, & A > 170 \end{cases}$$

$\beta$  — as described above.

The graphical representation of  $B(A)$ ,  $F(Z)$  and  $F(I)$  are shown in Fig. 2.

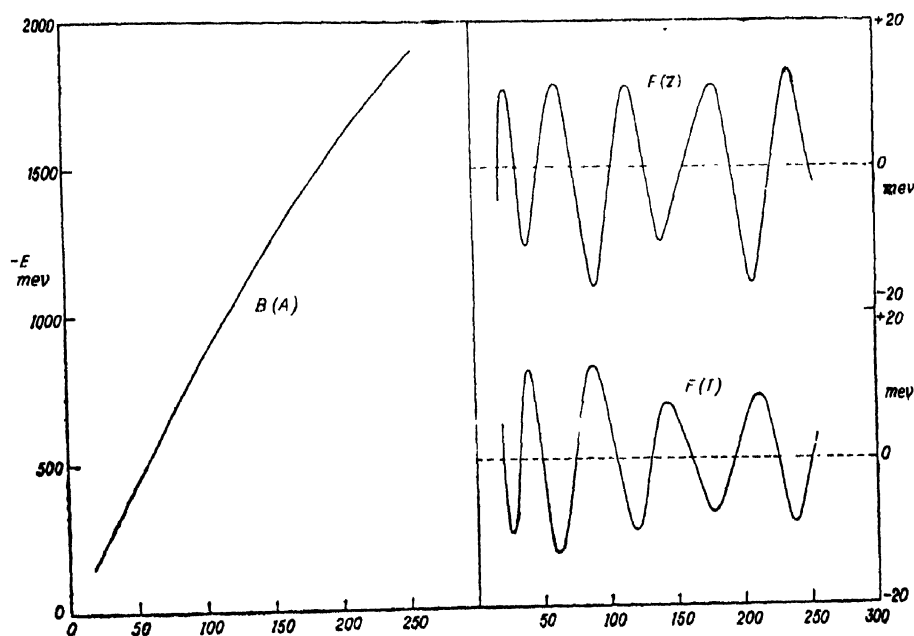


Fig. 2.

#### REFERENCES

- Dutta, A. K., Pal, B., Ganguly, P. and Banerjee, D. 1964, *Ind. J. Phys.*, **38**, 57.  
 König, L. A., Mattauch, J. H., Wapstra, A. H., 1962, *Nuclear Phys.*, **31**, 18.  
 Nuclear Data Sheets (1962), National Academy of Sciences, National Research Council, Washington, D.C.

# NUCLEAR ENERGY AND NUCLEAR CHARACTERISTICS (V)

A. K. DUTTA

PALIT PROFESSOR OF PHYSICS, CALCUTTA UNIVERSITY

92, ACHARYYA PRAFULLA CHANDRA ROAD, CALCUTTA-9.

(Received September 28, 1964, )

In a set of previous communications, I, II, III, IV (Dutta and others, 1963, 1964), we have analysed the formation and excitation energies of nuclei, available from the recent compilation works (Konig and others, 1962; Nuclear Data Sheets, 1962), and have found smooth relationships, to obtain the required magnitudes, to a fairly close approximation. The formation energy of nuclei, with optimum energy for any mass number, have been obtained by the combination of a basic curve of quadratic form in  $A$ , superposed by two periodic curves  $F(Z)$  and  $F(I)$  in nearly opposite phase. The deviation in energy of weakly bound isobaric nuclei is determined in terms of  $\beta(\Delta N)^2$ , i.e.  $\beta(N - N_0)^2$ , where  $\beta$  is the neutron-proton exchange energy and  $N_0$  is the optimum neutron number for a mass number. These values can be calculated from available binding energy data, as shown in relations (c), and (d), in III. Since the fluctuation in optimum energy from a smooth quadratic relationship, never surpasses the magnitude of about 10 mev., in the whole range from -80 to -1800 mev., it is considered that such splitting up of the total energy into components is imperative, unlike the process implied in "one particle model". Weizsacker (1938) had suggested that in nuclear energy study, one should understand the deviation from the smooth course indicative of a liquid drop model. The collective nuclear model (Bohr and Mottelson 1953) also realises the importance of the basic liquid drop contribution.

Of the two potential energy curves  $F(Z)$  and  $F(I)$  shown in Fig. (2), IV, the potential curve  $F(Z)$  primarily determines the energy of formation of weakly bound nuclei, as also the excitation energy, through close association of the obtained relations, with the maxima and minima positions of the curve  $F(Z)$ . Since the immediate determining factors in any transition, are the involved state functions, controlled mainly by the charge distributions, we have stamped the associated curve as  $F(Z)$ . The only other possible variable parameter for the associated periodic curve could be (I), the excess neutrons, which should determine the shape of the nuclei. The close correlationship of  $F(I)$  with shape would be apparent from the fact that the quadrupole moment maxima are generally placed

at the minima of the  $F(I)$  curve. This would be elaborated further, later. It is also, to be realised on these grounds, that the energy change to the  $F(Z)$  curve is immediate, followed by a deferred redistribution, corresponding to excess neutrons or shape, determined by the  $F(I)$  function.

The minima positions of the controlling  $F(Z)$  curve, in mass numbers, occur at 16, 40, 90, 140 and 208, corresponding to neutron-proton numbers as 8-8, 20-20; 50-40, 82-58, and 126-82. They correspond to the magic numbers of the shell model, 8, 20, 50 and 82 neutrons or protons, except that the proton number 50, corresponding to a mass number of about 118, is not a minimum of the  $F(Z)$  curve. It is, on the contrary, the position of a maximum, along with the mass numbers 27, 60, 177 and 235. The absence of a shell closure or strong binding near 50-protons is corroborated on other considerations as follows :

When one observes the excitation energies of odd-mass nuclei (fig. 1, IV), it would be noted that all excitation energies jump up to large magnitudes at all other shell closure positions, except at 50-proton positions. The excitation energies of even-even nuclei also obtain subdued excitation energies in this region, compared to other shell closure positions. Absence of a shell closure at 50 protons is thus indicated. Already studied thermal (Flowers 1952) or fast neutron (Hughes *et al.*, 1953) cross sections against neutron numbers point to the same direction. The plottings of deviations from Bethe-Weizsacker relation (Green, 1958) strongly confirms weak binding near 50 protons, in contrast to strong binding at 50 and 82 neutrons and 82 protons.

Further, the very obstinate nature of assymmetric nuclear fission finds an easy explanation now, as the mass number in the region of 120, is a maximum of the periodic curve  $F(Z)$  and thus would not be favoured for a transition. Indeed, Fong (1953, 1956) corrects the nuclear mass relation of symmetric fission product nuclei, such that it is less strongly bound than the assymmetric fission product nuclei, and proceeds to justify the assymetry on shell model. Hill and Wheeler (1953), however, rules out the possibility of explanation on shell basis and proposes assymetry on hydrodynamic consideration. As we have just noted, symmetric and assymmetric fission products follow automatically on the basis of  $F(Z)$  potential curve. It is also clear that the symmetric fission products, with a higher energy level, would be favoured with high excitation energies, as obtains in the case of dissociation of molecules, with constituents associated with excited energy.

Moreover, the argument of measured isotopic abundances in favour of magic numbers, when properly read, goes against the idea of 50-proton nuclei as being near a strongly bound position. One observes that the maximum of isotopic abundance generally tends to move to higher neutron-number isotopes as one moves to heavier elements, except that at the shell closure positions, even the lightest isotope obtains the largest abundance. It indicates the large probability

of transition to these nuclei, on account of their low potential energy. Thus, the nuclei  $^{18}\text{A}^{40}(99\%)$ ,  $^{20}\text{Ca}^{40}(97\%)$ ,  $^{38}\text{Sr}^{88}(83\%)$ ,  $^{40}\text{Zr}^{90}(52\%)$ ,  $^{56}\text{Ba}^{138}(72\%)$  and  $^{58}\text{Ce}^{140}(88\%)$ , the heaviest and lightest isotopes of the two elements grouped together, obtain the large abundances shown, on account of their shell closure positions, while  $^{50}\text{Sn}^{120}$  obtains only 30% abundance and  $^{52}\text{Te}^{120}$  is rare (Kaplan, 1963). It does not favour any strong transition probability near mass number 120 with about 50 protons.

Further, on account of the close relationship (Dutta *et al* IV) between neutron-proton exchange energy  $\beta$ , with the excitation energy and hence also with the ionisation energy of nuclei, one would consider that the mass numbers on the maximum of the  $F(Z)$  curve, which are weakly bound, particularly when  $\beta$  value itself is low, should have fewer isobaric nuclei. This is corroborated by very few isobaric nuclei in the region of mass number 155 to 200, around  $F(Z)$  maximum at 177. At the shell closure regions, corresponding to mass numbers 16, 40, 90, 120, 140 and 208, the average numbers of tabulated (Konig, *et al*, 1962) nuclei are respectively 3.5, 4.5, 5.5, 3.5, 5.5, 5, respectively. The number of isobaric nuclei near mass number 60 another  $F(Z)$  maximum position is also 3.5. It points out again proton-50 nuclei as not in strongly bound region.

The reason for considering proton 50 region as shell closure, is primarily the large number of stable isotopes, for the elements with charge values near 50, corresponding to mass numbers 115 to 135. Since the most strongly bound nuclei of any mass number is measured in terms of the smallness of the expression  $\beta(\Delta N)^2$ , it is apparent that if the rate of variation of  $N_0$  is nearly as high as the rate of variation of  $N$ , for successive mass numbers, an element would remain in the nearly optimum condition of energy for a series of mass numbers, giving a large number of isotopes. The increase in the calculated values of  $N_0$  with mass number may be obtained by relation (d, III). It is observed that the rate of increase of  $N_0$  is approximately 0.4, 0.8, 0.4 and 0.6, near about the mass numbers 90 ( $N = 50$ ), 118 ( $Z = 50$ ), 138 ( $N = 82$ ) and 208 ( $Z = 82$ ). The average number of stable isotopes in these regions are 5, 9, 5 and 4, in accordance with expectation. The number of isotopes is thus, not a criterion of strongly bound condition, unless the large value for the rate of change of  $N_0$  can be considered to be a criterion for that and this evidently it is not, according to the above. The rate of increase of  $N_0$  is actually determined by structural development.

The difficulty of the shell model, in view of the uncertainty of the 50-proton shell closure as also in view of the unsatisfactory explanation of magnetic and quadrupole moments, cannot be avoided by switching over to the collective nuclear model (A. Bohr and Mottelson 1953). Its correlation of excitation of even-even nuclei with the rotational energy expression, in the range of mass numbers 150 to 190, definitely fails for the nuclei  $^{64}\text{Gd}^{152}$ ,  $^{74}\text{W}^{180}$ , and  $^{78}\text{Pt}^{190}$ , in a systematic fashion. They are weakly bound even-even nuclei in this region by



the criterion of  $\beta(\Delta N)^2$  magnitude, and obtains a drop from the ratio of 3.3 for 2nd and 1st excitation energies to less than 2. This suggests explanation for the change in excitation energies here, to other causes than the change in rotational quantum numbers. A new orientation in the ideas about the structural development, is, thus necessary.

To understand the process of growth of nuclei, we note that the half periods of the periodic function  $F(Z)$ , mentioned before occur at steps of  $Z_0$  values, which remain roughly constant at about 10.5 units of charge after two initial lower steps at mass numbers 16 and 40. Such small and nearly constant half period values of nuclear charge could not be accounted for by any form of evenly distributed neutrons and protons at appropriate distances, over continuously increasing size of nuclei. It compels one to suggest that the growth in nuclear structure should be in the form of quasi-crystalline development, with variable units to increase the size during a period of growth, gradually.

Such a process of growth is also envisaged by Wigner's (1933) ideas on the short range nuclear force. It had been suggested by Wigner and emphasised by Weizsacker (1938) and others that the rapid rise in bindings energy per nucleon of  $2\text{He}^4$  from that of  $1\text{H}^2$ , through the nuclei  $1\text{H}^3$  and  $2\text{He}^3$  is on account of the increase in bonds between nucleons and the consequent closeness of internucleonic distance. Such large binding energy per nucleon as in  $2\text{He}^4$  obtains again at  $4\text{Be}^8$  and then from  $6\text{C}^{12}$ , onwards. The intervening nuclei from  $2\text{He}^4$  upto  $6\text{C}^{12}$ , except  $4\text{Be}^8$  have much lower binding energies per nucleon and must possess a more open structure, with less bonds per nucleon. The increase in binding energy of  $2\text{He}^4$ ,  $4\text{Be}^8$ ,  $6\text{C}^{12}$  and onwards, would then be on account of doubling up character, such that the bonds per nucleon are increased. Nuclei like  $6\text{C}^{13}$ ,  $7\text{N}^{14}$ ,  $8\text{O}^{17}$ , which also obtain large binding energies per nucleon could be considered as doubling up of known nuclei, such that symmetry of structure is also maintained.

For further growth and maintenance of symmetry we could always consider the even-even nucleus as doubled up structure of two groups, as in  $2\text{He}^4$  and  $4\text{Be}^8$  and an odd mass nucleus as a composition of three groups of nuclei, generally, held by internucleonic bonds. The nucleons in each group could also obtain spinning and orbital motion, on account of exchange of neutrons and protons to give the nucleus a liquid drop character.

Group formation as a recourse to the explanation of short range forces was suggested by Wefelmeyr (1937) and Fano (1937), in the form of an  $\alpha$ -particle model of solid crystal type. Weizsacker (1938) had brought out the comparative advantages, of such model over one particle model. It was also proposed by Wheeler (1937) and rejected by him (1941), on account of some obvious inconsistencies. A larger nucleus is not likely to be built up with strongly bound units like  $\alpha$ -particle, of nonflexible nucleonic content. The inconsistencies are often

on account of that. It is more reasonable to build up larger nuclei with a nucleonic composition of 3, 4 and 5 units of charge and associated neutrons, which are all weakly bound, ( $4\text{Be}^8$  would have been also weakly bound, if it were an open structure and not double up) and satisfy group association through internucleonic bondages, unlike the schemes with  $\alpha$ -particles as interacting entities.

Such building up process gives us the cohesive forces of the proper order of magnitude also (Dutta *et al* 1962). This limitation in size of the small units helps us in understanding the periodic structure, through a process of rearrangement that keep the nucleons always compact and hence nearer the spherical shape. Such a process of structural growth also helps us in understanding the correlation between nuclear orbital and magnetic moments as also the quadrupole moments. This will be discussed in the following communication.

#### REFERENCES

- Bohr A. and Mottelson B. R. 1953, *Kgl. D. V. Selskab Mat fys* **27**, No. 16  
 Dutta A. K., I, 1963, *Ind. J. Phys.* **37**, 183.  
 Dutta A. K., Pal B., Ganguly P., Banerjee D., II, 1963, *Ind. J. Phys.*, **37**, 543.  
 Dutta A. K., Pal B., Ganguly P., Banerjee D., III, 1964, *Ind. Phys.*, **38**, 57.  
 Dutta A. K., Pal B., Ganguly P., Banerjee D., IV, 1964, *Ind. J. Phys.*, **38**, 519.  
 Dutta A. K., Pal, B., Das Gupta, A., Chaudhury, N., 1962, *Ind. J. Phys.*, **36**, 497.  
 Fano, V. 1937, *Naturwiss* **25**, 602.  
 Fong P. 1953, *Phys. Rev.* **89**, 332.  
 Fong P. 1956, *Phys. Rev.* **102**, 434.  
 Green, A. E. S., 1958, *Rev. Mod. Phys.*, **30**, 569.  
 Hill, D. L. and Wheeler, A. H. 1953, *Phys. Rev.* **89**, 1102.  
 Hughes, D. J., Garth, R. C., Levin J. S., 1953, *Phys. Rev.* **91**, 1423.  
 Kaplan, I. Nuclear Phys. Addison Wesley Pub. Co. 1963, p. 210.  
 Konig, L. A., Mattauch J. H., Wapstra, A. H., 1962, *Nuclear Phys.*, **31**, 18.  
 Nuclear data sheets 1962, National Acad. Sci., Washington.  
 Weizsacker, von, C. F. V. 1938, *Naturwiss* **26**, 209, 255.  
 Wefelmeyer, W. 1937, *Naturwiss* **25**, 525.  
 Wheeler, A. H., 1937 *Phys. Rev.* **52**, 1083.  
 Wheeler, A. H., 1941 *Phys. Rev.* **59**, 16, 27.

# ON NUCLEAR STRUCTURE AND NUCLEAR MOMENTS (VI)

A. K. DUTTA

PALIT PROFESSOR OF PHYSICS, CALCUTTA UNIVERSITY,  
92, ACHARYYA PRAFULLA CHANDRA ROAD, CALCUTTA-9.

(Received September 28, 1964).

Nuclear moments which are determined by the structure of the nuclei, should give us, ultimately, the proper form of nuclear structure, when the magnitudes of these moments and their interrelations are clearly understood. In view of the accuracy of the experimental results, a suitable theory should approach the measured values closely. It is well known that the total orbital moments of the nuclei or their  $i$ -values are more or less in accordance with the shell model. Indeed the shell model is based on these measured  $i$ -values and the magic numbers and the agreement is expected. Even, then, there are disagreements of some experimental  $i$ -values (Strominger *et al.*, 1958) with the allowed values proposed initially in each group. The already known moments of the nuclei  $F^{19}$ ,  $Na^{23}$ ,  $Mn^{55}$  and the more recently determined moments of  $Ne^{21}$ ,  $Ti^{47}$ ,  $Se^{79}$ ,  $Hf^{179}$  contradict the allowed values, with an agreement for 3 out of 6 measured values in  $2d_{5/2}$  shell, upto now. Further, the interrelation between the orbital and magnetic moments expected on shell theory, on the basis of Schmidt model (Schmidt, 1937) is not supported by experimental values, although there are attempts to explain them. This has been clearly pointed out by Blatt and Weisskopf (1952, p. 772). Other procedures for correlating " $i$ " and " $\mu$ " values (Rose and Bethe 1937, Margenau and Wigner 1940) have not proved to be of much consequence. The explanation of quadrupole moments, on any theory, is yet in a very unsatisfactory position, inspite of some attempts at explanation on shell theory (Gordy 1949, Hill 1949, Townes 1949). It is, therefore, quite reasonable to state that we have not yet understood nuclear structure as we have failed to correlate the nuclear moments and even to put forward a satisfactory explanation for the origin of rapidly fluctuating quadrupole moments with mass number.

It would perhaps be helpful to study the experimental findings on the " $i$ " and " $\mu$ " values and their interrelation for different nuclei, critically, before formulating any plan for their interrelations. To understand these interrelations it is considered advantageous to have an overall picture for the whole set of nuclei before partitioning them as light, medium and heavy nuclei. Before proceeding in that direction, we may accept the experimental values for the magnetic

moments of proton and neutron as +2.793 and -1.913 respectively, giving us the corresponding Lande-g-factors as 5.59 and -3.83 respectively. The Lande g-factors for the orbital moments of the proton and the neutron are considered generally, to be 1 and 0 respectively, on the basis of our knowledge of electrodynamic relations. In view of various complicated relationships cropping up in the nuclear dimensions it would have been better if these g-factors could be substantiated on grounds of experimental results and they are actually so substantiated as would be shown in the following.

We tabulate for this purpose the numbers of nuclei observed with an approximate value of  $\mu$  for the different "i" values (Strominger *et al*, 1958), both for the odd proton and the odd neutron nuclei, as shown in Table I. The outlying rare cases have been left out in this tabulation.

TABLE I

		Numbers(odd proton nuclei)							Numbers (odd neutron nuclei)						
i	$\mu \rightarrow$	-.2	.5	1.5	2.5	3.5	4.5	5.5	-1	.5	0	+.6	1		
$\downarrow$	1/2	6	0	4					3	3	4	8	0		
	3/2		10	3	10				1	4	0	3	2		
	5/2			5	2	8			4	6	0	3	2		
	7/2				8	0	6		3	4	1	2	1		
	9/2						1	4	4	1	0	0	0		

It would be seen from the table that the major groups for odd proton nuclei lie on diagonal lines, decreasing the magnetic moment " $\mu$ " by unity for a corresponding decrease in the "i" value, whereas for nuclei with odd neutron, the major groups do not seem to change their magnetic moments when the "i" value is decreased by unity. The tabulated values, therefore, substantiate from experimental data the generally held ideas about the Lande-g-factors for orbital motion of protons and neutrons, in a gross way. Further, the table indicates that the behaviour of light and heavy nuclei, which are all mixed up here, are perfectly alike in their interrelation between "i" and " $\mu$ " values and only one general principle of interrelation between these moments should hold for all nuclei.

Secondly, one finds from the tabulated values (Strominger *et al*, 1958) a small and systematic change in the magnetic moments of isotopic nuclei with the same "i" values. To cite only a few cases we have the observed data for "i" and " $\mu$ " as follows :  $^{17}\text{O}^{135,37}$ , (3/2), .8, .68;  $^{47}\text{Ag}^{105,111}$ , (1/2), -.11 to -.14;  $^{50}\text{Sn}^{115,119}$ , (1/2), -.9 to -1.04;  $^{56}\text{Ba}^{135,137}$ , (3/2), .83, .93. Such a change for isotopic nuclei with the same "i" values, is likely to be caused only by a variation of values of gyromagnetic-ratio for spinning motion, with the neutron content of the nuclei. The data, in general, tend to require that the magnetic moment for spin of the proton should vary from 2.8 to 2.5 units and that for spin of the neutron should change from -1.85 to -2.15, with increase of neutron content of the nuclei. The requirement of some such, correction is well known in connection with the

$i$  — relationship for  $1H^2$ , and have been discussed by Blatt and Weisskopf (1952, p. 251).

We may now consider the process of development of nuclear structure (Dutta V. 1964), discussed before and try to find how far the observed magnetic and quadrupole moments are in accordance with that scheme of development. For this purpose we consider all nuclei upto a charge content of 5 units as primary and the rest as compositions from them, with additional neutrons. The nuclei  $4Be^8$ ,  $6C^{12,13}$ ,  $7N^{11,15}$  have been considered as doubled up structures from the point of view of their binding energies.

Any even-even nucleus would be regarded as a composition of two groups of nuclei, with opposite moments to balance each other and give the resultant effect as zero, in accordance with observed results. When one considers the moment of nuclei on any other basis than the one particle model, it would be difficult to obtain neutralised effects for all even-even nuclei. It is also known that one particle model does not satisfy the requirement of  $i - \mu$  relationship for all nuclei. Group formation with opposite moments is thus, the only other alternative for all even-even nuclei.

For odd mass nuclei, we consider the development of structure as superposition of equivalent groups, with opposite moments, on the primary nuclei, beginning from neutrons and protons at the earlier stages. Additional groups, symmetrically placed would then build up heavier nuclei. Thus, from oxygen nucleus, onwards, we may have two groups of  $4Be^8$ , with opposite moment, superposed on the primary nuclei to compose heavier nuclei, at the initial stage. In such a case there should be close correspondence between the magnetic moments of the base and the composed nuclei. A variation in the orbital quantum number for the developed structure is not unlikely, changing the orbital and magnetic moments by integral numbers and thus the correspondence would be in the non-integral portions. Small changes due to the neutron content, as already pointed out, is also expected. From these points of view, the magnetic moments of a set of nuclei, which may be considered as the base and the composed structure, make favourable comparison as follows :

Nuclei	$\mu$	Nuclei	$\mu$
$On^1$	-1.92	$3Li^7$	3.26
$8017$	-1.90	$11Na^{23}$	2.20
		$19K^{39}$	0.30
$1H^3$	2.79	$4Be^9$	-1.18
$9F^{19}$	2.60	$12Mg^{25}$	-0.85
		$20Ca^{43}$	-1.30
$3Li^6$	0.82		
$11Na^{22}$	1.75	$5B^{11}$	2.69
		$13Al^{27}$	3.60
$6C^{13}$	0.70	$21Sc^{45}$	4.7
$14Si^{29}$	0.55		

It must be noted, however, that one cannot go on adding small nuclei to heavier nuclei for composition, as those would be gradually more composite in structure, so as not to form bonds with smaller groups.

We may note, further, that the doubled up structures of  $6\text{C}^{13}$  and  $7\text{N}^{15}$  make  $14\text{Si}^{29}$  and  $15\text{P}^{31}$ , as four group nuclei instead of the three group nuclei of  $13\text{Al}^{27}$ , with 4 : 5 : 4 units of charge. One may consider that the three group system is saturated at  $\text{Al}^{27}$  and is followed by four and five group systems. From the nature of charge distribution and charge saturation, such nuclei should have comparatively large quadrupole moments as observed and weaker binding represented by a maximum of the  $F(Z)$  curve, shown in previous works (Dutta and others IV, 1964). It is expected to be followed by a comparative spread of the group and negative quadrupole moment, as in 3 : 3 : 5 : 3 : 3 charge distribution proposed for chlorine nucleus. The maxima of the  $F(Z)$  curve, near mass numbers 59, 117, 177 and 235, already noted (Dutta IV, V) are associated with large values of quadrupole moments in these positions. They correspond to the charges 27, 49, 71 and 92 and should be followed by a possible change over in structural groups, suitable for even and odd charges, which are symmetrically placed and held together by mutual bonds. These considerations would be substantiated.

It may be pointed out also that large quadrupole moments for even charge nuclei are very often not associated with those for the odd charge nuclei. This should be on account of the particular group systems and the characteristics of particular compositions necessary for odd and even nuclei. They obtain large positive or negative quadrupole moments for these nuclei by correlation with the concentration of charge in a structure, as has been just indicated. The large quadrupole moment at  $34\text{Sc}^{79}$  corresponds perhaps to the saturation of some even -group system. Odd charge nuclei has a subdued maxima in this region.

It may be remarked, finally, that with appropriate orbital and spin quantum numbers, associated with the major subdivisions, one may build up the magnetic moments of all nuclei by superposition of structures, keeping in view the observed quadrupole moments also. What is necessary and of importance however, is to associate the changes in quantum numbers with associated properties. The problem is being looked into.

#### REFERENCES

- Strominger, D., Hollander, J. M., Seaborg G. T. 1958, *Rev. Mod. Phys.* **30**, 585.  
 Blatt, J. M. and Weisskopf V. F. 1952, *Theoretical Nuclear Physics*, John Wiley and Sons.  
 Rose, M. E., Bethe, H. A., 1937, *Phys. Rev.* **51**, 205.  
 Margenau, H. and Wigner E. P. 1940, *Phys. Rev.* **58**, 103.  
 Dutta A. K. 1964, *Ind. J. Phys.* **38**, 521.  
 Dutta, A. K., Pal, B., Ganguly P., Banerjee D., 1964, IV *Ind. J. Phys.* **38**, 519.  
 Schmidt, T. 1937, *Zeits fur Physik* **106**, 358.  
 Gordy, W. 1949, *Phys. Rev.* **76**, 139.  
 Hill, R. D. 1949, *Phys. Rev.* **76**, 998.  
 Townes, C. H., Foley, H. M., Low, W., 1949, *Phys. Rev.* **76**, 1415.

# QUASI-CRYSTALLINE STRUCTURE AND INTERRELATION BETWEEN NUCLEAR MOMENTS (VII)

A. K. DUTTA,

PALIT PROFESSOR OF PHYSICS, CALCUTTA UNIVERSITY  
ACHARYA PRAFULLA CHANDRA ROAD, CALCUTTA 9.

(Received September 28, 1964).

We propose to examine, now, the possibility of interrelating magnetic and orbital moments on the basis of a quasi-crystalline structure, which considers (Dutta V, 1964) larger nuclei to be composed of elementary or primary nuclei. These are in circulating motion presumably on account of neutron-proton exchange and thus obtain magnetic and orbital moments.

The observed total orbital momentum for the nuclei are only integral or half-integral. This suggests that the relative spins of all the nucleons, both for the primary and the composite nuclei could be only parallel or antiparallel. They are designated, usually, with positive and negative signs to indicate correlation with the signs of the magnetic moments. The spins of the nucleons should be grouped separately for the protons and the neutrons, on account of their different Lande-g-factors to determine magnetic moments. The numbers of protons and neutrons taking opposite spin character would not be largely different and, thus, the resultant spin quantum numbers for protons and neutrons, in any nucleus are not expected to be large. The numbers, so aligned in opposite directions, are ascertainable from the resultant spin and nucleon number in the two groups.

We have been considering the composite nucleus as a superposition of close packed elementary nuclei, with the internucleonic spacings expected from the density. Such an arrangement would put the orbital momentum vectors for both the protons and the neutrons as parallel or antiparallel only, as in the case of nucleonic spins. Further, according to the scheme of composition of even-even nuclei from the subnuclei of opposite moments, we require to have both the spins and the orbital momenta oppositely aligned to bring the resultant to zero. It requires that the mechanical moments of the nuclei would be both positive and negative and a combination of these in the subnuclei imply attraction and formation of a larger nucleus. Also, in a symmetrical disposition of nucleonic spins and orbital momenta, it is not expected that the resultant spins and orbital moments would set themselves in any oblique direction with respect to each other. We, therefore, assume that the orbital momentum 'L' and the spin momentum 'S', align themselves along the same line, in parallel or antiparallel directions.

The experimentally observed total momentum " $\vec{L}$ ", would be, as a consequence, the algebraic sum of the orbital and spin momentum of the neutrons and protons and the total magnetic moment (Strominger *et al.*, 1958) for such alignment would be obtained by summing up the products of the respective mechanical moments with the corresponding Lande-g-factors.

The Lande-g-factor for orbital motion have been considered to be  $+1$  and  $0$  for protons and neutrons, and have been discussed before (Dutta VI, 1964). The Lande-g-factors for nucleonic spins are considered to be variable with a tendency to decrease with concentrated charge and also with the increase of neutrons in isotopes. The range of variations is not large as would be observed, further, in the table herewith.

As we have already observed in a previous communication (Dutta V, 1964), we consider all nuclei upto a charge content of 5 units as elementary nuclei. Of these the elements with a charge amounting to 2, 3, 4, or 5 units are considered to be of circulating type. All nuclei from carbon are of composite form, as discussed previously. A composition would, naturally, imply the summation or subtraction of the characteristics, determined by the quantum numbers. It is, however, unlikely, that all the characteristics would be maintained even after composition. It is observed, generally, that spin characteristic are maintained while the orbital quantum numbers suffer a change with respect to the composing units. The requisite tentative distribution of resultant spin and orbital quantum numbers, to satisfy the interrelation, as also the corresponding Lande-g-factors for the spinning motion, have been given in the following table for some primary and composed nuclei.

To obtain the different quantum numbers necessary for the correlation between orbital and magnetic moments, we proceed first to fix up the resultant spins for the protons and the neutrons, such that with the respective Lande-g-factors the algebraic sum gives us the fractional part in magnetic moment, keeping in view the probable odd-even character of composition. Orbital quantum number for the protons would then be decided by the integral part in magnetic moment. The total orbital moment would finally give the orbital quantum number of the neutron. Alternative arrangements are sometimes possible.

Regarding the characteristics to be satisfied by the orbital quantum numbers, we may state that the resultant orbital momentum of the composite nucleus is made up as the algebraic sum of the  $l$ -values for the different circulating units. The orbital quantum numbers must be distributed to the circulating units, in a way, that does not impair the symmetry of the nucleus. This implies that the resultant orbital quantum number can be odd or even for circulating systems of 1, 3, or 5 units and should be even only, for systems with 2 or 4 circulating units. This is true both for protons and neutrons. We have indicated the number of circulating units and the tentative composition in the adjoined table.



TABLE I  
Correlation between nuclear moments and composition

Nucleus	Experimental values			Proposed total quantum numbers			Lande-g factors $q \begin{cases} 1, p=1, & 1, n=0 \\ S_p & -S_n \end{cases}$	Symbols, units	Composition
	$i$	$\mu$	$q$	$S_p$	$L_p$	$L_n$			
H <sup>2</sup>	1	0.86	+ .003	1/2	0	0	5.56 3.84	H, 0	—
Li <sup>7</sup>	3/2	3.26	+ .020	3/2	-1	0	5.40, 3.84	Li, 1	—
Be <sup>9</sup>	3/2	-1.18	- .020	0	1	0	— 4.36	Be, 1	—
"	"	"	"	1	3/2	-1	5.52, 3.80	" "	—
B <sup>11</sup>	3/2	2.69	- .036	1/2	0	1	5.38, —	B, 1	—
C <sup>13</sup>	1/2	0.70	—	1	3/2	1	5.40, 3.80	C, 3	3He <sup>4</sup> (1)
N <sup>14</sup>	1	0.40	—	3/2	-2	0	5.40, 3.80	N, 3	H <sup>2</sup> (0)+3He <sup>4</sup> (1).
O <sup>17</sup>	5/2	-1.90	- .027	0	1/2	0	— 3.80	0, 4	n(0)+4He <sup>4</sup> (1).
Ne <sup>21</sup>	3/2	-0.66	—	-1	-3/2	2	5.44 3.86	Ne, 3	Be(1)+2Li(1).
N <sup>23</sup>	3/2	2.22	+ .10	3/2	-2	1	5.40, 3.88	Na, 3	Li(1)+0(2).
Al <sup>27</sup>	5/2	3.60	+ .15	1/2	1	1	5.20, —	Al, 3	B(1)+0(2).
S <sup>33</sup>	3/2	0.64	- .07	1	3/2	1	5.40 3.82	S, 5	Be(1)+4Li(1).
S <sup>35</sup>	3/2	0.64	- .05	-1	-3/2	4	5.36, 4.00	S, 4	n(0)+4Be(1).
Cl <sup>37</sup>	3/2	0.70	- .07	1/2	0	3	5.40, —	Cl, 5	B(1)+4Li(1)
Mn <sup>55</sup>	5/2	3.50	- .40	1/2	1	-2	5.20, 4.10	Mn, 5	B(1)+4(B,1)
Co <sup>59</sup>	7/2	4.60	+ .50	1/2	1	-6	5.20, 4.00	Co, 6	H(0)+2Al(3).
Cu <sup>63</sup>	3/2	2.20	- .16	3/2	-2	1	5.40, 3.90	Cu, 9	Na(3)+6Li(1).

It would be observed from the table that sometimes the Lande-g-factors for the primary nucleus, which acts as the basis, persists with very minor changes, in the composite nucleus also. In the case of  $6\text{C}^{13}$ , expected to be a composition from two Li nuclei, the even value for the orbital quantum number is associated with a comparatively large reduction of Lande-g-factor  $g(s_p)$ . The other possible scheme with odd numbers for orbital quantum numbers and Lande-g-factors of proper magnitudes, suggests a system of three circulating units, on account of odd values for the required orbital quantum number. It is however to be noted also, that the Lande-g-factor  $g(s)$  obtains a drop when a structure is saturated with charge as in  $\text{Al}^{27}$ ,  $\text{Mn}^{53}$  and  $\text{Co}^{57}$ . We have given two possible modes of composition for  $16\text{S}^{33,35}$ . A change over to a larger structure is expected to be associated with a drop in quadrupole moments (Dutta VI, 1960). The quadrupole moments of  $16\text{S}^{23,53}$  are negative and positive respectively. This suggests that  $16\text{S}^{33}$  conform to the five unit system in the free state. The distribution of moments, consistent with symmetry, lead us also to the probable structures of nuclei.

It would appear from the above that there is a close correlation between the nuclear moments on the basis of such quasi-crystalline structure of the nuclei. The scheme, therefore, calls for serious consideration. The structural development is based on the idea of cohesion of primary nuclei, with particular disposition of constituents. The nuclei so formed grow into larger nuclei, as, gradually, larger primary nuclei replace smaller ones. During such a process of growth by replacement, for a particular number of associated units, the potential energy decreases to a minimum and then increases to a maximum, when a bigger structure, with a larger number of units, begin to operate.

#### REFERENCES

- Dutta A. K. 1964, *Ind. J. Phys.* V, VI **38**: 522, 527.  
 Strominger, D., Hollander, J. M., Seaborg G. T., 1958, *Rev. Mod. Phys.* **30**, 585.

# A MINIATURE JOULE-THOMSON CASCADE LIQUEFIER CRYOSTAT FOR HELIUM

## ERRATA

(An Analysis of the *J*-Phenomenon in X-Rays, Part I)

February Issue 1964

Page 64	foot note	read $\frac{c}{v'}$	instead of $\frac{c}{v}$ .
„ 67	line 11	read $\left(\frac{\mu}{\rho}\right)_s$	„ „ $\left(\frac{\mu}{\rho}\right)$ .
	line 15	read $c_n$	„ „ $u_n$
„ 68	line 19	read $y_s$	„ „ $y_x$
	line 29	delete 'if'	after "in case"
„ 70	fig. 2	read $y_s$ (along ordinate axis)	instead of $y_x$
		read $y_y$ (along abscissa axis)	„ „ $y_r$
„ 71	lines 15 and 16,	read $A_s$	instead of $AX$
„ 73	fig 3	read $y$ (along r.h.s. ordinate axis)	instead of $y_r$ .

Hydrogen gas which may be helpful to workers in this field particularly in this country.

Hydrogen gas of fairly high purity (99.5% or more) is commercially available in this country in cylinders at a pressure of 1980 lbs./in<sup>2</sup> and is quite cheap. Be-

It would be observed from the table that sometimes the Lande-g-factors for the primary nucleus, which acts as the basis, persists with very minor changes, in the composite nucleus also. In the case of  $6\text{C}^{13}$ , expected to be a composition from two Li nuclei, the even value for the orbital quantum number is associated with a comparatively large reduction of Lande-g-factor  $g(s_p)$ . The possible solution for this is that the  $6\text{C}^{13}$  nucleus has a small number of

# A MINIATURE JOULE-THOMSON CASCADE LIQUEFIER CRYOSTAT FOR HELIUM

B. N. SRIVASTAVA, J. K. N. SHARMA, S. CHATTERJEE AND  
S. K. SEN

INDIAN ASSOCIATION FOR THE CULTIVATION OF SCIENCE, CALCUTTA-32

(Received October 9, 1964)

**ABSTRACT.** A miniature cascade helium liquefier cryostat has been described and various constructional details given. The liquefier is designed to enable experiments at liquid helium temperatures to be performed in an ordinary laboratory and uses only liquid oxygen for the initial cooling. The liquid hydrogen needed to cool the helium below its inversion temperature is provided by a hydrogen circuit liquefying hydrogen continuously within the same machine. Compressed cylinder hydrogen is used avoiding the necessity of compressor or gasometer for hydrogen.

## INTRODUCTION

The recent widespread interest in cryogenic research has resulted in the development of inexpensive small laboratory made liquefiers for helium, using liquid hydrogen externally or internally the three proprietary liquefiers of Collins (1947), Meissner (1957) and Weil (1955) being too expensive and not within the resources of most laboratories. Most of these cheap liquefiers therefore utilise the Joule-Thomson effect and the principal of regenerative cooling. The general principles underlying the practical design of the Joule-Thomson hydrogen or helium liquefiers are well-known (Croft 1961) and the construction of the usual liquefiers has been fully described (Ahlberg *et al* 1937, Rollin 1936, Ruhemann 1930, Starr 1941 Fairbank 1946, Daunt and Mendelssohn 1948, Chester and Jones 1953). For occasional work it is simpler and much less expensive to construct a double liquefier in which both hydrogen and helium are continuously liquefied, rather than set up separate liquefiers for hydrogen and helium. Thus starting only with liquid air, liquid oxygen or liquid nitrogen, a small quantity of hydrogen sufficient to obtain the necessary starting temperature for the helium stage is liquefied inside the apparatus itself. In the present paper a miniature Joule-Thomson Cascade liquefier for helium based on this principle is described, whose prototype is the liquefier of Chester and Jones (1953), but a few novel features have been employed. Further a few details of design and operation have been presented here which may be helpful to workers in this field particularly in this country.

Hydrogen gas of fairly high purity (99.5% or more) is commercially available in this country in cylinders at a pressure of 1980 lbs./in<sup>2</sup> and is quite cheap. Be-

cause of the relatively high cost of compressor-gasometer system, it is sound economy to use this commercially compressed gas for small scale liquefaction and to let off the low pressure hydrogen to the atmosphere. The standard 165 cu.ft. capacity cylinders at 135 atmospheres could be used down to 35-40 atmospheres. At our special request Messrs. Indian Oxygen Ltd. agreed to supply us Standard Purity (purged) locally manufactured hydrogen with impurities not exceeding 0.3% and this was available in any quantity. This greatly facilitated our work and involved very little cost.

### GENERAL DESCRIPTION OF THE APPARATUS

A simplified diagram of the liquefier is given in figure 1. In common with most other inexpensive liquefiers, the hydrogen liquefaction circuit is fed from a manifold of high pressure hydrogen cylinders, and the hydrogen gas is subjected to

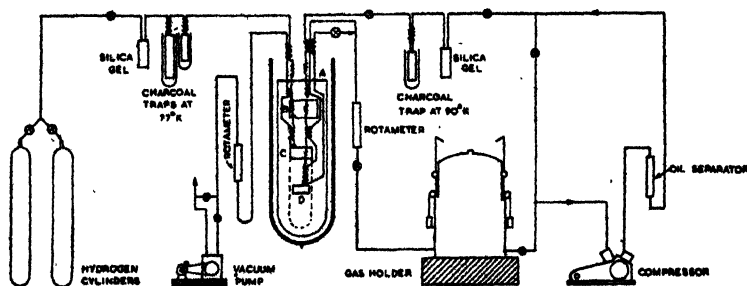


Fig. 1. Schematic diagram of the liquefier.

Joule-Thomson expansion in an open circuit. For the helium liquefaction circuit a small compressor is used, which delivers compressed helium at 40 atmospheres and this expands through the J. T. Valve in a closed circuit producing liquefaction.

The oxygen vessel B, the hydrogen vessel C and the helium vessel D are all made of brass and are suspended inside a vacuum case A, also of brass, which is attached by an easily demountable seal of Wood's metal. The vessel B is maintained at 62°K by constantly boiling liquid oxygen contained in it at a reduced pressure of about one cm. of mercury. The desired vacuum is produced with the help of Edwards 1S150 pump using tricresyl phosphate as the pump oil. An automatic valve actuated by metal bellows dispenses liquid oxygen via a gauze filter from the outer dewar to the vessel B and is of the same type as used by Chester and Jones (1953). The pumping speed was adjusted by a Saunders valve and the inflow of liquid oxygen in B was carefully adjusted by suitably fixing the rod which controls the valve seating. A general view of the assembly with the vacuum case removed is given in Fig. 2.

High pressure hydrogen and high pressure helium (25-30 atmospheres) are first cooled by the out-going low pressure hydrogen and helium in their respective

heat exchangers before entering the liquefier proper. The hydrogen exchanger is of special construction. The high pressure coils are wound round a rod and the

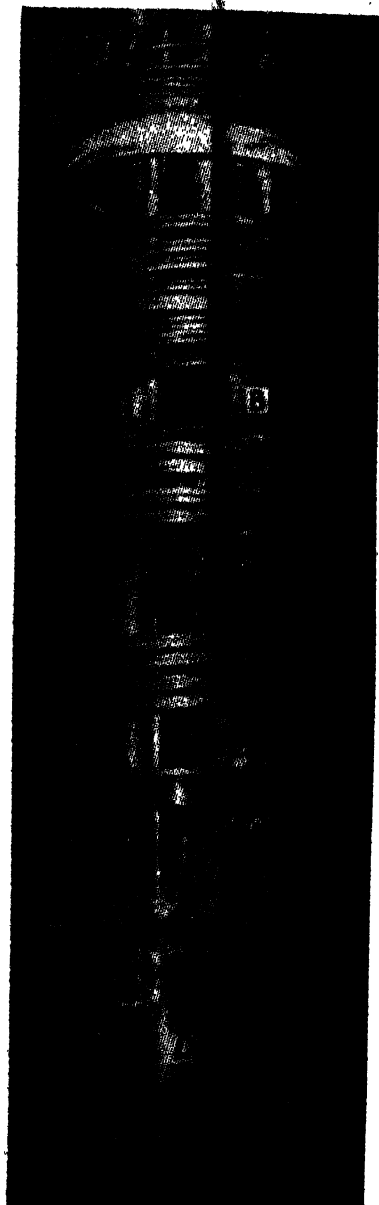


Fig. 2. General view of exchangers. (Photo with vacuum case removed.)

rod is inserted in a wide tube carrying the outgoing low pressure hydrogen. Next the high pressure hydrogen and the high pressure helium coil round in liquid oxygen in the dewar and finally enter the vacuum space. Here the high pressure hydrogen and helium coils are respectively solder-bonded to their low pressure

oils and these bonded coils of hydrogen and helium are arranged ~~anternately~~ and coiled round the liquid oxygen vessel B but not soldered to it. Then the high pressure hydrogen and the high pressure helium coils are both soldered to the lower part of B and thus leave it at temperature of B. Next the high pressure gases are again cooled by the respective outgoing gases through solder-bonding exchangers in the same manner as explained before. Then the high pressure hydrogen gas expands at the J.T. Valve, where it ultimately liquefies and the liquid collects in the vessel C. The outgoing gas passes out through the various exchangers thereby cooling the incoming gas and is finally let out to the atmosphere through the rotameter so that the rate of flow of the gas can be measured. When the vessel C is filled with liquid hydrogen at 20°K, the hydrogen pump (Edwards SI50) is started and the liquid allowed to boil at a pressure of 12 cm. of mercury producing a temperature of 15°K.

The high pressure helium after leaving the exchangers traverses through coils soldered to the lower part of C. The helium gas thereafter enters the final exchanger at about 15°K and subsequently expands at the Joule-Thomson valve where part of it liquefies and collects in the vessel D. The vessel D is surrounded by a radiation shield which is in metallic contact with the bottom of the vessel D and thus the heat leak into D is minimised. The helium stage is also provided with a by-pass return path for helium in 1/4" tube, which in turn sheaths the control rod of the expansion valve; this tube can be used as a low resistance pumping tube to lower the temperature of liquid helium below 4.2°K.

A critical discussion of the performance of various types of heat exchangers has been given by Jacobs and Collins (1940) from which it will be evident that a highly efficient interchanger is expensive and difficult to construct. For ordinary purposes it is therefore usual to construct heat exchanges either in the form of concentric tubes or solder-bonded high and low pressure tubes. The latter design was preferred due to its simplicity of construction and two cupro-nickel tubes (H.P. tubes : 3/32 in o.d., 26 s.w.g. ; L. P. tubes : 1/8 in, o.d., 26 s.w.g. ; length 1-2m.) hard soldered together and suitably coiled were used.

All joints in the inter-changer systems were hard-soldered with "Easy-Flo" silver solder (Johnson, Mathey and Co., Ltd.). For reasons of safety the same solder was used for all other parts of high pressure line. For low temperature soft soldering, the solder used has only tin and lead (no bismuth) in the ratio of 40 Sn and 60 Pb.

#### HELIUM DISTRIBUTION AND PURIFYING CIRCUIT

Figure 3 shows the lay-out of the helium distribution system used in our liquefier. Chester and Jones used a small oil-free gas-tight compressor in a closed helium circuit which included a dry gas-holder in the form of a large rubber bellows. We have found that the ordinary oil-lubricated HOSSE two-stage, single-acting



compressor (manufactured by Reavell and Co. Ltd., Ranelagh Works, Ipswich) originally meant for compressing air to 1000 lbs/in<sup>2</sup> with a capacity of 9 cu. ft.

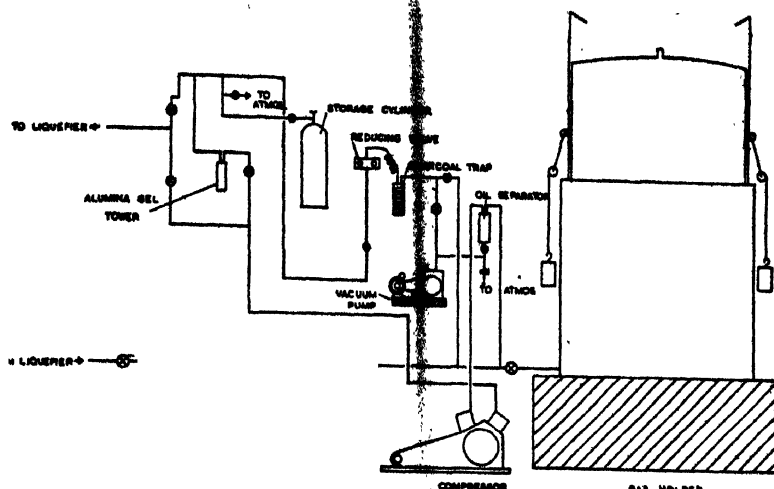


Fig. 3. Helium distribution system and Auxiliary purification circuit.

per minute when running at 1000 r.p.m. can be easily adapted for our purpose with slight modifications and is much cheaper. It is driven at 320 r.p.m. through V belts from a squirrel cage motor running at 950 r.p.m. and is capable of compressing 40 litres per min. of helium to a pressure of 40 atmospheres. It is fitted with enclosed relief valve on each stage with connections for piping back to the suction supply and a special seal at the point where the crankshaft passes through the casing so that there is no loss of helium. The usual rod for gauging the oil level in the crankcase has been replaced by a gauge glass and a special arrangement for adding oil without opening the crankcase to the atmosphere. Further the crankcase has to be joined to the gas-holder by tubing and the air hole is closed.

As the ratio of the two specific heats is larger for helium than for air, more heat will be produced during the compression of helium, and therefore a positive system of water circulation must be used to protect the compressing system from damage. For this reason our compressor has been fitted with an automatic switch designed (Sharma 1959) in this laboratory to break an electric circuit when the flow of liquid in the cooling pipe reaches a predetermined minimum.

The low pressure intake line to the compressor consists of a 1" copper pipe and connects it to the gasometer. The helium gas can be had from the gas-holder of 12 cu.ft. capacity. The dry gas-holders i.e. rubber bellows, as used by Jones and others are liable to develop leak and therefore a metallic gasometer supplied by Messrs. Tickford Ltd., is used and the gas is collected over transformer oil. Suitable alarm controls have been designed (Sharma 1961) and fitted to the gas-holder to indicate the maximum and minimum limits beyond which it is not to be used.

The high pressure helium leaves the compressor through 3/8" o.d., 1/4" i.d. copper tubing and passes through an after-cooler of the conventional type i.e. the gas is passed through a copper tube immersed in water, followed by an oil separator in which the velocity of the gas is slowed down, so that it does not carry forward the oil and moisture. The compressed helium next passes to the distribution panel from which it can be sent to the liquefier, to the storage cylinders, or through a reducing valve, to the purification circuit and the gasometer as may be seen from figure 3.

As an added precaution for preventing the contamination of charcoal through oil vapours, the dry helium gas from the distribution panel is further allowed to pass through a porous ceramic cylinder of pore size 7.5 to 10.0 microns which serves to remove any traces of oil. Finally a silica gel tower is used to remove completely any moisture from the gas. An alumina gel tower is inserted between the distributing panel, and the storage cylinder for removing oil and moisture, so that the helium stored in the storage cylinders is dry and oil-free.

*Auxiliary purification Circuit.* Before starting a liquefaction run, the helium in the gas holder should be carefully purified. This is done with the help of the auxiliary purification circuit. First all the gas from the gas-holder is transferred by the compressor to the storage cylinders, and from there it is passed through a reducing valve which reduces the pressure to about 4 atoms. Thereafter the gas goes through the charcoal trap C kept immersed in liquid oxygen, so that it is purified by the activated charcoal and finally the purified gas collects in the gas holder. This process is repeated three times before every liquefaction run. It may be mentioned that B.O.R. 13 (supplied by Indian Oxygen Ltd.) which gives an outlet pressure ranging from 0 to 200 lbs/sq. in is quite convenient to use as a reducing valve in this circuit and has been used by us for this purpose.

#### OTHER CONSTRUCTION DETAILS

*Charcoal traps.* The charcoal pot is made from vibrac steel bottles supplied by Messrs. Vickers Armstrongs. It is packed with about 500 cc. of activated charcoal supplied by M/s. British Carbo-Norit Union of grade ULTRASORB S. C. 11. The open end (i.e. lower one) is sealed with screwed plugs of the same material and soft-soldered in place. This allows for easy refilling when necessary. A filter inserted in the charcoal vessel prevents particles of charcoal or dust being carried further by the gas streams. The incoming and the outgoing lines support the pot and are joined to the circuit by detachable unions. The finished bottle is hydraulically tested to twice the working pressure when it should show no distortion.

In our experiments using locally manufactured hydrogen the J-T valve occasionally got choked showing that the degree of purification attained was not sufficient. We, therefore, inserted an additional charcoal pot of capacity about 400 cc. Using both of these in series there was never any trouble of blocking.

*Porous Ceramic Cylinders.* Porous ceramic cylinder (Aerox Ltd., U.K.) of porsilux Grade P.35 filter elements, 10" long  $\times$  2" o.d.  $\times$  1 $\frac{1}{2}$ " i.d., open at both ends were used for removing oil from gaseous helium at 40 atmosphere pressure. The filter casing is made of copper and is suitably mounted in the high pressure line of helium. The ceramic element is easily replaceable by removing the body of the filter unit from its head by releasing the retaining bolts, and then unscrewing the locking nuts and cap.

*For Low pressure line purification.* Wire gauze filters packed along the tube are generally used but this reduces the suction capacity of the compressor. Activated alumina also has the same disadvantage. We have, therefore, employed a simple oil separator made out of ordinary copper pipe length 10 $\frac{1}{2}$ ", 2" o.d. 1 $\frac{1}{2}$ " i.d. inside which are mounted several fins on a vertical axis. The whole is surrounded by ice and the oil vapour, if any, condenses and can be drained off. This is, however, not very essential as we are not using an oil free compressor and any oil vapour carried forward from the gas holder is not likely to do any great harm.

*Joule-Thomson Valves.* Unlike the apparatus of Chester and Jones we have used an adjustable expansion valve in the hydrogen stage which is further provided with a locking device as a precautionary measure to prevent excessive opening of the valve. This allows us to adjust the rate of flow of hydrogen and is useful at the time of blocking of the valve. The helium valve is also adjustable. These valves are the usual type of needle valves with long stem and seat. The top part of the valve is threaded and can be easily unscrewed and withdrawn. The two tubes sheathing the control rods are provided with relief valves at the upper end; this protects the hydrogen and helium liquid vessels from any high pressure accidentally developed. The valves are so constructed that the whole valve including the seating, can be withdrawn after only two simple soldered joints have been broken.

Apart from the Joule-Thomson valves already mentioned, the high pressure valves used are the M.K. VIII (M/s. Nico-light) valves while the low pressure valves are the Saunders valves with vacuum reinforced T and S grade

## INDICATORS

Gauges are permanently mounted to measure the intake pressure of cylinder hydrogen and compressed helium, and the pressure on the high and low pressure sides of the Joule-Thomson valve in both circuits. The temperature of the liquid hydrogen can be measured by the hydrogen-thermometer acting as a vapour thermometer and the temperature of helium vessel is measured by means of a

The high pressure helium leaves the compressor through 3/8" o.d., 1/4" i.d. copper tubing and passes through an after-cooler of the conventional type i.e. the gas is passed through a copper tube immersed in water, followed by an oil separator in which the velocity of the gas is slowed down, so that it does not carry forward the oil and moisture. The compressed helium next passes to the distribution panel from which it can be sent to the liquefier, to the storage cylinders, or through a reducing valve, to the purification circuit and the gasometer as may be seen from figure 3.

As an added precaution for preventing the contamination of charcoal through oil vapours, the dry helium gas from the distribution panel is [further allowed to pass through a porous ceramic cylinder of pore size 7.5 to 10.0 microns which serves to remove any traces of oil. Finally a silica gel tower is used to remove completely any moisture from the gas. An alumina gel tower is inserted between the distributing panel, and the storage cylinder for removing oil and moisture, so that the helium stored in the storage cylinders is dry and oil-free.

*Auxiliary purification Circuit.* Before starting a liquefaction run, the helium in the gas holder should be carefully purified. This is done with the help of the auxiliary purification circuit. First all the gas from the gas-holder is transferred by the compressor to the storage cylinders, and from there it is passed through a reducing valve which reduces the pressure to about 4 atoms. Thereafter the gas goes through the charcoal trap C kept immersed in liquid oxygen, so that it is purified by the activated charcoal and finally the purified gas collects in the gas holder. This process is repeated three times before every liquefaction run. It may be mentioned that B.O.R. 13 (supplied by Indian Oxygen Ltd.) which gives an outlet pressure ranging from 0 to 200 lbs/sq. in is quite convenient to use as a reducing valve in this circuit and has been used by us for this purpose.

#### OTHER CONSTRUCTION DETAILS

*Charcoal traps.* The charcoal pot is made from vibrac steel bottles supplied by Messrs. Vickers Armstrongs. It is packed with about 500 cc. of activated charcoal supplied by M/s. British Carbo-Norit Union of grade ULTRASORB S. C. 11. The open end (i.e. lower one) is sealed with screwed plugs of the same material and soft-soldered in place. This allows for easy refilling when necessary. A filter inserted in the charcoal vessel prevents particles of charcoal or dust being carried further by the gas streams. The incoming and the outgoing lines support the pot and are joined to the circuit by detachable unions. The finished bottle is hydraulically tested to twice the working pressure when it should show no distortion.

In our experiments using locally manufactured hydrogen the J-T valve occasionally got choked showing that the degree of purification attained was not sufficient. We, therefore, inserted an additional charcoal pot of capacity about 400 cc. Using both of these in series there was never any trouble of blocking.

*Porous Ceramic Cylinders.* Porous ceramic cylinder (Aerox Ltd., U.K.) of porsilex Grade P.35 filter elements, 10" long  $\times$  2" o.d.  $\times$  1 $\frac{1}{2}$ " i.d., open at both ends were used for removing oil from gaseous helium at 40 atmosphere pressure. The filter casing is made of copper and is suitably mounted in the high pressure line of helium. The ceramic element is easily replaceable by removing the body of the filter unit from its head by releasing the retaining bolts, and then unscrewing the locking nuts and cap.

*For Low pressure line purification.* Wire gauze filters packed along the tube are generally used but this reduces the suction capacity of the compressor. Activated alumina also has the same disadvantage. We have, therefore, employed a simple oil separator made out of ordinary copper pipe length 10 $\frac{1}{2}$ ", 2" o.d. 1 $\frac{7}{8}$ " i.d. inside which are mounted several fins on a vertical axis. The whole is surrounded by ice and the oil vapour, if any, condenses and can be drained off. This is, however, not very essential as we are not using an oil free compressor and any oil vapour carried forward from the gas holder is not likely to do any great harm.

*Joule-Thomson Valves.* Unlike the apparatus of Chester and Jones we have used an adjustable expansion valve in the hydrogen stage which is further provided with a locking device as a precautionary measure to prevent excessive opening of the valve. This allows us to adjust the rate of flow of hydrogen and is useful at the time of blocking of the valve. The helium valve is also adjustable. These valves are the usual type of needle valves with long stem and seat. The top part of the valve is threaded and can be easily unscrewed and withdrawn. The two tubes sheathing the control rods are provided with relief valves at the upper end; this protects the hydrogen and helium liquid vessels from any high pressure accidentally developed. The valves are so constructed that the whole valve including the seating, can be withdrawn after only two simple soldered joints have been broken.

Apart from the Joule-Thomson valves already mentioned, the high pressure valves used are the M.K. VIII (M/s. Nico-light) valves while the low pressure valves are the Saunders valves with vacuum reinforced T and S grade diaphragms.

#### INDICATORS

Gauges are permanently mounted to measure the intake pressure of cylinder hydrogen and compressed helium, and the pressure on the high and low pressure sides of the Joule-Thomson valve in both circuits. The temperature of the liquid hydrogen can be measured by the hydrogen-thermometer acting as a vapour thermometer and the temperature of helium vessel is measured by means of a

helium thermometer, acting either as a gas thermometer or a vapour pressure thermometer.

Rotameters, with duralumin floats supplied by Rotameter Manufacturing Co. are suitably inserted in the low pressure lines to measure the rate of flow of the gas in each circuit.

For check on the vacuum in the metal case A jacketing the liquefier unit, a Cathedon combined Pirani and Ionisation gauge (W. G. Pye and Co.) was mounted with both probes inserted. This served as a rugged and satisfactory indicator throughout the range. A vacuum of the order of  $5 \times 10^{-6}$  mm. of mercury was maintained inside the casing by a fractionating oil diffusion pump (F 203, W. Edwards and Co.) and thus a good thermal insulation was obtained.

#### HELIUM EVAPORATION CIRCUIT

For attaining temperatures lower than 4.2°K, it is necessary to evaporate liquid helium under reduced pressure. For this purpose a parallel circuit is provided for pumping the liquid helium in D through the helium by-pass tube and the helium gas going out of the pump is taken through an oil separator to the gas holder, the direct connection to the gas holder being closed. If desired, the degree of vacuum in D is controlled by pumping through a micro-meter valve of Nagretti and Zambra type.

#### OPERATION AND PERFORMANCE

Preparatory to a run, the charcoal pots and other high pressure circuits of the liquefier are carefully checked for leaks under the highest operating pressure. Next the hydrogen and the helium charcoal cleaners are kept at about 200°C for at least two hours and pumped continuously. During this reactivation of charcoal the bottom plugs of the cleaners are kept moistened to prevent the soldered joints from softening. Heating is then stopped and when the system has cooled, the pumps are turned off and the high pressure gases admitted to their respective systems.

Just before putting the plant in operation the low pressure and high pressure lines of both the hydrogen and the helium circuits are evacuated by their respective pumps and the charcoal cleaners are surrounded with liquid oxygen. Each system is then flushed with the respective gas purified by charcoal cooled by liquid oxygen. The process of evacuation and flushing is repeated several times and finally the liquefier is filled with pure gas in each system. Next the outer case A of the liquefier is connected to the rotary pump (the diffusion pump is kept ready) and after about ten minutes hydrogen exchange gas is introduced into the vacuum case. Then it is surrounded with liquid oxygen in a glass

dewar. The approximate timings of subsequent events in a typical run is as follows :

<i>Time</i>	
0 min.	Dewar vessel containing liquid oxygen is put on to the apparatus and the circulation of helium gas (30 litres/min) started with the helium by-pass open.
15 min. :	At this instant the temperatures of B, C and D will be 90°K. Liquid oxygen pump is started. Also high vacuum pump for evacuating the case started.
25 min. :	Vessel B at 62°K (Helium flow is continued). Hydrogen flow (30 litres/min) also started.
30 min. :	Vessel C at 62°K and D a little higher. Helium flow stopped.
37 min. :	Liquid hydrogen in C. Hydrogen pump started and the helium (15 litres/min) also started through the helium heat inter-changers with by-pass closed.
42 min. :	Hydrogen flow is reduced to 10 litres per minute and helium flow is continued as before.
55 min. :	Liquid helium in D.

The only departure we made from Jones procedure was that once liquid hydrogen had been formed and hydrogen pump started, the helium circulation was re-started with the by-pass closed rather than open. This slightly lengthened the cooling time, but is thermodynamically more efficient. Another advantage of this procedure is that there is no risk of liquid hydrogen completely evaporating in vessel C as the helium flow is kept down.

When once the initial difficulty of handling the apparatus had been overcome, it was found possible to maintain helium temperatures steadily for several hours. By boiling liquid helium at a reduced pressure of about 50 cm. a temperature of 3.25°K was attained and maintained for several hours. Only three cylinders of 165 cu.ft at 1980 lb/in<sup>2</sup> and 25 litres of liquid oxygen were necessary for a run of about 5 hours at a temperature 3.25°K. For maintaining a temperature of 4.2°K for several hours one to two cylinders of hydrogen and about 15 litres of liquid oxygen would be sufficient. The rate of production of liquid helium in our apparatus is about 2.8 cc/min. with an efficiency of about 0.13 which is about 87% of the theoretical yield.

The construction and installation of the liquefier was mainly due to the inspiration, encouragement and foresight of the late Professor M. N. Saha, D.Sc., F.R.S. One of the authors (B.N.S) expresses his grateful thanks to the late Professor Sir Francis Simon, Kt., O.B.E., F.R.S. and his colleagues of the Clarendon Laboratory, Oxford, for their kind hospitality and co-operation during his stay in

Oxford, and to Professor G. O. Jones of Queen Mary College, London, for a detailed discussion of the design of the liquefier. We record our thanks to the staff of our workshop for their skilful handling of various difficulties and their enthusiastic cooperation.

## REFERENCES

- Ahlberg, J. E., Eastermann, I., and Lundberg, W. O., 1937, *Rev. Sci. Instr.*, **8**, 422.  
Chester, P. F. and Jones, G. O., 1953, *Proc. Phys. Soc.*, **66B**, 296.  
Collins, S. C., 1947, *Rev. Sci. Instrum.*, **18**, 157.  
Croft, A. J., *Progress in Cryogenics*, Vol. **3**, p. 3.  
Daunt, J. G., and Mendelsohn, K., 1948, *J. Sci. Instrum.*, **20**, 122.  
Fairbank, H. A., 1946, *Rev. Sci. Instr.*, **17**, 473.  
Jacobs, R. B., and Collins, S. C., 1940, *J. Appl. Phys.*, **11**, 491.  
Lacaze, A., and Weil, L., 1955, IXth Conference of Refrigeration, Paris, p. 1.  
Meissner, W., Schmeissner, F., and Wiedemann, W., 1957, *Kaltetechnik*, **9**, 194.  
Rollin, B. V., 1936, *Proc. Phys. Soc. (London)*, **48**, 18.  
Ruhemann, M., 1930, *Zeits. f. Physik*, **65**, 67.  
Sharma, J. K. N., 1959, *J. Sci. Inst.*, **36**, 50.  
Sharma, J. K. N., 1961, *J. Sci. Ind. Res.*, **20D**, 356.  
Starr, C. J., 1941, *Rev. Sci. Instr.*, **12**, 193.



# DIELECTRIC ABSORPTION OF 7.7 mm MICROWAVES IN SOME POLAR LIQUIDS

## Part I—Alkyl Benzenes

J. BHATTACHARYYA, S. B. ROY AND G. S. KASTHA

OPTICS DEPARTMENT, INDIAN ASSOCIATION FOR THE CULTIVATION OF SCIENCE, CALCUTTA-32

(Received October 7, 1964)

**ABSTRACT.** Measurements on dielectric loss ( $\tan \delta$ ) at 38.8 KMc/s have been carried out on toluene, ethyl benzene, isopropyl benzene, *o*-xylene and *m*-xylene in the liquid state at different temperatures. Debye equation for solutions between  $\tan \delta$  and  $\tau$  has been changed into an expression between  $\tan \delta$  and  $\eta$  with the help of the rate equations in the form

$$\frac{T \tan \delta}{c\mu^2} = \frac{(\epsilon + 2)^2}{\epsilon} \cdot \frac{4\pi N\alpha\omega}{27k} \cdot \frac{\eta^\gamma}{1 + \alpha^2\omega^2\eta^2\gamma}$$

The applicability of the Debye equation has been justified in the case of pure liquids having dipole moments less than 1 D. from the superposition of the plots of  $\frac{T \tan \delta}{c\mu^2}$  ( $\tan \delta$  obtained experimentally) vs  $\eta$  over the theoretical curves derived from the left hand side expression of the above equation with  $\gamma = 1$  and suitable values of  $\alpha$ .

The values of relaxation time, the activation energies for viscous flow and dielectric relaxation have been determined. It has been found that the volumes of the rotors at any temperature for the various alkyl benzenes calculated with the help of the Debye relation between  $\tau$  and  $\eta$  do not show any quantitative correlation with the molar volumes of the respective compounds at the corresponding temperatures.

## INTRODUCTION

The validity of the Debye expression for dielectric loss ( $\tan \delta$ ) accompanying absorption of microwaves by polar molecules in dilute solutions in nonpolar solvents, where dipole-dipole interactions could be expected to be negligible, has been well established. But in the case of pure liquids the stronger dipolar interactions render the applicability of the Debye expression uncertain. However, in the case of pure liquids having molecules with small dipole moments the dipolar interactions will be weaker. Whiffen and Thompson (1946) studied the absorption of microwaves of wavelength 1.27 cm in toluene, *o*-xylene and a few other organic compounds in the pure liquid state. They considered the liquids as cent-percent solutions in non-polar solvents and using the Debye equation determined the dipole moments which were in agreement with the (corresponding) literature values. Petro and Smyth (1957) on the other hand measured dielectric constants

and losses at wavelengths 1.25 cm, 3.22 cm and 10 cm at three different temperatures in the case of some alkyl benzenes and other polar organic compounds in the pure liquid state and determined the values of  $\lambda_m$  at these temperatures for all these compounds by using Cole-Cole arc plot method. They discussed the dependence of relaxation times and viscosities on molecular shapes and sizes. Whiffen and Thompson as well as Petro and Smyth tacitly assumed the validity of the Debye expression for dielectric loss for all the polar liquids studied by them. However, though the values of dipole moments obtained by the authors from the Debye equation are in fair agreement with each other, the values of  $\tau$  for a certain compound at a certain temperature are quite different. As the conclusions arrived at by these authors about molecular size and other molecular properties would depend upon the correctness of the values of  $\tau$ , it would be desirable to test the accuracy of the value of  $\lambda_m$  reported by Petro and Smyth. For this purpose the measurements in the present case have been made at still higher microwave frequencies so that the maximum absorption in the alkyl benzenes which is expected to occur within a range of 100°C may be observed experimentally. Moreover, as the study of the pure liquids is likely to provide new data about the packing of molecules in the state of aggregation, where the "solvent effect" in dilute solutions (Müller, 1932; Jenkins, 1936) could be avoided, a careful study of the applicability of the Debye equation in the case of pure liquids is necessary. Even the deviations from the validity of the equation may bring out the degree of importance of dipolar interactions in the pure liquids and may throw light on the structure of liquids. With these objects in view, a programme of work was undertaken to investigate the dielectric loss in the still lower microwave region (7.7 mm) in the case of some polar liquids having widely different dipole moments. The present paper discusses the results obtained with some polar benzene derivatives in the pure liquid state, where the values of the dipole moments of the molecules lie within a limit of one Debye unit.

#### EXPERIMENTAL

The polar liquids studied in the present investigation are toluene, ethyl benzene, isopropyl benzene, *o*-xylene and *m*-xylene. All the chemicals, obtained from reputed firms, were of chemically pure quality. These were first fractionated and the proper fractions were repeatedly distilled under reduced pressure and dried by usual methods before being used in the investigations. The experimental arrangement for the determination of dielectric loss was the same as described in an earlier paper (Bhattacharyya *et al.*, 1964). Absorption of microwaves (38.8 K Mc/s) by the pure liquids taken in a U-shaped cell was measured at different temperatures in terms of  $dh$ , which were then converted into  $\tan \delta$ -values. In the case of all the polar compounds absorption maxima were obtained within the range of temperature variations produced in the bath. The values of the static dielectric constants at different temperatures were taken from the Inter-

national Critical Tables. The values of viscosity and density at different temperatures for all the compounds excepting isopropyl benzene were taken from the Landolt Börnstein Tables, while those for isopropyl benzene were determined experimentally.

## RESULTS AND DISCUSSION

The values of the dielectric loss ( $\tan \delta$ ) for all the polar liquids at different temperatures along with the corresponding macroscopic viscosity  $\eta$ , time of relaxation  $\tau$  (calculated by the method described in the following section) and the ratio  $\tau/\eta$  are given in Tables (I-V). The plots of  $\frac{T \tan \delta}{c}$  against  $T$  in some cases are shown in Figures 1, 2 and 3.

TABLE I

Toluene

6 cc of the liquid in the cell. Frequency—38.8 KMc/sec.

Temp. °C	$\tan \delta \times 10^3$	$\tau \times 10^{12}$ sec.	$\eta$ in c.poise	$\tau/\eta \times 10^{10}$
1	18.39	9.60	0.75	12.7
12	18.93	8.70	0.65	13.4
32	20.01	6.46	0.51	12.7
44	20.38	5.25	0.44	11.9
52	20.02	5.03	0.41	12.3
62	19.64	4.10	0.37	11.1
74	18.54	3.55	0.33	10.8
84	17.75	3.48	0.31	11.2

TABLE II

Ethyl benzene

5 cc. of the liquid in the cell Frequency—38.8 KMc/sec

Temp. °C	$\tan \delta \times 10^3$	$\tau \times 10^{12}$ sec	$\eta$ in c.poise	$\tau/\eta \times 10^{10}$
30	22.95	8.25	0.59	13.98
40	23.75	7.18	0.555	10.96
50	25.39	5.45	0.475	11.48
60	24.84	5.00	0.43	11.62
70	24.08	4.46	0.395	11.30
80	23.31	4.10	0.36	11.39
90	21.95	3.61	0.33	10.93
95	21.58	3.56	0.32	11.12

TABLE III

Isopropyl benzene

5 cc of the liquid in cell. Frequency—38.8 KMc/sec

Temp. °C	$\tan \delta \times 10^3$	$\tau \times 10^{12}$ sec	$\eta$ in c.poise	$\tau/\eta \times 10^{10}$
31	22.10	9.30	0.69	13.48
44	23.00	8.01	0.57	14.05
54	23.96	6.86	0.52	13.19
60	24.46	6.26	0.50	12.52
70	25.20	4.89	0.45	10.86
75	25.01	4.67	0.44	10.61
80	24.57	4.10	0.41	10.00
85	24.01	3.60	0.39	9.23
90	23.41	3.35	0.37	9.05
98	22.15	2.98	0.35	8.51

TABLE IV

*o*-Xylene

3 cc of the liquid in cell. Frequency—38.8 KMc/sec

Temp. °C	$\tan \delta \times 10^3$	$\tau \times 10^{12}$ sec	$\eta$ in c.poise	$\tau/\eta \times 10^{10}$
2	39.13	12.32	1.08	11.4
32	42.51	9.21	0.69	13.3
50	43.90	7.66	0.56	13.6
60	44.53	7.03	0.50	14.1
70	45.24	6.18	0.45	13.7
80	45.20	5.49	0.415	13.2
95	44.64	4.10	0.355	11.6
110	41.93	3.54	0.34	10.4

TABLE V

*m*-Xylene

6 cc of the liquid in cell. Frequency—38.8 KMc/sec

Temp. °C	$\tan \delta \times 10^3$	$\tau \times 10^{12}$ sec	$\eta$ in c.poise	$\tau/\eta \times 10^{10}$
2	13.53	12.34	0.74	15.7
17	14.32	10.56	0.64	16.5
33	14.80	9.01	0.53	17.0
54	15.08	7.68	0.43	17.8
70	15.32	6.42	0.37	17.3
80	15.54	5.50	0.34	16.2
90	15.29	5.06	0.31	16.3
98	15.13	4.10	0.29	14.1
115	13.59	2.98	0.27	11.1

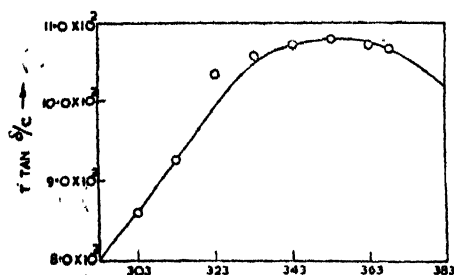


Fig. 1. Variation of  $T \tan \delta/c$  with  $T$  for Ethylbenzene in the liquid state.

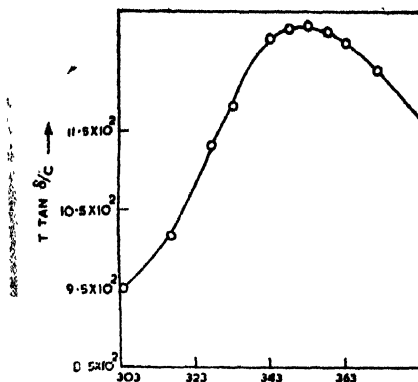


Fig. 2. Variation of  $T \tan \delta/c$  with  $T$  for Propylbenzene in the liquid state.

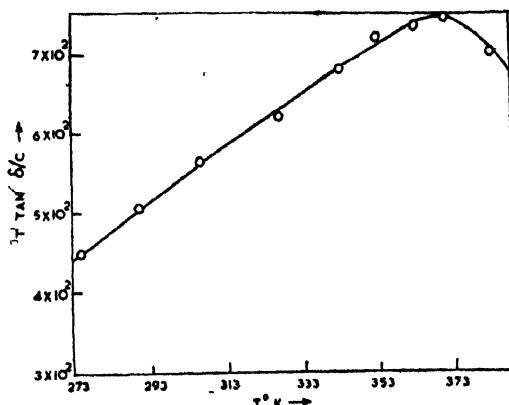


Fig. 3. Variation of  $T \tan \delta/c$  with  $T$  for *m*-Xylene in the liquid state.

(a) *Applicability of the Debye equation for dielectric loss to some polar alkyl benzenes in liquid state.*

The Debye equation for dielectric loss in the case of polar liquids is given by

$$\tan \delta = \frac{(\epsilon_1 - \epsilon_0)x}{\epsilon_1 + \epsilon_0 x^2} \quad \dots (1)$$

with  $x = \frac{\epsilon_1 + 2}{\epsilon_0 + 2} \omega \tau$ , where  $\epsilon_1$  and  $\epsilon_0$  are dielectric constants at static field and infinite frequency respectively. For the polar liquids studied in the present investigation  $\epsilon_1 \approx \epsilon_0$  and the dipole moments being small in all the cases the internal field acting on the molecules of each liquid becomes almost equal to the externally applied field and the Debye equation reduces to the simple form (Fröhlich)

$$\tan \delta = \frac{\epsilon_1 - \epsilon_0}{\epsilon_1} \cdot \frac{\omega \tau}{1 + \omega^2 \tau^2} \quad \dots (2)$$

Now the polar liquids are considered as cent percent solutions in non-polar solvents (Whiffen and Thompson, 1946) and the equation (2) takes the well known form in the case of dilute solutions,

$$\tan \delta = \frac{(\epsilon+2)^2}{\epsilon} \cdot \frac{4\pi N c \mu^2}{27kT} \cdot \frac{\omega\tau}{1+\omega^2\tau^2} \quad \dots (3)$$

where the various symbols have their usual meaning.

As  $\tau$  can not be measured by any other independent method, eqn. (3) can not be used to verify directly its validity in the case of polar liquids studied in the present investigation. However, using the rate equations for viscous flow and dielectric relaxation (Whiffen and Thompson, 1946)  $\tau$  may be expressed as a function of viscosity in the form  $\tau = \alpha\eta^\gamma$  ( $\gamma = \frac{E\tau}{E\eta}$ ) and the Debye equation (3) can be expressed as,

$$\frac{T \tan \delta}{c\mu^2} = \frac{(\epsilon+2)^2}{\epsilon} \cdot \frac{4\pi N \alpha \omega}{27k} \cdot \frac{\eta^\gamma}{1+\alpha^2\omega^2\eta^{2\gamma}} \quad (4)$$

With suitable values of  $\alpha$  and  $\gamma$  used as parameters and values of  $\epsilon$  taken from literature, the L.H.S. of eqn. (4) has been plotted as a function of  $\eta$  for some of

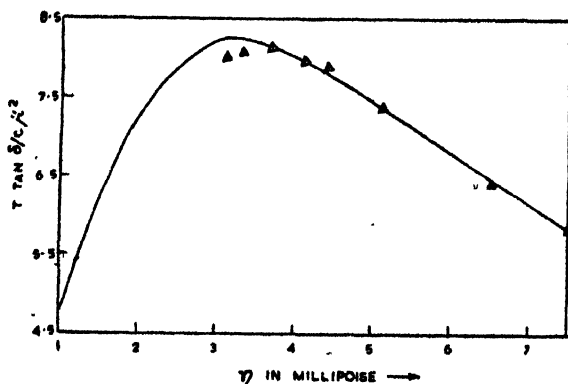


Fig. 4. Graph of  $T \tan \delta / c\mu^2$  against  $\eta$  for Toluene. Solid line denotes theoretical curve.  $\Delta$ —Experimental points.

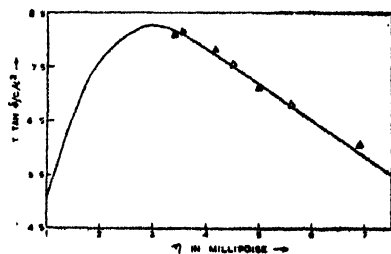


Fig. 5. Graph of  $T \tan \delta / c\mu^2$  against  $\eta$  for o-Xylene. Solid line denotes theoretical curve.  $\Delta$ —Experimental points.

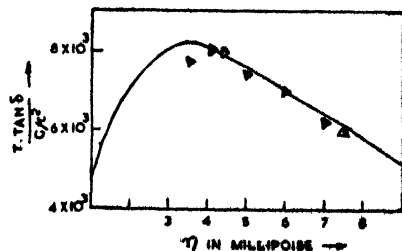


Fig. 6. Graph of  $T \tan \delta / c\mu^2$  against  $\eta$  for Isopropylbenzene. Solid line denotes theoretical curve.  $\Delta$ —Experimental points.

the compounds as shown in figures 4, 5 and 6. With experimentally observed values of  $\tan \delta$  and the values of  $\mu$  reported by Altshuller (1954), the plots of  $\frac{T \tan \delta}{c\mu^2}$  against viscosities at different temperatures are again made. It is seen that the experimental points lie very nearly on the theoretical curves in all the cases. However, the values of  $\alpha$  are different for different compounds. The superposition of the experimental curves over the theoretical ones in the case of polar liquids under investigation shows that the modified Debye eqn. (4) for dielectric loss is valid in the case of polar liquids having dipole moments less than 1 D. However, in the present case the value of  $\gamma$  is taken to be unity for all the liquids. This gives a linear dependence of  $\tau$  on  $\eta$  as is also implied in the Debye relation  $\tau = 4\pi\eta a^3/kT$  and therefore, the validity of eqn. (4) may be taken to imply the validity of the Debye eqn. (3) itself.

Incidentally, it may be pointed out that since for each of the liquids only one Debye curve satisfactorily describes the dependence of dielectric loss on viscosity, only one mode of relaxation is necessary for the molecules composing each of the liquids.

(b) Calculation of  $\mu$ ,  $\tau$ ,  $E\tau$  and  $E\eta$ .

The values of dipole moment  $\mu$  for each of the polar liquids have been calculated from Eqn. (3) by using  $\omega\tau = 1$  for the maximum of the graph of  $T \tan \delta$  against  $T$ . The values of  $\mu$  obtained here along with those reported by other workers (Petro and Smyth 1957; Whiffen, 1946; Altshuller 1954) are given in Table VI. The agreement is quite satisfactory. The value of  $\tau$  at any temperature  $T$  has been calculated with the relation

$$\left( \frac{T \tan \delta}{c} \right)_T \bigg/ \left( \frac{T \tan \delta}{c} \right)_{max} = \frac{2\omega\tau}{1 + \omega^2\tau^2}$$

TABLE VI

Dipole moments in Debye unit obtained by various workers

Substance	Present authors	Petro & Smyth	Whiffen & Thompson	Altshuller
Toluene	0.30	0.31	0.32	0.31
Ethyl benzene	0.36	0.37	—	0.37
Isopropyl benzene	0.40	0.39	—	0.37
<i>o</i> -Xylene	0.51	0.52	0.53	0.50
<i>m</i> -Xylene	0.30	0.31	—	0.31

The values of  $\tau$  for the compounds studied at different temperatures are given in Tables (I-V). It is seen from the Tables (I-V) that in each case  $\tau/\eta$  is almost constant, which is different for different compounds.

The values of molar activation energy  $E_\tau$  for dielectric relaxation and that for viscous flow  $E_\eta$  have been obtained respectively from the plots of  $\log \tau$  vs  $1/T$

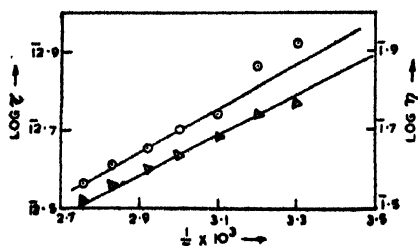


Fig. 7. Ethylbenzene

O —Plot of  $\log_{10} \tau$  against  $1/T$ .

Δ —Plot of  $\log_{10} \eta$  against  $1/T$ .

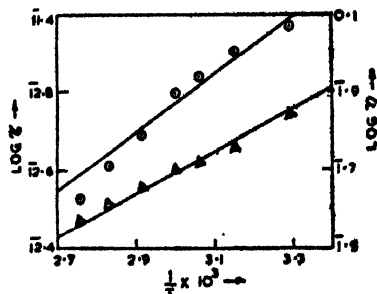


Fig. 8. Isopropylbenzene

O —Plot of  $\log_{10} \tau$  against  $1/T$ .

Δ —Plot of  $\log_{10} \eta$  against  $1/T$ .

and  $\log \eta$  vs  $1/T$  as usual (Figs. 7 and 8). The values of  $E_\eta$  and  $E_\tau$  are given in Table VII. It is seen that in almost all the cases  $E_\tau \approx E_\eta$  within experimental error. The value of the parameter  $\gamma = \frac{E_\tau}{E_\eta} \approx 1$  used to calculate the theoretical values of  $\frac{T \tan \delta}{c\mu^2}$  is thus justified.

It can be seen from Tables I-V that the values of time of relaxation  $\tau$  for the alkyl benzenes at any temperature increase in the order of toluene < ethylbenzene < isopropylbenzene < *o*-xylene < *m*-xylene. The values of  $\tau$  for toluene and *o*-xylene at different temperatures obtained in the present investigation agree well with those reported by Whiffen and Thompson (1946). But the values of  $\tau$  reported by Petro and Smyth (1957) in the case of ethyl benzene, isopropylbenzene, ortho- and meta-xylenes are much different from those obtained in the present case, although the values of  $\tau$  for toluene at different temperatures are almost the same in both cases. It may also be noted that the order of increase in the values of  $\tau$  for toluene, ethyl benzene and isopropyl benzene are similar in both cases. The  $\tau$ -values for ortho- and meta-xylenes are largest in the present investigation while those reported by Petro and Smyth (1957) are smaller than those for ethyl benzene and isopropyl benzene.

From a comparison of the values of dielectric loss ( $\tan \delta$ ) at different temperatures for *o*-Xylene, calculated from the values of  $\epsilon'$  and  $\epsilon''$  given by Petro and Smyth, with those reported by Whiffen and Thompson, it is found that the  $\tan \delta$  values in the former case are lower by 10-15% than those in the latter case and consequently, the former  $\tau$ -values are lower than the latter. Petro and Smyth used the Cole-Cole arc plot to obtain the values of critical wavelength ( $\lambda_m$ ) from measurements of  $\epsilon'$  and  $\epsilon''$  at only two microwave frequencies (1.25 cm and 3.22 cm). Thus the accuracy in the measurement of  $\lambda_m$  is very limited. Moreover, it has been observed in the present investigation that the values of  $\lambda_m$



for various alkyl benzenes occur at 7.7 mm at temperatures much lower than those to be expected from the data given by Petro and Smyth. So it appears that the inaccuracy in the determination of  $\lambda_m$  has resulted in the inaccurate values of  $\tau$  reported by them.

Petro and Smyth attempted to show that the  $\tau$ -values of various benzene compounds increase in the order of their molar volumes  $V (= M/d)$ . In the case of toluene, ethyl benzene, isopropyl benzene where the various alkyl group are substituted at the same *C*-atom of the benzene ring, the above correlation between  $\tau$  and  $V$  has also been observed to hold qualitatively in the present investigation. But in the case of ortho- and meta-xylenes where the methyl groups are substituted at two different *C*-atoms of the benzene ring, even such qualitative correlation is not observed.

TABLE VII

		$\tau \times 10^{12}$ sec.	$\eta$ milli-poise	$\tau/\eta \times 10^9$	Molar Vol. (V) cc.	Volume of the rotor in Å <sup>3</sup>	$E\tau$ K.Cal/ mole	$E\eta$ K.Cal/ mole
Toluene	a	4.1	3.7	1.11	111.0	16.9	2.15	2.05
	b	4.6	3.8	1.21		—	1.9	2.0
	c	4.1	3.8	1.09		—	2.2	2.2
Ethyl benzene	a	5.0	4.3	1.16	127.6	17.7	2.62	2.40
	b	—	—	—		—	—	—
	c	6.2	4.4	1.57		—	2.5	2.1
Isopropyl benzene	a	6.26	5.0	1.25	145.2	19.2	3.45	2.62
	b	—	—	—		—	—	—
	c	9.8	4.9	2.00		—	3.1	2.3
o-Xylene	a	7.03	5.0	1.41	125.4	21.4	2.16	2.26
	b	6.9	5.0	1.38		—	1.9	2.3
	c	5.3	5.0	1.06		—	2.1	2.3
m-Xylene	a	7.0	4.0	1.75	127.9	26.7	1.95	1.97
	b	—	—	—		—	—	—
	c	5.3	4.1	1.30		—	2.3	2.0

a—Present authors, b—Whiffen and Thompson (1946), and c—Petro and Smyth (1957).  
The values of  $\tau$ ,  $\eta$  and  $V$  given above are for 333°K in each case.

However, it is found from Table VII that the order of increase of  $\tau$ -values from toluene to *m*-xylene is the same as that of the corresponding  $\tau/\eta$ -values. By using the Debye relation  $a^3 = \frac{kT}{4\pi} \cdot \tau/\eta$ , the volume of the rotor at 333°K in case of each of the benzene derivatives has been calculated. These are given in Table VII along with the values of the molar volume for the respective compounds at the same temperature.

It is seen that there is no quantitative correlation between the two sets of values as regards either their relative order or their actual values. This makes

the identification of the rotor with the whole molecule uncertain. This uncertainty renders any inference about the molecular sizes and the degree of packing of the molecules in the liquid state rather unjustified. In conclusion, it is again stressed that very accurate determinations of the times relaxation for the various polar molecules in the liquid state over a wide range of temperature are necessary in order that reasonable quantitative values of certain molecular parameters may be obtained.

#### ACKNOWLEDGMENT

The authors wish to express their thanks to Prof. S. C. Sirkar, D.Sc., F.N.I. for helpful discussions.

#### REFERENCES

- Altshuller, A. P., 1954, *J. Phys. Chem.*, **58**, 392.  
Jenkins, H. O., 1936, *J. Chem. Soc.*, 862.  
Müller, A., 1932, *Physik, Z.*, **33**, 731.  
Petro, A. J. and Smyth, C. P., 1957, *J. Am. Chem. Soc.*, **79**, 6142.  
Bhattacharyya, J., Sinha, B., Roy, S. B. and Kastha, G. S., 1964, *Ind. J. Phys.*, **38**, 413.  
Whiffen, D. H. and Thompson, H. W., 1946, 'Dielectrics', a general discussion held by Faraday Soc., p. 122.

# STUDY OF PROPERTIES OF FLEXIBLE ARTIFICIAL DIELECTRIC

S. S. GUPTA AND M. N. SHARMA

DEPARTMENT OF PHYSICS, UNIVERSITY OF LUCKNOW, LUCKNOW

(Received August 13, 1964)

**ABSTRACT.** Flexible artificial dielectrics have been constructed by embedding metal powders in polythelene. The dielectric constant and loss tangents of these dielectrics have been determined experimentally at radio frequency (10.75 MC/s). Variation of the modulus of elasticity with percentage of metal particles of the metal embedded media have been studied. Results show that there is a simple relationship between modulus of elasticity and the dielectric constant. These flexible dielectrics may prove more advantageous than those constructed by embedding microscopic conducting particles in wax, due to former's mechanical properties, moulding ease and the wide temperature range within which they can be used.

## INTRODUCTION

There are two well known types of artificial dielectrics, one consists of an array of wave guides and the second one comprises of a cubic lattice of conducting particles having a size and separation small compared with the wave length. Such a medium was proposed by Kapzov as early as 1922 and Kock (1948) gave it a practical form. Carruthers (1951) later on proposed a dielectric medium, suitable for very short wavelengths, consisting of light weight medium embedded with some fine metal powder. Kelly and coworkers (1953) measured the dielectric properties of metal powders in paraffin wax using the microwave technique. Same type of work has been reported by Negebauer (1952), Peppiatt (1953), Mayer *et al.* (1956) and Mickaelion (1955). The dielectric properties of such media are affected by (a) volume fraction of conducting particles (b) size and shape of metal particles and (c) binding medium. Recently Pradhan and Gupta (1961) have shown that it also depends on the elemental spacing distribution of particles.

Most of the workers used paraffin wax as binding medium due to ease with which it could be handled, but we have used polythelene as binding medium in the construction of flexible artificial dielectrics, although polythelene is tough in handling but is more advantageous due to its mechanical properties, ease in moulding, resistance to moisture and the wide temperature range within which it can be used.

## EXPERIMENTAL PROCEDURE

**Preparation of samples :** Polythelene granules ( $\epsilon = 2.3$ ,  $\tan \delta = 0.001 \times 10^{-4}$ , density,  $d = 0.91$  gm/mL and modulus of elasticity,  $E = 9.83 \times 10^8$  dynes/cm<sup>2</sup>) and metal powder each were weighed in calculated quantity for a particular sample.

The mixture of polyethelene granules and metal powder was put in a air tight vessel, having a mechanical mixing arrangement. The vessel was heated in a temperature regulated electrical oven for about 30 minutes, keeping the temperature of oven at about 110°C. This process melted the polyethelene. The molten mixture was continuously stirred and then it was cooled till it solidified. The solid mass was removed with a scraper, the scraped mass was dessicated for 36 hours and then was moulded under compression in a hot brass cast in the form of disc. These moulded samples were grinded and polished.

*Procedure :* The method of Hartshorn and Ward (1936), for the measurement of dielectric constant and loss tangent at radio frequencies was used. The dielectric constant and loss tangent of different samples were determined at 10.75 MC/S as described in detail by Sharma (1960), Pradhan and Sharma (1960) and Sharma and Gupta (1962).

The dielectric constant  $K$  of a solid sample is given by

$$K = \frac{3.6C_s t}{r^2} \quad (1)$$

where  $C_s$  is capacitance of the sample in  $\mu\mu F$ ,  $t$  the thickness of the sample and  $r$  is the radius of the electrodes (2.5 Cms).

The loss tangent is given by

$$\tan \delta = \frac{\Delta C_1 - \Delta C_0}{2C_s} \quad \dots (2)$$

where  $\Delta C_1$  is capacitance change corresponding to half of the maximum deflection with sample in between the two copper electrodes and  $\Delta C_0$  is the capacitance change corresponding to half of the maximum deflection without the sample.

The moduli of elasticity of various samples were determined as follows :

The scraped mixture of polyethelene and conducting particles used for dielectric samples was moulded in the form of thin rods having circular cross-section (about 10 Cms. long and 1 mm. thick). One end of the rod was clamped to a rigid support and at the other end of the rod the stress was applied. The lengths between the two clamps, radius and elongation of each sample were measured with a travelling microscope having a least count of 0.0001 Cm. Thus, knowing stress and strain, elastic moduli for different samples were calculated.

## RESULTS AND DISCUSSION

Experimental determination of dielectric  $K_s$  and loss tangent for different metal powder artificial dielectrics has been carried out at 10.75 MC/S. for different concentrations of metal powders. Values are given in Tables I and II. Variation of dielectric constant  $K_s$  and loss tangent for aluminium, copper, antimony and zinc with concentration are shown in Figs. 1 and 2 respectively.

Microscopic examination of particle used, showed that aluminium particles ( $9\mu \times 7\mu \times 8\mu$ ) were in the shape of the discs, copper ( $18\mu \times 10\mu \times 9\mu$ ) and antimony

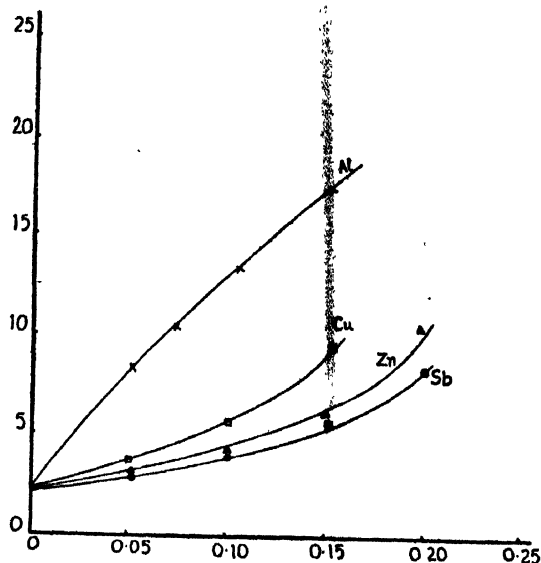


Fig. 1. Variation of dielectric constant with volume fraction.

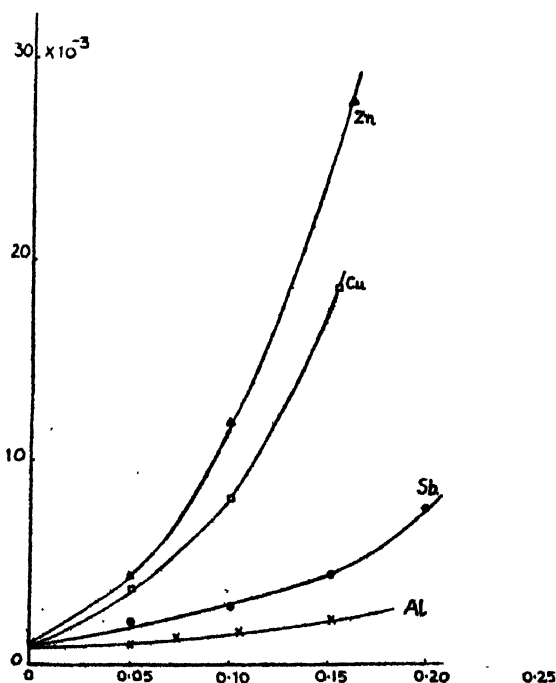


Fig. 2. Variation of loss tangent of met. l powder artificial dielectrics with volume fraction.

( $5\mu \times 4\mu \times 2\mu$ ) particles were irregular in form while zinc ( $5\mu$  in diameter) particles were more or less spherical. From theoretical considerations, it may be noted

that for the same volume fraction of conducting particles, aluminium dielectrics should have highest dielectric constant while copper dielectrics should have dielectric constant higher than those of antimony and zinc. For the last two materials, i.e., for antimony and zinc, the antimony dielectrics should have higher dielectric constant. Experimental results verify expectations for aluminium and copper dielectrics but in case of antimony and zinc dielectrics the case is just reversed.

On calculating  $\alpha_s/\epsilon_0$ , for aluminium, zinc and antimony mixtures from the Clausius-Mossotti relation

$$\frac{K_s - K}{K_s + K} = \frac{N}{3} (\alpha_s/\epsilon_0) \quad (3)$$

and plotting it against the fractional volume of conducting particles (Fig. 3),

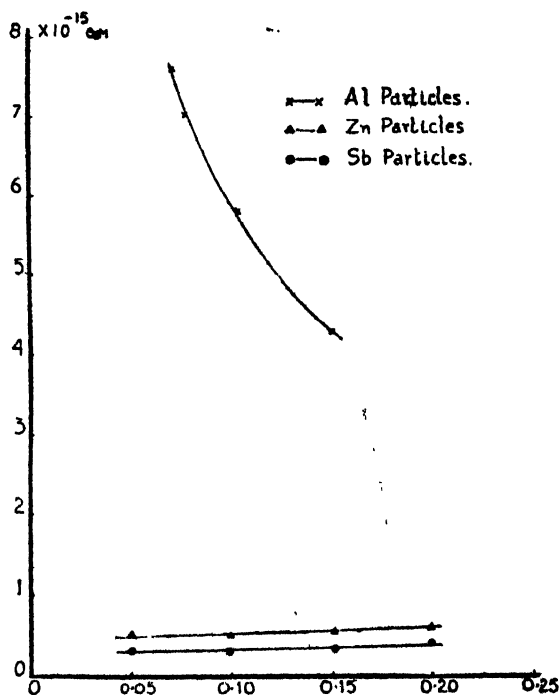


Fig. 3. Variation of polarizability with fractional volume of particles.

we observe that the polarizability in case of aluminium particles decreases with increasing concentration which may be attributed to change in shape of aluminium disc particles to ellipsoidal form. For zinc particles the polarizability increases with concentration, showing that particle shape is altered due to agglomeration of particles. The distribution of particles is also such that there is considerable interaction between the particles. The resulting curve of polarizability for antimony particles is horizontal, pointing out that the polarizability remains constant with variation in volume fraction, although it should have increased due to agglomeration. This indicates that either there is no agglomeration or there is no interaction between the particles.

Let us consider the case of copper, antimony and zinc dielectrics, i.e., which are constructed by embedding particles of heavier metals. For the same volume fraction of conducting particles, the dielectric constant was highest for copper dielectrics and lowest for antimony dielectrics i.e. highest for the dielectric shaving

$$25 \times 10^8$$

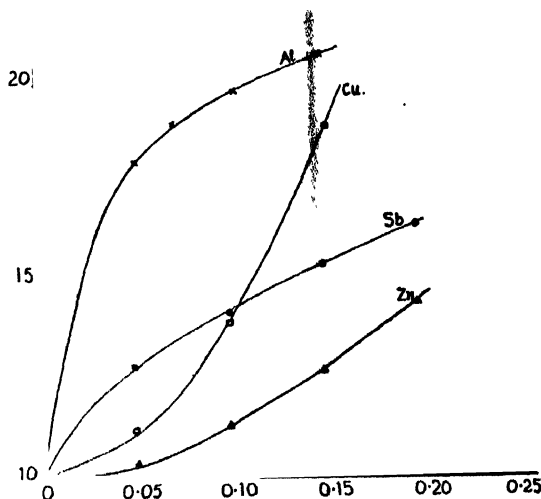


Fig. 4. Variation of modulus of elasticity with concentration of metal particles.

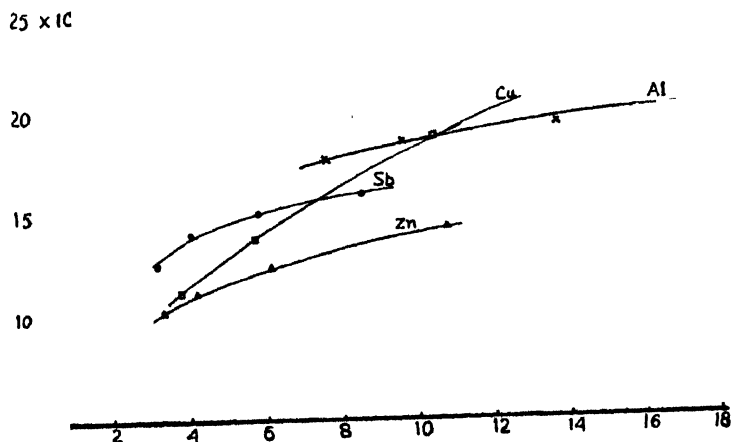


Fig. 5. Variation of mechanical strength of metal artificial dielectrics with dielectric constant.

particles of highest electrical conductivity and vice-versa. This indicates that the dielectric constant of artificial dielectric also depends on the electrical conductivity of the metallic particles used.

The variation of modulus of elasticity with concentration of conducting particles and with the dielectric constant are shown in Figs. 4 and 5. The curves show that a simple relationship exists between the modulus of elasticity and the dielectric constants of these artificial dielectrics.

Interesting results might be obtained if measurements on these flexible artificial dielectrics are extended to microwave region.

TABLE I

Variation of dielectric constant of metal powder artificial dielectrics with concentration.

Aluminium		Copper		Antimony		Zinc	
Fractional volume	$K_e$	Fractional volume	$K_e$	Fractional volume	$K_e$	Fractional volume	$K_e$
4.930	8.53	4.885	3.764	4.957	3.089	4.974	3.214
7.231	10.36	9.951	5.654	9.988	3.957	9.856	4.130
10.401	13.66	15.290	9.621	15.120	5.712	14.950	6.091
15.220	17.61	—	—	19.950	8.958	19.070	10.700

TABLE II

Variation of loss tangent of metal powder artificial dielectrics with concentration.

Aluminium		Copper		Antimony		Zinc	
Fractional volume	$\tan \delta \times 10^4$	Fractional volume	$\tan \delta \times 10^4$	Fractional volume	$\tan \delta \times 10^4$	Fractional volume	$\tan \delta \times 10^4$
4.930	10.32	4.885	38.05	4.957	22.31	4.974	42.30
7.231	14.94	9.951	80.28	9.988	26.80	9.856	119.10
10.401	15.54	15.290	189.50	15.120	44.31	14.950	283.60
15.220	23.12	—	—	19.950	79.29	19.070	733.00

## ACKNOWLEDGMENT

Authors are indebted to Professor P. N. Sharma for his kind interest and encouragement. Authors are also grateful to Dr. B. P. Pradhan for supervision of the work.

## REFERENCES

- Carruthers, J. A., 1951, United States Air Force Contract No. AF 19(122)81, Eaton Electronic Research Laboratory Rep. No. 5.  
 Hartshorn, L. and Ward, W. H., 1936, *Proc. Inst. elect. Engrs.*, **79**, 597.  
 Kapzov, N., 1922, *Ann. Phys., Lpz.*, **69**, 112.  
 Kelly, J. M., Stenoien, J. O. and Isbell, D. E., 1953, *J. appl. Phys.*, **24**, 258.  
 Kock, W. E., 1948, *Bell. Syst. Tech. J.*, **27**, 58.  
 Meyer, E., Schmitt, H. J. and Severin, H. 1956., *Z. angew. Phys.*, **8**, 257.  
 Mikaelian, A. L., 1955, *Radiotekhnika*, Moscow, **10**, 1.  
 Neugebauer, H. E. J., 1952, Air Force Contract No. AF19(122)81, Eaton Electronic Research Laboratory Rep. No. 6.  
 Peppiatt, H. J., 1953, United States Air Force Contract No. AF19(122)81, Cambridge Research Centre Rep. No. D6.  
 Pradhan, B. P. and Sharma, M. N., 1960, *Proc. Nat. Inst. Sci.*, **26 A**, 560.  
 Pradhan, B. P. and Gupta, R. C. 1961, *J. Sci. industr. Res.* **20B**, 581.  
 Sharma, M. N., 1960, *J. sci. industr. Res.*, **19B**, 5.  
 Sharma, M. N. and Gupta, S.S. 1963, *Ind. J. Phys.*, **37**, 33.



# SIMULTANEOUS OSCILLATIONS AT THREE FREQUENCIES IN A REGENERATIVE CIRCUIT WITH A LIMITER TYPE NON-LINEAR ELEMENT\*

B. N. BISWAS

DEPARTMENT OF PHYSICS, THE UNIVERSITY OF BURDWAN, WEST BENGAL.

(Received August 10, 1964)

**ABSTRACT.** In this paper the phenomenon of simultaneous oscillations at three anharmonically related frequencies in a regenerative loop, containing a limiter type non-linear element, has been analysed. The effects of finite selectivity of the modes on the locking range have been studied. The response of such a loop to an external input has also been analysed. A possible method for the elimination of the 'three-frequency effect' in such a circuit has been suggested. An experimental arrangement of such a regenerative loop, containing adjustable selectivity and gain control arrangement, has been described. Experimental results have also been presented in support of the conclusions of the analysis

## INTRODUCTION

The weak-signal suppression effect in non-linear regenerative tuned circuits has been examined by many authors. It is known that compression type characteristics are mutually destructive and expander type characteristics, on the other hand, are mutually supporting.

In this paper it will be shown that the compression type characteristics of a limiter may sometimes become mutually supporting in nature with respect to signals having certain phase and amplitude relationship among themselves. In particular, if the input to the limiter consists of three components the frequencies of which are anharmonically related and the phases are related as in a phase modulated wave and further if the amplitudes of the different signals are properly related, then the stronger signals may help the growth of the weaker ones. Thus with respect to such signals the destructive character of the limiter is lost. Therefore if the limiter is incorporated in a regenerative loop containing adjustable frequency selective networks and further if the gain of the loop for different modes is properly adjusted, then simultaneous oscillations at three anharmonically related frequencies can be maintained.

---

\* This work has been done at the Institute of Radio Physics and Electronics, University of Calcutta, Calcutta.

This is a desirable result where continuously variable stable frequency oscillations are needed, e.g., in frequency synthesis. In some cases, however, it may cause serious trouble, e.g., in Automatic phase control circuits, where depending upon the gain and transmission characteristics of bandpass tuned circuits, the system may break into simultaneous oscillations at different frequencies.

In section 2 the transmission characteristics of two types of non-linear elements one having the limiter type non-linear transference and the other having the expander type non-linear transference—in the presence of three signals having certain phase relationships among themselves, have been briefly studied. It has been pointed out that it is possible to realise simultaneous oscillations at three frequencies in a feedback circuit which can independently support three distinct modes and contains a limiter type non-linear element in the loop. The region of amplitude stability has also been found out theoretically.

In section 3 the effects of finite selectivity of the modes on the shifts of the frequencies of oscillations from the resonant frequencies of the tuned circuits have been studied. The possibility of having continuously variable stable frequency oscillations has also been suggested.

Section 4 deals with the effect of an external input, having a frequency nearly equal to that of any one of the free running modes. Expressions for the critical value of the amplitude of the external input for quenching action and the corresponding expression for locking range have been found out.

In section 5, a method has been discussed for converting the regenerative loop, sustaining simultaneous oscillations at three-frequency, into a degenerative one with respect to the undesired components with the help of a non-linear phase shifting network.

In section 6, experimental arrangement of the regenerative loop containing the limiter type non-linear element has been described and experimental data with respect to the region of stable oscillations have also been presented, which are in good agreement with the region of amplitude stability found in Section 2.

## TRANSMISSION CHARACTERISTICS

### *"Three frequency effect" in a non-linear element or Internal synchronisation*

The phenomenon that gives rise to the loss of destructive character of a limiter with respect to three signals which have certain phase and amplitude relationship among themselves, is called the "three frequency effect". It is well known that when two non-coherent signals are applied to a limiter type non-linear transference, the strong signal will be captured and the weak signal will be rejected. The expander type characteristics, on the other hand, helps the weaker signal to build up. But if the phases of the components of the signal to the limiter are related as in a phase modulated wave and further if the amplitudes are properly

related, then the compressor type characteristic of the limiter type non-linear element will fail to be mutually destructive in nature, i.e. the presence of the stronger signals will help the growth of the weaker one. In this section this phenomenon will be briefly studied with respect to two types of non-linear elements one having the limiter type non-linear transference and the other having the expansion type non-linear transference.

Let us consider that the inputs to the non-linear elements are

$$\begin{aligned} e_A &= A \cos(\omega_A t + \phi_1) = A \cos \psi_A, \quad e_B = B \cos(\omega_B t + \phi_2) = B \cos \psi_B, \\ e_C &= C \cos(\omega_C t + \phi_3) = C \cos \psi_C, \end{aligned} \quad \dots (2.1a)$$

where  $A, B, C$  are the peak amplitudes of the signals and  $\psi_A, \psi_B$  and  $\psi_C$  are their instantaneous phases which are related as

$$\psi_A + \psi_C = 2\psi_B + \phi. \quad \dots (2.1b)$$

The input output characteristic of the non-linear element having the compressor type characteristics is assumed to be given by

$$X_{out} = a_1 X_{in} - a_3 X_{in}^3, \quad \dots (2.2)$$

and that of the expander type non-linear element is of the form

$$X_{out} = \sinh(X_{in}), \quad \dots (2.3)$$

where ' $X_{in}$ ' and ' $X_{out}$ ' are respectively the input and output of the non-linear element.

Therefore the outputs of the expander type non-linear element consisting of frequencies  $\omega_A = d\psi_A/dt$ ,  $\omega_B = d\psi_B/dt$  and  $\omega_C = d\psi_C/dt$  are given respectively by

$$T_A = 2[I_0(B)I_0(C)I_1(A) + I_0(A)I_2(B)I_1(C) \cos \phi], \quad \dots (2.3a)$$

$$T_B = 2[I_0(A)I_0(C)I_1(B) + I_1(A)I_1(B)I_1(C) \cos \phi], \quad \dots (2.3b)$$

$$T_C = 2[I_0(A)I_0(B)I_1(C) + I_0(C)I_1(A)I_2(B) \cos \phi], \quad \dots (2.3c)$$

where  $I_k(Z)$  is modified Bessel Function of order ' $k$ ' and argument ' $Z$ '. Taking  $\phi = (2n+1)\pi$  for the steady state, Eqs. (2.3a) (2.3b) and (2.3c) reduce to

$$T_A = 2[I_0(B)I_0(C)I_1(A) - I_0(A)I_2(B)I_1(C)], \quad \dots (2.3d)$$

$$T_B = 2[I_0(A)I_0(C)I_1(B) - I_1(A)I_1(B)I_1(C)], \quad \dots (2.3e)$$

$$T_C = 2[I_0(A)I_0(B)I_1(C) - I_0(C)I_2(B)I_1(A)]. \quad \dots (2.3f)$$

The plots of  $T_A$ ,  $T_B$  and  $T_C$  are shown in Fig. 1 for the case when  $A = C$  for different values of  $B$ . If the input to the expander type non-linear element consists of three components  $e_A$ ,  $e_B$  and  $e_C$ , and further if one assumes that the amplitude of  $e_A$  is equal to that of  $e_C$  and the amplitude of  $e_B$  is less than that of either  $e_A$

or  $e_0$  then one can find from the plots of Fig. 1 that after sometime all the signals will be found to grow, particularly the weaker one. Thus expander type characteristics help building up of weaker ones.

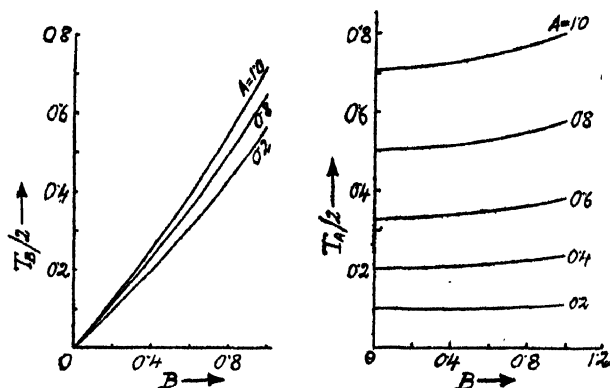


Fig. 1(a) & 1(b): The input-output characteristics for the three different components of a composite signal of an expander type non-linear element. The components of the composite signal bear a definite phase relationship among themselves, namely  $\psi_A + \psi_C = 2\psi_B + \pi$

Let us now consider the limiter type characteristic as represented by Eq. (2.2).

The outputs of the limiter type non-linear element consisting of frequencies  $\omega_A = d\psi_A/dt$ ,  $\omega_B = d\psi_B/dt$  and  $\omega_C = d\psi_C/dt$  are respectively given by

$$T_A = [A - \{A^3 + 2(B^2 + C^2)A + B^2C \cos \phi\}], \quad (2.4a)$$

$$T_B = [B - \{B^3 + 2(A^2 + C^2)B + 2ABC \cos \phi\}], \quad (2.4b)$$

$$T_C = [C - \{C^3 + 2(B^2 + A^2)C + AB^2 \cos \phi\}]. \quad (2.4c)$$

When the signals are non-coherent the  $\cos \phi$  terms drop out and the corresponding outputs are given by

$$T_A = [A - \{A^3 + 2(B^2 + C^2)A\}], \quad \dots \quad (2.5a)$$

$$T_B = [B - \{B^3 + 2(A^2 + C^2)B\}], \quad \dots \quad (2.5b)$$

$$T_C = [C - \{C^3 + 2(A^2 + B^2)C\}]. \quad \dots \quad (2.5c)$$

Now for the case when the phases are related as in Eq. (2.1b) taking  $\phi = (2n+1)\pi$  for the steady state, we have the following expressions for the output of the limiter type non-linear element for the different frequencies:

$$T_A = [A - \{A^3 + 2(B^2 + C^2)A - B^2C\}], \quad \dots \quad (2.4d)$$

$$T_B = [B - \{B^3 + 2(A^2 + C^2)B - 2ABC\}], \quad \dots \quad (2.4e)$$

$$T_C = [C - \{C^3 + 2(A^2 + B^2)C - AB^2\}]. \quad \dots \quad (2.4f)$$

The plots of  $T_A$ ,  $T_B$  and  $T_C$  given by Eqs. (2.4d), (2.4e) and (2.4f) are shown in Fig. 2. It is seen from the plot for the case where  $A = C$ , that when this type

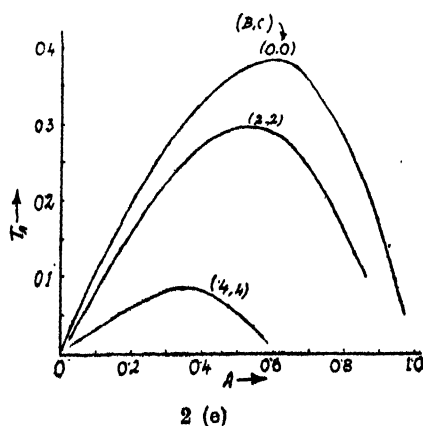
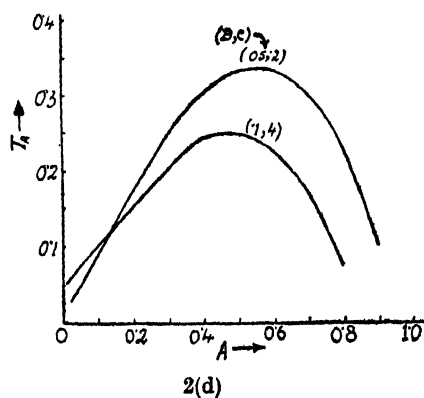
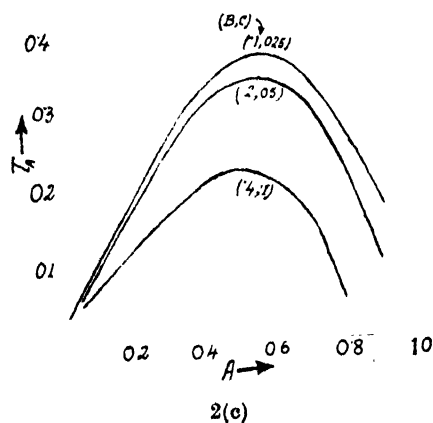
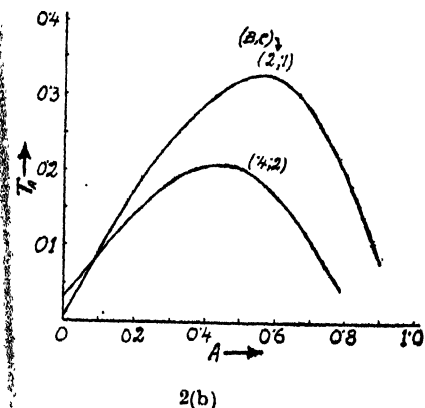
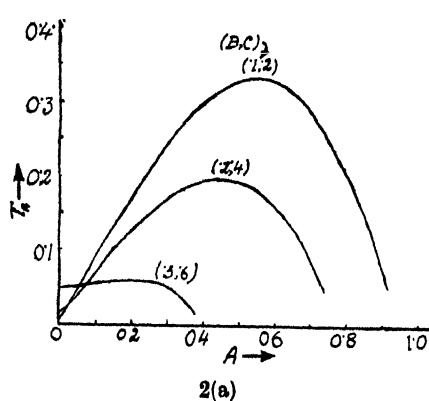


Fig. 2(a)-2(e): Transfer characteristic of a limiter for the component 'A' of a composite signal consisting of three components that bear the phase relationship  $(\psi_A + \psi_C = 2\psi_B + \pi)$  among themselves.

of limiter type non-linear element is incorporated in a regenerative loop and when  $B$  is greater than  $A$  or  $C$ , it does not help the growth of either  $A$  or  $C$ . For example if  $B = 0.8$  and  $A = 0.1$  then it is seen that  $A$  becomes non-existent after

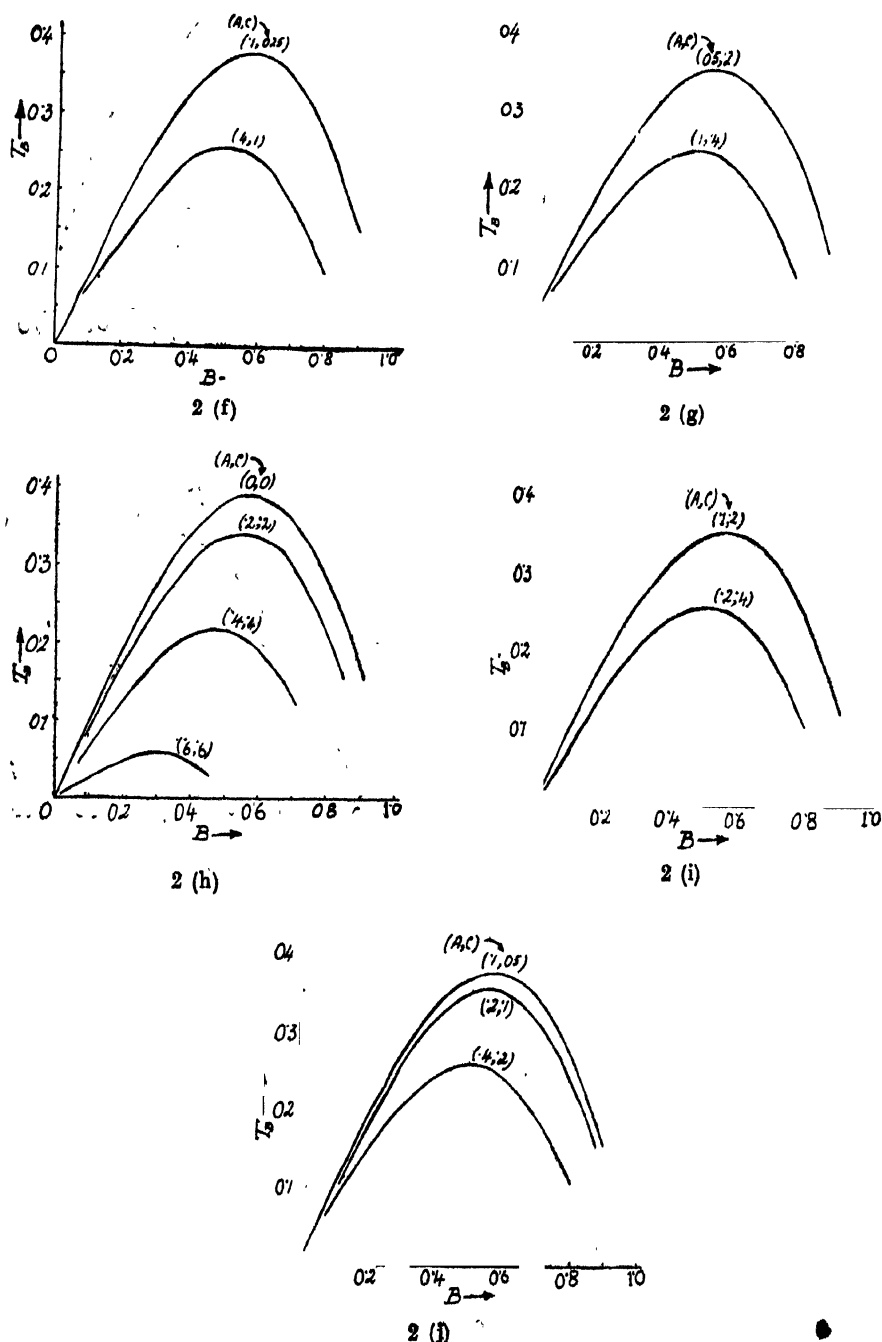


Fig 2(f)-2(j): Transfer characteristic of a limiter for the component 'B' of a composite signal consisting of three components that bear the phase relationship  $(\psi_A + \psi_C = 2\psi_B + \pi)$  among themselves]

sometime. But when  $A$  or  $C$  is greater than  $B$  then it is seen from the plots that  $A$  helps the growth of  $B$ . But it is to be noted that when  $A$  is much greater than  $B$  then the loop acts in such a way as to help the elementation of  $B$ . Thus there are limits to the value of the ratio  $A/B$  for which the loop may act in such way as to help building up of the weaker one. From the above discussion it is clear that if the non-linear element is placed in a regenerative loop having certain gain-frequency relations, the loop may break into simultaneous oscillations at the three frequencies  $\omega_A$ ,  $\omega_B$  and  $\omega_C$ . A schematic diagram of a circuit for producing simultaneous oscillations at three frequencies is shown in Fig. (3), which contains three gain control arrangements for the oscillations at frequencies  $\omega_A$ ,  $\omega_B$  and  $\omega_C$  respectively and three frequency selective networks for the oscillating components  $A$ ,  $B$ , and  $C$  respectively.

### *Region of Stability of Amplitudes*

From the above discussion it is evident that simultaneous oscillations at three frequencies will be maintained in the regenerative loop containing the limiter type non-linear element if the gain, phase and transmission characteristics of the loop for a particular component bear certain relationships with those of the others. Further the presence of any one of the components will have pronounced effect on the gain, phase and the transmission characteristics of the others. Hence if the amplitude of oscillation of any one of the components is changed, the corresponding transmission characteristics of the other will be modified, as a result of which all the modes may exist with a modified amplitude distribution. The above situation will occur if the gains of the loop for different components bear certain relationship among themselves. In this selection this region of amplitude stability has been found out.

Let us consider the regenerative loop shown in Fig. 3. It contains gain control arrangements  $G_A$ ,  $G_B$  and  $G_C$  respectively for the components  $e_A$ ,  $e_B$  and  $e_C$  and

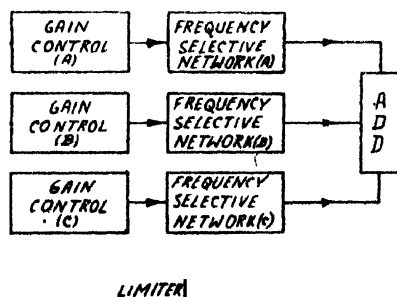


**Fig 3:** Schematic diagram of a regenerative loop with the limiter for simultaneous oscillations at three anharmonically related frequencies.

a limiter type non-linear element. The input-output relation of the compressor type non-linear element is assumed to be given by

$$X_{out} = a_1(X_{in}) - a_3(X_{in})^3, \quad \dots (2.5)$$

where

$$X_{in} = A \cos \psi_A + B \cos \psi_B + C \cos \psi_C. \quad \dots (2.6)$$

Then the instantaneous amplitude and phase equations can be written as:

$$(1 - a_1 G_A)A + T \frac{dA}{dt} = -\frac{3}{4} a_3 G_A [A^3 + 2(B^2 + C^2)A + B^2 C \cos \phi], \quad \dots (2.7)$$

$$(1 - a_1 G_B)B + T \frac{dB}{dt} = -\frac{3}{4} a_3 G_B [B^3 + 2(A^2 + C^2)B + 2ABC \cos \phi], \quad (2.8)$$

$$(1 - a_1 G_C)C + T \frac{dC}{dt} = -\frac{3}{4} a_3 G_C [C^3 + 2(A^2 + B^2)C + AB^2 \cos \phi], \quad (2.9)$$

and

$$T \frac{d\phi}{dt} = 3a_3 \left[ G_B A C + \frac{1}{4} \left( G_A \frac{A}{C} + G_C \frac{C}{A} \right) \right] \sin \phi, \quad \dots (2.10)$$

where  $T$  is an appropriate constant.

Putting

$$\begin{aligned} \frac{4}{3} \cdot \frac{a_1 G_A - 1}{a_3 G_A} &= K_A \\ \frac{4}{3} \cdot \frac{a_1 G_B - 1}{a_3 G_B} &= K_B \\ \frac{4}{3} \cdot \frac{a_1 G_C - 1}{a_3 G_C} &= K_C \end{aligned} \quad \dots (2.11)$$

and  $\phi = (2n+1)\pi$ , we have in the steady state

$$3A^3 - 6A^2 C + (4C^2 + K_A - 2K_B)A + (K_B - 2C^2)C = 0, \quad \dots (2.12)$$

$$\text{and} \quad 3C^3 - 6AC^2 + (4A^2 + K_C - 2K_B)C + (K_B - 2A^2)A = 0. \quad \dots (2.13)$$

Let us assume that the frequencies of the components  $A$  and  $C$  are symmetrically situated with respect to the frequency of oscillation of the component  $B$ . In general ' $A$ ' is not equal to ' $C$ ' and so let us assume that

$$C = mA \quad \dots (2.14)$$

where ' $m$ ' is a positive number. Substituting the value of  $C$  from (2.14), in the steady state we have

$$B^2 = \frac{K_A - (1 + 2m^2)A^2}{2 - m}, \quad \dots (2.15a)$$



$$= \frac{K_C - (m^2 + 2)A^2}{2 - 1/m} \quad \dots (2.15b)$$

and

$$A^2 = \frac{K_A - (2 - m)K_B}{2m^3 - 4m^2 + 6m - 3}, \quad \dots (2.16a)$$

$$= \frac{mK_C - (2m - 1)K_B}{2 - 4m + 6m^2 - 3m^3} \quad \dots (2.16b)$$

The above equations have been plotted in Fig. 4 where the region of stable oscillation which lies within the bounding curves corresponding to  $A^2 = 0$  and

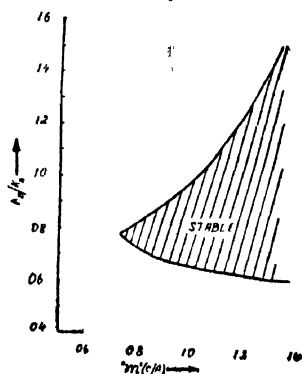


Fig 4: Amplitude stability diagram showing the amplitude relationship among the three components for simultaneous oscillations at three anharmonically related frequencies

$B^2 = 0$ . Now if the gains are symmetrically distributed around the frequency of oscillation of 'B' i.e.  $K_A = K_C$  and  $A = C$ , we have

$$(2.17)$$

$$B = \sqrt{2K_B - 2K_A}. \quad (2.18)$$

Therefore for simultaneous oscillations at three frequencies in the symmetrical case we must have

$$K_A = K_C > K_B, \quad (2.19)$$

and

$$3K_B > 2K_A. \quad (2.20)$$

In the above discussion nothing has been said about the stability of the amplitudes of oscillations. To study the question of stability of the modes we shall follow the Liapunoff technique. We imagine that the amplitudes 'A', 'B' and 'C' are given respectively increments of 'x', 'y' and 'z' about their mean values

of the amplitude of oscillations i.e.  $A_0$ ,  $B_0$  and  $C_0$ . If it is found that these increments ultimately die out we call the oscillation modes stable and otherwise unstable. Thus we have the incremental equations for the three components from

$$T \frac{\partial x}{\partial t} = -\frac{3}{4} a_3 G_A \{(5A_0^2 + 2B_0^2 - K_A)x + 2A_0 B_0 y + (4A_0^2 - B_0^2)z\}, \quad \dots \quad (2.21)$$

$$T \frac{\partial y}{\partial t} = -\frac{3}{4} a_3 G_B \{(3B_0^2 + 4A_0^2 - K_B)y + 2A_0 B_0 x + 2A_0 B_0 z\}, \quad \dots \quad (2.22)$$

$$T \frac{\partial z}{\partial t} = -\frac{3}{4} a_3 G_C \{(5A_0^2 + 2B_0^2 - K_C)z + (4A_0^2 - B_0^2)x + 2A_0 B_0 y\}. \quad \dots \quad (2.23)$$

Putting  $p = d/\partial t$  the characteristic equation can be written, for the simple case when  $A = C$ , i.e.  $K_A = K_C$ , as

$$p^2 + \frac{3}{4} a_3 T [G_B(2K_B - K_A) + 6G_A(K_A - K_B)]p + \left( \frac{3}{4} a_3 \right)^2 G_A G_B [2(K_A - K_B)^2 + 4(K_A - K_B)(3K_B - 2K_A)] = 0 \quad \dots \quad (2.24)$$

From the above Eq. (2.24) it is seen that the coefficients are real and positive when the conditions of Eqs. (2.19) and (2.20) are satisfied. Therefore Eqs. (2.19) and (2.20) give the correct criteria of simultaneous oscillations at three frequencies in the loop.

#### EFFECT OF TUNED CIRCUITS ON THE LOCKING RANGE

In the above analysis we have assumed that all the three oscillations occur at the resonant frequencies of the three tuned circuits. If only one mode exists the oscillation does occur at the resonant frequency of the corresponding tuned circuits. If, however, the three modes are present simultaneously it is possible that the frequencies of oscillations will differ from the resonant frequencies. Now from the analysis in section 2, it is clear that frequency and phase condition in Eq. (2.1b) must be satisfied. It is also evident that the amount of detuning present in the different tuned circuits will have a marked effect on the overall characteristics. This effect is studied in this section.

Let us suppose that the three tuned circuits which have been incorporated in the loop have sufficiently high  $Q$ -values and the three frequencies of oscillations that are simultaneously present in it, are chosen in such a way that the gain of any of the tuned circuits at its centre frequency is considerably large compared to that at other two frequencies which are away from the centre frequency.

Considering the loop shown in Fig. 3, one finds that for the simultaneous oscillations to occur at the three frequencies, the linear and non-linear gains of the loop for the three frequencies are to be related at

$$A = G_A(p)T_A(A, B, C), \quad \dots \quad (3.1)$$

$$B = G_B(p)T_B(A, B, C), \quad \dots \quad (3.2)$$

$$C = G_C(p)T_C(A, B, C), \quad \dots \quad (3.3)$$

where  $G_A(p)$ ,  $G_B(p)$  and  $G_C(p)$  are the linear gains of the loop for the component  $A$ ,  $B$  and  $C$  respectively  $\frac{1}{A} T_A(A, B, C)$ ,  $\frac{1}{B} T_B(A, B, C)$  and  $\frac{1}{C} T_C(A, B, C)$  are the corresponding non-linear gains of the loop. From Eqs. (3.1), (3.2) and (3.3) one can write the corresponding amplitude and phase equations as (see Appendix A)

$$\frac{2}{\alpha_A} \cdot \frac{dA}{dt} \simeq G_{A_0} \left[ a_1 A - \frac{3}{4} a_3 \{ A^3 + 2(B^2 + C^2)A + B^2 C \cos \phi \} \right] - A, \quad \dots \quad (3.4)$$

$$\frac{2}{\alpha_B} \cdot \frac{dB}{dt} \simeq G_{B_0} \left[ a_1 B - \frac{3}{4} a_3 \{ B^3 + 2(A^2 + C^2)B + 2ABC \cos \phi \} \right] - B, \quad \dots \quad (3.5)$$

$$\frac{2}{\alpha_C} \cdot \frac{dC}{dt} \simeq G_{C_0} \left[ a_1 C - \frac{3}{4} a_3 \{ C^3 + 2(A^2 + B^2)C + AB^2 \cos \phi \} \right] - C, \quad \dots \quad (3.6)$$

and

$$\frac{d\phi}{dt} \simeq 2\Delta\omega_B - (\Delta\omega_A + \Delta\omega_C) + K \sin \phi, \quad \dots \quad (3.7)$$

where 
$$K \simeq \frac{3}{8} \cdot a_3 \left[ \alpha_A G_{A_0} \frac{C}{A} + \alpha_C G_{C_0} \frac{A}{C} + 2\alpha_B G_{B_0} AC \right], \quad \dots \quad (3.8)$$

and  $\Delta\omega_A$ ,  $\Delta\omega_B$  and  $\Delta\omega_C$  are respectively the detuning from the centre frequencies of components  $A$ ,  $B$  and  $C$ .  $\alpha_A$  and  $\alpha_B$  and  $\alpha_C$  are proportional to the quality factors of the three tuned circuits, viz.,

$$\alpha_A = \frac{\omega_0 A}{Q_A}, \quad \alpha_B = \frac{\omega_0 B}{Q_B} \quad \text{and} \quad \alpha_C = \frac{\omega_0 C}{Q_C}.$$

In the steady state  $d\phi/dt = 0$  and the equilibrium phase  $\phi$  is given by

$$K \sin \phi = 2\Delta\omega_B - (\Delta\omega_A + \Delta\omega_C), \quad \dots \quad (3.9)$$

or, 
$$\frac{2\Delta\omega_B - (\Delta\omega_A + \Delta\omega_C)}{K} < 1. \quad \dots \quad (3.9a)$$

Obviously for entrainment the value of  $K$  must be greater than  $|2\Delta\omega_B - (\Delta\omega_A + \Delta\omega_C)|$

This defines the limits of detuning permissible. Beyond this limit the phase relations change to a value that the feedback circuit acts in a way so as to capture the strong signal and to reject the small signal.

The amplitude equations are given by

$$KA_o = A^2 + 2(B^2 + C^2) + B^2 \frac{C}{A} \cos \phi, \quad \dots \quad (3.10)$$

$$KB_o = B^2 + 2(A^2 + C^2) + 2AC \cos \phi, \quad \dots \quad (3.11)$$

$$KB_o = C^2 + 2(A^2 + B^2) + B^2 \frac{A}{C} \cos \phi. \quad \dots \quad (3.12)$$

In general  $A$  is not equal to  $C$  taking  $C = mA$  where ' $m$ ' is a positive number (integer or fraction) one can write from Eqs (3.10), (3.11) and (3.12) the following relations.

$$B^2 = \frac{KA_o - (1 + 2m^2)A^2}{2 + m \cos \phi}, \quad (3.13a)$$

$$= \frac{KC_o - (2 + m^2)A^2}{2 + 1/m \cos \phi}, \quad (3.13b)$$

$$= KB_o - \{2(1 + m^2) - 2m \cos \phi\}A^2, \quad (3.13c)$$

and

$$A^2 = \frac{KA_o - (2 + m \cos \phi)KB_o}{(1 + 2m^2) - 2(1 + m^2 + \cos \phi \cdot m)(2 + m \cos \phi)}, \quad \dots \quad (3.14a)$$

$$= KC_o - KA_o - \left( \frac{1}{m} - m \right) B^2 \cos \phi, \quad \dots \quad (3.14b)$$

and therefore the limiting value of the equilibrium phase  $\phi$  is given by

$$\cos \phi \approx 5 \frac{KA_o - KB_o}{KB_o - 2KA_o} \quad (3.15)$$

From a study of the above equations it is clear that if the tuned circuits have finite selectivity, then simultaneous oscillations at three frequencies may occur in the regenerative loop at frequencies which are not necessarily the resonant frequencies of the respective tuned circuits. In such a case the amounts of detuning from the resonant frequencies will be automatically adjusted by the loop in accordance with the amplitudes of the different modes, the selectivity of the tuned

circuits and the type of non-linear characteristic used. Ordinarily due to power supply variation, temperature fluctuations etc., the frequency of oscillation of the different modes will try to drift. But in this case the tendency will be influenced by the mutual coupling between the modes (vide Eq. 3.9).

We have so far considered the case when all the tuned circuits have more or less the same amount of selectivity. Let us now consider the case when one of the tuned circuits has a very high selectivity. For example, let us take case when the selectivity of the circuit sustaining the mode *B* is high, then the Eq. (3.7) reduces to

$$\frac{d\phi}{dt} \simeq -(\Delta\omega_A + \Delta\omega_C) + K \sin\phi. \quad \dots (3.16)$$

In the steady state it is seen from Eqs. (3.8) and (3.16) that the sum of the detunings of the mode *A* and the mode *C* from their respective centre frequencies is approximately constant. This means that if either the mode *A* or the mode *C* tries to drift in frequency then the other mode will drift in frequency in the opposite sense. This phenomenon gives an amount of stability to frequencies of simultaneous oscillations at three frequencies in regenerative loop containing the limiter type non-linear element.

#### EFFECT OF AN EXTERNAL INPUT

It is obvious that the first effect of the application of the external input to the system will be to cause an output at the frequency of excitation to appear. The amplitude of this output will depend upon the relative amplitudes of the free-running modes and the exciting signal at the input to the non-linearity and the linear response of the system at the exciting frequency. It is evident, for example, that if the exciting signal has a very large amplitude it may cause suppression of the internal modes and the output will then depend entirely on the input strength.

In general the effect of the external input will be to cause a reduction of the non-linear gains of the system. If the frequency of the external signal is close to that of any of the internal modes, there may also be an amount of energy exchange which may result in synchronisation of that internal mode with the applied signal. It can be readily shown that the effective gain of the relevant mode when it is locked to the external signal is increased by a factor that depends on the output and the phase difference between the two. The amplitude and phase equations of section 3 will have to be modified to take into account these effects, viz., reduction of the non-linear gains, the energy exchange and consequent frequency pulling. The relevant equations are presented in appendix B.

Although it is possible to solve those equations and treat the problem in all its generality it is considered advisable, for reasons of simplicity, to analyse only the following simple cases.

In the first case we assume that the loops for two of the modes are first disconnected and that for the other whose frequency is close to that of the exciting signal is closed and further that the amplitude and frequency of the external signal are such as to cause synchronisation. The loops for other two modes are subsequently closed after lock has been attained. Obviously we have to consider the phenomenon of single frequency synchronisation. The frequency of the free-running mode (say,  $B$ ) will be pulled into synchronism with the external signal and consequently the amplitude of the relevant mode will change to  $B'$ , given by

$$B' = B + E \cos \theta \quad (4.1)$$

where  $B$  is the amplitude of the free-running mode  $B$  in absence of the external input and  $E$  is the amplitude of the external signal at the input to the non-linearity and  $\phi$  is the steady state phase difference between the external input and the free-running mode and is given by

$$\sin \theta = \Omega \cdot \frac{E \cdot 2\omega_0}{B \cdot Q_B} \quad (4.2)$$

where  $\Omega$  is the difference of frequency between the external input and the free-running mode  $B$  and  $Q_B$  is quality factor of the tuned circuit sustaining the mode  $B$ . In this simple case the analysis of section 3 can be applied. It is to be remembered that  $B$  is to be changed to  $B'$ . Thus the amplitude of the external input necessary for quenching of oscillations at other two frequencies can be found out from the analysis of section 3.

In the second case we assume that the external input is applied to the system after internal synchronisation has been attained. Further it will be assumed that the amplitude and frequency relations of the external input with respect to any of the free running modes are such that it does not lock with any one of them. In this case also the external input will change the non-linear gains of the regenerative loop (in a way shown in appendix B). As a result the amplitude relations among the free-running modes will be altered in order that all the modes can be excited. Thus it follows from the discussion of section 3 that the frequencies of oscillations of all the free-running modes will be pulled to different values as permitted by the bandwidth of the tuned circuits. Analytical expressions for the modified amplitudes of the free-running modes and the different amount of detunings for the different modes can be found out from the analysis of section 3. It is to be remembered that  $KZ_0$  of section 3 should be replaced by  $(KZ_0 - 2E^2)$  (see appendix B) where  $z$  stands for either  $A$ ,  $B$  or  $C$ . Thus it is clear that if the exciting signal has such a large amplitude that internal synchronisation is lost then it will cause suppression of the internal modes and the output will depend entirely on the input strength and linear response of the system at the frequency of the external signal. If, however, the frequency of the external input is such that it lies at the centre of those of any two of the free-running modes and further

if the linear response of the system at the frequency of the external input is adequate then there is a possibility of oscillations of the two internal modes in presence of the external signal.

### ELIMINATION OF THREE FREQUENCY EFFECT

From the discussion of section 2 it is clear that a loop incorporating a limiter type non-linear element will help strong signals to build up and suppress the weaker ones. But if the net signal is a phase modulated one then the compressor type characteristics of the limiter will fail to be mutually destructive in nature. Thus the loop may still remain a regenerative one depending upon the amplitude and phase relationships among the various components. In this section a method has been discussed for converting the loop into a degenerative one with respect to the undesired components.

It has been shown in section 2 that simultaneous oscillations at three frequencies can be maintained if the gains at the three frequencies bear certain relationships depicted in Fig. 4 and the phase relations are such as in a phase modulated wave i.e.,

$$\psi_B - \psi_A = \psi_C - \psi_B. \quad (5.1)$$

This comes about because the suppression effect of the limiter is practically non-existent if the total instantaneous voltage has negligible amplitude variation with time and resembles a phase modulated wave. The above suggests a possibility of elimination of the weaker components by converting the phase modulated wave into an amplitude modulated one and amplitude limiting the latter. This conversion can be effected by means of a non-linear phase shifting network which

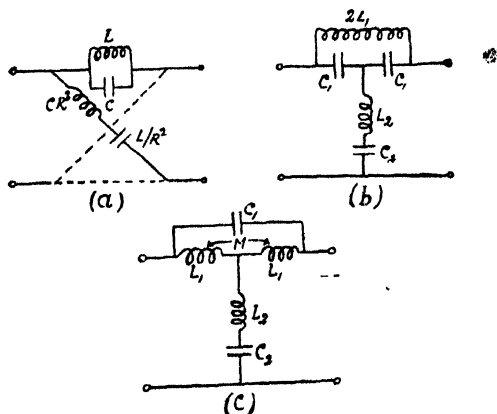


Fig 5(a): All pass lattice section

Fig 5(b): Bridged-T equivalent of Fig 5(a) for  $\omega_1/K_1 > \sqrt{3}$

Fig 5(c): Bridged-T equivalent of Fig 5(a) for  $\omega_1/K_1 < \sqrt{3}$

introduces a phase difference of  $180^\circ$  between the so-called side band components. It will be evident that other phase shifter circuits will have to be incorporated after the limiter in order to make the total phase shift at each of the frequencies equal to a multiple of  $2\pi$  radians for the loop to be still regenerative.

The theory of the non-linear phase shifter is outlined below.

It is known that the total phase shift due to an allpass lattice composed of a parallel resonant circuit in the series arm and constant resistance inverse impedance in the shunt arm (Fig. 5a) is given by

$$\phi = 2 \left[ \tan^{-1} \left( \frac{\omega + \omega_1}{K_1} \right) + \tan^{-1} \left( \frac{\omega - \omega_1}{K_1} \right) \right], \quad \dots (5.2)$$

$$\text{where } 2K_1 = \frac{L}{R}, \quad \dots (5.3)$$

$$K_1^2 + \omega_1^2 = \omega_0^2.$$

To obtain an unbalanced equivalent of this network we apply the technique of conversion of lattice into a bridged  $T$  (see Fig. 5b). From the study of equation (5.1) it is evident that the nature of the phase shift depends on the parameter  $K$ . Fig. (6) shows the phase shift characteristics obtained with lattice or a bridged

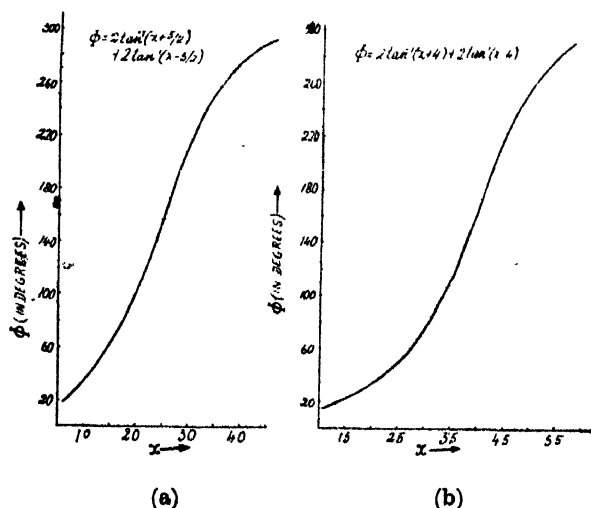


Fig 6: Phase-shift characteristics of the bridged-T network of Fig 5(a)

$T$  having  $\omega_1/K_1 = 5/2, 4$ . It should be pointed out that when  $\omega_1/K_1$  is less than  $\sqrt{3}$  the form shown in Fig. 5b cannot be used and one has to take recourse to the form shown in Fig. 5c. It should be mentioned that such phase shift characteristic can also be realised by active networks consisting of  $R-C$  elements only.



Now putting  $\omega/K_1 = x$  and  $\omega_1/K_1 = q$  we have from (5.2)

$$\phi(x) = 2 \tan^{-1} \left[ \frac{2x}{1+q^2-x^2} \right]. \quad \dots (5.4)$$

Now for converting a phase modulated wave to a corresponding amplitude modulated one we have the condition

$$\phi_A + \phi_C - 2\phi_B = \pi, \quad \dots (5.5)$$

where  $\phi_A$ ,  $\phi_B$  and  $\phi_C$  are the corresponding phase shifts for the components A, B and C respectively as they pass through the phase shifter and  $n$  is the number of stages utilised to obtain the required phase shift of  $\pi$  radian. Now comparing (5.3) and (5.4) we have

$$2 \frac{x_A(1+q^2-x_C^2)+x_C(1+q^2-x_A^2)}{(1+q^2-x_A^2)(1+q^2-x_C^2)-4x_Ax_C} = - \frac{\tan(\pi/2n)+\tan(\phi_B)}{\tan(\pi/2n)\tan(\phi_B)-1}. \quad \dots (5.6)$$

For  $n = 2$ , one can write from Eq. (5.6)

$$2 \frac{x_A(1+q^2-x_C^2)+x_C(1+q^2-x_A^2)}{(1+q^2-x_A^2)(1+q^2-x_C^2)-4x_Ax_C} = \frac{1+\tan\phi_B}{1-\tan\phi_B}. \quad \dots (5.7)$$

Therefore knowing the values of  $x_A$ ,  $x_B$  and  $x_C$  the corresponding value of  $C$  can be found from Eq. (5.7).

## EXPERIMENTAL SET-UP AND RESULTS

The experimental set up is shown in Fig. 7. The regenerative circuit consists of three variable gain and variable selectivity amplifiers and a limiter type non-

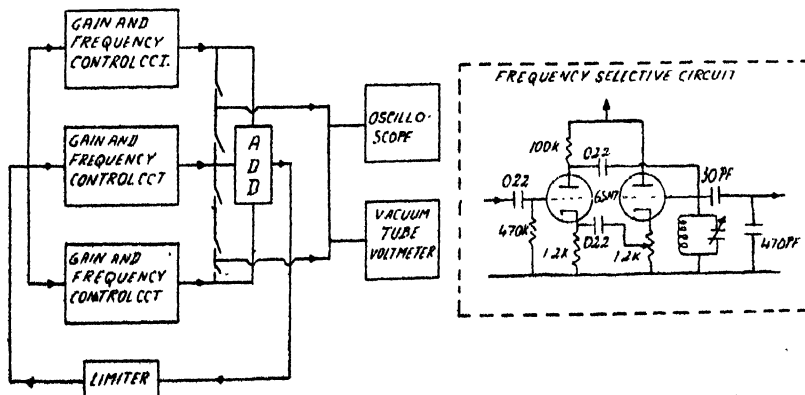


Fig 7: Experimental set-up The circuit diagram of the frequency selective network is also shown

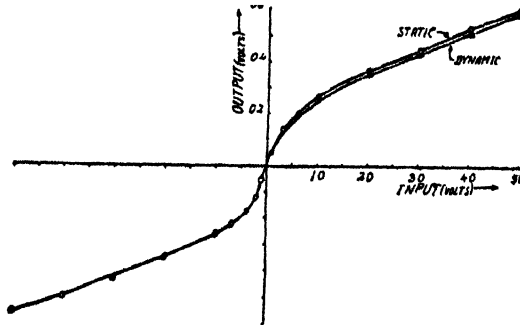


Fig 8: Experimentally obtained static and dynamic transfer characteristics of a limiter type non-linear element consisting of a pair of crystal diodes (1N34) connected back to back

linear element. The input-output characteristic of the limiter, consisting of a pair of crystal diodes (1N34) connected back to back, is shown in Fig. 8 and may be represented to a fair degree of approximation by

$$x_{out} = 0.42x_{in} - 0.16x_{in}^3, \quad x_{in} \leq 1$$

Now the gains for different modes were adjusted in such way as to cause the loop to break into simultaneous oscillations at three anharmonically related frequencies, viz.  $f_A = 156$  Kc/s,  $f_B = 184$  Kc/s and  $f_C = 212$  Kc/s. The corresponding gains at frequencies  $f_A$ ,  $f_B$  and  $f_C$  and their respective amplitudes were then measured. Thus knowing the values of the gains  $G_A$ ,  $G_B$  and  $G_C$  and the values of the constant ' $a_1$ ' and ' $a_3$ ' the corresponding values of ' $K_A$ ' and ' $K_B$ ' were found out from Eq. (2.11). The ratios  $K_B/K_A$  and corresponding  $C/A$  have been plotted in Fig. 9. The equilibrium points, so found experimentally, lie within

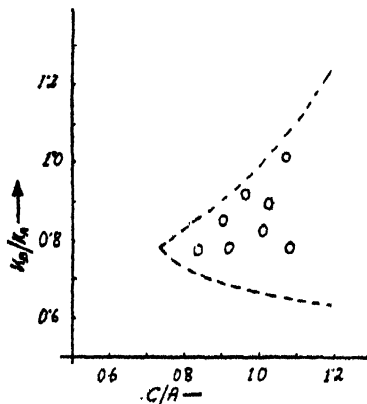


Fig 9: Amplitude stability diagram showing experimentally observed stable points. The computed bounding curve is shown dotted.

the region of amplitude stability found theoretically in section 2 and shown by the dotted line in the same figure for comparison.

The method of elimination of 'three frequency effect' in a regenerative loop containing a limiter type non-linear element, as discussed in section 5, requires a non-linear phase-shifting network  $N_1$  (see Fig. 10a) for introducing a phase shift

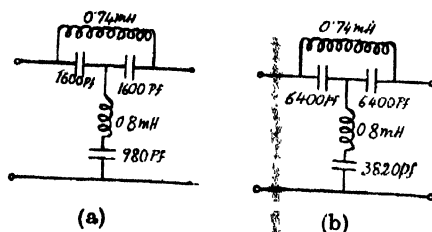


Fig 10 : Shows one of the two identical sections of the bridged-T phase shifter

Fig. 10(a) :  $R=1.0K \Omega$ ,  $\omega_{1,1}/K_1=4$ ,  $\omega_{01}/K_1=\sqrt{17}$ ,  $\omega_{01}=\sqrt{\frac{17}{9}} \omega_B$ ,  $f_B=150Kc/s$ .

Fig. 10(b) :  $R=500 \Omega$ ,  $\omega_{1,2}/K_2=4$ ,  $\omega_{02}/K_2=\sqrt{17}$ ,  $\omega_{02}=\sqrt{\frac{17}{36}} \omega_B$ ,  $f_B=150Kc/s$ .

of  $180^\circ$  between the so-called side-band components and it further requires a second non-linear phase shifting network  $N_2$  (see Fig. 10b) to ensure that the net phase shifts suffered by the different modes in passing through the network are even multiples of  $\pi$ . The complete arrangement of the non-linear phase-shifting network with the limiter is shown in Fig. 11. To get rid of the 'three-frequency effect' in the regenerative loop, the non-linear phase shifting arrangement (Fig. 11) is to be introduced in the loop in the position shown dotted in Fig. 3.

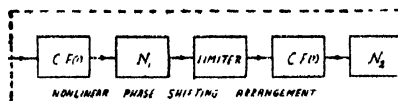


Fig 11 : Arrangement of the non-linear phase shifting network with the limiter to be introduced for the elimination of the three-frequency-effect

As the components of the signals pass through this non-linear phase shifting network, they become incoherent in nature and the regenerative loop containing the limiter type non-linear element, will favour oscillation of that mode having the highest amplitude before the introduction of the non-linear phase shifter. The experiment performed fully confirmed the speculation.

## CONCLUSION

Simultaneous oscillations at three anharmonically related frequencies in a regenerative loop containing a limiter type non-linear element have been analysed. The amplitude relations among the three modes for the co-existence have also been found out. Experimental results regarding their amplitude-relations have been presented and it has been found that the experimental results are in quite good agreement with those of the analysis. A possible method for the elimination of the three-frequency effect has also been suggested. The possibility of simul-

taneous oscillations at four and five frequencies in such a loop will be considered in a future communication.

#### ACKNOWLEDGMENT

The author takes the opportunity of thanking Mr. N. B. Chakrabarti of the Institute of Radio Physics and Electronics for suggesting the problem and for supervision of the work described. The author is indebted to Prof. J. N. Bhar, D.Sc., F.N.I., Head of the Institute of Radio Physics and Electronics for his kind interest and providing him with all the research facilities. The author also wishes to thank Prof. A. Mukherjee, D.Sc., Head of the Department of Physics, University of Burdwan, for his kind interest and encouragement.

#### APPENDIX

##### A.I. Derivation of the loop equations for the case when the tuned circuits have finite $Q$ -values :

Let us consider the loop as shown in Fig. 3. The loop equations for different modes can be written as

$$A = G_A(p)T_A(A, B, C), \quad \dots \quad (\text{A.1})$$

$$B = G_B(p)T_B(A, B, C), \quad \dots \quad (\text{A.2})$$

$$C = G_C(p)T_C(A, B, C), \quad \dots \quad (\text{A.3})$$

where the symbols have their usual significance as mentioned in the text. Now we have,

$$T_A(A, B, C) = [X_{out}]_A, \quad \dots \quad (\text{A.4})$$

$$\frac{1}{G_A(p)} = \frac{1}{G_{A0}} \left[ 1 + \frac{p + \omega_{0A}^2 p}{\alpha_A} \right] \quad \dots \quad (\text{A.5})$$

$$\psi_A + \psi_C = 2\psi_B + \phi, \quad \dots \quad (\text{A.6})$$

where  $\omega_{0A}$  is the resonant angular frequency of the tuned circuits sustaining the mode  $A$ ,  $G_{A0}$  is the gain at the resonant frequency and  $\psi_A$ ,  $\psi_B$  and  $\psi_C$  are respectively the instantaneous phases of the modes  $A$ ,  $B$  and  $C$  putting  $p = j\omega_A + S$  one can write from (A-5)

$$\frac{1}{G_A(p)} \simeq \left[ 1 + \frac{2}{\alpha_A} S + j \frac{\omega_A^2 - \omega_{0A}^2}{\alpha_A \omega_A} \right], \quad \dots \quad (\text{A.7})$$

where  $S$  represents an operator in a slow time scale and  $\alpha_A$  is given by

$$\alpha_A = \omega_{0A}/Q_A \quad \dots \quad (\text{A.8})$$

Hence from Eqs. (A.1) and (A.7) we have

$$\frac{2}{\alpha_A} \frac{dA}{dt} \simeq G_{A0} \left[ a_1 A - \frac{3}{4} a_3 \left\{ A^3 + 2(B^2 + C^2)A + B^2 C \cos \phi \right\} \right] - A, \quad \dots \quad (\text{A.9})$$

and

$$\frac{2}{\alpha_A} \frac{d\psi_A}{dt} \simeq -\Delta\omega_A + \frac{3}{4} a_3 G_{A0} B^2 \frac{C}{A} \sin \phi. \quad \dots \quad (\text{A.10})$$

Similarly for other modes one can easily write the following equations

$$\frac{2}{\alpha_B} \cdot \frac{dB}{dt} = G_{B0} \left[ a_1 B - \frac{3}{4} a_3 \{ B^3 + 2(A^2 + C^2)B + 2ABC \cos \phi \} \right] - B, \quad \dots \quad (\text{A.11})$$

$$\frac{2}{\alpha_C} \cdot \frac{dC}{dt} = G_{C0} \left[ a_1 C - \frac{3}{4} a_3 \{ C^3 + 2(A^2 + B^2)C + B^2 A \cos \phi \} \right] - C, \quad \dots \quad (\text{A.12})$$

and

$$\frac{2}{\alpha_B} \cdot \frac{d\psi_B}{dt} \simeq \Delta\omega_B - \frac{3}{4} a_3 G_{B0} A C \sin \phi, \quad (\text{A.13})$$

$$\frac{2}{\alpha_C} \cdot \frac{d\psi_C}{dt} \simeq \Delta\omega_C + \frac{3}{4} a_3 G_{C0} B^2 \frac{A}{C} \sin \phi. \quad (\text{A.14})$$

Comparing (A.10), (A.13) and (A.14) with (A.9) one can write

$$\frac{d\phi}{dt} \simeq 2\Delta\omega_B - (\Delta\omega_A + \Delta\omega_C) + K \sin \phi, \quad (\text{A.15})$$

where

$$K = \frac{3}{8} a_3 \left[ B^2 \left( \alpha_A G_{A0} \frac{C}{A} + \alpha_C G_{C0} \frac{A}{C} \right) - 2\alpha_B G_{B0} A C \right]. \quad \dots \quad (\text{A.16})$$

#### B.I. Derivation of the loop equations with the External input :

Let us consider the loop with the external input  $E' \cos \omega t$ . Assuming the instantaneous phases of the free-running modes and external input to be as

$$\psi_A + \psi_C = 2\psi_B + \phi \quad \dots \quad (\text{B.1})$$

and

$$\psi = \psi_B + \theta \quad \dots \quad (\text{B.2})$$

where  $\psi$  is the instantaneous phase of the external signal and  $\theta$  is the phase difference between the mode  $B$  and the external input. The loop equations can be written as

$$T_A(A, B, C, E) G_A(p) = A, \quad \dots \quad (\text{B.3})$$

$$T_B(A, B, C, E) + E \cos \theta = \frac{B}{G_B(p)}, \quad (\text{B.4})$$

$$T_C(A, B, C, E) G_C(p) = C, \quad \dots \quad (\text{B.5})$$

where  $E$  is the amplitude of the external at the input to the non-linearity and the other symbols have their usual significances. From appendix A one can write the following expression for  $G_A(p)$ ,  $G_B(p)$  or  $G_C(p)$

$$G_Z(p) \left[ 1 + \frac{2}{\alpha_Z} S + j \frac{\omega_Z^2 - \omega_0^2}{\alpha_Z \omega} \right], \quad \dots \quad (\text{B.6})$$

where  $Z = A, B$  or  $C$ .

Hence from equations (B.1) to (B.6) one can write

$$\frac{2}{\alpha_A} \cdot \frac{dA}{dt} \simeq G_{A0} \left[ a_1 A - \frac{3}{4} a_3 \{A^3 + 2(B^2 + C^2 + E^2)A + B^2 C \cos \phi\} \right] - A, \quad (\text{B.7})$$

$$\frac{2}{\alpha_B} \cdot \frac{dB}{dt} \simeq G_{B0} \left[ a_1 B - \frac{3}{4} a_3 \{B^3 + 2(A^2 + C^2 + E^2)B + 2ABC \cos \phi\} \right] - B, \quad (\text{B.8})$$

$$\frac{2}{\alpha_C} \cdot \frac{dC}{dt} \simeq G_{C0} \left[ a_1 C - \frac{3}{4} a_3 \{C^3 + 2(A^2 + B^2 + E^2)C + B^2 A \cos \phi\} \right] - C, \quad (\text{B.9})$$

$$\frac{d\phi}{dt} = 2\Delta\omega_B - (\Delta\omega_A + \Delta\omega_C) + K \sin \phi, \quad \dots (\text{B.10})$$

and

$$\frac{d\theta}{dt} \simeq \Omega - \frac{E}{B} \cdot \frac{\omega_{0B}}{2Q_B} \cdot \sin \theta, \quad \dots (\text{B.11})$$

where  $\theta$  is the instantaneous phase difference between the free-running mode and the external input and  $\Omega/2\pi$  is instantaneous difference of frequency between them. Putting

$$\frac{4}{3} \cdot \frac{a_1 G_{Z0} - 1}{a_3 G_{Z0}} = K_{Z0} \quad \dots (\text{B.12})$$

where  $Z = A, B$  or  $C$ .

We have from Eqs. (B.7), (B.8) and (B.9)

$$\frac{2}{\alpha_A} \cdot \frac{dA}{dt} \simeq \frac{3}{4} a_3 G_{A0} A \left[ K_{A0} - \left\{ A^2 + 2(B^2 + C^2 + E^2) + B^2 \frac{C}{A} \cdot \cos \phi \right\} \right], \dots (\text{B.13})$$

$$\frac{2}{\alpha_B} \cdot \frac{dB}{dt} \simeq \frac{3}{4} a_3 G_{B0} B \left[ K_{B0} - \{B^2 + 2(A^2 + C^2 + E^2) + 2AC \cos \phi\} \right], \quad \dots (\text{B.14})$$

$$\frac{2}{\alpha_C} \cdot \frac{dC}{dt} \simeq \frac{3}{4} a_3 G_{C0} C \left[ K_{C0} - \left\{ C^2 + 2(A^2 + B^2 + E^2) + B^2 \frac{A}{C} \cos \phi \right\} \right] \dots (\text{B.15})$$

## REFERENCES

- Chakrabarti, N. B., "Generation of pulse-like functions by means of lumped equivalent of delay lines" 1961-62, Research Report, Vol. XIV, pp. 9-. (Institute of Radio Physics and Electronics).
- Chakrabarti, N. B. and Biswas, B. N., 1964, *Ind. Jour. Phys.*, **38**, 148-173,
- Dishman, M. I., 1958, *Proc. I.R.E.*, **46**, 895-.
- Fredendall, G. L., 1954, *Proc. I.R.E.*, pp. 258.
- Met, V., 1957, *Proc. I.R.E.*, **45**, 1119.

# Letters to the Editor

The Board of Editors does not hold itself responsible for opinions expressed in the letters published in this section. The notes containing short reports of original investigations communicated to this section should not contain many figures and should not exceed 500 words in length. The contributions reaching the Secretary by the 15th of any month may be expected to appear in the issue for the next month. No proof will be sent to the author.

25

## VELOCITY OF ULTRASONIC WAVES IN SOLUTIONS OF ELECTROLYTES — A COMMENT.

M. SURYANARAYANA\*

DEPT. OF PHYSICS, NIZAM COLLEGE, HYDERABAD (A.P.)

(Received February 4, 1963)

An equation for the velocity  $V$  of ultrasonic wave in a solution of an electrolyte of density  $\rho$  was derived by Satyaprakash and Srivastava (1958), abbreviated as S S hereafter. According to this equation,  $(V\rho)^{\frac{1}{2}}$  of an electrolyte solution should vary linearly with  $\mu$ , the ionic strength of the solution, the gradient of this linear variation remaining the same for different salts of the same valency type. They supported their theory by considering the velocity and density data given by Mohanty and Deo (1955) for zinc and magnesium sulphate solutions.

In their treatment, S S have made use of a simpler expression for the potential,  $\psi_i$ , of an ion which is valid only for very dilute solutions. Using, however, a more elaborate expression,

$$\psi_i = \pm \frac{z_i e}{D} \frac{1}{1 + r\kappa}$$

one can, following the same treatment, arrive at the equation,

$$(V\rho)^{\frac{1}{2}} = \frac{P}{(2I)^{\frac{1}{2}}} + \frac{A}{(2I)^{\frac{1}{2}}} \left( \frac{\mu^{\frac{1}{2}}}{1 + Br\mu^{\frac{1}{2}}} \right)^2$$

where  $r$  is the mean radii of the ions and  $A$  and  $B$  are constants, the rest of the symbols having the same meaning as given by S S. For aqueous solutions at room temperature, the value of  $B$  is  $0.33 \times 10^8$ . Taking the ultrasonic velocity data of sodium chloride solutions given by Weissler and DelGrasso (1951) and

---

\*Present address : Department of Physics, Osmania University, Hyderabad, (A.P.)

making use of  $r = 2.2 \text{ \AA.u}$  for this salt, it is found that the graph of  $(V\rho)^{\frac{1}{2}}$  vs  $\left(\frac{\mu^{\frac{1}{2}}}{1+Br\mu^{\frac{1}{2}}}\right)^2$  is a curve even from the lowest concentration and not a straight line as required by the above equation. This prompted the author to verify the original equation of *SS* with regard to other electrolyte solutions.

Ultrasonic velocities for various aqueous solutions of electrolytes determined by Mohanty and Deo, Weissler and DelGrasso, Marks (1960) and the author (1962) are considered and it is found in all these cases that  $(V\rho)^{\frac{1}{2}}$  varies linearly as the ionic strength of the solutions but in no case the corresponding gradient for this linear variation is nearly the same for electrolytes of the same valency type.

Mohanty and Deo have recorded the concentration of zinc sulphate solutions in molal and that of magnesium sulphate in twice molal. This fact was not taken into account by *SS* in using the data to support their theory and hence, by sheer coincidence, they obtained the same gradient for the linear variation of  $(V\rho)^{\frac{1}{2}}$  with the ionic strengths of these two solutions.

It is now a well established fact (Suryanarayana 1962) that  $V\rho$ , the specific acoustic impedance of aqueous solutions of electrolytes, varies linearly as the normality of the solutions with different gradients depending on the ionic radii. This shows that at least for strong electrolytes of uni-univalent type,  $(V\rho)^{\frac{1}{2}}$  cannot at the same time vary linearly as  $\mu$ , much less have a common gradient.

The various factors mentioned above show that the theory proposed by *SS* need a revision and is engaging the attention of the author.

#### REFERENCES

- Marks, G. W., 1960, *J. Acoust. Soc. Amer.* **32**, 327.  
 Mohanty, B. S. and Deo, B. B., 1955 *Ind. J. Phys.* **29**, 578.  
 Satya Prakash and Srivastava, S. S., 1958, *Ind. J. Phys.* **32**, 62.  
 Suryanarayana, M. 1962, *J. Sci. & Ind. Res.* **21B**, 57.  
 Weissler, A. and DelGrasso, V. A., 1951, *J. Acoust. Soc. Amer.* **23**, 219.



# PREPARATION AND CRYSTALLOGRAPHIC STUDIES OF STRONTIUM PLUTONATE

D. M. CHACKRABURTTY and N. C. JAYADEVAN

RADIOCHEMISTRY AND ISOTOPE DIVISION, ATOMIC ENERGY

ESTABLISHMENT, TROMBAY, BOMBAY

(Received September 11, 1964)

Although complex oxide systems of plutonium with divalent metal ions have been found to be possible in number of cases (Russell *et al* 1960; Chackraburttty *et al* 1963), yet so far no definite crystallographic studies have been reported about the complex oxide system of plutonium with strontium ion.

Specpure strontium carbonate was heated to its oxide, which was mixed with freshly prepared plutonium dioxide in the ratio necessary for the formation of  $\text{SrPuO}_3$  and finally was heated to  $1300^\circ\text{C}$ – $1500^\circ\text{C}$  in tantalum crucible in a resistance furnace similar to that described by Drummond *et al* (1957). The diffraction patterns of the samples were taken in a 19 cm. Unicam camera in copper radiation. In addition to diffraction lines due to unreacted plutonium dioxide, extra lines were noticed which could be partly indexed by a cubic cell. By assuming simple shear of the cubic cell leaving 'a' and 'c' axis equal but 'b' axis slightly different, a monoclinic cell was obtained which could explain the data with a  $a = 4.280 \pm 0.006 \text{ \AA}$ ,  $b = 4.276 \pm 0.006 \text{ \AA}$ ,  $c = 4.280 \pm 0.006 \text{ \AA}$  and  $\beta = 92^\circ 28'$ , having one formula unit per cell. The substance was found to be isostructural with  $\text{CaTiO}_3$  (Megaw 1946, Naray Szabo 1943). Geometrically, the above lattice so obtained could have ortho-rhombic symmetry and could be referred to a new  $a$  and  $c$  axes which were the diagonals of the (010) face of the monoclinic cell. The orthorhombic cell, derived from this consideration, has the following values:  $a = 5.980 \pm 0.006 \text{ \AA}$ ,  $b = 4.276 \pm 0.006 \text{ \AA}$  and  $c = 6.114 \pm 0.006 \text{ \AA}$ . The 'b' face, in this case, appeared to be face-centred. Indexing of the lines could be done on this basis, and from the consideration of symmetrical lattice obtained, the present (orthorhombic) indexing seems to be more preferable. For comparison, indexed data on monoclinic and orthorhombic cells are presented in Table I. Spectrophotometric studies indicated the valency of plutonium in IV state, hence it was concluded that strontium plutonate with a molecular formula  $\text{SrPuO}_3$  was a complex oxide system in the group of perovskite compounds.

TABLE I  
Date for  $\text{SrPuO}_3$  ( $\lambda=1.5418 \text{ \AA}$ )  
Orthorhombic unit cell is derived from monoclinic cell

$d\text{\AA}^*$	$q_0^2 \times 10^{-4}$	$q_c^2 \times 10^{-4}$	Monoclinic indexing** hkl	Orthorhombic indexing*** hkl	Intensity
4.278	325	325	100	010, 101	
3.046	641	636	101	002	v.w.
3.015	645	650	011	111	v.s.
2.982	668	664	101	200	w*
2.498	954	961	111 $\bar{}$	012	w $\bar{}$
2.461	981	989	111	210	w.
2.133	1306	1300	200	020	m+
1.756	1926	1922	211 $\bar{}$	113	m.
1.739	1977	1978	211	311	m+
1.536	2536	2544	202 $\bar{}$	004	w.
1.512	2601	2600	022	212	m.w.
1.497	2656	2653	202	400	m.w $\bar{}$
1.350	3260	3250	031	131, 313	m+
1.281	3619	3617	311	412	v.w.
1.186	4224	4225	032	323	w.
1.137	4598	4592	321	422	w.

\*For unreacted plutonium dioxide the following  $d(\text{\AA})$  values are obtained (in brackets estimated intensities are given): 3.112(m+); 2.698 (w); 1.910(m+); 1.628 (m); 1.558(w $\bar{}$ ); 1.239 (w); 1.208 (w); 1.104 (w); 1.039 (w $\bar{}$ ); 0.913 $\alpha_1$ , (w+); 0.855 $\alpha_1$ , (w); 0.824 $\alpha_1$  (w). These lines could be indexed with cubic cell  $a=5.40 \text{ \AA}$  (fluorite type).

\*\*For monoclinic indexing, as  $a^*=b^*=c^*$ , by equivalence number of hkl indices are possible for many of the indexing planes.

\*\*\*From the indexed data in orthorhombic case, the possible conditions limiting the reflections are, for hkl planes,  $h+l=2n$  present; hoo planes,  $h=2n$  present and 00l planes,  $l=2n$  present. This could indicate a B centred lattice.

#### ACKNOWLEDGEMENT

Sincere thanks are due to the Head, Radiochemistry and Isotope Division, for his keen interest in the work.

#### REFERENCES

- Chackraburty, D. M., Jayadevan, N. C., and Sivaramakrishnan, C. K., 1963, *Acta Cryst.* **16**, 1060.  
 Drummond, J. L., McDonald, B. J., Ockenden H. M., and Welch, G. A., 1957, *J. Chem. Soc.*, p. 4785.  
 Megaw, H. D., 1946, *Proc. Phys. Soc.*, **58**, 133.  
 Naray Szabo, S., 1943, *Naturwissenschaften* **31**, 203.  
 1943, *naturwissenschaften* **31**, 466.  
 Russell, L. E., Harrison, J. D. L., and Brett, N. H., 1960, *J. Nucl. Mater.* **2**, 310.

# PHASE TRANSFORMATION IN ERBIUM ETHYL SULPHATE SINGLE CRYSTAL WITH LOWERING OF TEMPERATURE

T. MOOKHERJI

PHYSICS LABORATORY, THE UNIVERSITY OF BURDWAN, W.B., INDIA

In course of investigations on the magnetic behaviour of rare earth (Mookherji 1949) and iron (Bose 1948) group of ions in crystals, considerable change of the direction of the principal magnetic axes with change of temperature was observed in several monoclinic crystals. A change of orientation as large as 63.5 degrees for a change of temperature of 100°K was observed in the case of  $\text{Pr}_2(\text{SO}_4)_3 \cdot 8\text{H}_2\text{O}$  crystal, (Mookherji, 1949) having a magnetic anisotropy of 26% of the mean susceptibility. The earlier workers however, did not detect any change of the direction of the principal magnetic axes in hexagonal, tetragonal and trigonal crystals. We also had not so far detected any such change with hexagonal crystals like neodymium ethyl sulphate. Hence it is of considerable interest to find very recently a change of  $\sim 75^\circ$  in the setting angle (Table I) with single crystal of  $\text{Er}_2(\text{C}_2\text{H}_5\text{SO}_4)_6 \cdot 18\text{H}_2\text{O}$ , belonging to hexagonal class having 9% magnetic anisotropy at 300°K.

TABLE I

Magnetic Anisotropy  $\Delta\chi$ , change of setting angle and mean moment  $\mu$

T°K	300	250	200	150	100	80
$\Delta\chi \cdot 10^6$	3225	5227	8800	15124	32500	46227
$\mu$	8.847	8.660	8.197	7.809	7.299	7.078
Change in Setting Angle	0	8.1°	16.7°	57.8°	73.2°	69.0°

Measurements on the magnetic anisotropy,  $\Delta\chi = (\chi_{\perp} - \bar{\chi}_{\parallel})$ ; where  $\chi_{\parallel}$  represents gram molecular susceptibility along hexagonal axis of the crystal and  $\chi_{\perp}$  that normal to it and the change in setting angle were carried out by a modi-

fication of Stout and Griffel's (1950) method; and the mean magnetic moment

$$\mu = \frac{\mu_1^2 + 2\mu_2^2}{3}, \text{ by a modified Curie balance (Bose et al., 1963). Temperature}$$

control for  $\Delta\chi$  measurements was affected by a thermostatic device due to Bose (1948).

Jordahl's theory (1934) to explain this change of the direction of the principal magnetic axis can account only for a change of about 5 degrees where the difference of temperature is about 100°K, and that too only in cases of symmetry less orthorhombic.

Following Bose et al (1957) if this change is attributed to the instability in the crystal structure brought about mainly by anisotropic thermal expansion of the crystal, it may be concluded that there is a gradual change of crystal structure, from one phase to another within the range of study as there is no unexpected thermal variation in the magnetic anisotropy (Table I). Table I further shows that  $\Delta\chi$  and  $\mu$  at 300°K have almost the same values as those obtained by Krishnan and Mookherji (1938) for the same crystal.

When the crystal was suspended with its hexagonal axis vertical no appreciable anisotropy at 300°K was observed as is expected of a hexagonal crystal. However an appreciable anisotropy (1.0%) was observed at 80°K. The setting angle also changed continuously with temperature. All these go to support our view that the symmetry of the crystal was changing from hexagonal to either monoclinic or triclinic with the change of temperature.

In order to ascertain whether this gradual phase change is of permanent character, measurements were first taken on  $\Delta\chi$  in direct order (i.e. from 300°K to 80°K) and then in reverse order (i.e. from 80°K to 300°K). The anisotropy followed the same path suggesting that the rate of change of phase is the same in both the order i.e. there is no lag in the transformation.

Details will be published elsewhere.

#### REFERENCES

- Bose, A., 1948, *Ind. J. Phys.*, **22**, 73.  
 Bose, A., Datta Roy, S. K., Ghosh, P. K. and Mitra, S., 1963, *Ind. J. Phys.*, **37**, 505  
 Bose, A., 1947, *Ind. J. Phys.*, **21**, 276.  
 Bose, A., Mitra, S. C., Datta, S. K., 1957, *Proc. Roy. Soc.* **239**, 165.  
 Jordahl, 1934, *Phys. Rev.* **45**, 87.  
 Krishnan, K. S. and Mookherji, A., 1948, *Phil. Trans.* **237**, 185.  
 Mookherji, A., 1949, *Ind. J. Phys.* **23**, 217, 309, 410.  
 Stout, J. W. and Griffel, M., 1950, *J. Chem. Phys.* **50**, 1449.

# THE EFFECTS OF GAUSSIAN NOISE ON THE FREQUENCY RESPONSE CHARACTERISTICS OF A NONLINEAR FEEDBACK CONTROL SYSTEM

ASIM K. SEN

INSTITUTE OF RADIO PHYSICS AND ELECTRONICS, UNIVERSITY OF CALCUTTA

(Received September 15, 1964)

**ABSTRACT.** In this paper, a quasi-linearisation technique is described which gives a parameter for approximately representing a memory-type nonlinearity on the basis of an input containing a sinusoidal signal and a Gaussian noise with mean value zero. The parameter is termed 'complex equivalent gain' and this is used for investigating the effects of a Gaussian noise on the frequency response characteristics of a stable feedback control system incorporating the nonlinearity. A simple second-order position control system with backlash in the output coupling is considered as an example and the results obtained are verified experimentally with the help of an electronic analogue computer.

## INTRODUCTION

When the input of a stable feedback control system incorporating a memory-type nonlinearity is subjected to a sinusoidal signal, the frequency response characteristics of the system can be determined approximately by the use of linearisation techniques (Stein and Thaler 1958, Sen, 1964). In the application of these techniques, a quasi-linearised transfer function is used to represent the nonlinear element in the system which is called 'complex describing function'.

But, when the input of the nonlinear system considered becomes contaminated with a Gaussian noise then it is found that all the parameters of the frequency response characteristics, namely, the bandwidth, resonant frequency and the height of the resonant peak previously obtained for a particular value of the impressed sinusoidal amplitude, change considerably. This is due to the fact that the transmission property of the nonlinearity alters due to the presence of the noise. In this paper, an analytical method will be proposed for investigating these effects of the Gaussian noise on the frequency response characteristics of a memory-type nonlinear system, where the nonlinearity considered is assumed to be amplitude-sensitive alone. The importance of this investigation arises from the fact that the inputs of all practical control systems are usually contaminated with such external disturbances.

In order to carry out the above analytical investigation, a quasi-linearisation technique will be adopted in which a 'complex equivalent gain' (Sen, 1955) will be obtained for making an approximate representation of the nonlinearity under

the assumption that the input is composed of only a sinusoidal signal and a Gaussian noise with mean value zero. An outline of the proposed quasi-linearisation technique has been presented in the following section.

#### THE PROPOSED QUASI-LINEARISATION TECHNIQUE

When a linear element is subjected to an input consisting of a sine wave and a Gaussian signal of mean value zero it is found that the response of the element will also contain only the components of the input signal and the original shape of the input wave will be maintained at the output. But, when the element becomes nonlinear, distortion will appear in the shape of the output wave and it will become difficult to make any rigorous analysis of the response of the element in this case. However, it can be seen that, for the assumed input, the response of the nonlinearity can be separated into two parts—one representing the correlated component that exactly reproduces the input spectrum, while the remainder is called the 'distortions' comprising the harmonics and intermodulation components and then a quasi-linearisation technique can be adopted to make an approximate representation of the nonlinearity. The use of this linearisation technique assumes the presence of only the correlated component at the output and defines a quasi-linearised transfer function for the nonlinearity that relates the input to the output correlated component. For the case of nonlinearities that involve memory, phase-shift will be introduced to each of the frequency components at the output and therefore, in such cases, the quasi-linearised transfer function obtained for the nonlinearity becomes a complex quantity and may be called 'complex equivalent gain'. The magnitude of this complex equivalent gain is given by the ratio of the r.m.s. value of the output correlated component to that of the input, while the phase is assumed to be frequency-independent. The above definition of a 'complex equivalent gain' has been made for a memory type nonlinearity under the assumption that the components of the signal assumed at the input of the nonlinearity lie within a narrowband frequency spectrum.

In order to determine the phase function attributed to the quasi-linearised model of the nonlinearity, the simple procedure as outlined below is to be adopted. Consider a nonlinear element (Fig. 1), the input of which is impressed upon by a signal  $z$  comprising a sine wave  $z_1 = A_z \sin \omega_c t$  and a Gaussian noise  $z_2$  having mean value zero and variance  $\sigma_n^2$ . If the component of the Gaussian noise is expressed in the form  $z_2 = \sum_{n=0}^{\infty} a_n \sin(\omega_n t + \phi_n)$  where  $a_n$  describes the power spectrum of the noise and  $\phi_n$  is randomly distributed with a uniform probability distribution from 0 to  $2\pi$ , then, neglecting the harmonics and intermodulation components, the approximate output of the nonlinearity can be written as :

$$y = |H(\sigma)| [A_z \sin \{\omega_c t + \theta(\sigma)\} + \sum_{n=0}^{\infty} a_n \sin \{\omega_n t + \phi_n + \theta(\sigma)\}] \quad \dots \quad (1)$$

where  $|H(\sigma)|$  is the magnitude and  $\theta(\sigma)$  the phase of the complex equivalent gain defined for the nonlinearity. In order to attribute the proper sign to the phase function  $\theta(\sigma)$ , it should be remembered that  $\theta(\sigma)$  is negative for those nonlinearities that introduce a lagging phase-shift to the output frequency components for a sinusoidal input, while it is positive for those introducing a leading phase-shift.

Now, the difference between the approximate output and the input multiplied by the magnitude of the complex equivalent gain is given by

$$e - y = |H(\sigma)| z$$

$$= 2 |H(\sigma)| \sin \frac{\theta(\sigma)}{2} \left[ A_z \cos \left\{ \omega_e t + \frac{\theta(\sigma)}{2} \right\} + \sum_{n=0}^{\infty} a_n \cos \left\{ \omega_n t + \phi_n + \frac{\theta(\sigma)}{2} \right\} \right] \quad \dots (2)$$

or, the rms value of the quantity  $e$  is given by

$$\sigma_e = 2 |H(\sigma)| \sigma_z \sin \frac{\theta(\sigma)}{2} \quad \dots (3)$$

whence

$$\theta(\sigma) = 2 \sin^{-1} \frac{\sigma_e}{2 |H(\sigma)| \sigma_z} \quad \dots (4)$$

where  $\sigma_z$  represents the rms value of the total signal at the nonlinearity input.

In practice, however, as the magnitude of the complex equivalent gain defined for the nonlinearity, cannot be easily determined, an approximate measure of the parameter can be obtained by taking the ratio of the rms value of the actual output to that of the input of the nonlinearity. Evidently, this measurement will give a somewhat increased value of the parameter  $|H(\sigma)|$  due to the presence of the distortion components at the output of the nonlinearity.

Thus, the procedure for having an approximate measure of the complex equivalent gain of a memory-type nonlinearity for the assumed input can be summarised as follows :

(1) The rms values of the input and the output of the nonlinearity are first measured and then the parameter  $|H(\sigma)|$  is computed for different rms values of the input.

(2) The rms values of the quantity  $e$  are measured for different values of the input by arranging the set-up as shown in Fig. 1, each time using proper value of the quantity  $|H(\sigma)|$  obtained from the procedure in step (1).

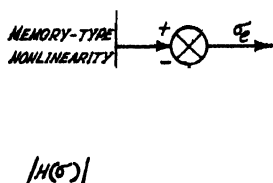


Fig. 1. Set-up for measuring the phase of complex equivalent gain.

(3) Finally, eqn. (4) is used to compute the parameter  $\theta(\sigma)$  of the complex equivalent gain.

For different values of the quantities  $A_z/\delta$  and  $\sigma_n/\delta$  the complex equivalent gain of a simple backlash as measured by the above method is presented in Fig. 2, where  $\delta$  represents the backlash half-width.

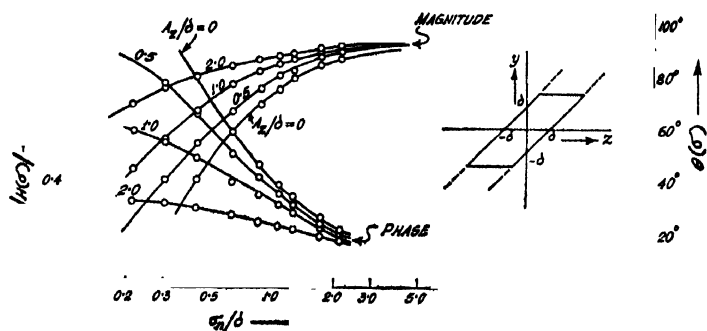


Fig. 2. The complex equivalent gain of a simple backlash.

#### APPLICATION OF THE PROPOSED QUASI-LINEARISATION TECHNIQUE

In the preceding section, a quasi-linearisation technique has been developed which yields a 'complex equivalent gain' as a parameter for approximately representing a memory-type nonlinearity with an input function comprising a sinusoidal signal and a Gaussian noise with mean value zero. When the nonlinear element considered occurs as a part of a feedback system which is also subjected to a similar input, the application of the quasi-linearisation technique is facilitated by replacing the nonlinearity with the help of the quasi-linearised gain and then the analysis is carried out by obtaining two separate linearised versions for the over-all nonlinear system—one for the sinusoidal portion and the other for the Gaussian component of the impressed signal (Sawaragi and Sugai, 1959). The justification in using the two separate linearised systems for the analysis can be seen from the fact that, in either case, the effect of the remaining signal simultaneously present in the system is included in the quasi-linearised gain obtained for the nonlinearity. Though the presence of the nonlinearity will destroy the nature of the signals impressed upon the system, but it will be assumed that the signal feedback to the input of the nonlinearity will contain only a sinusoidal and a Gaussian component, and, possibly, this assumption will be justified in practice because of the narrow-band characteristic of the feedback system.

#### A POSITION CONTROL SYSTEM WITH BACKLASH

Consider a position control system as shown in Fig. 3, incorporating backlash in the output coupling and is subjected to a sinusoidal and a Gaussian signal at



the point in the loop as indicated in the figure. Assuming the signal at the input of the nonlinearity to contain only the components of the impressed wave, the

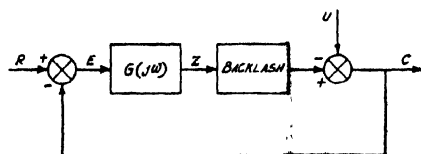


Fig. 3. A position control system with backlash.

application of the quasi-linearisation technique yields the two linearised versions of the nonlinear system as presented in Figs. 4(a) and 4(b).

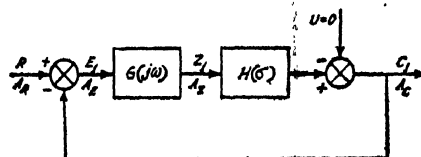


Fig. 4(a). The linearised version of the position control system for sinusoidal portion of the impressed input.

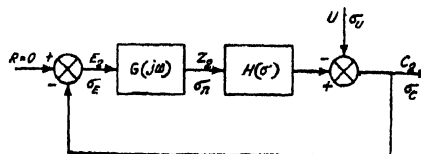


Fig. 4(b). The linearised version of the position control system for Gaussian component of the impressed input.

Confining our attention to the evaluation of the frequency response characteristics of the nonlinear system at the point 'Z' alone, we get from Fig. 4(a),

$$z_1 = \frac{RG(jw)}{1 + H(\sigma)G(jw)} \quad \dots (5)$$

while Fig. 4(b) gives

$$\psi z_2(s) = \psi_U(s) \cdot \frac{G(s)}{1 + H(\sigma)G(s)} \quad \dots (6)$$

where  $\psi z_2(s)$  represents the complex frequency spectrum of the Gaussian noise assumed at the point  $z$ , which is the input of the nonlinearity and  $\psi_U(s)$  is the complex frequency spectrum of the impressed noise. Of the above two equations, it can be readily seen that the first equation gives the required frequency response characteristics of the nonlinear system for different assumed values of the amplitudes of the sine wave and also the Gaussian noise at the input of the nonlinearity, while, with the help of the second equation, the rms values of the impressed noise are computed in terms of the rms noise present at the input point 'Z' of the nonlinearity.

# THE USE OF NICHOLS' CHART

When the transfer functions for the linear and the nonlinear part of the system considered are given as plots on the conventional magnitude-phase plane (shown in Fig. 5), then the frequency response characteristics of the closed-loop system

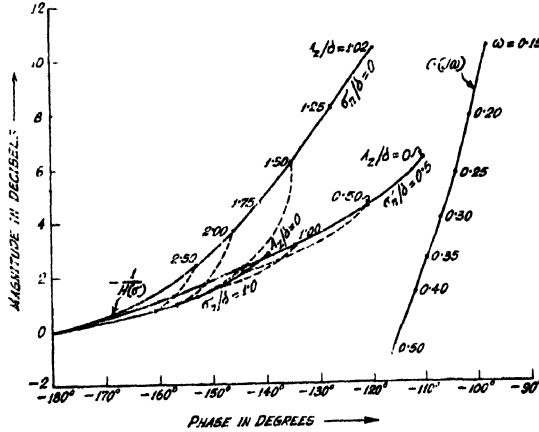


Fig. 5. The magnitude-phase plane plots of the transfer functions for the linear and the nonlinear parts of the position control system.

as given by eqn. (5) can be easily determined by the use of Nichols' chart. Two different approaches can be followed in using the chart as outlined below :

(a) In one approach, the given loci on the magnitude-phase plane are first utilised to obtain different families of curves for the combined transference  $H(\sigma) G(j\omega)$  of the linear and the nonlinear components of the system, each family corresponding to a particular value of the rms noise at the input of the nonlinearity. The procedure for obtaining these families of curves for the combined transfer function can be explained as follows :

If the magnitude of the quantity  $H(\sigma) G(j\omega)$  be expressed in decibels and its phase in degrees, then denoting the respective quantities as  $M_{H\omega}$  and  $\theta_{H\omega}$ , we have

$$M_{H\omega} = |H(\sigma)| + |G(j\omega)|$$

$$= - \frac{1}{|H(\sigma)|} + |G(j\omega)| \quad (7)$$

and

$$Q_{H\omega} = |H(\sigma) + G(j\omega)|$$

$$= - \left[ 180^\circ + \left| - \frac{1}{H(\sigma)} \right| \right] + |G(j\omega)| \quad \dots (8)$$

Since the values of the quantities  $\frac{1}{|H(\sigma)|}$  and  $\left| - \frac{1}{H(\sigma)} \right|$  are directly obtainable from the loci of  $\left| - \frac{1}{H(\sigma)} \right|$  on the magnitude-phase plane and

are known for the values of the parameters  $A_z/\delta$  and  $\sigma_n/\delta$  marked on these loci, substitution of these values in the above equations gives the values of both the magnitude and phase of the combined transference for different values of the frequency, and thus, the required families of curves are obtained at different selected values of  $A_z/\delta$  and  $\sigma_n/\delta$ , each curve being graduated with different values of the frequency.

For a particular selected value of the rms noise  $\sigma_n/\delta$  and with different values of  $A_z/\delta$  as a parameter, the family of curves obtained for the combined transference are now superimposed on the contour system of a Nichols' Chart and the points of intersection of these curves with the contours on the Nichols' chart are noted which give the frequency response characteristics for the transfer function

$$\frac{A}{B} = \frac{H(\sigma) G(j\omega)}{1 + H(\sigma) G(j\omega)} \quad \dots (9)$$

at the selected value of  $\sigma_n/\delta$  and for the different chosen values of  $A_z/\delta$ .

The same procedure as outlined above is then followed for different selected values of  $\sigma_n/\delta$ .

Knowing the frequency response characteristics for the transfer function  $A/B$  with the help of the Nichols' chart, the frequency response characteristics of the system given by eqn. (5) can now be easily computed and this can be done by determining the values of the parameter  $H(\sigma)$  from Fig. 5 at the different selected values of  $\sigma_n/\delta$  and  $A_z/\delta$  and by substituting those values in the relation :

$$\frac{Z_1}{R} = \frac{A}{B} \cdot \frac{1}{H(\sigma)} \quad \dots (10)$$

(b) In the other approach, on the other hand, as suggested by Stein and Thaler (1958), the contour system of the Nichol's chart is superimposed on the given plots of the transfer function of the system, locating its origin on the selected values of  $\sigma_n/\delta$  and  $A_z/\delta$  as marked on the  $\left[ -\frac{1}{H(\sigma)} \right]$ -loci and the same results as represented in eqn. (9) are obtained by observing the points of intersection between the chart-contour and the locus of the given linear transference  $G(j\omega)$  of the system considered. It should be noted, however, that though this latter approach will be useful only when the Nichols' chart is available as contours drawn on a transparent template, but it will be more convenient because of the fact that the laborious computation of the families of curves for the combined transference  $H(\sigma) G(j\omega)$  will not be required in this case.

#### AN EXAMPLE OF A SECOND-ORDER SYSTEM WITH BACKLASH

If the position control system considered in the preceding section be of second order with its linear part having the transfer function  $G(j\omega) = K_v/j\omega(j\omega + 1)$ , then the family of curves for the combined transfer function  $H(\sigma) G(j\omega)$  obtained

at a selected value of  $\sigma_n/\delta$  and superimposed on the Nichols' chart will be as shown in Fig. 6. Taking the value of the velocity error constant  $K_v = 0.5$ , the amplitude

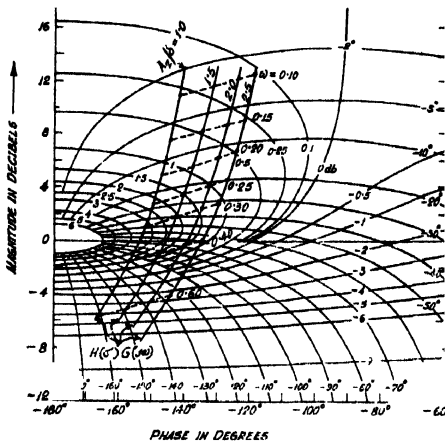


Fig. 6. The loci of the combined transfer function for the linear and nonlinear components of a second-order system superimposed on the contour system of a Nichols' chart.

and the phase response characteristics of the system have been evaluated for different chosen values of  $\sigma_n/\delta$  and  $A_z/\delta$  and the particular characteristics obtained for  $\sigma_n/\delta = 0.5$  and for a set of selected values of  $A_z/\delta$  are presented in Figs. 7 and 8, respectively, where  $A_z/A_R$  represents the amplitude response and  $\phi_z$  the phase response of the system at the point Z. With the help of these characteristics evaluated at different constant values of  $A_z/\delta$ , the frequency response characteristics of the system can be easily determined for different constant values of the amplitude  $A_R/\delta$  of the sinusoidal signal impressed upon the system and this can be done by first designating at each position of the amplitude response characteristics obtained above with the proper value of  $A_R/\delta$  and then drawing the locus

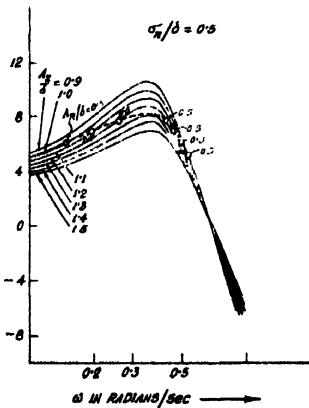


Fig. 7. The amplitude response characteristics of the second-order system for  $\sigma_n/\delta = 0.5$  and for  $A_z/\delta = 0.9, 1.0, 1.1, 1.2, 1.3, 1.4, 1.5$ . (The dotted curve shows the corresponding amplitude response characteristics for  $A_R/\delta = 0.5$ ).

of constant  $A_R/\delta$  on these characteristics. This is illustrated in Fig. 7. Knowing from the figure the values of  $w$  and  $A_z/\delta$  at different positions on the constant

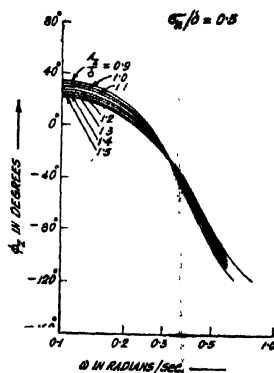


Fig. 8. The phase response characteristics of the second-order system for  $\sigma_n/\delta = 0.5$  and for  $A_z/\delta = 0.9, 1.0, 1.1, 1.2, 1.3, 1.4, 1.5$ .

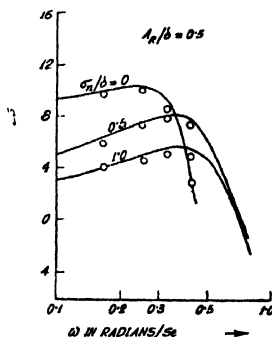


Fig. 9. The amplitude response characteristics of the second-order system for  $A_R/\delta = 0.5$  and for  $\sigma_n/\delta = 0, 0.5$  and  $1.0$ .  
— analytical values  
○ experimental values.

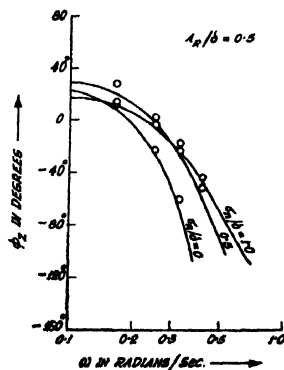


Fig. 10. The phase response characteristics of the second-order system for  $A_R/\delta = 0.5$  and for  $\sigma_n/\delta = 0, 0.5$  and  $1.0$ .  
— analytical values.  
○ experimental values.

$A_R/\delta$  locus, the corresponding phase response characteristics of the system is then determined with the help of Fig. 8. Thus the amplitude and the phase response characteristics of the system are determined for different constant values of  $A_R/\delta$  and the characteristics evaluated at  $A_R/\delta = 0.5$  and for a set of selected values of  $\sigma_n/\delta$  are presented in Figs. 9 and 10, respectively.

Since, in the present system considered, the noise impressed upon the system occurs at the output point  $C$ , the rms values of the impressed noise corresponding to the different selected values of the rms noise at the point  $Z$  are to be determined and this will be done by the use of eqn. (6). Substituting the expression for  $G(jw)$ , eqn. (6) can be written as

$$\psi_{Z_2}(s) = \psi_U(s) \cdot \frac{K_v}{s(s+1) + K_v H(\sigma)} \quad \dots (11)$$

Therefore, for a particular input spectrum given by

$$\psi_U(w) = \frac{\omega_0 n}{j\omega + \omega_0} \cdot \frac{\omega_0 n}{-j\omega + \omega_0} \quad \dots (12)$$

where  $s = jw$  and  $\omega_0$  is the half-power frequency and  $n$  the low frequency amplitude of the noise spectrum, the normalised values of the impressed rms noise in terms of the rms noise at the point  $z$  are obtained from the relation :

$$\frac{\sigma_U}{\delta} = \frac{\sigma_n}{\delta} \sqrt{\left| \frac{H(\sigma)}{K_v} \left\{ \omega_0 + \frac{K_v}{\omega_0 + 1} H(\sigma) \right\} \right|} \quad \dots (13)$$

Since the parameter  $H(\sigma)$  in the above equation is determined by the values of both  $\sigma_n/\delta$  and  $A_z/\delta$ , a set of curves are drawn for the particular system considered by plotting the different values of  $\sigma_n/\delta$  as abscissa and the corresponding values of  $\sigma_U/\delta$  as ordinate and taking the values of  $A_z/\delta$  as a parameter. This is shown in Fig. 11. With the help of these curves, it will be possible to obtain the values of  $\sigma_U/\delta$  corresponding to the selected values of  $\sigma_n/\delta$  and  $A_z/\delta$  in the above

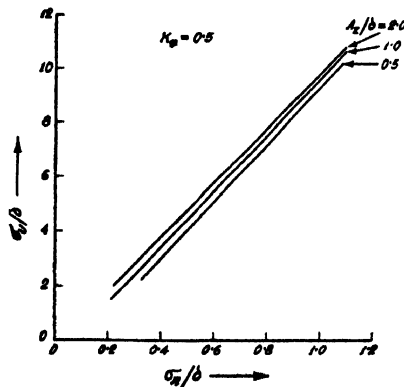


Fig. 11. The plots of  $\sigma_U/\delta$  vs.  $\sigma_n/\delta$  with different values  $A_z/\delta$  as a parameter.

analysis or, conversely, for a given value of  $\sigma_u/\delta$ , the values of  $\sigma_n/\delta$  and  $A_z/\delta c$  can also be selected with the help of these curves.

### COMPUTER STUDY

In order to have an experimental check on the results obtained analytically, the nonlinear system considered in the example, is simulated on an electronic analogue computer and the arrangements as shown in Fig. 12, is made for measur-

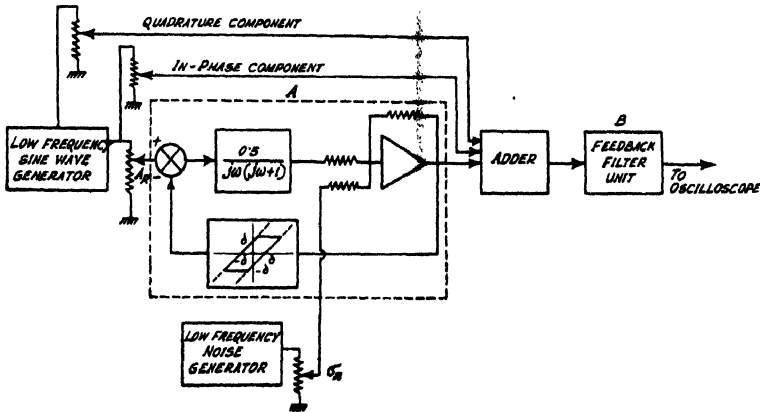


Fig. 12. The experimental arrangement for measuring the amplitude and phase response characteristics of the second-order system with noise injected at the nonlinearity input.

ing both the amplitude and the phase response characteristics of the system for different values of the rms noise present at the point Z in the system loop.

In the arrangement, the block A is the simulated system, under investigation, where the output terminal represents the point Z in the system loop at which the frequency response characteristics are proposed to be evaluated. The block B represents a feedback filter unit having a very narrow pass-band around a centre frequency equal to  $\omega_c$  and the centre frequency is ganged to the frequency of the oscillator supplying the sinusoidal signal impressed upon the input of the simulated system. The filter unit will be used in conjunction with an oscilloscope for detection of the condition of balance of the fundamental component of the impressed sine wave present at the output of the simulated system.

The procedure adopted for the measurement can be outlined as follows : First of all, the amplitude of the sine wave of a particular frequency and also the rms value of noise impressed upon the system is set at the selected values and then the fundamental component appearing at the output of the simulated system due to the impressed sine wave is balanced out by the addition of suitable fractions of the in-phase and quadrature -components of the same sinusoidal signal and the balance is detected with the help of the oscilloscope. As the output

point of the simulated system will be contaminated with noise, the point of exact balance will not correspond to zero output of the filter unit, but, instead, a low frequency noise component will appear on the oscilloscope due to the finite bandwidth of the filter. However, the adjustments could be made such that the departure from the point of balance could readily be detected for a few millivolts change in the fundamental balancing signal from the value at which the balance is obtained. Finally, the amplitude values of the in-phase and the quadrature components of the fundamental balancing signal corresponding to the point of balance are noted and these are used for computing the required amplitude and phase response of the system at the particular value of the frequency of the impressed sine wave.

The above procedures are then repeated for different frequencies and at different selected rms values of the impressed noise and the results obtained are presented and are indicated as circles on Figs. 9 and 10.

### CONCLUSION

The quasi-linearisation technique described in the first part of this paper has been found to be useful for investigating the effect of a Gaussian noise on the frequency response characteristics of a feedback control system incorporating a memory-type nonlinearity. As a graphical aid to the evaluation of the closed-loop equation for obtaining the frequency response characteristics of the system, Nichols' chart has been used and the two possible ways of using the chart have been outlined. It has been observed that, by assuming the Gaussian noise to be impressed at the input of the nonlinearity, the effect of the rms noise is to decrease both the amplitude and the phase response characteristics of the system at the lower frequencies, while increasing them towards the high frequency end of the characteristics. The experimental results obtained from a computer study of the system are found to corroborate the above observations.

### ACKNOWLEDGMENT

The author is grateful to Prof. J. N. Bhar, D.Sc., F.N.I., for his keen interest in the work and to Dr. A. K. Choudhury, M.Sc., D.Phil. for his guidance and many helpful suggestions and discussions. The author also thankfully acknowledges the award of a research fellowship by the Council of Scientific and Industrial Research, New Delhi.

### REFERENCES

- Stein, W. A. and Thaler, G. J., 1958, *Trans. A.I.E.E.*, **77**, Part 2, 91-96.
- Sen, A. K., 1964, *Control*, **8**, 77, 566-569.
- Sen, A. K., 1965, *Trans. I.E.E.E. on Automatic Control*, to be published.
- Sawaragi, Y. and Sugai, N., 1959, *Memoirs of the Faculty of Engineering, Kyoto University*, Vol. XXI, Part 2,



# DETERMINATION OF THE DIELECTRIC CONSTANT OF A TUBULAR MATERIAL AT 3KMc/s

S. K. SEN, J. BASU\* AND A. K. GHOSHAL

INSTITUTE OF RADIO PHYSICS & ELECTRONICS, UNIVERSITY OF CALCUTTA

(Received September 22, 1964)

**ABSTRACT.** The paper describes two methods for determining the resonant behaviour of cylindrical cavity with a tubular dielectric material introduced coaxially in it. The first method tends to give the exact value of the dielectric constant of the material. The second one, based on a perturbation theory, yields somewhat approximate results.

Experiments carried out at a microwave frequency of 3 KMc/s on two tubes of Pyrex glass, show that the inaccuracy in determining the dielectric constant arising out of the approximation inherent in the perturbation theory, is, in these cases, so small as to be compatible with the inaccuracy due to experimental limitations.

## INTRODUCTION

The treatment on the resonant behaviour of a cylindrical cavity when partially filled with a solid dielectric rod, has been given by Horner *et al* (1946). With the help of this, an exact evaluation of the dielectric constant of the rod specimen can be made by solving the transcendental equation relating the dielectric constant and the resonant frequency of the cavity with the rod placed coaxially inside. An approximate analysis on the basis of a perturbation theory was also presented by Slater (1946), with which the dielectric constant can be measured from the change in resonant frequency of the cavity with and without the specimen. This analysis can be utilised to measure the dielectric constant of a fluid (liquid, gas or plasma) in a tubular container (Biondi and Brown, 1949); the evaluation of the dielectric constant of the container is not required. For an exact evaluation, however, it is necessary to determine the dielectric constant of the container.

In the present work the treatment developed by Horner *et al* (1946), as well as the approximate analysis given by Slater (1946), valid for a solid cylindrical dielectric, are extended for a lossless dielectric in the form of a tube. These methods have been used at a microwave frequency of 3 KMc/s to measure the dielectric constant of two pyrex glass tubes, subsequently to be used as plasma containers.

## THEORETICAL CONSIDERATIONS

The cavity is operated in the lowest frequency mode i.e.  $TM_{010}$  mode. The boundaries of the cavity are assumed to be perfectly conducting.

---

\* Present Address: Saha Institute of Nuclear Physics, Calcutta

## (a) Exact solution

Maxwell's equations valid for the interior of the cavity are, in cylindrical coordinates  $(z, r, \theta)$ . :

$$\left. \begin{aligned} j\omega \mu H_\theta &= \frac{\partial E_z}{\partial r} \\ (\sigma + j\omega k) E_z &= \frac{1}{r} \frac{\partial}{\partial r} (r H_\theta) \end{aligned} \right\} \dots (1)$$

where  $\mu$ ,  $k$  and  $\sigma$  are the permeability, permittivity and conductivity of the homogeneous dielectric medium filling the cavity and  $\omega$  is the angular frequency. All the parameters are expressed in rationalised M.K.S. units.

Solutions of the above equations for  $E_z$  and  $H_\theta$  are :

$$\left. \begin{aligned} E_z &= \frac{K}{\sigma + j\omega k} A J_0(Kr) e^{j\omega t} \text{ volts/metre} \\ H_\theta &= A J_1(Kr) e^{j\omega t} \text{ amp/metre} \end{aligned} \right\} \dots (2)$$

in which  $J_0$ ,  $J_1$  are the Bessel functions of the first kind,  $A$  is the constant of integration governed by the strength of excitation and the propagation constant  $K$  is given by

$$K^2 = -j\omega\mu(\sigma + j\omega k) \dots (3)$$

Let the cavity contain three lossless media ( $\sigma = 0$ ) 1, 2, and 3, having permittivities  $k_1$ ,  $k_2$ ,  $k_3$  respectively, as shown in Fig. 1. and permeabilities equal to

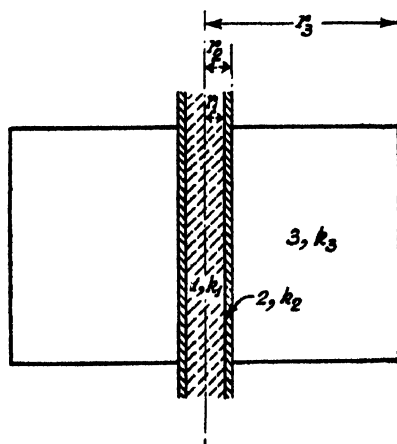


Fig 1 Cavity with glass tube

that of free space,  $\mu_0$ . The propagation constants for the media are, from eqn. (3),

$$\begin{aligned} K_1 &= \omega\sqrt{\mu_1 k_1} = \omega\sqrt{\mu_0 k_1} = \beta_1(\text{say}) \\ K_2 &= \omega\sqrt{\mu_2 k_2} = \omega\sqrt{\mu_0 k_2} = \beta_2 \\ K_3 &= \omega\sqrt{\mu_3 k_3} = \omega\sqrt{\mu_0 k_3} = \beta_3 \end{aligned} \quad \dots (4)$$

Solutions of Maxwell's equations for the electric and magnetic fields, can be written as follows :

For medium 1

$$\left. \begin{aligned} EZ_1 &= \frac{\beta_1}{j\omega k_1} B_1 J_0(\beta_1 r) e^{j\omega t} \\ H_{\theta_1} &= B_1 J_1(\beta_1 r) e^{j\omega t} \end{aligned} \right\} \quad \dots (5)$$

For medium 2

$$\left. \begin{aligned} E_2 &= \frac{\beta_2}{j\omega k_2} [B_2 J_0(\beta_2 r) + C_2 Y_0(\beta_2 r)] e^{j\omega t} \\ H_{\theta_2} &= [B_2 J_1(\beta_2 r) + C_2 Y_1(\beta_2 r)] e^{j\omega t} \end{aligned} \right\} \quad \dots (6)$$

For medium 3

$$\left. \begin{aligned} EZ_3 &= \frac{\beta_3}{j\omega k_3} [B_3 J_0(\beta_3 r) + C_3 Y_0(\beta_3 r)] e^{j\omega t} \\ H_{\theta_3} &= [B_3 J_1(\beta_3 r) + C_3 Y_1(\beta_3 r)] e^{j\omega t} \end{aligned} \right\} \quad \dots (7)$$

Here  $B$ 's and  $C$ 's are constants of integration depending upon the strength of excitation and  $Y_0, Y_1$  are the Bessel functions of the second kind. Equation (5) does not contain the second kind Bessel functions as they become infinite at the axis of the cavity.

The boundary conditions for the cavity system are :

- (1) The tangential component of the electric field at the cavity wall vanishes.
- (2) There is continuity of electric and magnetic fields at the boundaries of the media 3, 2 and 2, 1. Applying these conditions we get from equations (5), (6) and (7)

$$B_3 J_0(\beta_3 r_3) + C_3 Y_0(\beta_3 r_3) = 0$$

$$\frac{\beta_3}{k_3} [B_3 J_0(\beta_3 r_2) + C_3 Y_0(\beta_3 r_2)] = \frac{\beta_2}{k_2} [B_2 J_0(\beta_2 r_2) + C_2 Y_0(\beta_2 r_2)]$$

$$B_3 J_1(\beta_3 r_2) + C_3 Y_1(\beta_3 r_2) = B_2 J_1(\beta_2 r_2) + C_2 Y_1(\beta_2 r_2) \quad (8)$$

$$\frac{\beta_2}{k_2} [B_2 J_0(\beta_2 r_1) + C_2 Y_0(\beta_2 r_1)] = \frac{\beta_1}{k_1} B_1 J_0(\beta_1 r_1)$$

$$B_2 J_1(\beta_2 r_1) + C_2 Y_1(\beta_2 r_1) = B_1 J_1(\beta_1 r_1)$$

Now, from equation (4)

$$\beta_1 = \beta_3 \sqrt{\frac{k_1}{k_3}} \quad (9)$$

and

$$\beta_2 = \beta_3 \sqrt{\frac{k_2}{k_3}}$$

Eliminating the constants in equation (8) and using eqn. (9), we get the following transcendental equation relating the dielectric constants of the different media.

$$\begin{aligned} & \left[ J_0(\beta_2 r_2) - \sqrt{\frac{k_2}{k_3}} F J_1(\beta_2 r_2) \right] \left[ Y_0(\beta_2 r_1) J_1(\beta_1 r_1) - \sqrt{\frac{k_2}{k_1}} J_0(\beta_1 r_1) Y_1(\beta_2 r_1) \right] \\ &= \left[ \sqrt{\frac{k_2}{k_3}} F Y_1(\beta_2 r_2) - Y_0(\beta_2 r_2) \right] \left[ \sqrt{\frac{k_2}{k_1}} J_0(\beta_1 r_1) J_1(\beta_2 r_1) - J_0(\beta_2 r_1) J_1(\beta_1 r_1) \right] \dots \quad (10) \end{aligned}$$

where

$$F = \frac{J_0(\beta_3 r_2) Y_0(\beta_3 r_3) - J_0(\beta_3 r_3) Y_0(\beta_3 r_2)}{J_1(\beta_3 r_2) Y_0(\beta_3 r_3) - J_0(\beta_3 r_3) Y_1(\beta_3 r_2)}$$

Assuming that the medium 3 is air, we get a transcendental equation from (10) which gives the dielectric constant of medium 1 in terms of that of 2 and vice versa, provided  $\omega$ , the resonant frequency of the composite system is known.

Further, if we assume that the dielectric medium 1, enclosed by the tube represented by the medium 2, is air, we can find  $k_2/k_0 = \epsilon_2$ , the dielectric constant of the tubular material from the following equation, the permittivity of air being taken equal to that of free space,  $k_0$ .

$$\begin{aligned} & \left[ J_0(\beta_2 r_2) - \sqrt{\frac{k_2}{k_0}} F' J_1(\beta_2 r_2) \right] \left[ Y_0(\beta_2 r_1) J_1(\beta_0 r_1) - \sqrt{\frac{k_2}{k_0}} J_0(\beta_0 r_1) Y_1(\beta_2 r_1) \right] \\ &= \left[ \sqrt{\frac{k_2}{k_0}} F' Y_1(\beta_2 r_2) - Y_0(\beta_2 r_2) \right] \left[ \sqrt{\frac{k_2}{k_0}} J_0(\beta_0 r_1) J_1(\beta_2 r_1) - J_0(\beta_2 r_1) J_1(\beta_0 r_1) \right] \dots \quad (11) \end{aligned}$$

$$\text{where } F' = \frac{J_0(\beta_0 r_2) Y_0(\beta_0 r_3) - J_0(\beta_0 r_3) Y_0(\beta_0 r_2)}{J_1(\beta_0 r_2) Y_0(\beta_0 r_3) - J_0(\beta_0 r_3) Y_1(\beta_0 r_2)}$$

and  $\beta_0 = w\sqrt{\mu_0 \epsilon_0} = \frac{w}{c}$ ,  $c$  being the velocity of light in free space.

### (b) Solution based on a Perturbation Theory

When the electric or magnetic field within a cavity is perturbed by insertion of a material within it, a change occurs in the distribution of the electromagnetic field. Consequently the resonant frequency of the cavity changes. This change of resonant frequency,  $\Delta f$ , is related to the dielectric constant of the material inserted.

Let a dielectric tube be placed coaxially within the cavity. For  $TM_{010}$  mode being used, the electric field only is disturbed. Following Slater (1946), the perturbation equation is

$$\frac{\Delta f}{f_0} = - \frac{\int_{v_s} (\epsilon - 1) E^2 dv}{\int_{v_c} E^2 dv} \quad \dots (12)$$

where  $f_0$  is the resonant frequency and  $E$  is the electric field intensity of the unperturbed cavity,  $\Delta f$  is the change in frequency due to the introduction of the tube.  $v_s$  refers to integration over the volume of the tube and  $v_c$  that over the volume of the cavity. It should, however, be noted that this equation is valid only if the perturbation is small i.e. the dielectric constant of the material under study is not very high and the radius of the tube is small compared to that of the cavity.

Now, using cylindrical coordinates ( $z, r, \theta$ ), the solution of Maxwell's equation for the electric field in a cylindrical cavity operating in  $TM_{010}$  mode is, in absence of any perturbation,

$$E = DJ_0(K_0 r) \quad \dots (13)$$

where  $K_0$  is the propagation constant and  $D$  is a constant of integration depending upon the strength of excitation.

From equations (12) and (13)

$$\begin{aligned} \frac{\Delta f}{f_0} &= - \frac{1}{2} \frac{\int_z \int_r \int_\theta (\epsilon - 1) D^2 J_0^2(K_0 r) dr \cdot r d\theta \cdot dz}{\int_z \int_r \int_\theta D^2 J_0^2(K_0 r) dr \cdot r d\theta \cdot dz} \\ &= - \frac{1}{2} \frac{(\epsilon - 1) D^2 2\pi \cdot L \int_{r_1}^{r_2} r J_0^2(K_0 r) dr}{D^2 \cdot 2\pi \cdot L \int_0^{r_3} r J_0^2(K_0 r) dr} \quad \dots (14) \end{aligned}$$

$L$  represents the length of the cavity.  $r_1, r_2$  are the internal and external radii of the tube and  $r_3$  is the radius of the cavity (Fig. 1).

From equation (14)

$$\frac{\Delta f}{f_0} = -\frac{1}{2}(\epsilon - 1) \frac{\int_{r_1}^{r_2} r J_0^2(K_0 r) dr}{\int_0^{r_3} r J_0^2(K_0 r) dr}$$

$$\begin{aligned} \text{or,} \quad \epsilon &= 1 - \frac{2\Delta f}{f_0} \frac{\int_0^{r_3} r J_0^2(K_0 r) dr}{\int_{r_1}^{r_2} r J_0^2(K_0 r) dr} \\ &= 1 - \frac{2\Delta f}{f_0} \cdot \frac{r_3^2 [J_0^2(K_0 r_3) + J_1^2(K_0 r_3)]}{r_2^2 [J_0^2(K_0 r_2) + J_1^2(K_0 r_2)] - r_1^2 [J_0^2(K_0 r_1) + J_1^2(K_0 r_1)]} \quad \dots (15) \end{aligned}$$

As the cavity wall is assumed to be perfectly conducting, the electric field at  $r = r_3$  is zero. Therefore, from equation (13),  $J_0(K_0 r_3) = 0$ . Since the cavity is operated in the  $TM_{010}$  mode,  $K_0 r_3 = 2.405$ , the value at which the first zero of  $J_0$  occurs.

Equation (15) becomes

$$\begin{aligned} \epsilon &= 1 - \frac{2\Delta f}{f_0} \frac{r_3^2 [J_1^2(2.405)]}{r_2^2 \left[ J_0^2\left(2.405 \frac{r_2}{r_3}\right) + J_1^2\left(2.405 \frac{r_2}{r_3}\right) \right] - r_1^2 \left[ J_0^2\left(2.405 \frac{r_1}{r_3}\right) + J_1^2\left(2.405 \frac{r_1}{r_3}\right) \right]} \quad \dots (16) \end{aligned}$$

## EXPERIMENT

The block diagram of the experimental arrangement is shown in Fig. 2.

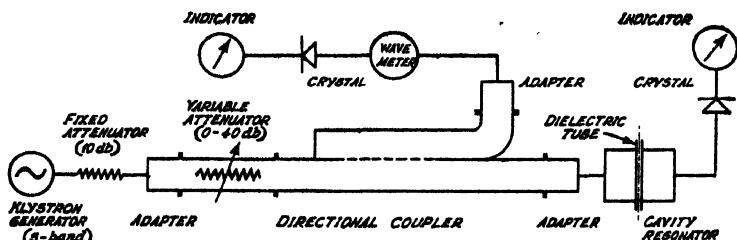


Fig. 2 Experimental arrangement.

Two pyrex glass tubes were chosen as dielectric samples and each of them, in turn, was placed coaxially inside the cavity. The resonant frequencies of the cavity with and without each of the samples were measured. The resonant frequency, in each case, is given by the frequency at which the transmission through the cavity is maximum. The frequency meter gives an accurate reading within  $\pm 0.3$  Mc/sec.

### RESULTS

The resonant frequency of the empty cavity in  $TM_{010}$  mode as measured experimentally ( $f_0'$ ) is found to be slightly different from that calculated from its dimensions ( $f_0$ ). The discrepancy is assumed to be due to the presence of holes in the cavity wall provided for insertion of the samples and the coupling loops. It is therefore evident that the measured resonant frequency of the cavity with a sample ( $f'$ ) is also affected by the holes and needs correction, the corrected value being taken as

$$f = f' + (f_0 - f_0')$$

The frequencies  $f_0, f_0', f', f$  and the difference frequency  $\Delta f = (f' - f_0')$  are given in Table I.

Radius of the cavity  $r_3 = 3.837$  cm.

Sample I. Internal radius,  $r_1 = 0.145$  cm

External radius,  $r_2 = 0.233$  cm.

Sample II. Internal radius,  $r_1 = 0.389$  cm.

External radius,  $r_2 = 0.501$  cm.

The internal radii were calculated from the volume of Mercury filling the tubes as described by Worsnop and Flint (1961).

TABLE I

Sample	$f_0$ Mc/sec	$f_0'$ Mc/sec	$f'$ Mc/sec	$f$ Mc/sec	$\Delta f$ Mc/sec
I	2992.7	2999.0	2950.7	2944.4	48.3
II	2992.7	3004.5	2874.7	2862.9	129.8

Equation (11) is used for determining the exact value of the dielectric constant of the samples, putting  $\omega = 2\pi f$  where  $f$  is obtained from Table I. With the help of equation (16) based on the perturbation theory, the dielectric constant is again calculated;  $f_0$  and  $\Delta f$  are given by Table I. Dielectric constant for two pyrex glass tubes as determined by the above methods, are recorded in Table II. Its percentage deviation for the solution based on the perturbation theory, with respect to the value obtained from the exact solution, is also recorded.

TABLE II

Sample	Dielectric constant		percentage deviation $\frac{b-a}{a} \times 100\%$
	from	from	
	exact	perturbation	
	solution	theory	
	<i>a</i>	<i>b</i>	
I	4.80	4.86	1.25
II	4.58	4.59	0.22

## CONCLUDING REMARKS

The value of the dielectric constant of pyrex glass is found to be in conformity with that reported earlier (Von Hippel, 1954; Forsythe, 1956; Knoll, 1959). It appears from Table II that the composition of the two tube samples is slightly different.

The result for the tubes, as obtained from the solution based on the perturbation theory, differs, by less than 2%, from that given by the exact solution. It may be concluded that the inaccuracy due to the approximation inherent in the perturbation method is, in these cases, so small as to be compatible with the inaccuracy due to experimental limitations. However, if the perturbation is large, i.e., if the material under study is of high dielectric constant or if the thickness of the tubewall is appreciable, compared to the radius of the cavity resonator, the perturbation theory fails to hold. The exact method described in section (a) of theoretical consideration would, then, have to be followed.

The dielectric material discussed in this paper is assumed to be completely lossless. For a material with a low loss tangent, the methods described for determining the dielectric constant may still be applicable with a fair degree of accuracy; the loss tangent can be determined by measuring the 'Q' of the cavity with and without the specimen and applying, in an extended form, the perturbation method (Slater, 1946) or, for a more accurate evaluation, the method described by Horner *et al* (1946).

## ACKNOWLEDGMENT

The authors are indebted to Prof. J. N. Bhar, D.Sc., F.N.I., for his keen interest in the work and for valuable discussions,



REFERENCES

- Biondi, M. A., and Brown, S. C., 1949, *Phys. Rev.* **75**, 1700
- Forsythe, William Elmer, 1956, *Smithsonian Physical Tables*, Smithsonian Institution, Washington, 534
- Horner, F., Taylor, T. A., Dunsmair, R., Lamb, T., and Jackson, Willis, 1946, *Jour Inst Elec Eng*, **93**, Part III, 53
- Knoll, Mex., 1959 *Materials and Processes of Electron Devices*, Springer-Verlag, Berlin/Göttingen/Heidelberg, 219
- Slator, J. C., 1946, *Review of Modern Physics*, **18**, 441
- Von Hippel., Arthur R., 1954, *Dielectric Materials and Applications*, Technology Press of MIT and John Wiley and Sons, Inc., New York, 310
- Worsnop, B. L., and Flint, H. T., 1961, *Advanced Practical Physics for Students*, Methuen and Co. Ltd., London, 26.

# ON THE INFRARED SPECTRA OF FLUORO-, CHLORO-, BROMO- AND IODOBENZENE IN THE VAPOUR STATE

S. C. SIRKAR, D. K. MUKHERJEE and P. K. BISHUI

INDIAN ASSOCIATION FOR THE CULTIVATION OF SCIENCE, CALCUTTA-32.

(Received, 30.11.64)

**ABSTRACT.** The infrared spectra of fluorobenzene, chlorobenzene, bromobenzene and iodobenzene in the vapour state have been studied using a Perkin-Elmer one metre gas cell and Model 21 spectrophotometer and compared with the spectra of the pure liquids and of their solutions in carbon tetrachloride and chloroform. Significant changes are observed with the change of state. From the spectra of fluorobenzene and chlorobenzene in the different states it has been concluded that in both these cases the vapour consists of both monomeric and dimeric molecules and the liquid consists almost wholly of dimers. In the other two cases the vapour consists predominantly of monomeric molecules and in the liquid state there is a smaller percentage of monomeric molecules and a greater proportion of dimeric molecules. From a comparison of the spectra with the Raman spectra, some of the bands not assigned by previous workers have been assigned to relevant modes of vibration of the molecules.

## INTRODUCTION

The Raman and infrared spectra of monohalogen substituted benzenes in the state of aggregation and also in solution have been studied by many previous workers (Landolt-Börnstein, 1951; Lecomte, 1937; Mortimer *et al.*, 1947; Plyler, 1949). As the molecules are strongly polar some intermolecular association in the state of aggregation is expected in all these cases. The Raman spectra of chlorobenzene in the vapour and liquid states were studied by Sponer and Kirby-Smith (1941) who observed that in the spectrum due to the vapour some of the lines due to the liquid were shifted and some other lines were absent. Such an effect was also observed by them in the case of three isomeric dichlorobenzenes. As the Raman spectrum of the vapour is generally very weak a definite conclusion regarding the disappearance of some of the lines cannot be drawn. The strength of the infrared absorption in the spectra of the vapour can, however, be increased by increasing the length of the cell. Further, a comparative study of the infrared absorption spectra of the different halogen substituted benzenes in the vapour and liquid states might show whether any significant changes depending on the chemical affinity of the substituent halogen atoms take place with the change from the vapour to the liquid state. With this object in view the infrared spectra of fluorobenzene, chlorobenzene, bromobenzene and iodobenzene in the vapour and liquid states and in solution in different solvents have been studied in the present investigation.

# EXPERIMENTAL

The liquids were of chemically pure quality and were distilled under reduced pressure before use. A Perkin-Elmer Model 21 double beam infrared spectrophotometer was used to record the spectra. In the case of the vapours a Perkin-Elmer multiple reflection gas cell with total absorbing path of 100 cm was used. The spectra of the solutions of the compounds in  $\text{CCl}_4$ ,  $\text{CHCl}_3$  and  $\text{CS}_2$  were also recorded using compensation cells in the reference beam. In the case of the pure liquids, thin films enclosed between two NaCl plates were used.

## RESULTS AND DISCUSSION

The absorption curves due to the four compounds in the vapour and liquid states are reproduced in Figs. 1, 2, 3 and 4 respectively. The wave numbers in  $\text{cm}^{-1}$  of the bands are given in Tables I, II, III and IV in which the positions of some of the bands of solutions in different solvents have also been included. The changes observed in the spectra with the change of state and also with dissolution in different solvents are discussed in the following sections.

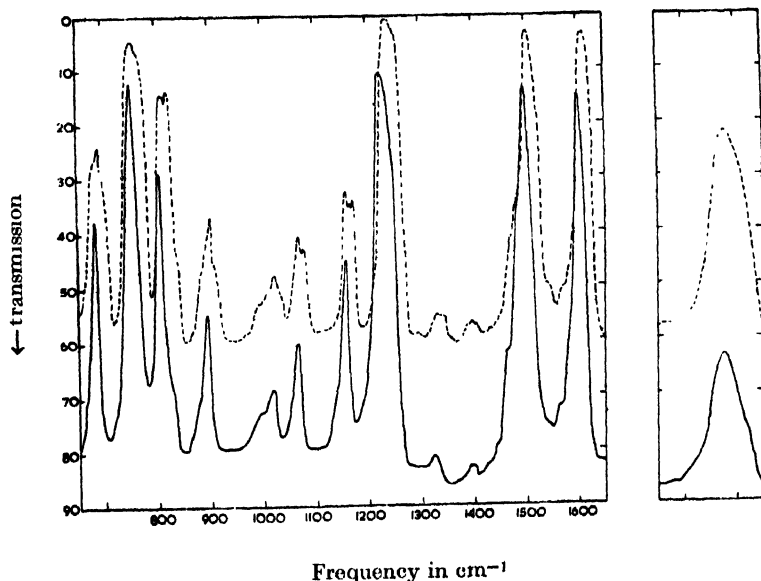


Fig. 1. Infrared spectra of fluorobenzene.

..... vapour.  
——— liquid.

### (a) Fluorobenzene

The curves in Fig. 1 show that most of the bands due to the vapour are well resolved while the rest are asymmetric and broad. In the spectrum of the liquid on the other hand, each of the doublets is replaced by a single band. For instance, the liquid gives a strong band  $805\text{ cm}^{-1}$  in place of the two bands at  $810$  and  $820\text{ cm}^{-1}$  due to the vapour. In the Raman spectrum of the liquid there is a

TABLE I  
Fluorobenzene  
 $\nu$  in  $\text{cm}^{-1}$

Liquid	Vapour	3% Soln. in $\text{CHCl}_3$	4% Soln. in $\text{CCl}_4$	4% Soln. in $\text{CS}_2$
670 (vw)	675 (w)	665 (w) 675 (w)		670 (w)
682 (s)	680 (m, b) 690 (s) 695 (m)	682 (s)	682 (s)	680 (s)
752 (vs)	752 (vs, b) 768 (s)	710 (m) 752 (s)	728 (s)	750 (vs)
805 (s)	810 (s) 820 (s)	795 (vs) 820 (w)	810 (s, b)	802 (s)
825 (w)		840 (vw)		
895 (m)	885 (w) 900 (m) 908 (w)	895 (m)	892 (m)	850 (w) 890 (m)
998 (vw)	992 (w) 1005 (w)	925 (w) 1000 (vw)		
1020 (w)	1020 (m)	1020 (w)	1000 (w, b)	1020 (vw)
1065 (m)	1065 (m) 1078 (m)	1065 (m)	1065 (m)	1065 (w)
1155 (s)	1155 (m) 1170 (m)	1155 (s)	1157 (s)	1155 (m)
1225 (vs, b)		1215 (vs, b) 1225 (vs, b)	1224 (vs)	1222 (vs)
	1238 (vs, b) 1250 (vs)		1235 (m) 1250 (vw)	1235 (m)
1326 (vw)	1330 (w) 1340 (w)	1325 (w)	1328 (vvw)	
1398 (vw)	1395 (w, b)			
1435 (vw)		1425 (w)	1450 (vvw)	
1465 (w)	1470 (w)	1465 (w)	1465 (w)	
1482 (w)	1485 (w)	1480 (m)	1480 (m)	
1498 (vs)	1502 (vs) 1510 (s) 1540 (vw)	1498 (vs) 1515 (vw) 1530 (vw)	1498 (vs)	
1565 (vvw)	1570 (vw) 1580 (vw) 1590 (vw)	1585 (vw)	1585 (w)	
1600 (vs)		1600 (vs)	1600 (vs)	
	1615 (s) 1635 (vvw) 1695 (vw)			
1700 (vw, b)	1708 (w, b) 1770 (w, b)			
1850 (vw)	1850 (w) 1862 (w) 1938 (w)			
1950 (vw)	1952 (m, b)			
2035 (vvw)	2160 (w) 2470 (vw) 2575 (vvw) 2630 (vvw) 2890 (vvw)			
		3040 (s)		
3078 (m, b)	3078 (vs, b) 3100 (s)	3100 (w)	3070 (w, b)	3060 (vw)

strong line at  $806\text{ cm}^{-1}$  which is assigned to the C-F stretching oscillation (Mecke/ and Kerkhof, 1951). Hence it can be concluded from the observed results that there are two types of molecules in the vapour giving two C-F stretching frequencies and only one of these two types persists in the liquid. Probably, these are the single molecules, and the dimers and the wave number  $820\text{ cm}^{-1}$  is to be assigned to the single free molecule and  $810\text{ cm}^{-1}$  to the dimer. Again, in place of the two bands  $752\text{ cm}^{-1}$  and  $768\text{ cm}^{-1}$  given by the vapour only one band at  $752\text{ cm}^{-1}$  is given by the liquid. As this band at  $752\text{ cm}^{-1}$  is very strong and its frequency is lower than the Raman frequency  $759\text{ cm}^{-1}$  given by the liquid, the mode giving the band is different from that giving the Raman line. Probably, the band is due to the mode corresponding to mode No. 18 B of benzene (Pitzer and Scott, 1943) and the band at  $752\text{ cm}^{-1}$  is to be assigned to this mode of the dimer.

The strong band at  $1502\text{ cm}^{-1}$  given by the vapour has an unresolved companion at  $1510\text{ cm}^{-1}$  and there are weak satellites at  $1470$ ,  $1480$  and  $1485\text{ cm}^{-1}$  respectively. The spectrum due to the liquid shows a sharp and strong band at  $1498\text{ cm}^{-1}$  and two moderately strong satellites at  $1465$  and  $1482\text{ cm}^{-1}$  respectively. This group of bands is due to the mode corresponding to the  $e_u^-$  mode No. 19B of benzene. Evidently, the band at  $1510\text{ cm}^{-1}$  is due to the single molecule and that at  $1502\text{ cm}^{-1}$  to dimers which persist in the vapour. In the liquid the latter frequency diminishes to  $1498\text{ cm}^{-1}$  probably owing to formation of hydrogen bonds between neighbouring molecules. The components at  $1482\text{ cm}^{-1}$  and  $1465\text{ cm}^{-1}$  in the spectrum due to the liquid are stronger than any of the three components given by the vapour. The symmetry of the mode is  $B_1$  in the present case and the two-fold axis in the plane of the molecule passes through the halogen atom. It may be possible, however, that there is small probability of similar alternative sets of displacements taking place with respect to axes passing through diametrically opposite C-H groups in the molecule and the bands at  $1485\text{ cm}^{-1}$  and  $1470\text{ cm}^{-1}$  may be due to such modes in the single molecules present in the vapour and those at  $1480\text{ cm}^{-1}$  and  $1565\text{ cm}^{-1}$  might be due to those in the dimer. The slight dependence of the frequency of this mode on the weight of the substituent atom is indicated by the corresponding Raman frequencies of these four halogen substituted compounds. The other component of symmetry  $A_1$  of this mode gives the two bands at  $1235\text{ cm}^{-1}$  and  $1250\text{ cm}^{-1}$  in the case of the vapour and only a single band at  $1225\text{ cm}^{-1}$  in the spectrum due to the liquid, the latter frequency being that of the dimer. The alternative displacements of this mode referred to above would give rise to modes having frequencies near about those of the  $B_1$  mode mentioned above.

It has to be pointed out that the strong band at  $1608\text{ cm}^{-1}$  due to the vapour is also accompanied by an unresolved companion at  $1615\text{ cm}^{-1}$  and three weak satellites at  $1590$ ,  $1580$  and  $1570\text{ cm}^{-1}$  respectively. As this band is due to the  $B_1$  mode corresponding to the  $e_g^+$  mode No. 8B of benzene and the dependence

of the frequency of the vibration on the weight of the substituent atom is very small, the frequency of the dimer is not much different from that of the monomer to show a splitting of the bands  $1608\text{ cm}^{-1}$  and  $1615\text{ cm}^{-1}$ , the latter being due to the monomer. In this case also, alternative sets of displacements with respect to diametral axes not passing through the halogen atom may occur with a small probability, the satellites  $1590\text{ cm}^{-1}$  and  $1580\text{ cm}^{-1}$  being the frequencies of such modes in the single molecule. The frequencies of the corresponding modes of the dimer present in the vapour diminish a little in the liquid due probably to intermolecular hydrogen bonding. Other doublets in the region  $1000\text{ cm}^{-1}$ — $1200\text{ cm}^{-1}$  due to C—H bending oscillations observed in the case of the vapour also appear as single lines in the spectrum due to the liquid. The C—H stretching vibrations of the vapour give bands at  $3078\text{ cm}^{-1}$  and  $3100\text{ cm}^{-1}$  while in the liquid there is a broad band at  $3078\text{ cm}^{-1}$ . This latter band is due to the vibration of the dimer corresponding to mode No. 20B of benzene, the frequency of the monomer being  $3100\text{ cm}^{-1}$ .

It can, therefore be concluded from the results that the liquid consists of only dimers and in the vapour there are dimers and monomers almost in equal proportions. The bands observed in the spectra of the solutions in chloroform, carbon tetrachloride and carbon disulphide show that they correspond to the bands given by the pure liquid. In the case of the solution in chloroform the frequency of C—H stretching vibration corresponding to mode 20B is reduced to  $3040\text{ cm}^{-1}$ , which shows that hydrogen bonding takes place between the solvent and solute molecules. This band is very weak in the spectra due to solutions in the other two solvents, which shows that in those solutions also the molecules are not free..

#### (b) *Chlorobenzene*

The spectra due to chlorobenzene in the vapour state and in the liquid state reproduced in Fig. 2 show that the bands at  $690$ ,  $712$ ,  $810$ ,  $905$  and  $1465\text{ cm}^{-1}$  disappear when the vapour is liquefied. The other bands of the vapour of frequencies below  $1600\text{ cm}^{-1}$  are broad and asymmetric on the higher frequency side, which suggests that there are unresolved companions on this side. These companions at  $750$ ,  $1035$ ,  $1100$ ,  $1250$ ,  $1495$ ,  $1605$  and  $3095\text{ cm}^{-1}$  also disappear when the vapour is liquefied. Thus, in this case also it appears that the vapour consists of both associated and single molecules, while the liquid consists wholly of dimers. The frequency of the C—Cl stretching vibration of the single molecule is therefore,  $712\text{ cm}^{-1}$  and that of the dimer is  $702\text{ cm}^{-1}$  and the latter frequency diminishes to  $700\text{ cm}^{-1}$  in the case of the liquid. This shows the formation of intermolecular H...Cl bond in the liquid.

The strong band at  $738\text{ cm}^{-1}$  of the liquid may be due to the mode corresponding to mode No. 18B of benzene, the frequency of vibration in the monomer being  $750\text{ cm}^{-1}$  represented by an unresolved companion of the band given by the vapour. The bands are broader in the spectrum due to the vapour probably

TABLE II  
Chlorobenzene  
 $\nu$  in  $\text{cm}^{-1}$

Liquid at 28°C	Vapour at 28°C	3% Soln. in $\text{CHCl}_3$	3% Soln. in $\text{CCl}_4$
668 (w)		665 (w)	
682 (s)	680 (w)	685 (s)	680 (s)
	690 (m)		
600 (s)	702 (s)	700 (s)	700 (s)
	712 (m)	710 (w)	
			725 (m)
738 (vs)	738 (vs, b)		
	750 (s)		
800 (vvw)	810 (m, b)		
898 (m)	895 (m)	900 (vw)	900 (w)
	905 (w)		
		930 (w)	930 (vw)
1002 (w)	1002 (vw, b)	1000 (vw)	1000 (vw)
1022 (s)	1024 (s)	1025 (s)	1020 (m)
	1035 (m)		
1070 (m)	1070 (w)	1070 (w)	1070 (w)
1082 (s)	1090 (vs)	1085 (vs)	1085 (vs)
	1100 (m)		
1120 (w)	1225 (m)	1120 (w)	1120 (vw)
1155 (vvw)	1150 (vw)		
1170 (vvw)	1170 (vw)		
1235 (m)	1238 (vs)	1225 (vs)	
	1250 (s)		
1430 (vw)	1430 (vvw)	1430 (vw)	
1450 (s)	1450 (w)	1450 (m)	
	1465 (w)		
1480 (vs)	1485 (vs)	1485 (vs)	
	1495 (s)		
1550 (vw)	1550 (vvw)		
1565 (w)	1570 (w)		
1585 (s)	1585 (w)?		
		1590 (m)	
	1598 (vs)		
	1605 (s)		
	1780 (w)		
1860 (vw)			
	1870 (w)		
1950 (vw)	1950 (w)		
	3000 (w)		
3040 (w)		3040 (s)	3035 (vw)
	3050 (w)		
3075 (m, b)	3070 (w)	3075 (w)	
			3080 (w)
	3095 (vs, b)		

because the molecules are free to rotate about the two-fold axis. The band at  $1090\text{ cm}^{-1}$  of the vapour is produced by the  $A_1$  component of the mode corresponding to mode No. 19 A of benzene and the  $B_1$  component gives the band at  $1485\text{ cm}^{-1}$ . Both the bands are asymmetric on the high frequency side as mentioned earlier, but the latter band is accompanied by weaker satellites

at 1450 and 1465  $\text{cm}^{-1}$  respectively. The main band shifts to 1480  $\text{cm}^{-1}$ , the band at 1465  $\text{cm}^{-1}$  disappears and that at 1450  $\text{cm}^{-1}$  becomes stronger when the

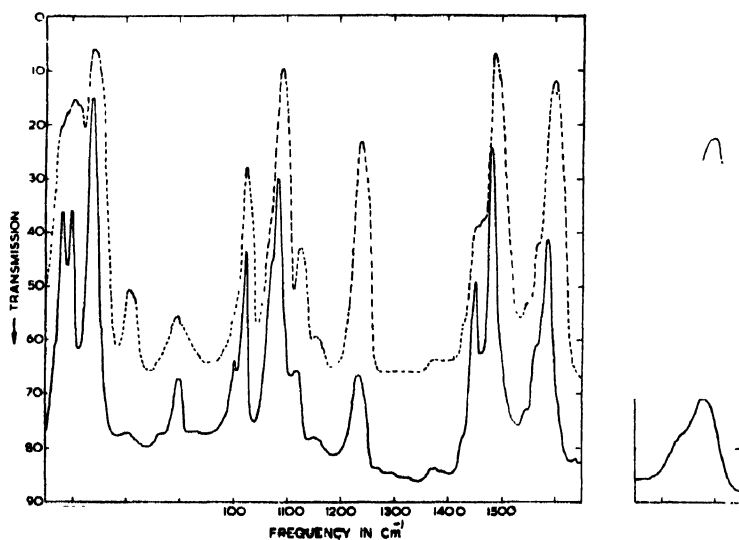


Fig. 2. Infrared spectra of chlorobenzene.  
 ..... vapour.  
 — liquid.

vapour is liquefied. As suggested in the case of fluorobenzene these satellites may be due to alternative sets of displacements with respect to the axes passing through diametrically opposite C—H groups of the molecule and the strengthening of the band at 1450  $\text{cm}^{-1}$  of the liquid shows that in the dimer such alternative sets of displacements become more probable. The band at 1598  $\text{cm}^{-1}$  due to the vapour has similarly weaker companions at 1570  $\text{cm}^{-1}$  and 1550  $\text{cm}^{-1}$ . The strong band shifts to 1586  $\text{cm}^{-1}$  and the other two to 1565  $\text{cm}^{-1}$  and 1545  $\text{cm}^{-1}$  respectively in the case of the liquid. The corresponding Raman frequency of the molecule in the liquid state is 1584  $\text{cm}^{-1}$  and it has been assigned to the  $A_1$  component corresponding to mode No. 8A of benzene by Meeke and Kerkhof (1951). Hence this frequency is to be assigned to the dimer.

The strong bands at 3095  $\text{cm}^{-1}$  and the weaker one at 3050  $\text{cm}^{-1}$  given by the vapour are due to vibrations corresponding to modes 20B and 7B of benzene respectively. These bands appear to be due to the monomer, the corresponding bands due to the dimer are weak and have frequencies 3070  $\text{cm}^{-1}$  and 3040  $\text{cm}^{-1}$  respectively. In the spectrum due to the liquid there are a moderately strong band at 3075  $\text{cm}^{-1}$  and a weak band at 3038  $\text{cm}^{-1}$ . So, it appears that the C—H vibration is partially suppressed in the dimers present in the liquid. In the spectrum due to the 3% solution in chloroform the band at 3040  $\text{cm}^{-1}$  is much stronger than that at 3075  $\text{cm}^{-1}$ . The former band is thus due to the molecules associated with the chloroform molecules through weak H...Cl bond.



(c) *Bromobenzene*

The bands due to bromobenzene in the vapour and liquid states reproduced in Fig. 3 show remarkable changes in the spectra with the change of state. The strong band at  $1483\text{ cm}^{-1}$  due to the vapour has two weak companions at  $1460$  and  $1448\text{ cm}^{-1}$  respectively. In the spectrum due to the liquid on the other hand, the band at  $1447\text{ cm}^{-1}$  is the strongest and there are a weaker companion at  $1472\text{ cm}^{-1}$  and another still weaker component at  $1485\text{ cm}^{-1}$ . These changes can be explained on the assumption that in the case of the vapour the very strong band at  $1483\text{ cm}^{-1}$  is due to the  $B_1$  mode in the single molecule corresponding to mode 19B of benzene and the weak band at  $1448\text{ cm}^{-1}$  is due to the same vibration in one of the molecules in the small percentage of dimers present in the vapour. In the liquid the percentage of dimers is larger than that of the monomeric molecule and therefore the band at  $1448\text{ cm}^{-1}$  becomes much stronger than that at  $1483\text{ cm}^{-1}$ . The intermediate band at  $1472\text{ cm}^{-1}$  may be due to the same vibration in the second molecule in the dimer. Similarly, the band at  $1590\text{ cm}^{-1}$  due to the vapour has a weak component at  $1570\text{ cm}^{-1}$  which becomes very strong in the spectrum due to the liquid, while the component at  $1590\text{ cm}^{-1}$  becomes very weak. This latter band is thus due to the single molecule and the band at  $1570\text{ cm}^{-1}$  is due to the dimer. The group of bands at  $1020\text{ cm}^{-1}$  due to the

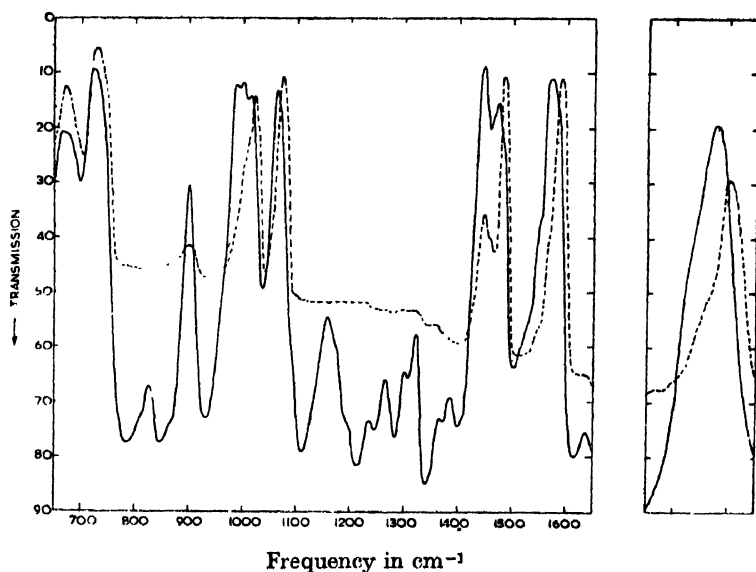


Fig. 3. Infrared spectra of bromobenzene.

..... vapour.

— liquid.

vapour also undergoes remarkable changes with the change from vapour to the liquid state. In the case of the vapour the strong band at  $1022\text{ cm}^{-1}$  has two weak companions at  $1010\text{ cm}^{-1}$  and  $1000\text{ cm}^{-1}$  respectively. In the spectrum

due to the liquid the band at  $1000\text{ cm}^{-1}$  becomes the strongest and there are a strong new band at  $990\text{ cm}^{-1}$  and a slightly weaker band at  $1015\text{ cm}^{-1}$ . In the Raman spectrum of the liquid there is a strong line at  $1000\text{ cm}^{-1}$  due to the breathing vibration of the ring, but this vibration gives a very weak band at the same position in the infrared spectra due to fluoro- and chlorobenzene in the liquid state. The other band at  $1022\text{ cm}^{-1}$  is due to the  $A_1$  mode corresponding to mode No. 12 of benzene. The band at  $1072\text{ cm}^{-1}$  due to the vapour only shifts to  $1065\text{ cm}^{-1}$  without any change in its strength. The Raman line of this frequency-shift is very strong and it has been assigned by previous workers to the  $A_1$  mode corresponding to mode No. 19A of benzene. It appears, however, that the structure of the band at  $1072\text{ cm}^{-1}$  does not change with the change of state, and therefore, this band may be due to the C-H bending vibration. In that case the band at  $1010\text{ cm}^{-1}$  may be due to the  $A_1$  component mentioned above in the single molecule and the band at  $990\text{ cm}^{-1}$  may be due to the same mode in the dimer. The band at  $1000\text{ cm}^{-1}$  is then to be assigned to the breathing vibration of the ring both in the monomeric and dimeric molecules.

The C-H stretching vibrations in the vapour give a very strong band  $3105\text{ cm}^{-1}$  and two weak bands at  $3075$  and  $3065\text{ cm}^{-1}$  respectively. In the spectrum due to the liquid the strong band shifts to  $3075\text{ cm}^{-1}$  and there is a weak band at  $3040\text{ cm}^{-1}$ . The band  $3075\text{ cm}^{-1}$  is thus to be assigned to a mode in the dimer corresponding to mode No. 20B of benzene. The corresponding band due to the single molecules in the liquid seems to be extremely weak.

The spectra due to the solutions of bromobenzene in carbon tetrachloride and chloroform are slightly different from the spectrum due to the pure liquid. The band  $725\text{ cm}^{-1}$  of the liquid shifts to  $718\text{ cm}^{-1}$  and  $710\text{ cm}^{-1}$  respectively in the spectra of the two solutions. As this band is also due to a C-H bending oscillation, the shifts mentioned above indicate the formation of weak hydrogen bonds with the chlorine atoms of the solvent molecules. The relative strengths as well as frequencies of the bands  $1485$  and  $1470\text{ cm}^{-1}$  of the liquid also undergo changes when the liquid is dissolved in the two solvents mentioned above. The strong band  $1470\text{ cm}^{-1}$  of the liquid shifts to  $1465\text{ cm}^{-1}$  and becomes weaker while weaker band  $1485\text{ cm}^{-1}$  shifts to  $1475\text{ cm}^{-1}$  and becomes very strong in the cases of both the solutions. Such changes are also observed in the cases of the bands  $1585\text{ cm}^{-1}$  and  $1570\text{ cm}^{-1}$  of the liquid which shift to  $1575$  and  $1565\text{ cm}^{-1}$  respectively in the spectra of both the solutions. Finally, the band  $3040\text{ cm}^{-1}$  due to C-H stretching oscillation in the liquid shifts to  $3030\text{ cm}^{-1}$  and becomes stronger while the band  $3075\text{ cm}^{-1}$  shifts to  $3080$  and becomes very weak when the liquid is dissolved in chloroform.

#### (d) *Iodobenzene*

It can be seen from Fig. 4 that although the absorption due to the vapour is weak owing to the low vapour pressure in the cell, the relative strengths of some

TABLE III  
Bromobenzene  
 $\nu$  in  $\text{cm}^{-1}$

Liquid at 28°C	Vapour at 28°C	4% Solution in $\text{CCl}_4$	3% Solution in $\text{CHCl}_3$
665 (s)			
	670 (m)	670 (vs)	670 (s, vb)
674 (s)			
	678 (m)	680 (m)	
725 (vs, b)	728 (vs, b)	718 (s)	710 (m)
825 (vw)			875 (w)
900 (s)	900 (vw)	900 (w)	900 (vw)
990 (vs)		990 (s)	990 (vw)
1000 (vs)	1000 (m)	1000 (s)	1000 (w)
	1010 (m)		
1016 (s)	1020 (s)	1018 (vs)	1020 (s)
			1045 (m)
1064 (vs)	1072 (vs)	1065 (vs)	1065 (s)
1160 (m)			
1175 (m)			
1175 (m)			
1195 (w)			
1235 (vw)			
1265 (w)			
1300 (vw)			
1322 (m)			
1362 (vw)			
1385 (w)			
			1400 (w)
		1428 (w)	1425 (w)
1447 (vs)	1448 (m)	1448 (vs)	1445 (vs)
1470 (s)	1460 (w)	1465 (w)	1465 (w)
		1475 (vs)	1475 (vs)
1485 (m)	1484 (vs)		
1515 (vw)		1515 (vw)	
1530 (w)		1530 (vw)	
1550 (m)	1550 (vw)	1550 (m)	1550 (vw)
1570 (vs)	1570 (m)	1565 (s)	1565 (s)
		1575 (s)	1578 (vs)
1585 (s)	1588 (vs)		
1638 (w)	1640 (vw)		
1700 (vw)			
1726 (w)			
1775 (vw)	1775 (vw)		
1788 (w)	1788 (w)		
1862 (m)	1850 (vw)	1860 (w)	
	1870 (w)		
1880 (w)	1880 (w)		
1952 (m)	1952 (w)	1948 (w)	
1975 (w)	1970 (w)		
3040 (m)	3060 (w)	3040 (w)	3020 (s, vb)
3075 (vs, b)	3075 (w)	3075 (s)	3080 (vw)
	3102 (vs, b)		

of the bands are different from those of the corresponding bands due to the pure liquid. The very weak band at  $1445\text{ cm}^{-1}$  of the vapour becomes strong and the band  $1482\text{ cm}^{-1}$  shifts to  $1475\text{ cm}^{-1}$  in the spectrum due to the liquid. The band at  $1018\text{ cm}^{-1}$  of the vapour is accompanied by weaker bands at 1010, 1000, 986 and  $975\text{ cm}^{-1}$  respectively, but in the spectrum due to the liquid the band at  $998\text{ cm}^{-1}$  is stronger than the band  $1015\text{ cm}^{-1}$  while the band  $1010\text{ cm}^{-1}$  is absent. These changes can be explained on the assumptions that in this case also the vapour consists predominantly of monomeric molecules with a small percentage of dimers which increases when the vapour is liquefied and that the line  $998\text{ cm}^{-1}$  may be due to the  $A_1$  mode of the single molecule in the liquid corresponding to mode No. 19A of benzene and the band  $990\text{ cm}^{-1}$  may be the corresponding band of the dimer. Similarly, the band  $1018\text{ cm}^{-1}$  due to the vapour is to be assigned to mode No. 12 of the benzene ring and the corresponding band of the dimer may be identified with the weak band  $1010\text{ cm}^{-1}$ . In the spectrum due to the liquid the strengthening of the latter band and slight shift of the former band may be responsible for producing a single strong band at  $1013\text{ cm}^{-1}$ . The bands  $1475$  and  $1443\text{ cm}^{-1}$  of the liquid may also be due respectively to the monomeric and dimeric molecules in the liquid. The formation of hydrogen bond in the liquid is indicated by the fact that the strong band  $3090\text{ cm}^{-1}$  due to C-H vibration corresponding to mode 20B of benzene shifts to  $3075\text{ cm}^{-1}$  and becomes relatively weak in the spectrum due to the liquid.

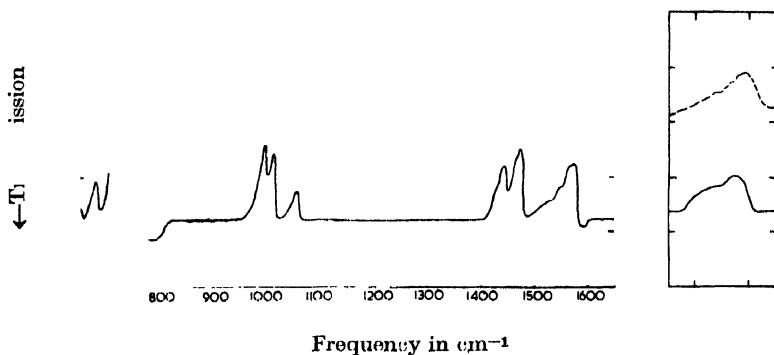


Fig. 4. Infrared spectra of iodobenzene.

..... vapour.

— — — liquid.

In the case of the solution in carbon tetrachloride the band  $1442\text{ cm}^{-1}$  becomes stronger than the band  $1472\text{ cm}^{-1}$  and the weak band  $1450\text{ cm}^{-1}$  of the vapour becomes quite strong. Also the line due to C-H valence oscillation shifts to  $3078\text{ cm}^{-1}$ . In the spectrum due to the solution in chloroform on the other hand the band  $3040\text{ cm}^{-1}$  is stronger than the band  $3073\text{ cm}^{-1}$  and there is a new band at  $2990\text{ cm}^{-1}$ . The diminution of the frequency from  $3090\text{ cm}^{-1}$  to  $3078\text{ cm}^{-1}$  in the case may be due to the formation of weak H..Cl bond between the solvent and solute molecules.

*On the Infrared Spectra of Fluoro-, Chloro-, Bromo-, etc.* 621

TABLE IV  
Iodobenzene  
 $\nu$  in  $\text{cm}^{-1}$

Liquid at 28°C	Vapour at 28°C	Solution in $\text{CCl}_4$	Solution in $\text{CHCl}_3$
640 (vw)			
650 (w)	650 (m, b)	652 (m)	650 (s)
670 (vw)		670 (w)	675 (m)
680 (m)	680 (w)	680 (s)	
723 (vs)	725 (s)	720 (vs)	700 (m)
900 (vw)	890 (vw)	890 (vw)	895 (vvw)
	915 (vw)		920 (vvw)
	975 (vw)		
990 (w)	986 (vw)	998 (vs)	997 (vs)
998 (s)			
	1000 (m)		
1013 (s)	1010 (w)		
	1018 (s)	1012 (s)	1012 (vs)
1060 (m)	1062 (m)	1058 (s)	1055 (m)
		1320 (vw)	1300 (vw)
1430 (w)			1425 (w)
1443 (s)	1445 (vvw)	1440 (vs)	1440s(vs)
1465 (m)		1465 (w)	1465 (w)
1475 (s)	1470 (w)	1470 (s)	1470 (s)
	1482 (s)		
1530 (vw)			
1550 (w)	1550 (vvw)	1550 (m)	1545 (w)
1565 (m)	1570 (m)	1565 (s)	1565 (m)
1576 (s)	1585 (s)		1573 (s)
			2990 (w)
3025 (w, b)	3040 (vw)	3040 (vw)	3038 (vs)
3075 (m, b)	3070 (vw)	3080 (vs)	3075 (w)
	3090 (s)		

It can thus be concluded from the results discussed in the previous sections that the frequencies of the modes of vibration of the single molecules of the four monohalogen substituted benzenes can be obtained only from the spectra of the compounds in the vapour state and that these frequencies are

invariably larger than the corresponding frequencies observed in the spectra of the compounds in the liquid state. The results also show that the intermolecular interaction in the liquid state is stronger in the cases of fluorobenzene and chlorobenzene than in the other two cases and this is in conformity with the larger chemical affinity of these two substituent halogen atoms.

#### ACKNOWLEDGMENT

The work was done under a scheme sanctioned by the Council of Scientific and Industrial Research and two of the authors (S.C.S. and P.K.B.) are thankful to the Council for the financial help. They are also indebted to the authorities of the Indian Association for the Cultivation of Science for the facilities for carrying out the investigation.

#### REFERENCES

- Landolt-Börnstein, 1951, Tables of Constants Auf. 6, Band 1, Teil 2.  
Lecomte, J., 1937, *J. de Physique*, **7**, 889.  
Mecke-Kerkhof, 1951, Landolt-Börnstein Tables, Auf. 6, Band 1, Teil 2.  
Mortimer, F. S., Blodgett, R. B. and Farrington, D., 1947, *J. Amer. Chem. Soc.*, **69**, 822.  
Pitzer, K. S. and Scott, D. W., 1943, *J. Amer. Chem. Soc.*, **65**, 803.  
Plyler, E. K., 1949, *J. Chem. Phys.*, **17**, 218.  
Sponer, H. and Kirby-Smith, J. S., 1941, *J. Chem. Phys.*, **9**, 667.

## ORIENTED TRANSFORMATION OF MAGNESITE

D. R. DASGUPTA

GEOLOGICAL SURVEY OF INDIA

29, CHOWRINGHEE, CALCUTTA-16

(Received November 11, 1964)

## Plate XI

**ABSTRACT.** The transformation of magnesite into periclase under heat treatment has been studied by single crystal X-ray diffraction method. It was observed that a single crystal of magnesite, when heated to about 450°C, transformed into a single crystal of periclase with orientational relationships between the two phases. One of the triad axes of rhombohedral crystal of magnesite became parallel to one of the triad axes of cubic crystal of periclase with three diad axes of both the phases being interchanged.

## INTRODUCTION

Magnesite ( $\text{MgCO}_3$ ) falls in the calcite group of minerals. Though no single crystal structure analysis of this particular mineral has been done, its difference from that of calcite is only in its cell dimensions, the positions of calcium ions being replaced by magnesium ions in magnesite. A pure magnesite should have a chemical formula like  $\text{MgCO}_3$ ; but in nature a slight amount of  $\text{Mg}^{++}$  is always replaced by other divalent ions such as  $\text{Fe}^{++}$ ,  $\text{Mn}^{++}$ ,  $\text{Ca}^{++}$  etc. Thermal decomposition of magnesite had been studied by different workers (Cuthbert and Rowland, 1947; Weiden, 1954) and in the d.t.a. curve for magnesite an endothermic peak at around 650°C and a small exothermic peak at a slightly higher temperature were observed. The endothermic peak was due to the decomposition of magnesite into periclase ( $\text{MgO}$ ) and  $\text{CO}_2$ ; the exothermic peak was explained as due to the crystallisation of periclase. Kulp, Kent and Kerr (1951) observed that the peak temperature for endothermic reaction varied within a range of 660° to 690°C. Beck (1950) had ascribed the inflection on the downward sweep in the d.t.a. curve, after the main endothermic peak, to the formation of an intermediate carbonate such as  $\text{MgO.MgCO}_3$ . But his X-ray study did not provide any conclusive evidence. Cramer and Bachman (1955) studied the transformation of  $\text{MgCO}_3$  under various pressures of  $\text{CO}_2$ . Their observation under the electron microscope showed the following: The shape of magnesite grains remained unchanged during the decomposition.  $\text{MgO}$  was first formed on the outer side of  $\text{MgCO}_3$  grains as a fluffy layer of small crystallites. With increasing  $\text{CO}_2$  pressure, the size of  $\text{MgO}$  crystallites increased and the velocity of decomposition decreased. The thermal transformation of siderite ( $\text{FeCO}_3$ ), a mineral belonging to the same structural group, was studied by Bernal, Dasgupta and Mackay (1959) and Dasgupta

(1960) by X-ray diffraction method. Cleavage rhombohedron of siderite was sealed in a tube under vacuum and heated to about 550°C. After rapid cooling it was observed that the crystal, without changing its shape, became highly magnetic and the X-ray examination of the same crystal revealed the presence of oriented intergrowths of FeO and Fe<sub>3</sub>O<sub>4</sub>. However, upto the present time no work on the transformation of magnesite by single crystal X-ray diffraction method has come to the author's notice. The present work was, therefore, intended for finding out if magnesite would also transform into periclase with orientational relationships between the two phases.

#### EXPERIMENTAL

Beautiful milky white single crystals of rhombohedral shape were separated from sample (Ind. Mus. Reg. No. 8677, found at Dhoba and Delwaidhar, Almora Dt., Uttar Pradesh). The sample as a whole, when examined by X-ray powder diffraction method, proved to be mainly magnesite with minor amount of dolomite and traces of talc. However, single crystals, separated from that sample, did not contain dolomite or talc. Rotation photograph of one such crystal, taken along the two-fold axis of the rhombohedral crystal in a 3 cm. radius cylindrical camera with Ni-filtered Cu-radiation, is shown in Fig. 1. Similar crystals were heated in a covered porcelain crucible at about 450°C for five hours and then cooled down to room temperature. It was observed that the crystals decrepitated and had broken down into small fragments. The colour of the small fragments turned slightly pinkish but the rhombohedral shape was still maintained in those small fragments. A 30° oscillation photograph of one such crystal along the same axis as before was taken in the same camera with similar radiation (Fig. 2). It was seen that the crystal was partly transformed into periclase. The sharp spots in Fig. 2 were due to untransformed magnesite, while the powder diffraction arcs showing definite preferred orientation were due to periclase. Measurement of periodicity from the fibre pattern due to periclase showed that the direction of preferred orientation coincided with a two-fold axial direction of the cubic crystal of periclase. It has been already stated that the crystals of magnesite heated to 450°C turned slightly pinkish. But when such crystals were powdered, it was observed that the inner portions of the crystals were still milky white, indicating that the surface of the crystal was affected first during the transformation. This seems to be in agreement with Cremer and Bachman's (1955) observation. Powder diffraction photograph of crystals of magnesite heated to 600°C for five hours showed complete conversion of magnesite into periclase with a slight change in the degree of crystallisation.

#### DISCUSSIONS

The orientational relationship, which was observed during the transformation of magnesite to periclase, can be explained from structural point of view. Magnesite, which has a face-centred rhombohedral structure, can be very well



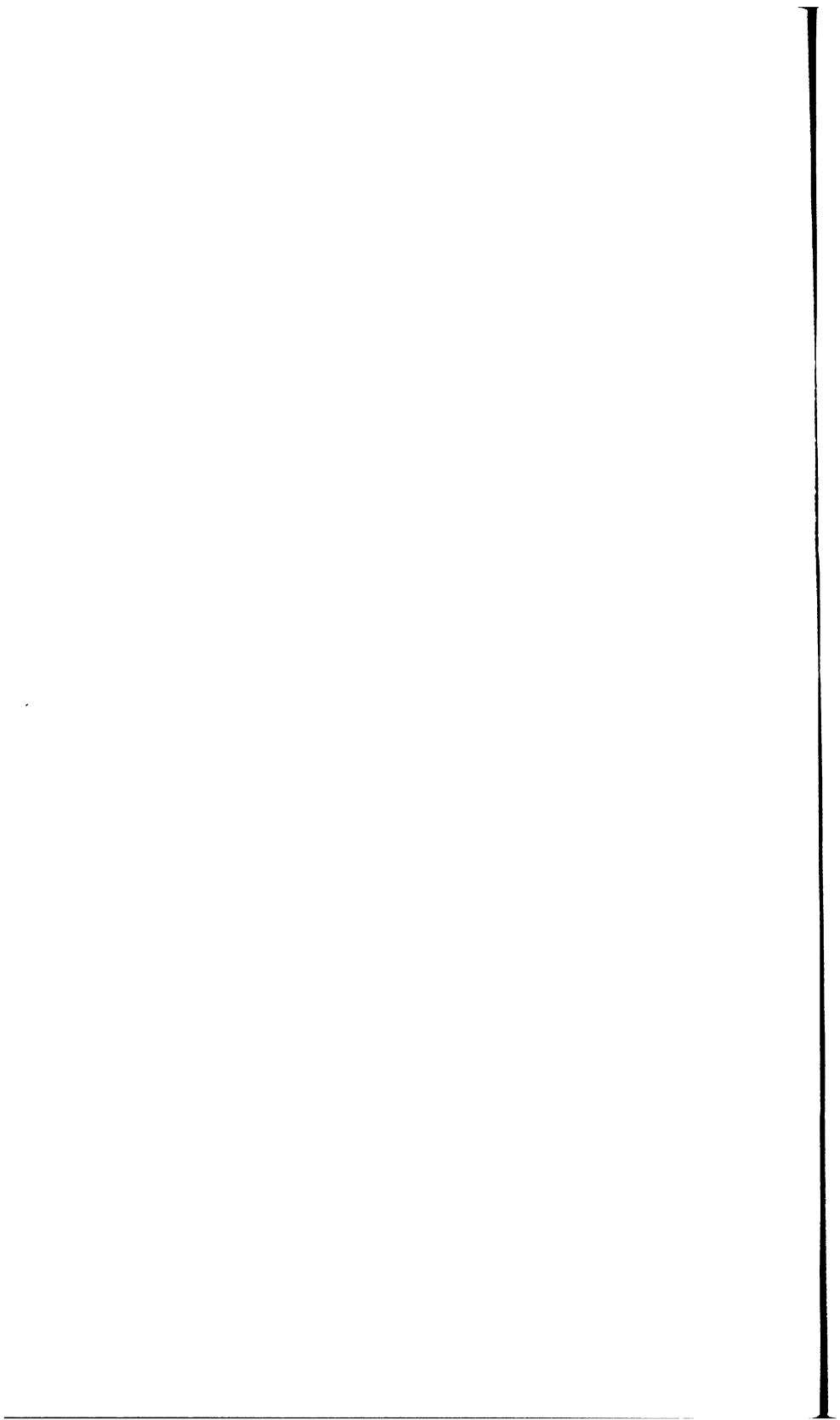


Fig 1

Fig. 2

Fig. 1. Rotation photograph of single crystal of magnesite taken along a diad axis of the rhombohedral crystal with Ni-filtered Curadiation

Fig. 2. Rotation photograph of single crystal of magnesite heated to 450°C. taken along the same direction with same radiation.





compared to a distorted NaCl structure. If the  $\text{MgCO}_3$  structure is considered along a threefold axis of the rhombohedral crystal, it can be seen that the  $\text{CO}_3$  ions are arranged in cubic closed-packed (ABCABCABCA...) layers with  $\text{Mg}^{++}$  ions in octahedral positions in between layers. The oblate shape of the  $\text{CO}_3^{--}$  ions makes the crystal to be rhombohedral instead of being cubic. Periclase, on the other hand, has a simple NaCl structure. The arrangements of  $\text{CO}_3$  and  $\text{O}^{--}$  along the three-fold axis of magnesite and periclase are shown in Fig. 3.

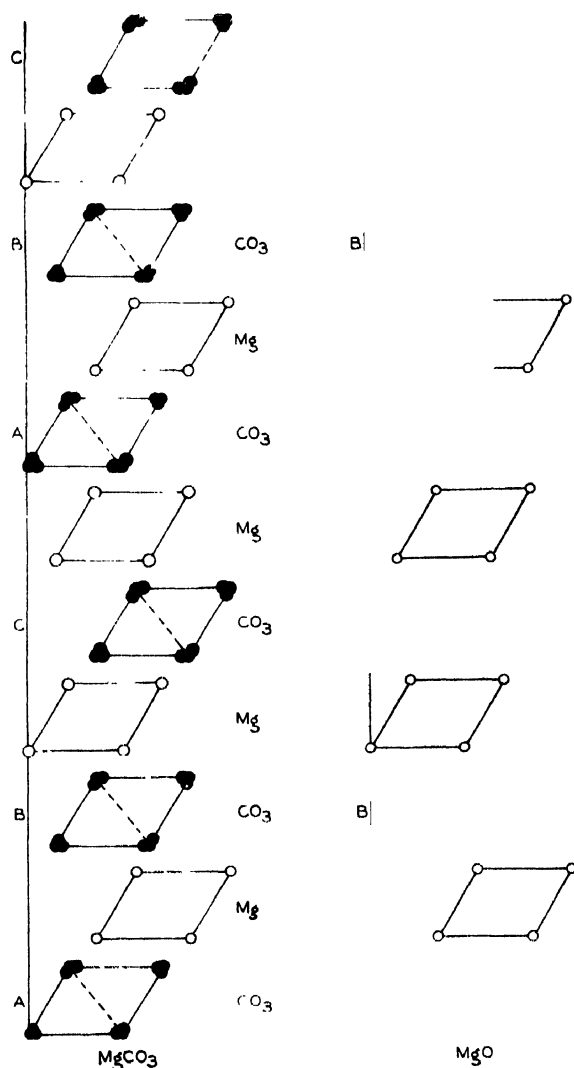
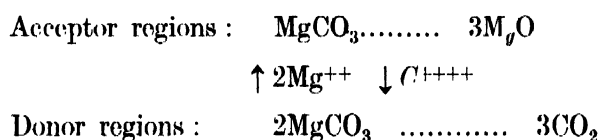


Fig. 3. Arrangements of  $\text{CO}_3$  and O layers along three-fold axis in Magnesite and Periclase Mg layers are placed in octahedral position in between  $\text{CO}_3$  and O layers.

To arrive at the structure of periclase from that of magnesite, all one has to do is to press the structure along the three-fold axis till the edges meeting that axis make angles equal to  $90^\circ$  to each other. So, when magnesite is heated,  $\text{CO}_2$

begins to come out from the  $\text{CO}_3^{--}$  layers as a result of which a strain is produced along the three-fold axis. With the complete expulsion of  $\text{CO}_2$ , the rhombohedral cell changes into a cubic cell of periclase. Thus, a three-fold axis of the rhombohedral magnesite crystal becomes a three-fold axis of the cubic periclase crystal, the three diad axes of both the phases being interchanged with each other. The effect of strain in changing the rhombohedral cell into a cubic cell is very much evident from the X-ray photograph due to periclase.

It may be pointed out here that in the case of  $\text{FeCO}_3$  a similar sort of oriented decarbonation occurred (Bernal, Dasgupta and Mackay, 1959; Dasgupta, 1960) and attention was drawn to the difficulty of reconciling this with the fact that two-thirds of the oxygen was lost during the decomposition. Ball and Taylor (1961) suggested that this difficulty could be removed if an inhomogeneous mechanism of transformation is considered in this case. The fact that the surface of the magnesite crystal was affected first during the transformation may be an indication for an inhomogeneous mechanism. In that case one is tempted to think that there are acceptor and donor regions in the magnesite crystals and the migrations of ions from these regions may take place in the following way :



However, it will be very much premature to describe the mechanism of transformation like this unless a complete study is made with other minerals of the calcite group.

#### ACKNOWLEDGMENT

The author is very much grateful to Dr. M. V. N. Murthy, Superintending Geologist, Central Petrological Laboratories, Geological Survey of India, for his sincere encouragement during the progress of the work.

#### REFERENCES

- Bock, C. W., 1950, *Amer. Min.* **35**, 985.  
 Bernal, J. D., Dasgupta, D. R. and Mackay, A. L., 1959, *Clay Min. Bull.* **4**, 15.  
 Cremer, E. and Bachman, L. 1955, *Z. Electrochem.* **59**, 407.  
 Cuthbert, F. L., Rowland, R. A. 1947, *Amer. Min.*, **32**, 111.  
 Dasgupta, D. R. 1960, *Ind. Jour. Phys.* **35**, No. 8, 401.  
 Kulp, J. L. Kent, P and Kerr, P. F., 1951, *Amer. Min.* **36**, 643.  
 Ball, M. C. and Taylor, H. F. W., 1961, *Min. Mag.* **32**, No. 253, 754.  
 Weiden, P., 1954, *Tschermak, Min. Pel. Mitt. Ser 3*, **5**, 85 (Abstract)

# A STUDY OF THE ANGLE OF SPREAD OF THE DOWNCOMING RADIO-WAVES

N. N. SH

DEPT OF PHYSICS, BIRLA INST. OF TECH. AND SCIENCE, PILANI (INDIA)

(Received November 1, 1964)

## Plate XII

**ABSTRACT.** The angle of spread has been measured for the vertical-incidence pulsed radio-waves returned from both the *E*- and the *F*-regions of the ionosphere on two undisturbed days. Observations cover all the hours of the day and night.

In the case of the *E*-region returns, the value of the angle of spread is found to occur between 50' and 7" with an average value of 4° 20'. The most preferred range of this angle is found to be 4° to 5°.

In the case of the *F*-region returns, the value of the angle of spread is found to occur between 30' and 10" with an average value of 4° 50'. The most preferred range of this angle is again found to be 4° to 5°.

## INTRODUCTION

From the findings of Ratcliffe *et al.* (1933) and Pawsey (1935), Ratcliffe (1948) concluded that radio waves are returned by a process of diffractive reflection from the ionospheric irregularities. On account of the presence of these irregularities which act as scattering centres, there is a cone of radio waves scattered to the receiving point. The fading of a singly-reflected wave can then be attributed to the changing interference conditions between the various elementary wavelets scattered from the different scattering centres within the cone. The semiangle of this cone is called the angle of spread of the scattered components.

A method of determination of the angle of spread was described by Briggs *et al.* (1950). Later Briggs (1951) described another much simpler but slightly approximate method for the determination of the angle of spread. Assuming the horizontal movement of the ionospheric irregularities to be the main cause of fading, he deduced the relation

$$N = \frac{2V}{\lambda} \sin \theta$$

where  $N$  = number of maxima of the fading pattern per second.

$V$  = horizontal drift velocity of the ionospheric irregularities.

$\lambda$  = wave-length of the sounding radio-wave.

and  $\theta$  = angle of spread.

The above relation has been used in the present investigations to measure the angle of spread.

#### EXPERIMENTAL DETAILS

The records were taken at Waltair (Geographic Lat.  $17^{\circ} 43' \text{ N}$ ; long.  $83^{\circ} 18' \text{ E}$ ; Geomag. lat.  $7.4^{\circ} \text{ N}$ ) with the vertical-incidence pulsed radio-waves by the three spaced-receivers technique of Mitra (1949). The transmitting antenna was of multiple-wire delta-type and the receiving antennas were three tuned dipoles fixed parallel to one another at the three corners of a right angled isocles triangle. The two equal sides of the triangle were each of 108 meters and were oriented along the East-West and North-South directions. Each record was of 4 to 6 minutes duration. A typical record is shown in Fig. 1.

The horizontal drift velocity,  $V$ , of the ionospheric layer was determined using all the three fading curves by the similar fade method of Mitra (1949), and the number of maxima of the fading pattern per second,  $N$  was obtained using only the central fading curve.

The records on the days of magnetic disturbance or solar flare were rejected. The angle of spread of the downcoming radio waves was determined with fifty records in all. Twenty five of these were due to the  $F$ -region returns and were taken on 15th December 1959. The remaining twenty five were due to the  $E$ -region returns and were taken on 17th December 1959. On these two days no solar flare was recorded at Kodaikanal (lat.  $10^{\circ} 14' \text{ N}$ , long.  $77^{\circ} 29' \text{ E}$ , Geomag. lat.  $00^{\circ} 44' \text{ N}$ ) and no magnetic disturbance was recorded at Alibag (lat.  $18^{\circ} 38' \text{ N}$ , long.  $72^{\circ} 52' \text{ E}$ , Mag. Lat.  $9^{\circ} \text{ N}$ )\*. The International Magnetic Character figures for 15th December and 17th December 1959 are respectively 1 and 0. The records of both the days cover all the hours of the day and night.

For the  $E$ -region returns the operating frequency was 2.5 Mc/s and for the  $F$ -region returns the operating frequency was 5.6 Mc/s during the day-light hours and 2.5 Mc/s during the night hours. The records in the night hours of  $E$ -region are due to reflection from sporadic  $E$ -layer. The reflection height for  $E$ -region was between 100 to 120 km. and that for  $F$ -region between 255 to 315 km.

#### EXPERIMENTAL RESULTS

In the case of the  $E$ -region returns, the values of the angle of spread have been found to occur between  $50'$  and  $7^{\circ}$  with an average value of  $4^{\circ} 20'$ . In the case of the  $F$ -region returns, the values have been found to be between  $30'$  and  $10^{\circ}$ , with an average of  $4^{\circ} 50'$ .

From the histograms (Fig. 2) it is observed that the most preferred range of the angle of spread for the returns from both the regions is  $4^{\circ}$  to  $5^{\circ}$ . In the case of the  $E$ -region returns the angle of spread does not go beyond  $7^{\circ}$ , but in the case

---

\*The geomagnetic latitudes of Waltair and Alibag are very nearly the same.

ST.

F-LAYER

2. '59



0 sec

qu

in b

ord

yp























